INTERPLAY BETWEEN IMMUNITY AND FIBROSIS

EDITED BY: Anna-Maria Hoffmann-Vold, Oliver Distler and
Jeska Kirsten De Vries-Bouwstra
PUBLISHED IN: Frontiers in Immunology

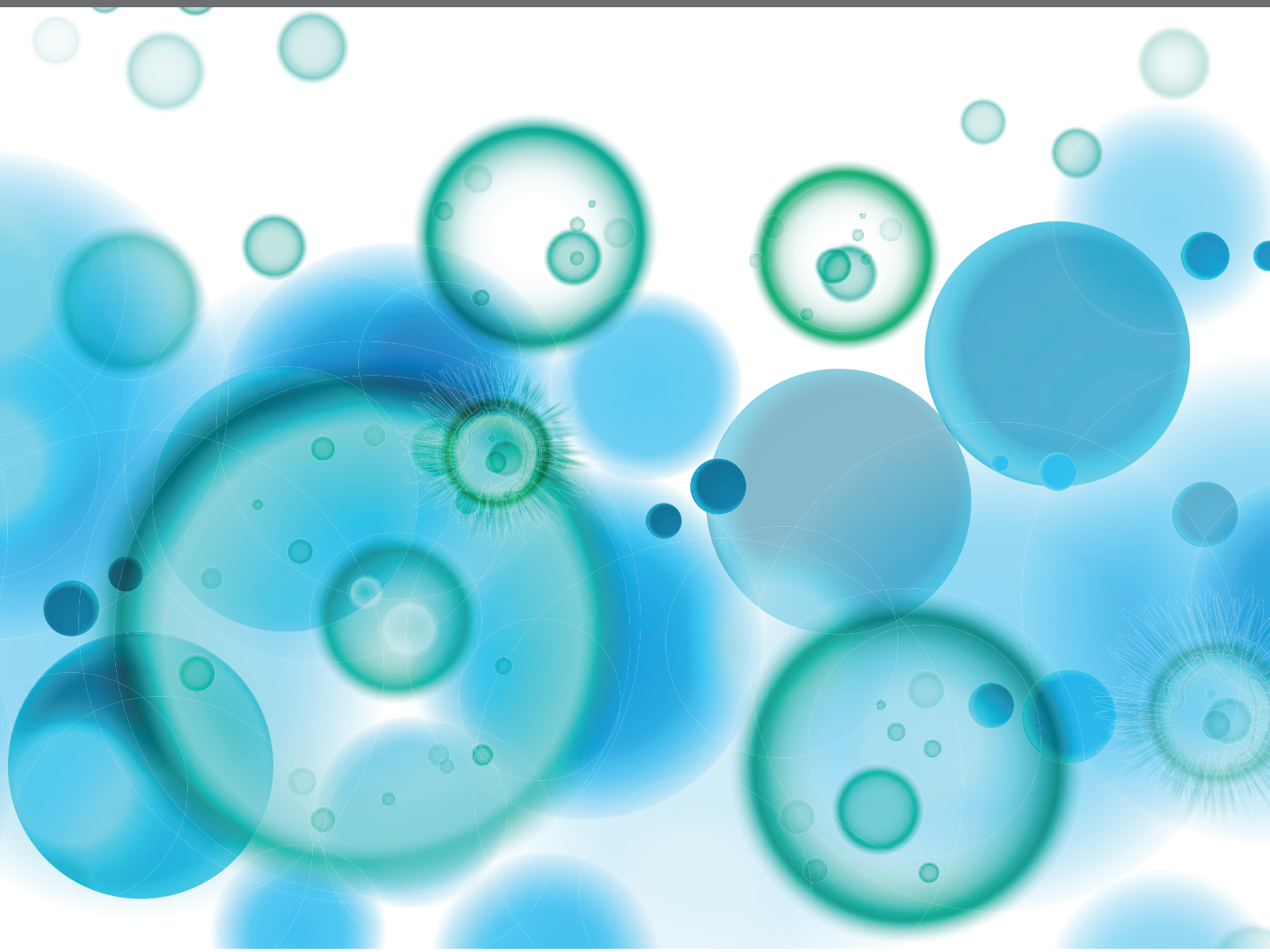

frontiers Research Topics

frontiers

ISSN 1664-8714
ISBN 978-2-88971-833-7
DOI 10.3389/978-2-88971-833-7

About Frontiers

Frontiers is more than just an open-access publisher of scholarly articles: it is a pioneering approach to the world of academia, radically improving the way scholarly research is managed. The grand vision of Frontiers is a world where all people have an equal opportunity to seek, share and generate knowledge. Frontiers provides immediate and permanent online open access to all its publications, but this alone is not enough to realize our grand goals.

Frontiers Journal Series

The Frontiers Journal Series is a multi-tier and interdisciplinary set of open-access, online journals, promising a paradigm shift from the current review, selection and dissemination processes in academic publishing. All Frontiers journals are driven by researchers for researchers; therefore, they constitute a service to the scholarly community. At the same time, the Frontiers Journal Series operates on a revolutionary invention, the tiered publishing system, initially addressing specific communities of scholars, and gradually climbing up to broader public understanding, thus serving the interests of the lay society, too.

Dedication to Quality

Each Frontiers article is a landmark of the highest quality, thanks to genuinely collaborative interactions between authors and review editors, who include some of the world's best academicians. Research must be certified by peers before entering a stream of knowledge that may eventually reach the public - and shape society; therefore, Frontiers only applies the most rigorous and unbiased reviews.
Frontiers revolutionizes research publishing by freely delivering the most outstanding research, evaluated with no bias from both the academic and social point of view. By applying the most advanced information technologies, Frontiers is catapulting scholarly publishing into a new generation.

What are Frontiers Research Topics?

Frontiers Research Topics are very popular trademarks of the Frontiers Journals Series: they are collections of at least ten articles, all centered on a particular subject. With their unique mix of varied contributions from Original Research to Review Articles, Frontiers Research Topics unify the most influential researchers, the latest key findings and historical advances in a hot research area! Find out more on how to host your own Frontiers Research Topic or contribute to one as an author by contacting the Frontiers Editorial Office: frontiersin.org/about/contact

INTERPLAY BETWEEN IMMUNITY AND FIBROSIS

Topic Editors:
Anna-Maria Hoffmann-Vold, Oslo University Hospital, Norway
Oliver Distler, University of Zurich, Switzerland
Jeska Kirsten De Vries-Bouwstra, Leiden University Medical Center, Netherlands

Topic Editor Prof. Oliver Distler received financial support from Actelion, Bayer, Boehringer Ingelheim, Mitsubishi Tanabe Pharma companies. All other Topic Editors declare no competing interests with regards to the Research Topic subject.

Citation: Hoffmann-Vold, A.-M., Distler, O., De Vries-Bouwstra, J. K., eds. (2021). Interplay Between Immunity and Fibrosis. Lausanne: Frontiers Media SA.
doi: 10.3389/978-2-88971-833-7

Table of Contents

frontiers in Immunology

ORIGINAL RESEARCH
published: 22 November 2019
doi: 10.3389/fimmu.2019.02724

^{18}F-AzaFol for Detection of Folate Receptor-β Positive Macrophages in Experimental Interstitial Lung Disease—A Proof-of-Concept Study

Janine Schniering[1], Martina Benešová[2,3], Matthias Brunner[1], Stephanie Haller[2], Susan Cohrs[2], Thomas Frauenfelder[4], Bart Vrugt[5], Carol Feghali-Bostwick[6], Roger Schibli[2,3], Oliver Distler[1], Cristina Müller[2,3†] and Britta Maurer[1*†]*

[1] Department of Rheumatology, Center of Experimental Rheumatology, University Hospital Zurich, Zurich, Switzerland, [2] Center for Radiopharmaceutical Sciences, Paul Scherrer Institute, Villigen, Switzerland, [3] Department of Chemistry and Applied Biosciences, ETH Zurich, Zurich, Switzerland, [4] Institute of Diagnostic and Interventional Radiology, University Hospital Zurich, Zurich, Switzerland, [5] Institute of Pathology and Molecular Pathology, University Hospital Zurich, Zurich, Switzerland, [6] Division of Rheumatology & Immunology, Medical University of South Carolina, Charleston, SC, United States

Background: Interstitial lung disease (ILD) is a common and severe complication in rheumatic diseases. Folate receptor-β is expressed on activated, but not resting macrophages which play a key role in dysregulated tissue repair including ILD. We therefore aimed to pre-clinically evaluate the potential of ^{18}F-AzaFol-based PET/CT (positron emission computed tomography/computed tomography) for the specific detection of macrophage-driven pathophysiologic processes in experimental ILD.

Methods: The pulmonary expression of folate receptor-β was analyzed in patients with different subtypes of ILD as well as in bleomycin (BLM)-treated mice and respective controls using immunohistochemistry. PET/CT was performed at days 3, 7, and 14 after BLM instillation using the ^{18}F-based folate radiotracer ^{18}F-AzaFol. The specific pulmonary accumulation of the radiotracer was assessed by *ex vivo* PET/CT scans and quantified by *ex vivo* biodistribution studies.

Results: Folate receptor-β expression was 3- to 4-fold increased in patients with fibrotic ILD, including idiopathic pulmonary fibrosis and connective tissue disease-related ILD, and significantly correlated with the degree of lung remodeling. A similar increase in the expression of folate receptor-β was observed in experimental lung fibrosis, where it also correlated with disease extent. In the mouse model of BLM-induced ILD, pulmonary accumulation of ^{18}F-AzaFol reflected macrophage-related disease development with good correlation of folate receptor-β positivity with radiotracer uptake. In the *ex vivo* imaging and biodistribution studies, the maximum lung accumulation was observed at day 7 with a mean accumulation of 1.01 ± 0.30% injected activity/lung in BLM-treated vs. control animals (0.31 ± 0.06% % injected activity/lung; $p < 0.01$).

OPEN ACCESS

Edited by:
Kutty Selva Nandakumar, Southern Medical University, China

Reviewed by:
Philip S. Low, Purdue University, United States
Adriaan Anthonius Lammertsma, VU University Medical Center, Netherlands

***Correspondence:**
Cristina Müller
cristina.mueller@psi.ch
Britta Maurer
britta.maurer@usz.ch

†These authors have contributed equally to this work

Specialty section:
This article was submitted to Autoimmune and Autoinflammatory Disorders, a section of the journal Frontiers in Immunology

Received: *14 August 2019*
Accepted: *06 November 2019*
Published: *22 November 2019*

Citation:
Schniering J, Benešová M, Brunner M, Haller S, Cohrs S, Frauenfelder T, Vrugt B, Feghali-Bostwick C, Schibli R, Distler O, Müller C and Maurer B (2019) ^{18}F-AzaFol for Detection of Folate Receptor-β Positive Macrophages in Experimental Interstitial Lung Disease—A Proof-of-Concept Study. Front. Immunol. 10:2724. doi: 10.3389/fimmu.2019.02724

Conclusion: Our preclinical proof-of-concept study demonstrated the potential of ^{18}F-AzaFol as a novel imaging tool for the visualization of macrophage-driven fibrotic lung diseases.

Keywords: interstitial lung disease, imaging biomarkers, animal model of lung fibrosis, macrophages, folate receptor, positron emission tomography, inflammation, folate-based ^{18}F-PET tracer

INTRODUCTION

In the US, 45% of deaths can be attributed to fibrotic disorders including pulmonary fibrosis (1), for which a global rise in mortality is observed (2). This large and heterogeneous group of parenchymal lung disorders, termed interstitial lung disease (ILD) shares the common feature of pulmonary fibrosis resulting in impaired respiratory function and often failure. The most prevalent forms of ILD are idiopathic pulmonary fibrosis (IPF) and ILD associated with connective tissue diseases (CTD-ILD). CTDs commonly complicated by ILD include systemic sclerosis (SSc) (3), idiopathic inflammatory myopathies (4), rheumatoid arthritis (5), systemic lupus erythematous (6), Sjögren's syndrome (7), mixed connective tissue disease (8), and undifferentiated connective tissue disease (9). Among the different CTD-ILDs, ILD is most prevalent in SSc with 70–90% of SSc patients developing ILD (10). The life expectancy is markedly reduced, especially in IPF and SSc-ILD, with a median survival of 2–3 years from diagnosis (2, 10).

Despite their clinical heterogeneity, increasing data suggest that in ILD fibrosis develops due to the same dysregulation of wound-healing mechanisms (11, 12).Whereas cell death of alveolar epithelial cells is considered the key trigger of ILD (13, 14), a growing body of (pre-)clinical data point to a similarly crucial pathogenic role of pulmonary macrophages and macrophage-released factors (15, 16). Macrophage activation was shown throughout different stages of ILD including early/mild (17), intermediate (18) as well as end-stage/severe stages (19), and also in different ILD etiologies (20). These observations argue either for a persistent role of macrophages throughout the disease process or for the existence of "inflammatory" or "macrophage-driven" subtypes of ILD (21, 22). Importantly, the persistence of macrophages seems to correlate with poor prognosis and reduced overall survival (17, 23). Thus, the development of macrophage-targeted imaging techniques for prognostic and treatment purposes in ILD might represent a valuable approach to improve the deleterious disease outcome (15).

Molecular imaging, including nuclear imaging approaches such as positron emission tomography (PET) are sensitive and allow the non-invasive visualization of pathophysiologic processes in real-time. This is a unique advantage over conventional morphological imaging modalities such as high resolution computed tomography (HRCT) scans or magnetic resonance imaging (MRI) (24). These conventional imaging techniques depict anatomical changes in organ architecture with high spatial resolution. They can, however, neither provide information on whether the observed changes are signs of inactive or active tissue remodeling, nor discriminate inflammatory from fibrotic processes, a crucial information for informed clinical decision making (12, 25). An example is the presence of ground glass opacities, which commonly are considered to reflect alveolitis. However, the notion of alveolitis being synonymous to inflammation has been abandoned in fibrosing ILD, since early fibrotic interstitial changes have the same appearance on HRCT (26).

In recent years, several studies have investigated the potential of 2-deoxy-2-[^{18}F]fluoro-D-glucose [^{18}F]FDG-PET/CT for diagnosis of ILD. [^{18}F]FDG is an unspecific, metabolic radiotracer for the assessment of cellular glucose metabolism, which has been shown to be elevated in ILD (27, 28). A disadvantage for its use in diagnosis and monitoring of ILD is that [^{18}F]FDG signals reflect metabolic activity, which can arise from both inflammatory and fibrotic cell types and can occur during different disease stages including those of stabilization or repair. This lacking discrimination of pathophysiologic stages of ILD diminishes the value of [^{18}F]FDG-PET/CT for informed treatment decisions and monitoring of therapeutic responses (29, 30).

In contrast, imaging approaches using target-specific radiotracers ideally aiming at a single key cell type in ILD may overcome this limitation of [^{18}F]FDG-PET/CT. So far, only few approaches have been successfully applied pre-clinically in ILD (31–36).

Activated macrophages express folate receptor-β (FR-β) in various pathological conditions including cancer and inflammatory diseases (37–39), whereas the number of FR-β-expressing macrophages is very low under physiological conditions (37, 40).

FR-β is a glycosylphosphatidylinositol (GPI)-anchored protein, which binds folic acid and folate-linked molecules with high affinity and internalizes them via endocytosis. Imaging

Abbreviations: ILD, Interstitial lung disease; PET/CT, Positron emission computed tomography/computed tomography; BLM, Bleomycin; IPF, Idiopathic pulmonary fibrosis; CTD-ILD, Connective tissue disease-associated interstitial lung disease; SSc, Systemic sclerosis; HRCT, High resolution computed tomography; MRI, Magnetic resonance imaging; [^{18}F]FDG, [^{18}F]fluorodeoxyglucose; FR-β, Folate receptor-β; GPI, Glycosylphosphatidylinositol; ^{18}F-AzaFol, 3′-Aza-2′-[^{18}F]-fluoro-folic acid; RT, Room temperature; HE, Hematoxylin and eosin; IHC, Immunohistochemistry; DAB, Diaminobenzidine; AEC, 3-Amino-9-ethylcarbazole; IF, Immunofluorescence; DAPI, 4′,6-Diamidino-2-phenylindole; RT-qPCR, Quantitative reverse transcription polymerase chain reaction; mRNA, Messenger RNA; Rplp0, 60S acidic ribosomal protein P0; p.i., Post injection; % IA/g, Percentage of the injected activity per gram of tissue mass; % IA/organ, Percentage of the injected activity per organ; MLEM, Maximum-likelihood expectation maximization IQR, Interquartile range; S.D., Standard deviation; UIP, Usual interstitial pneumonia; NSIP, Non-specific interstitial pneumonia; HP, Hydroxyproline.

of FR-β can be realized with folate radiotracers. A number of folic acid-based radiotracers have been used pre-clinically for the imaging of activated macrophages in non-pulmonary, inflammatory conditions including e.g., rheumatoid arthritis, activated osteoarthritis, or atherosclerosis (41–47), FR-targeted radiopharmaceuticals have, however, not been evaluated yet in the context of ILD. Furthermore, the number of clinical studies making use of FR-targeting nuclear imaging strategies is limited including one exploratory trial in rheumatoid arthritis patients (48), since no folate-based radiotracer for PET imaging is currently available for clinical application.

A novel ^{18}F-based folate PET radiotracer 3′-Aza-2′-[^{18}F]-fluoro-folic acid, herein referred to as ^{18}F-AzaFol), has recently been developed at the Center for Radiopharmaceutical Sciences ETH-PSI-USZ for FR imaging. The rationale to test this radiotracer instead of previously investigated macrophage imaging markers such as translocator protein (TSPO) was based on several disadvantages compared with ^{18}F-AzaFol: TSPO (a) is mainly expressed in the outer mitochondrial membrane (49), thus it is not a cell surface receptor, (b) exhibits a high multicellular, basal expression in the lungs (50), and (c) TSPO-targeting PET tracers are still facing difficulties for clinical implementation. While the first generation of TSPO PET tracers showed high non-specific binding due to their lipophilic character (51), newer TSPO targeted radiotracers with improved binding specificity and affinity have still limitations due to the allelic dependency of the binding capability resulting from TSPO polymorphisms (52–54).

In this preclinical proof-of-concept study, we aimed to evaluate the potential of ^{18}F-AzaFol-PET/CT for the specific visualization of macrophage-driven pathophysiologic processes in experimental ILD.

METHODS

Human Subjects

Surgical lung biopsies from patients with IPF (n = 39) and CTD-ILD (n = 14), who underwent lung transplantation, were analyzed for the expression of FR-β. Lung sections from excess tissue from lung organ donors served as controls (n = 26). The patients' characteristics including demographic and clinical data are summarized in the data supplement (**Supplementary Table 1**).

The local ethics committee approved the study (BASEC-No. 2017-01298), and informed consent was obtained from all patients.

Murine Model of Bleomycin-Induced Lung Fibrosis

As a representative animal model for experimental ILD, we used the well-established mouse model of BLM-induced lung fibrosis in this study. In the BLM model, inflammation peaks around day 7, whereas fibrosis reaches its maximum between days 14-21 (33, 35, 55). M1-like macrophages dominate the early inflammatory phase, whereas M2-like macrophages are most abundant in the pro-fibrotic phase, although they might appear as early as day 7 (56, 57).

Female C57BL/6J-rj mice (5–7 weeks old) were purchased from Janvier (Le Genest-Saint-Isle, France) and housed at the institutional animal facilities under defined temperature, humidity, and light conditions, and received *ad libitum* a standard rodent diet. After an acclimatization period of at least 7 days, lung fibrosis was induced in 8-week-old mice by instilling intratracheally a single dose of bleomycin sulfate (4 U/kg of body weight, Baxter, cantonal pharmacy Zurich, Switzerland) dissolved in sterile saline solution under isoflurane anesthesia (33–35). Control mice received equivalent volumes of 0.9% NaCl (50 μl). At days 3, 7, and 14 after the BLM instillation, biodistribution, and imaging studies were performed. Perfused lungs of separate animals were harvested for immunostainings, histological, and molecular analyses.

All animal experiments performed in this study were approved by the cantonal veterinary offices and conducted in strict compliance with the Swiss animal welfare guidelines. For all experiments, mice were randomized into the different study groups in a non-blinded manner.

Histology

For histology, perfused middle, caudal, and accessory lobes of the right mouse lung were inflated with 10% neutral-buffered formalin solution and fixed overnight at room temperature (RT). After embedding in paraffin, lung sections were cut at a thickness of 4 μm and stained with hematoxylin and eosin (HE) for analysis of the lung architecture and the presence of cellular infiltrates, and with Picrosirius Red to detect collagen deposition using standard protocols.

Immunohistochemistry on Murine Lung Tissues

For immunohistochemistry (IHC) on murine tissues, lung sections were deparaffinized and rehydrated, and then subjected to heat-mediated antigen retrieval with 10 mM sodium citrate buffer (pH = 6.0) at 95°C for 15 min. After blocking of endogenous peroxidase activity with 3% hydrogen peroxide (15 min, RT), sections were blocked with 10% normal goat serum (1 h, RT) followed by blocking of endogenous biotin using an Avidin/Biotin blocking kit (Vector Laboratories, Burlingame, CA, United States). Afterwards, primary antibodies for F4/80 (rat anti-mouse F4/80, clone Cl:A3-1, 1:100, AbD Serotec; Kidlington, United Kingdom), and FR-β (rabbit anti-mouse FR-β, 1:400, Genetex, Irvine, CA, United States) were applied on the specimens and incubated overnight at 4°C. Isotype- and concentration-matched IgGs served as negative controls. Next, biotin-labeled goat anti-rat or anti-rabbit secondary antibodies (all from Vector Laboratories) were applied (30 min, RT). This was followed by incubation with the Vectastain ABC Elite HRP kit for 30 min at RT (Vector Laboratories). Finally, stainings were visualized using 3,3′-diaminobenzidine (DAB) in case of F4/80, or 3-amino-9-ethylcarbazole (AEC) (all from Vector Laboratories) in case of FR-β, and sections were counterstained with Mayer's hematoxylin (J.T. Baker, Deventer, Netherlands).

Immunohistochemistry on Human Lung Tissues

Immunohistochemistry was performed using an automated single-staining procedure (Benchmark Ultra; Ventana Medical Systems). Briefly, 4 μm thick sections were stained using mouse monoclonal anti-human antibodies directed against CD68 (clone PG-M1, Dako, 1:50) and FR-β (clone OTI8G1, Origen, 1:50). Detection was completed with respective secondary antibodies and the OptiView DAB Kit (Ventana Medical Systems).

Immunofluorescence

Immunofluorescence (IF) stainings were performed using the MaxDouble IF staining kits for rat and rabbit primary antibodies (MaxVision Biosciences Inc., Bothell, WA, United States). In brief, after blocking of auto-fluorescence for 5 min at RT, heat-mediated antigen retrieval with 10 mM sodium citrate buffer was performed for 15 min at 95°C. After antigen retrieval, primary antibodies for FR-β (rabbit anti-mouse FR-β, 1:800, Genetex), and F4/80 (rat anti-mouse F4/80, clone Cl:A3-1, 1:800, AbD Serotec), or concentration matched IgG isotype controls were applied and incubated overnight at 4°C. Next, specimens were incubated with rat and rabbit signal amplifier for 30 min at RT followed by washing and linkage to the respective fluorophores for 60 min at RT in the dark (anti-rat MaxFluor488 and anti-rabbit MaxFlour594). Cell nuclei were counterstained with 4′,6-diamidino-2-phenylindole (DAPI).

Microscopy and Image Analysis

Histological and immunohistochemical stainings were recorded automatically with the AxioScan.Z1. slidescanner (Carl Zeiss, Feldbach, Switzerland) using a Plan-Apochromat 20×/0.8 M27 objective. For semi-quantitative expression analyses, per sample, six randomly selected high power fields were extracted with a 10× objective using the *Zen 2.0 lite* (blue edition) software. The percentage of positively stained pixels was automatically quantified using an in-house designed *MATLAB* script (Mathworks, *MATLAB* R2016b) to avoid observer bias. This script quantified the target-positive (=brown or red) pixels and cell nuclei-positive (=blue) pixels and calculated the percentage of positively stained pixels in relation to the total number of image pixels. To account for increased cell numbers and tissue consolidations, also the percentage of positively stained pixels in relation to the total number of colored image (brown or red + blue) pixels was calculated (**Supplementary Figure 1**).

For semi-quantitative assessment of murine and human lung fibrosis, the Ashcroft Score was applied on Picrosirius Red stained lung sections as described previously (58). Two blinded examiners performed the scorings in duplicates. If deviations of more than 1 score were observed, the respective slides were re-assessed to reach consensus.

Immunofluorescent pictures were recorded at 630× magnification (oil immersion) using the Olympus BX53 microscope in fluorescence mode (Olympus, Volketswil, Switzerland).

The total number of double positive (FR-β+/F4/80+) cells was quantified by both automated and manual image analyses using Orbit image analyses software version 3.15 (Objection Detection and Object Classification Module) (59) or manual counting by two blinded examiners, respectively.

RNA Extraction and Quantitative Reverse Transcription PCR

For RNA extraction from mouse lungs, perfused cranial lobes were homogenized using the Qiagen TissueLyser and total RNA was isolated with the RNeasy Fibrous Tissue Mini Kit from Qiagen (Hombrechtikon, Switzerland). For quantitative reverse transcription PCR (RT-qPCR), 120 ng RNA were reverse-transcribed into complementary DNA with the Transcriptor First Strand cDNA Synthesis Kit from Roche (Basel, Switzerland) using anchored-oligo$(dT)_{18}$ primer. Messenger RNA (mRNA) expressions were analyzed by SYBR Green qPCR on a Stratagene Mx3005P qPCR System (Agilent Technologies, Santa Clara, California, USA) using the SYBR Green GoTaq qPCR Master mix from Promega (Dübendorf, Switzerland) and specific primers for murine *Folr2* (forward primer: 5′-CCAGCAAGTGGACCA GAGTT-3′, reverse primer: 5′-CAGTCCCAGCCTTTATGCCA-3′; Microsynth, Balgach, Switzerland). As a housekeeping gene 60S acidic ribosomal protein P0 (*Rplp0;* forward primer: 5′-GCAGGTGTTTGACAACGGCAG-3′, reverse primer: 5′-GAT GATGGAGTGTGGCACCGA-3; Microsynth) was used. The fold change of mRNA expression was calculated using the $2^{-\Delta\Delta Ct}$ method. False positive results due to primer dimers or genomic contamination were excluded by dissociation curve analysis and non-template controls, or by minus-reverse transcriptase controls, respectively.

Hydroxyproline Assay

Collagen contents in lungs of BLM-treated mice and saline controls were quantified by hydroxyproline assay as described previously (60). Briefly, after homogenization, left lung lobes were digested in 6 M HCl for 3 h at 120°C and subsequently neutralized with 6 M NaOH. Next, samples were mixed with a 60 mM chloramine T solution and incubated for 20 min at RT. After addition of 3.15 M perchloric acid (5 min, RT), p-Dimethylaminobenzaldehyd (20% w/v) was added and samples were incubated for 20 min at 60°C. The absorbance was measured at 560 nm with a spectrophotometer (*GloMax-Multi Detection System*, Promega, Dübendorf, Switzerland).

Radiosynthesis of ^{18}F-AzaFol

3′-Aza-2′-[^{18}F]-fluoro-folic acid (^{18}F-AzaFol) was produced on an automated synthesis module at the ETH Zurich (Switzerland) according to a previously reported method (61). ^{18}F-AzaFol was applied at ∼5 MBq (in 100 μL, 0.25–0.5 pmol/mouse) for biodistribution studies and at ∼10 MBq (in 100 μL, 0.5–1 pmol/mouse) for *in vivo* and *ex vivo* PET/CT imaging. The *in vivo* stability of the tracer has been demonstrated in previous studies, in which only the intact parent radiotracer was detected. No downstream radiometabolites in blood plasma, urine, or liver samples were detectable (61, 62).

TABLE 1 | Scan parameters for *in vivo* and *ex vivo* PET scans using *G8* bench-top PET/CT scanner.

Energy window	150–650 keV
Isotope	Fluorine 18
Framing sequence	Static
Duration of static PET scans	
In vivo (chest region)	10 min
Ex vivo (isolated whole lungs)	20 min
Normalization	Yes
Dead time correction	Yes
Decay correction	Yes
Scatter correction	No
Image reconstruction	
Number of iterations	60
Attenuation correction	Yes

In vivo and ex vivo scans were performed 1 h after the injection of ^{18}F-AzaFol (∼10 MBq in 100 μL, 0.5–1 pmol/per mouse).

Biodistribution Studies

As an accurate means to quantify radiotracer uptake (31), biodistribution studies were performed. ^{18}F-AzaFol was administrated via the lateral tail vein of mice. Receptor-blocking studies were performed by pre-injection of folinic acid (leucovorin; 300 nmol, 100 μL) ∼30 min before the injection of ^{18}F-AzaFol. Mice were sacrificed 1 h post injection (p.i.) of ^{18}F-Azafol. Tissues and organs of interest were collected, weighed and counted for activity using a γ-counter (*Wallac Wizard 1480*, Perkin Elmer, Germany). The results were calculated as a percentage of the injected activity per gram of tissue mass (% IA/g) or expressed as a percentage of the injected activity per organ (% IA/organ). Thereafter, the already counted lungs were subjected to *ex vivo* PET/CT scans as described below.

Ex vivo and *in vivo* PET/CT Scans

The *ex vivo* PET/CT scans of collected lungs (obtained from mice used for the biodistribution study) were performed using a small-animal bench-top PET/CT scanner (*G8*, Perkin Elmer, Massachusetts, USA; **Table 1**). Static PET scans of 20 min duration were acquired using the G8 acquisiton software (version 2.0.0.10) followed by CT scans of 1.5 min duration. The energy window ranged from 150 to 650 keV. The PET data were corrected for random coincidences, decay, and dead time and reconstructed with maximum-likelihood expectation maximization (MLEM). A correction for scatter was not made. The images were prepared using VivoQuant post-processing software (version 3.0, inviCRO Imaging Services and Software, Boston, USA). A Gauss post-reconstruction filter (FWHM = 1 mm) was applied to the PET images. The *ex vivo* PET/CT scans and biodistribution studies were performed in a separate experiment as the *in vivo* PET/CT scans. For *in vivo* imaging, static PET scans were performed 1 h p.i. of the radiotracer and lasted for 10 min followed by a CT of 1.5 min duration. During the *in vivo* PET/CT scans, the mice were anesthetized with a mixture of isoflurane and oxygen. The *in vivo* images were visualized using a dedicated 3D-rendering software (Ziostation2, Ziosoft, Tokyo, Japan).

For both, biodistribution studies/*ex vivo* scans and the *in vivo* scans per each time point the following numbers of mice have been used: $n = 3$–4 for saline-treated mice, $n = 3$–4 for BLM-treated mice and $n = 2$–4 for BLM-treated mice receiving leucovorin for FR blockade.

Statistics

Statistical analysis was performed using GraphPad Prism 7 software (version 7.04). Unless otherwise indicated, non-parametric data were expressed as median ± interquartile range (IQR) and parametric data were expressed as mean ± standard deviation (S.D.). For non-parametric non-related data, the Mann–Whitney *U*-test for comparison of two groups, or the Kruskal–Wallis test followed by Dunn's multiple correction for comparison of multiple groups was employed. For parametric non-related data, an unpaired *t*-test was applied for comparison between two groups, or a One-Way ANOVA with Tukey's *post-hoc* test for comparison between multiple groups was performed. For correlation analysis, Spearman rank correlation was performed. *P*-values < 0.05 were considered statistically significant.

RESULTS

FR-β Expression Is Upregulated in Human ILD and Correlates With Disease Severity

To assess the presence of FR-β-positive macrophages in human ILD, we performed IHC for FR-β on lung explants derived from patients with IPF ($n = 39$) and CTD-ILD ($n = 14$), who underwent lung transplantation. Lung sections from excess tissue from lung organ donors served as controls ($n = 26$) (**Supplementary Table 1**).

As anticipated, the histopathological analysis of lung tissues from both patients with IPF and CTD-ILD revealed severe damage of the normal tissue architecture with increased numbers of mononuclear inflammatory infiltrates and excessive interstitial collagen deposition as assessed by HE or Picrosirius Red staining (**Figure 1A**), respectively. This was also reflected in the semi-quantitative Ashcroft score of pulmonary fibrosis with a median score of 6.125 (Q1, Q3 = 5.625, 6.5; $p < 0.0001$) for IPF and a median score of 5 (Q1, Q3 = 4.219, 6.531; $p < 0.0001$) for CTD-ILD patients (**Figure 1B**). In most cases, lung remodeling in IPF and CTD-ILD patients had histological features of usual interstitial pneumonia (UIP) characterized by patchy fibrosis and areas of honeycombing, whereas only the minority of patients displayed patterns of non-specific interstitial pneumonia (NSIP), characterized by a more uniformly spread fibrosis and better preserved lung architecture (**Supplementary Table 1**). In these highly inflammatory and fibrotic lung sections, presence of FR-β was significantly increased (**Figure 1A**) with median increases of ∼ 3- to 4-fold in both IPF and CTD-ILD patients (**Figure 1C**, **Supplementary Figure 2A**; $p < 0.0001$). To confirm the expression of FR-β on macrophages (40, 63), we additionally performed IHC for CD68, a human pan-macrophage marker, on sequential lung sections from healthy controls, IPF and CTD-ILD patients. In accordance with the increased FR-β expression, we also found increased CD68 expression in lung sections

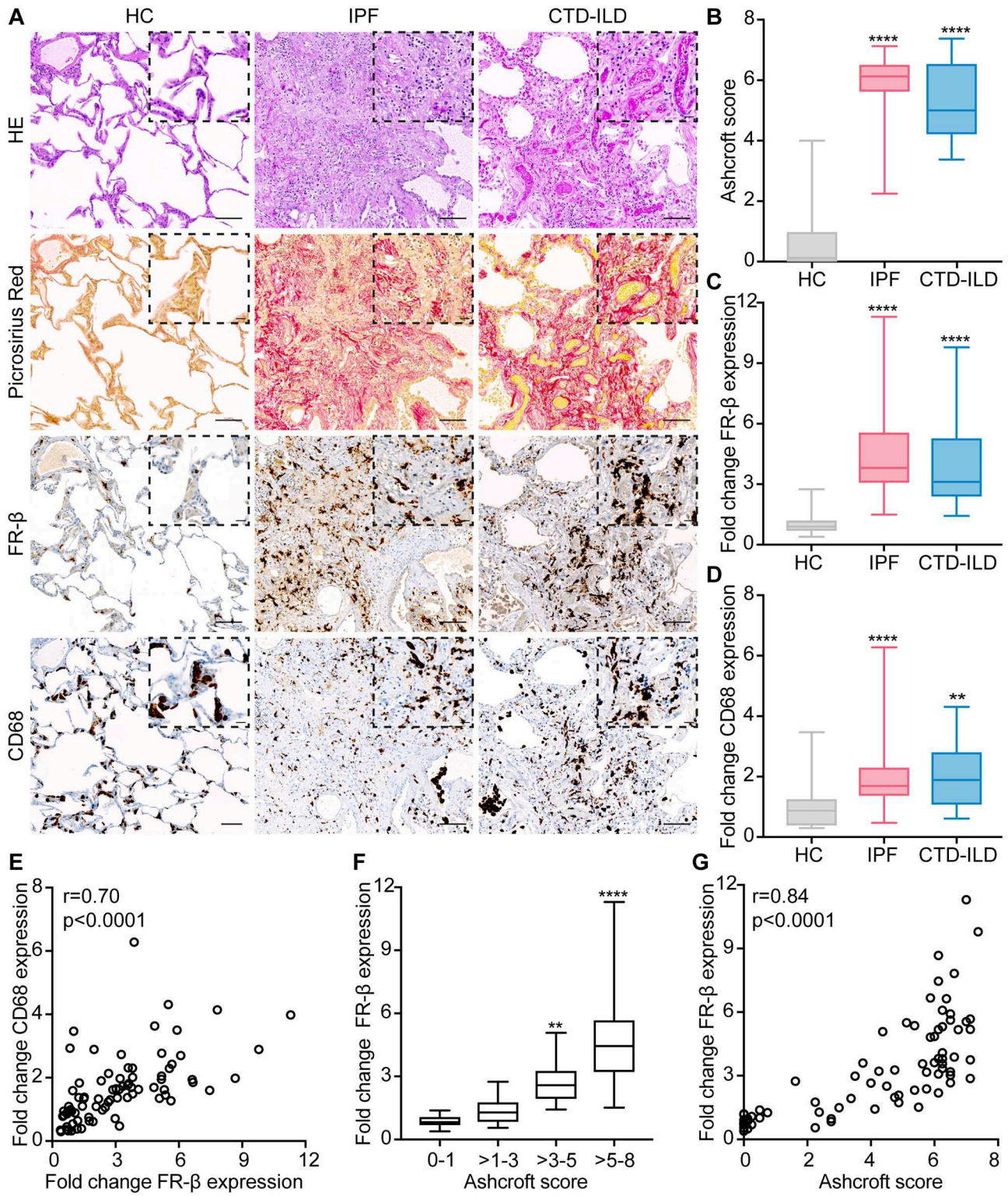

FIGURE 1 | FR-β expression is increased in human ILD and correlates with the severity of lung remodeling. **(A)** Representative images of lung sections from healthy controls (HC) and patients with IPF and CTD-ILD stained with hematoxylin and eosin (HE, first panel), Picrosirius Red (collagen = red, second panel), FR-β (brown, third panel) and CD68 (brown, fourth panel). Representative pictures at 100× magnification (scale bars: 100 μm) and at higher magnification (400×, scale bars: 20 μm) are shown. **(B)** Semi-quantification of pulmonary fibrosis by Ashcroft score. **(C)** Semi-quantification of FR-β tissue expression by automatic image analysis. **(D)** Semi-quantification of CD68 tissue expression by automatic image analysis. **(E)** Spearman correlation of FR-β expression with the CD68 expression. **(F)** Analysis of

(Continued)

FIGURE 1 | FR-β expression according to the severity of lung remodeling as defined by the Ashcroft score (score 0–1: no fibrosis, scores >1–3: mild fibrosis, scores >3–5: moderate fibrosis, scores >5–8: severe fibrosis). **(G)** Spearman correlation of FR-β expression with the Ashcroft score. For **(B–D,F)** data are displayed as box plots with min/max values. For statistical analysis, the Kruskal–Wallis test with Dunn's multiple correction was applied (*$p < 0.05$, **$p < 0.01$, ***$p < 0.001$, ****$p < 0.0001$). For all experiments: $n = 26$ for healthy controls, $n = 39$ for IPF patients, and $n = 14$ for CTD-ILD patients.

from both IPF and CTD-ILD patients with median increases of 1.69-fold (Q1, Q3 = 1.37, 2.29; $p < 0.0001$) and 1.89-fold (Q1, Q3 = 1.09, 2.8; $p < 0.01$), respectively (**Figure 1D**, **Supplementary Figure 2B**). Consistently, FR-β expression also strongly correlated with the CD68 expression ($r = 0.70$, $p < 0.0001$; **Figure 1E**). Whereas, a strong expression of CD68 was observed on macrophages in the alveolar spaces, FR-β was mostly expressed in the lung interstitium (**Figure 2**). Furthermore, while the upregulation of CD68 and FR-β in IPF and CTD-ILD patients was independent of the histological subtype (**Supplementary Figure 3**), the expression of FR-β significantly increased with the severity of lung remodeling (**Figure 1F**) and positively correlated with the Ashcroft score as measure of lung remodeling ($r = 0.84$, $p < 0.0001$; **Figure 1G**).

FR-β Expression Is Also Upregulated in Experimental ILD and Changes With Disease Development

Next, we assessed whether the expression of FR-β was mirrored in a representative mouse model of human ILD, the BLM-induced lung fibrosis model.

Upon a single intratracheal BLM administration, mice progressively developed lung remodeling with inflammation (days 3–7) preceding the development of pulmonary fibrosis (day 14). As early as day 3, the histopathological examination of lung sections from BLM-treated mice vs. saline controls revealed the presence of mononuclear cell infiltrates (**Figure 3A**) around the vessels and bronchi with increased numbers of macrophages as assessed by IHC with the murine macrophage marker F4/80 (**Figure 3B**). In contrast, only minimal fibrous thickening of the alveolar and bronchial walls (**Figure 3C**) was detected, which was also reflected by a low median Ashcroft score of 2.5 (Q1, Q3 = 2, 3; $p < 0.01$; **Figure 3D**). With disease progression, the number of macrophages increased in BLM-treated lungs and peaked at day 7 with a median 4.11-fold increase (Q1, Q3 = 2.38, 10.65; $p < 0.001$; **Figure 3E**, **Supplementary Figure 2D**) and subsided thereafter. Consistently, pulmonary fibrosis gradually increased with extensive interstitial collagen deposition characterized by the formation of fibrous bands and larger fibrous masses in subpleural as well as perivascular and peribronchial areas (**Figure 3C**). Maximally established fibrosis was detected at day 14 as demonstrated by a high median Ashcroft score of 5 (Q1, Q3 = 4.25, 5.5; $p < 0.001$). The lung collagen content as assessed by hydroxyproline (HP) assay increased over time in BLM-treated mice with a median 1.32-fold (Q1, Q3 = 1.17, 1.42; $p < 0.05$) increase at day 14 (**Figure 3F**).

In accordance with the expression in human ILD and the time course of the appearance of pulmonary macrophages in this animal model, FR-β expression significantly increased over time in lungs of BLM-treated mice (**Figure 4A**). While FR-β was only weakly expressed in the lungs of saline-treated controls, FR-β expression was significantly upregulated in lungs of BLM-treated mice with peak at day 3 at the mRNA level (**Figure 4B**) and at day 7 at the protein level (**Figures 4A,C**, **Supplementary Figure 2C**) and thus in the inflammatory phase in this animal model with a median increase of 1.98-fold (Q1, Q3 = 1.61, 2.19; $p < 0.001$) and 4.41-fold (Q1, Q3 = 2.4, 6.83; $p < 0.01$), respectively. The expression of FR-β on murine lung macrophages was confirmed by immunofluorescent double staining using an antibody for murine macrophages, F4/80 (**Figure 4D**, **Supplementary Figure 4**).

As in human ILD patients, the expression of FR-β also positively correlated with the Ashcroft score ($r = 0.64$, $p < 0.0001$; **Figure 4E**) and, hence, with the degree of lung remodeling (**Figure 4F**).

Pulmonary Accumulation of ^{18}F-AzaFol, a Surrogate Marker for FR-β-Positive Macrophages, Reflects Macrophage-Related Disease Development in Experimental ILD

Having established the time course of FR-β expression in this mouse model, we next performed nuclear imaging experiments to assess whether macrophage-related disease development could be visualized by ^{18}F-AzaFol.

In strong correlation with the expression changes of FR-β at the tissue level, BLM-treated mice showed increased pulmonary accumulation of ^{18}F-AzaFol from days 3 to 14, as assessed by *ex vivo* biodistribution studies at 1 h p.i. of ^{18}F-AzaFol (**Figures 5A,B**). The maximum lung accumulation was observed at day 7 with a mean total uptake of 1.01 ± 0.30% injected activity per lung (% IA/lung) and 3.33 ± 0.77% injected activity per tissue mass (% IA/g) in BLM-treated vs. control animals (0.31 ± 0.06% IA/lung and 1.78 ± 0.15% IA/g; $p < 0.01$ and $p < 0.05$, respectively). The specificity of the pulmonary tissue uptake of ^{18}F-AzaFol was validated by receptor blockade using folinic acid (leucovorin) administrated to mice 30 min prior to the injection of the radiotracer. This significantly reduced the lung accumulation of ^{18}F-AzaFol in BLM-treated mice, resulting in pulmonary radioactivity accumulation comparable to saline-treated controls. *Ex vivo* PET/CT scans of isolated lungs also clearly distinguished diseased from healthy lungs and confirmed the successful receptor blockade (**Figure 5C**). *In vivo* PET/CT scans of the chest region of the animal showed a generally low pulmonary accumulation of ^{18}F-AzaFol with background signals in bone and muscles in both NaCl-treated controls and BLM-treated mice. A slightly increased signal intensity compared with control mice was observed in lungs of BLM-treated mice at the maximum of inflammation at day 7 (**Supplementary Figure 5**).

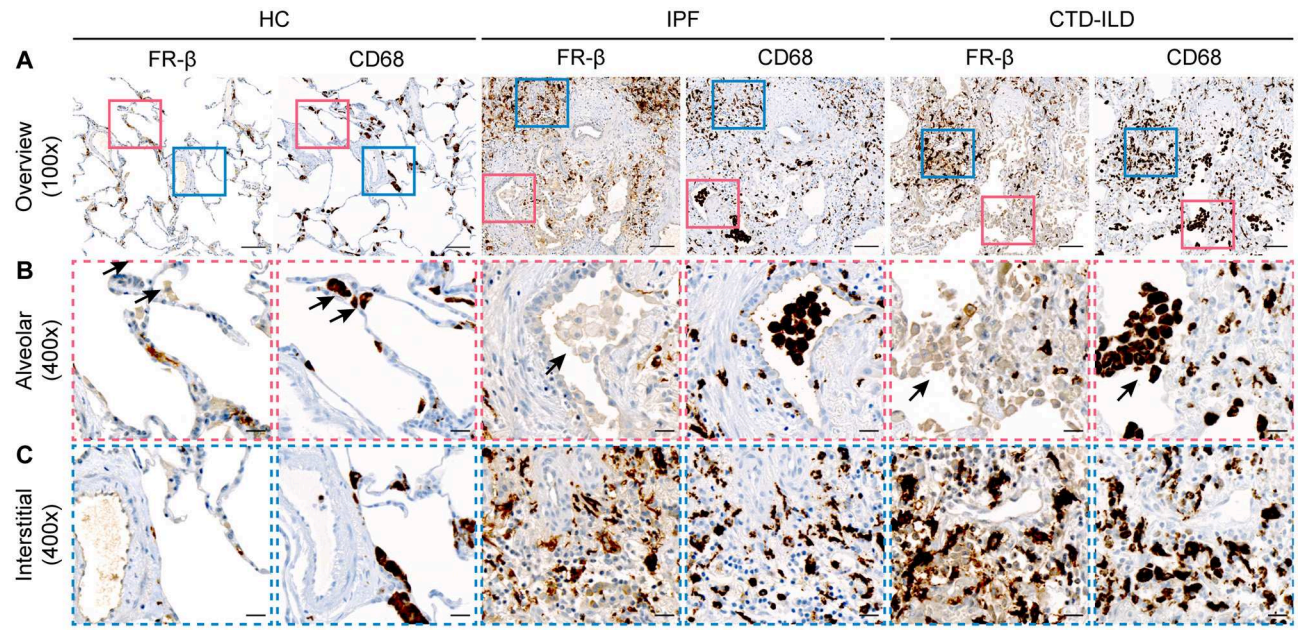

FIGURE 2 | FR-β is mostly expressed in the lung interstitium in human ILD. Representative images of sequential lung sections from healthy controls (HC, $n = 26$) and patients with IPF ($n = 39$) and CTD-ILD ($n = 14$) that were stained with FR-β and the human macrophage marker CD68. **(A)** Overview images at 100× magnification are shown (scale bars: 100 μm). Colored squares indicate regions of interest for the higher magnification images depicted in **(B,C)**. **(B)** Higher magnification images at 400× magnification (scale bars: 20 μm) indicating the only weak to undetectable expression of FR-β on macrophages located in alveolar spaces (arrows). **(C)** Higher magnification images at 400× magnification (scale bars: 20 μm) indicating the strong expression of FR-β on macrophages located in the lung interstitium.

The distribution of ^{18}F-AzaFol in other organs besides the lungs was comparable between BLM-treated mice and saline-treated control animals at day 7 (**Figure 5D**, **Supplementary Tables 2, 3**). The slightly increased uptake in both experimental groups in lymphoid organs (e.g., thymus, lymph nodes), which may have been also affected by the BLM treatment (64), is most likely caused by the presence of activated macrophages expressing FR–β (65, 66), a phenomenon, previously observed in lymph nodes of tumor-bearing mice (61). The high basal liver uptake of ^{18}F-AzaFol observed in both controls and BLM-treated mice can be explained by the fact that folate vitamins are physiologically stored in the liver. Since ^{18}F-AzaFol is not a conjugate of folic acid, as this is the case with other folate radioligands, ^{18}F-AzaFol may also be transported through carrier systems such as the proton-coupled folate transporter. A relatively high liver uptake and potential signs of metabolism were also shown in our previous studies, in which we evaluated ^{18}F-AzaFol for the first time (61).

The distinct drop in activity after treatment with the FR blocking agent in both liver and lymph nodes further argues for a folate-specific effect rather than an unspecific accumulation mechanism.

DISCUSSION

In different types of ILD, an increased lung uptake of [^{18}F]FDG was observed in pathologically changed areas of reticulation/honeycombing and ground-glass opacities, but also in radiologically normal-appearing lung areas (28, 29, 67–71). [^{18}F]FDG uptake, especially in normal appearing lung parenchyma, was shown to be of prognostic value and to correlate with overall disease severity in IPF patients (28, 68, 70). However, [^{18}F]FDG-PET/CT has also important limitations for the diagnosis and monitoring of ILD since it visualizes changes in glucose metabolism in a non-specific, cell-type-independent manner (25, 26, 67), and does not allow to draw conclusions on the pathophysiological disease stage (30, 72). In our study, ^{18}F-AzaFol visualized macrophage-related ILD development in the mouse model of BLM-induced lung fibrosis in *ex vivo* PET/CT scans and tissue expression of FR-β showed good correlation with the pulmonary radiotracer uptake in the biodistribution studies. This has important clinical implications.

As ILDs are highly heterogeneous on molecular level, such a targeted molecular imaging approach could be used in the future for a molecular stratification of ILD patients, i.e., the identification of subgroups of patients, who are likely to benefit from macrophage-oriented therapies and who will be eligible for subsequent monitoring of therapeutic responses. This is of particular interest due to the recent or imminent approval of such therapies for ILD (73–75). These include pirfenidone and nintedanib, which have pre-clinically shown to exert their anti-fibrotic effects at least partially by targeting pulmonary macrophages and/or their products (75–77) as well as tocilizumab, which was assessed in recent phase II and III randomized controlled studies (78). In addition, the ability to identify ILD patients based

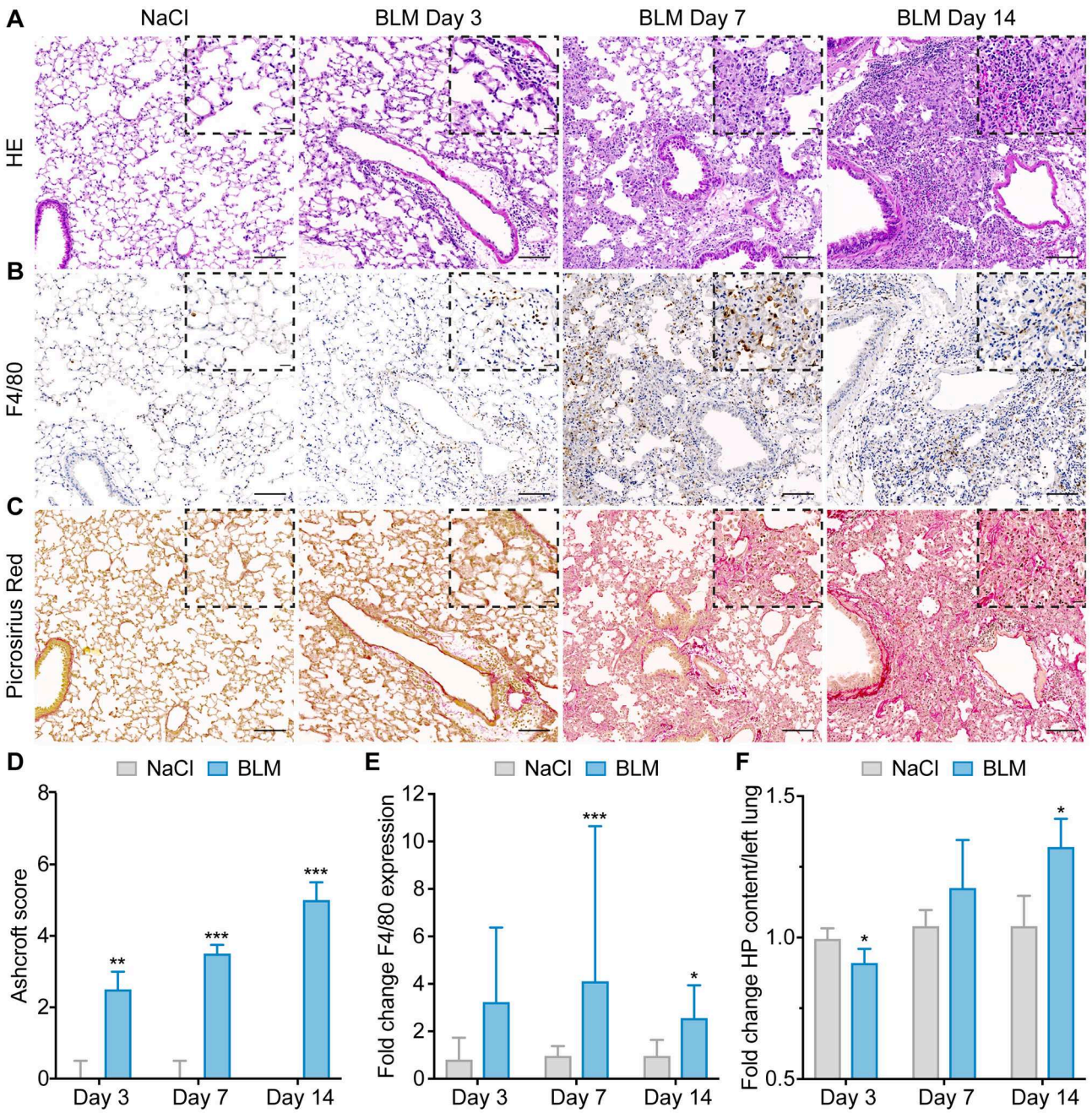

FIGURE 3 | Intratracheal instillation of bleomycin in mice induces progressive lung remodeling characterized by increased numbers of macrophages. **(A)** Representative images of lung sections from saline-treated controls and BLM-treated mice at days 3, 7, and 14 stained with hematoxylin and eosin (HE), **(B)** the murine macrophage marker F4/80 (brown), and **(C)** Picrosirius Red (collagen = red). **(D)** Semi-quantitative assessment of lung fibrosis by Ashcroft score. **(E)** Semi-quantification of pulmonary macrophages by automatic image analysis of F4/80 expression. **(F)** Quantification of left lung collagen content by hydroxyproline (HP) assay. For **(A–C)** representative pictures at 100× magnification (scale bars: 100 μm) and at higher magnification (400×, scale bars: 20 μm) are shown. For **(D–F)** data are presented as medians ± IQR. For statistical analysis, the Mann–Whitney U-test was applied (*$p < 0.05$, **$p < 0.01$, ***$p < 0.001$). For all experiments: n = 4–6 for saline controls and n = 6–10 for BLM-treated mice.

on their underlying molecular and cellular subtype without the need of lung biopsies might also have relevance for clinical trial design by allowing the definition of (more) homogenous patients' subgroups and by serving as a primary/secondary readout for macrophage-orientated treatment studies. To this end, additional preclinical studies to confirm the suitability for ^{18}F-AzaFol for predicting and monitoring therapeutic efficacy will have to be performed. The alterations of tissue uptake of ^{18}F-AzaFol throughout the development of experimental ILD were in strong accordance

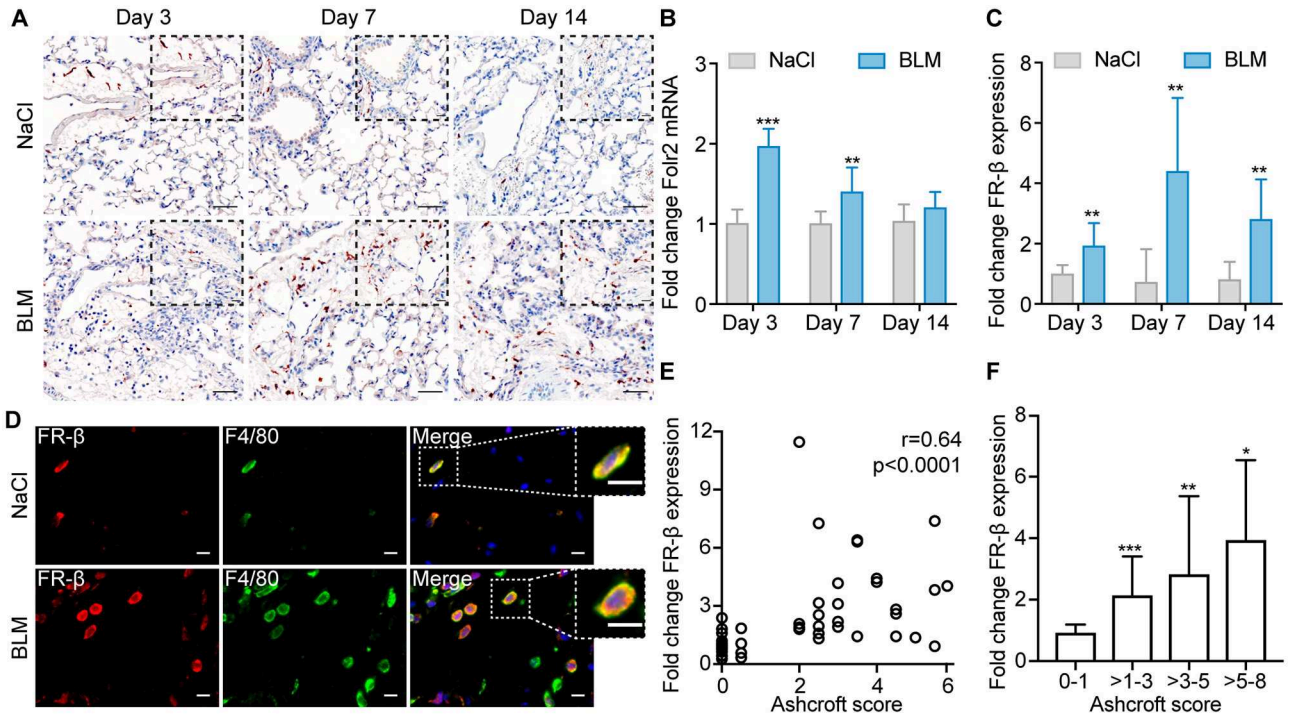

FIGURE 4 | FR-β expression is increased in experimental ILD and correlates with the severity of lung remodeling. **(A)** Representative images of lung sections from saline-treated controls and BLM-treated mice at days 3, 7, and 14 stained for FR-β (red). Representative pictures at 100× magnification (scale bars: 100 μm) and at higher magnification (400×, scale bars: 20 μm) are shown. **(B)** Fold change of mRNA expression of *Folr2* in BLM-treated mice vs. saline-treated controls at days 3, 7, and 14. **(C)** Semi-quantification of FR-β tissue expression by automatic image analysis. **(D)** Representative images of immunofluorescent double staining of FR-β (red) with the murine macrophage marker F4/80 (green) performed on lung sections from saline-treated controls and BLM-treated mice at day 7. For **(D)** representative images from three mice each at 630× magnification are shown (scale bars: 10 μm). **(E)** Spearman correlation of FR-β expression with the Ashcroft score. **(F)** Analysis of FR-β expression according to the severity of lung remodeling as defined by the Ashcroft score (score 0–1: no fibrosis, scores >1–3: mild fibrosis, scores >3–5: moderate fibrosis, scores >5–8: severe fibrosis). For **(B,C,F)** data are presented as medians ± IQR. For statistical analysis the Kruskal–Wallis test with Dunn's multiple correction or the Mann–Whitney *U*-test was applied (*$p < 0.05$, **$p < 0.01$, ***$p < 0.001$). For all experiments: $n = 6$ for saline-treated controls, $n = 9$–10 for BLM-treated mice.

with the time course of macrophage presence on tissue level, which documents a good sensitivity to change. This quality is an important prerequisite for the monitoring of macrophage-targeted treatment responses, which we have not yet tested pre-clinically.

Another important finding of this study was that the numbers of (FR-β-positive) macrophages were substantially increased in human ILD patients, irrespective of the underlying etiology. This observation has some interesting implications. Firstly, it supports the re-evaluation of the pathophysiology of fibrotic ILD as immune-mediated and thus, as potentially amenable to immune-targeted therapies (12). Secondly, the persistence of macrophages throughout different stages of experimental ILD and their presence in late disease stages in the human disease points to an important role in the whole process of tissue remodeling (79). Thus, the characterization of macrophage subpopulations, particularly of FR-β-positive macrophages, might further elucidate the mechanisms of fibrosis in ILD and identify novel macrophage- or macrophage-related therapeutic targets (15) including FR-β-targeted molecular therapies (40, 80–82).

The exploratory character of our study accounts for some of its limitations. The model of BLM-induced lung fibrosis, although extensively used and widely acknowledged as a valuable model of experimental ILD, does not reflect the chronic disease course in human patients, since following the single instillation of BLM, fibrosis gradually resolves over 4–8 weeks (55). Furthermore, the imaging analyses have been limited to the stages of active disease and later time points of resolution of fibrosis (days 21–28) have not been investigated. For pathophysiologic studies to elucidate the whole process of macrophage-related tissue remodeling in ILD in detail, FR-β-targeted nuclear imaging would have to be performed (a) in the phase of tissue repair in the acute BLM model and (b) in non-resolving, chronic disease models of ILD (83). Numerous studies, however, are now focusing on the acute, pro-inflammatory phase and the role of macrophages in fibrosis development in this model (15, 56, 57), which support the importance and comparability of its early stages to certain aspects of human ILD.

Another important limitation of our proof-of-concept study is that our nuclear imaging experiments are largely based on *ex vivo* analyses and quantifications. Furthermore, the performance

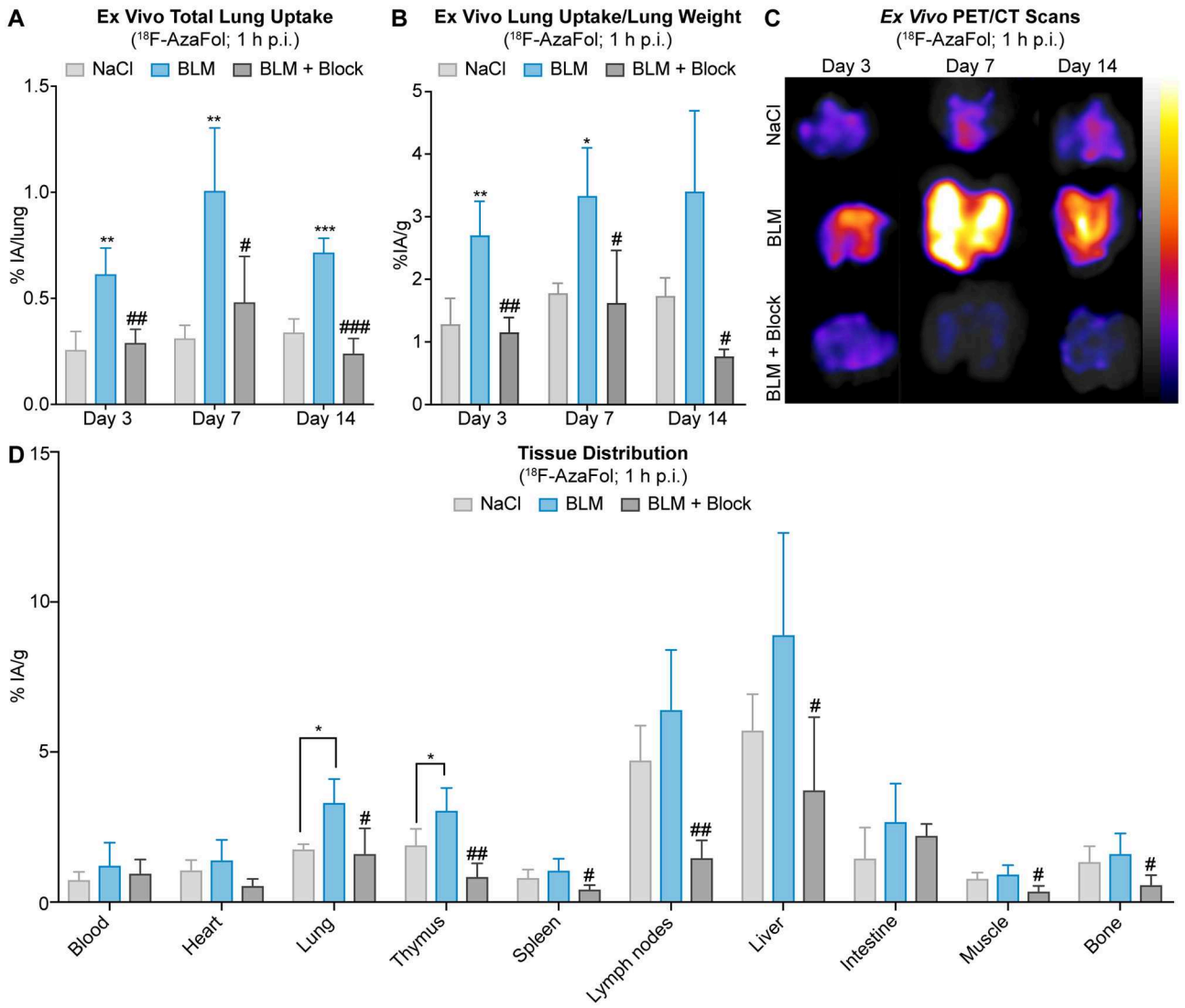

FIGURE 5 | Pulmonary accumulation of ^{18}F-AzaFol reflects macrophage-related disease development in experimental ILD. **(A)** *Ex vivo* lung uptake of ^{18}F-AzaFol (1 h p.i.) shown as percentage of injected activity per lung (% IA/lung) or **(B)** shown as percentage of injected activity per lung mass (% IA/g) in lungs from saline-treated controls and BLM-treated mice with and without receptor blockade at days 3, 7, and 14. **(C)** *Ex vivo* PET/CT scans of lungs from saline controls and BLM-treated mice with and without receptor blockade at days 3, 7, and 14 that were collected 1 h after injection of ^{18}F-AzaFol. Scans are shown as maximum intensity projections. **(D)** Representative tissue distribution of ^{18}F-AzaFol (1 h p.i.) in organs of interest of saline-treated controls and BLM-treated mice. Biodistribution data are shown for day 7, when the strongest pulmonary accumulation of ^{18}F-AzaFol was observed. Data are expressed as percentage of injected activity per gram of tissue (% IA/g). For **(A,B,D)** data are presented as means ± S.D. For statistical analysis, the One Way ANOVA test with Tukey's multiple correction was applied (*$p < 0.05$, **$p < 0.01$, ***$p < 0.001$, vs. saline; $^{\#}p < 0.05$, $^{\#\#}p < 0.01$, $^{\#\#\#}p < 0.001$, vs. BLM). For all experiments: $n = 3$–4 for saline-treated controls, $n = 3$–4 for BLM-treated mice, and $n = 2$–4 for BLM-treated mice receiving receptor blockade.

of static PET scans did not allow the correction for changes in pulmonary blood flow. Elevated blood flow and increased vascular leakage are cardinal features of lung inflammation and fibrosis (34, 84). These phenomena could have contributed non-specifically to the pulmonary accumulation of ^{18}F-AzaFol in BLM-treated mice. The fact that receptor blockade with folinic acid lowered the radiotracer uptake to the level of control mice, however, points to a receptor-specific rather than a non-specific pulmonary uptake of ^{18}F-AzaFol.

In future preclinical experiments to further support the specificity of ^{18}F-AzaFol-PET/CT, (a) the quality of the *in vivo* imaging should be improved by using gated respiration during the acquisition of the nuclear images to reduce motion artifacts, which could affect tissue density, (b) dynamic PET scans should be performed to account for blood flow-related changes, and (c) signal intensities should be also quantified *in vivo* e.g., by calculating the standardized uptake values (84, 85). These additional studies would allow to better

estimate the clinical applicability of ^{18}F-AzaFol-PET/CT. For the extrapolation of our preclinical data to humans, it is further important to note that the endogenous folate levels largely differ between rodents and humans (∼15–40 fold higher in mice). In our study, this could have led to an underestimation of the actual ^{18}F-AzaFol tissue uptake since endogenous folate might also compete with ^{18}F-AzaFol for binding to the FR (86).

In general, the transferability of results from animal models, which, even though representative of certain aspects, never cover the whole complexity of a human disease, is always a matter of debate. However, previous studies using the murine BLM-induced lung fibrosis model provided evidence for its suitability for both imaging (33, 87) and molecular analyses (88) and our own data showed similarly high pulmonary expression levels of FR-β in experimental and (end-stage) human ILD.

In conclusion, our proof-of-concept study showed that nuclear imaging using ^{18}F-AzaFol can visualize macrophage-related experimental ILD. The fact that FR-β—apart from being a cellular rather than a metabolic marker—is only expressed on activated macrophages in disease states such as inflammatory disorders or malignancies, supports ^{18}F-AzaFol as a more specific alternative to [^{18}F]FDG in ILD. Since ^{18}F-AzaFol-PET/CT has been tested for targeting FR-positive tumors in a Swiss multi-center trial (NCT03242993; www.clinicaltrials.gov), its clinical availability, including first-in-human clinical trials for imaging of ILD, is impending.

DATA AVAILABILITY STATEMENT

All datasets generated for this study are included in the article/**Supplementary Material**.

ETHICS STATEMENT

The studies involving human participants were reviewed and approved by Ethics committee Zurich. The patients/participants provided their written informed consent to participate in this study. The animal study was reviewed and approved by Swiss veterinary office. The local ethics committee approved the study (BASECNo. 2017-01298), and informed consent was obtained from all patients.

AUTHOR CONTRIBUTIONS

JS made substantial contributions to the conception of the study and the acquisition, analysis and the interpretation of data, and was involved in drafting and revising the manuscript. MBe, MBr, SH, SC, TF, BV, and CF-B were centrally involved in the acquisition and analysis of data and in revising the manuscript. RS and OD made contributions to the conception and design of the study, the interpretation of the data, and the revision of the manuscript. CM and BM made substantial contributions to conception, design of the study and were centrally involved in the acquisition, analysis and interpretation of data, and in drafting and revising the manuscript.

FUNDING

This work was supported by the Swiss National Science Foundation: grant: CRSII3_154490 and grant: 310030_156803, Hartmann-Mueller Foundation (BM), Swiss Personalized Health Network Grant 2017DRI09 (OD), Prof. Max Cloetta Foundation (BM), and by the National Institutes of Health grant P30 AR061271 (CF-B).

ACKNOWLEDGMENTS

We thank Maria Comazzi (Center of Experimental Rheumatology, University Hospital Zurich, Switzerland) for her technical assistance and Susanne Geistlich und Annette Krämer for the production of ^{18}F-AzaFol for this study. Microscopic image recording was performed with equipment maintained by the Center for Microscopy and Image Analysis, University of Zurich.

SUPPLEMENTARY MATERIAL

The Supplementary Material for this article can be found online at: https://www.frontiersin.org/articles/10.3389/fimmu.2019.02724/full#supplementary-material

REFERENCES

1. Wynn TA. Fibrotic disease and the T(H)1/T(H)2 paradigm. *Nat Rev Immunol*. (2004) 4:583–94. doi: 10.1038/nri1412
2. Hutchinson JP, McKeever TM, Fogarty AW, Navaratnam V, Hubbard RB. Increasing global mortality from idiopathic pulmonary fibrosis in the twenty-first century. *Ann Am Thorac Soc*. (2014) 11:1176–85. doi: 10.1513/AnnalsATS.201404-145OC
3. Hoffmann-Vold AM, Fretheim H, Halse AK, Seip M, Bitter H, Wallenius M, et al. Tracking impact of interstitial lung disease in systemic sclerosis in a complete nationwide cohort. *Am J Respir Crit Care Med*. (2019). doi: 10.1164/rccm.201903-0486OC
4. Long K, Danoff SK. Interstitial lung disease in polymyositis and dermatomyositis. *Clin Chest Med*. (2019) 40:561–72. doi: 10.1016/j.ccm.2019.05.004
5. Brito Y, Glassberg MK, Ascherman DP. Rheumatoid arthritis-associated interstitial lung disease: current concepts. *Curr Rheumatol Rep*. (2017) 19:79. doi: 10.1007/s11926-017-0701-5
6. Tselios K, Urowitz MB. Cardiovascular and pulmonary manifestations of systemic lupus erythematosus. *Curr Rheumatol Rev*. (2017) 13:206–18. doi: 10.2174/1573397113666170704102444
7. Roca F, Dominique S, Schmidt J, Smail A, Duhaut P, Levesque H, et al. Interstitial lung disease in primary Sjogren's syndrome. *Autoimmun Rev*. (2017) 16:48–54. doi: 10.1016/j.autrev.2016.09.017
8. Reiseter S, Gunnarsson R, Mogens Aalokken T, Lund MB, Mynarek G, Corander J, et al. Progression and mortality of interstitial lung disease in mixed connective tissue disease: a long-term observational nationwide cohort study. *Rheumatology*. (2018) 57:255–62. doi: 10.1093/rheumatology/kex077
9. Fischer A, Brown KK. Interstitial lung disease in undifferentiated forms of connective tissue disease. *Arthritis Care Res*. (2015) 67:4–11. doi: 10.1002/acr.22394

10. Wallace B, Vummidi D, Khanna D. Management of connective tissue diseases associated interstitial lung disease: a review of the published literature. *Curr Opin Rheumatol*. (2016) 28:236–45. doi: 10.1097/BOR.0000000000000270
11. Maher TM, Wells AU, Laurent GJ. Idiopathic pulmonary fibrosis: multiple causes and multiple mechanisms? *Eur Respir J*. (2007) 30:835–9. doi: 10.1183/09031936.00069307
12. Wells AU, Denton CP. Interstitial lung disease in connective tissue disease–mechanisms and management. *Nat Rev Rheumatol*. (2014) 10:728–39. doi: 10.1038/nrrheum.2014.149
13. Sisson TH, Mendez M, Choi K, Subbotina N, Courey A, Cunningham A, et al. Targeted injury of type II alveolar epithelial cells induces pulmonary fibrosis. *Am J Respir Crit Care Med*. (2010) 181:254–63. doi: 10.1164/rccm.200810-1615OC
14. Plataki M, Koutsopoulos AV, Darivianaki K, Delides G, Siafakas NM, Bouros D. Expression of apoptotic and antiapoptotic markers in epithelial cells in idiopathic pulmonary fibrosis. *Chest*. (2005) 127:266–74. doi: 10.1378/chest.127.1.266
15. Byrne AJ, Maher TM, Lloyd CM. Pulmonary macrophages: a new therapeutic pathway in fibrosing lung disease? *Trends Mol Med*. (2016) 22:303–16. doi: 10.1016/j.molmed.2016.02.004
16. Aran D, Looney AP, Liu L, Wu E, Fong V, Hsu A, et al. Reference-based analysis of lung single-cell sequencing reveals a transitional profibrotic macrophage. *Nature Immunol*. (2019) 20:163–72. doi: 10.1038/s41590-018-0276-y
17. Christmann RB, Sampaio-Barros P, Stifano G, Borges CL, de Carvalho CR, Kairalla R, et al. Association of interferon- and transforming growth factor beta-regulated genes and macrophage activation with systemic sclerosis-related progressive lung fibrosis. *Arthritis Rheumatol*. (2014) 66:714–25. doi: 10.1002/art.38288
18. Schupp JC, Binder H, Jager B, Cillis G, Zissel G, Muller-Quernheim J, et al. Macrophage activation in acute exacerbation of idiopathic pulmonary fibrosis. *PLoS ONE*. (2015) 10:e0116775. doi: 10.1371/journal.pone.0116775
19. Hsu E, Shi H, Jordan RM, Lyons-Weiler J, Pilewski JM, Feghali-Bostwick CA. Lung tissues in systemic sclerosis have gene expression patterns unique to pulmonary fibrosis and pulmonary hypertension. *Arthritis Rheum*. (2011) 63:783–94. doi: 10.1002/art.30159
20. Cai M, Bonella F, He X, Sixt SU, Sarria R, Guzman J, et al. CCL18 in serum, BAL fluid and alveolar macrophage culture supernatant in interstitial lung diseases. *Respir Med*. (2013) 107:1444–52. doi: 10.1016/j.rmed.2013.06.004
21. Mahoney JM, Taroni J, Martyanov V, Wood TA, Greene CS, Pioli PA, et al. Systems level analysis of systemic sclerosis shows a network of immune and profibrotic pathways connected with genetic polymorphisms. *PLoS Comput Biol*. (2015) 11:e1004005. doi: 10.1371/journal.pcbi.1004005
22. Taroni JN, Greene CS, Martyanov V, Wood TA, Christmann RB, Farber HW, et al. A novel multi-network approach reveals tissue-specific cellular modulators of fibrosis in systemic sclerosis. *Genome Med*. (2017) 9:27. doi: 10.1186/s13073-017-0417-1
23. Thomeer MJ, Vansteenkiste J, Verbeken EK, Demedts M. Interstitial lung diseases: characteristics at diagnosis and mortality risk assessment. *Respir Med*. (2004) 98:567–73. doi: 10.1016/j.rmed.2003.10.015
24. Basu S, Zhuang H, Torigian DA, Rosenbaum J, Chen W, Alavi A. Functional imaging of inflammatory diseases using nuclear medicine techniques. *Semin Nucl Med*. (2009) 39:124–45. doi: 10.1053/j.semnuclmed.2008.10.006
25. Hansell DM, Goldin JG, King TE Jr, Lynch DA, Richeldi L, Wells AU. CT staging and monitoring of fibrotic interstitial lung diseases in clinical practice and treatment trials: a position paper from the Fleischner Society. *Lancet Respir Med*. (2015) 3:483–96. doi: 10.1016/S2213-2600(15)00096-X
26. Goldin J, Elashoff R, Kim HJ, Yan X, Lynch D, Strollo D, et al. Treatment of scleroderma-interstitial lung disease with cyclophosphamide is associated with less progressive fibrosis on serial thoracic high-resolution CT scan than placebo: findings from the scleroderma lung study. *Chest*. (2009) 136:1333–40. doi: 10.1378/chest.09-0108
27. Win T, Lambrou T, Hutton BF, Kayani I, Screaton NJ, Porter JC, et al. ^{18}F-Fluorodeoxyglucose positron emission tomography pulmonary imaging in idiopathic pulmonary fibrosis is reproducible: implications for future clinical trials. *Eur J Nucl Med Mol Imaging*. (2012) 39:521–8. doi: 10.1007/s00259-011-1986-7
28. Nobashi T, Kubo T, Nakamoto Y, Handa T, Koyasu S, Ishimori T, et al. ^{18}F-FDG uptake in less affected lung field provides prognostic stratification in patients with interstitial lung disease. *J Nucl Med*. (2016) 57:1899–904. doi: 10.2967/jnumed.116.174946
29. Bellando-Randone S, Tartarelli L, Cavigli E, Tofani L, Bruni C, Lepri G, et al. ^{18}F-fluorodeoxyglucose positron-emission tomography/CT and lung involvement in systemic sclerosis. *Ann Rheum Dis*. (2018) 78:577–8. doi: 10.1136/annrheumdis-2018-eular.3748
30. Bondue B, Castiaux A, Van Simaeys G, Mathey C, Sherer F, Egrise D, et al. Absence of early metabolic response assessed by ^{18}F-FDG PET/CT after initiation of antifibrotic drugs in IPF patients. *Respir Res*. (2019) 20:10. doi: 10.1186/s12931-019-0974-5
31. Desogere P, Tapias LF, Hariri LP, Rotile NJ, Rietz TA, Probst CK, et al. Type I collagen-targeted PET probe for pulmonary fibrosis detection and staging in preclinical models. *Sci Transl Med*. (2017) 9:eaaf4696. doi: 10.1126/scitranslmed.aaf4696
32. Golestani R, Razavian M, Ye Y, Zhang J, Jung JJ, Toczek J, et al. Matrix metalloproteinase-targeted imaging of lung inflammation and remodeling. *J Nucl Med*. (2017) 58:138–43. doi: 10.2967/jnumed.116.176198
33. Schniering J, Benesova M, Brunner M, Haller S, Cohrs S, Frauenfelder T, et al. Visualisation of interstitial lung disease by molecular imaging of integrin $\alpha_v\beta_3$ and somatostatin receptor 2. *Ann Rheum Dis*. (2019) 78:218–27. doi: 10.1136/annrheumdis-2018-214322
34. Schniering J, Borgna F, Siwowska K, Benesova M, Cohrs S, Hasler R, et al. *In vivo* labeling of plasma proteins for imaging of enhanced vascular permeability in the lungs. *Mol Pharm*. (2018) 15:4995–5004. doi: 10.1021/acs.molpharmaceut.8b00606
35. Schniering J, Guo L, Brunner M, Schibli R, Ye S, Distler O, et al. Evaluation of ^{99m}Tc-rhAnnexin V-128 SPECT/CT as a diagnostic tool for early stages of interstitial lung disease associated with systemic sclerosis. *Arthritis Res Ther*. (2018) 20:183. doi: 10.1186/s13075-018-1681-1
36. Withana NP, Ma X, McGuire HM, Verdoes M, van der Linden WA, Ofori LO, et al. Non-invasive imaging of idiopathic pulmonary fibrosis using cathepsin protease probes. *Sci Rep*. (2016) 6:19755. doi: 10.1038/srep19755
37. Han W, Zaynagetdinov R, Yull FE, Polosukhin VV, Gleaves LA, Tanjore H, et al. Molecular imaging of folate receptor beta-positive macrophages during acute lung inflammation. *Am J Respir Cell Mol Biol*. (2015) 53:50–9. doi: 10.1165/rcmb.2014-0289OC
38. Paulos CM, Turk MJ, Breur GJ, Low PS. Folate receptor-mediated targeting of therapeutic and imaging agents to activated macrophages in rheumatoid arthritis. *Adv Drug Deliv Rev*. (2004) 56:1205–17. doi: 10.1016/j.addr.2004.01.012
39. Low PS, Kularatne SA. Folate-targeted therapeutic and imaging agents for cancer. *Curr Opin Chem Biol*. (2009) 13:256–62. doi: 10.1016/j.cbpa.2009.03.022
40. Nagai T, Tanaka M, Hasui K, Shirahama H, Kitajima S, Yonezawa S, et al. Effect of an immunotoxin to folate receptor beta on bleomycin-induced experimental pulmonary fibrosis. *Clin Exp Immunol*. (2010) 161:348–56. doi: 10.1111/j.1365-2249.2010.04182.x
41. Silvola JMU, Li XG, Virta J, Marjamaki P, Liljenback H, Hytonen JP, et al. Aluminum fluoride-18 labeled folate enables *in vivo* detection of atherosclerotic plaque inflammation by positron emission tomography. *Sci Rep*. (2018) 8:9720. doi: 10.1038/s41598-018-27618-4
42. Piscaer TM, Müller C, Mindt TL, Lubberts E, Verhaar JA, Krenning EP, et al. Imaging of activated macrophages in experimental osteoarthritis using folate-targeted animal single-photon-emission computed tomography/computed tomography. *Arthritis Rheum*. (2011) 63:1898–907. doi: 10.1002/art.30363
43. Jager NA, Westra J, Golestani R, van Dam GM, Low PS, Tio RA, et al. Folate receptor-beta imaging using ^{99m}Tc-folate to explore distribution of polarized macrophage populations in human atherosclerotic plaque. *J Nucl Med*. (2014) 55:1945–51. doi: 10.2967/jnumed.114.143180
44. Chandrupatla D, Jansen G, Mantel E, Low PS, Matsuyama T, Musters RP, et al. Imaging and methotrexate response monitoring of systemic inflammation in arthritic rats employing the macrophage PET Tracer [^{18}F]Fluoro-PEG-Folate. *Contrast Media Mol Imaging*. (2018) 2018:8092781. doi: 10.1155/2018/8092781
45. Ayala-Lopez W, Xia W, Varghese B, Low PS. Imaging of atherosclerosis in apoliprotein e knockout mice: targeting of a folate-conjugated

radiopharmaceutical to activated macrophages. *J Nucl Med*. (2010) 51:768–74. doi: 10.2967/jnumed.109.071324
46. Winkel LC, Groen HC, van Thiel BS, Müller C, van der Steen AF, Wentzel JJ, et al. Folate receptor-targeted single-photon emission computed tomography/computed tomography to detect activated macrophages in atherosclerosis: can it distinguish vulnerable from stable atherosclerotic plaques? *Mol Imaging*. (2014) 13. doi: 10.2310/7290.2013.00061
47. Kelderhouse LE, Robins MT, Rosenbalm KE, Hoylman EK, Mahalingam S, Low PS. Prediction of response to therapy for autoimmune/inflammatory diseases using an activated macrophage-targeted radioimaging agent. *Mol Pharm*. (2015) 12:3547–55. doi: 10.1021/acs.molpharmaceut.5b00134
48. Kraus VB, McDaniel G, Huebner JL, Stabler TV, Pieper CF, Shipes SW, et al. Direct in vivo evidence of activated macrophages in human osteoarthritis. *Osteoarthr Cartilage*. (2016) 24:1613–21. doi: 10.1016/j.joca.2016.04.010
49. Papadopoulos V, Baraldi M, Guilarte TR, Knudsen TB, Lacapere JJ, Lindemann P, et al. Translocator protein (18kDa): new nomenclature for the peripheral-type benzodiazepine receptor based on its structure and molecular function. *Trends Pharmacol Sci*. (2006) 27:402–9. doi: 10.1016/j.tips.2006.06.005
50. Largeau B, Dupont AC, Guilloteau D, Santiago-Ribeiro MJ, Arlicot N. TSPO PET imaging: from microglial activation to peripheral sterile inflammatory diseases? *Contrast Media Mol Imaging*. (2017) 2017:6592139. doi: 10.1155/2017/6592139
51. Canat X, Guillaumont A, Bouaboula M, Poinot-Chazel C, Derocq JM, Carayon P, et al. Peripheral benzodiazepine receptor modulation with phagocyte differentiation. *Biochem Pharmacol*. (1993) 46:551–4. doi: 10.1016/0006-2952(93)90535-5
52. Owen DR, Yeo AJ, Gunn RN, Song K, Wadsworth G, Lewis A, et al. An 18-kDa translocator protein (TSPO) polymorphism explains differences in binding affinity of the PET radioligand PBR28. *J Cereb Blood Flow Metab*. (2012) 32:1–5. doi: 10.1038/jcbfm.2011.147
53. Owen DR, Gunn RN, Rabiner EA, Bennacef I, Fujita M, Kreisl WC, et al. Mixed-affinity binding in humans with 18-kDa translocator protein ligands. *J Nucl Med*. (2011) 52:24–32. doi: 10.2967/jnumed.110.079459
54. Owen DR, Howell OW, Tang SP, Wells LA, Bennacef I, Bergstrom M, et al. Two binding sites for [^{3}H]PBR28 in human brain: implications for TSPO PET imaging of neuroinflammation. *J Cereb Blood Flow Metab*. (2010) 30:1608–18. doi: 10.1038/jcbfm.2010.63
55. Schiller HB, Fernandez IE, Burgstaller G, Schaab C, Scheltema RA, Schwarzmayr T, et al. Time- and compartment-resolved proteome profiling of the extracellular niche in lung injury and repair. *Mol Syst Biol*. (2015) 11:819. doi: 10.15252/msb.20156123
56. Misharin AV, Morales-Nebreda L, Mutlu GM, Budinger GR, Perlman H. Flow cytometric analysis of macrophages and dendritic cell subsets in the mouse lung. *Am J Respir Cell Mol Biol*. (2013) 49:503–10. doi: 10.1165/rcmb.2013-0086MA
57. Ayaub EA, Dubey A, Imani J, Botelho F, Kolb MRJ, Richards CD, et al. Overexpression of OSM and IL-6 impacts the polarization of pro-fibrotic macrophages and the development of bleomycin-induced lung fibrosis. *Sci Rep*. (2017) 7:13281. doi: 10.1038/s41598-017-13511-z
58. Ashcroft T, Simpson JM, Timbrell V. Simple method of estimating severity of pulmonary fibrosis on a numerical scale. *J Clin Pathol*. (1988) 41:467–70. doi: 10.1136/jcp.41.4.467
59. Seger S, Stritt M, Vezzali E, Nayler O, Hess P, Groenen PMA, et al. A fully automated image analysis method to quantify lung fibrosis in the bleomycin-induced rat model. *PLoS ONE*. (2018) 13:e0193057. doi: 10.1371/journal.pone.0193057
60. Woessner JF Jr, Boucek RJ. Connective tissue development in subcutaneously implanted polyvinyl sponge. I. Biochemical changes during development. *Arch Biochem Biophys*. (1961) 93:85–94. doi: 10.1016/0003-9861(61)90319-8
61. Betzel T, Müller C, Groehn V, Müller A, Reber J, Fischer CR, et al. Radiosynthesis and preclinical evaluation of 3′-Aza-2′-[^{18}F]fluorofolic acid: a novel PET radiotracer for folate receptor targeting. *Bioconjug Chem*. (2013) 24:205–14. doi: 10.1021/bc300483a
62. Boss SD, Müller C, Siwowska K, Schmid RM, Groehn V, Schibli R, et al. Diastereomerically pure 6R- and 6S-3′-Aza-2′-^{18}F-Fluoro-5-Methyltetrahydrofolates show unprecedentedly high uptake in folate receptor-positive KB tumors. *J Nucl Med*. (2019) 60:135–41. doi: 10.2967/jnumed.118.213314
63. Xia W, Hilgenbrink AR, Matteson EL, Lockwood MB, Cheng JX, Low PS. A functional folate receptor is induced during macrophage activation and can be used to target drugs to activated macrophages. *Blood*. (2009) 113:438–46. doi: 10.1182/blood-2008-04-150789
64. van den Brule S, Huaux F, Uwambayinema F, Ibouraadaten S, Yakoub Y, Palmai-Pallag M, et al. Lung inflammation and thymic atrophy after bleomycin are controlled by the prostaglandin D2 receptor DP1. *Am J Respir Cell Mol Biol*. (2014) 50:212–22. doi: 10.1165/rcmb.2012-0520OC
65. Bellomo A, Gentek R, Bajenoff M, Baratin M. Lymph node macrophages: scavengers, immune sentinels and trophic effectors. *Cell Immunol*. (2018) 330:168–74. doi: 10.1016/j.cellimm.2018.01.010
66. Junt T, Moseman EA, Iannacone M, Massberg S, Lang PA, Boes M, et al. Subcapsular sinus macrophages in lymph nodes clear lymph-borne viruses and present them to antiviral B cells. *Nature*. (2007) 450:110–4. doi: 10.1038/nature06287
67. Groves AM, Win T, Screaton NJ, Berovic M, Endozo R, Booth H, et al. Idiopathic pulmonary fibrosis and diffuse parenchymal lung disease: implications from initial experience with ^{18}F-FDG PET/CT. *J Nucl Med*. (2009) 50:538–45. doi: 10.2967/jnumed.108.057901
68. Win T, Screaton NJ, Porter JC, Ganeshan B, Maher TM, Fraioli F, et al. Pulmonary ^{18}F-FDG uptake helps refine current risk stratification in idiopathic pulmonary fibrosis (IPF). *Eur J Nucl Med Mol Imaging*. (2018) 45:806–15. doi: 10.1007/s00259-017-3917-8
69. Win T, Thomas BA, Lambrou T, Hutton BF, Screaton NJ, Porter JC, et al. Areas of normal pulmonary parenchyma on HRCT exhibit increased FDG PET signal in IPF patients. *Eur J Nucl Med Mol Imaging*. (2014) 41:337–42. doi: 10.1007/s00259-013-2514-8
70. Justet A, Laurent-Bellue A, Thabut G, Dieudonne A, Debray MP, Borie R, et al. [^{18}F]FDG PET/CT predicts progression-free survival in patients with idiopathic pulmonary fibrosis. *Respir Res*. (2017) 18:74. doi: 10.1186/s12931-017-0556-3
71. Motegi SI, Fujiwara C, Sekiguchi A, Hara K, Yamaguchi K, Maeno T, et al. Clinical value of ^{18}F-fluorodeoxyglucose positron emission tomography/computed tomography for interstitial lung disease and myositis in patients with dermatomyositis. *J Dermatol*. (2019) 46:213–8. doi: 10.1111/1346-8138.14758
72. Bondue B, Sherer F, Van Simaeys G, Doumont G, Egrise D, Yakoub Y, et al. PET/CT with ^{18}F-FDG- and ^{18}F-FBEM-labeled leukocytes for metabolic activity and leukocyte recruitment monitoring in a mouse model of pulmonary fibrosis. *J Nucl Med*. (2015) 56:127–32. doi: 10.2967/jnumed.114.147421
73. Khanna D, Tashkin DP, Denton CP, Lubell MW, Vazquez-Mateo C, Wax S. Ongoing clinical trials and treatment options for patients with systemic sclerosis-associated interstitial lung disease. *Rheumatology*. (2018) 58:567–79. doi: 10.1093/rheumatology/key151
74. Kolb M, Bonella F, Wollin L. Therapeutic targets in idiopathic pulmonary fibrosis. *Respir Med*. (2017) 131:49–57. doi: 10.1016/j.rmed.2017.07.062
75. Distler O, Highland KB, Gahlemann M, Azuma A, Fischer A, Mayes MD, et al. Nintedanib for systemic sclerosis-associated interstitial lung disease. *N Engl J Med*. (2019) 380:2518–28. doi: 10.1056/NEJMoa1903076
76. Huang J, Maier C, Zhang Y, Soare A, Dees C, Beyer C, et al. Nintedanib inhibits macrophage activation and ameliorates vascular and fibrotic manifestations in the Fra2 mouse model of systemic sclerosis. *Ann Rheum Dis*. (2017) 76:1941–8. doi: 10.1136/annrheumdis-2016-210823
77. Toda M, Mizuguchi S, Minamiyama Y, Yamamoto-Oka H, Aota T, Kubo S, et al. Pirfenidone suppresses polarization to M2 phenotype macrophages and the fibrogenic activity of rat lung fibroblasts. *J Clin Biochem Nutr*. (2018) 63:58–65. doi: 10.3164/jcbn.17-111
78. Khanna D, Denton CP, Lin CJF, van Laar JM, Frech TM, Anderson ME, et al. Safety and efficacy of subcutaneous tocilizumab in systemic sclerosis: results from the open-label period of a phase II randomised controlled trial (faSScinate). *Ann Rheum Dis*. (2018) 77:212–20. doi: 10.1136/annrheumdis-2017-211682
79. Byrne AJ, Mathie SA, Gregory LG, Lloyd CM. Pulmonary macrophages: key players in the innate defence of the airways. *Thorax*. (2015) 70:1189–96. doi: 10.1136/thoraxjnl-2015-207020

80. Li H, Nagai T, Hasui K, Matsuyama T. Depletion of folate receptor beta-expressing macrophages alleviates bleomycin-induced experimental skin fibrosis. *Mod Rheumatol.* (2014) 24:816–22. doi: 10.3109/14397595.2013.879415
81. Feng Y, Shen J, Streaker ED, Lockwood M, Zhu Z, Low PS, et al. A folate receptor beta-specific human monoclonal antibody recognizes activated macrophage of rheumatoid patients and mediates antibody-dependent cell-mediated cytotoxicity. *Arthritis Res Ther.* (2011) 13:R59. doi: 10.1186/ar3312
82. Lynn RC, Feng Y, Schutsky K, Poussin M, Kalota A, Dimitrov DS, et al. High-affinity FRbeta-specific CAR T cells eradicate AML and normal myeloid lineage without HSC toxicity. *Leukemia.* (2016) 30:1355–64. doi: 10.1038/leu.2016.35
83. Cao Z, Lis R, Ginsberg M, Chavez D, Shido K, Rabbany SY, et al. Targeting of the pulmonary capillary vascular niche promotes lung alveolar repair and ameliorates fibrosis. *Nat Med.* (2016) 22:154–62. doi: 10.1038/nm.4035
84. Chen DL, Cheriyan J, Chilvers ER, Choudhury G, Coello C, Connell M, et al. Quantification of lung PET images: challenges and opportunities. *J Nucl Med.* (2017) 58:201–7. doi: 10.2967/jnumed.116.184796
85. Guerra L, Ponti E, Morzenti S, Spadavecchia C, Crivellaro C. Respiratory motion management in PET/CT: applications and clinical usefulness. *Curr Radiopharm.* (2017) 10:85–92. doi: 10.2174/1874471010666170519165918
86. Reddy JA, Xu LC, Parker N, Vetzel M, Leamon CP. Preclinical evaluation of ^{99m}Tc-EC20 for imaging folate receptor-positive tumors. *J Nucl Med.* (2004) 45:857–66.
87. Vande Velde G, Poelmans J, De Langhe E, Hillen A, Vanoirbeek J, Himmelreich U, et al. Longitudinal micro-CT provides biomarkers of lung disease that can be used to assess the effect of therapy in preclinical mouse models, and reveal compensatory changes in lung volume. *Dis Models Mech.* (2016) 9:91–8. doi: 10.1242/dmm.020321
88. Aichler M, Kunzke T, Buck A, Sun N, Ackermann M, Jonigk D, et al. Molecular similarities and differences from human pulmonary fibrosis and corresponding mouse model: MALDI imaging mass spectrometry in comparative medicine. *Lab Invest.* (2018) 98:141–9. doi: 10.1038/labinvest.2017.110

Conflict of Interest: ^{18}F-AzaFol is patent pending (WO 2013/167653 A1) and the patent is owned by Merck & Cie, Switzerland, an affiliate of Merck KGaA, Darmstadt, Germany. RS and CM are co-inventor on this patent. RS received funding for the development of ^{18}F-AzaFol from Innosuisse (grant no.: CTI-Project 13877.1 PFLS-LS). CM received funding from Merck & Cie for the performance of preclinical studies with ^{18}F-AzaFol. OD had consultancy relationships with Actelion, AnaMar, Bayer, Boehringer Ingelheim, Catenion, CSL Behring, ChemomAb, Roche, GSK, Inventiva, Italfarmaco, Lilly, medac, Medscape, Mitsubishi Tanabe Pharma, MSD, Novartis, Pfizer, Sanofi, and UCB in the area of potential treatments of scleroderma and its complications. Additionally, OD has research funding from Actelion, Bayer, Boehringer Ingelheim, Mitsubishi Tanabe Pharma, and Roche. In addition, OD has a patent mir-29 for the treatment of systemic sclerosis registered. BM had grant/research support from AbbVie, Protagen, Novartis, congress support from Pfizer, Roche, and Actelion. In addition, BM has a patent mir-29 for the treatment of systemic sclerosis registered. The real or perceived potential conflicts listed above are accurately stated.

The remaining authors declare that the research was conducted in the absence of any commercial or financial relationships that could be construed as a potential conflict of interest.

frontiers in Immunology

ORIGINAL RESEARCH
published: 18 February 2020
doi: 10.3389/fimmu.2020.00219

Crystalline Silica Impairs Efferocytosis Abilities of Human and Mouse Macrophages: Implication for Silica-Associated Systemic Sclerosis

Alain Lescoat[1,2†], *Alice Ballerie*[1,2†], *Marie Lelong*[1], *Yu Augagneur*[1], *Claudie Morzadec*[1], *Stéphane Jouneau*[1,3], *Patrick Jégo*[1,2], *Olivier Fardel*[1,4], *Laurent Vernhet*[1] *and Valérie Lecureur*[1*]

[1] Univ Rennes, CHU Rennes, Inserm, EHESP, Irset (Institut de Recherche en Santé, Environnement et Travail) – UMR_S 1085, Rennes, France, [2] Department of Internal Medicine and Clinical Immunology, Rennes University Hospital, Rennes, France, [3] Department of Respiratory Diseases, Rennes University Hospital, Rennes, France, [4] Pôle Biologie, Rennes University Hospital, Rennes, France

OPEN ACCESS

Edited by:
Jeska Kirsten De Vries-Bouwstra, Leiden University Medical Center, Netherlands

Reviewed by:
Seyed Mahmoud Hashemi, Shahid Beheshti University of Medical Sciences, Iran
Jillian M. Richmond, University of Massachusetts Medical School, United States

***Correspondence:**
Valérie Lecureur
valerie.lecureur@univ-rennes1.fr

[†] These authors have contributed equally to this work

Specialty section:
This article was submitted to Autoimmune and Autoinflammatory Disorders, a section of the journal Frontiers in Immunology

Received: 02 October 2019
Accepted: 27 January 2020
Published: 18 February 2020

Citation:
Lescoat A, Ballerie A, Lelong M, Augagneur Y, Morzadec C, Jouneau S, Jégo P, Fardel O, Vernhet L and Lecureur V (2020) Crystalline Silica Impairs Efferocytosis Abilities of Human and Mouse Macrophages: Implication for Silica-Associated Systemic Sclerosis. Front. Immunol. 11:219. doi: 10.3389/fimmu.2020.00219

Inhalation of crystalline silica (SiO_2) is a risk factor of systemic autoimmune diseases such as systemic sclerosis (SSc) and fibrotic pulmonary disorders such as silicosis. A defect of apoptotic cell clearance (i.e., efferocytosis, a key process in the resolution of inflammation) is reported in macrophages from patients with fibrotic or autoimmune diseases. However, the precise links between SiO_2 exposure and efferocytosis impairment remain to be determined. Answering to this question may help to better link innate immunity and fibrosis. In this study, we first aim to determine whether SiO_2 might alter efferocytosis capacities of human and mouse macrophages. We secondly explore possible mechanisms explaining efferocytosis impairment, with a specific focus on macrophage polarization and on the RhoA/ROCK pathway, a key regulator of cytoskeleton remodeling and phagocytosis. Human monocyte-derived macrophages (MDM) and C57BL/6J mice exposed to SiO_2 and to CFSE-positive apoptotic Jurkat cells were analyzed by flow cytometry to determine their efferocytosis index (EI). The effects of ROCK inhibitors (Y27632 and Fasudil) on EI of SiO_2-exposed MDM and MDM from SSc patients were evaluated *in vitro*. Our results demonstrated that SiO_2 significantly decreased EI of human MDM *in vitro* and mouse alveolar macrophages *in vivo*. In human MDM, this SiO_2-associated impairment of efferocytosis, required the expression of the membrane receptor SR-B1 and was associated with a decreased expression of M2 polarization markers (CD206, CD204, and CD163). F-actin staining, RhoA activation and impairment of efferocytosis, all induced by SiO_2, were reversed by ROCK inhibitors. Moreover, the EI of MDM from SSc patients was similar to the EI of *in vitro*- SiO_2-exposed MDM and Y27632 significantly increased SSc MDM efferocytosis capacities, suggesting a likewise activation of the RhoA/ROCK pathway in SSc. Altogether, our results demonstrate that SiO_2 exposure may contribute to the impairment of efferocytosis capacities of mouse and human macrophages but also of MDM in SiO_2-associated autoimmune diseases and fibrotic disorders such as SSc; in this context, the silica/RhoA/ROCK pathway may constitute a relevant therapeutic target.

Keywords: crystalline silica, efferocytosis, macrophage polarization, rho kinase, systemic sclerosis

INTRODUCTION

Exploring the pathogenesis of silica-associated fibrotic and autoimmune disorders may help to decipher the link between fibrotic diseases and autoimmunity. Indeed, the consequences of crystalline silica (SiO_2) on health firstly include respiratory disorders, and more specifically, silicosis, a granulomatous and fibrotic interstitial lung disease (1). Beyond these direct pulmonary effects, independent epidemiological studies show that exposure to crystalline silica increases the risk of autoimmune connective tissue diseases (CTD) with chronic inflammation such as systemic sclerosis (SSc) or systemic lupus erythematosus (SLE) (2–4). SSc is considered as the main autoimmune disorder associated with silica exposure and, among rheumatic diseases, this chronic inflammatory and fibrotic disease involving lung and skin, has the highest case-specific mortality (5). Almost 50% of men suffering from SSc may have a history of silica exposure (6, 7). Crystalline silica is an oxide of silicon commonly found in nature as quartz. Exposure to crystalline silica particles especially occurs in occupational settings when materials containing crystalline silica are reduced to dust (1). More than 30% of workers could suffer from silica hazards in primary industries and high-risk sectors in developing countries (8). The pathogenic links between silica inhalation and the onset of fibrotic autoimmune disorders such as SSc are still to be determined.

Lungs and respiratory tracts constitute the first tissue interacting with SiO_2 after inhalation. As pulmonary macrophages (MΦ) phagocyte SiO_2 particles, they are considered the main cellular targets of this airborne contaminant (9). Via interaction with the membrane scavenger receptor B1 (SR-B1), SiO_2 exerts pro-inflammatory effects on MΦ through activation of the NLRP3 inflammasome (10, 11). MΦ are also involved in the resolution of inflammation. They can indeed adopt various phenotypes or activation states, either pro- or anti-inflammatory (i.e., M1 or M2 MΦ, respectively), according to their surrounding microenvironment. An altered MΦ polarization has been described in SSc (12) and in SLE (13) and also in fibrotic pulmonary diseases such as idiopathic pulmonary fibrosis (IPF) (14). Nonetheless, the effects of SiO_2 on the polarization states and associated phenotypes of MΦ are further to be explored.

Among MΦ properties, the process of efferocytosis, i.e., the specialized recognition and ingestion of apoptotic cells, is also essential for tissue homeostasis. Efferocytosis is a key process in the resolution of inflammation. By processing the clearance of apoptotic bodies, MΦ limit inflammation by preventing the secondary necrosis of apoptotic cells. Impaired efferocytosis can also participate to the release of auto-antigens, such as intra-nuclear components of apoptotic cells, which can directly contribute to the triggering of systemic autoimmunity (15–17). Interestingly, an impaired efferocytosis has been documented in monocyte-derived macrophages (MDM) from patient with systemic autoimmune disorders such as SLE (18–20) or SSc (21) but also in fibrotic diseases such as IPF (22). Efferocytosis could represent a key pathogenic process at the crossroads of systemic auto-immunity, MΦ and fibrosis. As SiO_2 is an airborne contaminant associated with both systemic autoimmunity and pulmonary fibrosis, exploring the consequences of SiO_2 on MΦ polarization and function may provide new insights on the link between autoimmunity, chronic inflammation and fibrosis. Nonetheless, the direct impact of SiO_2 exposure on efferocytosis capacities and polarization of MΦ has never been studied to date. In the present study, we first aim to determine whether SiO_2 might alter efferocytosis capacities of human and mouse MΦ. We secondly explore possible mechanisms that could explain an impaired efferocytosis, with a specific focus on MΦ polarization and on the RhoA/ROCK pathway, a key regulator of cell adhesion, cytoskeleton remodeling and phagocytosis, that has been recently advanced as a promising therapeutic target in fibrotic disease and especially in SSc (23, 24).

MATERIALS AND METHODS

Reagents

Crystalline silica particles (SiO_2, DQ 12; $d_{50} = 2.2\,\mu m$, DMT GmbH & Co.KG, Essen, Germany) and Tungsten carbide (WC) particles ($d_{50} = 1\,\mu m$) were heated at 200°C for 2 h to remove any possible endotoxin contamination, suspended in sterile water at the concentration of 100 mg/ml and were then sonicated for 30 min. Human recombinant cytokine IFNɤ, IL-4, and IL-13 were purchased from Peprotech (Neuilly sur Seine, France) and human recombinant GM-CSF and M-CSF were obtained from Sanofi-Aventis (Montrouge, France) and Miltenyi Biotec SAS (Paris, France), respectively. Camptothecin, propidium iodide (IP) and Lipopolysaccharide (LPS) from *E. coli* (serotype: 055:B5) were purchased from Sigma-Aldrich (St-Quentin Fallavier, France). FITC-Annexin V was purchased from BD Biosciences (Le Pont de Claix, France). Fasudil was obtained from MedchemExpress whereas the Rho-associated protein kinase (ROCK) inhibitor (+)-C-trans-4-(1-aminoethyl)-N- (4-pyridyl) cyclohexane carboxamide (Y27632) was purchased from Santa cruz Biotechnology, INC (Heidelberg).

Preparation of Human Monocyte-Derived Macrophages (MDM)

Patients With SSc and Healthy Donors (HD)

Peripheral blood mononuclear cells were obtained from HD or SSc patients through Ficoll gradient centrifugation. SSc patients from the department of Internal Medicine and Clinical Immunology of Rennes University Hospital were consecutively included after written informed consent. All patients fulfilled the 2013 ACR/EULAR classification criteria for SSc (25). Patients with overlapping syndrome with Sjögren syndrome or SLE were not included. Blood buffy coats of healthy donors were provided by Etablissement Français du Sang (Rennes, France) after consent. All healthy donors included in this study answered a medical questionnaire; allowing the exclusion of any pathologic condition (acute or chronic).

Differentiation of Blood Monocytes in MDM and Treatment

In all experiments, monocytes were selected after a 1 h adhesion step and were differentiated into MΦ for 6 days

using GM-CSF(400 IU/ml) or M–CSF (50 ng/ml) in RPMI 1640 medium GlutaMAX (Gibco, Life technologies SAS, Courtaboeuf, France) supplemented with 10 % heat-inactivated fetal bovine serum (FBS, Lonza, Levallois-Perret, France), 20 IU/ml penicillin and 20 μg/ml streptomycin (ThermoFisher Scientific, Courtaboeuf, France). Unless otherwise indicated, M0-MDM from HD were exposed *in vitro* to SiO_2 as follows: particles were re-suspended by vortexing before their addition to the medium for 4 h, MDM were then washed and subsequent experiments were performed.

In vitro Polarization of MDM

For M1 polarization, MDM were activated for additional 24 h by the addition of IFNγ (20 ng/ml) and LPS (20 ng/ml). For M2a polarization, MDM were activated for additional 24 h by the addition of IL-4 (20 ng/ml) and IL-13 (20 ng/ml). Before treatment, all MDM were placed in medium with 5% of FBS. For experiments described in **Figure 7**, M-CSF was replaced by GM-CSF (400 IU/ml) in the same conditions, to obtain GM-MDM (26).

Cell Viability

Cytotoxic effects of SiO_2 treatment on human MDM were assessed using reagent WST-1 colorimetric assay (Cell proliferation Reagent, Roche, Mannheim, Germany). Briefly, 4-day MDM were seeded in 96-well-plates at 0.4×10^5 cells/well to achieve their differentiation. Six day-old MDM were then exposed for 24 h to various concentrations of particles. After silica exposure, cells were washed twice, and 100 μL of medium with 10% of WST-1 was added in each well. Absorbance of soluble formazan formed products was measured after 60 min and 90 min at 450 nm using SPECTROstar Nano (BMG Labtech, Ortenberg, Germany). For some experiment, MDM cell viability was also evaluated by flow cytometry through the analysis of the percentage of Annexin-V-IP staining positive cells as previously described (21).

Animal Protocols

Female C57BL/6J mice weighing between 18 and 20 gr, used at 8 weeks of age, purchased from Janvier Labs (Le Genest Saint Isle, France) were randomly divided into 3 groups ($n = 5$ per experimental group). The animals were housed in positive pressure air-conditioned units (25°C, 50% relative humidity) on a 12-h light/dark cycle. For instillation, animals were anesthetized with a mix of ketamine and xylazine (respectively, 60 and 10 mg/kg). Particles were suspended in NaCl 0.9% and 1.5 mg of particles (SiO_2 or WC) per mouse (50 μl/mouse) were instilled into the lungs via trachea by transoral instillation. Control mice were instilled with the corresponding volume of NaCl. Four days after particle instillation, 5×10^6 $CFSE^{pos}$ apoptotic Jurkat cells in 50 μl saline were administered into the lungs by transoral instillation. Mice were sacrificed 3 h after apoptotic cell instillation with an overdose of ketamine and xylazine (respectively, 100 and 20 mg/kg). Bronchoalveolar lavages (BAL) were performed by cannulating the trachea (with a 21G needle) and infusing the lungs five times with 1 ml of NaCl 0.9%. The BAL fluids were centrifuged (800 g, 10 min, 4°C) and cell pellets were re-suspended in PBS-2% FBS for flow cytometry analyses with determination of the efferocytosis index (EI).

Efferocytosis Assays

Human Jurkat CD4 T-lymphocyte cells (1.10^6 cells/ml), cultured in RPMI 1640 Glutamax culture medium with 10 % FBS, 20 IU/ml penicillin and 20 μg/ml streptomycin, were stained for 15 min with 100 ng/ml CellTrace™ CFSE (Invitrogen), washed and then exposed for 4 h to 10 μM camptothecin to induce apoptosis as previously described (21).

Human MDM Analysis

CFSE-stained apoptotic and non-apoptotic Jurkat cells were added to MDM plated in 12-well-tissue culture plates, in 10:1 ratio (apoptotic cells/MΦ) for 90 min at 37°C in a 5% CO_2 humidified incubator. After co-culture, Jurkat cells were removed, MΦ were washed at least 3 times with phosphate-buffered saline (PBS), detached using Accutase™ (BioLegends, Paris, France) and incubated with Fc-block (Miltenyi Biotech SAS) in a PBS supplemented with 2% FBS solution. The staining of Jurkat cells with human anti-CD3-PE antibody (BD Biosciences) was used to exclude MΦ with unengulfed lymphocytes bound to their surface. Engulfment efficiency was measured by flow cytometry. EI was calculated according to the following equation: EI = (number of $CD3^{neg}$ $CFSE^{pos}$ MΦ /number of total MΦ) ×100.

BAL Fluids Analysis

As previously described, mouse cells from BAL were re-suspended in PBS supplemented with 2% FBS solution containing Fc block and then stained with human anti-CD3-PE, mouse anti-CD11b-PE-Cy7 (BD Biosciences) and anti-Gr1-V450 (eBiosciences SAS, Paris) antibodies. Engulfment efficiency was measured by flow cytometry. EI was calculated according to the following equation: EI = (number of $CD3^{neg}$ $Gr1^{int}$ $CD11b^{Int}$ $CFSE^{pos}$ cells /number of total $CD3^{neg}$ $Gr1^{int}$ $CD11b^{Int}$ cells) × 100.

Cell Surface Marker Analyses by Flow Cytometry

After cell detachment using Accutase™, MDM were first blocked in PBS supplemented with 2% FBS solution and with Fc block, then re-suspended and incubated with specific antibodies or appropriate isotypic controls for 30 min at 4°C. Cells were then washed once with PBS and analyzed on a LSR II cytometer with FACSDiva software (BD Biosciences). Surface marker expression was evaluated using the following antibodies: anti-CD163-FITC, anti-CD206-PE (BD Biosciences), anti-CD204-PE (R&D Systems, Abingdon, UK), anti-CD91-vioBright FITC, anti-CD44-vioBlue, anti-SR-B1-APC, anti-integrin αV, β5, or β3 (all from Miltenyi Biotec, SAS). Results were expressed as a ratio of median fluorescence intensity (MFI) calculated as follows: median fluorescence (mAb of interest)/ median fluorescence (isotype control mAb).

Transfection of siRNA

SMARTpool of individual siRNAs directed against human SCARB1 (SR-B1) (L-010592-00-0005) and a non-targeting pool (siRNA Ct), used as control, were purchased from Dharmacon (GE Healthcare Europe GmbH-FR, Velizy-Villacoublay, France). MDM were transfected using Lipofectamine RNAiMax reagent (Invitrogen) with siRNA at 5 pmol for 24 h. Silencing efficiency of siRNA SR-B1 was analyzed at the protein level using the anti-SR-B1-APC antibody (Miltenyi Biotec, SAS) by flow cytometry on a LSR II cytometer.

Analysis of F-actin Expression

Four-days MDM were trypsinized with Accutase^{TM} and then plated at 18×10^3 cells/cm^2 on a Lab-Tek^{TM} chamber slide system (Thermo Fisher Scientific, France) for additional 24 h. Twenty-four hours before treatment, cell culture medium was changed and replaced by a medium with 1% of FBS. MDM were next pre-treated or not with 20 μM of Y27632 for 1 h and, they were untreated or treated with 25 μg/cm^2 of SiO_2 or they were polarized into M1 MDM. Cells were fixed with 4% paraformaldehyde for 20 min at room temperature, washed three times with PBS and permeabilized in a 0.2% Triton X100 for 5 min and blocked in PBS containing 4% BSA for 1 h at room temperature. MDM were then incubated with Alexa fluor 568-phalloidin (Life Technologies SAS), to detect F-actin filaments, in a blocking solution for 2 h at room temperature and then washed with PBS. Thereafter, cells were co-stained with DAPI (Thermo Fisher Scientific), a fluorescent dye specific for DNA, for 10 min. After washings, coverslips were mounted with Dako Fluorescence mounting medium (Agilent Technologies France). Fluorescent-labeled cells were captured with a fluorescence microscope (Zeiss Apotome, Axio Imager Z1) and quantification of phalloidin staining was performed with Image J 1.52a software (NIH, USA).

Western Blotting

MDM were harvested and lysed on ice in RIPA buffer supplemented with phosphatase inhibitor cocktail 2 and 3 (Sigma-Aldrich) and a cocktail of protein inhibitors (Roche Diagnostic, Meylan, France). Then, cell lysates were sonicated on ice and protein concentration was measured using the Bradford's method. Samples were heated for 5 min at 100°C, loaded in a 4 % stacking gel and then separated by a 8% sodium dodecyl sulfate polymerase gel electrophoresis (SDS-PAGE). Gels were electroblotted overnight onto nitrocellulose membranes. After blocking the membrane with a Tris-buffered saline solution supplemented with 0.1% tween-20 and 5% bovine serum albumin, membranes were hybridized with primary antibodies overnight at 4°C and incubated with appropriate horseradish peroxidase-conjugated (HRP) secondary antibodies. Primary antibodies used were directed against anti-P-MYPT1 (Thr696) (Ozyme SAS, Saint Quentin-en-Yvelines, France) and anti-HSC70 (Santa Cruz Biotechnology, Inc. Heidelberg, Germany). Immunolabeled proteins were finally visualized by chemiluminescence. Full scans of the entire original gels are provided as supplementary material. Densitometry with ImageJ 1.40g software (National Institutes of Health, Bethesda, MD, USA) was used for quantifying intensities of stained bands and normalization to HSC70 content.

RhoA-GTP Pull-Down Assay

Twenty-four hours before treatment, MDM culture medium was changed and replaced by a medium with 1 % of FBS. RhoA-GTP levels were measured using the RhoA activation assay biochem kit^{TM} (Cytoskeleton, Tebu-bio, Le Perray-en Yvelines, France). Briefly, cells were rapidly lysed at 4°C and equal volumes of 300 μg total cellular proteins were incubated with 50 μg of Rhotekin-RBD beads to specifically pull-down RhoA-GTP. After washing, the beads were re-suspended in Laemmli buffer, boiled, and subjected to Western-blot analysis. SDS-PAGE and Western blotting were performed as described above, by using primary anti-RhoA or anti-HSC70 antibodies.

Statistical Analysis

Data are presented as means ± standard error on the mean (SEM). Comparison between more than 2 groups were performed by one-way analysis of variance followed by Dunnett's or Newman–Keuls multiple comparison *post-hoc* tests. Depending on conditions and Gaussian distribution, Student's *t* test, paired-*t*-test or Mann–Whitney test were used to compare 2 groups. A $P < 0.05$ was considered significant. Data analyzes were performed with GraphPad Prism 5.0 software (GraphPad Software, La Jolla, CA, USA).

RESULTS

Impaired Efferocytosis Capacities of Human SiO_2-Exposed MDM and Alveolar Macrophages of Mice Exposed to SiO_2

MDM exposed to 25 μg/cm^2 of SiO_2 were less able to engulf apoptotic Jurkat cells (M0 SiO_2 + apoJ) than untreated MDM (M0 + apoJ), as the EI of SiO_2-exposed MDM was significantly lower (17.6 ± 1.7) than the EI of untreated MDM (32.4 ± 2.2) (**Figure 1A**). This decrease of apoptotic Jurkat cells engulfment and the phagocytosis of SiO_2 by human MDM was illustrated on **Figure 1B** (right) when compared to untreated MDM (**Figure 1B,** left). The EI of human MDM exposed to apoptotic Jurkat cells (M0 + apoJ) was significantly higher (32.4 ± 2.2) than the EI of MDM exposed to non-apoptotic Jurkat cells (M0 + J) (11.1 ± 1.1), confirming the specificity of this efferocytosis assay (**Figure 1A**). The decrease of efferocytosis in SiO_2-exposed MDM was specific, as human MDM exposed to the same concentration of tungsten carbide (WC) particles had preserved efferocytosis capacities (38.6 ± 5.0 in M0 Ct + apoJ vs. 33.2 ± 4.5 in M0 + WC + apoJ) (**Figure 2A**). This impairment of efferocytosis by SiO_2 in human MDM was dose-dependent (**Figure 2B**). No toxicity of a 4 h-exposure to various SiO_2 concentrations (from 1.65 to 33 μg/cm^2) was observed using a WST1 cell viability assay (**Figure 2C**), thus suggesting that the impact of 25 μg/cm^2 of SiO_2 on efferocytosis was not the consequence of a decreased cell viability in our model of MDM. Moreover, MDM could not retrieve their efferocytosis capacities 24 h (D1) after a 4 h-exposure to SiO_2 (D0) (**Figure 2D**) and this effect was not due to an impact of SiO_2 on cell viability

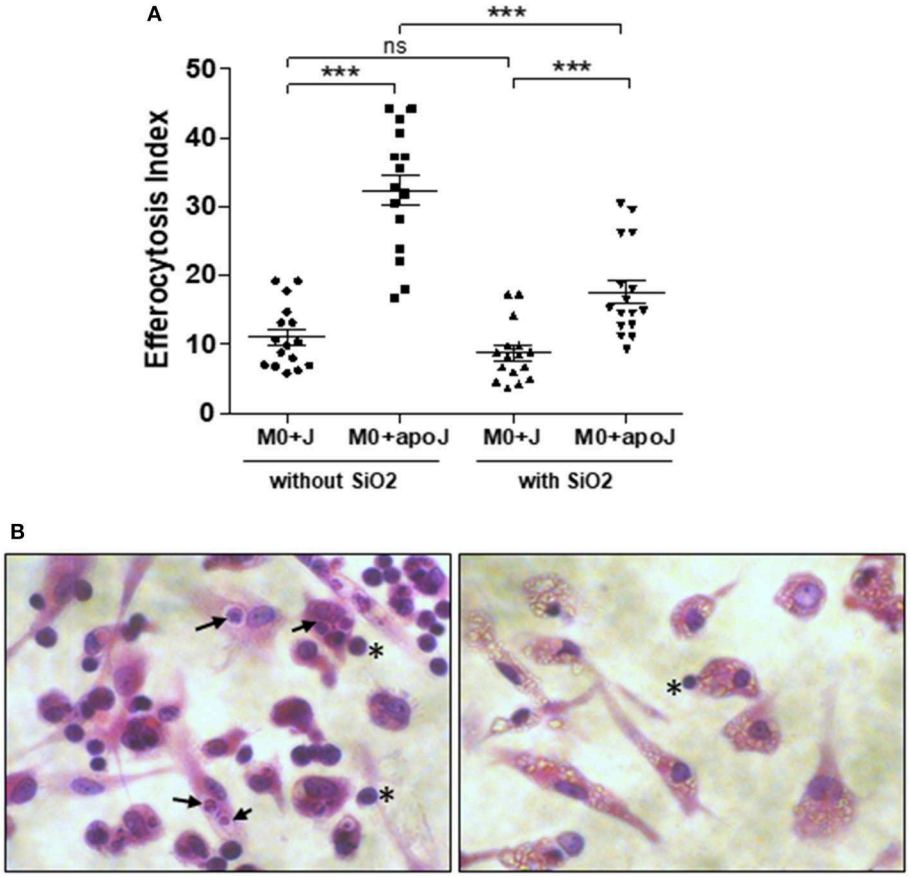

FIGURE 1 | *In vitro* impaired efferocytosis capacities of silica-exposed MDM. **(A)** EI of M0 MDM from the same healthy donors untreated or treated by 25 $\mu g/cm^2$ of SiO_2 for 4 h and then exposed to apoptotic Jurkat (apoJ) or live Jurkat (J) cells. Efferocytosis assay was performed on MDM from 16 different healthy donors. **(B)** Pictures of optical microscopy: M0 MDM were untreated (left) or treated with 25 $\mu g/cm^2$ of SiO_2 for 4 h (right), secondly exposed to apoptotic Jurkat cells for 90 min and then stained by HES. Black arrows and stars indicate the localization of Jurkat cells inside or outside MDM, respectively. SiO_2 particles are easily visualized in MDM cytoplasm on the right picture. ***$p < 0.001$; ns, not significant.

(**Figure 2E**). In accordance with these findings in human MDM, the relative EI of alveolar MΦ ($CD3^{neg}$ $Gr1^{Int}$ $CD11b^{Int}$ $CFSE^{pos}$) as defined in the gating strategy (**Figure 3A**) from mice exposed *in vivo* to $CFSE^{pos}$ apoptotic Jurkat cells 4 days after inhalation of SiO_2 (63.2 ± 9.2), was significantly lower than after inhalation of NaCl as control (100 ± 2.0) or WC particles (110.1 ± 4.1) (**Figure 3B**).

SiO_2-Reduced Phagocytosis of Apoptotic Jurkat Cells Requires SR-B1

Because SR-B1 has been demonstrated as a SiO_2 membrane receptor of MΦ (11), we further determined the role of this receptor on the modulation of efferocytosis capacities in SiO_2-exposed human MDM. A transient transfection of RNAi against SR-B1 significantly reduced endogenous SR-B1 expression in MDM in comparison with cells transfected with a non-targeting siRNA (Ct) (**Figure 4A**). SiO_2 significantly reduced the EI in siRNA Ct-transfected MDM but not in siRNA SR-B1-transfected MDM (**Figure 4B**), demonstrating that SiO_2-induced reduction of efferocytosis in human MDM is SR-B1 dependent.

Effects of SiO_2 on MDM Polarization Markers and on the Expression of Membrane Receptors Involved in Efferocytosis

We secondly explored the possible mechanisms involved in this SiO_2-related impairment of efferocytosis in human MDM. Because pro-inflammatory M1 MΦ exhibit impaired efferocytosis capacities (21, 27), we first compared the EI of polarized MDM with SiO_2-exposed MDM. Such as M1 MDM, SiO_2-exposed MDM had a significant lower EI than M2a MDM (**Figure 5A**). Three markers down-regulated in M1 MDM (CD206, CD163, and CD204) were also significantly reduced in SiO_2-exposed MDM when compared to M2a MDM, whereas their expression was similar in SiO_2-exposed MDM and M1 MDM (**Figure 5B**). Moreover, SiO_2 increased the secretion levels of pro-inflammatory M1-related cytokines IL-6, IL-8, and TNFα but not those of CCL18, a typical M2a marker. By contrast, WC had no effect on the secretions of these cytokines (**Figure S1**). Altogether these results suggest that SiO_2 modulates the polarization state toward a M1 like-phenotype.

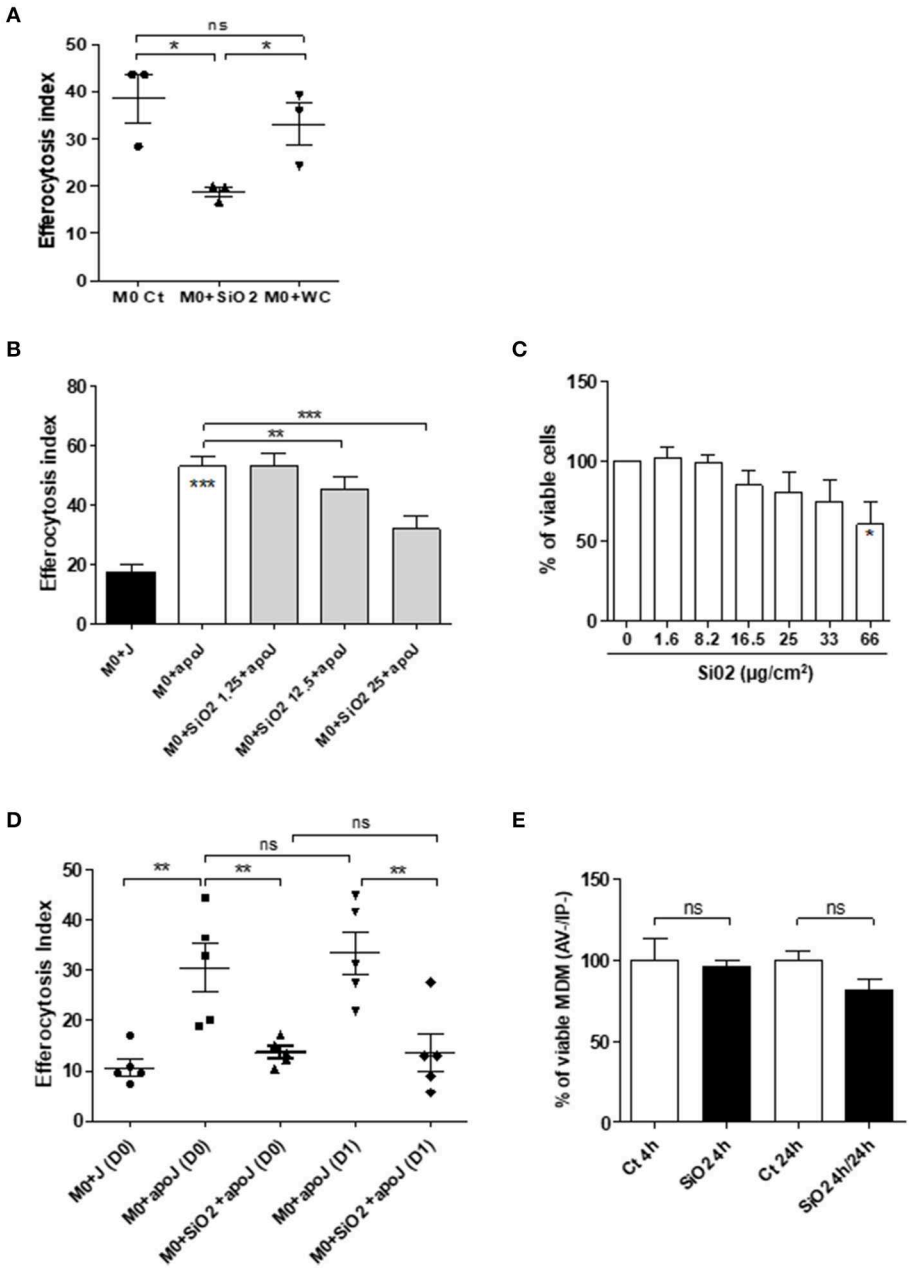

FIGURE 2 | Impaired efferocytosis capacities of silica-exposed MDM *in vitro* is specific, dose dependent, irreversible and is not directly due to the impact of SiO_2 on cell viability. **(A)** EI of M0 MDM from the same healthy donors, untreated or treated by 25 $\mu g/cm^2$ of SiO_2 or WC for 4 h and then exposed to apoptotic Jurkat (apoJ) or live Jurkat (J) cells (Experiment on MDM from 3 different healthy donors). **(B)** EI of M0 MDM from the same healthy donors, untreated or treated by the indicated concentrations of SiO_2 for 4 h and then exposed to apoptotic Jurkat (apoJ) (Experiment on MDM from 3 different healthy donors). **(C)** Determination of MDM cell viability by a WST-1 assay; data expressed in percentage of viable cells (Experiment on MDM from 4 different healthy donors). **(D)** EI of M0 MDM untreated or treated with 25 $\mu g/cm^2$ of SiO_2 for 4 h, washed and then exposed to apoptotic Jurkat (apoJ) or live Jurkat (J) cells for 90 min the same day (D0) or 24 h later (D1) (Experiment on MDM from 5 different healthy donors). **(E)** Determination, by flow cytometry, of MDM cell viability by AV/IP staining after exposure to 25 $\mu g/cm^2$ of SiO_2 for 4 h only or, 4 h followed by a 24 h period without SiO_2 (Experiment on MDM from 4 different healthy donors). $^*p < 0.05$; $^{**}p < 0.01$; $^{***}p < 0.001$; ns, not significant.

Several membrane receptors are involved in the recognition of apoptotic bodies by MΦ (28) and a decrease of their expression has been involved in the impairment of efferocytosis in M1 MDM (21). Therefore, we evaluated the impact of SiO_2 exposure on the expression of some of these membrane receptors and we compared their expression with M1 and M2a MDM. Membrane expression of CD91 and ITGβ5 were significantly reduced in M1 MDM when compared to M2a or SiO_2-exposed MDM (**Figure 5C**). The expressions of CD91, ITGβ5, CD44, ITGβ3, and ITGαV were similar in

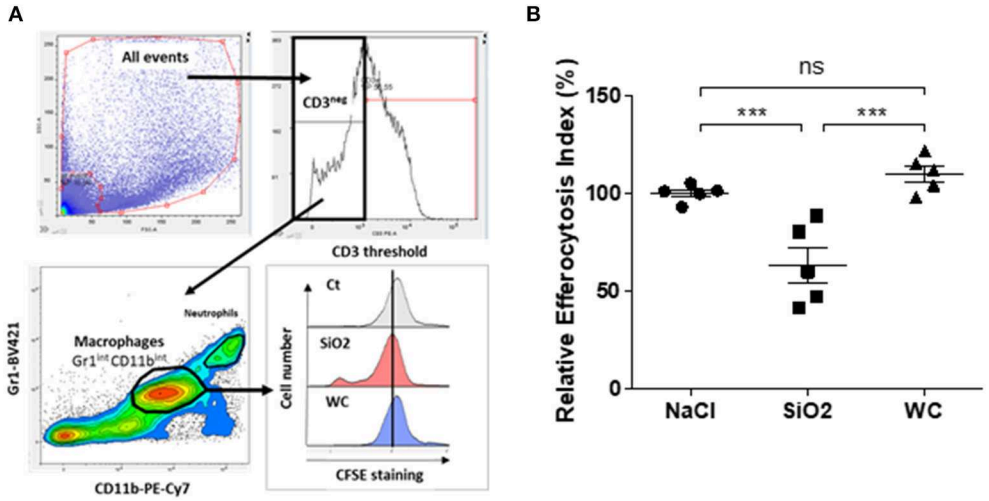

FIGURE 3 | Impaired efferocytosis capacities of alveolar MΦ from mice exposed *in vivo* to SiO_2. **(A)** Gating strategy used to evaluate efferocytosis capacities of alveolar MΦ from mice. EI of BAL cells obtained from mice exposed to NaCl or to 1.5 mg of SiO_2 or WC for 4 days and then exposed *in vivo* to $CFSE^{pos}$ apoptotic Jurkat (apoJ) cells, were analyzed by flow cytometry. **(B)** EI of alveolar MΦ which have engulfed apoptotic $CFSE^{pos}$ Jurkat cells ($CD3^{neg}$ $Gr1^{int}$ $CD11b^{int}$ $CFSE^{pos}$ cells). Efferocytosis of mice treated with NaCl as control was set as 100% ($n = 5$ mice in each group). $^{***}p < 0.001$; ns, not significant.

M2a MDM and in SiO_2-treated MDM (**Figure 5C**). These results suggest that the effect of SiO_2 on efferocytosis is not due to a SiO_2 mediated down-expression of these efferocytosis receptors.

SiO_2 Induces RhoA/ROCK Pathway in Human MDM

Considering that the RhoA/ROCK pathway modulates cytoskeleton in MDM (29) and that RhoA/ROCK inhibitors may shift M1 into M2 MΦ (30–32) and could restore efferocytosis reduced by chemical pollutants (33, 34), we explored the role of the RhoA/ROCK pathway in the impairment of efferocytosis induced by SiO_2 exposure. Firstly, a 10 min- SiO_2 exposure as well as M1 polarization, induced a higher staining for F-actin in comparison with untreated M0 suggesting a cytoskeletal rearrangement (**Figure 6A** and **Figure S2**). Pre-treatment by Y27632, a ROCK inhibitor, suppressed F-actin staining both in M1 polarized MDM and SiO_2-exposed MDM, suggesting that cytoskeletal rearrangements observed in M1 and in SiO_2-exposed MDM may involve an activation of RhoA/ROCK (**Figure 6A** and **Figure S2**). Secondly, SiO_2 exposure significantly increased RhoA expression in MDM (**Figure 6B**). The phosphorylation of myosin binding subunit of myosin phosphatase (MYPT), a known target of RhoA/ROCK, increased significantly from 30 min of SiO_2 exposure (**Figure 6C**), and this effect was inhibited in the presence of Y27632 (**Figure 6D**). Thirdly, we observed that, in the presence of Y27632, the membrane expressions of CD206 and CD204 were significantly restored in MDM exposed to SiO_2. Nonetheless, the expression of CD163 remained unchanged (**Figure 6E**). Altogether, these data indicate that SiO_2 activates RhoA/ROCK and that inhibition of this pathway may, at least in part, prevent the loss of M2a polarized markers in SiO_2-exposed MDM. To

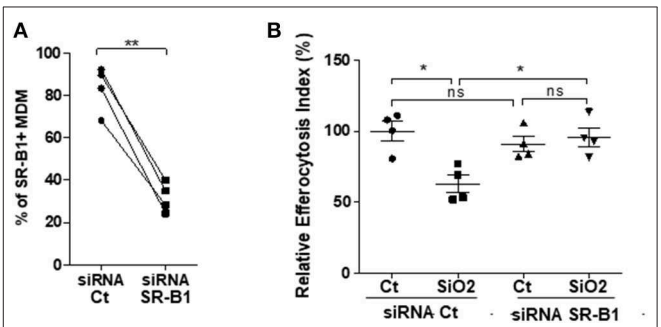

FIGURE 4 | Impairment of efferocytosis by silica in MDM requires SR-B1 expression. M0 MDM from the same healthy donors, were transfected with siRNA Ct or siRNA for SR-B1 for 24 h. Percentages of SR-B1 positive MDM **(A)** and EI of MDM from the same 4 healthy donors **(B)**, untreated or treated to SiO_2 and then exposed to apoptotic Jurkat (apoJ) or live Jurkat (J) cells for 90 min, were both determined by flow cytometry (Experiment on MDM from 4 different healthy donors). $^{*}p < 0.05$; $^{**}p < 0.01$; ns, not significant.

support these results on RhoA/ROCK and efferocytosis we also explored EI of GM-CSF derived MDM. Indeed, GM-CSF can activate RhoA/ROCK (35) and GM-CSF MDM are considered as another model of M1 MDM (26, 36). We firstly demonstrated that GM-MDM (GM-M0) had decreased efferocytosis capacities in comparison with M-M0 (**Figure S3A**). We also demonstrated that GM-M0 had a significantly decreased membrane expressions of CD204 and CD163, therefore confirming their M1-like phenotype (**Figure S3B**). We lastly confirmed that GM-M0 had a significant higher staining for F-actin (**Figure S3C**) supporting a GM-CSF mediated activation of RhoA/ROCK, as previously described (35). Altogether, our data support the crucial role of cytoskeleton in the control of MΦ polarization (37).

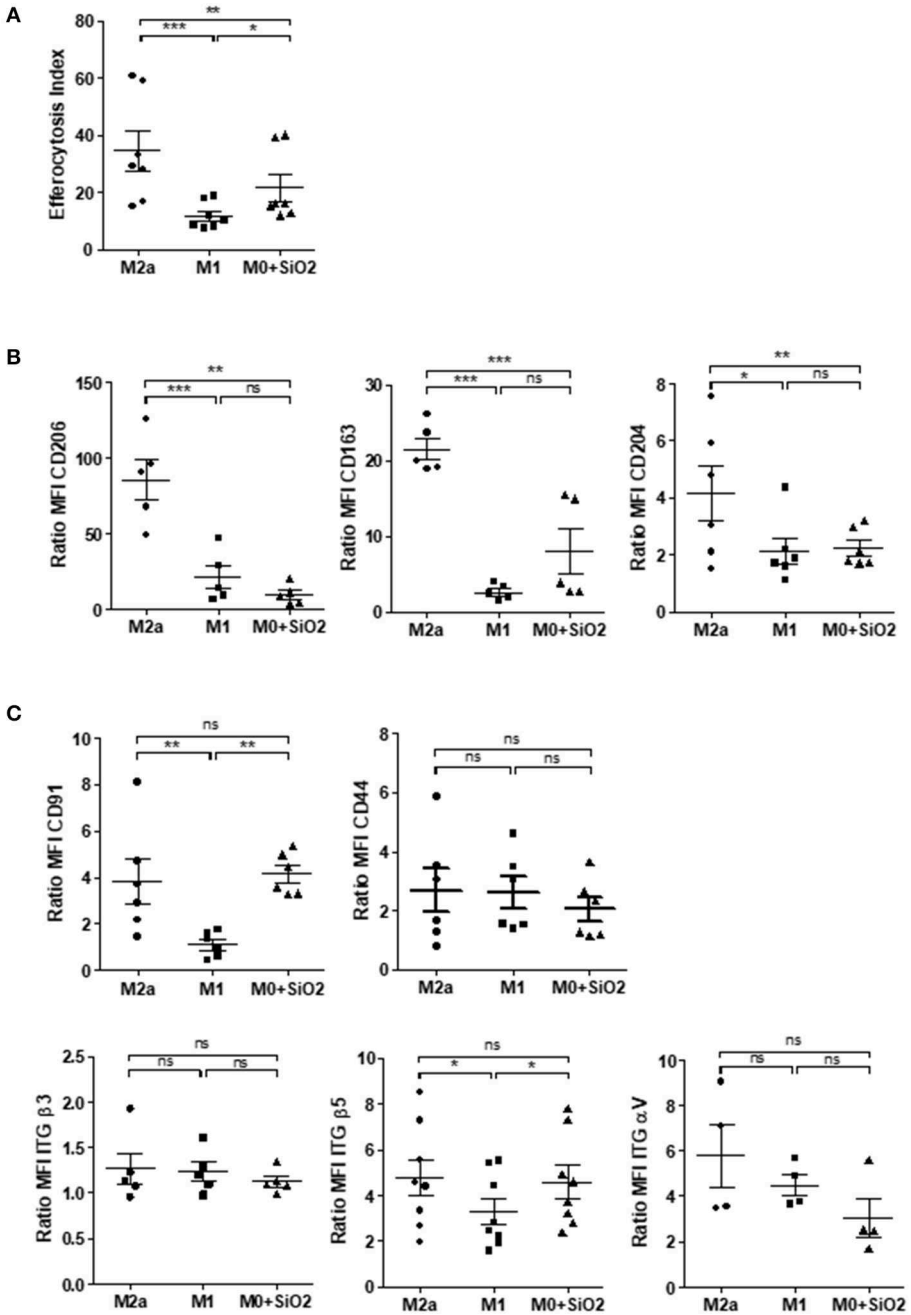

FIGURE 5 | Silica-exposed MDM have a M1-like phenotype. **(A)** EI of M0 MDM from the same healthy donors treated by 25 $\mu g/cm^2$ of SiO_2 for 4 h or of MDM polarized for 24 h into M2a or M1 and then exposed to apoptotic Jurkat for 90 min (Experiment on MDM from 7 different healthy donors). **(B)** Membrane expressions of CD206, CD163, and CD204 or **(C)** of CD91, CD44, ITGβ5, ITGβ3, and ITGαV in M0 MDM treated by 25 $\mu g/cm^2$ of SiO_2 for 4 h or in MDM polarized for 24 h into M2a or M1 were determined by flow cytometry; data are expressed as ratio of MFI (Experiment on MDM from 4 to 8 different healthy donors). $^*p < 0.05$; $^{**}p < 0.01$; $^{***}p < 0.001$; ns, not significant.

Rock Inhibition Partially Restores Impaired Efferocytosis in SiO_2-Exposed MDM and in MDM From SSc Patients

The EI of SiO_2-exposed MDM in the presence of RhoA/ROCK inhibitors such as Y27632 (**Figure 7A**) or Fasudil (**Figure 7B**) were significantly higher than the EI of SiO_2-exposed MDM without these inhibitors. This improvement of efferocytosis capacities by Y27632 or Fasudil in SiO_2-exposed MDM was not explained by a variation of SR-B1 expression (**Figures 7C,D**), suggesting that the effect of these two inhibitors was not related

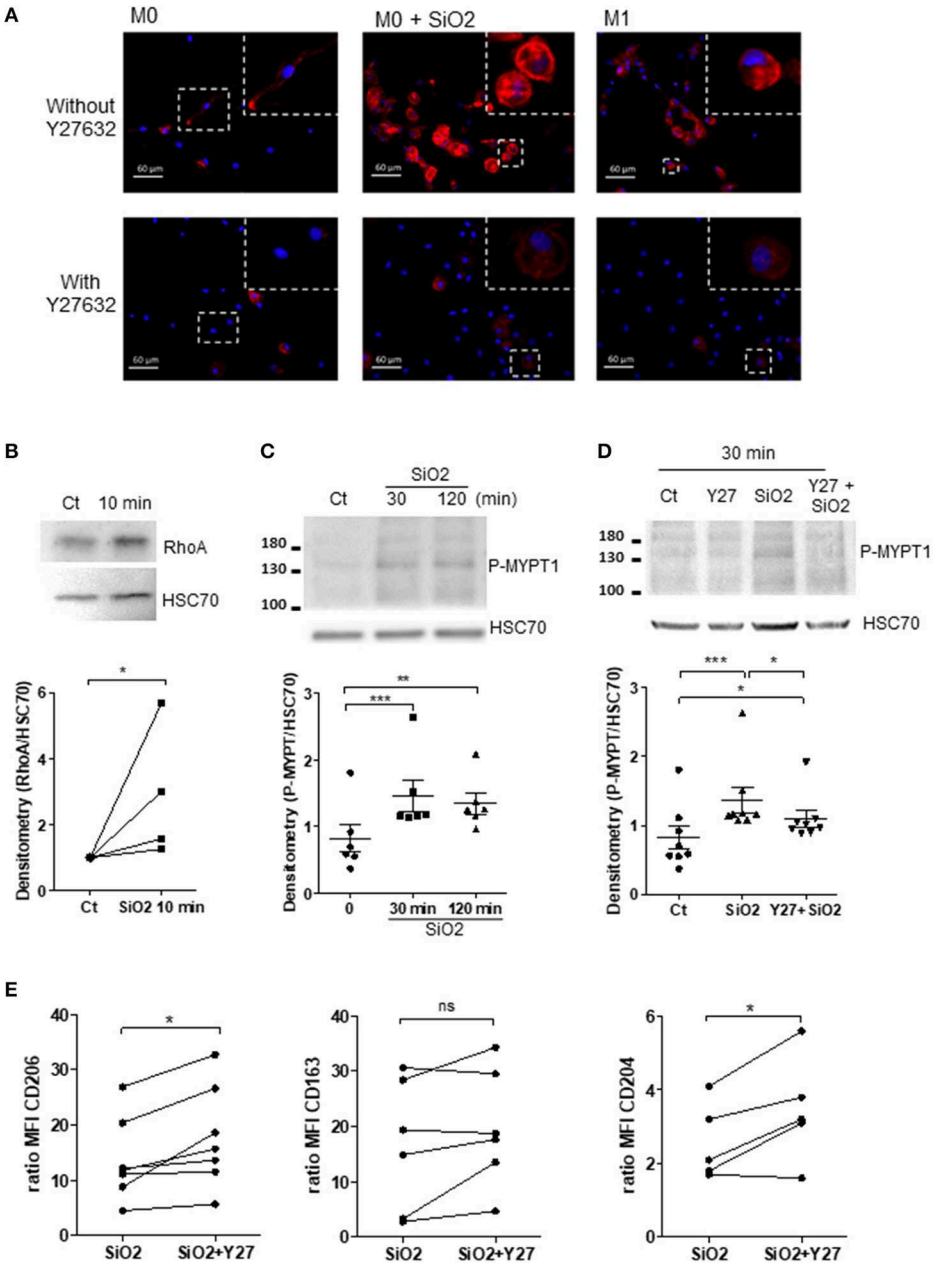

FIGURE 6 | Silica exposure induces cytoskeleton remodeling and alteration of MΦ polarization through activation of the RhoA/ROCK pathway. **(A)** Representative pictures of fluorescence microscopy: F-actin and nuclei were stained by Alexa Fluor 568-phalloidin (red) and DAPI (blue), respectively. M0-MDM were untreated or treated with 25 $\mu g/cm^2$ of SiO_2 for 10 min or polarized into M1 cells for 24 h. MDM were also pre-treated or not 1 h with the ROCK inhibitor Y27632 at 20 μM. **(B–D)** M0-MDM (Ct) from the same healthy donors were pre-treated or not with 20 μM Y27632 and then untreated or not with 25 $\mu g/cm^2$ of SiO_2 for the indicated time. The GTP-binding fraction of RhoA was pulled-down as described in Materials and Methods. **(C,D)** Western-blot analyzes of Phospho-MYPT1 expression were performed on whole-cell lysates. The relative levels of the proteins were determined by densitometry (Experiment on MDM from 4 to 8 different healthy donors). **(E)** Effect of Y27632 on the membrane expression of CD206, CD163, and CD204. MDM from the same healthy donors were pre-treated or not 1 h with the ROCK inhibitor Y27632 at 20 μM before exposure to 25 $\mu g/cm^2$ of SiO_2 for 4 h; data determined by flow cytometry are expressed as ratio of MFI (Experiment on MDM from 5 to 7 different healthy donors). $^*p < 0.05$; $^{**}p < 0.01$; $^{***}p < 0.001$; ns, not significant.

to a modulation of the interaction of SiO_2 with SR-B1, but was more likely due to its direct impact on the RhoA/ROCK pathway. **Figure 8A** shows that the EI of MDM from patients with SSc, an autoimmune fibrotic disease associated with SiO_2 exposure, was decreased in comparison with the EI of MDM from HD. This impairment of efferocytosis in SSc MDM was similar to the decrease of efferocytosis induced by an *in vitro* exposure to SiO_2 in HD MDM. Moreover, EI of SSc MDM was partially

restored after treatment by Y27632 (**Figure 8B**), suggesting that inhibiting RhoA/ROCK pathway may also improve efferocytosis in SSc.

DISCUSSION

This is the first study evaluating the direct effects of SiO_2 on the efferocytosis capacities of human and mouse MΦ. We demonstrate in this work that SiO_2 impairs capacities of human MDM and of mouse alveolar MΦ to clear apoptotic Jurkat cells. In human MDM, this effect of SiO_2 is dose-dependent and requires the scavenger receptor SR-B1. This reduced efferocytosis after SiO_2 exposure is associated with an induction of a pro-inflammatory M1-like phenotype in human MDM. Moreover, SiO_2 activates the RhoA/ROCK pathway and ROCK inhibition partly restores efferocytosis capacities of SiO_2-exposed MDM, demonstrating that RhoA/ROCK pathway is involved in this SiO_2 induced-impairment of efferocytosis (**Figure 6**). A reduced efferocytosis may lead to persistent apoptotic cells that may undergo subsequent necrosis leading to a pro-inflammatory environment with delayed resolution of inflammation (17) and fibrosis (**Figure 9**). Moreover, this persistence of apoptotic cells due to SiO_2-impaired efferocytosis may concur to the release of intranuclear components that could activate innate and adaptive immunity, triggering or exacerbating SiO_2-associated systemic autoimmune diseases such as SSc and SLE. In accordance with this hypothesis, MDM from SSc patients have reduced efferocytosis capacities and a treatment by the ROCK inhibitor Y27632 partly restores this defective efferocytosis, confirming the involvement of RhoA/ROCK in this SiO_2-associated fibrotic disorder.

The link between fibrosis and a defective efferocytosis is strengthened by the existence of a similar impairment of efferocytosis in IPF (22). Moreover, instillation of an excess of apoptotic cells, followed by active efferocytosis, in the early phase of the bleomycin mouse model of pulmonary fibrosis is associated with a less severe progression of the disease in comparison of saline-instilled mice, also suggesting that an effective efferocytosis in the early stage of the disease is protective from subsequent fibrosis (39). Therefore, inhalation of SiO_2 could inversely result in an intense pulmonary inflammation associated with a defect of efferocytosis leading to a delayed or impaired resolution of inflammation and to fibroblast activation resulting in fibrosis. Impaired efferocytosis by alveolar MΦ would therefore constitutes a key player in the pathogenesis of SiO_2-induced fibrosis but the direct link between such efferocytosis defect and fibrosis is still to be demonstrated especially *in vivo*. In our study, exposure to SiO_2 reduced the EI of mouse alveolar MΦ and human MDM in a similar intensity (1.6- and 1.8-fold, respectively). However, we also observed some variation in SiO_2 effects on EI in some mice; as it is inherent to *in vivo* experiments, the variability of such effects could be partly due to the variable efficiency of the transoral instillation of the particles. The concentration of SiO_2 in human MDM (25 $\mu g/cm^2$) was similar to previous studies evaluating the impact of SiO_2 on alveolar MΦ (40). The concentration of SiO_2 used *in vivo* (1.5 mg/mice), although lower than the concentrations used in mouse models of silicosis (2.5 to 10 mg/mice) (41–43), was able to induce granuloma formation (data not shown). We can thus hypothesize that the observed defect of efferocytosis at 1.5

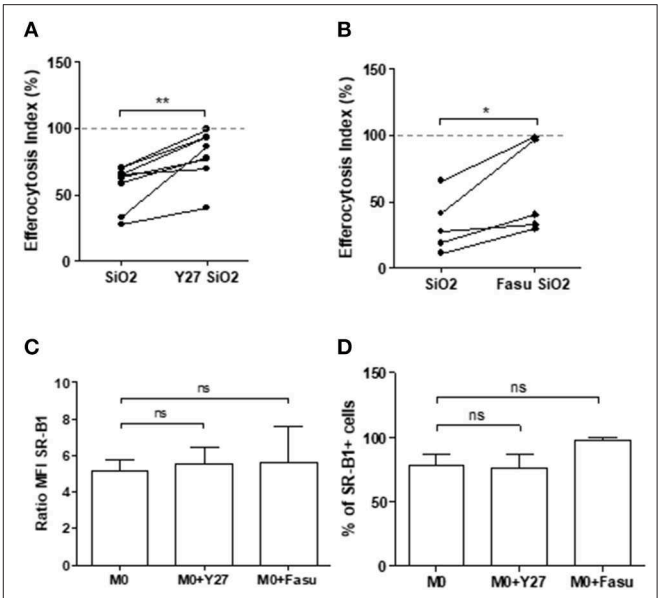

FIGURE 7 | RhoA/ROCK pathway inhibition enhances efferocytosis capacities of silica-exposed MDM and this effect is not due to a down expression of SR-B1 after RhoA/ROCK inhibition. **(A,B)** EI of MDM pre-treated or not with the ROCK inhibitors **(A)** Y27632 or **(B)** fasudil at 20 μM and treated with 25 $\mu g/cm^2$ of SiO_2 for 4 h and then exposed to apoptotic Jurkat cells for 90 min (Experiment on MDM from at least 5 different healthy donors). **(C,D)** Expression of SR-B1 expressed as **(C)** ratio of MFI and **(D)** percentage of positive cells of MDM treated or not with the ROCK inhibitor Y27632 and Fasudil at 20 μM for 4 h analyzed by flow cytometry (Experiment on MDM from 2 to 5 different healthy donors). *$p < 0.05$; **$p < 0.01$; ns, not significant.

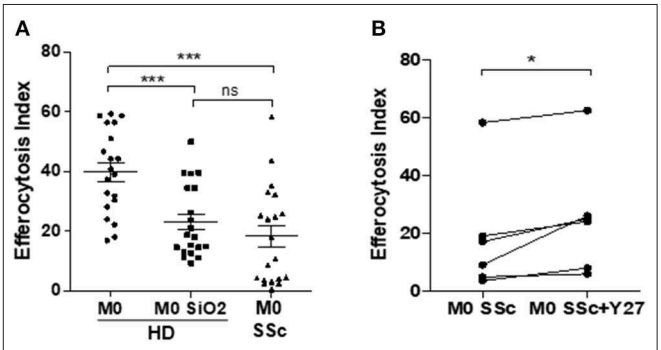

FIGURE 8 | RhoA/ROCK pathway inhibition by Y27632 enhances efferocytosis capacities of MDM from patients with systemic sclerosis. **(A)** EI of M0 MDM from healthy donors untreated or treated with 25 $\mu g/cm^2$ of SiO_2 for 4 h and of M0 MDM from SSc patients (Experiment on MDM from 20 different healthy donors and 20 different SSc patients). **(B)** EI of M0 MDM from SSc patients pre-treated or not with 20 μM Y27632 before exposure to apoptotic Jurkat cells (apoJ) for 90 min (Experiment on MDM from 6 different healthy donors). *$p < 0.05$; **$p < 0.01$; ***$p < 0.001$; ns, not significant.

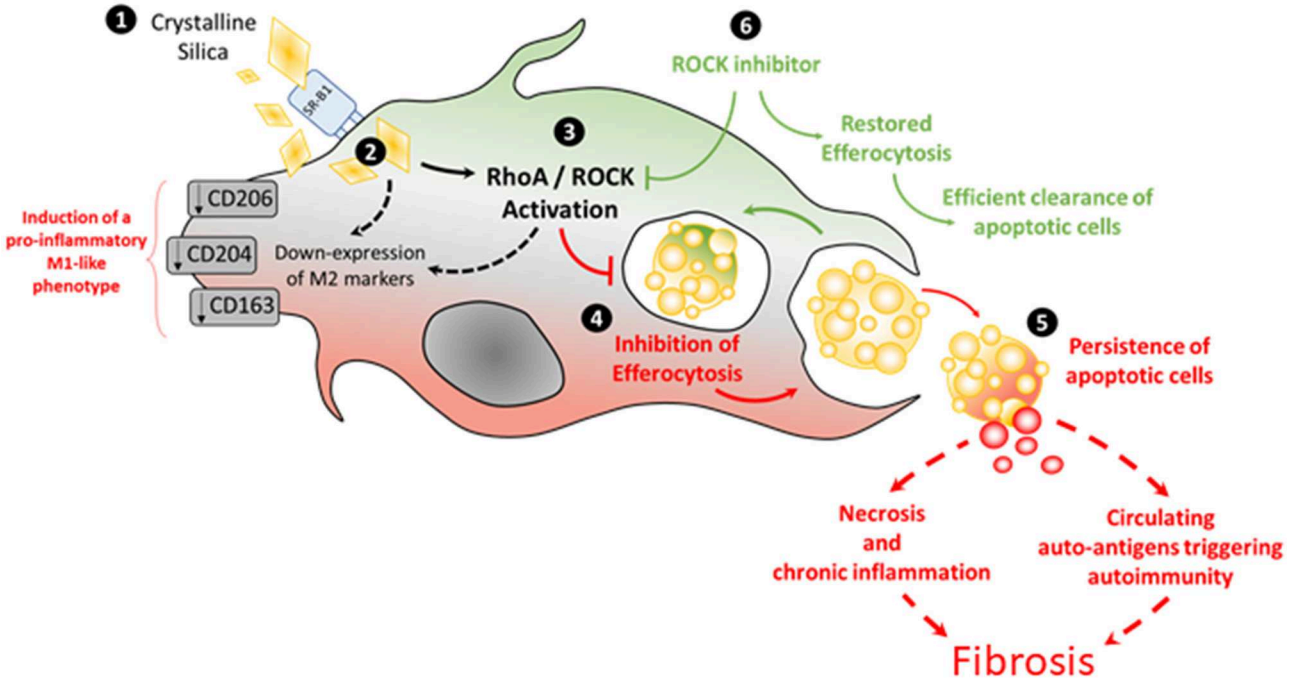

FIGURE 9 | Pathways involved in silica-impaired efferocytosis abilities of MDM [adapted from Lescoat et al. (38), license number: 4681481154582].

mg/mice may also occur with higher concentrations of SiO_2. Other airborne contaminants, such as cigarette smoke, associated with inflammatory lung diseases can also impair efferocytosis (34, 44). Nonetheless, SiO_2 may have a more significant impact *in vivo*, since, as a mineral particle, it remains persistent in lung tissues and in mediastinal lymphadenopathies of silica-exposed workers many years after exposure cessation (1). In our work, the effect of SiO_2 on efferocytosis persisted 24 h after discontinuation of SiO_2 exposure in human MDM, suggesting that the impact of SiO_2 on the clearance of apoptotic cells is long-lasting. The phagocytic capacity of dendritic cells, also considered as professional efferocytosis cells, was decreased after a direct exposure to SiO_2 at a concentration similar to the concentration we used in our study, suggesting that silica may also probably alter efferocytosis abilities of these myeloid cells (45). Interestingly, among particles, this effect of SiO_2 on efferocytosis appeared specific, as another crystalline dust, WC particles, had no significant impact on efferocytosis. WC does not induce pulmonary inflammation or fibrosis after tracheal instillation in mice models (41) and is therefore a crystalline dust considered as non-toxic, especially for MΦ (46). Altogether, these data suggest that it is the nature of the particles rather than their accumulation in MΦ that participates in the disruption of efferocytosis.

The limitations of this study include the use of only one type of crystalline silica; indeed, other types of crystalline silica may have different effects than DQ12. Nonetheless, DQ12 is largely used in the literature *in vitro* and *in vivo* to assess silica hazards (41). Moreover, as the exposure to amorphous silica is not associated with autoimmune diseases, it could be interesting to evaluate its effects on efferocytosis to confirm that it does not impair this function, contrarily to crystalline silica. The incomplete expression analysis of the efferocytosis receptors is also another limitation of this study. Indeed, since the role of efferocytosis is crucial for tissue homeostasis, there are numerous types of such receptors at the cell surface and, an extent analysis of SiO_2 impact on all of them was beyond the scope of this study.

Considering the issue of MΦ polarization in CTDs, our results are concordant with previous studies. Indeed, in our work, SiO_2 affected MΦ phenotype and shifted them into MΦ sharing some phenotypic characteristics of M1 MΦ as suggest by the down-expression of the M2 membrane markers CD206, CD204, and CD163 and by the upregulation of pro-inflammatory cytokines. Blood MDM in SLE are characterized by a similar down-regulation of CD206 (47). As SSc is both a fibrotic and inflammatory disorder, the polarization profile is more complex, although blood MDM are also characterized by some phenotypic features associated with M1 polarization such as a down-expression of CD204 (12). On the contrary, in fibrotic tissues such as lungs and skin in SSc, tissue MΦ express M2 markers such as CD163. It has been recently highlighted that the patients with SSc had higher blood levels of silica particle in comparison healthy controls (48). We hypothesize that for some patients this circulating silica could participate both to the alteration of polarization profile in SSc-MDM and to the impairment of their efferocytosis capacities.

The activation of RhoA/ROCK by SiO_2 is concordant with the involvement of this pathway in autoimmune disorders classically associated with silica exposure in human and characterized by a defective efferocytosis with production of antinuclear antibodies (ANA). Indeed, in mouse models of SLE, ROCK1/2 are spontaneously up-regulated and Y27632 significantly reduces serum levels of pro-inflammatory cytokines. Efferocytosis and activation of RhoA/ROCK could represent a key pathogenic process at the crossroads of systemic autoimmunity, MΦ and silica exposure: in mouse models of SLE, SiO_2 inhalation is associated with more severe visceral manifestations of the disease and higher levels of ANA (43, 49, 50). ANA produced after SiO_2 exposure specifically target apoptotic cells (51) and an altered efferocytosis after SiO_2 inhalation could lead to an excess of uncleared apoptotic cells with subsequent increased production of these ANA. Consistently, in a mouse model of SSc, fasudil, another ROCK inhibitor, significantly reduces lung inflammation, fibrosis and also serum levels of anti-DNA-topoisomerase-1 ANA (24). The links between a possible restoration of efferocytosis and this reduction of autoimmune features and/or fibrotic manifestations by ROCK inhibitors in SLE and SSc have never been established to date. Interestingly, significant associations between ROCK1/2 and RhoA gene polymorphisms and SSc have been reported, which also strengthens the possible role of this pathway in this systemic autoimmune disorder (52). New Rho inhibitors have been recently design for the treatment of SSc with promising results on dermal fibrosis in the bleomycin SSc mouse model (23). Beyond fibroblasts, the authors announce that identifying other biological targets of these new Rho inhibitors is a new key step for scleroderma research (23). Our results suggest that MΦ could constitute such relevant targets. Concerning the direct link between autoimmunity and fibrosis, defective efferocytosis might contribute to an excess of autoantigens with subsequent higher amount of immune-complexes (IC) and, recently, a direct activation of scleroderma fibroblasts by IC has been described [(53); **Figure 9**], strengthening the hypothesis that enhancing efferocytosis to reduce circulating IC could be a relevant strategy to limit fibrosis, at least in the early phase of the disease and/or in patients with uncontrolled inflammation. In our work, MDM from SSc patients had impaired efferocytosis capacities and this impairment was similar to the defective efferocytosis capacities of *in vitro* SiO_2-treated MDM from HD. Treatment by Y27632 11enhanced efferocytosis in SSc MDM, suggesting that an activation of ROCK may be involved in the reduced clearance of apoptotic cells by SSc MDM. Nonetheless, the relevance and the clinical impact of such an enhancement of efferocytosis in SSc patients is still to be determined. Although, the direct links between SiO_2 exposure and ROCK activation in SSc cannot be established in our study, more than 25% of SSc patients from our cohort have a history of silica exposure (54). Nonetheless, a detailed evaluation of the history of silica exposure, with precise dating of the time and duration of exposure and their correlation with impaired efferocytosis would be necessary to evaluate if this impairment could be considered as a biomarker of silica exposure and silica hazards in our SSc patients. Moreover, the impact of SiO_2 exposure and the exploration of efferocytosis in mouse models of CTDs in future studies may help to better characterize the interactions between SiO_2, RhoA/ROCK and defective clearance of apoptotic cells.

DATA AVAILABILITY STATEMENT

The datasets generated for this study are available on request to the corresponding author.

ETHICS STATEMENT

The studies involving human participants were reviewed and approved by Committees for protection of persons (CPP) Ouest-V France, CPP approval N°: 2015-A01221-48; study N°.15/26-988. The patients/participants provided their written informed consent to participate in this study. This animal study was reviewed and approved by Committee on the Ethics of Animal Experiments of the French government (agreement of V. Lecureur #17011).

AUTHOR CONTRIBUTIONS

AL, AB, and VL conceived and designed experiments. AL, AB, ML, YA, CM, and VL performed experiments. AL, AB, ML, VL, LV, and OF analyzed the data. PJ and SJ contributed reagents and materials. All the authors have contributed to the drafting and writing of the manuscript and added substantial modifications to the manuscript.

FUNDING

This work was supported by the Groupe Francophone de la Recherche sur la Sclerodermie.

ACKNOWLEDGMENTS

The authors thank the animal house facilities (ARCHE), the platform of Flow cytometry and the Platform of Histo-Pathology Hight Precision (H_2P_2) (Biosit, Rennes, France). We would also like to thank S. Dion (IRSET, Rennes, France) for providing us with mouse antibodies, K. Pouxvielh for ELISA and N. Gouault (Institut des sciences chimiques de Rennes) for silica sterilization. We thank F. Huaux (Louvain Centre for Toxicology and Applied Pharmacology, Brussels, Belgium) for providing us WC particles and for teaching us transoral instillation. The authors thank the nurses, the medical team and the patients from the Department of Internal Medecine and Clinical Immunology from Rennes University Hospital.

SUPPLEMENTARY MATERIAL

The Supplementary Material for this article can be found online at: https://www.frontiersin.org/articles/10.3389/fimmu.2020.00219/full#supplementary-material

REFERENCES

1. Leung CC, Yu ITS, Chen W. Silicosis. *Lancet Lond Engl.* (2012) 379:2008–18. doi: 10.1016/S0140-6736(12)60235-9
2. Blanc PD, Järvholm B, Torén K. Prospective risk of rheumatologic disease associated with occupational exposure in a cohort of male construction workers. *Am J Med.* (2015) 128:1094–101. doi: 10.1016/j.amjmed.2015.05.001
3. Miller FW, Alfredsson L, Costenbader KH, Kamen DL, Nelson LM, Norris JM, De Roos AJ. Epidemiology of environmental exposures and human autoimmune diseases: findings from a National Institute of Environmental Health Sciences Expert Panel Workshop. *J Autoimmun.* (2012) 39:259–71. doi: 10.1016/j.jaut.2012.05.002
4. Pollard KM. Silica, silicosis, and autoimmunity. *Front Immunol.* (2016) 7:97. doi: 10.3389/fimmu.2016.00097
5. Denton CP, Khanna D. Systemic sclerosis. *Lancet Lond Engl.* (2017) 390:1685–99. doi: 10.1016/S0140-6736(17)30933-9
6. Smith V, Vanthuyne M, Vander Cruyssen B, Van Praet J, Vermeiren F, Smets H, et al. Over-representation of construction-related occupations in male patients with systemic sclerosis. *Ann Rheum Dis.* (2008) 67:1448–50. doi: 10.1136/ard.2008.088419
7. De Decker E, Vanthuyne M, Blockmans D, Houssiau F, Lenaerts J, Westhovens R, et al. High prevalence of occupational exposure to solvents or silica in male systemic sclerosis patients: a Belgian cohort analysis. *Clin Rheumatol.* (2018) 37:1977–82. doi: 10.1007/s10067-018-4045-y
8. The Lancet Respiratory Medicine null. The world is failing on silicosis. *Lancet Respir Med.* (2019) 7:283. doi: 10.1016/S2213-2600(19)30078-5
9. Gilberti RM, Joshi GN, Knecht DA. The phagocytosis of crystalline silica particles by macrophages. *Am J Respir Cell Mol Biol.* (2008) 39:619–27. doi: 10.1165/rcmb.2008-0046OC
10. Dostert C, Pétrilli V, Van Bruggen R, Steele C, Mossman BT, Tschopp J. Innate immune activation through Nalp3 inflammasome sensing of asbestos and silica. *Science.* (2008) 320:674–7. doi: 10.1126/science.1156995
11. Tsugita M, Morimoto N, Tashiro M, Kinoshita K, Nakayama M. SR-B1 is a silica receptor that mediates canonical inflammasome activation. *Cell Rep.* (2017) 18:1298–311. doi: 10.1016/j.celrep.2017.01.004
12. Lescoat A, Ballerie A, Jouneau S, Fardel O, Vernhet L, Jego P, et al. M1/M2 polarisation state of M-CSF blood-derived macrophages in systemic sclerosis. *Ann Rheum Dis.* (2018) 78:e127. doi: 10.1136/annrheumdis-2018-214333
13. Ma C, Xia Y, Yang Q, Zhao Y. The contribution of macrophages to systemic lupus erythematosus. *Clin Immunol Orlando Fla.* (2019) 207:1–9. doi: 10.1016/j.clim.2019.06.009
14. Joshi S, Singh AR, Wong SS, Zulcic M, Jiang M, Pardo A, et al. Rac2 is required for alternative macrophage activation and bleomycin induced pulmonary fibrosis; a macrophage autonomous phenotype. *PloS ONE.* (2017) 12:e0182851. doi: 10.1371/journal.pone.0182851
15. Muñoz LE, Lauber K, Schiller M, Manfredi AA, Herrmann M. The role of defective clearance of apoptotic cells in systemic autoimmunity. *Nat Rev Rheumatol.* (2010) 6:280–9. doi: 10.1038/nrrheum.2010.46
16. Radic M. Clearance of apoptotic bodies, NETs, and Biofilm DNA: implications for autoimmunity. *Front Immunol.* (2014) 5:365. doi: 10.3389/fimmu.2014.00365
17. Abdolmaleki F, Farahani N, Gheibi Hayat SM, Pirro M, Bianconi V, Barreto GE, et al. The role of efferocytosis in autoimmune diseases. *Front Immunol.* (2018) 9:1645. doi: 10.3389/fimmu.2018.01645
18. Potter PK, Cortes-Hernandez J, Quartier P, Botto M, Walport MJ. Lupus-prone mice have an abnormal response to thioglycolate and an impaired clearance of apoptotic cells. *J Immunol.* (2003) 170:3223–32. doi: 10.4049/jimmunol.170.6.3223
19. Tas SW, Quartier P, Botto M, Fossati-Jimack L. Macrophages from patients with SLE and rheumatoid arthritis have defective adhesion *in vitro*, while only SLE macrophages have impaired uptake of apoptotic cells. *Ann Rheum Dis.* (2006) 65:216–21. doi: 10.1136/ard.2005.037143
20. Reefman E, Horst G, Nijk MT, Limburg PC, Kallenberg CGM, Bijl M. Opsonization of late apoptotic cells by systemic lupus erythematosus autoantibodies inhibits their uptake via an Fcgamma receptor-dependent mechanism. *Arthritis Rheum.* (2007) 56:3399–411. doi: 10.1002/art.22947
21. Ballerie A, Lescoat A, Augagneur Y, Lelong M, Morzadec C, Cazalets C, et al. Efferocytosis capacities of blood monocyte-derived macrophages in systemic sclerosis. *Immunol Cell Biol.* (2018) 97:340–7. doi: 10.1111/imcb.12217
22. Morimoto K, Janssen WJ, Terada M. Defective efferocytosis by alveolar macrophages in IPF patients. *Respir Med.* (2012) 106:1800–3. doi: 10.1016/j.rmed.2012.08.020
23. Kahl DJ, Hutchings KM, Lisabeth EM, Haak AJ, Leipprandt JR, Dexheimer T, et al. 5-Aryl-1,3,4-oxadiazol-2-ylthioalkanoic acids: a highly potent new class of inhibitors of Rho/Myocardin-Related Transcription Factor (MRTF)/Serum Response Factor (SRF)-mediated gene transcription as potential antifibrotic agents for scleroderma. *J Med Chem.* (2019) 62:4350–69. doi: 10.1021/acs.jmedchem.8b01772
24. Bei Y, Hua-Huy T, Nicco C, Duong-Quy S, Le-Dong NN, Tiev KP, et al. RhoA/Rho-kinase activation promotes lung fibrosis in an animal model of systemic sclerosis. *Exp Lung Res.* (2016) 42:44–55. doi: 10.3109/01902148.2016.1141263
25. van den Hoogen F, Khanna D, Fransen J, Johnson SR, Baron M, Tyndall A, et al. 2013 classification criteria for systemic sclerosis: an American College of Rheumatology/European League against Rheumatism collaborative initiative. *Arthritis Rheum.* (2013) 65:2737–47. doi: 10.1002/art.38098
26. Jaguin M, Houlbert N, Fardel O, Lecureur V. Polarization profiles of human M-CSF-generated macrophages and comparison of M1-markers in classically activated macrophages from GM-CSF and M-CSF origin. *Cell Immunol.* (2013) 281:51–61. doi: 10.1016/j.cellimm.2013.01.010
27. Michlewska S, Dransfield I, Megson IL, Rossi AG. Macrophage phagocytosis of apoptotic neutrophils is critically regulated by the opposing actions of pro-inflammatory and anti-inflammatory agents: key role for TNF-alpha. *FASEB J.* (2009) 23:844–54. doi: 10.1096/fj.08-121228
28. Penberthy KK, Ravichandran KS. Apoptotic cell recognition receptors and scavenger receptors. *Immunol Rev.* (2016) 269:44–59. doi: 10.1111/imr.12376
29. Liu Y, Tejpal N, You J, Li XC, Ghobrial RM, Kloc M. ROCK inhibition impedes macrophage polarity and functions. *Cell Immunol.* (2016) 300:54–62. doi: 10.1016/j.cellimm.2015.12.005
30. Liu C, Li Y, Yu J, Feng L, Hou S, Liu Y, et al. Targeting the shift from M1 to M2 macrophages in experimental autoimmune encephalomyelitis mice treated with fasudil. *PloS ONE.* (2013) 8:e54841. doi: 10.1371/journal.pone.0054841
31. Zandi S, Nakao S, Chun KH, Fiorina P, Sun D, Arita R, et al. ROCK-isoform-specific polarization of macrophages associated with age-related macular degeneration. *Cell Rep.* (2015) 10:1173–86. doi: 10.1016/j.celrep.2015.01.050
32. Xie Y, Zhao D, Dong P, Lai L. Macrophage-targeting Fasudil treatment protects liver from the ischemia/reperfusion injury by promoting M2 macrophage polarization. *Biosci Rep.* (2018). doi: 10.1042/BSR20171734. [Epub ahead of print].
33. Richens TR, Linderman DJ, Horstmann SA, Lambert C, Xiao YQ, Keith RL, et al. Cigarette smoke impairs clearance of apoptotic cells through oxidant-dependent activation of RhoA. *Am J Respir Crit Care Med.* (2009) 179:1011–1021. doi: 10.1164/rccm.200807-1148OC
34. Boé DM, Richens TR, Horstmann SA, Burnham EL, Janssen WJ, Henson PM, et al. Acute and chronic alcohol exposure impair the phagocytosis of apoptotic cells and enhance the pulmonary inflammatory response. *Alcohol Clin Exp Res.* (2010) 34:1723–32. doi: 10.1111/j.1530-0277.2010.01259.x
35. Kohno Y, Tanimoto A, Cirathaworn C, Shimajiri S, Tawara A, Sasaguri Y. GM-CSF activates RhoA, integrin and MMP expression in human monocytic cells. *Pathol Int.* (2004) 54:693–702. doi: 10.1111/j.1440-1827.2004.01682.x
36. Verreck FAW, de Boer T, Langenberg DML, Hoeve MA, Kramer M, Vaisberg E, et al. Human IL-23-producing type 1 macrophages promote but IL-10-producing type 2 macrophages subvert immunity to (myco)bacteria. *Proc Natl Acad Sci USA.* (2004) 101:4560–5. doi: 10.1073/pnas.0400983101
37. McWhorter FY, Wang T, Nguyen P, Chung T, Liu WF. Modulation of macrophage phenotype by cell shape. *Proc Natl Acad Sci USA.* (2013) 110:17253–8. doi: 10.1073/pnas.1308887110
38. Lescoat A, Ballerie A, Lelong M, Augagneur Y, Morzadec C, Jouneau S, et al. THU0003 crystalline silica impairs efferocytosis capacities of human monocyte-derived macrophages through RhoA-rock activation. *Ann Rheum Dis.* (2019) 78:267–268. doi: 10.1136/annrheumdis-2019-eular.5370
39. Yoon YS, Kim SY, Kim MJ, Lim JH, Cho MS, Kang JL. PPARγ activation following apoptotic cell instillation promotes resolution of lung inflammation

and fibrosis via regulation of efferocytosis and proresolving cytokines. *Mucosal Immunol.* (2015) 8:1031–46. doi: 10.1038/mi.2014.130
40. Li J, Yao W, Zhang L, Bao L, Chen H, Wang D, et al. Genome-wide DNA methylation analysis in lung fibroblasts co-cultured with silica-exposed alveolar macrophages. *Respir Res.* (2017) 18:91. doi: 10.1186/s12931-017-0576-z
41. Huaux F, Lardot C, Arras M, Delos M, Many MC, Coutelier JP, et al. Lung fibrosis induced by silica particles in NMRI mice is associated with an upregulation of the p40 subunit of interleukin-12 and Th-2 manifestations. *Am J Respir Cell Mol Biol.* (1999) 20:561–72. doi: 10.1165/ajrcmb.20.4.3342
42. Hamilton RF, Thakur SA, Mayfair JK, Holian A. MARCO mediates silica uptake and toxicity in alveolar macrophages from C57BL/6 mice. *J Biol Chem.* (2006) 281:34218–26. doi: 10.1074/jbc.M605229200
43. Mayeux JM, Escalante GM, Christy JM, Pawar RD, Kono DH, Pollard KM. Silicosis and silica-induced autoimmunity in the diversity outbred mouse. *Front Immunol.* (2018) 9:874. doi: 10.3389/fimmu.2018.00874
44. Hodge S, Hodge G, Ahern J, Jersmann H, Holmes M, Reynolds PN. Smoking alters alveolar macrophage recognition and phagocytic ability: implications in chronic obstructive pulmonary disease. *Am J Respir Cell Mol Biol.* (2007) 37:748–55. doi: 10.1165/rcmb.2007-0025OC
45. Liu S, Hao C, Bao L, Zhao D, Zhang H, Hou J, et al. Silica particles mediate phenotypic and functional alteration of dendritic cells and induce Th2 cell polarization. *Front Immunol.* (2019) 10:787. doi: 10.3389/fimmu.2019.00787
46. Lison D, Lauwerys R. *In vitro* cytotoxic effects of cobalt-containing dusts on mouse peritoneal and rat alveolar macrophages. *Environ Res.* (1990) 52:187–98. doi: 10.1016/S0013-9351(05)80253-1
47. Deng W, Chen W, Zhang Z, Huang S, Kong W, Sun Y, et al. Mesenchymal stem cells promote CD206 expression and phagocytic activity of macrophages through IL-6 in systemic lupus erythematosus. *Clin Immunol.* (2015) 161:209–16. doi: 10.1016/j.clim.2015.07.011
48. Ferri C, Artoni E, Sighinolfi GL, Luppi F, Zelent G, Colaci M, et al. High serum levels of silica nanoparticles in systemic sclerosis patients with occupational exposure: Possible pathogenetic role in disease phenotypes. *Semin Arthritis Rheum.* (2018) 48:475–81. doi: 10.1016/j.semarthrit.2018.06.009
49. Brown JM, Archer AJ, Pfau JC, Holian A. Silica accelerated systemic autoimmune disease in lupus-prone New Zealand mixed mice. *Clin Exp Immunol.* (2003) 131:415–21. doi: 10.1046/j.1365-2249.2003.02094.x
50. Wang Y, Lu Y, Chai J, Sun M, Hu X, He W, et al. Y-27632, a Rho-associated protein kinase inhibitor, inhibits systemic lupus erythematosus. *Biomed Pharmacother Biomedecine Pharmacother.* (2017) 88:359–66. doi: 10.1016/j.biopha.2017.01.069
51. Pfau JC, Brown JM, Holian A. Silica-exposed mice generate autoantibodies to apoptotic cells. *Toxicology.* (2004) 195:167–76. doi: 10.1016/j.tox.2003.09.011
52. Pehlivan Y, Yolbas S, Cetin GY, Alibaz-Oner F, Cagatay Y, Yilmaz N, et al. Investigation of the association between Rho/Rho-kinase gene polymorphisms and systemic sclerosis. *Rheumatol Int.* (2016) 36:421–7. doi: 10.1007/s00296-015-3400-4
53. Raschi E, Chighizola CB, Cesana L, Privitera D, Ingegnoli F, Mastaglio C, et al. Immune complexes containing scleroderma-specific autoantibodies induce a profibrotic and proinflammatory phenotype in skin fibroblasts. *Arthritis Res Ther.* (2018) 20:187. doi: 10.1186/s13075-018-1689-6
54. Ballerie A, Cavalin C, Lederlin M, Nicolas A, Garlantezec R, Jouneau S, et al. FRI0331 history of silica dust exposures and association with chest hrct and clinical characteristics in systemic sclerosis. *Ann Rheum Dis.* (2019) 78:847–848. doi: 10.1136/annrheumdis-2019-eular.7632

Conflict of Interest: The authors declare that the research was conducted in the absence of any commercial or financial relationships that could be construed as a potential conflict of interest.

frontiers in Immunology

ORIGINAL RESEARCH
published: 10 March 2020
doi: 10.3389/fimmu.2020.00383

Prominence of IL6, IGF, TLR, and Bioenergetics Pathway Perturbation in Lung Tissues of Scleroderma Patients With Pulmonary Fibrosis

Ludivine Renaud[1], *Willian A. da Silveira*[2], *Naoko Takamura*[1], *Gary Hardiman*[1,2] *and Carol Feghali-Bostwick*[1]*

[1] *Department of Medicine, Medical University of South Carolina, Charleston, SC, United States,* [2] *School of Biological Sciences, Institute for Global Food Security, Queens University Belfast, Belfast, United Kingdom*

Scleroderma-associated pulmonary fibrosis (SSc-PF) and idiopathic pulmonary fibrosis (IPF) are two of many chronic fibroproliferative diseases that are responsible for nearly 45% of all deaths in developed countries. While sharing several pathobiological characteristics, they also have very distinct features. Currently no effective anti-fibrotic treatments exist that can halt the progression of PF or reverse it. Our goal is to uncover potential gene targets for the development of anti-fibrotic therapies efficacious in both diseases, and those specific to SSc-PF, by identifying universal pathways and molecules driving fibrosis in SSc-PF and IPF tissues as well as those unique to SSc-PF. Using DNA microarray data, a meta-analysis of the differentially expressed (DE) genes in SSc-PF and IPF lung tissues (diseased vs. normal) was performed followed by a full systems level analysis of the common and unique transcriptomic signatures obtained. Protein-protein interaction networks were generated to identify hub proteins and explore the data using the centrality principle. Our results suggest that therapeutic strategies targeting IL6 trans-signaling, *IGFBP2*, *IGFL2*, and the coagulation cascade may be efficacious in both SSc-PF and IPF. Further, our data suggest that the expression of matrikine-producing collagens is also perturbed in PF. Lastly, an overall perturbation of bioenergetics, specifically between glycolysis and fatty acid metabolism, was uncovered in SSc-PF. Our findings provide insights into potential targets for the development of anti-fibrotic therapies that could be effective in both IPF and SSc-PF.

Keywords: scleroderma, systemic sclerosis, pulmonary fibrosis, idiopathic, microarray, interstitial lung disease

OPEN ACCESS

Edited by:
Oliver Distler,
University Hospital Zürich, Switzerland

Reviewed by:
Carlo Chizzolini,
Université de Genève, Switzerland
Theresa T. Lu,
Hospital for Special Surgery,
United States

***Correspondence:**
Carol Feghali-Bostwick
feghalib@musc.edu

Specialty section:
This article was submitted to Autoimmune and Autoinflammatory Disorders, a section of the journal Frontiers in Immunology

Received: *16 December 2019*
Accepted: *18 February 2020*
Published: *10 March 2020*

Citation:
Renaud L, da Silveira WA, Takamura N, Hardiman G and Feghali-Bostwick C (2020) Prominence of IL6, IGF, TLR, and Bioenergetics Pathway Perturbation in Lung Tissues of Scleroderma Patients With Pulmonary Fibrosis. Front. Immunol. 11:383. doi: 10.3389/fimmu.2020.00383

INTRODUCTION

Systemic sclerosis (SSc), commonly known as scleroderma, is a chronic and systemic autoimmune connective tissue disease characterized by proliferative/obliterative vasculopathy, immune dysregulation, and the development of fibrosis in the skin, lungs and other internal organs. SSc-associated pulmonary fibrosis (SSc-PF) is one of the leading causes of death in patients with SSc (1). SSc-PF is diffuse and displays inflammatory cell infiltration of the alveoli, interstitium and peribronchiolar tissues along with excessive proliferation of fibroblasts leading to extensive deposition of various extracellular matrix (ECM) proteins by mesenchymal cells, such as collagen

type I and III, fibronectin and tenascin (2, 3). SSc is one of many chronic fibroproliferative diseases that are responsible for nearly 45% of all deaths in developed countries (4). No effective therapy currently exists that can halt the progression of fibrosis or reverse it.

SSc-PF shares pathobiologic characteristics with other lung diseases, especially with idiopathic pulmonary fibrosis (IPF), but also has distinct features (5). Results from clinical trials emphasized the differences in pathogenesis that exist between SSc-PF and IPF. Immunosuppressive therapies are more effective in SSc-PF than in IPF, i.e., cyclophosphamide, mycophenolate mofetil (MMF) (6, 7), and drugs targeting fibrotic pathways in PF have shown some benefits in IPF, i.e., nintedanib and pirfenidone (8, 9). Recently, nintedanib has also been shown to inhibit macrophage activation and ameliorate SSc-PF (10, 11). Treatment with an antagonist to lysophosphatidic acid receptor 1 (LPA1) showed promising results in a murine model of SSc-PF and in clinical trial of IPF patients by improving forced vital capacity (FVC) and reducing fibrosis and inflammation, even though the trial was terminated early (12, 13). Therapy with the anti-oxidant N-acetylcysteine (NAC) ameliorated pulmonary function in both SSc-PF and IPF patients (14, 15). Despite similar pathological features, the pursuit of a treatment that would be equally beneficial in IPF and SSc-PF has been challenging.

This study aims to characterize universal pathways and molecules driving fibrosis in SSc-PF and IPF lung tissues and identify potential gene targets for the development of anti-fibrotic therapies that could improve lung function in both diseases. In doing so, we will also identify the unique gene signature of SSc-PF and characterize therapeutic targets specific to SSc-PF. To achieve this goal, we performed a meta-analysis of the differentially expressed (DE) genes in SSc-PF and IPF lung tissues (diseased vs. normal) using microarray data, followed by a full systems level analysis of the common and unique transcriptomic signatures obtained. Gene, protein and metabolite interactions are key to decipher the biological meaning of systems (16). Using STRING (17), a database of known and predicted protein-protein interactions, we identified functionally important hub genes in shared and unique datasets for IPF and SSc-PF. Results from this analysis provide insights for the development of anti-fibrotic therapies that could be effective in both IPF and SSc-PF.

MATERIALS AND METHODS

Study Population

Lung tissue samples were obtained from patients with SSc-PF ($n = 13$) and IPF ($n = 13$) who underwent lung transplantation at the University of Pittsburgh Medical Center, under a protocol approved by the Institutional Review Board. All patients with SSc met the American College of Rheumatology criteria for the diagnosis of SSc (18). Severe PF in SSc was defined as the presence of restrictive physiology, with a forced vital capacity (FVC) <55% of predicted. Patients with IPF were confirmed to have usual interstitial pneumonia (UIP) pathology without evidence of other known causes and no associated pulmonary arterial hypertension (PAH). Normal lung tissue specimens ($n = 9$) were obtained from organ donors whose lungs were not used for lung transplantation. Lung tissues were frozen prior to the extraction of total RNA.

RNA Extraction and qRT-PCR Validation

Total RNA was extracted from frozen lung tissues using TRIzol (Thermo Fisher Scientific, USA) and purified using the RNeasy Kit (Qiagen, USA). RNA quality was determined by agarose gel electrophoresis as well as analysis of samples using an Agilent 2100 Bioanalyzer with an RNA integrity number ≥6. For cDNA synthesis, 1,000 ng of total RNA was used with these reagents (Invitrogen, USA): Oligo(dT)12-18 Primer (Catalog # 18418012) and SuperScript™ IV (Catalog # 18090010). For qRT-PCR, the TaqMan™ Gene Expression Master Mix (Applied Biosystems, USA, Catalog # 4369016) was used along with the following primers: *IGFBP2* (Hs01040719_m1); *IGFL2* (Hs01389017_m1); *IL-6* (Hs00985639_m1); *TLR8* (Hs00152972_m1); *B2M* as housekeeping gene (Hs00187842_m1) on a StepOnePlus real time PCR system (Applied Biosystems, USA). The sample size for qRT-PCR validation was $n = 8$ for NL and SSc-PF, and $n = 12$ for IPF. For statistical analysis, a Kruskal-Wallis test was performed followed by Dunn's multiple comparisons test with significance set at $p < 0.05$. Error bars indicate standard error of the mean (SEM).

Gene Level Analysis: Microarray

Gene expression profiling was performed by microarray analysis using HumanRef-8 v3.0 BeadChips (Illumina, USA) containing 25,440 annotated genes. After sample hybridization, BeadChips were scanned using an Illumina BeadChip Array Reader. Intensity data was loaded in Limma version 3.40.2 in R version 3.6.0 and normalization between arrays was performed using the quantile method. Normalized expression was log2 transformed before being fitted to a linear model and differential expression analysis was performed for the following comparisons: SSc-PF vs. normal (NL) and IPF vs. NL. For each gene, Limma reported the estimated log2 fold change (log2FC) and provided a false discovery rate (FDR) adjusted q-value. FDR is the expected fraction of false positive tests among significant tests and was calculated using the Benjamini-Hochberg multiple testing adjustment procedure. Differentially expressed (DE) genes were identified based on the following criteria: $q < 0.1$, log2FC > 1: upregulated (equivalent to linear FC increase of 2), log2FC < -1: downregulated (equivalent to linear FC decrease of 2). The dataset is deposited on the Gene Expression Omnibus database with GSE48149 accession number (https://www.ncbi.nlm.nih.gov/geo/). The Genotype-Tissue Expression (GTEx) Portal (https://gtexportal.org/home/) was accessed on 05/01/2019 to obtain information on IGFBP2 and IGFL2 genes.

Hierarchical clustering was generated using MORPHEUS, a versatile matrix visualization and analysis software (https://software.broadinstitute.org/morpheus). The normalized data for all 425 DE genes (common and unique to both diseases) was uploaded to the site and the parameters hierarchical clustering, one minus cosine similarity based, linkage method on average and cluster on columns were selected (relative color scheme 0.63).

Systems Level Analysis

Functional Enrichment and Gene Ontology (GO)

Functional enrichment was performed on DE genes (q < 0.1, linear fold change of 2) using ToppFun (19) (ToppGene Suite), a portal for gene list enrichment analysis and candidate gene prioritization based on functional annotations and protein interactions network. ToppFun specifically extracts information from transcriptome, gene ontology (GO) and biological pathway annotations. GO terms were then visualized using REViGO (20), a tool that summarizes long lists of GO terms by removing redundant ones. The remaining terms were visualized in semantic similarity-based scatterplots and treemaps, a two-level hierarchy of GO terms that grouped cluster representatives under "superclusters" of related terms.

Protein-Protein Interaction Network (STRING)

The Search Tool for the Retrieval Of Interacting Genes/Proteins (STRING) is a database purposely designed to gather information on protein-protein interactions (direct experimental evidence and *de novo* predictions via computational approaches) and protein associations in the context of metabolic, signaling or transcriptional pathways (17). DE genes were entered (q < 0.1, linear FC of 2) using the following settings: lines thickness indicates the strength of data support (high confidence 0.7), the active interaction sources selected were textmining, experiments, databases, coexpression and gene fusion, number of interactors in the 1st shell were limited to query proteins only and in the 2nd shell were limited to 2 interactors; disconnected nodes were hidden in the network. In this study, hub genes are defined as genes with at least 5 links (connections).

Pathway Impact Analyses and Coherent Cascades

Pathway impact analysis was performed using iPathwayGuide (Advaita) on DE genes (q < 0.1, linear fold change of 1.5 to capture biologically significant perturbations of relevant pathways) to include important biological factors such as the magnitude of the expression change of each gene, the position of the DE genes in the given pathways, the topology of the pathway that describes how these genes interact, and the type of signaling interactions between them (21). This approach better captures the enrichment and perturbation of a given pathway and applies coherent cascade analysis to identify putative mechanisms. The impact analysis is modeled on KEGG Pathways.

RESULTS

Differential Expression Analysis

Differential expression analysis revealed 312 DE genes in the SSc-PF vs. NL comparison, and 352 DE genes in the IPF vs. NL comparison (q < 0.1, log2FC > |1|, **Supplementary Tables 1, 2**). Out of 425 DE genes identified (common and unique lists combined), 239 DE genes were commonly deregulated in both diseases (**Figure 1**, intersection), representing 56.2% of all DE genes. Conversely, 113 and 73 DE genes were exclusively perturbed in IPF and SSc-PF, respectively.

Hierarchical clustering of all 425 DE genes showed 3 main clusters: cluster-1 contains all NL samples, cluster-2 and cluster-3 comprise IPF and SSc-PF samples intertwined together (**Figure 2**), emphasizing that IPF and SSc-PF patients have a similar transcriptomic perturbation. Heatmaps of common and unique DE genes were also generated (**Supplementary Figures 1–3**).

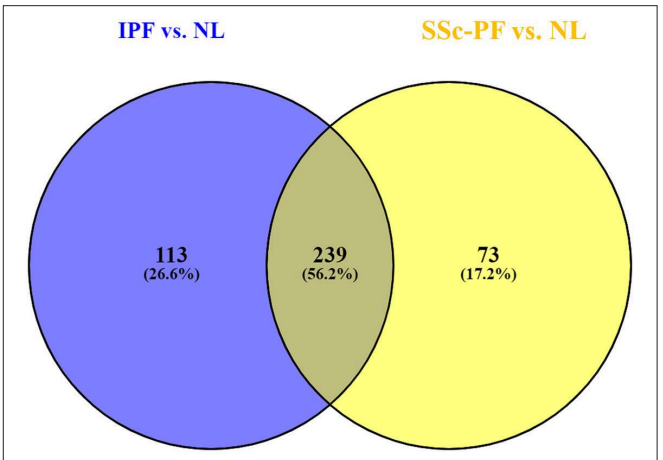

FIGURE 1 | Meta-analysis of DE genes in IPF and SSc-PF. Differential expression analysis revealed 312 DE genes in the SSc-PF vs. NL comparison, and 352 DE genes in the IPF vs. NL (q < 0.1, log2FC > |1|); 239 DE genes were commonly deregulated in both diseases (intersection), representing 56.2% of all DE genes (intersection and unique lists combined = 425). Conversely, 113 and 73 DE genes were exclusively perturbed in IPF and SSc-PF, respectively.

Upregulation of IGFBP2 and IGFL2 Is Common to Both Diseases

We and others have previously shown that the insulin-like growth factors (IGFs) and their binding proteins (IGFBPs) are key players in the development and progression of pulmonary fibrosis (22–27). *IGFBP3*, *IGFBP5*, and *IGFBP7* have been previously shown to be upregulated in both lung tissues and lung fibroblasts from patients with SSc-PF and IPF (24–26). *IGFBP4* is downregulated in SSc lung fibroblasts (27), and upregulated in IPF lung tissues (28, 29). Here we describe perturbation of the IGF signaling system in SSc-PF and IPF, specifically upregulation of *IGFBP2* and *IGF-like family member 2* (*IGFL2*) (**Table 1**). At homeostasis, *IGFBP2* is detectable in several organs and without obvious gender differences in fibroblasts, lung and skin, while *IGFL2* is highly expressed in healthy skin samples of both male and female donors **(Supplementary Figures 4, 5)**.

Perturbation of Matrikine-Producing Collagens in SSc-PF and IPF

Collagen-derived matrikines are peptides generated by partial proteolysis of certain collagens that can regulate cell activity (30). Out of the 9 DE collagen genes identified in the intersection of SSc-PF and IPF (**Table 2**), 4 have been identified as sources of matrikines: *COL1A1*, *COL1A2*, *COL15A1,* and *COL17A1* (30, 31). Note that all 4 collagens are upregulated in both diseases by at least a linear fold change increase of 2.

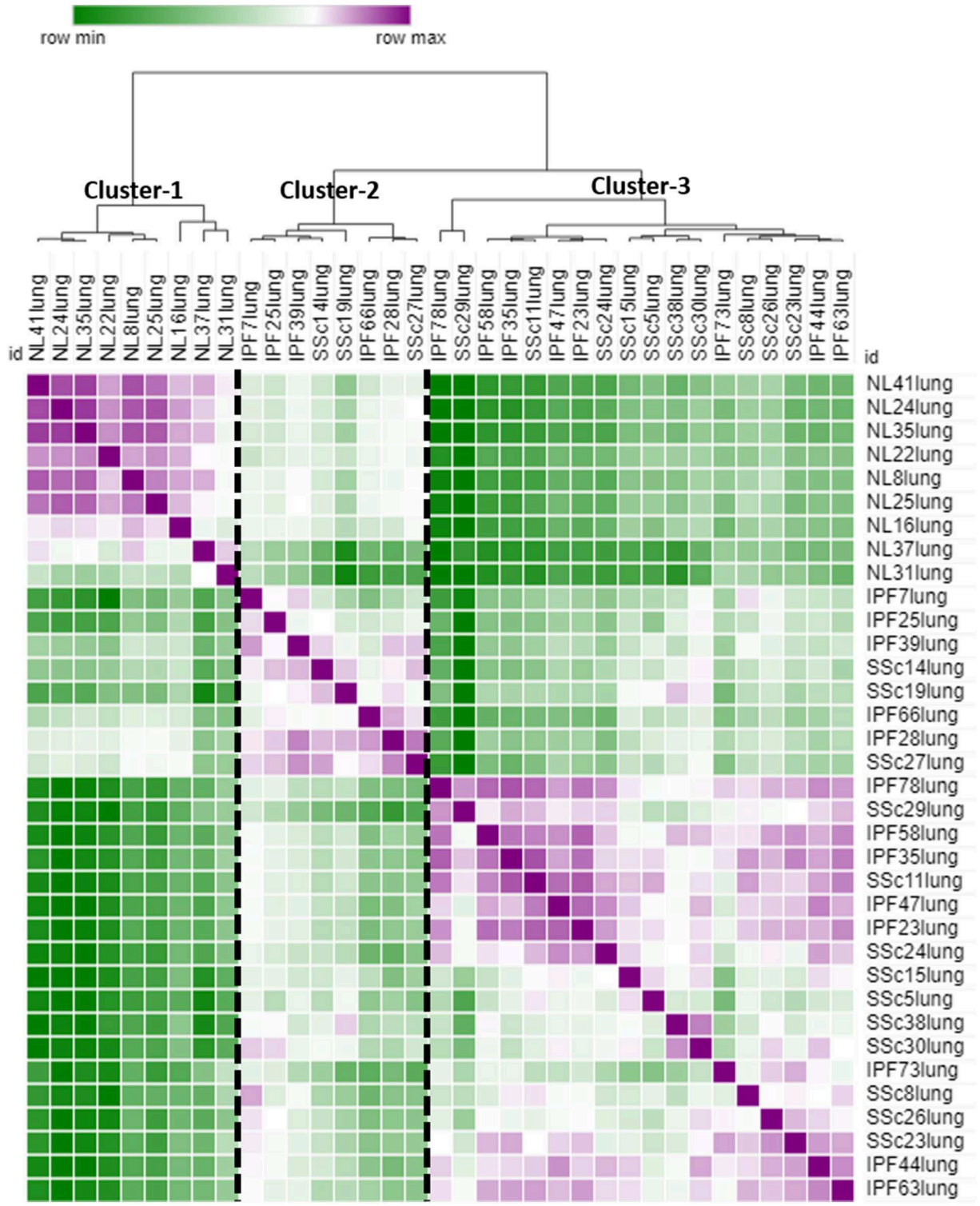

FIGURE 2 | Similarity matrix. The raw data for all 425 DE genes (common and unique to both diseases) was uploaded to MORPHEUS to generate a similarity matrix. Three main clusters are apparent, cluster-1 made up of NL samples only, cluster-2 and cluster-3 made up of SSc-PF and IPF samples intertwined, emphasizing that the gene signatures of these 2 diseases are very similar.

TABLE 1 | Genes deregulated in the IGF pathway.

SSc-PF vs. NL				IPF vs. NL			
Symbol	**Entrez_ID**	**log2FC**	***q*-value**	**Symbol**	**Entrez_ID**	**log2FC**	***q*-value**
IGFBP2	3485	1.50	2.16E-05	*IGFBP2*	3485	1.27	2.30E-04
IGFBP4	3487	0.95	8.37E-04	*IGFBP4*	3487	0.90	1.58E-03
IGFBP7	3490	0.63	2.24E-03	*IGFL2*	147920	1.17	4.04E-03
IGFL2	147920	1.07	7.97E-03	*IGFBP7*	3490	0.56	6.55E-03
IGFL1	374918	0.39	2.72E-02	*IGFBP5*	3488	0.77	4.70E-02
IGFBP5	3488	0.78	4.24E-02	*IGFL1*	374918	0.31	8.34E-02
IGF1	3479	0.42	1.07E-01	*IGF2BP3*	10643	−0.26	1.09E-01
				IGF1	3479	0.41	1.22E-01

DE upregulated genes are highlighted in red ($q < 0.1$, $log2FC > |1|$, representing a 2 linear fold change increase in gene expression). Genes are sorted by q-value from smallest to largest.

TABLE 2 | Perturbation of matrikine-producing collagen genes.

SSc-PF vs. NL				IPF vs. NL			
Symbol	**Entrez_ID**	**log2FC**	***q*-value**	**Symbol**	**Entrez_ID**	**log2FC**	***q*-value**
COL9A2	1298	1.12	1.91E-05	*COL9A2*	1298	1.10	2.60E-05
COL7A1	1294	2.14	3.20E-05	***COL1A1****	1277	2.29	4.71E-05
COL15A1*	1306	1.96	5.14E-05	***COL17A1****	1308	1.94	1.31E-04
COL17A1*	1308	2.06	5.21E-05	*COL7A1*	1294	1.92	1.56E-04
COL1A1*	1277	2.09	1.42E-04	***COL15A1****	1306	1.59	6.54E-04
COL10A1	1300	1.31	5.53E-04	***COL1A2****	1278	1.69	1.71E-03
COL1A2*	1278	1.68	1.63E-03	*COL10A1*	1300	1.18	1.79E-03
COL3A1	1281	1.84	5.43E-03	*COL3A1*	1281	1.83	6.12E-03
COL5A2	1290	1.13	1.46E-02	*COL5A2*	1290	1.08	1.96E-02

DE upregulated genes are highlighted in red ($q \leq 0.1$, $log2FC \geq 1$ representing a linear fold change of 2). Genes are sorted by q-value from smallest to largest. Bold matrikine-producing collagen genes.*

Systems Level Analysis

Our systems level analysis examined gene ontology and pathway impact analysis to try to decipher the biological relevance of the gene perturbation observed by taking into consideration the position and role of every gene in the pathway, the direction and type of signal from one gene to another, and feedback mechanisms that may exist (21). The meta-analysis revealed 56 enriched pathways in the IPF vs. NL comparison, and 67 in the SSc-PF vs. NL. A total of 48 pathways were commonly enriched in both diseases (intersection), while 8 and 19 pathways were exclusively perturbed in IPF and SSc-PF, respectively (**Supplementary Figure 6**).

We also analyzed STRING-generated networks for protein-protein interactions to identify hub genes in the intersection and unique gene sets using the principle of "network centrality" which states that genes with the highest degree of centrality (more connected) are three times more likely to be essential than genes with a smaller number of connection to other genes (32, 33).

Intersection

The meta-analysis revealed 239 DE genes at the intersection of IPF and SSc-PF. GO analysis of these genes revealed perturbation of "immune response," "extracellular matrix organization," and "collagen metabolism" biological processes as well as enrichment of "ECM-receptor interaction," "cytokine-cytokine receptor interaction," "chemokine," and "IL-17" signaling pathways (**Figure 3A** and **Supplementary Figures 6, 7**), reflecting ongoing inflammatory immune responses in both IPF and SSc-PF, even at such a late stage of pulmonary fibrosis.

Hub proteins identified in the functional protein association network generated using STRING (**Figure 3B**) included interleukin 6 (IL6), several CXC chemokine family members (CXCL8, CXCL10, CXCL12), two CC motif chemokine ligands (CCL2, CCL19), APLNR, SERPIND1, VCAM1, several coagulation factor fibrinogens (FGA, FGB, FGG), CDH2, SPP1 and several collagens proteins (COL1A1, COL1A2, COL3A1, COL5A2, COL7A1, COL9A2, COL10A1, COL15A1, COL17A1). Note that CXCL8, APLNR, FGA, and FGB were not DE genes but were hub proteins in the network as 2nd shell interactors. All identified hub proteins in this network were upregulated genes, except *FGG* which was downregulated (**Supplementary Table 3**) in both DE analyses, showing that these genes are similarly regulated in both diseases.

The fibrinogens and VCAM1 are involved in all 3 major biological processes "extracellular structure organization,"

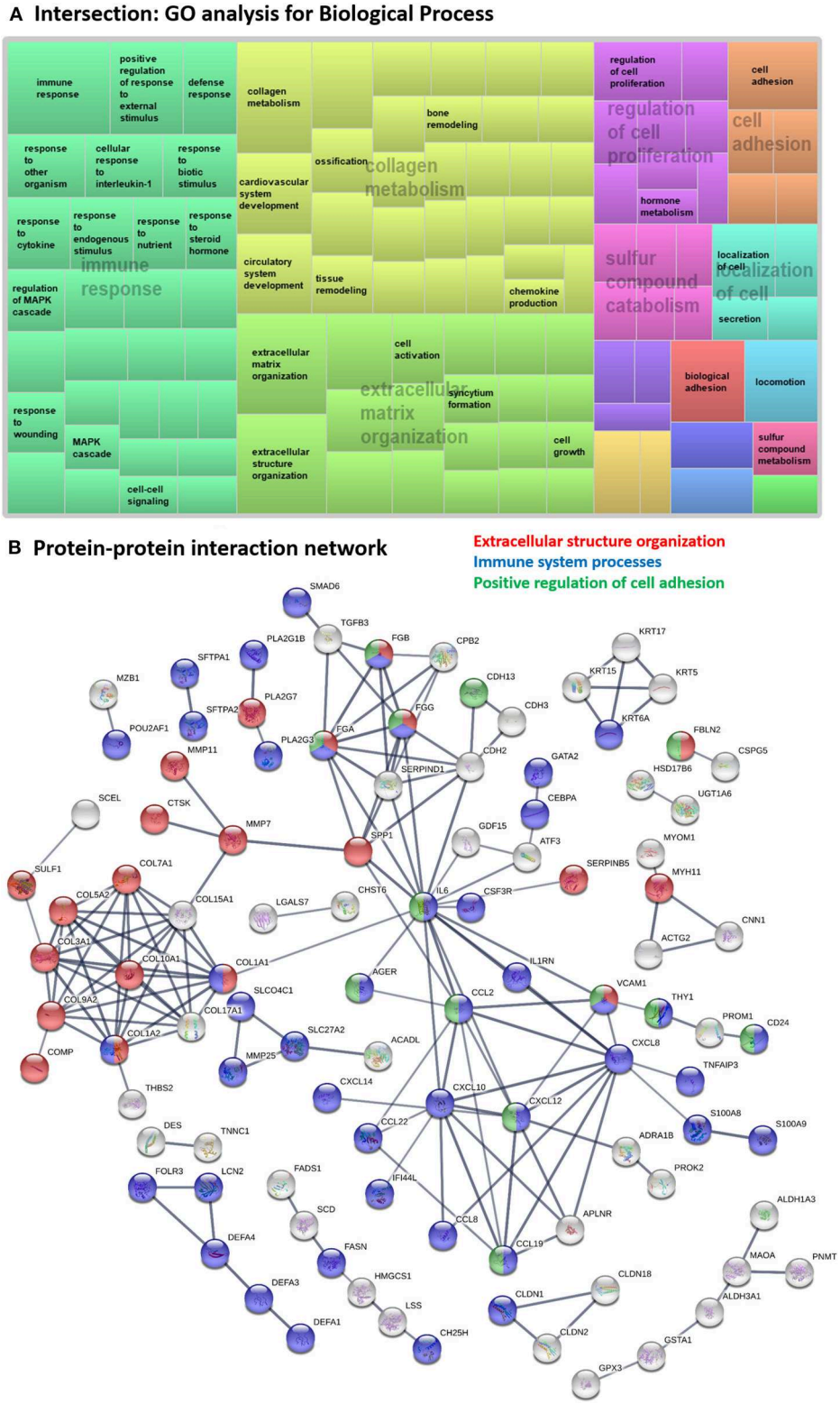

FIGURE 3 | Systems level analysis—intersection. **(A)** Gene ontology analysis for biological process. Data obtained from ToppFun and visualized with REViGO treemaps (abs_log10_pvalue). **(B)** Protein-protein interaction network generated by STRING.

"immune system processes," and "positive regulation of cell adhesion," while IL6, CCL2, CCL19, and CXCL12 are involved in both "immune system processes" and "positive regulation of cell adhesion" terms. COL1A1 and COL1A2 are hit genes in "extracellular structure organization" and "immune system processes" GO terms.

Unique to SSc-PF

The 73 DE genes exclusive to SSc-PF mainly pertained to "regulation of vasculature development" and "response to endogenous stimulus" biological processes as these terms were super clusters in the GO analysis (**Figure 4A** and **Supplementary Figure 7**). Pathways related to immunity and inflammation were also enriched, including "C-type lectin receptor," "TNF," and "PI3K-Akt" signaling pathways, suggesting that both innate and adaptive immune responses are still active in SSc-PF even in late stage disease (**Supplementary Figure 6**). Additionally, pathways related to metabolism and bioenergetics were also perturbed in SSc-PF, including "fatty acid (FA) degradation," "biosynthesis of unsaturated FA," and "glycolysis/gluconeogenesis" (**Table 3**). **Figure 5** is a heatmap showing the DE genes associated with these pathways and how they cluster. For column clustering, all NL and all SSc-PF samples clustered together except for NL31 that clustered with SSc-PF samples. For row clustering, several of the DE genes involved were downregulated in SSc-PF as compared to NL (*ACSS2, PCK2, PTPLA, DCI, SCD, FASN, FADS1, ADH1A, ADH1B,* and *ACADL*). On the other end, *ALDH1A3, ALDH3A1, ALDH3B2, CPT1C, PFKP, BAAT,* and *ADH7* were upregulated in SSc-PF. These findings reflect an overall deregulation of FA metabolism and glycolysis in SSc-PF patients.

Several hub proteins were evident in the STRING network generated (**Figure 4B**), including toll-like receptor 8 (TLR8), myeloperoxidase (MPO), prostaglandin-endoperoxide synthase 2 (PTGS2 aka COX2), arginase 1 (ARG1), and endothelin 1 (EDN1) genes. PTGS2, ARG1, and EDN1 are associated with several enriched GO terms: "regulation of localization," "tube development," "regulation of response to external stimulus," and "system development." PTGS2 and EDN1 are also present in "blood circulation" process. All identified hub proteins in this network were downregulated genes, except *PTGS2* which was upregulated (**Supplementary Table 4**). Note that EDN1 was not a DE gene but was a hub gene in the network as a 2nd shell interactor.

Unique to IPF

One hundred and thirteen DE genes were unique to IPF and these generated the super-cluster "lymphocyte chemotaxis" in the GO analysis (**Figure 6A** and **Supplementary Figure 7**), emphasizing the importance of the immune response to external stimuli in IPF. The immune signature was also present in the unique pathways to SSc-PF, such as "intestinal immune network for IgA production," "toll-like receptor signaling pathway," emphasizing on-going innate immune response (**Supplementary Figure 6**).

Several hub proteins are associated with multiple enriched GO terms, including "response to oxygen-containing compound," "microtubule-based movement," "inflammatory response," "lymphocyte migration," and "response to lipopolysaccharide": CSF2, CCR7, CCL3, CCL4L1, CCL13, CXCL13, CCL5, and NLRP3 (**Figure 6B**). APOE and CCDC114 were hub proteins only associated with "response to oxygen-containing compound" and "microtubule-based movement," respectively. All identified hub proteins in this network were upregulated DE genes, except *CSF2* which was downregulated (**Supplementary Table 5**). Note that CCDC114 was not a DE gene but was a hub gene in the network as a 2nd shell interactor.

Validation of IGFBP2, IGFL2, IL6, and TLR8 by qRT-PCR

The DE and systems level analyses emphasized the deregulation and importance of *IGFBP2*, *IGFL2,* and *IL6* in both diseases, as well as *TLR8* in SSc-PF. Using qRT-PCR, these genes of interest were validated (**Figure 7**). In both SSc-PF and IPF lung samples, the expression levels of *IGFBP2*, *IGFL2,* and *IL6* were significantly increased compared to NL (**Figures 7A–C**), and *TLR8* was noticeably decreased in SSc-PF lungs, albeit not significantly (**Figure 7D**). These results are consistent with and validate the microarray data.

Comparing Inflammatory Responses in IPF and SSc-PF

Next, we aimed to tease out similarities and differences in the inflammatory response signature of both diseases by specifically looking at two biological pathways present in the intersect: "Cytokine-cytokine receptor interaction" and "IL-17 signaling pathway" (**Figure 8** and **Supplementary Figures 8–11**). At first glance, the inflammatory response in both diseases looked very similar and nearly all of the hit genes in these pathways were differentially expressed in both diseases with the same direction of regulation. However, subtle differences were captured, especially in the pathway impact analysis that revealed perturbations and coherent cascades. Specifically, in the SSc-PF "cytokine-cytokine receptor interaction" pathway under TNF Family (**Supplementary Figure 8**), *TNFSF14*-associated perturbation (labeled LIGHT) that leads to upregulation of *LTBR, HVEM,* and *DCR3* was not observed in IPF (**Supplementary Figure 10**). Additionally, upregulation of LIF that cascades to upregulation of *LIFR* and *IL6ST* was exclusive to SSc-PF. In the "IL-17" signaling pathway, all DE chemokines, cytokines and anti-microbial genes were the same in both diseases (**Supplementary Figures 9, 11**), but upstream of this cascade *IL-17RA* and *FOSB* (labeled *API*) were only differentially expressed in IPF (**Supplementary Figure 11**). Together these findings revealed overall similar inflammatory responses in IPF and SSc-PF with subtle differences in TNF and IL6/IL12/IL17 signaling pathways.

DISCUSSION

SSc-PF and IPF are distinct diseases but they do share several pathobiologic characteristics (5). The goal of this study was to (1) characterize the similarities existing in the development of pulmonary fibrosis in scleroderma and IPF to find potential

A Unique to SSc-PF: GO analysis for Biological Process

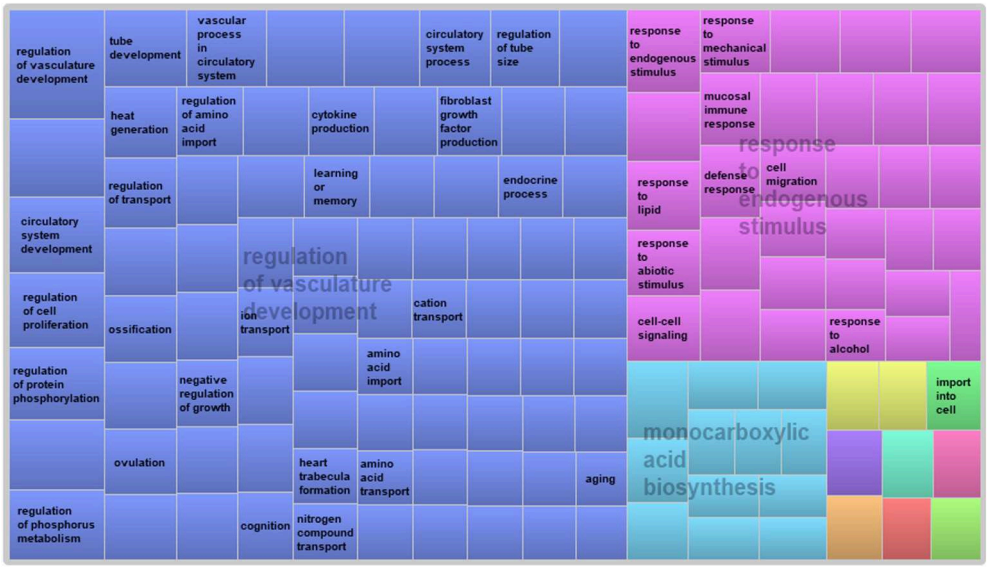

B Protein-protein interaction network

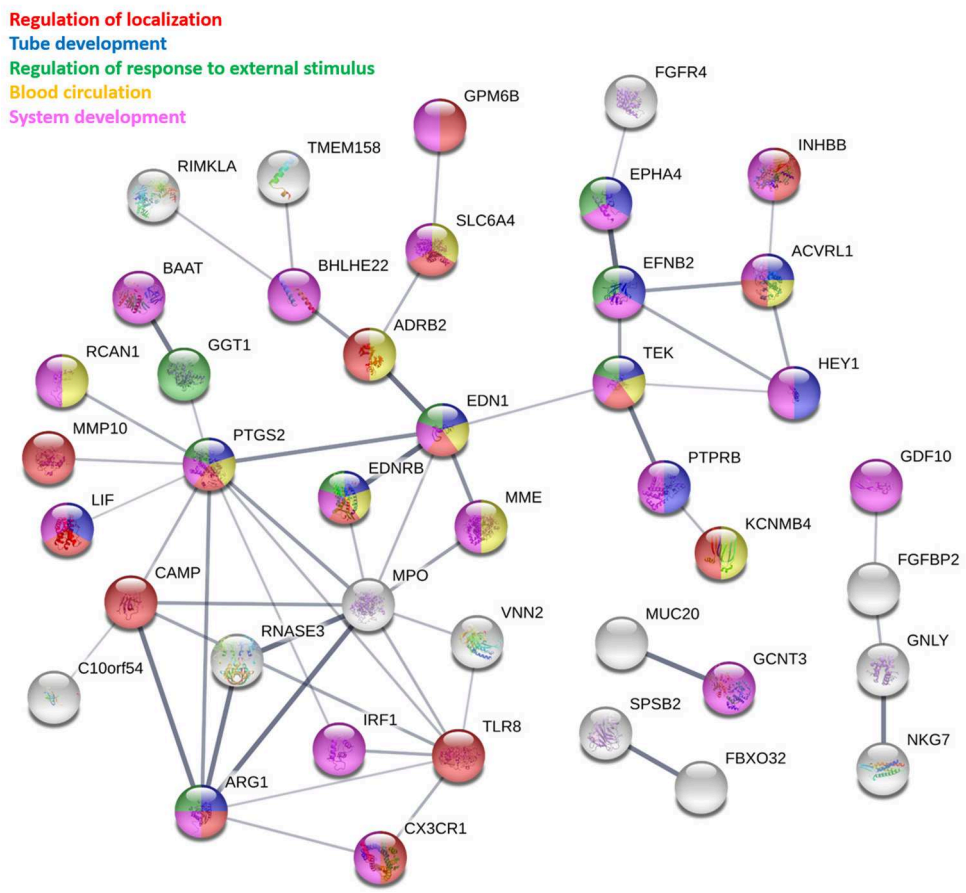

FIGURE 4 | Systems level analysis—unique to SSc-PF. **(A)** Gene ontology analysis for biological process. Data obtained from ToppFun and visualized with REViGO treemaps (abs_log10_pvalue). **(B)** Protein-protein interaction network generated by STRING.

therapeutic targets that could be beneficial in both diseases, and (2) to tease out the exclusive signature that each disease has, using a systems level and protein-protein interaction network approach. In both diseases, inflammation and immune responses were highly enriched, revealing that even at an advanced stage of pulmonary fibrosis, these "first-response" feedback mechanisms are still active and on-going.

The Intersection Signature Highlights Potential Therapeutic Targets Beneficial for Both SSc-PF and IPF

The systems level analysis we performed on the DE genes in the intersection between IPF and SSc-PF was dominated by "immune response," "collagen metabolism," and "ECM organization" super clusters (**Figure 3**) and most of the query genes entered in the network were hit genes in "immune system processes" term, including hub proteins IL6, COL1A1, COL1A2, VCAM1, CXCL10, CXCL12, CCL2, CCL19, and FGG. Our data also showed that the IGF family members *IGFBP2* and *IGFL2* are significantly upregulated in both SSc-PF and IPF lung tissues, and that the coagulation cascade was a prominent protein-protein interaction sub-network in the intersection signature.

TABLE 3 | Enriched pathways in SSc-PF pertaining to FA metabolism and glycolysis.

Pathway	SSc-PF vs. NL (*p*-value)
Fatty acid degradation	0.044
Biosynthesis of unsaturated fatty acids	0.022
Glycolysis/gluconeogenesis	0.006

p < 0.05.

Interleukin 6 (IL6) and Its Role in Autoimmunity, Inflammation, and Fibrogenesis

The IL17 signaling pathway is critical for the activation of inflammatory genes and production of chemokines and cytokines such as IL6 (**Supplementary Figures 9, 11**) (34). IL6 is a multi-faceted pro-inflammatory cytokine synthesized by fibroblasts, peripheral blood mononuclear cells (PBMCs), B cells, macrophages, dendritic cells, monocytes and mast cells, that plays a role in chronic inflammation, autoimmunity, endothelial cell dysfunction, vascularization/angiogenesis and fibrogenesis (35–41). We characterized *IL6* as a hub protein upregulated in both IPF and SSc-PF tissues (**Supplementary Table 3**) that has a strong influence on the immune response. *IL6* is overexpressed in dermal fibroblasts, PBMCs, mononuclear and endothelial cells of SSc patients (37, 38, 42). Interestingly, few effector cells express the functional membrane IL6 receptor (IL6R); lymphocytes, hepatocytes, monocytes, B cells, neutrophils and a subset of

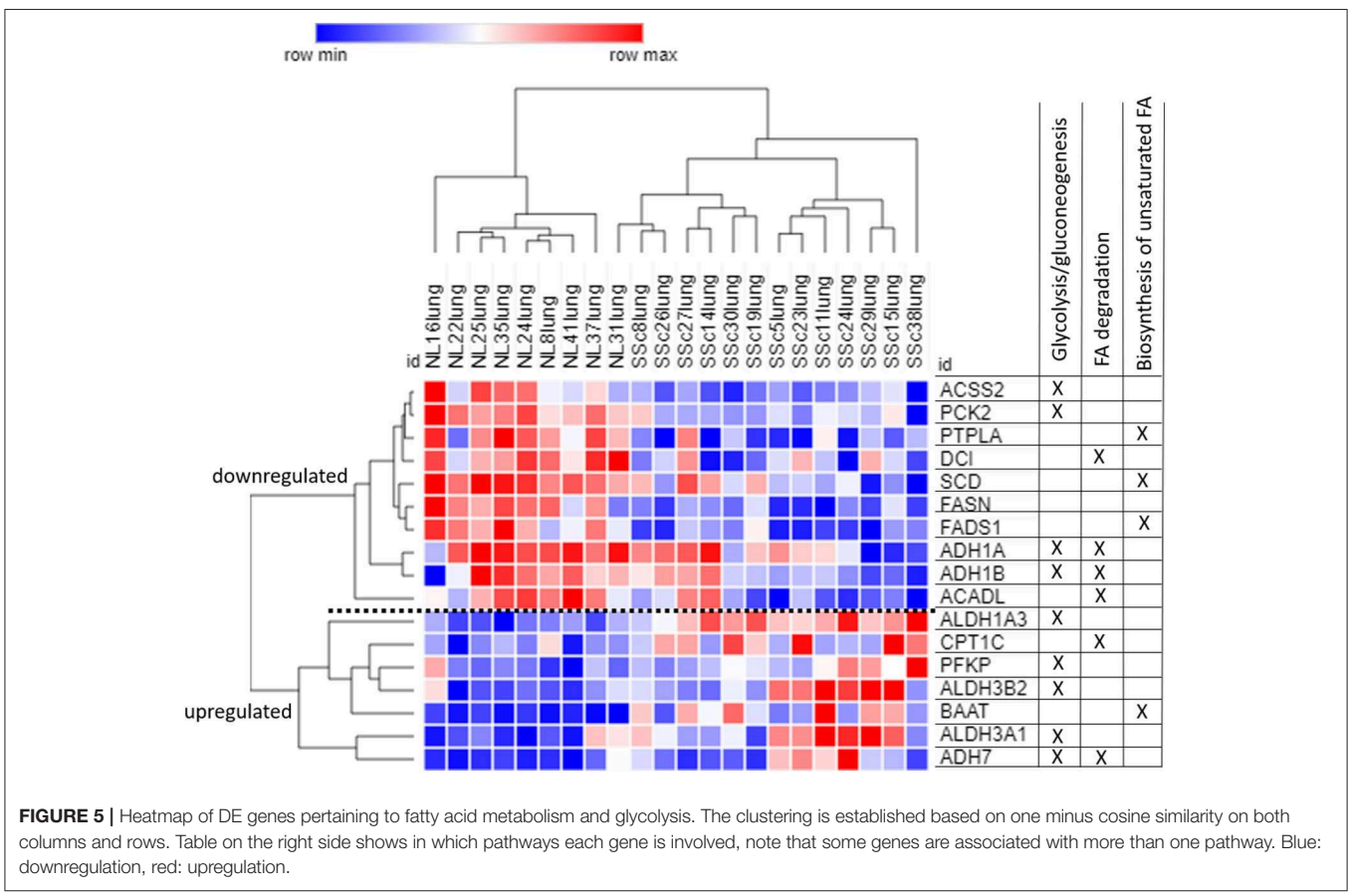

FIGURE 5 | Heatmap of DE genes pertaining to fatty acid metabolism and glycolysis. The clustering is established based on one minus cosine similarity on both columns and rows. Table on the right side shows in which pathways each gene is involved, note that some genes are associated with more than one pathway. Blue: downregulation, red: upregulation.

A Unique to IPF: GO analysis for Biological Process

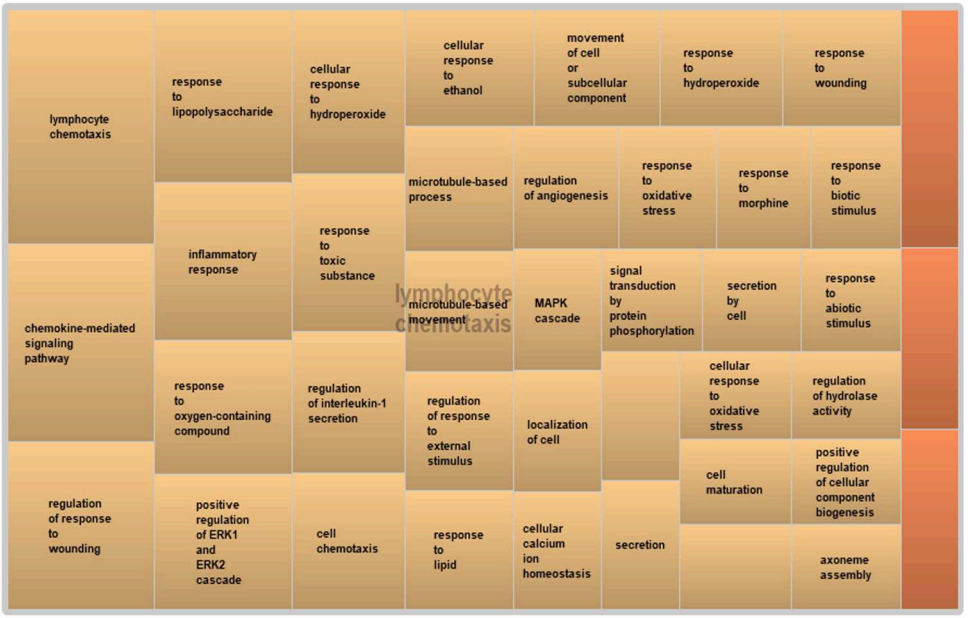

B Protein-protein interaction network

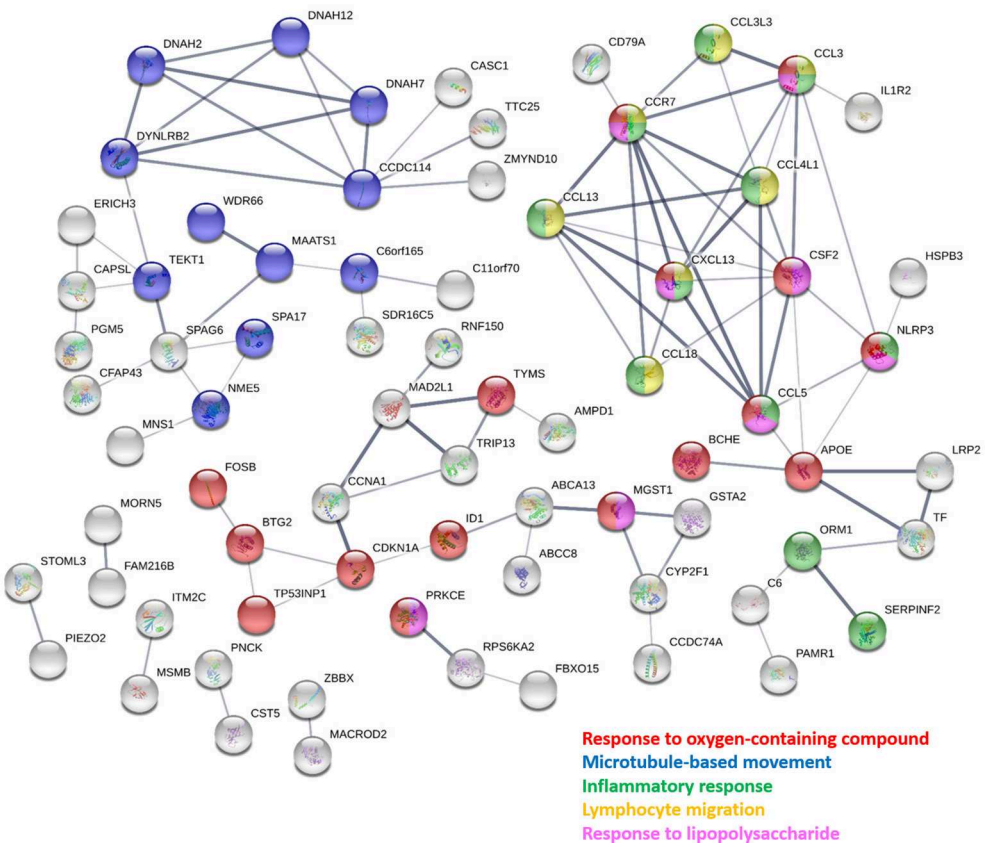

FIGURE 6 | Systems level analysis—unique to IPF. **(A)** Gene ontology analysis for biological process. Data obtained from ToppFun and visualized with REViGO treemaps (abs_log10_pvalue). **(B)** Protein-protein interaction network generated by STRING.

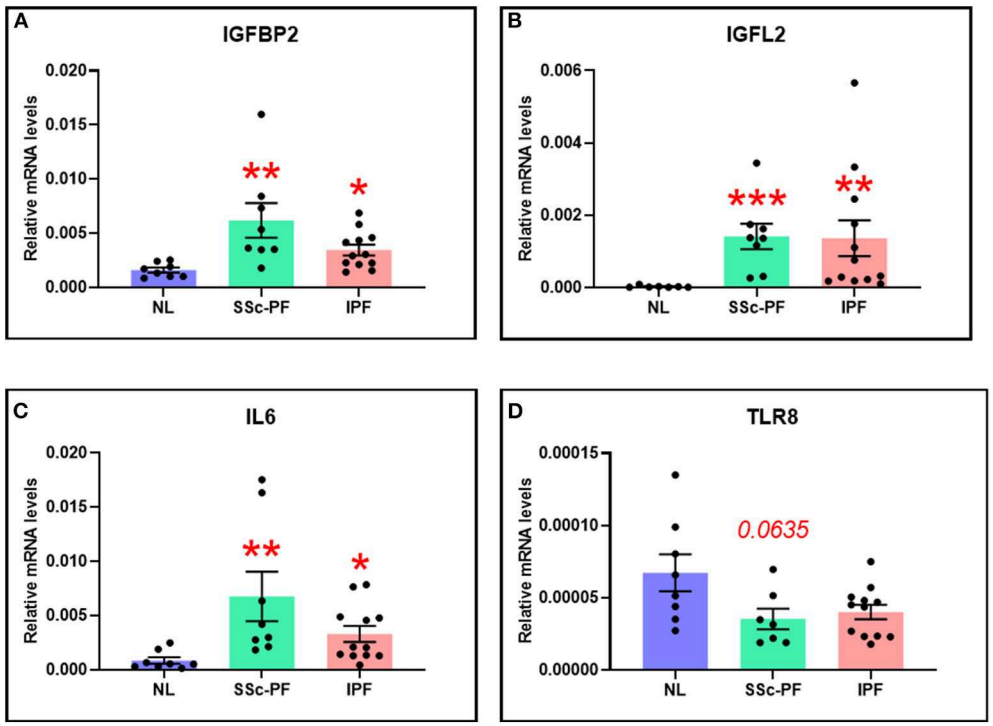

FIGURE 7 | The expression levels of **(A)** IGFBP2, **(B)** IGFL2, **(C)** IL6, and **(D)** TLR8 were quantified in tissue lysates from SSc-PF ($n = 8$) and IPF ($n = 12$) patients and healthy individuals (NL, $n = 8$). $^{*}p < 0.05$, $^{**}p < 0.01$, $^{***}p < 0.001$ vs. NL. Error bars = SEM.

T-cells (35). Other cell types that do not express IL6R (i.e., fibroblasts and endothelial cells) can still respond to IL6 due to trans-signaling of soluble IL6R (sIL6R) and gp130 receptor (39).

In both SSc-PF and IPF, the IL17 signaling pathway is enriched (**Supplementary Figures 9, 11**) and the expression of the ubiquitin-editing enzyme A20 (TNFAIP3), a major regulator of NFκB activation, is upregulated (43, 44). A20 reduces NFκB activation by inhibiting TNF receptor signaling and removing K63-linked ubiquitin chains conjugated to TRAF6 (45, 46). The observed upregulation of A20 suggests downregulation of the IL17 signaling pathway (47). However, several chemokines and cytokines downstream of IL17 signaling were upregulated (IL6, CXCL8, CXCL10, CCL2, and COX2), indicating that other regulatory mechanisms are likely at play that affect the expression of downstream genes in this pathway. Inhibition of TNFα signaling has shown promising results in many patients with inflammatory disorders (48), but has also generated adverse side effects (49), highlighting that TNFα signaling is a double-edged sword that can be both pro- and anti-inflammatory.

Serum IL6 is a predictive marker of early functional decline and mortality in SSc-PF (50). Here we found that *IL6* levels are still significantly increased in advanced SSc-PF and IPF, suggesting that IL6 lingers to stimulate more collagen synthesis and chronic inflammation, consistent with Koch et al. (51). Activated lung macrophages have also been shown to enhance IL6 trans-signaling via ADAM-17 leading to fibroblast proliferation and ECM deposition, and inhibition of sIL6Rα can attenuate pulmonary inflammation and fibrosis (52). In recent clinical trials, blocking IL6 trans-signaling using the monoclonal antibody tocilizumab showed promising trends in patients with SSc (53), suggesting that IL6 might be a viable therapeutic target in SSc. Our current findings also suggest that targeting IL6 trans-signaling may be a suitable therapeutic approach for the treatment of IPF.

Targeting IGFBP2 and IGFL2

We show here that the IGF family members *IGFBP2* and *IGFL2* are significantly upregulated in both SSc-PF and IPF lungs tissues. IGFBP2 is secreted into the bloodstream where it binds IGF1 and IGF2 with high affinity, can interact with several different ligands, and can be localized intracellularly (54). Guiot et al. showed that IGFBP2 levels are increased in serum and sputum samples of IPF patients, and characterized IGFBP2 as a biomarker of IPF severity (55, 56). In patients with diffuse cutaneous SSc (dcSSc), IGFBP2 levels are also increased in both serum and skin biopsies (57). Additionally, IGFBP2 is abundant in collagen1-stimulated peripheral blood mononuclear cells (PBMCs) from juvenile and adult dcSSc patients (58).

Findings with IGFBP2 are consistent with our previous studies showing increased expression of *IGFBP3* and *IGFBP5* in IPF and SSc-PF (25, 26) and reinforced the crucial role that IGFBPs and the IGF pathway play in the development and perpetuation of pulmonary fibrosis (22–24). Note however that IGFBPs can also signal via membrane bound proteins such as integrins in a IGF-independent pathway (59). We previously showed that IGFBP5 induces fibrosis by promoting

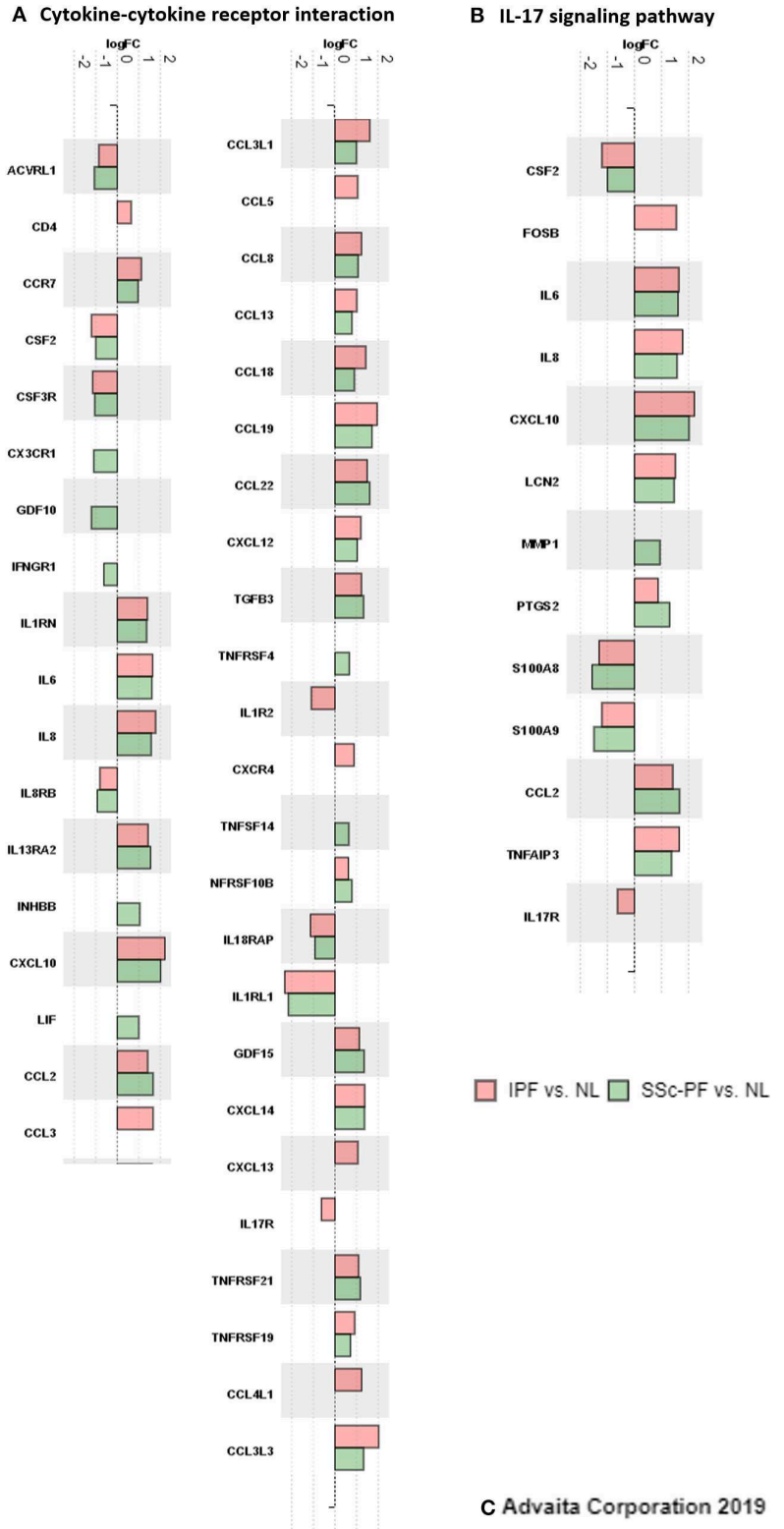

FIGURE 8 | Inflammatory response signatures in IPF and SSc-PF. DE genes ($q < 0.1$, log2FC > |0.6|, linear FC of 1.5) that are hit genes in the "cytokine-cytokine receptor interaction" and "IL-17 signaling" pathways are shown here, color-coded by DE analysis. Peach: IPF vs. NL, and green: SSc-PF vs. NL.

fibroblast activation into myofibroblasts and recruitment of pro-inflammatory cells (60, 61) via p44/p42 mitogen-activated protein kinase (MAPK) pathway and induction of EGR1 and DOK5 (62, 63). Additionally, IGFBP5 induces the expression of collagen 1, fibronectin, CTGF and lysyl oxidase, as well as its own expression by positive feedback mechanism (26).

IGFBP3 induces tenascin C (TNC), a biomarker of SSc-PF (3). Importantly, both IGFBP3 and IGFBP5 contribute to extracellular (ECM) deposition in IPF (25) and promote fibrosis in human skin maintained in organ culture (64), demonstrating direct relevance to the human disease. Targeting IGFBPs that are elevated in SSc-PF and IPF is an appealing therapeutic strategy yet no clinical trials employing this approach have been reported.

IGFL2 expression is also increased in SSc-PF and IPF, however its biological function is not well-characterized. IGFL2 does not have a transmembrane domain, it is found in secreted form in the ECM, and it may play a critical role in cellular energy metabolism as well as in growth and development (65). In human skin fibroblasts undergoing mitochondrial depletion, *IGFL2* levels are substantially decreased (dataMED, ID: E-GEOD-24945), suggesting a connection between mitochondrial physiology and IGFL2 secretion. Its specific role in SSc-PF and IPF remains to be elucidated.

Collagen-Derived Matrikines

Collagen-derived matrikines are peptides generated by partial proteolysis of certain collagens that can regulate cell activity (30). Out of the 9 DE collagen genes identified in the intersection of SSc-PF and IPF, 4 have been identified as sources of matrikines: *COL1A1, COL1A2, COL15A1,* and *COL17A1* (30, 66, 67).

Two matrikines are derived from COL1A1: DGGRYY peptide that can inhibit human neutrophil activation by collagen (68), and COL1 matricryptin p1158/1159 that has recently shown promising results in generating new ECM and stimulating angiogenesis post myocardial infarction (69).

The tripeptide GHK is produced from cleavage of COL1A2 and forms the complex GHK-Cu due to its high affinity to copper ions (30). This complex regulates a plethora of biological processes relevant for ECM remodeling: (1) chemoattraction of repair cells, (2) anti-inflammation, (3) synthesis of collagen, elastin, MMPs, anti-proteases, VEGF, FGF2, NGF, and EPO, (4) stimulation of angiogenesis, and (5) proliferation of fibroblasts and keratinocytes (70). Recently, the GHK-Cu complex was shown to inhibit bleomycin-induced PF in mice by suppressing TGFβ1/Smad-mediated epithelial to mesenchymal transition (71).

Restin is a COL15-derived matrikine that can inhibit endothelial cell proliferation and has anti-angiogenic properties similar to endostatin, with the latter being a cleavage product of COL18 (72, 73).

COL17A1 sheds a soluble triple-helical ectodomain (aka BP180) under the regulation of ADAM9 and ADAM10 (67, 74). Less is known about the function of BP180. BP180 acts as a core anchor protein due to its multiple binding sites (i.e., extracellular domains of integrin α6, cytoplasmic domains of integrin β4, laminin-5 and plectin) connecting intra- and extra-cellular hemidesmosomal proteins and playing a role in the development of bullous pemphigoid (75). Cleavage of BP180 enhances neutrophil chemotaxis and initiates the release of inflammatory factors (75, 76).

Fibrinogen Hub Proteins

Fibrinogen proteins FGA, FGB, and FGG are essential for a variety of processes, including blood clot formation, wound healing, inflammation and blood vessel growth (77). When fibrinogen is cleaved by thrombin into insoluble fibrin polymer, the formation of a fibrin clot occurs, a process that is essential for hemostasis and wound healing. As part of the fibrinolytic system, fibrin binds and cleaves plasminogen into plasmin, leading to fibrin digestion and removal of fibrin clots.

In this study, we found that FGG was a hub protein in the protein-protein network interacting with IL6, FGA, FGB, CDH2, CPB2, SPP1, TGFβ3, and SERPIND1 that was significantly downregulated in both IPF and SSc-PF lung tissues (**Figure 3**), in agreement with recent work by Vukmirovic et al. (78). During PF, impaired coagulation cascade plays a role in orchestrating inflammatory and tissue repair responses as well as fibrogenesis via activation of proteinase-activated receptors (79). Additionally, the fibrinolytic pathway has been shown to have anti-fibrotic actions in PF thanks to COX2 induction by plasminogen leading to prostaglandin E2 synthesis and repression of collagen expression (80).

TLR8: Autoimmunity, Fibrosis, and Angiogenesis

Because the respiratory airways are constantly exposed to environmental pathogens and other elements, TLRs play a crucial role in innate immunity to endogenous and exogenous ligands (81). TLR2 and TLR4 have been shown to trigger immune and fibrotic responses in PF (82). TLR4 activation induces the release of profibrotic and proangiogenic chemokines from anti-fibroblast antibodies stimulated fibroblasts (83). Furthermore, activation of TLR4 signaling in skin and lung fibroblasts increased TGFβ1 sensitivity and ECM production, both processes contributing to persistent fibrogenesis in SSc (84).

In this study, we determined that TLR8 was a hub protein in the SSc-PF network (**Figure 4**) that was downregulated at the transcript level in both SSc-PF and IPF, albeit not significantly. Another study examining TLR expression levels in bronchoalveolar lavage fluid of patients with IPF and fibrotic interstitial pneumonias associated with collagen tissue disorders reported no significant difference in TLR8 levels in these 2 patient cohorts as compared to a control group (85). The role of TLR8 during the development of SSc-PF remains elusive, but TLR8 activation has been shown to promote inflammatory responses and fibrogenesis in skin fibrosis and lung injury (86, 87). Together this suggests that TLR8 expression may be upregulated in early and intermediate stages of PF when inflammation is more prominent, and its activation contributes to enhanced inflammation and fibrogenesis, whereas TLR8 expression returns to low levels in late stages of PF, when inflammation is less evident. In the skin of SSc patients, the infiltration and

activation of plasmacytoid dendritic cells (pDCs) via PI3Kδ pathway leads to aberrant expression of TLR8 (otherwise not expressed in pDCs) that induces CXCL4, IFN-α, IL6, and TNF secretion contributing to skin fibrosis and autoimmunity (87). Inhibitors of PI3Kδ have been approved for treatment of cancer, inflammatory and autoimmune diseases (88), and our data provide rationale to further explore the targeting of the PI3Kδ-TLR8 axis in SSc-PF and IPF, via repurposing drugs used for cancer treatment.

TLR8 is a gene hit in the "Regulation of localization" biological process and has protein-protein interaction with other hub proteins including PTGS2, MPO, and ARG1 (**Figure 4**). In SSc-PF lungs, *TLR8, MPO* and *ARG1* are downregulated while *PTGS2* is upregulated (**Supplementary Table 4**). Expression profiling for these 4 hub proteins may indeed capture advanced stages of fibrosis in SSc-PF lungs, emphasizing that the damage caused by inflammation and fibrosis is so far advanced that lung transplantation is necessary and justified.

The Unique Transcriptomic Signature in SSc-PF Relates to Vasculature Development and Perturbation of Bioenergetics

Even though SSc-PF and IPF have common characteristics, SSc-PF has a unique transcriptomic signature and features (5). Here we found that "regulation of vasculature development" was a Biological Process super cluster in the GO analysis of DE genes unique to SSc-PF, and PTGS2, ARG1 and EDN1 were related hub proteins under the subcategories "tube development" and "blood circulation." This is consistent with vascular complications and angiogenesis impairment being trademarks in SSc patients (89), and with structural disintegration of vasculature and loss of endothelial cell numbers observed in late stage of SSc-PF (2).

ARG1

ARG1 is a key enzyme in the urea cycle that converts L-arginine to L-ornithine, which is further metabolized into proline and polyamines, drivers of collagen synthesis (90). ARG1 is also a marker of activated macrophages (M2), producers of angiogenic factors (91, 92). Macrophages have been shown to regulate the rate of conversion to proline and IL4Rα-induced stimulation of macrophages increases ARG1, proline output and fibrosis sequentially (93). Targeting ARG1 metabolism is an emerging therapeutic strategy in the treatment of inflammation-induced suppression of T lymphocyte proliferation (immunosuppression) (94).

PTGS2 (Aka COX2)

Cyclooxygenase (COX) enzymes contribute to the release of lipid mediators in arachidonic acid metabolism, and PTGS2/COX2 plays a key role not only in prostaglandin signaling, but also in the fibrinolytic pathway and fibrogenesis, as well as in inflammatory cytokine-induced angiogenesis (80, 95). *PTGS2/COX2* was exclusively upregulated in SSc-PF lung tissues (**Supplementary Table 4**) and is a hub protein that interacts with TLR8, IRF1, ARG1, CAMP, LIF, MMP10, RCAN1, GGT1, EDN1, and MPO. Prostaglandin signaling has been shown to promote PF independently of TGFβ and loss of the prostaglandin F receptor reduced fibrosis in the bleomycin-induced PF model without affecting alveolar inflammation (96). Additionally, *PTGS2/COX2* selective inhibitors markedly reduced IL1β-induced angiogenesis *in vivo* (95). Together these data suggest that targeting *PTGS2/COX2* with a therapeutic drug could modulate both fibrosis and angiogenesis in SSc patients.

Overall Perturbation of FA Metabolism and Glycolysis in SSc-PF

Altered cellular bioenergetics as a driving force behind fibrogenesis is an emerging field (97–100). Here we found that FA metabolism (FA degradation and biosynthesis of unsaturated FA) and glycolysis pathways were significantly perturbed in SSc-PF lungs.

Metabolic reprogramming is a hallmark of cancer that is also observed during immune response and inflammation during which glycolysis becomes the alternative pathway to oxidative phosphorylation for ATP production (101, 102). Interestingly, inhibition of glycolysis has been shown to attenuate lung fibrosis (103), suggesting that metabolic reprogramming also plays a crucial role in the development of PF. Additionally, Selvarajah et al. (99) concluded that glycolysis (but not mitochondrial respiration) was necessary for TGFβ1-induced collagen deposition in primary human lung fibroblasts. This may also be true for other cell types that are present in whole lung tissue.

Fluctuation between glycolysis and fatty acid oxidation (FAO) has been shown to govern macrophages and dendritic cells as well as fibroblasts during inflammation and ECM remodeling, respectively (100, 102). In fact, the FA transporter CD36 has been identified as crucial mediator of COL1 internalization and degradation that can be targeted to reduce murine skin fibrosis (100). Our data show that biosynthesis of unsaturated FA and FA degradation, the steps that ultimately generate acetyl-CoA required for the citric acid cycle to produce energy within mitochondria, are significantly deregulated in SSc-PF. Interestingly, this signature has also been uncovered in renal epithelial cells from patients with kidney fibrosis (104). Additionally, in TGFβ1-induced fibrotic models, suppression of FAO and enhancement of glycolysis are observed (99, 104), highlighting that a shift in bioenergetics, similar to the Warburg effect characteristic of cancer cells, is ongoing during fibrogenesis.

In all, metabolic reprogramming appears to hijack energy production of several cell types that are the drivers of inflammation, fibrogenesis and ECM remodeling, disturbing the homeostatic balance between glycolysis and FAO, ultimately shifting the cellular fuel source and activating pathological processes. Once key players regulating this reprogramming are identified, the development of anti-fibrotic therapies targeting metabolic molecules will be possible. Such potential therapeutic

targets have already been identified and tested in experimental PF models (100, 103).

CONCLUSION

By conducting differential expression analyses on lung tissues from IPF and SSc-PF, we were able to compare the gene signature of these two pulmonary fibrotic diseases that share many pathobiologic features and identify shared features as well as exclusive characteristics for each disease. Our data suggest that therapeutic strategies targeting IL6 trans-signaling, *IGFBP2*, *IGFL2,* and the coagulation cascade may be efficacious in both SSc-PF and IPF. In SSc-PF, additional potential targets include mediators of fatty acid metabolism and glycolysis as well as *TLR8*.

DATA AVAILABILITY STATEMENT

The datasets generated for this study can be found in the NCBI GEO GSE48149.

ETHICS STATEMENT

The studies involving human participants were reviewed and approved by the University of Pittsburgh Institutional Review Board. The patients/participants provided their written informed consent to participate in this study.

AUTHOR CONTRIBUTIONS

Study design and manuscript editing: LR and CF-B. Differential expression analysis (microarray)—gene level analysis: WS, LR, and GH. Systems level analysis and protein-protein interaction network: LR. Validation qRT-PCR: NT. Writing of the manuscript and generation of figures with statistics and heatmaps: LR, NT, and CF-B. Reviewing the draft and comments: WS, NT, and GH.

FUNDING

This project was supported by NIH grants K24 AR060297 R01 HL121262 (CF-B) and T32 AR050958 (LR), as well as the SmartState® and Kitty Trask Holt Endowment (CF-B). GH acknowledges support from NIH/NIDA U01-DA045300.

ACKNOWLEDGMENTS

We would like to thank Ms. Deborah Hollingshead at the University of Pittsburgh Genomics Research Core for performing the microarray analysis.

SUPPLEMENTARY MATERIAL

The Supplementary Material for this article can be found online at: https://www.frontiersin.org/articles/10.3389/fimmu.2020.00383/full#supplementary-material

REFERENCES

1. Steen VD, Medsger TA. Changes in causes of death in systemic sclerosis, 1972–2002. *Ann Rheum Dis.* (2007) 66:940–4. doi: 10.1136/ard.2006.066068
2. Beon M, Harley R, Wessels A, Silver R, Ludwicka-Bradley A. Myofibroblast induction and microvascular alteration in scleroderma lung fibrosis. *Clin Exp Rheumatol.* (2004) 22:733–42.
3. Brissett M, Veraldi KL, Pilewski JM, Medsger TA Jr, Feghali-Bostwick CA. Localized expression of tenascin in systemic sclerosis–associated pulmonary fibrosis and its regulation by insulin-like growth factor binding protein 3. *Arthritis Rheum.* (2012) 64:272–80. doi: 10.1002/art.30647
4. Wynn T. Cellular and molecular mechanisms of fibrosis. *J Pathol.* (2008) 214:199–210. doi: 10.1002/path.2277
5. Herzog EL, Mathur A, Tager AM, Feghali-Bostwick C, Schneider F, Varga J. Review: interstitial lung disease associated with systemic sclerosis and idiopathic pulmonary fibrosis: how similar and distinct? *Arthritis Rheum.* (2014) 66:1967–78. doi: 10.1002/art.38702
6. Kondoh Y, Taniguchi H, Yokoi T, Nishiyama O, Ohishi T, Kato T, et al. Cyclophosphamide and low-dose prednisolone in idiopathic pulmonary fibrosis and fibrosing nonspecific interstitial pneumonia. *Eur Respir J.* (2005) 25:528–33. doi: 10.1183/09031936.05.00071004
7. Tzouvelekis A, Bouros E, Ekonomou A, Ntolios P, Zacharis G, Kolios G, et al. Effect and safety of mycophenolate mofetil in idiopathic pulmonary fibrosis. A retrospective study. *Eur Respir Soc.* (2011) 38:178. doi: 10.1164/ajrccm-conference.2011.183.1_MeetingAbstracts.A1537
8. King TE Jr, Bradford WZ, Castro-Bernardini S, Fagan EA, Glaspole I, Glassberg MK, et al. A phase 3 trial of pirfenidone in patients with idiopathic pulmonary fibrosis. *N Engl J Med.* (2014) 370:2083–92. doi: 10.1056/NEJMoa1402582
9. Richeldi L, Du Bois RM, Raghu G, Azuma A, Brown KK, Costabel U, et al. Efficacy and safety of nintedanib in idiopathic pulmonary fibrosis. *N Engl J Med.* (2014) 370:2071–82. doi: 10.1056/NEJMoa1402584
10. Huang J, Maier C, Zhang Y, Soare A, Dees C, Beyer C, et al. Nintedanib inhibits macrophage activation and ameliorates vascular and fibrotic manifestations in the Fra2 mouse model of systemic sclerosis. *Ann Rheum Dis.* (2017) 76:1941–8. doi: 10.1136/annrheumdis-2016-210823
11. Distler O, Highland KB, Gahlemann M, Azuma A, Fischer A, Mayes MD, et al. Nintedanib for systemic sclerosis–associated interstitial lung disease. *N Engl J Med.* (2019). 380:2518–28. doi: 10.1056/NEJMoa1903076
12. Castelino FV, Seiders J, Bain G, Brooks SF, King CD, Swaney JS, et al. Amelioration of dermal fibrosis by genetic deletion or pharmacologic antagonism of lysophosphatidic acid receptor 1 in a mouse model of scleroderma. *Arthritis Rheum.* (2011) 63:1405–15. doi: 10.1002/art.30262
13. Palmer SM, Snyder L, Todd JL, Soule B, Christian R, Anstrom K, et al. Randomized, double-blind, placebo-controlled, phase 2 trial of BMS-986020, a lysophosphatidic acid receptor antagonist for the treatment of idiopathic pulmonary fibrosis. *Chest.* (2018) 154:1061–9. doi: 10.1016/j.chest.2018.08.1058
14. Fen F, Zhang J, Wang Z, Wu Q, Zhou X. Efficacy and safety of N-acetylcysteine therapy for idiopathic pulmonary fibrosis: an updated systematic review and meta-analysis. *Exp Ther Med.* (2019) 18:802–16. doi: 10.3892/etm.2019.7579
15. Rosato E, Rossi C, Molinaro I, Giovannetti A, Pisarri S, Salsano F. Long-term N-acetylcysteine therapy in systemic sclerosis interstitial lung disease: a retrospective study. *Int J Immunopathol Pharmacol.* (2011) 24:727–33. doi: 10.1177/039463201102400319
16. Kitano H. Systems biology: a brief overview. *Science.* (2002) 295:1662–4. doi: 10.1126/science.1069492

17. von Mering C, Jensen LJ, Snel B, Hooper SD, Krupp M, Foglierini M, et al. STRING: known and predicted protein–protein associations, integrated and transferred across organisms. *Nucleic Acids Res.* (2005) 33(Suppl. 1):D433–7. doi: 10.1093/nar/gki005
18. Masi AT, Rodnan G, Medsger T Jr, Altman R, D'Angelo W, Fries J. Subcommittee for scleroderma criteria of the american rheumatism association diagnostic and therapeutic criteria committee. preliminary criteria for the classification of systemic sclerosis (scleroderma). *Arthritis Rheum.* (1980) 23:581–90. doi: 10.1002/art.1780230510
19. Chen J, Bardes EE, Aronow BJ, Jegga AG. ToppGene Suite for gene list enrichment analysis and candidate gene prioritization. *Nucleic acids Res.* (2009) 37(Suppl. 2):W305–11. doi: 10.1093/nar/gkp427
20. Supek F, Bošnjak M, Škunca N, Šmuc T. REVIGO summarizes and visualizes long lists of gene ontology terms. *PloS ONE.* (2011) 6:e21800. doi: 10.1371/journal.pone.0021800
21. Draghici S, Khatri P, Tarca AL, Amin K, Done A, Voichita C, et al. A systems biology approach for pathway level analysis. *Genome Res.* (2007) 17:1537–45. doi: 10.1101/gr.6202607
22. Hamaguchi Y, Fujimoto M, Matsushita T, Hasegawa M, Takehara K, Sato S. Elevated serum insulin-like growth factor (IGF-1) and IGF binding protein-3 levels in patients with systemic sclerosis: possible role in development of fibrosis. *J Rheum.* (2008) 35:2363–71. doi: 10.3899/jrheum.080340
23. Hsu E, Feghali-Bostwick CA. Insulin-like growth factor-II is increased in systemic sclerosis-associated pulmonary fibrosis and contributes to the fibrotic process via Jun N-terminal kinase-and phosphatidylinositol-3 kinase-dependent pathways. *Am J Pathol.* (2008) 172:1580–90. doi: 10.2353/ajpath.2008.071021
24. Hsu E, Shi H, Jordan RM, Lyons-Weiler J, Pilewski JM, Feghali-Bostwick CA. Lung tissues in systemic sclerosis have gene expression patterns unique to pulmonary fibrosis and pulmonary hypertension. *Arthritis Rheum.* (2011) 63:783–94. doi: 10.1002/art.30159
25. Pilewski JM, Liu L, Henry AC, Knauer AV, Feghali-Bostwick CA. Insulin-like growth factor binding proteins 3 and 5 are overexpressed in idiopathic pulmonary fibrosis and contribute to extracellular matrix deposition. *Am J Pathol.* (2005) 166:399–407. doi: 10.1016/S0002-9440(10)62263-8
26. Nguyen X-X, Muhammad L, Nietert PJ, Feghali-Bostwick C. IGFBP-5 promotes fibrosis via increasing its own expression and that of other pro-fibrotic mediators. *Front Endocrinol.* (2018) 9:601. doi: 10.3389/fendo.2018.00601
27. Su Y, Nishimoto T, Hoffman S, Nguyen XX, Pilewski JM, Feghali-Bostwick C. Insulin-like growth factor binding protein-4 exerts antifibrotic activity by reducing levels of connective tissue growth factor and the C-X-C chemokine receptor 4. *FASEB BioAdv.* (2019) 1:167–79. doi: 10.1096/fba.2018-00015
28. Selman M, Pardo A, Barrera L, Estrada A, Watson SR, Wilson K, et al. Gene expression profiles distinguish idiopathic pulmonary fibrosis from hypersensitivity pneumonitis. *Am J Respir Crit Care Med.* (2006) 173:188–98. doi: 10.1164/rccm.200504-644OC
29. Zuo F, Kaminski N, Eugui E, Allard J, Yakhini Z, Ben-Dor A, et al. Gene expression analysis reveals matrilysin as a key regulator of pulmonary fibrosis in mice and humans. *Proc Natl Acad Sci USA.* (2002) 99:6292–7. doi: 10.1073/pnas.092134099
30. Maquart F-X, Pasco S, Ramont L, Hornebeck W, Monboisse J-C. An introduction to matrikines: extracellular matrix-derived peptides which regulate cell activity: implication in tumor invasion. *Crit Rev Oncol Hemat.* (2004) 49:199–202. doi: 10.1016/j.critrevonc.2003.06.007
31. Ricard-Blum S, Salza R. Matricryptins and matrikines: biologically active fragments of the extracellular matrix. *Exp Dermatol.* (2014) 23:457–63. doi: 10.1111/exd.12435
32. Koschützki D, Schreiber F. Centrality analysis methods for biological networks and their application to gene regulatory networks. *Gene Regul Syst Biol.* (2008) 2:S702. doi: 10.4137/GRSB.S702
33. Jeong H, Mason SP, Barabási AL, Oltvai ZN. Lethality and centrality in protein networks. *Nature.* (2001) 411:41–2. doi: 10.1038/35075138
34. Hwang S-Y, Kim J-Y, Kim K-W, Park M-K, Moon Y, Kim W-U, et al. IL-17 induces production of IL-6 and IL-8 in rheumatoid arthritis synovial fibroblasts via NF-κB-and PI3-kinase/Akt-dependent pathways. *Arthritis Res Ther.* (2004) 6:R120–8. doi: 10.1186/ar1038
35. Barnes TC, Anderson ME, Moots RJ. The many faces of interleukin-6: the role of IL-6 in inflammation, vasculopathy, and fibrosis in systemic sclerosis. *Int J Rheumatol.* (2011) 2011:721608. doi: 10.1155/2011/721608
36. Lukacs NW, Hogaboam C, Chensue SW, Blease K, Kunkel SL. Type 1/Type 2 cytokine paradigm and the progression of pulmonary fibrosis. *Chest.* (2001) 120(Suppl. 1):S5–8. doi: 10.1378/chest.120.1_suppl.S5
37. Feghali C, Bost K, Boulware D, Levy L. Mechanisms of pathogenesis in scleroderma. I. Overproduction of interleukin 6 by fibroblasts cultured from affected skin sites of patients with scleroderma. *J Rheumatol.* (1992) 19:1207–11.
38. Giacomelli R, Cipriani P, Danese C, Pizzuto F, Lattanzio R, Parzanese I, et al. Peripheral blood mononuclear cells of patients with systemic sclerosis produce increased amounts of interleukin 6, but not transforming growth factor beta 1. *J Rheum.* (1996) 23:291–6.
39. Romano M, Sironi M, Toniatti C, Polentarutti N, Fruscella P, Ghezzi P, et al. Role of IL-6 and its soluble receptor in induction of chemokines and leukocyte recruitment. *Immunity.* (1997) 6:315–25. doi: 10.1016/S1074-7613(00)80334-9
40. Sakkas LI, Bogdanos DP. Systemic sclerosis: new evidence re-enforces the role of B cells. *Autoimmun Rev.* (2016) 15:155–61. doi: 10.1016/j.autrev.2015.10.005
41. Wermuth PJ, Jimenez SA. The significance of macrophage polarization subtypes for animal models of tissue fibrosis and human fibrotic diseases. *Clin Transl Med.* (2015) 4:1–19. doi: 10.1186/s40169-015-0047-4
42. Khan K, Xu S, Nihtyanova S, Derrett-Smith E, Abraham D, Denton CP, et al. Clinical and pathological significance of interleukin 6 overexpression in systemic sclerosis. *Ann Rheum Dis.* (2012) 71:1235–42. doi: 10.1136/annrheumdis-2011-200955
43. Vereecke L, Beyaert R, van Loo G. The ubiquitin-editing enzyme A20 (TNFAIP3) is a central regulator of immunopathology. *Trends Immunol.* (2009) 30:383–91. doi: 10.1016/j.it.2009.05.007
44. Zou X-L, Pei D-A, Yan J-Z, Xu G, Wu P. A20 overexpression inhibits lipopolysaccharide-induced NF-κB activation, TRAF6 and CD40 expression in rat peritoneal mesothelial cells. *Int J Mol Sci.* (2014) 15:6592–608. doi: 10.3390/ijms15046592
45. Lin S-C, Chung JY, Lamothe B, Rajashankar K, Lu M, Lo Y-C, et al. Molecular basis for the unique deubiquitinating activity of the NF-κB inhibitor A20. *J Mol Biol.* (2008) 376:526–40. doi: 10.1016/j.jmb.2007.11.092
46. Wertz IE, O'Rourke KM, Zhou H, Eby M, Aravind L, Seshagiri S, et al. De-ubiquitination and ubiquitin ligase domains of A20 downregulate NF-κB signalling. *Nature.* (2004) 430:694–9. doi: 10.1038/nature02794
47. Urbano PCM, Aguirre-Gamboa R, Ashikov A, van Heeswijk B, Krippner-Heidenreich A, Tijssen H, et al. TNF-α-induced protein 3 (TNFAIP3)/A20 acts as a master switch in TNF-α blockade–driven IL-17A expression. *J Allergy Clin Immunol.* (2018) 142:517–29. doi: 10.1016/j.jaci.2017.11.024
48. Monaco C, Nanchahal J, Taylor P, Feldmann M. Anti-TNF therapy: past, present and future. *Int Immunol.* (2015) 27:55–62. doi: 10.1093/intimm/dxu102
49. Ko JM, Gottlieb AB, Kerbleski JF. Induction and exacerbation of psoriasis with TNF-blockade therapy: a review and analysis of 127 cases. *J Dermatolog Treat.* (2009) 20:100–8. doi: 10.1080/09546630802441234
50. De Lauretis A, Sestini P, Pantelidis P, Hoyles R, Hansell DM, Goh NS, et al. Serum interleukin 6 is predictive of early functional decline and mortality in interstitial lung disease associated with systemic sclerosis. *J Rheumatol.* (2013) 40:435–46. doi: 10.3899/jrheum.120725
51. Koch AE, Kronfeld-Harrington LB, Szekanecz Z, Cho MM, Haines K, Harlow LA, et al. *In situ* expression of cytokines and cellular adhesion molecules in the skin of patients with systemic sclerosis. *Pathobiology.* (1993) 61:239–46. doi: 10.1159/000163802
52. Le T-TT, Karmouty-Quintana H, Melicoff E, Le T-TT, Weng T, Chen N-Y, et al. Blockade of IL-6 *Trans* signaling attenuates pulmonary fibrosis. *J Immunol.* (2014) 193:3755–68. doi: 10.4049/jimmunol.1302470
53. Khanna D, Denton CP, Lin CJ, van Laar JM, Frech TM, Anderson ME, et al. Safety and efficacy of subcutaneous tocilizumab in systemic sclerosis: results from the open-label period of a phase II randomised controlled trial (faSScinate). *Ann Rheum Dis.* (2018) 77:212–20. doi: 10.1136/annrheumdis-2017-211682

54. Dupont J, Holzenberger M. Biology of insulin-like growth factors in development. *Birth Defects Res C.* (2003) 69:257–71. doi: 10.1002/bdrc.10022
55. Guiot J, Henket M, Corhay J-L, Louis R. Serum IGFBP2 as a marker of idiopathic pulmonary fibrosis. *Eur Respiratory Soc.* (2015). 46:PA3840. doi: 10.1183/13993003.congress-2015.PA3840
56. Guiot J, Bondue B, Henket M, Corhay JL, Louis R. Raised serum levels of IGFBP-1 and IGFBP-2 in idiopathic pulmonary fibrosis. *BMC Pulm. Med.* (2016) 16:86. doi: 10.1186/s12890-016-0249-6
57. Rice LM, Mantero JC, Stifano G, Ziemek J, Simms RW, Gordon J, et al. A proteome-derived longitudinal pharmacodynamic biomarker for diffuse systemic sclerosis skin. *J Invest Dermatol.* (2017) 137:62–70. doi: 10.1016/j.jid.2016.08.027
58. Brown M, Postlethwaite AE, Myers LK, Hasty KA. Supernatants from culture of type I collagen-stimulated PBMC from patients with cutaneous systemic sclerosis versus localized scleroderma demonstrate suppression of MMP-1 by fibroblasts. *Clin Rheumatol.* (2012) 31:973–81. doi: 10.1007/s10067-012-1962-z
59. Denduluri SK, Idowu O, Wang Z, Liao Z, Yan Z, Mohammed MK, et al. Insulin-like growth factor (IGF) signaling in tumorigenesis and the development of cancer drug resistance. *Genes Dis.* (2015) 2:13–25. doi: 10.1016/j.gendis.2014.10.004
60. Yasuoka H, Jukic DM, Zhou Z, Choi AMK, Feghali-Bostwick CA. Insulin-like growth factor binding protein 5 induces skin fibrosis: a novel murine model for dermal fibrosis. *Arthritis Rheum.* (2006) 54:3001–10. doi: 10.1002/art.22084
61. Yasuoka H, Zhou Z, Pilewski JM, Oury TD, Choi AMK, Feghali-Bostwick CA. Insulin-like growth factor-binding protein-5 induces pulmonary fibrosis and triggers mononuclear cellular infiltration. *Am J Pathol.* (2006) 169:1633–42. doi: 10.2353/ajpath.2006.060501
62. Yasuoka H, Yamaguchi Y, Feghali-Bostwick CA. The membrane-associated adaptor protein DOK5 is upregulated in systemic sclerosis and associated with IGFBP-5-induced fibrosis. *PloS ONE.* (2014) 9:e87754. doi: 10.1371/journal.pone.0087754
63. Yasuoka H, Hsu E, Ruiz XD, Steinman RA, Choi AM, Feghali-Bostwick CA. The fibrotic phenotype induced by IGFBP-5 is regulated by MAPK activation and egr-1-dependent and-independent mechanisms. *Am J Pathol.* (2009) 175:605–15. doi: 10.2353/ajpath.2009.080991
64. Yasuoka H, Larregina AT, Yamaguchi Y, Feghali-Bostwick CA. Human skin culture as an *ex vivo* model for assessing the fibrotic effects of insulin-like growth factor binding proteins. *Open Rheumatol J.* (2008) 2:17–22. doi: 10.2174/1874312900802010017
65. Emtage P, Vatta P, Arterburn M, Muller MW, Park E, Boyle B, et al. IGFL: a secreted family with conserved cysteine residues and similarities to the IGF superfamily. *Genomics.* (2006) 88:513–20. doi: 10.1016/j.ygeno.2006.05.012
66. Karsdal MA, Nielsen SH, Leeming D, Langholm L, Nielsen M, Manon-Jensen T, et al. The good and the bad collagens of fibrosis–their role in signaling and organ function. *Adv Drug Deliv Rev.* (2017) 121:43–56. doi: 10.1016/j.addr.2017.07.014
67. Schäcke H, Schumann H, Hammami-Hauasli N, Raghunath M, Bruckner-Tuderman L. Two forms of collagen XVII in keratinocytes: a full-length transmembrane protein and a soluble ectodomain. *J Biol Chem.* (1998) 273:25937–43. doi: 10.1074/jbc.273.40.25937
68. Monboisse J-C, Bellon G, Randoux A, Dufer J, Borel J-P. Activation of human neutrophils by type I collagen. Requirement of two different sequences. *Biochem J.* (1990) 270:459–62. doi: 10.1042/bj2700459
69. Lindsey ML, Iyer RP, Zamilpa R, Yabluchanskiy A, DeLeon-Pennell KY, Hall ME, et al. A novel collagen matricryptin reduces left ventricular dilation post-myocardial infarction by promoting scar formation and angiogenesis. *J Am Coll Cardiol.* (2015) 66:1364–74. doi: 10.1016/j.jacc.2015.07.035
70. Pickart L. The human tri-peptide GHK and tissue remodeling. *J Biomater Sci Polym Ed.* (2008) 19:969–88. doi: 10.1163/156856208784909435
71. Zhou X-M, Wang G-L, Wang X-B, Liu L, Zhang Q, Yin Y, et al. GHK peptide inhibits bleomycin-induced pulmonary fibrosis in mice by suppressing TGF?1/SMAD-mediated epithelial-to-mesenchymal transition. *Front Pharmacol.* (2017) 8:904. doi: 10.3389/fphar.2017.00904
72. Marneros AG, Olsen BR. The role of collagen-derived proteolytic fragments in angiogenesis. *Matrix Biol.* (2001) 20:337–45. doi: 10.1016/S0945-053X(01)00151-2
73. John H, Radtke K, Ständker L, Forssmann W-G. Identification and characterization of novel endogenous proteolytic forms of the human angiogenesis inhibitors restin and endostatin. *Biochim Biophys Acta.* (2005) 1747:161–70. doi: 10.1016/j.bbapap.2004.10.013
74. Franzke C-W, Bruckner-Tuderman L, Blobel CP. Shedding of collagen XVII/BP180 in skin depends on both ADAM10 and ADAM9. *J Biol Chem.* (2009) 284:23386–96. doi: 10.1074/jbc.M109.034090
75. Liu Y, Li L, Xia Y. BP180 is critical in the autoimmunity of bullous pemphigoid. *Front Immunol.* (2017) 8:1752. doi: 10.3389/fimmu.2017.01752
76. Lin L, Betsuyaku T, Heimbach L, Li N, Rubenstein D, Shapiro SD, et al. Neutrophil elastase cleaves the murine hemidesmosomal protein BP180/type XVII collagen and generates degradation products that modulate experimental bullous pemphigoid. *Matrix Biol.* (2012) 31:38–44. doi: 10.1016/j.matbio.2011.09.003
77. Weisel JW. Fibrinogen and fibrin. *Adv Protein Chem.* (2005) 70:247–99. doi: 10.1016/S0065-3233(05)70008-5
78. Vukmirovic M, Herazo-Maya JD, Blackmon J, Skodric-Trifunovic V, Jovanovic D, Pavlovic S, et al. Identification and validation of differentially expressed transcripts by RNA-sequencing of formalin-fixed, paraffin-embedded (FFPE) lung tissue from patients with idiopathic pulmonary fibrosis. *BMC Pulm Med.* (2017) 17:15. doi: 10.1186/s12890-016-0356-4
79. Chambers RC, Scotton CJ. Coagulation cascade proteinases in lung injury and fibrosis. *Proc Am Thorac Soc.* (2012) 9:96–101. doi: 10.1513/pats.201201-006AW
80. Bauman KA, Wettlaufer SH, Okunishi K, Vannella KM, Stoolman JS, Huang SK, et al. The antifibrotic effects of plasminogen activation occur via prostaglandin E2 synthesis in humans and mice. *J Clin Invest.* (2010) 120:1950–60. doi: 10.1172/JCI38369
81. Lafferty EI, Qureshi ST, Schnare M. The role of toll-like receptors in acute and chronic lung inflammation. *J Inflamm.* (2010) 7:57. doi: 10.1186/1476-9255-7-57
82. Karampitsakos T, Woolard T, Bouros D, Tzouvelekis A. Toll-like receptors in the pathogenesis of pulmonary fibrosis. *Eur J Pharmacol.* (2017) 808:35–43. doi: 10.1016/j.ejphar.2016.06.045
83. Fineschi S, Goffin L, Rezzonico R, Cozzi F, Dayer JM, Meroni PL, et al. Antifibroblast antibodies in systemic sclerosis induce fibroblasts to produce profibrotic chemokines, with partial exploitation of toll-like receptor 4. *Arthritis Rheum J Am Coll Rheumatol.* (2008) 58:3913–23. doi: 10.1002/art.24049
84. Bhattacharyya S, Kelley K, Melichian DS, Tamaki Z, Fang F, Su Y, et al. Toll-Like receptor 4 signaling augments transforming growth factor-β responses: a novel mechanism for maintaining and amplifying fibrosis in scleroderma. *Am J Pathol.* (2013) 182:192–205. doi: 10.1016/j.ajpath.2012.09.007
85. Margaritopoulos GA, Antoniou KM, Karagiannis K, Samara KD, Lasithiotaki I, Vassalou E, et al. Investigation of Toll-like receptors in the pathogenesis of fibrotic and granulomatous disorders: a bronchoalveolar lavage study. *Fibrogenesis Tissue Repair.* (2010) 3:20. doi: 10.1186/1755-1536-3-20
86. Evankovich J, Lear T, Baldwin C, Chen Y, White V, Villandre J, et al. Toll-like receptor 8 stability is regulated by ring finger 216 in response to circulating microRNAs. *Am J Respir Cell Mole Biol.* (2020) 62:157–67. doi: 10.1165/rcmb.2018-0373OC
87. Kioon MDA, Tripodo C, Fernandez D, Kirou KA, Spiera RF, Crow MK, et al. Plasmacytoid dendritic cells promote systemic sclerosis with a key role for TLR8. *Sci Transl Med.* (2018) 10:eaam8458. doi: 10.1126/scitranslmed.aam8458
88. Stark A-K, Sriskantharajah S, Hessel EM, Okkenhaug K. PI3K inhibitors in inflammation, autoimmunity and cancer. *Curr Opin Pharmacol.* (2015) 23:82–91. doi: 10.1016/j.coph.2015.05.017
89. Guiducci S, Giacomelli R, Cerinic MM. Vascular complications of scleroderma. *Autoimmun Rev.* (2007) 6:520–3. doi: 10.1016/j.autrev.2006.12.006
90. Barbul A. Proline precursors to sustain mammalian collagen synthesis. *J Nutr.* (2008) 138:2021–4S. doi: 10.1093/jn/138.10.2021S
91. Glueck B, Han Y, Cresci G. Tributyrin supplementation protects immune responses and vasculature and reduces oxidative stress in the proximal colon of mice exposed to chronic-binge ethanol feeding. *J Immunol Res.* (2018) 2018:9671919. doi: 10.1155/2018/9671919

92. Jetten N, Verbruggen S, Gijbels MJ, Post MJ, De Winther MPJ, Donners MMPC. Anti-inflammatory M2, but not pro-inflammatory M1 macrophages promote angiogenesis *in vivo*. *Angiogenesis.* (2014) 17:109–18. doi: 10.1007/s10456-013-9381-6
93. Barron L, Wynn TA. Macrophage activation governs schistosomiasis-induced inflammation and fibrosis. *Eur J Immunol.* (2011) 41:2509–14. doi: 10.1002/eji.201141869
94. Munder M. Arginase: an emerging key player in the mammalian immune system. *Br J Pharmacol.* (2009) 158:638–51. doi: 10.1111/j.1476-5381.2009.00291.x
95. Kuwano T, Nakao S, Yamamoto H, Tsuneyoshi M, Yamamoto T, Kuwano M, et al. Cyclooxygenase 2 is a key enzyme for inflammatory cytokine-induced angiogenesis. *FASEB J.* (2004) 18:300–10. doi: 10.1096/fj.03-0473com
96. Oga T, Matsuoka T, Yao C, Nonomura K, Kitaoka S, Sakata D, et al. Prostaglandin F 2α receptor signaling facilitates bleomycin-induced pulmonary fibrosis independently of transforming growth factor-β. *Nat Med.* (2009) 15:1426–30. doi: 10.1038/nm.2066
97. Bernard K, Logsdon NJ, Benavides GA, Sanders Y, Zhang J, Darley-Usmar VM, et al. Glutaminolysis is required for transforming growth factor-β1–induced myofibroblast differentiation and activation. *J Biol Chem.* (2018) 293:1218–28. doi: 10.1074/jbc.RA117.000444
98. Rangarajan S, Bone NB, Zmijewska AA, Jiang S, Park DW, Bernard K, et al. Metformin reverses established lung fibrosis in a bleomycin model. *Nat Med.* (2018) 24:1121–7. doi: 10.1038/s41591-018-0087-6
99. Selvarajah B, Azuelos I, Platé M, Guillotin D, Forty EJ, Contento G, et al. mTORC1 amplifies the ATF4-dependent *de novo* serine-glycine pathway to supply glycine during TGF-β1–induced collagen biosynthesis. *Sci Signal.* (2019) 12:eaav3048. doi: 10.1126/scisignal.aav3048
100. Zhao X, Psarianos P, Ghoraie LS, Yip K, Goldstein D, Gilbert R, et al. Metabolic regulation of dermal fibroblasts contributes to skin extracellular matrix homeostasis and fibrosis. *Nat Metab.* (2019) 1:147–57. doi: 10.1038/s42255-018-0008-5
101. O'Neill LA, Kishton RJ, Rathmell J. A guide to immunometabolism for immunologists. *Nat Rev Immunol.* (2016) 16:553–65. doi: 10.1038/nri.2016.70
102. Kelly B, O'neill LA. Metabolic reprogramming in macrophages and dendritic cells in innate immunity. *Cell Res.* (2015) 25:771–84. doi: 10.1038/cr.2015.68
103. Xie N, Tan Z, Banerjee S, Cui H, Ge J, Liu R-M, et al. Glycolytic reprogramming in myofibroblast differentiation and lung fibrosis. *Am J Respir Crit Care Med.* (2015) 192:1462–74. doi: 10.1164/rccm.201504-0780OC
104. Kang HM, Ahn SH, Choi P, Ko Y-A, Han SH, Chinga F, et al. Defective fatty acid oxidation in renal tubular epithelial cells has a key role in kidney fibrosis development. *Nat. Med.* (2015) 21:37–46. doi: 10.1038/nm.3762

Conflict of Interest: The authors declare that the research was conducted in the absence of any commercial or financial relationships that could be construed as a potential conflict of interest.

The handling editor declared a past co-authorship with one of the authors, CF-B.

frontiers in Immunology

SYSTEMATIC REVIEW
published: 06 May 2020
doi: 10.3389/fimmu.2020.00648

Interplay Between Keratinocytes and Fibroblasts: A Systematic Review Providing a New Angle for Understanding Skin Fibrotic Disorders

Barbara Russo[1], *Nicolò C. Brembilla*[1,2] *and Carlo Chizzolini*[1]*

[1] *Department of Pathology and Immunology, School of Medicine, University of Geneva, Geneva, Switzerland,* [2] *Dermatology, School of Medicine, University Hospital, Geneva, Switzerland*

Background/Objective: Skin fibrosis is the result of aberrant processes leading to abnormal deposition of extracellular matrix (ECM) in the dermis. In healthy skin, keratinocytes participate to maintain skin homeostasis by actively crosstalking with fibroblasts. Within the wide spectrum of fibrotic skin disorders, relatively little attention has been devoted to the role of keratinocytes for their capacity to participate to skin fibrosis. This systematic review aims at summarizing the available knowledge on the reciprocal interplay of keratinocytes with fibroblasts and their soluble mediators in physiological states, mostly wound healing, and conditions associated with skin fibrosis.

Methods: We performed a systematic literature search on PubMed to identify *in vitro and ex vivo* human studies investigating the keratinocyte characteristics and their interplay with fibroblasts in physiological conditions and within fibrotic skin disorders including hypertrophic scars, keloids, and systemic sclerosis. Studies were selected according to pre-specified eligibility criteria. Data on study methods, models, stimuli and outcomes were retrieved and summarized according to pre-specified criteria.

Results: Among the 6,271 abstracts retrieved, 73 articles were included, of which 14 were specifically dealing with fibrotic skin pathologies. Fifty-six studies investigated how keratinocyte may affect fibroblast responses in terms of ECM-related genes or protein production, phenotype modification, and cytokine production. Most studies in both physiological conditions and fibrosis demonstrated that keratinocytes stimulate fibroblasts through the production of interleukin 1, inducing keratinocyte growth factor (KGF) and metalloproteinases in the fibroblasts. When the potential of keratinocytes to modulate collagen synthesis by healthy fibroblasts was explored, the results were controversial. Nevertheless, studies investigating keratinocytes from fibrotic skin, including keloids, hypertrophic scar, and scleroderma, suggested their potential involvement in enhancing ECM deposition. Twenty-three papers investigated keratinocyte proliferation differentiation and production of soluble mediators in response to interactions with fibroblasts. Most studies showed that fibroblasts modulate keratinocyte viability, proliferation, and differentiation. The production of KGF by fibroblast was identified as key for these functions.

OPEN ACCESS

Edited by:
Oliver Distler,
University of Zurich, Switzerland

Reviewed by:
Richard Stratton,
University College London, United Kingdom
Gabriela Kania,
University Hospital Zürich, Switzerland

***Correspondence:**
Carlo Chizzolini
carlo.chizzolini@unige.ch

Specialty section:
This article was submitted to Autoimmune and Autoinflammatory Disorders, a section of the journal Frontiers in Immunology

Received: *17 February 2020*
Accepted: *23 March 2020*
Published: *06 May 2020*

Citation:
Russo B, Brembilla NC and Chizzolini C (2020) Interplay Between Keratinocytes and Fibroblasts: A Systematic Review Providing a New Angle for Understanding Skin Fibrotic Disorders. Front. Immunol. 11:648. doi: 10.3389/fimmu.2020.00648

Conclusions: This review condenses evidence for the active interaction between keratinocytes and fibroblasts in maintaining skin homeostasis and the altered homeostatic interplay between keratinocytes and dermal fibroblasts in scleroderma and scleroderma-like disorders.

Keywords: fibrosis, keratinocyte, fibroblast, systemic sclerosis, cytokine, extracellular matrix, homeostasis

INTRODUCTION

Fibrosis is a complex process characterized by abnormal deposition of extracellular matrix (ECM), which can lead to altered tissue architecture impacting organ function and survival (1). Fibroblasts are endowed with the full machinery allowing deposition and resorption of ECM, which under homeostatic conditions is continually renewed. Fibroblast synthetic and degradative capacities are modulated by a variety of stimuli, which include soluble factors, cell-to-cell interactions, matrix stiffness, and tensile forces, oxygen levels, epigenetic changes, cell aging, telomere length, and cell survival (2).

Most importantly, fibroblasts are under the influence of a variety of other cell types, which are specifically resident in the tissue undergoing fibrotic changes or professional inflammatory cells recruited in the tissue (3). Soluble mediators of inflammation and, in particular, cytokines and growth factors are deeply involved in regulating fibroblast migration, proliferation, metabolism, and ECM deposition (4). In particular, TGF-β is considered a master mediator of fibrosis (5) relevant for the recruitment and trans-differentiation of cell precursors into myofibroblasts. These are cells with contractile properties associated with the expression of α-smooth actin and with a very high capacity to synthetize and release ECM components such as type I and type III collagen, fibronectin, and tenascin among others (6–8).

Enhanced ECM deposition is physiologically important and part of the reparative process in damaged tissues. Tissue damage can result from infectious agent assaults, or traumatic wounds, or the effect of physico-chemical injuries. Thus, enhanced ECM deposition is part of normal reparative inflammatory processes, and the characterization of wound healing has historically been fundamental to understand processes leading to fibrosis. What distinguishes controlled ECM enhanced deposition from pathological fibrosis is that the many mechanisms, which are important to halt ECM deposition, are relatively deficient to oppose persistent stimulation (1). Thus, perturbed homeostasis resulting from a variety of origins may explain excessive ECM deposition and pathological tissue fibrosis.

The skin is a tissue that can undergo fibrosis in response to local stimuli but also, while more rarely, as a result of systemic inflammatory disorders. Systemic sclerosis (SSc) or scleroderma is a prototypic condition in which dysregulated inflammation associated with autoimmunity and widespread vascular dysfunction results in skin and internal organs' pathological fibrosis (9). Localized skin fibrosis is observed in Morphea, hypertrophic scars, keloids, and many other conditions with metabolic, vascular, or genetic origins (10). Since long, it is known that the traumatic loss of epithelial cells (keratinocytes) and the following process of re-epithelization are spatially and chronologically important events regulating fibroblast activation and ECM deposition (wound healing) (11). More recent and less developed is our understanding of the role of keratinocytes for their capacity to regulate ECM deposition in non traumatic skin fibrosis. Similarly, relatively little is known about the role of fibroblasts and ECM for their influence on keratinocyte proliferation, differentiation, and epidermis generation. The present work aims to systematically review published evidence on the reciprocal role of keratinocytes and fibroblasts and their soluble products under the angle of human skin fibrosis.

METHODS

Literature Search

We searched the literature on PubMed up to, and including, August 31, 2019. We conducted our search using a combination of free terms and controlled vocabulary terms by Boolean operators (AND, OR). The terms used were: ["myofibroblast" (Mesh) OR "mesangial cells" (Mesh) OR "fibroblast*" (tiab) OR "fibro*" (tiab)] AND ("dermis" (Mesh) OR "derm*" (tiab) OR "skin" (Mesh) OR "cutis*" (tiab) OR "cutan*" (tiab) OR "epithel*" (tiab) OR "keratin*" (tiab)]. Keywords were detected in titles and abstracts. We also reviewed reference lists of the included full text and of other reviews on the topic to find additional reports. The systematic review was performed according to the PRISMA guidelines (12).

Inclusion Criteria

Studies fulfilling the following inclusion criteria were included in the present review: *in vitro* or *ex vivo* studies on cells or tissues of human origin from healthy donors or individuals affected by fibrotic pathologies with the exclusion of tumors or cancers. The focus was put on the keratinocyte–fibroblast interactions and the methods used to investigate these interactions, with no restrictions.

Exclusion Criteria

We excluded studies on animals, animal tissues, animal cells, and animal pathologies. We excluded human studies on hair follicles, neoplastic conditions or neoplastic cell lines, as well as inflammatory skin pathologies with no evident fibrotic component. We excluded reviews and commentaries. We excluded studies not describing keratinocyte–fibroblast interactions. We excluded studies when the full text was not available and when the language was other than English.

Data Extraction

We used standardized data extraction forms. For each study, the following items were collected: first author, year of publication, type of experimental models and methods used for investigating keratinocyte–fibroblast interactions, type of culture medium, type of stimuli and their outcomes, and mediators potentially responsible for the observed effect. Initially, titles and abstracts of all identified citations were reviewed. Full text of potentially relevant articles was screened and checked for eligibility. Disagreements about the inclusion of articles were resolved by two of the authors (BR, CC). In detail, abstract and full texts were reviewed together by the authors to reach a shared decision in case of disagreement.

Summarizing and Interpreting the Data

Data were subdivided according to the main objective of the identified studies in two categories: studies reporting mainly the effects of keratinocytes on fibroblasts (**Table 1**), studies reporting mainly the effects of fibroblasts on keratinocytes (**Table 2**). Studies specifically addressing fibrotic skin disorders are summarized in **Table 3**. Reporting was focused on cell proliferation, differentiation, and migration, extracellular matrix components, and turnover, identification of soluble factors of inflammation and growth factors, skin pathology, type of activating stimuli. The studies describing reciprocal effects on both cells types were listed in both categories and tables.

Figures were generated using Biorender.com and Inkscape (http://www.inkscape.org/).

RESULTS

Literature Search

The literature search resulted in 6,250 hits from PubMed and 21 from reference screening. After the screening of titles, abstracts, and full texts, 73 articles were included in the present review as reported in the flowchart (**Figure 1**). Six studies examined simultaneously the reciprocal effect of keratinocytes on fibroblasts and of fibroblasts on keratinocytes. Fifty-six papers explored the effects of keratinocytes on fibroblasts, 19 of which investigating soluble factors of inflammation and growth factors, 17 reporting cell proliferation, differentiation, and migration, extracellular matrix components, and turnover, 10 reporting responses to soluble factors and physical stress, 14 referring to specific skin pathologies including SSc, keloids, hypertrophic scars.

Twenty-three studies investigated the effects of fibroblasts on keratinocytes, 14 of which investigated keratinocyte proliferation, differentiation, activation, survival, and adhesion; two investigated keratinocyte production of inflammatory mediators. Six papers focused on responses to soluble factors or altered expression of transcription factors. Two papers investigating the effect of fibroblasts on keratinocytes focused on pathological conditions (SSc and keloids).

Experimental Models Used to Assess the Crosstalk Between Keratinocytes and Fibroblasts

The experimental models used to assess the crosstalk between keratinocytes and fibroblasts are schematically reproduced in **Figure 2**, and analytically reported in **Tables 1**, **2**. Many papers combined two or more experimental models. The simplest and straightforward experimental approach used in 11 papers was based on the use of the conditioned medium (CM) to be transferred from a cell type to the other (**Figure 2A**). A potential drawback may be related to differential media requirements for optimal survival, proliferation, and differentiation of keratinocytes and fibroblasts. Two papers have used centrifugation of CM to enrich for keratinocyte microvesicles or exosomes to be tested on fibroblasts (20, 38). Physical coculture of keratinocytes with fibroblasts was used in 14 papers (**Figure 2B**). The Transwell technology has been adapted to assess many different cell combinations for a total of 16 papers. Thus, keratinocytes put in the upper well-could have been cultured in monolayers or could be grown to reach stratification and differentiation to become epidermal equivalents (EE) (**Figure 2C**). Similarly, fibroblasts put in the lower well could have been grown in monolayers adherent to plastic or embedded in a matrix, thus generating a dermal equivalent (DE) (**Figure 2C**). Skin equivalents generated in cultures based on air/liquid interphase have been used in 24 papers (**Figure 2D**). Finally, full skin organotypic culture has been used in three papers (**Figure 2E**) (13, 28, 60). The proportion of studies using these culture methods is reported in **Figure 2F**.

Effects of Keratinocytes on Fibroblasts

Effects of Keratinocytes on the Production by Fibroblast of Soluble Factors of Inflammation and Growth Factors

Enhanced interleukin (IL)-6 production by fibroblasts submitted to the influence of keratinocytes was robustly identified in eight studies of eight in healthy donors (HD) (13, 20, 23, 26, 32, 50, 64, 68). Enhanced production of IL-8 was identified in six studies of seven in HD (13, 18, 26, 29, 32, 64) with a decreased IL-8 production in one of seven (59). Enhanced production of monocyte chemotactic protein (MCP)-1 was identified in three studies of three (13, 18, 50). Enhanced production of cyclooxygenase (COX)2 was identified in two studies of two (23, 50). Enhanced production of IL-1 (IL-1α, or IL-1β, or IL-1 with no specification) was identified in four studies of six (26, 29, 59, 67), with a decreased IL-1 production in two of six (41, 64). Enhanced production of prostaglandin E2 (PGE2) (63), chemokine (C-X-C motif) ligand 1 (CXCL1) (29), and tumor necrosis factor (TNF)-α (41) by fibroblasts was identified in single studies. Enhanced keratinocyte growth factor (KGF), also known as fibroblast growth factor (FGF) 7, production by fibroblasts submitted to the influence of keratinocytes was identified in four studies of five in HD (27, 29, 55, 59), with a decreased KGF production in one of five (23). Enhanced

TABLE 1 | *In vitro* and *ex vivo* studies on the effect of human keratinocytes on dermal fibroblasts.

Ref	Type of cells or samples	Type of stimuli	Identified mediators	Experimental outcome
Dufour et al. (13)	NEK, HDF, SScF; K-CM; HD full skin explant	TGF-β, IL-17A	IL-1; TGF-β	Keratinocytes enhance IL-6, IL-8, and MCP-1, production by HDF and SScF. Keratinocytes enhance ECM turnover by enhancing MMP-1 and decreasing col-I. IL-17A increases these effects TGF-β reduces these effects
Fernando et al. (14)	HaCaT, HDF; HaCaT-CM	Particulate matter (PM) fucosterol		Increase of inflammatory responses (TNFα, IL-1β, IL-6, MMP1, MMP2, elastase, PGE2) in fibroblasts treated with media from HaCaT exposed to CPM. Fucosterol reduced these effects
Zhao et al. (15)	HaCaT; HDF; EE Transwell coculture Hypertrophic scar biopsies	Dehydration		HaCaT dehydration increases col-I and αSMA expression by HDF. HMGB1 KO in HaCaT decreases HDF activation induced by dehydration. Cytoplasm accumulation of HMGB1 in hypertophic scar
McCoy et al. (16)	SScK, NEK; HDF; K-CM		Not-TGF-β	SScK more than NEK enhance col-I and αSMA expression by HDF Microarray data on differences between SScK and NEK
Carr et al. (17)	NEK, HDF, HaCaT Transwell coculture K-CM	Differentiated and undifferentiated NEK	IL-1	NEK enhances G-CSF production by HDF Undifferentiated NEK have stronger effect than differentiated NEK
Brembilla et al. (18)	NEK, HDF, SScF K-CM	IL-22, TNFα		NEK and SScK promote HDF production of MMP-1, MCP-1, and IL-8. IL22 + TNFα enhances this effect
Zhong et al. (19)	HaCaT, foreskin K, foreskin F; Differentiated-K Transwell coculture Epidermal explant HD, keloids, hypertrophic scars biopsies	Low humidity/reduced hydration	S100A8/A9	S100A8/A9 is more expressed in epidermis from keloids and hypertrophic scars than HD HaCaT dehydration increases col-I and αSMA expression by HDF. Effect mediated by epidermal S100A8/A9, which expression is induced by reduced hydration
Huang et al. (20)	HaCaT, foreskin K, HDF Keratinocyte-derived microvesicles (K-MV)		Keratinocyte-derived microvesicles (K-MV)	K-MV enhance in HDF the expression of TGF-β-induced genes and of MMP-1, MMP-3, THBS1, IL-6, lumican; enhance HDF migration and matrix contraction, enhance HDF-dependent angiogenesis Decrease in HDF the expression of cadherin-2
Gauglitz et al. (21)	HDF keloid and normal skin biopsies 2D-culture		S100A7 S100A15	Compared to healthy skin reduced expression of S100A7 and S100A15 in keloids epidermis with reciprocal expression of COL1A1, COL1A2, COL3A1. S100A7 and S100A15 on HDF decrease COL1A1, COL1A2 and COL3A1, TGF-β1, TGF-β2, TGF-β3, laminin-β2 and α-SMA and HDF proliferation
Xu et al. (22)	HaCaT, foreskin k, foreskin F; Differentiated-K Transwell coculture Epidermal explants	Reduced hydration	ENaC, COX2, PGE2	HaCaT dehydration increases col-I and αSMA expression by HDF. Effects mediated by ENaC, COX2, PGE2
Arai et al. (23)	Foreskin-K, foreskin-F; EE DE (decellularized dermis) Skin equivalent EE-CM		IL-1α, IL-1β	PGE2 detected only in skin equivalent. PGE2 expressed by DD enhances keratinocytes proliferation EE-CM increases COX2, IL-6, and GM-CSF and decrease KGF expression in HDF
Nikitorowicz-Buniak et al. (24)	HD and SSc skin, HDF, SScF; HD, SSc epidermal and dermal explants; HD, SSc epidermal explant CM	S100A9	S100A9	Increase of CCN2, S100A9, HGF in SSc epidermis compared to dermis and HD epidermis; S100A9 enhances HDF and SScF proliferation, migration, and CTGF production
Li et al. (25)	HaCaT, HDF HaCaT-CM		Fibronectin	HaCaT–CM enhances HDF migration

(Continued)

TABLE 1 | Continued

Ref	Type of cells or samples	Type of stimuli	Identified mediators	Experimental outcome
Varkey et al. (26)	NEK; HDF EE DD (superficial (S)/or deep(D) HDF embedded in a GAG matrix) Skin equivalent			In organotypic cultures, the levels of col-I and fibronectin were lower and levels of TGFα, PDGF, IL-1 higher compared to embedded HDF only D-HDF produced higher levels of col-I higher levels of TGF-β activity and IL-6 compared to S-HDF S-HDF produced higher MMP-1 levels
Sun et al. (27)	HaCaT, fibroblast cell line CCD966SK 2D-culture		KGF, IL-19	IL-19 induces KGF expression in CCD966SK fibroblasts KGF enhances the production of IL-19 in HaCaT and promotes higher proliferation and migration
Canady et al. (28)	NEK, HDF, SScF, keloid fibroblasts, HD skin skin explant		KGF, OSM	KGF is increased in keloid and SSc fibroblasts and sera KGF induces keratinocytes to release OSM leading to fibroblast activation KGF increases the production of OSM, (fibroblast activator protein) FAP, col-I in cultured skin explants
Kolar et al. (29)	HaCaT, NEK, HDF EE; DE (collagen embedded HDF) Skin equivalent		IL-6, IL-8, CXCL-1	NEK-organotypic cultures enhance the expression of FGF-7, FGF-5, FGF-2, CXCL-1, IL-6, IL-8 in HDF
Rock et al. (30)	Female NEK and HDF K-CM		E2; E2 and UVB	E2 and E2 + UVB increase the production of EGF in NEK Conditioned medium from E2 and E2 + UVB-exposed KCM enhances hyaluronan synthase 3 and versican V2 and proliferation of HDF
Simon et al. (31)	K-from hypertrophic scars, NEK, HDF, hypertrophic scar F EE or EE-CM DE (F in a dermal matrix) Skin equivalent		TIMP-1	Compared to NEK, K from hypertrophic scars increase dermal matrix thickness, by enhanced production of TIMP-1
Do et al. (32)	Keloids-K, Keloid-F, NEK, HD Transwell coculture		IL-18	K form keloids more than NEK produce IL-18, fibroblasts from keloids and HDF enhance IL-18 production by keratinocytes IL-18 enhances col-I, IL-6, IL-8 production by HDF
Lai et al. (33)	NEK, HDF K-CM		Stratifin	Conditioned medium from NEK enhances the production by HDF of MMP-1, MMP-3, MMP-12, versican, TN-C, ITGA1, CTNNA1, FN NEK induce the upregulation of aminopeptidase N/CD13 in HDF as consequence of stratifin production
Tandara and Mustoe (34)	NEK; HDF Transwell coculture K-CM			K-CM enhance the production of MMP-1, MMP-8, MMP-13, MMP-2, MMP-10, TIMP-1, and TIMP-2 by HDF. NEK-hydration further increases the upregulation of MMPs and decreases TIMP-2
Koskela et al. (35)	NEK, HDF, EE DE (HDF embedded in collagen) Skin equivalent	TGF-β		Compared to HDF alone, organotypic cocultures increase MMP-1, MMP-3, uPA and decrease CTGF, col I, col III, FN, TIMP-2, αSMA, PAI, in the presence or absence of TGF-β
Aden et al. (36)	SSc and HD skin biopsies, HDF, SScF, SSc or HD epidermis explant DE (HDF embedded on collagen) Skin equivalent		IL-1, TGF-β, ET-1	Altered keratinocyte differentiation in SSc biopsies Compared to HD, SSc epidermal explants produce more IL-α resulting in enhanced gel contraction SSc and HD explants have similar levels of ET-1 or TGFβ. ET-1 and TGFβ have a role in CTGF production by HDF
Lim et al. (37)	Keloids-K, keloids-F, NEK, HDF. Monolayer, Transwell coculture			IL-6, IL-8, MCP1, TIMP-1, TIMP-2 detected in monocultures Angiogenin, OSM, VEGF, IGF-binding protein-1, OPG, and TGF-β2 detected in keloids-K-keloids-F, but absent in NEK–HDF cocultures
Chavez-Munoz et al. (38)	Differentiated and undifferentiated foreskin K, HDF K-Exosomes		14-3-3 (stratifin)	Exosomes generated from differentiated more than undifferentiated foreskin K enhance MMP-1 production by HDF. This effect is mediated by stratifin

(Continued)

TABLE 1 | Continued

Ref	Type of cells or samples	Type of stimuli	Identified mediators	Experimental outcome
Ghaffari et al. (39)	NEK, HDF Transwell coculture		keratinocyte-derived collagen-inhibitory factor of 30–50 kD (KD-CIF)	Keratinocyte-released factors reduce col-I production by HDF by KD-CIF Keratinocyte differentiation do not alter synthesis, release, or activity of KD-CIF
Wall et al. (40)	NEK, HDF DE (HDF) embedded in collagen gel Skin equivalent			In comparison to HDF cultured in monolayers, the production of MMP2, MMP9, uPA, uPAR is increased in organotypic cocultures, with no significant changes in contractile responses
Tandara et al. (41)	NEK, HDF Transwell coculture			Compared to HDF cultured in monolayers, col-I production is decreased, and KGF production increased in Transwell cultures, more so in hydrated cultures. Compared to NEK cultured in monolayers, TNF production is increased and IL-1 is decreased in Transwell cultures
Amjad et al. (42)	NEK, HDF, K-CM DE (HDF collagen embedded) Skin equivalent			NEK decrease TGFβ1 the production by HDF
Harrison et al. (43)	NEK, HDF Coculture			NEK conditioned medium and NEK coculture inhibit spontaneously, and IGF, bFGF-stimulated col-I production by HDF, TNF reduce this inhibition
Ghaffari et al. (44)	NEK, HDF Transwell coculture		Stratifin	Stratifin is produced only by NEK Stratifin and NEK-conditioned medium enhance MMPs, adhesion molecules, PAI1. PAI2, THSP1, FN (and other detected by microarray) by HDF
Harrison et al. (45)	NEK, HDF HD epidermal explants Coculture K-CM			Both NEK-conditioned medium and HD epidermal explants decrease HDF proliferation HD epidermal explants but not NEK-conditioned medium enhance FN production by HDF
Chinnathambi and Bickenbach (46)	NEK and HDF EE; DE (HDF collagen embedded) skin equivalent			Compared to HDF cultured in monolayers, the production of MMP1 is increased and MMP-2 is decreased in organotypic cocultures
Ghahary et al. (47)	NEK, HDF Transwell coculture		Stratifin	Compared to HDF cultured in monolayer, MMP1 is increased Stratifin induces MMP-1 Stratifin expression is higher in differentiated NEK
Sawicki et al. (48)	K-foreskin, HDF Transwell coculture			Compared to NEK cultured alone, HDF enhance the production of MMP-9 and MMP-2 by K. HDF cocultured with K produce MMP-9 TIMP-1, TIMP-2, and TIMP-3, but not, TIMP-4 levels are enhanced both in K and HDF when in coculture
Shephard et al. (49)	HaCaT, irradiated HDF Coculture			Compared to HDF cultured in monolayer, the contractile activity and αSMA expression is increased in coculture ET-1 enhances contraction and TGF-β enhances αSMA expression in cocultures
Shephard et al. (50)	HaCaT, NEK, irradiated and not irradiated HDF Coculture			Compared to HDF cultured alone, HDF in cocultures with HaCaT and NEK expresses more—*ENA-78*, and *MCP-1*, *IL-6*, *LIF*, *G-CSF*, *M-CSF*, *COX2*, PAI, and less *Cathepsin K, Cathepsin L, Cathepsin L2* *More col-I, col-IV, col-V, col-VI, hyaluran synthtease, lysine hydroxylase, transglutaminase 2, TN-C, decorin, syndecan 2, but less testican, tenascin XA, fibulin, thrombospondin a* SMA expression requires close proximity to keratinocytes
Ghahary et al. (51)	NEK, HDF, DE (HDF collagen embedded) Transwell coculture		Stratifin	Compared to HDF cultured alone, HDF in cocultures produce more MMP1 and enhance col-I digestion
Satish et al. (52)	K-foreskin, Hs68 Transwell coculture		CXCL11	CXCL11 (IP9) is induced by mechanical wounding in K CXCL11 reduces EGF-induced fibroblast motility and enhance EGF-induced keratinocytes motility

(Continued)

TABLE 1 | Continued

Ref	Type of cells or samples	Type of stimuli	Identified mediators	Experimental outcome
Funayama et al. (53)	NEK, keloid-K, HDF, keloid-F; Transwell coculture			Compared to NEK, keloid-K enhanced keloid-F proliferation, resistance to apoptosis (upregulation of Bcl-2) and TGF-β1 expression
Phan et al. (54)	Keloids-K, keloids-F, NEK, HDF. Transwell coculture		IGFBP-3	Compared to monocultures, HDF and keloid-F showed higher proliferation when cocultured with keloid-K. IGFBP-3 inhibition reduced keloid-F proliferation
Gron et al. (55)	NEK, HDF Coculture where NEK were grown on polycarbonate membrane coated with col-IV and added to HDF monolayers			Compared to HDF cultured alone, HDF in cocultures produce more HGF and KGF No difference in HDF proliferation
Lim et al. (56)	Keloids-K, keloids-F, NEK, HDF. Transwell coculture			HDF cocultured with keloid-K increased soluble col-I and col-III. Keloid-F cocultured with keloid-K increased both soluble and insoluble collagen
Lim et al. (57)	Keloids-K, keloids-F, HDF. Transwell coculture			Keloid-k induce proliferation HDF more than NEK
Niessen et al. (58)	Biopsies of normal and hypertrophic scars after breast surgery			High IL-1α expression at month 3 predicts normal scar, no relationship between IL-1β and TNF expression. High levels of PDGF and bFGF at 12 months correlate with hypertrophic scar
Maas-Szabowski et al. (59)	NEK, irradiated HDF, DE Coculture			Compared to HDF cultured alone, HDF in coculture expresses more KGF, IL-1α, IL-1β but less IL-8, TGF-β Compared to NEK cultured alone, NEK in col culture express more IL-1α, IL-8, bFGF, GM-CSF
Zhang et al. (60)	Skin explant culture Coculture (NEK seeded onto stratified HDF embedded on sterile nylon membrane)			Compared to HDF cultured alone, HDF have enhanced expression of epimorphin particularly beneath the keratinocyte layer
Garner (61)	NEK, HDF, Coculture			Compared to HDF cultured alone, col-I is decreased in cocultures
Ralston et al. (62)	NEK, DE Coculture			Coculture enhances matrix contraction and FN
Sato et al. (63)	NEK, HDF, DE Coculture		IL-1α	Compared to HDF cultured alone, PGE2 production is increased in cocultures via enhanced expression of COX-2 induced by IL-1α
Boxman et al. (64)	NEK, HDF K-CM			Compared to HDF cultured alone, IL-6, IL-8, production is higher and IL-1 lower in HDF exposed to NEK-conditioned medium
Chang et al. (65)	NEK, HDF, Transwell coculture			Compared to HDF cultured alone, col-I and GAG production is reduced in cocultures more so if NEK is hydrated
Lacroix et al. (66)	NEK, HDF, DE Coculture			Compared to HDF cultured alone, col-I and FN production is increased in coculture
Boxman et al. (67)	K-foreskin, HDF Coculture CM		IL-1α	Compared to HDF cultured alone, IL-1α production is increased in cocultures and K-foreskin conditioned medium
Waelti et al. (68)	NEK, irradiated HDF Coculture		IL-1β	Compared to HDF cultured alone, IL-6 production is increased in cocultures and NEK conditioned medium, effect mediated by IL-1β

The references are reported in inverse chronological order. αSMA, alpha-smooth muscle actin; bFGF, basic fibroblast growth factor; CCD966SK, fibroblast cell line; CCL, chemokine (C-C containing) motif; CCR, receptor; for CCL chemokines; CM, conditioned medium; Col, collagen; COX2, Cyclooxygenase 2; CTGF, connective tissue growth factor; CTNNA1, Catenin Alpha 1; CXCL, chemokine (C-X-C containing)motif ligand; DE, dermis equivalent; Differentiated-K, Differentiated keratinocytes; E2, estrogen; EE, epidermal equivalent; EGF, epidermal growth factor; ENaC, Epithelial sodium channel; ENA-78, Epithelial neutrophil-activating protein 78; ET-1, endothelin-1; FAP, fibroblast activation protein; FGF, fibroblast growth factor; FN, fibronectin; Foreskin K, newborn foreskin keratinocytes; G-CSF, granulocyte colony stimulating factor; GM-CSF, granulocyte-monocyte colony stimulating factor; HaCaT, human keratinocytes immortalized cell line; HD, healthy donor; HDF, healthy donor fibroblasts; HMGB1, high mobility group box-1; Hs68, foreskin fibroblasts cell line; IGF, insulin-like growth factor; IGFBP, insulin-like growth factor binding protein; IL, interleukin; ITGA1, alpha 1 subunit of integrin receptors; K-CM, keratinocytes conditioned medium; Keloids-F, keloids fibroblasts; Keloids-K, keloids keratinocytes; KGF, keratinocyte growth factor; K-MV, Keratinocyte-derived microvesicles; LIF, leukemia inhibitory factor; MCP-1, monocyte chemotactic protein-1; M-CSF, monocyte colony stimulating factor; MMP, metalloproteinase; NEK, healthy donor keratinocytes; OPG, osteoprotegerin; OSM, oncostatin M; PAI, plasminogen activator inhibitor; PDGF, platelet-derived growth factor; PGE2, Prostaglandin E2; S100A7, psoriasin; S100A8/A9, calprotectin; S100A15, koebnerisin; SSc, Systemic sclerosis; SSc-F, SSc fibroblasts; SSc-K, SSc keratinocytes; TGF, Transforming growth factor; THBS1, Thrombospondin 1; TN-C, tenascin C; TNFα, Tumor necrosis factor α; uPA, urokinase-type plasminogen activator; UVB, ultraviolet B radiation.

TABLE 2 | *In vitro* and *ex vivo* studies on the effect of human dermal fibroblasts on keratinocytes.

Ref	Type of cells or samples	Type of stimuli	Identified mediators	Experimental outcome
Kumtornrut et al. (69)	NEK, HDF Coculture	Testosterone	KGF2 (FGF10)	Androgen-stimulated HDF, reduce NEK differentiation (keratins), effect mediated by FGF10
Yang et al. (70)	NEK, HDF Skin equivalent	TGF-β bFGF	KGF	TGF-β enhanced αSMA, VEGF and reduced KGF and HGF expression in HDF. bFGF reduced αSMA, but increased KGF expression in HDF. In skin equivalent, bFGF enhanced epidermal differentiation via KGF
Quan et al. (71)	NEK, HDF Skin equivalent	SDF-1		SDF-1 is expressed selectively in HDF and is hyper expressed in psoriatic skin. SDF-1 overexpression increases epidermal thickness with increased keratinocytes layers, in skin equivalent. SDF activates ERK pathway on keratinocytes.
Fernandez et al. (72)	NEK, HDF Transwell coculture Skin equivalent	Keratinocytes UVB exposure		HDF enhance NEK survival, DNA repair, and reduce apoptosis after UVB exposure by reducing caspase-3 and enhancing p53 activities
Varkey et al. (73)	NEK, superficial (S) and deep (D) HD EE S- or D-DE (cross-linked col-I–GAG matrix) Skin equivalent			In skin equivalents either engineered from S- or D-HDF, the epidermal production of IL-1α, TGFα, PDGFα was increased compared to EE alone. Only skin equivalent engineered from D-HDF showed increased epidermal production of PDGF compared to EE alone. Skin equivalent engineered either from S- or D-HDF showed increased IL-6 and KGF production compared to S- or D-DE alone. Skin equivalent showed a reduced expression of col-I and active TGFβ1 compared to DE (mainly for D-DE)
Arai et al. (23)	NEK and HDF K-CM; F-CM; EE, DE (collagen matrix) Skin equivalent			IL-1α derived by keratinocytes increase expression of PGE2 and other IL-1 inducible genes (IL6, GM-CSF and KGF) by fibroblasts (shown in skin equivalent or K-CM model of K–F interaction). Dermis derived PGE2 promote epidermis proliferation.
Sun et al. (27)	HaCaT, CCD966SK (fibroblasts cell line); 2D cultures		KGF, IL-19	KGF enhances proliferation and IL-19 production by HaCaT and IL-19 induces KGF expression in CCD966SK fibroblasts.
Canady et al. (28)	NEK, HDF, SScF, keloid fibroblasts, K-CM, F-CM skin explant		KGF, OSM	KGF is increased in keloid and SSc fibroblasts and sera. Fibroblast-derived KGF induces keratinocytes to release OSM leading to fibroblast activation (increased col-I, FAP, and migration) (results from K- or-F-CM and 2D models of interaction). In *ex vivo* skin explant confirmed that KGF increases the production of OSM, FAP, col-I
Chowdhury et al. (74)	NEK, HDF, F-CM			Compared to monolayer, coculture enhances NEK adhesion and proliferation
Yang et al. (75)	NEK, HDF, skin equivalent			Epidermal differentiation is enhanced in the absence of myo-fibroblasts. bFGF reduces αSMA expression and enhanced keratin 10 but reduced keratin 16 and TGF-β in the epidermis
Wang et al. (76)	NEK, HDF, coculture or trans-well coculture		IL-1 + TGF-β1 (HDF) HB-EGF (NHK)	In coculture, HDF enhance NEK proliferation. This effect may be due to autocrine HB-EGF effect. Keratinocyte HB-EGF expression may be induced by fibroblast-derived IL-1α and TGF-β
Kolar et al. (29)	HaCaT, NEK, Transwell coculture K- or F-CM		IL-6, IL-8, CXCL-1	F-CM and IL-6, IL-8, CXCL-1 increase the expression of keratin-8 in NEK NEK enhances the expression of IL-6, IL-8, CXCL-1,KGF, bFGF, FGF-5 in HDF
Carr et al. (77)	NEK, HDF, coculture		Stratifin (14-3-3)	Compared to monolayers, HDF enhance 14-3-3σ 1 expression in NEK

(Continued)

TABLE 2 | Continued

Ref	Type of cells or samples	Type of stimuli	Identified mediators	Experimental outcome
Peura et al. (78)	NEK, CRL2088-F fibroblast cell line, HDF in fibrin matrix	CRL2088-F in fibrin matrix (=Finectra)	EGF	Compared to NEK cultured alone, CRL2088-F in fibrin matrix provides better NEK viability and migration. An inhibitor of EGFR/c-Met receptor tyrosine kinases abolished keratinocyte responses
Chong et al. (79)	NEK, HDF, DE (collagen matrix) skin equivalent		PPAR α/δ	Compared to wild-type skin equivalents, PPAR α/δ-deficient fibroblasts enhanced NEK proliferation, IL-1 expression, activation of TAK1 and up-regulation of AP-1 controlled mitogenic target genes
El Ghalbzouri and Ponec (80)	NEK, HDF, F-CM skin equivalent,		Soluble factors	Compared to conditioned medium generated form epidermal equivalents or HDF, conditioned media from skin equivalents (NEK + HDF) enhanced NEK viability and differentiation, and resulted in higher deposition of laminin 5 and nidogen in the basal membrane via the release of soluble factors
Sorrell et al. (81)	NEK, HDF, S-DE, D-DE, EE, S- or D-DE (collagen matrix) skin equivalent			Compared to D-DE, S-DE resulted in higher GM-CSF/KGF ratio and enhanced IL-6 production. NEK cultured in skin equivalents with S-HDF, compared to D-HDF, showed enhanced differentiation and formation of basement membrane
Maas-Szabowski et al. (82)	HaCaT, NEK, HDF, Skin equivalent	TGF-α	IL-1α, GM-CSF, KGF (FGF7)	IL-1 epidermal derived stimulate fibroblast production of AP1-related genes, among this KGF and GM-CSF stimulate keratinocytes proliferation and secretion of IL-1. Autocrine epidermal TGFα production induce epidermal expression of the receptor for KGF and GM-CSF. HaCaT differentiation in skin equivalent is impaired, as well as IL-1 production and response to KGF and GM-CSF. This effect is due to the lack of TGFα
El Ghalbzouri et al. (83)	NEK, HDF, EE, DE (repopulated dermis matrix) skin equivalent		KGF	Complete *in vitro* generation of a differentiated epidermis requires the presence of HDF in a repopulated dermal equivalent. Fibroblast presence promotes keratinocyte proliferation, downregulates K6 and abate K16 and K17 expression. The fibroblast presence can be substituted by KGF
el-Ghalbzouri et al. (84)	NEK, HDF, EE, DE (collagen matrix) skin equivalent			As El Ghalbzouri et al. However, the expression of integrin α6β4 and of E-CAD was not dependent on HDF.
Blomme et al. (85)	NEK; HDF 2D cultures	PTHrP		PTHrP produced by K increases KGF secretion by fibroblasts
Monical and Kefalides (86)	NEK; HDF Transwell coculture			Coculture promote NEK proliferation, compared to monolayer; coculture increased protein synthesis in both cell types, compared to monolayer. Production of laminin is modulated in coculture in both cell types
Smola et al. (87)	NEK; HDF DE (irradiated or not); skin equivalent coculture			NEK proliferation increases in coculture or in skin equivalent compared to EE alone) NEK increased HDF production of IL-6; KGF, GM-CSF, collagenase compared to 2D culture Irradiation affected GM-CSF production (lower in irradiated vs. not) and collagenase production (higher in irradiated vs. not)

The references are reported in inverse chronological order. 2D, 2-dimentions; AP-1, Activator protein 1; bFGF, basic fibroblasts growth factor; CCD966SK, human normal fibroblasts cell lines from adult; C-I, collagen I; CM, conditioned medium; CRL2088, human normal fibroblasts cell lines from foreskin; CXCL, chemokine (C-X-C containing) motif ligand; D-DE, deep dermis equivalent; DE, dermis equivalent; D-HDF= deep dermal fibroblasts; E-CAD, E-cadherin; EE, epidermal equivalent; EGF, epidermal growth factor; F, fibroblasts; FAP, fibroblast activating protein; FGF, fibroblasts growth factor; GAG, Glycosaminoglycan; GM-CSF, granulocyte-monocyte growth factor; HaCaT, human normal keratinocyte cell line from adult; HB-EGF, heparin binding EGF like growth factor; HDF, healthy donor fibroblasts; HGF, hepatocyte growth factor; IL, interleukin; K, keratinocytes; KGF, keratinocyte growth factor; NEK, normal epidermal keratinocytes; OSM, oncostatin M; PDGF, platelet-derived growth factor; PGE2, prostaglandin E2; PPAR, peroxisome proliferator-activated receptor; PTHrP, parathyroid hormone-related protein; rh, recombinant human; SCC marker, Squamous cell marker; S-DE, superficial dermis equivalent; SDF, stromal cell derived factor; S-HDF, superficial dermal fibroblasts; SMA, smooth muscle actin; TAK1, TGF activated kinase; TGF, transforming growth factor; VEGF, vascular endothelial growth factor.

TABLE 3 | Keratinocyte–fibroblast crosstalk in fibrotic pathologies.

References	Pathology	Experimental outcome
Dufour et al. (13)	SSc	SScF compared to HDF produce higher col-I when exposed to NEK-CM
McCoy et al. (16)	SSc	SScK compared to NEK induce higher col-I and αSMA expression by HDF
Nikitorowicz-Buniak et al. (24)	SSc	SSc epidermis expresses higher S100A9 compared to dermis and HD epidermis S100A9 enhances HDF and SScF proliferation, migration, and CTGF production
Aden et al. (36)	SSc	SSc epidermal explants produce more IL-1α resulting in enhanced gel contraction by HDF
Canady et al. (28)	SSc, keloid	SSc and keloid fibroblasts express higher levels of KGF KGF induces keratinocytes to release OSM leading to fibroblast activation
Gauglitz et al. (21)	Keloid	Keloid skin expresses lower levels of S100A7 and higher levels of COL1A1, COL1A2, COL3A1 in the dermis than HD. S100A7 decrease HDF production of COL1A1, COL1A2, COL3A1, TGF-β1, TGF-β2, TGF-β3, laminin-β2, α-SMA, and HDF proliferation
Do et al. (32)	Keloids	Keloids-K produce more IL-18 than NEK IL-18 enhances col-I, IL-6, IL-8 production by HDF
Lim et al. (37)	Keloids	Keloids-K and fibroblasts coculture produce angiogenin, OSM, VEGF, IGF-binding protein-1, OPG, and TGF-β2, and HD coculture does not
Funayama et al. (53)	Keloids	Keloid-K enhanced keloid-F proliferation, resistance to apoptosis (upregulation of Bcl-2) and TGF-β1 expression
Phan et al. (54)	Keloids	Keloid-K increased proliferation of HD and K-fibroblasts, on an IGFBP-3-dependent mechanism
Lim et al. (56)	Keloids	Keloid-K increased col-I and col-III production by HDF
Lim et al. (57)	Keloids	Keloids-k induced proliferation of HDF more than NEK
Simon et al. (31)	Hypertrophic scars	K from hypertrophic scars increase dermal matrix thickness by enhanced production of TIMP-1.
Niessen et al. (58)	Hypertrophic scars	High IL-1α expression at month 3 predicts normal scar; no relationship between IL-1β and TNF expression. High levels of PDGF and bFGF at 12 months correlate with hypertrophic scar

*The references are grouped per pathology. Additional details on culture conditions and mediators are reported in **Tables 1**, **2**. αSMA, alpha-smooth muscle actin; bFGF, basic fibroblast growth factor; Col, collagen; CTGF, connective tissue growth factor; FGF, fibroblast growth factor; HD, healthy donor; HDF, healthy donor fibroblasts; IGF, insulin-like growth factor; IGFBP, insulin-like growth factor binding protein; IL, interleukin; Keloids-F, keloids fibroblasts; Keloids-K, keloids keratinocytes; KGF, keratinocyte growth factor; MMP, metalloproteinase; NEK, healthy donor keratinocytes; OPG, osteoprotegerin; OSM, oncostatin M;PDGF, platelet-derived growth factor; S100A7, psoriasin; S100A8/A9, calprotectin; SSc, Systemic sclerosis; SSc-F, SSc fibroblasts; SSc-K, SSc keratinocytes; TGF, Transforming growth factor; THBS1, Thrombospondin 1; TIMP, tissue inhibitor of metalloproteinases; TNF, Tumor necrosis factor; VEGF, vascular endothelial growth factor.*

production of granulocyte-colony-stimulating factor (G-CSF) was identified in two of two in HD (17, 50), while transforming growth factor (TGF)-β was found to be decreased in two of two studies (42, 59). For connective tissue growth factor (CTGF), one study reported enhanced (26), and on other study decreased, production (35) by HD fibroblasts. Enhanced production of vascular endothelial growth factor (VEGF)-1, platelet-derived growth factor (PDGF)-1, hepatocyte growth factor (HGF), basic FGF (bFGF), monocyte (M)-CSF, granulocyte monocyte (GM)-CSF, and epimorphin were all found in single studies (17, 23, 26, 55, 60).

Effects of Keratinocytes on Fibroblast Proliferation, Differentiation, Migration, Extracellular Matrix Components, and Turnover

Type-I collagen (col-I) production by fibroblasts submitted to the influence of keratinocytes was found enhanced in four studies (13, 16, 32, 66) and decreased in eight of 12 studies in HD (26, 35, 39, 41, 43, 50, 61, 65). Fibronectin (FN) production was reported to be enhanced in five of six studies (33, 44, 45, 62, 66) and decreased in one of six (35). Other ECM components including tenascin, versican, lumican, and thrombospondin were variably reported to be increased in two or decreased in one of three studies (20, 33, 49). The production of matrix metalloproteinases (MMP) including MMP-1, MMP-2, MMP-3, MMP-8, MMP-9, and MMP-12 when investigated was always found to be increased in fibroblast under the influence of keratinocytes for a total of 12 studies (13, 18, 20, 34, 35, 38, 40, 44, 46–48, 51). The production of tissue inhibitor of metalloproteinases (TIMP)-1, TIMP-2, and TIMP-3 was variably reported to be increased in two (34, 48) or decreased in one of three studies (35). Decreased production of cathepsins was reported in one paper (50). The production of plasminogen activator inhibitor (PAI) was variably reported to be increased in two (44, 50) and decreased in one of three studies (35). Uroplasminogen (uPA) was increased in two of two papers (35, 40). Decreased proliferation of HD fibroblasts was reported in two (45, 57) and unchanged in one of three (55). Enhanced fibroblast migration

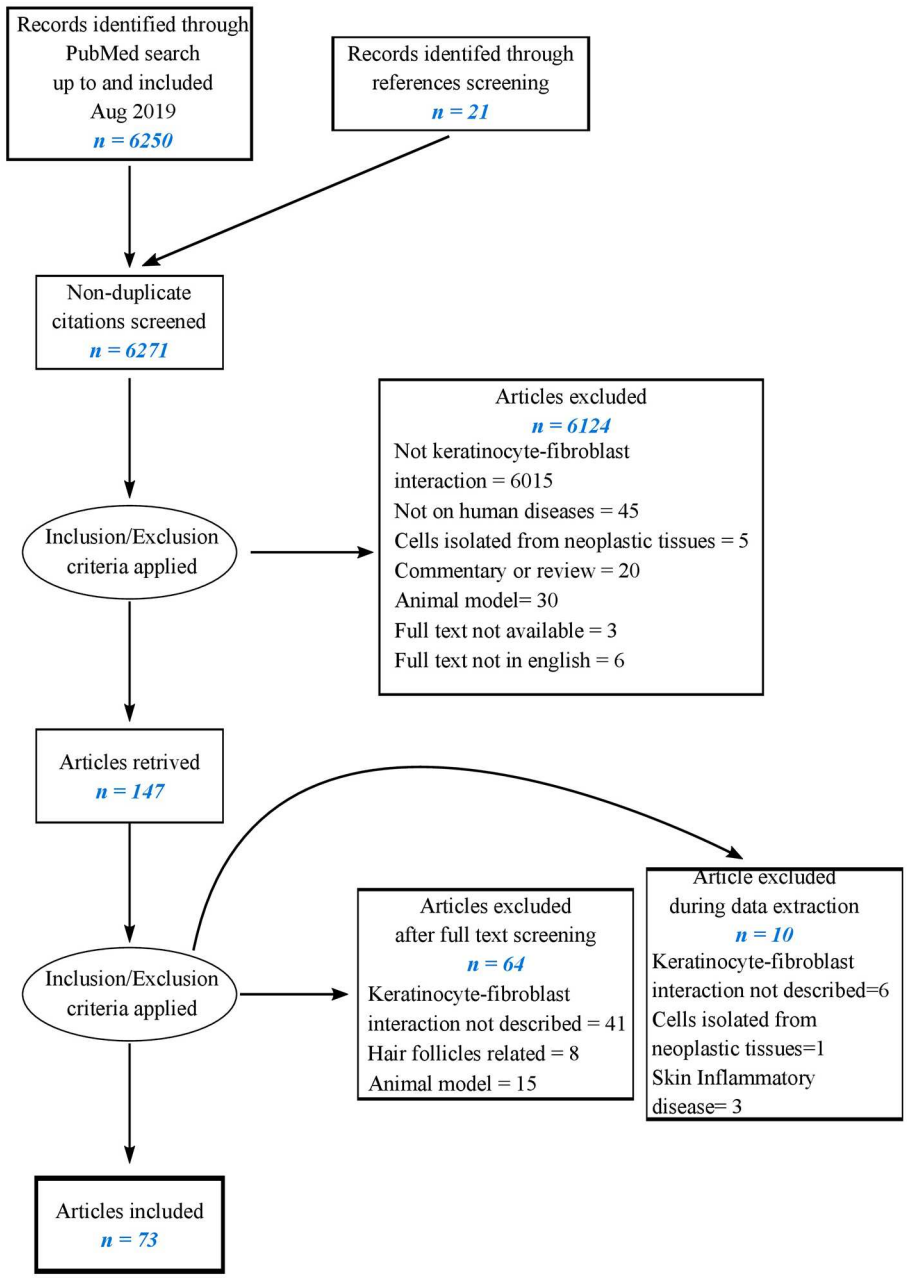

FIGURE 1 | Flow chart of the literature-searching strategy.

was reported in three of three papers (20, 25, 27). Four papers reported enhanced HD fibroblast proliferation mediated by keratinocyte produced S100A9 (24), or by UVB-exposed keratinocytes cultured in estradiol (30) or enhanced migration (25) mediated by microvesicles released by keratinocytes (20). Cell adhesion and cadherin expression were found increased in two papers each (20, 44), and gel contraction increased in three of three (20, 49, 62). The expression of α-smooth muscle actin (αSMA) was variably reported to be increased in two (49, 50) or decreased in one of three studies (35).

Effect of Soluble Factors and Physical Stress Acting on Keratinocytes for Their Influence on Fibroblasts

Within the context of wound healing, the effects on fibroblasts of dehydration or hyper-hydration of partially stratified keratinocytes was investigated in six papers (15, 19, 22, 34, 52). Robustly, five of them examining col-I production reported enhanced col-I production when keratinocytes were dehydrated compared to their normally hydrated counterpart. When tested, consistently with the results on col-I, αSMA expression was increased by dehydration in three of three papers (15, 19, 22).

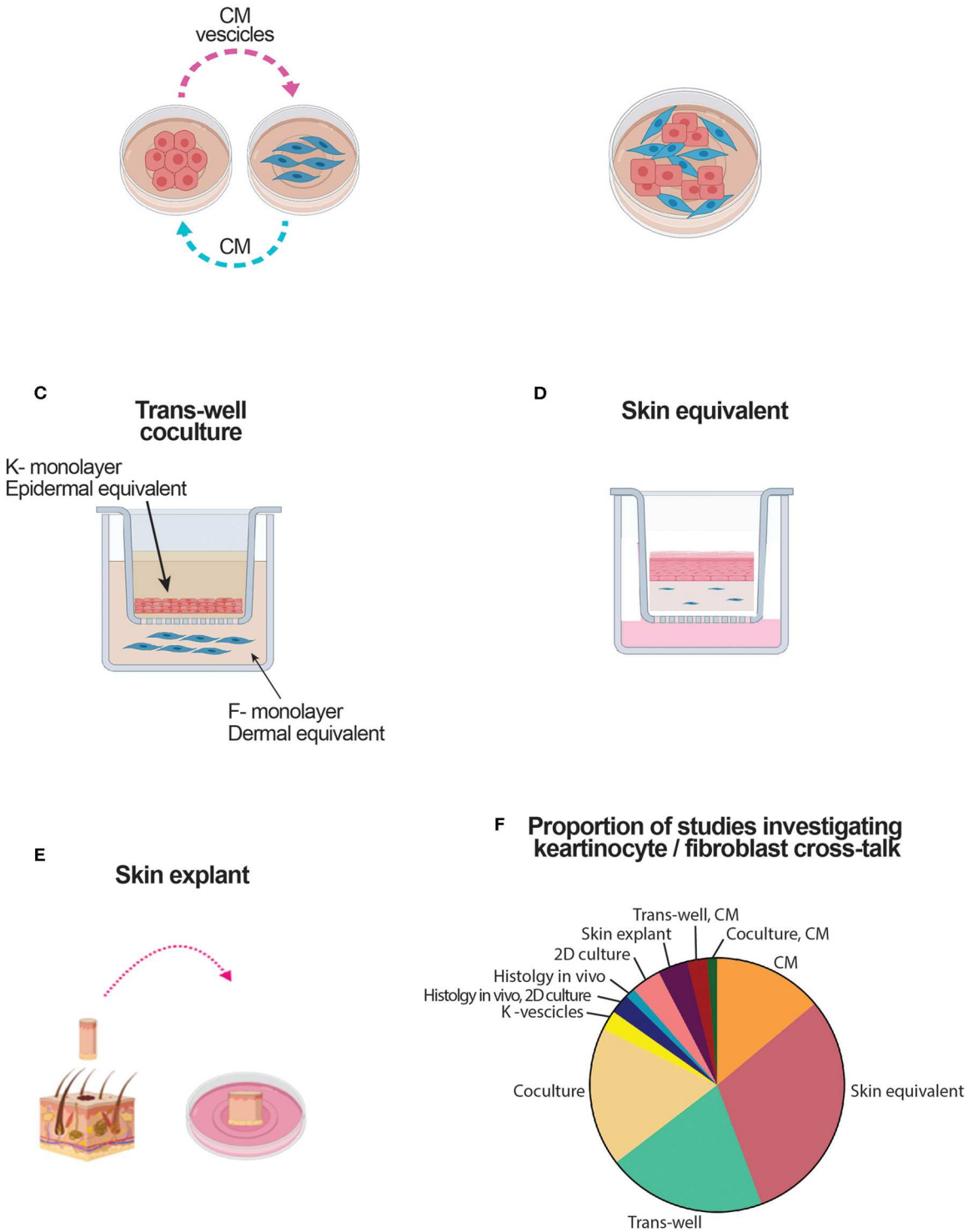

FIGURE 2 | Schematic representation of culture systems used to assess the crosstalk between keratinocytes and fibroblasts. CM, conditioned medium; DE, dermal equivalent; EE, epidermal equivalent; F, fibroblast; K, keratinocyte. **(A)** Culture based on the use of medium conditioned by one type of cell cultured in monolayer to modulate the response of the other cell type. **(B)** Culture based on a mix of keratinocytes and fibroblasts. **(C)** Culture based on the use of transwells. Keratinocytes either in monolayer, either in dermal equivalents are in the top well. Fibroblasts, either in monolayer either in dermal equivalent are in the bottom well. Soluble mediators cross the semipermeable transwell membrane. **(D)** Skin equivalent generated at the air liquid interphase. **(E)** Organotypic full skin culture obtained by skin biopsy. **(F)** Proportion of the studies addressing keratinocyte-fibroblast crosstalk which results are reviewed here.

One of these papers focused on MMPs and TIMP-1 showing that hydration enhances MMP1, MMP8, and MMP13 and decreases TIMP-1 production (34). One paper reported that hyper-hydration of partially stratified keratinocytes enhances the production of KGF by fibroblasts (34).

Physical stimuli were investigated in two papers. One focusing on keratinocyte exposure to UVB in the presence of estradiol (E2) reported that when exposed, fibroblasts responded by enhanced proliferation and EGF and lumican production (30). Another paper reported that keratinocytes exposed to micro-particles enhanced the fibroblast production of IL-1β, IL-6, TNF-α, PGE2, MMP-1, and MMP2 (14).

Keratinocytes primed with IL-17A were reported to enhance fibroblast production of IL-6, IL-8, MCP-1, and MMP-1 (13). Keratinocytes primed with IL-22 jointly with TNF-α were reported to enhance fibroblast production of IL-8, MCP-1, and MMP-1 when compared to keratinocytes unprimed or primed with IL-22 or TNF-α alone (18).

Specific Skin Pathologies (Table 3)

Five papers investigated the influence of keratinocytes on fibroblasts in SSc (13, 16, 24, 28, 36). Two reported increased col-I production compared to HD (16, 28), one of them indicating a TGF-β-independent enhancement (16), one reported enhanced IL-1-dependent gel contraction in which TGF-β and endothelin (ET)-1 were needed to observe gel contraction (36). One paper reported enhanced CTGF production, enhanced fibroblast migration, and proliferation with a role of S100A9 (24). SSc fibroblasts were reported to respond with higher production of col-I, similar production of MMP-1 with an increased ratio col-I over MMP-1, suggestive of decreased ECM turnover (13).

Eight papers investigated the influence of keratinocytes on fibroblasts in keloids. Three reported enhanced fibroblast proliferation (53, 54, 57) of which one also enhanced TGF-β production (53). One paper pointed to a reduced expression of S100A7 and S100A15, which were suggested to act as inhibitors (21); one concentrated on enhanced col-I production (56). A single paper reported enhanced production of TGF-β, oncostatin M (OSM), fibroblast-activating protein (FAP), αSMA, and laminin, compared to HD (37). Enhanced production of KGF by keloid keratinocytes resulting in enhanced release by fibroblasts of OSM, and col I was reported in one paper (28). One paper reported enhanced IL-18 production by keratinocytes resulting in enhanced production of IL-6, IL-8, and col-I by fibroblasts (32).

Two papers investigating the influence of keratinocytes on fibroblasts in hypertrophic scars reported an increase in matrix thickness, PDGF, and bFGF production compared to HD (31, 58).

Effects of Fibroblasts on Keratinocytes

Effect of Fibroblasts on Keratinocyte Proliferation, Survival, Adhesion, Keratin Expression

The effect of fibroblasts on keratinocyte proliferation was investigated in nine papers and reported to be increased in all of them (72, 74, 76, 82–84, 86, 87). Keratinocyte survival was reported to be enhanced in the presence of fibroblasts for reduced apoptosis, reduced expression of Bcl2, and enhanced expression of p53 (72, 78, 80). Keratinocyte adhesion and cadherin expression were reported to be enhanced in the presence of fibroblasts in two papers (72, 74). Keratinocyte differentiation was robustly reported to be enhanced in the presence of fibroblasts in four of four papers (73, 80–82), two of which specifically attributed this effect to fibroblasts from papillary compared to superficial dermis (73, 81). The influence of fibroblasts on keratin expression by keratinocytes was studied in two papers, one reporting enhanced expression of keratin 8 (29) and two others a reduced expression of keratins 6, 16, and 17 (80, 83). Fibroblasts were reported to enhance the deposition of basal membrane components by keratinocytes in three papers (73, 80, 81).

Effect of Soluble Factors or Altered Expression of Transcription Factors in Fibroblasts for Their Influence on Keratinocytes

Fibroblasts exposed to bFGF were reported to enhance keratinocyte differentiation in one study (70) and to reduce keratinocyte production of TGF-β in another study (75). Fibroblasts exposed to stromal cell-derived factor (SDF)-1 were reported to enhance keratinocyte proliferation and stratification in one study (71). Fibroblasts exposed to testosterone were reported to decrease keratinocyte differentiation in one study (69). Fibroblasts with inhibited expression of both peroxisome proliferator-activated receptor (PPAR)α and PPARδ were reported to enhance keratinocyte proliferation and their production of IL-1 and activator protein (AP)-1-targeted genes in one paper (79).

Specific Skin Pathologies (Table 3)

Fibroblasts from keloids and SSc were reported to enhance the production of oncostatin M (OSM) by HD keratinocytes in one paper (28).

Soluble Mediators of Inflammation Influencing the Crosstalk of Keratinocytes With Fibroblasts

Among the soluble mediators of inflammation produced by keratinocytes affecting fibroblast responses, IL-1 is robustly reported to be a relevant keratinocyte-derived mediator inducing fibroblast activation in eight of eight papers addressing this aspect (13, 17, 23, 36, 63–65, 82). Conversely, three of three papers reported that fibroblasts regulate epidermal homeostasis (proliferation and differentiation) through the secretion of KGF (28, 70, 83). Keratinocyte production of TGF-β by itself or in association with other mediators including IL-1 and ET-1 was reported to enhance col-I production by fibroblasts in three of four papers (13, 36, 49). The role of keratinocyte-derived stratifin, also known under the name 14.3.3 sigma, has been extensively investigated by one group that showed its role in enhanced MMPs and reduced col-I production by fibroblasts (33, 38, 39, 44, 45, 47, 51). Further, in the presence of fibroblasts, the same group showed enhanced stratifin production by keratinocytes (77). Keratinocytes were shown to produce fibronectin resulting in enhanced fibroblast migration (25). Keratinocytes were reported to produce IL-19, which resulted in enhanced KGF production

by fibroblasts. In its turn, KGF enhanced the IL-19 production by keratinocytes. Chemokine (C-C motif) ligand (CCL)26 (eotaxin-3) production by keratinocytes was reported to enhance fibroblast proliferation and motility (27). High mobility group box 1 (HMGB1) production by keratinocytes was reported to enhance fibroblast activation and αSMA expression (15). One study reported that parathyroid hormone-related protein (PTHrP) released by keratinocytes enhanced the production of KGF by fibroblasts (85). Finally, two studies reported that keratinocyte production of vesicles (whether microvesicles or exosomes) enhanced fibroblast activation with higher production of MMPs and a number of other mediators detected by microarrays (20, 38, 45).

Specific Skin Pathologies

In SSc, one paper reported enhanced col-I production induced by keratinocytes in a TGF-β-independent fashion (16), while a role for TGF-β was reported in two (13, 36). Expression of calprotectin, also known as S100A8/A9, was reported to be increased in keratinocytes from hypertrophic scars and SSc, resulting in enhanced fibroblast production of col-I and CTGF in two studies (19, 24). Psoriasin, also known as S100A7, was reported to be decreased in keratinocytes from keloids, a finding associated with increased col-I production by fibroblasts (21). Single papers have addressed the role of several other mediators. Collectively, the production by keratinocytes of IL-18 in keloids (32), PGE2 in dehydration (22), reduced TIMP production in hypertrophic scars (31), was associated with enhanced col-I production.

DISCUSSION

Our systematic review has retrieved 73 published papers investigating the interplay between keratinocytes and fibroblasts. Our main aim was to focus on fibrosis. While only 14 papers specifically aimed at skin fibrotic disorders, many focused on wound healing, which is a physiological condition considered to have several analogies with skin fibrosis, at least during the initial proliferative and synthetic phase (1). In this respect, it has to be underlined that the relatively little number of papers dedicated to this topic reflects, at least in part, the complexity of experimental settings needed to investigate the interactions between these two cell types with different requirements for optimal *in vitro* survival. This is particularly true for keratinocytes, which may undergo proliferation and differentiation under specific and mutually exclusive culture conditions. Not unexpectedly, compared to their undifferentiated counterpart, keratinocytes undergoing differentiation synthetize a distinct panel of proteins and soluble mediators and react differentially to exogenous stimuli, including those potentially provided by fibroblasts. For instance, a number of papers investigating the effect of keratinocytes on fibroblasts have used culture supernatants as effectors on fibroblasts. Furthermore, the supernatants may have been generated from non-primary keratinocyte cell lines, undifferentiated primary keratinocyte lines, and, in some instances, differentiated and stratified keratinocytes. Likely, the most physiologically relevant approaches to address the cross-talk between keratinocytes with fibroblasts were based on the use of epidermal equivalents or skin equivalents of full skin approaches. This information is provided in **Tables 1**, **2**, and **Figure 2F**. However, as limitation of our review, we have not weighted the relevance of the reported results based on the experimental assay used. Of particular importance to critically apprise the mutual relationship between keratinocytes and fibroblasts is the role of the basement membrane, which separates, holding together, the epidermis and dermis *in vivo* (88). In this respect, the papers specifically studying the structure and composition of the *in vitro*-generated basement membrane acquire additional value (73, 80, 81). The experimental settings leading to the results here reviewed were mostly based on the use of conditioned medium, skin equivalents, transwells, and cocultures each contributing to about one fifth of the total. Additional approaches took advantage on combinations of methods, histology on skin tissues, and more demanding skin explants. Given the existence of a basement membrane separating the epidermis from dermis, cell-to-cell contact effects between keratinocytes and fibroblasts could have limited physiological relevance. An additional point to consider is the possibility that dermal fibroblasts adapting to *in vitro* culture growth may lose some of their tissue-specific characteristics, then impacting on their effects on keratinocytes.

Notwithstanding these considerations, the wealth of retrieved papers clearly highlights the interest in the problematics of keratinocyte to fibroblast crosstalk and the capacity of these cell types to mutually influence each other. The majority of the retrieved papers investigated how keratinocytes interact with fibroblasts in the context of wound healing, using keratinocytes and fibroblasts generated from healthy individuals, with 14 papers investigating how this interaction is modified and characteristic of pathologic conditions. Overall, a large agreement characterizes the results indicating that also in homeostatic conditions, the crosstalk between keratinocytes and fibroblasts has an impact on both cell types and ultimately on the structure of both epidermis and dermis. However, the outcome of the interactions and the factors contributing to the crosstalk were heterogeneously investigated, and in some cases, the reported results were inconsistent.

Strong evidence supports a role for keratinocyte-produced IL-1 in inducing fibroblast production of KGF, GM-CSF, TGFα, IL-6, IL-8, IL-1, the expression of COX2 and PGE2 production (**Figures 3A–D**). In its turn, KGF, GM-CSF, and PGE2 promote keratinocyte proliferation and favor proper keratinocyte differentiation (**Figures 3A,B,D**). Simultaneously, TGFα enhances the expression on keratinocytes of both receptors for KGF (FGFR2b) and GM-CSF (GM-CSF-R), thus favoring keratinocyte responses to these ligands (**Figure 3B**). Furthermore, PGE2, IL-6, GM-CSF, and KGF produced by fibroblasts enhance IL-1 production by keratinocytes, thus promoting a positive forward amplification loop (**Figure 3D**). Not last, the autocrine production of IL-1 by fibroblasts may amplify fibroblast production of several mediators including KGF and GM-CSF (**Figures 3A,D**). It is of interest to notice that the circuitries here reported and highlighted in **Figure 3** all propose

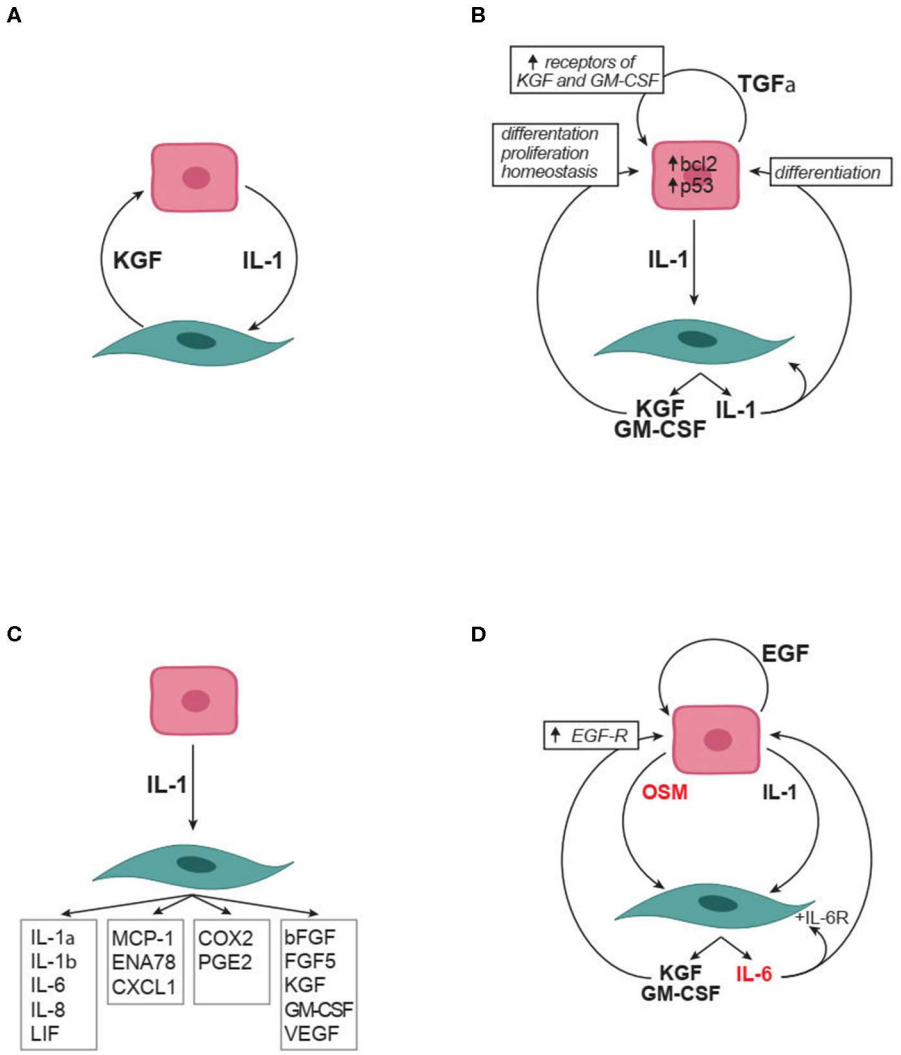

FIGURE 3 | Soluble factors in the crosstalk between keratinocytes and fibroblasts. **(A)** IL-1 and KGF are soluble mediators robustly identified as involved in the crosstalk. **(B)** Autocrine and paracrine effects relevant to IL-1 and KGF role in the crosstalk. **(C)** The many effects of keratinocyte produced IL-1 on fibroblasts. **(D)** Synergistic effect of IL-1 with IL-6 family members (in red) on the crosstalk. Arrowheads indicate enhancement. bFGF, basic fibroblast growth factor; COX2, Cyclooxygenase 2; CXCL, chemokine containing the CXC motif; EGF, epidermal growth factor which comprises multiple mediators including transforming growth factor-α, amphiregulin, heparin binding-EGF, and epiregulin; ENA-78, Epithelial neutrophil-activating protein 78; FGF, fibroblast growth factor; GM-CSF, granulocyte-monocyte colony stimulating factor IL, interleukin; KGF, keratinocyte growth factor (also known as FGF7); LIF, leukemia inhibitory factor; MCP-1, monocyte chemotactic protein-1; OSM, oncostatin M;PGE2, Prostaglandin E2; TGF, Transforming growth factor; VEGF, vascular endothelial growth factor.

positive feedforward effects. It is very unlikely that this reflects the reality since biological systems have inbuilt physiological modulators and inhibitors. Thus, further homeostatic factors and inhibitory mechanisms important in the crosstalk between keratinocytes and fibroblasts likely will be identified in future work. It is, however, true that feed-forward mechanisms may participate in pathological processes.

Several papers retrieved in our systematic review address the effect of keratinocytes on ECM component production by fibroblasts. Controversial are the results reported on collagen deposition and other ECM components. Thus, while a majority of studies (eight of 12) demonstrate an inhibitory role of keratinocytes, four of 12 papers reported an enhancing effect of keratinocytes on collagen production (**Figure 4A**). One paper proposed for the enhanced production of collagen a TGF-β-independent keratinocyte contribution (16), the others via TGF-β. It is difficult to reconcile these contradictory results; however, substantial differences in the experimental settings including the culture medium composition, the differentiation status of keratinocytes, as well as the methods used to quantify collagen may explain the differences observed. For future studies, it will be important to standardize further the experimental settings to allow robust comparisons across results.

Consistent with the majority of reports showing a decreased production of collagen by fibroblasts under the influence of keratinocytes, the fibroblast production of TGF-β and

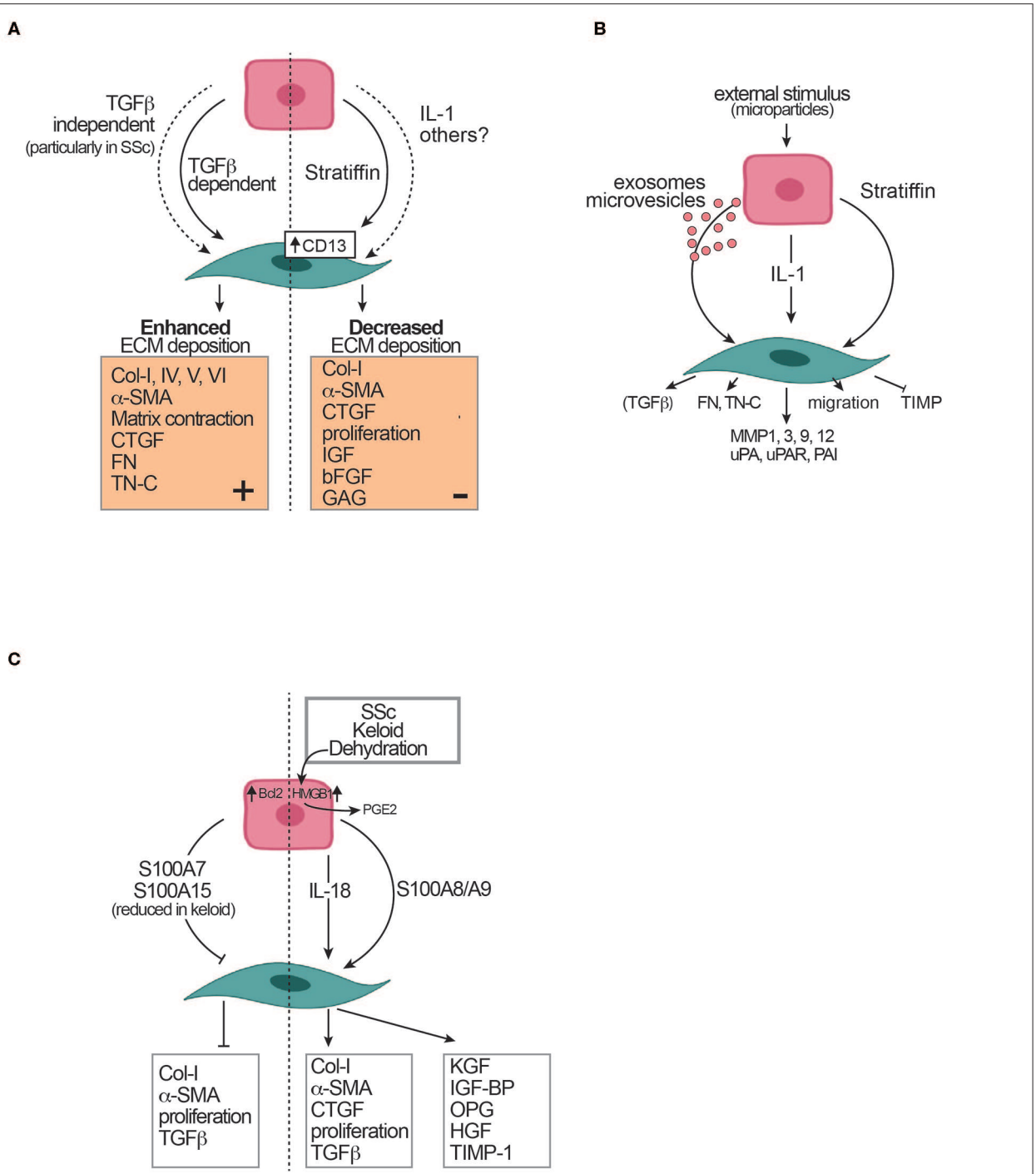

FIGURE 4 | Effects of keratinocytes on fibroblasts and extracellular matrix (ECM). **(A)** Controversial effects of keratinocytes on ECM deposition. **(B)** Mediators of keratinocyte effects on fibroblasts. **(C)** Skin pathological conditions and their effects on the crosstalk between keratinocytes and fibroblasts. The dotted vertical line separates controversial evidence. Arrowheads indicate enhancement. Blunted heads indicate inhibition. αSMA, alpha-smooth muscle actin; Bcl2, B-cell lymphoma 2; bFGF, basic fibroblast growth factor; Col, collagen; CTGF, connective tissue growth factor; FN, fibronectin; HGF, hepatocyte growth factor; HMGB1, high mobility group box-1; IGF, insulin-like growth factor; IGF-BP, insulin-like growth factor binding protein; KGF, keratinocyte growth factor; MMP, metalloproteinase; OPG, osteoprotegerin; OSM, oncostatin M; PAI, plasminogen activator inhibitor; PDGF, platelet-derived growth factor; PGE2, Prostaglandin E2; S100A7, psoriasin; S100A8/A9, calprotectin; S100A15,koebnerisin; SSc, Systemic sclerosis; SSc-F, SSc fibroblasts; SSc-K, SSc keratinocytes; TGF, Transforming growth factor; TIMP, tissue inhibitor of MMP; TN-C, tenascin C; TNFα, Tumor necrosis factor α; uPA, urokinase-type plasminogen activator; uPAR, urokinase-type plasminogen activator receptor.

CTGF was reported to be downregulated by keratinocytes. However, keratinocytes form keloids, hypertrophic scars, and SSc that distinctly showed enhanced expression of the alarmin S100A8/A9, which directly favored collagen and CTGF production and αSMA expression by fibroblasts, thus pointing to pathology-associated differences compared to controls (**Figure 4C**). Further, among the states of perturbed homeostasis, keratinocyte dehydration was frequently investigated and consistently found to favor profibrotic responses in fibroblasts (**Figure 4C**). Finally, decreased expression of S100A7 and S100A15 in keloids may mechanistically be linked to enhanced collagen production since they were reported to be inhibitory (21).

In contrast with the inconsistent results reported on collagen production, there was a strong agreement among reports showing that keratinocytes enhance MMP production by fibroblasts (**Figure 4B**). One paper reported, in addition, a decreased production of TIMP by fibroblasts under the influence of keratinocytes. Overall, the picture that emerges from these studies supports a model in which keratinocytes favor ECM turnover by favoring MMP over a concomitant decreased or alternatively increased collagen production by fibroblasts. Of interest, one paper exploring this issue reports that in SSc compared to healthy controls, the ratio of collagen over MMP-1 is distinctly in favor of enhanced deposition, such as an effect not being present in HD (13). IL-1 stands out among the soluble factors produced by keratinocytes involved in the enhanced production of MMPs by fibroblasts (**Figure 4B**). In addition, one group has devoted enormous attention to the role of stratifin expressed by keratinocytes in inducing MMP and decreasing collagen, CTGF, insulin-like growth factor (IGF), bFGF, glycosaminoglycan (GAG) production as well as the expression of αSMA by fibroblasts (**Figures 4A,B**). Of further interest, the possibility that exosomes released by keratinocytes may be, at least in part, mediators of this effect (38) and that soluble factors released by fibroblasts may modulate stratifin production by keratinocytes (77).

Concerning the influence of fibroblasts on keratinocytes, the literature provides solid and consistent evidence that, in the presence of fibroblasts, keratinocytes show enhanced proliferation, reduced apoptosis, physiological differentiation, enhanced basement membrane deposition (**Figure 5**). These effects are mediated mostly by KGF (**Figure 3A**). Other important soluble factors are HGF and PGE2 (**Figure 5**). Of interest, TGF-β and myofibroblasts exert an inhibitory role particularly on keratinocyte differentiation and proliferation. Further, the deficiency of PPARα and PPARδ in fibroblasts promotes keratinocyte proliferation and, among others, enhanced IL-1 production (**Figure 5**). However, only two papers provided data on the effect of fibroblasts on keratinocytes in fibrotic disorders (28, 37) showing stronger effects of fibroblasts from fibrotic disorders. The paucity of studies exploring this topic most likely may be explained by the fact that keratinocytes are not currently integrated in physiopathological models of fibrosis development. However, the recent documentation of altered keratinocyte differentiation and inflammatory response in skin fibrosis begs the question whether these abnormalities are primary or secondary to dermal fibrosis. Thus, at the moment, it remains an interesting area of research to investigate whether fibroblasts generated form SSc may affect keratinocyte behavior.

CONCLUSIONS

Evidence generated in recent years and reviewed here strengthen a role for keratinocytes in participating in dermal fibrosis. Whether this is a modulatory role rather than an initiation role remains to be established firmly. Murine models support the possibility that keratinocytes may indeed instruct fibroblast to enhance ECM deposition. For instance, Brakebusch et al., observed the development of dermal fibrosis in a mouse deficient for the β1 integrin subunit in keratinocytes (89). Similarly, the keratinocyte-specific genetic deletion of Friend leukemia virus integration 1 (Fli1) induced in mice a SSc-like phenotype with skin, esophageal, and lung involvement (90). To further

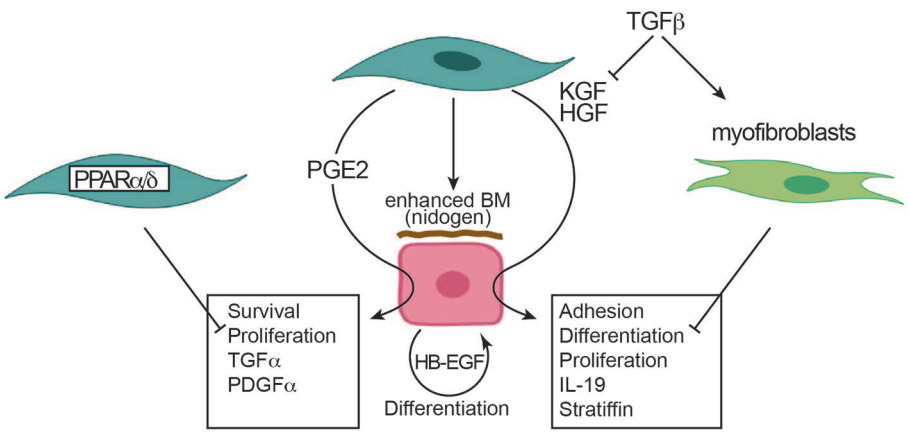

FIGURE 5 | Effects of fibroblasts on keratinocytes. Arrowheads indicate enhancement. Blunted heads indicate inhibition. BM, basal membrane; HB-EGF, heparin binding EGF like growth factor; HGF, hepatocyte growth factor; IL, interleukin; KGF, keratinocyte growth factor; PDGF, platelet derived growth factor; PGE2, prostaglandin E2; PPAR, peroxisome proliferator-activated receptor; TGF, transforming growth factor.

strengthen this point, a system level analysis based on consensus clustering of genes expressed in human SSc skin revealed that keratinocytes make major connections with the inflammation network, thus highlighting their role in SSc (91).

Further work is required to better understand the reciprocal role of keratinocytes and fibroblasts and their interactions at initiation and stabilization of skin fibrosis. In this respect, novel sophisticated technical approaches may provide important new information. For instance, the generation of human skin equivalents where keratinocytes, dermal fibroblasts, and endothelial cells are grown on a biological scaffold and perfused at physiological pressure have very recently been shown to respond to fibrotic stimuli (92). Thus, vascularized skin equivalents can replicate key features of fibrotic skin and may serve as a platform to better understand the interplay between different cell types including keratinocytes and fibroblasts in pathophysiologically relevant human setting. Skin generated from stem cells and human organoids or humanized mouse models may provide additional tools for approaching similar questions (93). A complementary *ex vivo* approach would be the use of precision cut slices of healthy and diseased human skin, which would recapitulate the organ architecture then analyzed by advanced imaging techniques (94). Further, single-cell mRNA studies from cells freshly obtained from healthy and diseased skin will expand our knowledge, particularly comparing wound healing to fibrotic skin disoders. These approaches will possibly capture the subtle mechanisms involved in rapid termination of ECM deposition, which very likely distinguish physiological reparative processes from pathological fibrosis. This may lead to the development of novel therapeutic strategies.

AUTHOR CONTRIBUTIONS

BR performed the systematic review of the literature. BR, NB, and CC drafted the manuscript, reviewed its contents, and approved its final version.

FUNDING

This work was supported, in part, by grant 310030-159999 from the Swiss National Science Foundation and by a grant from sclerodermie.ch (Swiss Scleroderma Patient organization) to CC. BR was supported, in part, by a grant from the Ernst and Lucie Schmidheiny Foundation.

REFERENCES

1. Rockey DC, Bell PD, Hill JA. Fibrosis–a common pathway to organ injury and failure. *N Engl J Med.* (2015) 372:1138–49. doi: 10.1056/NEJMra1300575
2. Distler JHW, Gyorfi AH, Ramanujam M, Whitfield ML, Konigshoff M, Lafyatis R. Shared and distinct mechanisms of fibrosis. *Nat Rev Rheumatol.* (2019) 15:705–30. doi: 10.1038/s41584-019-0322-7
3. Duffield JS, Lupher M, Thannickal VJ, Wynn TA. Host responses in tissue repair and fibrosis. *Annu Rev Pathol.* (2013) 8:241–76. doi: 10.1146/annurev-pathol-020712-163930
4. Boin F, Chizzolini C. Inflammation and immunity. In: Varga J, Denton C, Wigley F, Allanore Y, Kuwana M, editors. *Scleroderma: From Pathogenesis to Comprehensive Management*. New York, NY: Springer (2017). p. 161–96.
5. Lodyga M, Hinz B. TGF-β–a truly transforming growth factor in fibrosis and immunity. *Semin Cell Dev Biol.* (2020) 101:123–39. doi: 10.1016/j.semcdb.2019.12.010
6. Gabbiani G, Majno G. Dupuytren's contracture: fibroblast contraction? An ultrastructural study. *Am J Pathol.* (1972) 66:131–46.
7. Hinz B, Phan SH, Thannickal VJ, Galli A, Bochaton-Piallat ML, Gabbiani G. The myofibroblast: one function, multiple origins. *Am J Pathol.* (2007) 170:1807–16. doi: 10.2353/ajpath.2007.070112
8. Hinz B, Phan SH, Thannickal VJ, Prunotto M, Desmouliere A, Varga J, et al. Recent developments in myofibroblast biology: paradigms for connective tissue remodeling. *Am J Pathol.* (2012) 180:1340–55. doi: 10.1016/j.ajpath.2012.02.004
9. Gabrielli A, Avvedimento EV, Krieg T. Scleroderma. *N Engl J Med.* (2009) 360:1989–2003. doi: 10.1056/NEJMra0806188
10. Hummers LK, Tyndall A. Scleroderma mimics. In: Varga J, Denton C, Wigley F, Allanore Y, Kuwana M, editors. *Scleroderma: From Pathogenesis to Comprehensive Management*. New York, NY: Springer (2017). p. 115–23. doi: 10.1007/978-3-319-31407-5_9
11. Rousselle P, Braye F, Dayan G. Re-epithelialization of adult skin wounds: cellular mechanisms and therapeutic strategies. *Adv Drug Deliv Rev.* (2019) 146:344–65. doi: 10.1016/j.addr.2018.06.019
12. Moher D, Liberati A, Tetzlaff J, Altman DG. Preferred reporting items for systematic reviews and meta-analyses: the PRISMA statement. *PLoS Med.* (2009) 6:e1000097. doi: 10.1371/journal.pmed.1000097
13. Dufour AM, Borowczyk-Michalowska J, Alvarez M, Truchetet ME, Modarressi A, Brembilla NC, et al. IL-17A dissociates inflammation from fibrogenesis in systemic sclerosis (scleroderma). *J Invest Dermatol.* (2020) 140:103–12. doi: 10.1016/j.jid.2019.05.026
14. Fernando IPS, Jayawardena TU, Kim HS, Vaas A, De Silva HIC, Nanayakkara CM, et al. A keratinocyte and integrated fibroblast culture model for studying particulate matter-induced skin lesions and therapeutic intervention of fucosterol. *Life Sci.* (2019) 233:116714. doi: 10.1016/j.lfs.2019.116714
15. Zhao J, Yu J, Xu Y, Chen L, Zhou F, Zhai Q, et al. Epidermal HMGB1 activates dermal fibroblasts and causes hypertrophic scar formation in reduced hydration. *J Invest Dermatol.* (2018) 138:2322–32. doi: 10.1016/j.jid.2018.04.036
16. McCoy SS, Reed TJ, Berthier CC, Tsou PS, Liu J, Gudjonsson JE, et al. Scleroderma keratinocytes promote fibroblast activation independent of transforming growth factor beta. *Rheumatology.* (2017) 56:1970–81. doi: 10.1093/rheumatology/kex280
17. Carr MJ, Li Y, Rezakhanlou AM, Ghahary A. Keratinocyte-releasable factors stimulate the expression of granulocyte colony-stimulating factor in human dermal fibroblasts. *J Cell Biochem.* (2017) 118:308–17. doi: 10.1002/jcb.25638
18. Brembilla NC, Dufour AM, Alvarez M, Hugues S, Montanari E, Truchetet ME, et al. IL-22 capacitates dermal fibroblast responses to TNF in scleroderma. *Ann Rheum Dis.* (2016) 75:1697–705. doi: 10.1136/annrheumdis-2015-207477
19. Zhong A, Xu W, Zhao J, Xie P, Jia S, Sun J, et al. S100A8 and S100A9 are induced by decreased hydration in the epidermis and promote fibroblast activation and fibrosis in the dermis. *Am J Pathol.* (2016) 186:109–22. doi: 10.1016/j.ajpath.2015.09.005
20. Huang P, Bi J, Owen GR, Chen W, Rokka A, Koivisto L, et al. Keratinocyte microvesicles regulate the expression of multiple genes in dermal fibroblasts. *J Invest Dermatol.* (2015) 135:3051–9. doi: 10.1038/jid.2015.320
21. Gauglitz GG, Bureik D, Zwicker S, Ruzicka T, Wolf R. The antimicrobial peptides psoriasin (S100A7) and koebnerisin (S100A15) suppress extracellular matrix production and proliferation of human fibroblasts. *Skin Pharmacol Physiol.* (2015) 28:115–23. doi: 10.1159/000363579
22. Xu W, Hong SJ, Zeitchek M, Cooper G, Jia S, Xie P, et al. Hydration status regulates sodium flux and inflammatory pathways through epithelial sodium channel (ENaC) in the skin. *J Invest Dermatol.* (2015) 135:796–806. doi: 10.1038/jid.2014.477
23. Arai KY, Fujioka A, Okamura R, Nishiyama T. Stimulatory effect of fibroblast-derived prostaglandin E(2) on keratinocyte stratification in the skin equivalent. *Wound Repair Regen.* (2014) 22:701–11. doi: 10.1111/wrr.12228

24. Nikitorowicz-Buniak J, Shiwen X, Denton CP, Abraham D, Stratton R. Abnormally differentiating keratinocytes in the epidermis of systemic sclerosis patients show enhanced secretion of CCN2 and S100A9. *J Invest Dermatol.* (2014) 134:2693–702. doi: 10.1038/jid.2014.253
25. Li X, Qian H, Ono F, Tsuchisaka A, Krol RP, Ohara K, et al. Human dermal fibroblast migration induced by fibronectin in autocrine and paracrine manners. *Exp Dermatol.* (2014) 23:682–4. doi: 10.1111/exd.12447
26. Varkey M, Ding J, Tredget EE. Fibrotic remodeling. of tissue-engineered skin with deep dermal fibroblasts is reduced by keratinocytes. *Tissue Eng A.* (2014) 20:716–27. doi: 10.1089/ten.TEA.2013.0434
27. Sun DP, Yeh CH, So E, Wang LY, Wei TS, Chang MS, et al. Interleukin (IL)-19 promoted skin wound healing by increasing fibroblast keratinocyte growth factor expression. *Cytokine.* (2013) 62:360–8. doi: 10.1016/j.cyto.2013.03.017
28. Canady J, Arndt S, Karrer S, Bosserhoff AK. Increased KGF expression promotes fibroblast activation in a double paracrine manner resulting in cutaneous fibrosis. *J Invest Dermatol.* (2013) 133:647–57. doi: 10.1038/jid.2012.389
29. Kolar M, Szabo P, Dvorankova B, Lacina L, Gabius HJ, Strnad H, et al. Upregulation of IL-6, IL-8 and CXCL-1 production in dermal fibroblasts by normal/malignant epithelial cells *in vitro*: immunohistochemical and transcriptomic analyses. *Biol Cell.* (2012) 104:738–51. doi: 10.1111/boc.201200018
30. Rock K, Meusch M, Fuchs N, Tigges J, Zipper P, Fritsche E, et al. Estradiol protects dermal hyaluronan/versican matrix during photoaging by release of epidermal growth factor from keratinocytes. *J Biol Chem.* (2012) 287:20056–69. doi: 10.1074/jbc.M112.353151
31. Simon F, Bergeron D, Larochelle S, Lopez-Valle CA, Genest H, Armour A, et al. Enhanced secretion of TIMP-1 by human hypertrophic scar keratinocytes could contribute to fibrosis. *Burns.* (2012) 38:421–7. doi: 10.1016/j.burns.2011.09.001
32. Do DV, Ong CT, Khoo YT, Carbone A, Lim CP, Wang S, et al. Interleukin-18 system plays an important role in keloid pathogenesis via epithelial-mesenchymal interactions. *Br J Dermatol.* (2012) 166:1275–88. doi: 10.1111/j.1365-2133.2011.10721.x
33. Lai A, Ghaffari A, Li Y, Ghahary A. Paracrine regulation of fibroblast aminopeptidase N/CD13 expression by keratinocyte-releasable stratifin. *J Cell Physiol.* (2011) 226:3114–20. doi: 10.1002/jcp.22666
34. Tandara AA, Mustoe TA. MMP- and TIMP-secretion by human cutaneous keratinocytes and fibroblasts–impact of coculture and hydration. *J Plast Reconstr Aesthet Surg.* (2011) 64:108–16. doi: 10.1016/j.bjps.2010.03.051
35. Koskela A, Engstrom K, Hakelius M, Nowinski D, Ivarsson M. Regulation of fibroblast gene expression by keratinocytes in organotypic skin culture provides possible mechanisms for the antifibrotic effect of reepithelialization. *Wound Repair Regen.* (2010) 18:452–9. doi: 10.1111/j.1524-475X.2010.00605.x
36. Aden N, Nuttall A, Shiwen X, de Winter P, Leask A, Black CM, et al. Epithelial cells promote fibroblast activation via IL-1alpha in systemic sclerosis. *J Invest Dermatol.* (2010) 130:2191–200. doi: 10.1038/jid.2010.120
37. Lim CP, Phan TT, Lim IJ, Cao X. Cytokine profiling and Stat3 phosphorylation in epithelial-mesenchymal interactions between keloid keratinocytes and fibroblasts. *J Invest Dermatol.* (2009) 129:851–61. doi: 10.1038/jid.2008.337
38. Chavez-Munoz C, Kilani RT, Ghahary A. Profile of exosomes related proteins released by differentiated and undifferentiated human keratinocytes. *J Cell Physiol.* (2009) 221:221–31. doi: 10.1002/jcp.21847
39. Ghaffari A, Kilani RT, Ghahary A. Keratinocyte-conditioned media regulate collagen expression in dermal fibroblasts. *J Invest Dermatol.* (2009) 129:340–7. doi: 10.1038/jid.2008.253
40. Wall IB, Bhadal N, Broad S, Whawell SA, Mudera V, Lewis MP. Force generation and protease gene expression in organotypic co-cultures of fibroblasts and keratinocytes. *J Tissue Eng Regen Med.* (2009) 3:647–50. doi: 10.1002/term.206
41. Tandara AA, Kloeters O, Mogford JE, Mustoe TA. Hydrated keratinocytes reduce collagen synthesis by fibroblasts via paracrine mechanisms. *Wound Repair Regen.* (2007) 15:497–504. doi: 10.1111/j.1524-475X.2007.00257.x
42. Amjad SB, Carachi R, Edward M. Keratinocyte regulation of TGF-beta and connective tissue growth factor expression: a role in suppression of scar tissue formation. *Wound Repair Regen.* (2007) 15:748–55. doi: 10.1111/j.1524-475X.2007.00281.x
43. Harrison CA, Gossiel F, Bullock AJ, Sun T, Blumsohn A, Mac Neil S. Investigation of keratinocyte regulation of collagen I synthesis by dermal fibroblasts in a simple *in vitro* model. *Br J Dermatol.* (2006) 154:401–10. doi: 10.1111/j.1365-2133.2005.07022.x
44. Ghaffari A, Li Y, Karami A, Ghaffari M, Tredget EE, Ghahary A. Fibroblast extracellular matrix gene expression in response to keratinocyte-releasable stratifin. *J Cell Biochem.* (2006) 98:383–93. doi: 10.1002/jcb.20782
45. Harrison CA, Dalley AJ, Mac Neil S. A simple *in vitro* model for investigating epithelial/mesenchymal interactions: keratinocyte inhibition of fibroblast proliferation and fibronectin synthesis. *Wound Repair Regen.* (2005) 13:543–50. doi: 10.1111/j.1524-475X.2005.00076.x
46. Chinnathambi S, Bickenbach JR. Human skin and gingival keratinocytes show differential regulation of matrix metalloproteinases when combined with fibroblasts in 3-dimensional cultures. *J Periodontol.* (2005) 76:1072–83. doi: 10.1902/jop.2005.76.7.1072
47. Ghahary A, Marcoux Y, Karimi-Busheri F, Li Y, Tredget EE, Kilani RT, et al. Differentiated keratinocyte-releasable stratifin (14-3-3 sigma) stimulates MMP-1 expression in dermal fibroblasts. *J Invest Dermatol.* (2005) 124:170–7. doi: 10.1111/j.0022-202X.2004.23521.x
48. Sawicki G, Marcoux Y, Sarkhosh K, Tredget EE, Ghahary A. Interaction of keratinocytes and fibroblasts modulates the expression of matrix metalloproteinases-2 and−9 and their inhibitors. *Mol Cell Biochem.* (2005) 269:209–16. doi: 10.1007/s11010-005-3178-x
49. Shephard P, Hinz B, Smola-Hess S, Meister JJ, Krieg T, Smola H. Dissecting the roles of endothelin, TGF-beta and GM-CSF on myofibroblast differentiation by keratinocytes. *Thromb Haemost.* (2004) 92:262–74. doi: 10.1160/TH03-11-0669
50. Shephard P, Martin G, Smola-Hess S, Brunner G, Krieg T, Smola H. Myofibroblast differentiation is induced in keratinocyte-fibroblast co-cultures and is antagonistically regulated by endogenous transforming growth factor-beta and interleukin-1. *Am J Pathol.* (2004) 164:2055–66. doi: 10.1016/S0002-9440(10)63764-9
51. Ghahary A, Karimi-Busheri F, Marcoux Y, Li Y, Tredget EE, Taghi Kilani R, et al. Keratinocyte-releasable stratifin functions as a potent collagenase-stimulating factor in fibroblasts. *J Invest Dermatol.* (2004) 122:1188–97. doi: 10.1111/j.0022-202X.2004.22519.x
52. Satish L, Yager D, Wells A. Glu-Leu-Arg-negative CXC chemokine interferon gamma inducible protein-9 as a mediator of epidermal-dermal communication during wound repair. *J Invest Dermatol.* (2003) 120:1110–7. doi: 10.1046/j.1523-1747.2003.12230.x
53. Funayama E, Chodon T, Oyama A, Sugihara T. Keratinocytes promote proliferation and inhibit apoptosis of the underlying fibroblasts: an important role in the pathogenesis of keloid. *J Invest Dermatol.* (2003) 121:1326–31. doi: 10.1111/j.1523-1747.2003.12572.x
54. Phan TT, Lim IJ, Bay BH, Qi R, Longaker MT, Lee ST, et al. Role of IGF system of mitogens in the induction of fibroblast proliferation by keloid-derived keratinocytes *in vitro*. *Am J Physiol Cell Physiol.* (2003) 284:C860–9. doi: 10.1152/ajpcell.00350.2002
55. Gron B, Stoltze K, Andersson A, Dabelsteen E. Oral fibroblasts produce more HGF and KGF than skin fibroblasts in response to co-culture with keratinocytes. *APMIS.* (2002) 110:892–8. doi: 10.1034/j.1600-0463.2002.1101208.x
56. Lim IJ, Phan TT, Bay BH, Qi R, Huynh H, Tan WT, et al. Fibroblasts cocultured with keloid keratinocytes: normal fibroblasts secrete collagen in a keloidlike manner. *Am J Physiol Cell Physiol.* (2002) 283:C212–22. doi: 10.1152/ajpcell.00555.2001
57. Lim IJ, Phan TT, Song C, Tan WT, Longaker MT. Investigation of the influence of keloid-derived keratinocytes on fibroblast growth and proliferation *in vitro*. *Plast Reconstr Surg.* (2001) 107:797–808. doi: 10.1097/00006534-200103000-00022
58. Niessen FB, Andriessen MP, Schalkwijk J, Visser L, Timens W. Keratinocyte-derived growth factors play a role in the formation of hypertrophic scars. *J Pathol.* (2001) 194:207–16. doi: 10.1002/path.853
59. Maas-Szabowski N, Stark HJ, Fusenig NE. Keratinocyte growth regulation in defined organotypic cultures through IL-1-induced keratinocyte growth factor expression in resting fibroblasts. *J Invest Dermatol.* (2000) 114:1075–84. doi: 10.1046/j.1523-1747.2000.00987.x

60. Zhang L, Ishikawa O, Takeuchi Y, Yokoyama Y, Miyachi Y. Influences of keratinocyte-fibroblast interaction on the expression of epimorphin by fibroblasts *in vitro*. *J Dermatol Sci.* (1999) 20:191–6. doi: 10.1016/S0923-1811(98)00081-4
61. Garner WL. Epidermal regulation of dermal fibroblast activity. *Plast Reconstr Surg.* (1998) 102:135–9. doi: 10.1097/00006534-199807000-00021
62. Ralston DR, Layton C, Dalley AJ, Boyce SG, Freedlander E, MacNeil S. Keratinocytes contract human dermal extracellular matrix and reduce soluble fibronectin production by fibroblasts in a skin composite model. *Br J Plast Surg.* (1997) 50:408–15. doi: 10.1016/S0007-1226(97)90327-1
63. Sato T, Kirimura Y, Mori Y. The co-culture of dermal fibroblasts with human epidermal keratinocytes induces increased prostaglandin E2 production and cyclooxygenase 2 activity in fibroblasts. *J Invest Dermatol.* (1997) 109:334–9. doi: 10.1111/1523-1747.ep12335935
64. Boxman IL, Ruwhof C, Boerman OC, Lowik CW, Ponec M. Role of fibroblasts in the regulation of proinflammatory interleukin IL-1, IL-6, and IL-8 levels induced by keratinocyte-derived IL-1. *Arch Dermatol Res.* (1996) 288:391–8. doi: 10.1007/BF02507108
65. Chang CC, Kuo YF, Chiu HC, Lee JL, Wong TW, Jee SH. Hydration, not silicone, modulates the effects of keratinocytes on fibroblasts. *J Surg Res.* (1995) 59:705–11. doi: 10.1006/jsre.1995.1227
66. Lacroix M, Bovy T, Nusgens BV, Lapiere CM. Keratinocytes modulate the biosynthetic phenotype of dermal fibroblasts at a pretranslational level in a human skin equivalent. *Arch Dermatol Res.* (1995) 287:659–64. doi: 10.1007/BF00371739
67. Boxman I, Lowik C, Aarden L, Ponec M. Modulation of IL-6 production and IL-1 activity by keratinocyte-fibroblast interaction. *J Invest Dermatol.* (1993) 101:316–24. doi: 10.1111/1523-1747.ep12365474
68. Waelti ER, Inaebnit SP, Rast HP, Hunziker T, Limat A, Braathen LR, et al. Co-culture of human keratinocytes on post-mitotic human dermal fibroblast feeder cells: production of large amounts of interleukin 6. *J Invest Dermatol.* (1992) 98:805–8. doi: 10.1111/1523-1747.ep12499961
69. Kumtornrut C, Yamauchi T, Koike S, Aiba S, Yamasaki K. Androgens modulate keratinocyte differentiation indirectly through enhancing growth factor production from dermal fibroblasts. *J Dermatol Sci.* (2019) 93:150–8. doi: 10.1016/j.jdermsci.2019.01.007
70. Yang L, Zhang D, Wu H, Xie S, Zhang M, Zhang B, et al. Basic fibroblast growth factor influences epidermal homeostasis of living skin equivalents through affecting fibroblast phenotypes and functions. *Skin Pharmacol Physiol.* (2018) 31:229–37. doi: 10.1159/000488992
71. Quan C, Cho MK, Shao Y, Mianecki LE, Liao E, Perry D, et al. Dermal fibroblast expression of stromal cell-derived factor-1 (SDF-1) promotes epidermal keratinocyte proliferation in normal and diseased skin. *Protein Cell.* (2015) 6:890–903. doi: 10.1007/s13238-015-0198-5
72. Fernandez TL, Van Lonkhuyzen DR, Dawson RA, Kimlin MG, Upton Z. *In vitro* investigations on the effect of dermal fibroblasts on keratinocyte responses to ultraviolet B radiation. *Photochem Photobiol.* (2014) 90:1332–9. doi: 10.1111/php.12317
73. Varkey M, Ding J, Tredget EE. Superficial dermal fibroblasts enhance basement membrane and epidermal barrier formation in tissue-engineered skin: implications for treatment of skin basement membrane disorders. *Tissue Eng A.* (2014) 20:540–52. doi: 10.1089/ten.TEA.2013.0160
74. Chowdhury SR, Aminuddin BS, Ruszymah BH. Effect of supplementation of dermal fibroblasts conditioned medium on expansion of keratinocytes through enhancing attachment. *Indian J Exp Biol.* (2012) 50:332–9.
75. Yang L, Hashimoto K, Tohyama M, Okazaki H, Dai X, Hanakawa Y, et al. Interactions between myofibroblast differentiation and epidermogenesis in constructing human living skin equivalents. *J Dermatol Sci.* (2012) 65:50–7. doi: 10.1016/j.jdermsci.2011.10.008
76. Wang Z, Wang Y, Farhangfar F, Zimmer M, Zhang Y. Enhanced keratinocyte proliferation and migration in co-culture with fibroblasts. *PLoS ONE.* (2012) 7:e40951. doi: 10.1371/journal.pone.0040951
77. Carr M, Chavez-Munoz C, Lai A, Ghahary A. Dermal fibroblasts influence the expression profile of 14-3-3 proteins in human keratinocytes. *Mol Cell Biochem.* (2011) 353:205–14. doi: 10.1007/s11010-011-0788-3
78. Peura M, Siltanen A, Saarinen I, Soots A, Bizik J, Vuola J, et al. Paracrine factors from fibroblast aggregates in a fibrin-matrix carrier enhance keratinocyte viability and migration. *J Biomed Mater Res A.* (2010) 95:658–64. doi: 10.1002/jbm.a.32881
79. Chong HC, Tan MJ, Philippe V, Tan SH, Tan CK, Ku CW, et al. Regulation of epithelial-mesenchymal IL-1 signaling by PPARbeta/delta is essential for skin homeostasis and wound healing. *J Cell Biol.* (2009) 184:817–31. doi: 10.1083/jcb.200809028
80. El Ghalbzouri A, Ponec M. Diffusible factors released by fibroblasts support epidermal morphogenesis and deposition of basement membrane components. *Wound Repair Regen.* (2004) 12:359–67. doi: 10.1111/j.1067-1927.2004.012306.x
81. Sorrell JM, Baber MA, Caplan AI. Site-matched papillary and reticular human dermal fibroblasts differ in their release of specific growth factors/cytokines and in their interaction with keratinocytes. *J Cell Physiol.* (2004) 200:134–45. doi: 10.1002/jcp.10474
82. Maas-Szabowski N, Starker A, Fusenig NE. Epidermal tissue regeneration and stromal interaction in HaCaT cells is initiated by TGF-alpha. *J Cell Sci.* (2003) 116:2937–48. doi: 10.1242/jcs.00474
83. El Ghalbzouri A, Lamme E, Ponec M. Crucial role of fibroblasts in regulating epidermal morphogenesis. *Cell Tissue Res.* (2002) 310:189–99. doi: 10.1007/s00441-002-0621-0
84. el-Ghalbzouri A, Gibbs S, Lamme E, Van Blitterswijk CA, Ponec M. Effect of fibroblasts on epidermal regeneration. *Br J Dermatol.* (2002) 147:230–43. doi: 10.1046/j.1365-2133.2002.04871.x
85. Blomme EA, Sugimoto Y, Lin YC, Capen CC, Rosol TJ. Parathyroid hormone-related protein is a positive regulator of keratinocyte growth factor expression by normal dermal fibroblasts. *Mol Cell Endocrinol.* (1999) 152:189–97. doi: 10.1016/S0303-7207(98)00252-4
86. Monical PL, Kefalides NA. Coculture modulates laminin synthesis and mRNA levels in epidermal keratinocytes and dermal fibroblasts. *Exp Cell Res.* (1994) 210:154–9. doi: 10.1006/excr.1994.1023
87. Smola H, Thiekotter G, Fusenig NE. Mutual induction of growth factor gene expression by epidermal-dermal cell interaction. *J Cell Biol.* (1993) 122:417–29. doi: 10.1083/jcb.122.2.417
88. Has C, Nystrom A. Epidermal basement membrane in health and disease. *Curr Top Membr.* (2015) 76:117–70. doi: 10.1016/bs.ctm.2015.05.003
89. Brakebusch C, Grose R, Quondamatteo F, Ramirez A, Jorcano JL, Pirro A, et al. Skin and hair follicle integrity is crucially dependent on beta 1 integrin expression on keratinocytes. *EMBO J.* (2000) 19:3990–4003. doi: 10.1093/emboj/19.15.3990
90. Takahashi T, Asano Y, Sugawara K, Yamashita T, Nakamura K, Saigusa R, et al. Epithelial Fli1 deficiency drives systemic autoimmunity and fibrosis: possible roles in scleroderma. *J Exp Med.* (2017) 214:1129–51. doi: 10.1084/jem.20160247
91. Mahoney JM, Taroni J, Martyanov V, Wood TA, Greene CS, Pioli PA, et al. Systems level analysis of systemic sclerosis shows a network of immune and profibrotic pathways connected with genetic polymorphisms. *PLoS Comput Biol.* (2015) 11:e1004005. doi: 10.1371/journal.pcbi.1004005
92. Matei AE, Chen CW, Kiesewetter L, Gyorfi AH, Li YN, Trinh Minh T, et al. Vascularised human skin equivalents as a novel *in vitro* model of skin fibrosis and platform for testing of antifibrotic drugs. *Ann Rheum Dis.* (2019) 78:1686–92. doi: 10.1136/annrheumdis-2019-216108
93. Shultz LD, Keck J, Burzenski L, Jangalwe S, Vaidya S, Greiner DL, et al. Humanized mouse models of immunological diseases and precision medicine. *Mamm Genome.* (2019) 30:123–42. doi: 10.1007/s00335-019-09796-2
94. Alsafadi HN, Staab-Weijnitz CA, Lehmann M, Lindner M, Peschel B, Konigshoff M, et al. An *ex vivo* model to induce early fibrosis-like changes in human precision-cut lung slices. *Am J Physiol Lung Cell Mol Physiol.* (2017) 312:L896–902. doi: 10.1152/ajplung.00084.2017

Conflict of Interest: The authors declare that the research was conducted in the absence of any commercial or financial relationships that could be construed as a potential conflict of interest.

frontiers in Immunology

ORIGINAL RESEARCH
published: 12 May 2020
doi: 10.3389/fimmu.2020.00875

CASK, the Soluble Glomerular Permeability Factor, Is Secreted by Macrophages in Patients With Recurrent Focal and Segmental Glomerulo—Sclerosis

Xiaomeng Zhang[1,2†], *Florence Herr*[1,3,4†], *Amelia Vernochet*[1,3], *Hans K. Lorenzo*[1,3,5], *Séverine Beaudreuil*[1,5] *and Antoine Dürrbach*[1,3,4,6*]

[1] INSERM U1197, Villejuif, France, [2] Division of Internal Medicine, Department of Nephrology, Tongji Hospital, Tongji Medical College, Huazhong University of Science and Technology, Wuhan, China, [3] University of Paris-Saclay, Saint-Aubin, France, [4] Centre de Reference Maladie Rare du Syndrome Nephrotique Idiopatique, Paris, France, [5] Department of Nephrology, Bicêtre Hospital, Le Kremlin-Bicêtre, France, [6] Department of Nephrology, Henri Mondor Hospital, Creteil, France

OPEN ACCESS

Edited by:
Oliver Distler,
University of Zurich, Switzerland

Reviewed by:
George William Burke,
University of Miami, United States
Weici Zhang,
University of California, Davis, United States

***Correspondence:**
Antoine Dürrbach
antoine.durrbach@aphp.fr

[†]These authors have contributed equally to this work

Specialty section:
This article was submitted to Autoimmune and Autoinflammatory Disorders, a section of the journal Frontiers in Immunology

Received: 04 February 2020
Accepted: 16 April 2020
Published: 12 May 2020

Citation:
Zhang X, Herr F, Vernochet A, Lorenzo HK, Beaudreuil S and Dürrbach A (2020) CASK, the Soluble Glomerular Permeability Factor, Is Secreted by Macrophages in Patients With Recurrent Focal and Segmental Glomerulo—Sclerosis. Front. Immunol. 11:875. doi: 10.3389/fimmu.2020.00875

Introduction: Focal and segmental glomerulosclerosis (FSGS) is a frequent form of glomerulonephritis that may be caused by a soluble permeability factor and regulated by the immune system. We previously described a soluble form of calcium/calmodulin-dependent serine/threonine kinase (CASK) acting as a permeability factor in patients with recurrent FSGS (rFSGS). Here, we aimed to identify the immune cells associated with CASK secretion in patients with rFSGS.

Methods: FACS, western blotting and immunoprecipitation were performed to detect CASK in peripheral blood mononuclear cells, including $CD3^+$, $CD20^+$, and $CD14^+$subsets, from patients with rFSGS, healthy donors, transplant patients and patients with nephrotic syndrome due to diabetes mellitus, and in KHM2 cells.

Results: CASK was produced mostly by monocytes in patients with rFSGS but not by T or B lymphocytes. It was not detectein cells from control patients. CASK was also produced and secreted by M2 polarized macrophages and KMH2 cells, but not by M1 polarized macrophages. CASK secretion was not not inhibited by brefeldin A, suggesting an absence of classical secretion pathway involvement. Within cells, CASK was partly colocalized with ALIX, a molecule involved in exosome development, and these two molecules were coprecipitated from M2 macrophages. Moreover, exosomes derived from M2 macrophages induced podocyte cytoskeleton alterations and increased podocyte motility.

Conclusion: These results suggest that the soluble permeability factor CASK is secreted by monocytes and M2 macrophages, via exosomes, to alter the glomerular filtration barrier in rFSGS.

Keywords: CASK, focal and segmental glomerulosclerosis, macrophages, exosomes, idiopathic nephrotic syndrome

INTRODUCTION

Idiopathic nephrotic syndrome (iNS) is a group of diseases characterized by glomerular lesions and caused by various injuries leading to lesions of the basal membranes and podocytes (1). Focal segmental glomerulosclerosis (FSGS) is a major lesion that can lead to end-stage renal failure. It may occur secondary to hyperfiltration, viral infection, or may be associated with mutations of genes encoding podocyte proteins, such as nephrin, podocin, or alpha-actinin-4 (2). INS could also be associated with ectopic or altered expression of podocyte membrane protein including CD80 or SMPDL-3B that participated directly or indirectly to the regulation of actin cytoskeleton or the recruitment of circulating cells (3, 4). It may also be caused by the secretion of a permeability factor (PF) altering the glomerular basal membrane, characterized by massive proteinuria and hypoalbuminemia. FSGS accounts for 20% of nephrotic syndrome cases in children and 40% in adults and the disease can recur after transplantation in 30–50% of first kidney transplants and up to 90% of second grafts (5–8). Several PFs, including suPAR, cardiotrophin-like cytokine-1, angioprotein-like 4, and anti-CD40 autoantibodies, have been suggested to be implicated in FSGS, but none of these factors has been shown to be related to FGSG recurrence (rFSGS) (9–15). We recently reported that a soluble form of calcium/calmodulin-dependent serine/threonine kinase (CASK) acts as a PF in patients with rFSGS, and that this molecule can be removed by plasma exchange and immunoadsorption on protein A columns (16).

CASK, a member of the membrane-associated guanylate kinase (MAGUK) family, is a scaffolding protein that can link membrane receptors to cytoskeleton proteins, thereby regulating neuronal and epithelial cell polarity (17). CASK is widely expressed in the neuron, kidney and spleen (18). It has been reported to bind to CD98 in the extracellular space of intestinal epithelial cells, thereby modulating amino-acid transport or the organization of the actin cytoskeleton, depending on the coreceptor associated with CD98 (19, 20). In podocytes, the siRNA-mediated silencing of CD98 prevents the cytoskeleton alterations induced by CASK (16).

The cells responsible for releasing this molecule into the plasma of patients with rFSGS have yet to be identified. However, the immune system is thought to play a key role in this disease. iNS can be favored by viral disease or vaccination, but decreases in proteinuria have been observed after measles, which impairs the immune system, in patients with iNS (1, 21, 22). iNS has been also observed in patients with lymphoproliferative diseases (Hodgkin's disease and T-cell lymphoma), disappearing during the remission of these diseases (23, 24). Furthermore, current treatments include drugs targeting both the innate and adaptive immune systems, such as steroids, calcineurin inhibitors and rituximab (3, 25), and c-mip and NF-?? have been shown to be upregulated in T lymphocytes during relapses of the disease (26, 27).

In this study, we aimed to identify the cells producing and secreting CASK in patients with rFSGS, and to decipher the secretion mechanism. By analyzing peripheral blood mononuclear cells from patients with rFSGS, we found that CASK was secreted by monocytes (CD14-positive cells) and M2 macrophages from these patients.

MATERIALS AND METHODS

Patients

Group 1

Five patients with rFSGS after renal transplantation were included. The immunosuppressive regimen was thymoglobulin for induction, and tacrolimus, mycophenolate mofetil, and corticosteroids for maintenance therapy. Proteinuria recurred in all patients, and graft biopsy was performed to rule out acute rejection (**Table 1**). Renal biopsies showed minimal change disease or FSGS. The patients were treated with high-dose steroids and tacrolimus (with a tacrolimus trough level >13 ng/mL) for the recurrence of FSGS. Peripheral blood was collected from all patients at the time of recurrence.

Group 2

Seven kidney-transplant patients without FSGS were included. The causes of nephropathy in these patients were diabetes mellitus ($n = 2$), IgA nephropathy ($n = 3$), or unknown ($n = 2$). All had end-stage renal disease and had undergone transplantation. The patients were treated with tacrolimus, mycophenolate mofetil, and steroids. Their renal function was stable, with no acute or chronic rejection.

Group 3

Five patients with chronic kidney failure and nephrotic syndrome caused by type 2 diabetes were included. All had biopsy-proven diabetes associated with glomerulonephritis. Peripheral blood was collected from all patients.

Group 4

Peripheral blood samples were collected from eight healthy donors.

The project was approved by the local ethics committee ≪ Comité Consultatif de Protection des Personnes participant à une Recherche Biomédicale ≫ (n°4/010). All patients provided their written informed consent (patients from groups 1, 2, and 3). Healthy donors samples were collected by Etablissement Français du Sang after written informed consent. The informatic file developed for the research was approved by the national commission of informatic and liberty. None of the transplant donors were from a vulnerable population and none of them had declared their opposition for organ procurement accordingly to French law (Loi de Bioethique Article L. 1232- 1).

Reagents and Antibodies

Production of Recombinant CASK

The cDNA sequence for human CASK was kindly provided by Prof. Zenta Walther (Yale University, School of Medicine). The DNA was digested with *Bam*HI and *Eco*RI and inserted into the pTrcHis2C vector (Invitrogen) for expression and purification of the protein product in *Escherichia coli*. Gene expression and protein purification were performed by Genscript Services (Piscataway, NJ, USA). Briefly, the recombinant protein was

TABLE 1 | Patient's description.

	rFSGS	Stable Transplant Patient	Nephrotic syndrome	Healthy donors
Number	5	7	5	8
Age (year)	39.8 ± 7.3	53.7 ± 16.5	66.7 ± 6.4	44.2 ± 9.1
Sexe F/M	1/4	2/5	1/4	3/5
Kidney disease	Recurrent FSGS	• IgA-GN ($n = 1$) • Alport syndrome ($n = 2$) • NAS ($n = 2$) • Diabetes Type 2 ($n = 1$) • Unknown ($n = 1$)	Diabetes type 2	na
Hypertension (number)	5	7	5	0
Serum creatinine (μmol/l)	150.5 ± 101	202 ± 98	288 ± 162	na
Proteinuria (g/day)	6.8 ± 2.4	0.3 ± 0.22	4.9 ± 1.9	na
Time between Transplantation and Proteinuria (days)	22.8 ± 21.6	na	na	na
Time between Transplantation and blood samples (days)	27.8 ± 25	61.2 ± 32.1	na	na
Dialysis	No	No	No	na
Kidney transplant	5	7	No	na
CNI treatment	5	5	No	na

Na, non-applicable, NAS, nephroangiosclerosis, IGA-GN, IgA associated glomerulonephritis. CNI, calcineurin inhibitor.

purified by affinity chromatography on Ni-agarose columns followed by anion-exchange chromatography. The final purity was close to homogeneity (>95%) and endotoxin levels were below 0.10 EU.

Human IL-4 and M-CSF were obtained from ImmunoTools (Friesoythe, Germany) and human recombinant IFNγ was purchased from Miltenyi Biotec (BergischGladbach, Germany). Lipopolysaccharide and brefeldin A were purchased from Sigma-Aldrich (Saint-Louis, USA). Short interfering RNA (siRNA) sequences directed against human CASK were purchased from OriGene (Rockville, USA). The antibodies against CASK used for western blotting were from Santa Cruz Biotechnology (Dallas, USA) (H107, targeting amino acids 353–459) or from BD Biosciences (610782, targeting amino acids 353–486). The anti-CASK antibody used for Flow cytometry and microscopy was from Abcam (Cambridge, UK, ab126609). Antibodies against ALIX and LAMP2, were purchased from Abcam. Antibodies against actin and synaptopodin were purchased from Santa Cruz Biotechnology. Antibody against GAPDH was purchased from Sigma-Aldrich. Antibodies against Calnexin, GM-130, CD3-APC and CD3-FITC, CD20-APC, CD14-APC, and CD14-PE-Cy7, CD206-PE-Cy7, CD163-PE and isotype controls were purchased from BD Biosciences. Horseradish peroxidase-conjugatedsecondary antibodies for western blotting, or fluorescent conjugated secondary antibodies for immunofluorescence analysis were purchased from Jackson ImmunoResearch (West Grove, USA). Antibody against CD63 was kindly provided by Dr. Eric Rubinstein (INSERM).

Cell Culture

Podocyte

A conditionally immortalized mouse podocyte cell line was cultured, as described by Mundel et al. (28). Briefly, non-differentiated podocytes were cultured in RPMI supplemented with 10% fetal calf serum (FSC), 2 mM L-glutamine, 100 U/ml penicillin/streptomycin (Invitrogen, California,USA), 50 U/ml IFNγ (for the first two passages, and 10 U/ml IFNγ thereafter) at 33°C under an atmosphere containing 5% CO_2. Differentiation was induced by treating the podocytes with trypsin and culturing them in the same medium, without IFNγ, for 2 weeks at 37°C.

In experiments with cells microvesicules isolation, microvesicles were removed from the FCS by centrifugation at 100 000 × g for 2 h before addition to the culture medium.

Macrophage Polarization

Peripheral blood mononuclear cells (PBMCs) were isolated from healthy donors by Ficoll-Paque density-gradient centrifugation (GE Healthcare Life Sciences, Buckinghamshire, UK). Monocytes were isolated from PBMCs by two passages of adherence on plastic culture plates. Purity of monocyte were assessed by flow cytometry with anti-CD14mAbs (ImmunoTools, Friesoythe, Germany). Monocytes were maintained in culture at a density of $5 \times 10^5/cm^2$, in RPMI 1640 supplemented with 10% FCS, 2 mM L-glutamine, and 100 U/ml penicillin/streptomycin. M1-polarized macrophages were obtained by culturing the monocytes for 7 days with 1000 U/ml IFNγ. M2-polarized macrophages were obtained by culturing the monocytes for 7 days with 50 ng/ml M-CSF and 10 ng/ml IL-4. Cells displaying intermediate differentiation were cultured in the same medium supplemented with 50 ng/ml M-CSF for 7 days at 37°C, under an atmosphere containing 5% CO_2.

PBMCs Isolation

PBMCs were isolated from the blood of healthy volunteers, rFSGS patients, kidney-transplant patients and type 2 diabetes patients by density Ficoll-Paque gradient centrifugation. Briefly, blood collected in EDTA-coated tube was diluted in Hanks Balance Salt Solution (HBSS) at 1:1 ratio and layered on

Ficoll-Paque plus solution (GE Healthcare Life Sciences, Buckinghamshire, UK) (1 volume Ficoll-Paque: 2 suspension volumes). After centrifugation 400 g 30 min at room temperature the layer of mononuclear cells was transferred in a tube and washed two times in 10 volumes HBSS.

Exosome Purification

Exosomes were purified from cell supernatants by three successive centrifugations: an initial centrifugation at 10 000 × g (30 min) to eliminate cells and debris, followed by a concentration step with amicon Ultra centrifugal filter (Merk) at 4 000g and then an ultracentrifugation for 2 h at 100 000 × g. The exosome pellet was washed once in a 5 mL of PBS, centrifuged at 100 000 × g for 2 h and the resulting pellet was then resuspended in 50–200 μl PBS.

We used a modified version of the classical protocol to obtain plasma microvesicles, due to the viscosity of the plasma and the higher abundance of lipids in the plasma than in the cell supernatant. Plasma was centrifuged for 30 min at 500 × g, 45 min at 12 000 × g and 2 h at 100 000 × g. Pellets were resuspended in 5 mL of PBS, and the suspension was passed through a filter with 0.22 μm pores(Millipore, Massachusetts, USA) and centrifuged at 100 000 × g for 2 h. The resulting microvesicle pellets were washed once in 5 mL of PBS, centrifuged at 100 000 × g for 2 h and the final pellet was resuspended in 50–200 μl PBS.

Protein concentrations were determined with the BCA protein assay kit (Thermo Fisher Scientific, Massachusetts, USA) for immunocytochemistry, immunoblotting or functional assays. Exosomes were used as fresh preparations or after freezing and storage at −80°C.

Flow Cytometry

Cells

PBMCs isolated from healthy donors, patients with rFSGS, transplant patients without FSGS or from patients with nephrotic syndrome were analyzed. PBMCs were isolated from whole blood by Ficoll-Paque (GE Healthcare Life Sciences) density-gradient centrifugation. Phenotypic analyses were performed on the various subpopulations of PBMC as follows: cells were incubated with labeled primary antibody directed against a membrane protein or isotype control, and were then washed in PBS and fixed by incubation in 3% paraformaldehyde (PFA) for 30 min. After washing in PBS, Fc receptors were saturated by incubation with 10% AB-human serum (Life Technologies, California, USA). For the subsequent intracellular staining of CASK, cells were washed in PBS, incubated for 15 min in 100 mM NH_4Cl in PBS, permeabilized by incubation with 0.1% saponin in 0.2% BSA and stained with specific primary antibodies followed by secondary antibodies (goat anti-rabbit AlexaFluor-488). Anti-CD3, anti-CD20, and anti-CD14mAbs were purchased from ImmunoTools and rabbit anti-CASK antibodies were obtained from Abcam (Cambridge, USA). Cells were analyzed with aFACScalibur™ machine (BD Biosciences, Franklin, USA), with Cell Quest Analysis (BD Biosciences) and FlowJo (BD Lifesciences) software.

Exosomes

For FACS analysis, exosomes were incubated with sulfate latex beads (Life Technologies) at a ratio of 2 μg exosomes to 10 μl beads. The volume was made up to 500 μl with PBS and the mixture was incubated for 2 h at room temperature. The beads were blocked by incubation with glycine (100 mM) for 30 min and were then washed three times with 0.5% BSA in PBS. The exosome-coated beads were resuspended in 500 μl PBS. We then incubated 10 μl of bead suspension with the primary antibodies (anti-CASK, anti-CD9, anti-CD63, and anti CD81) at a dilution of 1/50, followed by the secondary antibody (goat anti-rabbit PE, goat anti-mouse APC; Jackson Immuno Research, Cambridgeshire, UK). FACS analysis was performed on a BD Accuri C6 flow cytometer with CFlow plus software (BD Lifesciences).

Immunofluorescence

Immunofluorescence of Cells

Podocytes were grown on coverslips and incubated with recombinant CASK or macrophage-derived exosomes for 24 h. For immunofluorescence staining, cells were washed three times in PBS and fixed by incubation with 3%PFA in PBS for 20 min. They were then washed in PBS and incubated for with 100 mM NH_4Cl in PBS for 10 min. Cells were permeabilized with 0.01% saponin, and then blocked by incubation with 3% BSA-0.01% saponin buffer for 1 h. Finally, the cells were incubated with the primary antibodies for 1 h at room temperature and washed three times before incubation with secondary antibodies or phalloidin 488. Cells were mounted in Mowiol 4–88 medium, and fluorescence was observed with a Leica DM-RXA23D microscope or Leica DM confocal microscope (Wechsler, Germany).

Gene silencing

For the CASK knockdown experiments, KM-H2 cells were transiently transfected, by electroporation, with a pool of three target-specific human siRNA (100 pmol) oligonucleotides against CASK according to the manufacturer's protocols (Lonza Amaxa, Basel, Germany).

Videomicroscopy

Cell motility analysis was performed by time-lapse video microscopy on an inverted microscope equipped with a 37°C chamber, under an atmosphere containing5% CO_2 (Nikon, Tokyo, Japan). Stacks of phase-contrast images were collected every 15 min for 24 h, at ×200 magnification. Cell migration was quantified with the manual tracking plug-in of ImageJ. Data were transferred to Excel for calculations and statistics. For each position, we analyzed at least 10 cells.

Immunoprecipitation

The cell culture supernatant was concentrated with Amicon ultracentrifugation filter units (Millipore, Massachusetts, USA) and precleaned by incubation with protein G-Sepharose (GE Healthcare Life Sciences, Buckinghamshire, UK) beads for 2 h at 4°C. The supernatant was incubated overnight with anti-CASK antibody (Santa Cruz, H-107) in a rotating mixer at 4°C.

Protein G-Sepharose beads were then added and the mixture was incubated for 2 h at 4°C. It was then centrifuged and the beads were washed. The complexes were recovered in 2× Laemmli buffer (BioRad, California, USA) and analyzed by SDS-PAGE.

For co-immunoprecipitation, cells (1.5×10^7) were lysed by incubation in ice-cold lysis buffer (25 mmol/L HEPES, 150 mmol/L NaCl) supplemented with 1% Brij 97 and a protease inhibitor cocktail (Thermo Fisher Scientific, Massachusetts, USA) for 1 h at 4°C. The lysate was centrifuged (10 min, 20000 × g), and 1 mL of the supernatant was then precleared by incubation with Protein G-Sepharose for 2 h at 4°C. The precleared lysates were incubated overnight at 4°C with 1 μg antibody. They were then incubated with Protein G-Sepharose for 2 h, and the immune complexes were washed five times in the lysis buffer. Immunoprecipitated proteins were analyzed by SDS-PAGE and western blotting.

Immunoblotting

Equal amounts of protein (5–30 μg) or immunoprecipitate were subjected to SDS–PAGE under reducing conditions. The resulting bands were electrophoretically transferred onto a PVDF membrane. They were then fixed in 3% acetic acid, and the membrane was saturated by incubation with 5% BSA in TBS-Tween (0.1%) and incubated with primary mouse antibodies against CASK, β-Actin, GAPDH or ALIX for 1 h at room temperature. The membrane was washed three times in TBS-Tween and incubated with horseradish peroxidase-conjugated secondary antibodies for detection by enhanced chemiluminescence (WBKLS0500, Substrate HRP Immobilon, Millipore SAS, Saint Quentin en Yvelines, France). Protein content was quantified with ImageJ software. The density of the bands was normalized against a reference protein (β-Actin or GAPDH).

STATISTICS

Quantitative values were compared in non-parametric Mann-Whitney U tests or ANOVA, qualitative values were compared in Chi^2 tests. We considered p-values below 0.05 to be significant.

RESULTS

Expression of CASK by PBMCs in rFSGS Patients

We investigated CASK levels in PBMCs by western blotting, to determine whether these cells might be responsible for CASK secretion. The immunoblot detected low levels of CASK, with an apparent molecular mass of 105 kDa in T cells, B cells and monocytes from the healthy donor (**Figure 1A**). In PBMCs from rFSGS patients, we detected CASK with a different apparent molecular mass, ∼90 kDa (**Figure 1A**), consistent with the size of CASK in the serum of patients with rFSGS (**Figure 1A**). KM-H2 cells, which are derived from a Hodgkin lymphoma, expressed constitutively CASK. We demonstrated the specificity of the CASK antibody by knocking down CASK expression in KM-H2 cells (**Figure 1B**).

For identification of the subpopulation of cells expressing CASK in patients, we performed FACS with antibodies specific for surface markers of leukocytes (CD3, CD20, and CD14) and intracellular staining for CASK. Significant CASK expression relative to healthy patients was detected in $11.6 \pm 1.4\%$ of $CD14^+$ cells from patients with rFSGS ($p < 0.0001$). Expression of CASK was also detectable in a small fraction of T cells ($1.3 \pm 0.6\%$) and B-lymphocytes ($2.8 \pm 1.1\%$) of rFSGS patients as compared to the other groups of patients (**Figures 1C,D**). CASK was not significantly detected in PBMCs from transplant patients or from patients with nephrotic syndrome due to diabetes mellitus glomerulonephritis. Comparing expression of CASK between CD14+ cells of rFSGS patients and those from patients with diabetes mellitus or transplant patients or healthy donors, we observed a higher expression in rFSGS CD14+ cells (**Figure 1D**). In addition, the fraction of cells expressing CASK in PBMC of rFSGS patients were substantially higher in the CD14 population than in T or B lymphocytes populations. Thus, we analyzed CASK expression by CD14+ derived cells.

CASK Expression in the M2 Macrophage Subset

Monocytes/macrophages constitute a heterogeneous population that can be separated into different subsets on the basis of cell development and phenotype. We investigated the macrophage subsets involved in CASK production, by promoting the differentiation of monocytes purified from healthy individuals and their polarization into M1 or M2 macrophage subpopulations (**Figure 2A**). The cells of the M2 subset were elongated, with a fibroblast-like morphology, contrasting with the classical "fried egg shape" of the cells of the M1 subset (**Figure 2A**). Furthermore, the cells of the M2 subset strongly expressed the prototypic markers CD206 and CD163, which were absent from the M1 subset (**Figure 2B**). The monocytes treated with M-CSF had an intermediate phenotype. FACS demonstrated stronger CASK expression in M2 macrophages than in M1 macrophages (**Figures 2C,D**). These results were confirmed by western blotting (**Figures 2E,F**).

Secretion of CASK by M2 Macrophages

We then investigated the secretion of CASK by these cells. We subjected the supernatants of KM-H2 cells and macrophages to immunoprecipitation for CASK before subjecting gel electrophoresis and western blotting. CASK was detected in the supernatant of KM-H2 cells, and in the supernatant of M2 cells, but much less strongly in the supernatant of M1 cells (**Figure 3A**).

Subcellular Localization of CASK

CASK is a membrane-associated cytoplasmic protein with no signal peptide. We therefore investigated the mechanism of CASK secretion in KM-H2 cells, in which CASK is cytoplasmic and not colocalized with GM 130, a *cis*-Golgi protein (**Figure 3B**). We investigated the role of the classical pathway in CASK secretion, by treating KM-H2 cells with

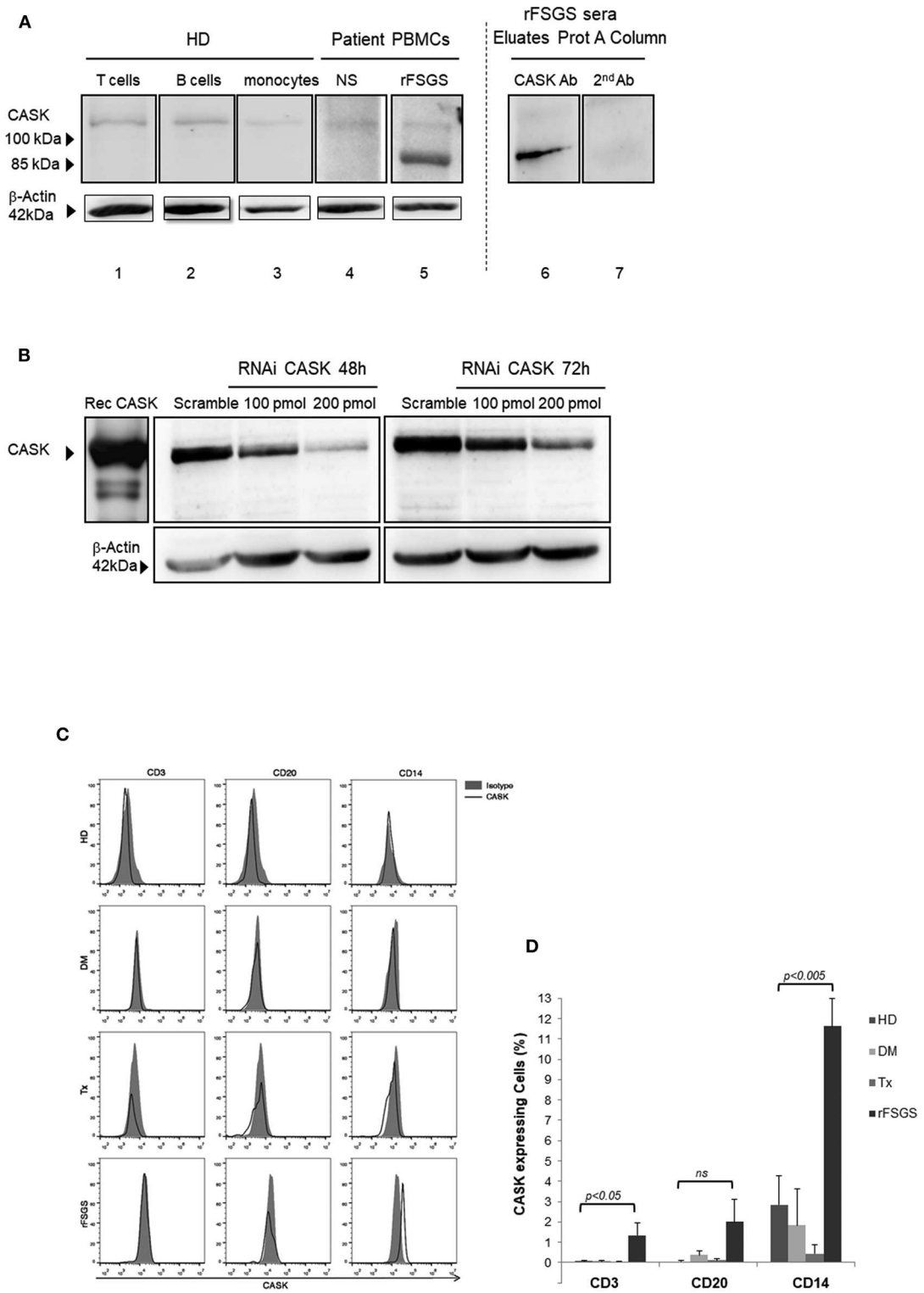

FIGURE 1 | CASK expression in PBMCs. **(A)** (lanes 1–3) T cells, B cells, and monocytes isolated from healthy donors (HD), (lanes 4,5) peripheral blood mononuclear cells (PBMCs) from patients with nephrotic syndrome (NS) due to diabetes mellitus or rFSGS patients, (lane 6,7) eluate from a patient treated with a protein A column, analyzed by immunoblotting with a commercial rabbit polyclonal anti-CASK antibody (lanes 1–6) or a secondary anti-rabbit IgG antibody (lane7). **(B)** Gel electrophoresis and western blotting with an anti-CASK antibody of recombinant CASK (rec CASK) or lysates of KM-H2 cells transfected with an anti-CASK or

(Continued)

FIGURE 1 | scrambled siRNA, at various time points. **(C)** Flow cytometry analysis of PBMCs from healthy donors (HD), patients with NS due to diabetes mellitus-associated nephropathy kidney transplant recipients without rFSGS (Tx), or rFSGS patients (rFSGS). Cells were labeled with anti-CASK antibody and either an antibody against CD3, CD20, or CD14. **(D)** Percentages of CASK$^+$ cells in the CD3$^+$, CD20$^+$, and CD14$^+$subsets were compared with those in healthy individuals ($n = 8$), diabetic patients ($n = 5$), kidney transplant recipients ($n = 7$) and rFSGS patients($n = 4$). Statistical differences were determined by ANOVA test for CD3, CD20, and CD14 cells populations (dotted line), and by unpaired student's *t*-test for patient groups among cells populations (solid line).

brefeldin A (BFA), a fungal metabolite that inhibits ER-to-Golgi trafficking. BFA did not inhibit the secretion of CASK or induce its intracellular accumulation (**Figure 3C**), suggesting the involvement of another release pathway.

Exosomes provide an alternative pathway for protein secretion. They are of endosomal origin and are formed by the inward budding of multivesicular bodies (MVBs) (29). We therefore investigated the distribution of CASK in these compartments by confocal microscopy with antibodies against CASK, CD63 (a late endosomal marker), LAMP2 (a lysosomal marker) or ALIX (an auxiliary component of the ESCRT: endosomal sorting complexes required for transport) (30) in the M2 macrophage subset. CASK had a diffuse cytosolic distribution (**Figure 4A**). It was not colocalized with CD63 or LAMP2. Partial colocalization was observed between CASK and ALIX. We then performed co-immunoprecipitation experiments with Brij97 detergent, to investigate the association of CASK with ALIX further. ALIX was co-immunoprecipitated with CASK and, conversely, CASK was co-immunoprecipitated with ALIX (**Figure 4B**). These results confirmed association between these two proteins.

Exosome-Associated CASK Release

To investigate the association of CASK with exosomes, we purified exosomes from the supernatant of M1 or M2 macrophages and subjected them to FACS analysis. We detected high levels of expression for exosomal markers, such as CD9 and CD63 (**Figure 5A**) in exosomes from macrophages and only CD63 in those purified from KM-H2 cells. None of the exosome preparations tested displayed an association with calnexin (**Figures 5B,C**), an ER membrane component. In KM-H2 cells, CASK was detected in the exosomal fraction (**Figure 5D**), mostly in exosomes from M2 subset. Quantification of the CASK/GAPDH density ratio revealed significantly higher levels of CASK expression in exosomes from the M2 subset (**Figure 5C**) than in those from the M1 fraction or undifferentiated macrophages. In KM-H2 cells, CASK knockdown with siRNA efficiently reduced CASK levels in both the cell lysate and exosomes (**Figure 5D**). For confirmation that the secreted CASK was mostly associated with exosomes, we compared CASK levels in the supernatant of KM-H2 cells or macrophage subsets before and after exosome removal. As expected, CASK was detected in the supernatant (SnExo$^+$) of KM-H2 cells, but not in the supernatant of these cells after ultracentrifugation to remove the exosomes (SnExo-) (**Figure 5E**). CASK was also not detected after its knock down with a specific siRNA. These results suggest that CASK release may be associated with exosomes in the cellular microenvironment.

Expression of CASK in the Plasma-Derived Exosomes of rFSGS Patient

We then investigated whether CASK was presenting exosomes from rFSGS patients. For this purpose, we purified exosomes from the sera of rFSGS patients, healthy controls and transplant patients without proteinuria. CASK was present in exosomes from rFSGS patients, but not in those from healthy donors, as shown by immunoblotting (**Figure 5F**). It was detected in control patients, but to a lesser degree. These results were confirmed by flow cytometry. For this purpose, exosomes were fixed on microbeads (see methods). Flow cytometry analysis revealed significantly higher levels of CASK expression on the exosomes from patients with rFSGS than on those from control patients ($p < 0.05$), whereas CD63 and CD9 levels were similar for the two groups (**Figure 5G**).

M2-derived Exosome-Induced Podocyte Alterations

Cytoskeleton Alterations

CASK induced cytoskeleton alterations in podocytes (16). We therefore investigated the impact of exosomes purified from macrophage subsets on the morphology of human podocytes. M2-derived exosomes induced a dose-dependent loss of actin stress fibers, with maintenance of the peripheral organization of F-actin (**Figure 6**). Similarly, exosomes affected synaptopodin, an actin-associated protein displaying liner codistribution with actin filaments in control cells (**Figure 6**). In the presence of M2-derived exosomes, synaptopodin staining was diffuse. By contrast, treatment with 40 μg/ml M1-derived exosomes had no effect on actin cytoskeleton organization (**Figure 6**).

Increase in Podocyte Motility

We investigated whether the disruption of the actin cytoskeleton observed after the addition of exosomes from the M2 subset was associated with a functional effect on podocytes, through video microscopy explorations of podocyte motility. Podocytes were grown on plates coated with collagen IV and treated with recombinant CASK, M1-derived exosomes or M2-derived exosomes. Both CASK and M2-derived exosomes induced an increase in podocyte motility (5.5 ± 1.531 μm/h and 6.8 ± 1.265 μm/h, respectively) relative to control podocytes (4.66 ± 1.068 μm/h) or podocytes treated with M1-derived exosomes (4.16 ± 1.075 μm/h)(**Figures 7A,B**; $p < 0.05$).

DISCUSSION

In a previous mass spectrometry study analyzing the proteins eluted from protein A columns used to treat rFSGS, we identified a serum form of CASK in rFSGS patients. Recombinant CASK

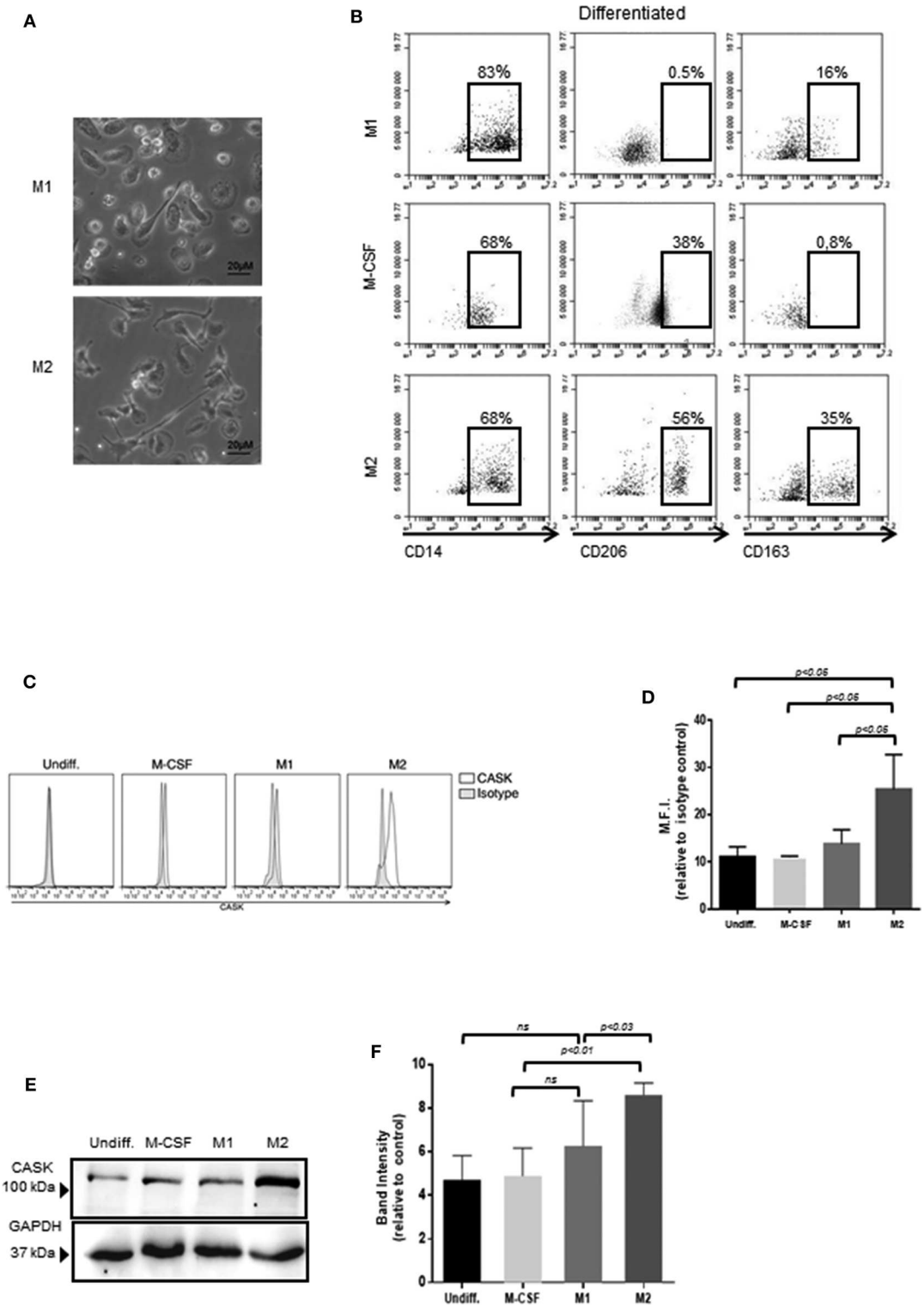

FIGURE 2 | Expression of CASK in the macrophage subsets. **(A)** The morphology of M1 and M2 macrophages was analyzed by phase-contrast microscopy with a ×20 objective. **(B)** Surface marker expression of M2, M1 and undifferentiated macrophages (CD14, CD206, CD163) was analyzed by flow cytometry ($n = 4$). **(C,D)** CASK expression of macrophage subsets was evaluated by intracellular staining and flow cytometry analysis and mean fluorescence intensity (M.F.I) was quantified, relative to isotype control ($n = 4$) **(E)** CASK expression was assessed by SDS-PAGE and immunoblot analysis in the different macrophage subsets. **(F)** Quantification of the intensity of the CASK band with Image J software ($n = 4$).

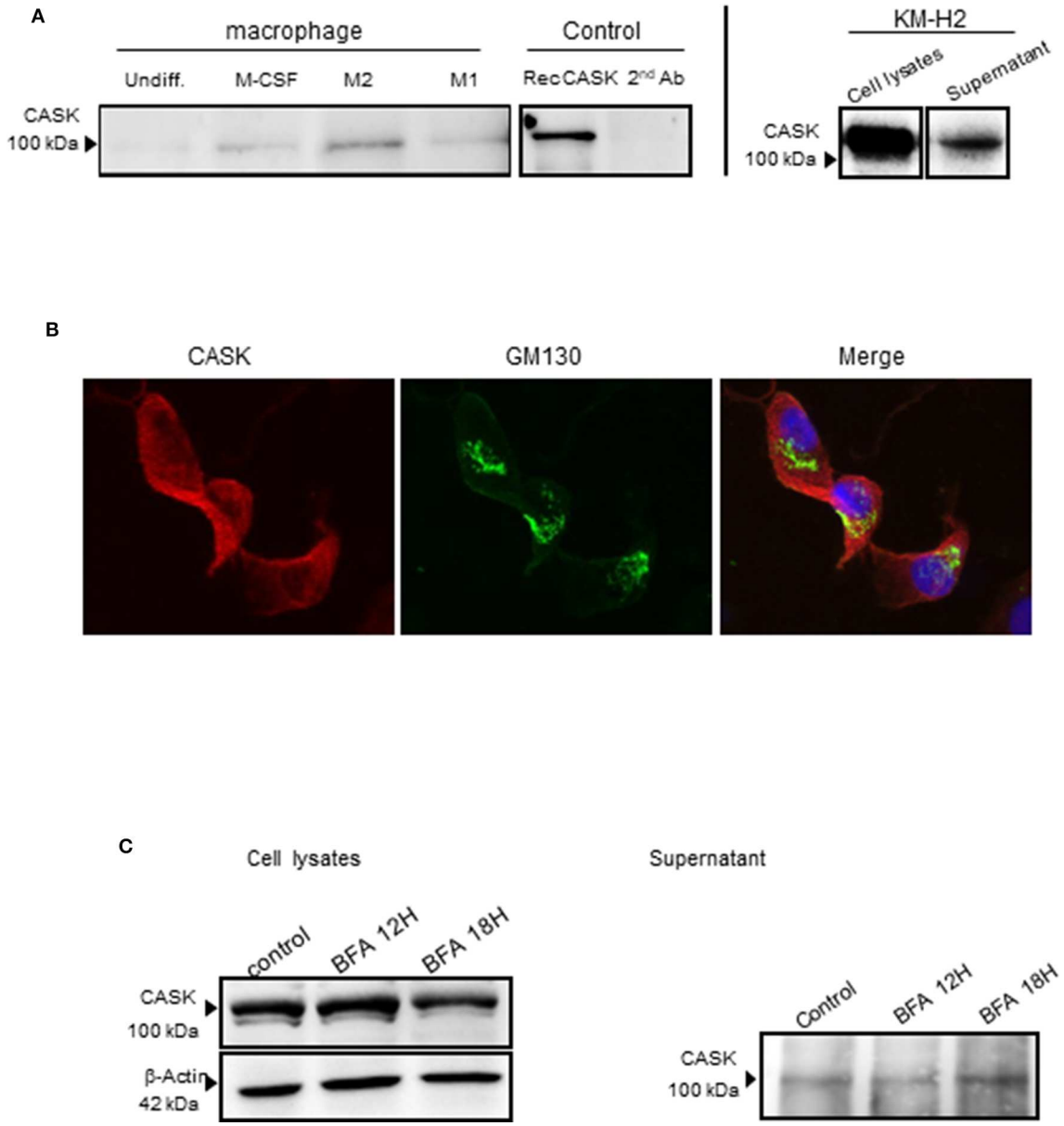

FIGURE 3 | CASK secretion by the macrophage subsets and KM-H2s. **(A)** Immunoprecipitation of CASK, with a rabbit polyclonal Ab, from the supernatant of different macrophage cultures and recombinant CASK, followed by immunoblotting with mouse anti-CASK antibody **(B)** M2 macrophages were stained with antibodies against CASK (red) and GM130 (green), a *cis*-Golgi matrix protein, ×63 magnification. **(C)** Protein transport from the endoplasmic reticulum to the Golgi apparatus was blocked by treating KM-H2 cells with brefeldin A (10 μg/ml) for 12 or 18 h. The production and secretion of CASK were evaluated by western blots of cell lysates and supernatants, respectively.

induced the impairment of podocytes *in vitro* (cytoskeleton alterations) and proteinuria and podocyte foot-process effacement in mice (16). Moreover, as our work suggests rFSGS may be a systemic disease involving the immune system. In this study, we found that CASK was expressed by $CD14^+$ cells from patients with rFSGS, but not by those of healthy donors or control patients treated with similar immunosuppressive drugs.

Given the frequency of its recurrence after transplantation, rFSGS is considered to correspond to a systemic disease with a specific effect on glomeruli. Its sensitivity to immunosuppressors and its recurrence after vaccination or viral infection have led to the hypothesis of a role for the immune system in initiating or maintaining the disease. The work of Grimbert et al. supported this view, by demonstrating an upregulation of c-mip in T cells and podocytes from patients with rFSGS (26). In addition, several molecules have been demonstrated to be ectopically expressed or up regulated suggesting that it could be direct or indirect target of the immune system (3, 4). Although, the expression of CD80

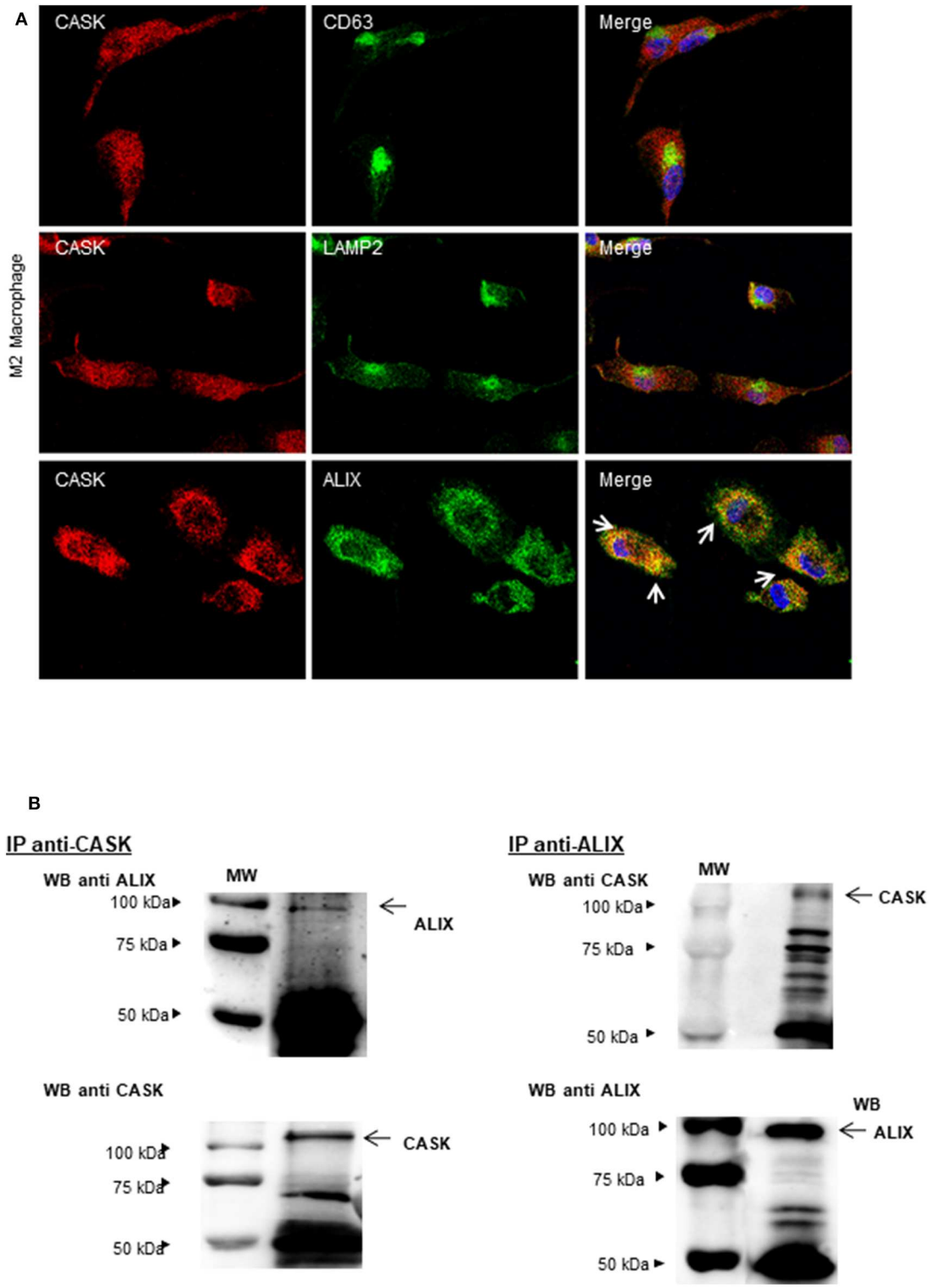

FIGURE 4 | Subcellular distribution of CASK and interaction between CASK and ALIX. **(A)** M2 macrophages were stained with antibodies against CASK and CD63, CASK, and LAMP2 or CASK and ALIX, and then with secondary antibodies labeled with Alexa Fluor 488 and Alexa Fluor 594. The samples were analyzed by confocal microscopy, with a ×63 objective. The co-distribution of two markers is indicated by arrows in the composite image. **(B)** Reciprocal co-immunoprecipitation was performed with antibodies against CASK and ALIX, in M2 macrophages. The immunoprecipitates were analyzed by western blotting with mAbs against CASK or ALIX ($n = 3$). IP: immunoprecipitation.

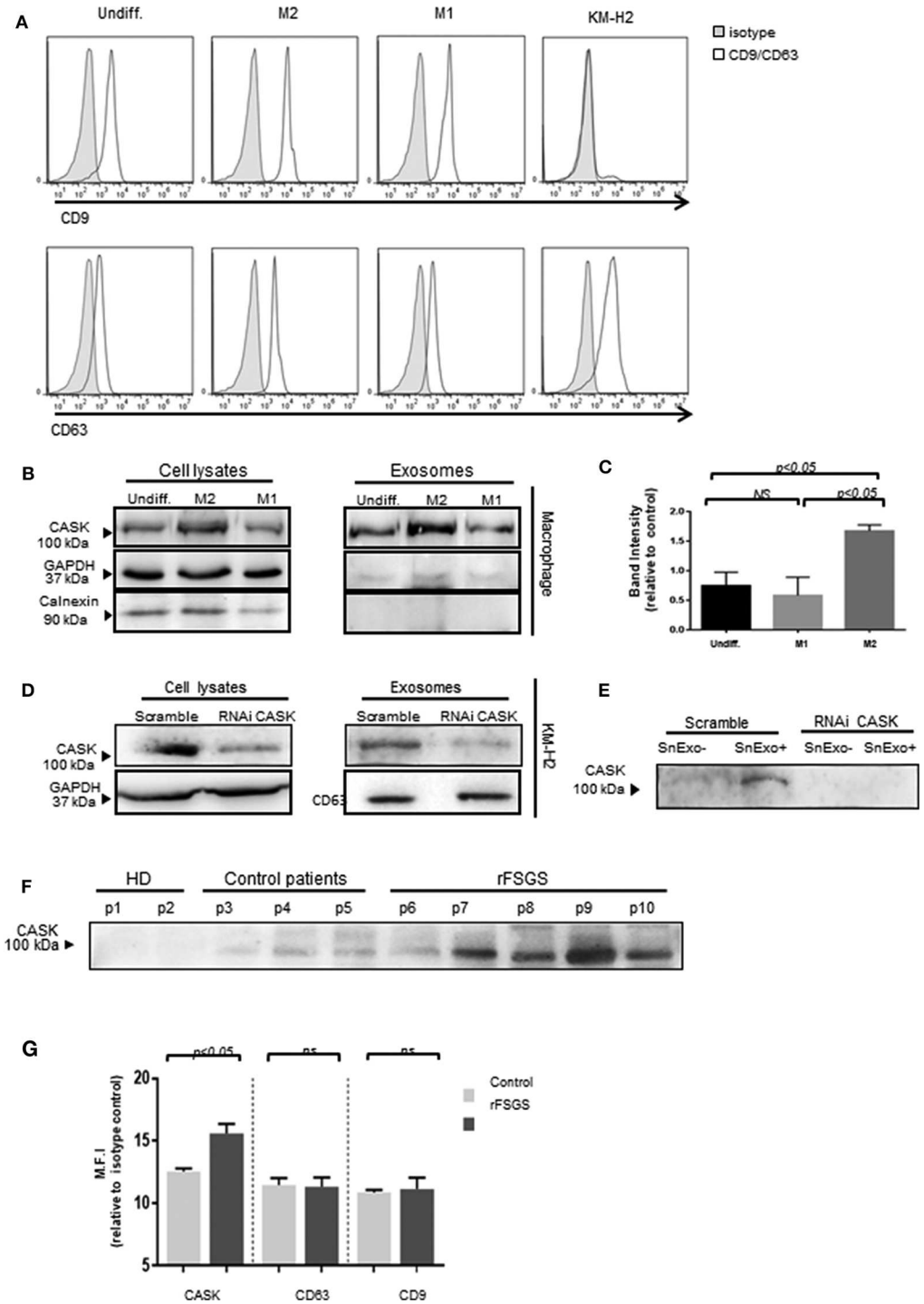

FIGURE 5 | Exosome-associated CASK release. Exosomes were purified from culture supernatants of KM-H2 cells and M1 and M2 macrophages, by differential ultracentrifugation. **(A)** Surface exosomal marker expression was analyzed by flow cytometry for CD9 and CD63 expression. **(B,D)** CASK levels were investigated in cell lysate or exosomes from macrophage subsets **(B)** and from KM-H2 cells transfected with a siRNA directed against CASK or with a scrambled sequence as a negative control **(D)** ($n = 3$). Total cell lysates and corresponding exosomes were analyzed by immunoblottingwith anti-CASK, anti-GAPDH or anti-calnexin antibodies. **(C)** CASK band intensity of **(B)** was quantified with Image J software, with normalization against GAPDH ($n = 4$). **(E)** Immunoblotting with anti-CASK antibody of exosome-containing supernatant ($SnExo^+$) and exosome-depleted supernatant ($SnExo^-$) from KM-H2 cells of **(D)** ($n = 4$). **(F)** Exosomes were purified from the plasma of healthy controls (HD) (P1–P2), control patients with NS due to diabetes mellitus (P3–P5) or rFSGS patients (P6–P10). CASK levels in these exosomes were analyzed by western blotting. **(G)** The expression of CASK, CD63, and CD9 in control patients ($n = 4$) and in rFSGS patients ($n = 5$) was analyzed by flow cytometry. Mean fluorescence intensity for CASK, CD63 andCD9 relative to isotype control, displayed as a histogram.

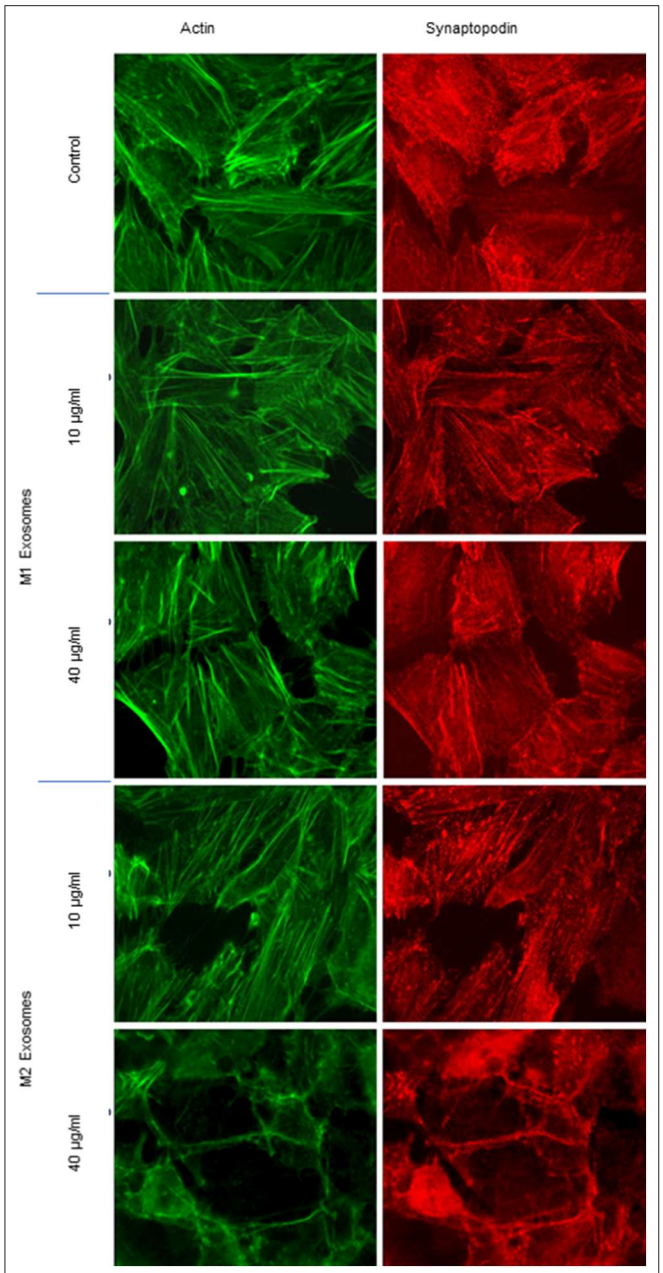

FIGURE 6 | Cytoskeleton alterations induced by exosomes from M1 or M2 macrophages. Exosomes from M1 and M2 macrophages were incubated with human podocytes at concentrations of 10 and 40 µg/ml. Immunostaining was performed with phalloidin (green) and anti-synaptopodin antibody (red). Analysis was performed by fluorescence microscopy with a ×63 objective.

is controversial during iSN, this molecule could participate to the interaction of podocytes and the immune system during iSN (31, 32). However, biopsies performed during active processes of rFSGS did not find infiltration of inflammatory cells but we cannot formally ruled out that transient interaction can take place directly or through cell mediators as microvesicles. For these reasons, we investigated the ability of immune system cells to produce CASK in patients with rFSGS, by analyzing CASK production by PBMCs. We found that a fraction of monocytes expressed CASK. Monocytes have a short half-life in blood, but serve as the precursors of macrophages and dendritic cells, which play key roles in innate and adaptive immunity (33, 34). *In vitro*, CASK was produced by M2 macrophages expressing CD206 and CD163. This finding is consistent with the expression of CASK in the spleen and with the demonstration ofTh2 polarization and activation during the development of iNS in Buffalo/Mna rats with minimal change lesion of glomeruli (35, 36).

Soluble CASK was detected in the supernatants of M2 macrophages and KM-H2 cells. It was not associated with markers of cell culture necrosis (data not shown), suggesting that it was secreted by PBMCs. However, CASK has no signal peptide, which suggests that it may not be secreted by the classical secretory pathway. This was indeed confirmed by the absence of CASK co-distribution with secretory pathway organelles, such as the Golgi apparatus and endoplasmic reticulum. Moreover, CASK secretion in KH-M2 cells was not affected by brefeldin A treatment, which blocks endoplasmic reticulum-to-Golgi apparatus transport.

We hypothesized that CASK might be secreted in exosomes, leading to its release into the extracellular environment. Exosome release is an alternative protein secretion pathway that has been suggested to play a major role in the release of IL-1β from murine bone marrow-derived macrophages (37). We detected CASK in exosomes purified from KM-H2 cells and different macrophage subsets. CASK levels were much lower (barely detectable) in the exosome-depleted supernatant than in the supernatant containing exosomes. This suggests that CASK secretion may be associated with exosomes. Before their release into the extracellular medium, exosomes accumulate in MVBs formed by the inward budding and scission of vesicles from the limiting membrane of late endosomes into the lumen. During this process, transmembrane and peripheral membrane proteins are incorporated into the invaginated membrane, whereas cytosolic components are engulfed and enclosed in the vesicles. CASK, which is known to be a membrane-associated cytoplasmic scaffold protein, had a diffuse cytoplasmic distribution pattern not restricted to endosomal compartments. Co-immunoprecipitation methods showed that a fraction of CASK was associated with ALIX. ALIX is connected to syndecans, providing a support for the packaging of cargoes for vesicle entry and triggering vesicle formation (38). CASK has been reported to bind to syndecan (17, 39). Thus, CASK may be recruited to exosomes through binding to ALIX and syndecan.

CASK was also detected in exosomes purified from patients with iNS, and was present in significantly larger amounts in exosomes from the rFSGS group and from M2 macrophages. This higher level of CASK in exosomes was correlated with higher levels of CASK in the cytoplasm of M2 macrophages *in vitro,* suggesting that the higher levels of CASK secretion are mostly due to higher levels of CASK production in the corresponding cells rather than an increase in the rate of transfer of CASK to exosomes.

We previously showed that recombinant CASK induced a reorganization of the actin cytoskeleton of cultured podocytes.

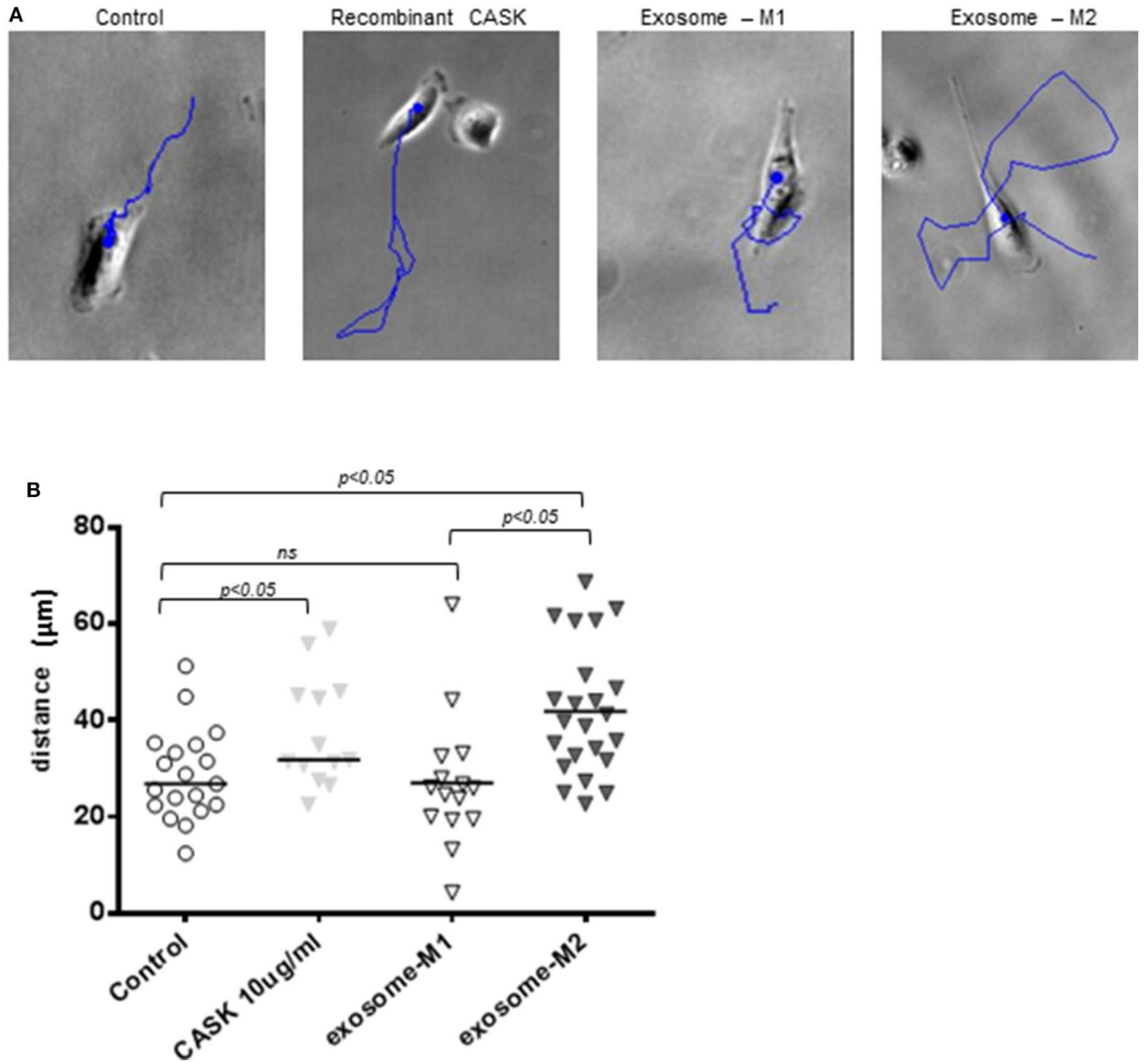

FIGURE 7 | Increase in podocyte motility induced by exosomes from M2 macrophages. Podocyte motility was evaluated by video microscopy for 24 h in the presence of recombinant CASK, M1 exosomes or M2 exosomes. **(A)** Blue lines show the displacement of single cells. **(B)** Image J analysis showing the distance migrated by podocytes. Statistical differences were determined by ANOVA test.

M2 macrophage-derived exosomes caused a loss of actin stress fibers and the redistribution of synaptopodinin the podocytes *in vitro*. The depletion of exosomes from the supernatant of M2 macrophages or KM-H2 cells (data not shown) was associated with an absence of change in actin stress fiber organization and synaptopodin redistribution, supporting the notion that exosomes bearing CASK play an important role. The alterations to the actin cytoskeleton in the presence of CASK or exosomes bearing CASK are associated with a motile phenotype of podocytes.

This study was a prospective study designed to collect PBMC of patients. Because of the small number of patients enrolled in this study, the results should be validated on a larger cohort of patients. However, our results defined a secretory pathway of CASK and increased the level of evidence of immune cells implication in rFSGS. In conclusion, we report here the synthesis of CASK by the $CD14^{+}$cells of rFSGS patients, and M2 polarized macrophages. These results highlighted the role of monocytes/macrophages in the pathology of rFSGS.

DATA AVAILABILITY STATEMENT

The datasets generated for this study are available on request to the corresponding author.

ETHICS STATEMENT

The studies involving human participants were reviewed and approved by Comité Consultatif de Protection des

Personnes participant à une Recherche Biomédicale ≫ (n°4/010). The patients/participants provided their written informed consent to participate in this study.

AUTHOR CONTRIBUTIONS

XZ performed the study and cell biology. AD designed the study and wrote the paper. SB was following patients. HL provided recombinant CASK and podocytes. AV performed western blotting. FH performed Flow cytometry.

FUNDING

The work was supported by grants from INSERM Transfer, the Association des Malades d'un Syndrome Néphrotique primitif ou idiopathique, la Fondation du Rein.

REFERENCES

1. sD'Agati VD, Kaskel FJ, Falk RJ. Focal segmental glomerulosclerosis. *N Engl J Med.* (2011) 365:2398–411. doi: 10.1056/NEJMra1106556
2. Crosson JT. Focal segmental glomerulosclerosis and renal transplantation. *Transpl Proc.* (2007) 39:737–43. doi: 10.1016/j.transproceed.2007.02.010
3. Fornoni A, Sageshima J, Wei C, Merscher-Gomez S, Aguillon-Prada R, Jauregui AN, et al. 3rd, Rituximab targets podocytes in recurrent focal segmental glomerulosclerosis. *Sci Transl Med.* (2011) 3:85ra46. doi: 10.1126/scitranslmed.3002231
4. Yu CC, Fornoni A, Weins A, Hakroush S, Maiguel D, Sageshima J, et al. Abatacept in B7-1-positive proteinuric kidney disease. *N Engl J Med.* (2013) 369:2416–23. doi: 10.1056/NEJMoa1304572
5. Beaufils H, Alphonse JC, Guedon J, Legrain M. Focal glomerulosclerosis: natural history and treatment. A report of 70 cases. *Nephron.* (1978) 21:75–85. doi: 10.1159/000181374
6. Canaud G, Dion D, Zuber J, Gubler MC, Sberro R, Thervet E, et al. Recurrence of nephrotic syndrome after transplantation in a mixed population of children and adults: course of glomerular lesions and value of the Columbia classification of histological variants of focal and segmental glomerulosclerosis (FSGS). *Nephrology Dialysis Transpl.* (2010) 25:1321–8. doi: 10.1093/ndt/gfp500
7. Dantal J, Bigot E, Bogers W, Testa A, Kriaa F, Jacques Y, et al. Effect of plasma protein adsorption on protein excretion in kidney-transplant recipients with recurrent nephrotic syndrome. *N Engl J Med.* (1994) 330:7–14. doi: 10.1056/NEJM199401063300102
8. Ponticelli C, Recurrence of focal segmental glomerular sclerosis (FSGS) after renal transplantation. Nephrology, dialysis, transplantation : official publication of the European *Dialysis Transpl Assoc.* (2010) 25:25–31. doi: 10.1093/ndt/gfp538
9. Delville M, Sigdel TK, Wei C, Li J, Hsieh SC, Fornoni A, et al. A circulating antibody panel for pretransplant prediction of FSGS recurrence after kidney transplantation. *Sci Transl Med.* (2014) 6:256ra136. doi: 10.1126/scitranslmed.3008538
10. Koliwad SK, Gray NE, Wang JC. Angiopoietin-like 4 (Angptl4): A glucocorticoid-dependent gatekeeper of fatty acid flux during fasting. *Adipocyte.* (2012) 1:182–7. doi: 10.4161/adip.20787
11. Michaud JL, Chaisson KM, Parks RJ, Kennedy CR. FSGS-associated alpha-actinin-4 (K256E) impairs cytoskeletal dynamics in podocytes. *Kidney Int.* (2006) 70:1054–61. doi: 10.1038/sj.ki.5001665
12. Reiser J, von Gersdorff G, Loos M, Oh J, Asanuma K, Giardino L, et al. Induction of B7-1 in podocytes is associated with nephrotic syndrome. *J Clin Invest.* (2004) 113:1390–7. doi: 10.1172/JCI20402
13. Wei C, El Hindi S, Li J, Fornoni A, Goes N, Sageshima J, et al. Circulating urokinase receptor as a cause of focal segmental glomerulosclerosis. *Nature Med.* (2011) 17:952–60. doi: 10.1038/nm.2411
14. Wei C, Moller CC, Altintas MM, Li J, Schwarz K, Zacchigna S, et al. Modification of kidney barrier function by the urokinase receptor. *Nat Med.* (2008) 14:55–63. doi: 10.1038/nm1696
15. Zhu P, Goh YY, Chin HF, Kersten S, Tan NS. Angiopoietin-like 4: a decade of research. *Biosci Rep.* (2012) 32:211–9. doi: 10.1042/BSR20110102
16. Beaudreuil S, Zhang X, Herr F, Harper F, Candelier JJ, Fan Y, et al. Circulating CASK is associated with recurrent focal segmental glomerulosclerosis after transplantation. *PLoS ONE.* (2019) 14:e0219353. doi: 10.1371/journal.pone.0219353
17. Cohen AR, Woods DF, Marfatia SM, Walther Z, Chishti AH, Anderson JM. Human CASK/LIN-2 binds syndecan-2 and protein 4.1 and localizes to the basolateral membrane of epithelial cells. *J Cell Biol.* (1998) 142:129–38. doi: 10.1083/jcb.142.1.129
18. Hata Y, Butz S, Sudhof TC. CASK: a novel dlg/PSD95 homolog with an N-terminal calmodulin-dependent protein kinase domain identified by interaction with neurexins. *J Neurosci.* (1996) 16:2488–94. doi: 10.1523/JNEUROSCI.16-08-02488.1996
19. Yan Y, Dalmasso G, Sitaraman S, Merlin D. Characterization of the human intestinal CD98 promoter and its regulation by interferon-gamma. *Am J Physio.* (2007) 292:G535–45. doi: 10.1152/ajpgi.00385.2006
20. Yan Y, Vasudevan S, Nguyen H, Bork U, Sitaraman S, Merlin D. Extracellular interaction between hCD98 and the PDZ class II domain of hCASK in intestinal epithelia. *J Membr Biol.* (2007) 215:15–26. doi: 10.1007/s00232-007-9001-8
21. Cunard R, Kelly CJ. T cells and minimal change disease. *J Am Soc Nephrol.* (2002) 13:1409–11. doi: 10.1097/01.ASN.0000016406.82019.B3
22. Sellier-Leclerc AL, Duval A, Riveron S, Macher MA, Deschenes G, Loirat C, et al. A humanized mouse model of idiopathic nephrotic syndrome suggests a pathogenic role for immature cells. *J Am Soc Nephrol.* (2007) 18:2732–9. doi: 10.1681/ASN.2006121346
23. Audard V, Zhang SY, Copie-Bergman C, Rucker-Martin C, Ory V, Candelier M, et al. Occurrence of minimal change nephrotic syndrome in classical Hodgkin lymphoma is closely related to the induction of c-mip in Hodgkin-Reed Sternberg cells and podocytes. *Blood.* (2010) 115:3756–62. doi: 10.1182/blood-2009-11-251132
24. Stephan JL, Deschenes G, Perel Y, Bader-Meunier B, Brunat-Mentigny M, Lejars O, et al. Nephrotic syndrome and Hodgkin disease in children: a report of five cases. *Eur J Ped.* (1997) 156:239–42. doi: 10.1007/s004310050592
25. Cattran DC, Alexopoulos E, Heering P, Hoyer PF, Johnston A, Meyrier A, et al. Cyclosporin in idiopathic glomerular disease associated with the nephrotic syndrome : workshop recommendations. *Kidney Int.* (2007) 72:1429–47. doi: 10.1038/sj.ki.5002553
26. Grimbert P, Valanciute A, Audard V, Pawlak A, Le gouvelo S, Lang P, et al. Truncation of C-mip (Tc-mip), a new proximal signaling protein, induces c-maf Th2 transcription factor and cytoskeleton reorganization. *J Exp Med.* (2003) 198:797–807. doi: 10.1084/jem.20030566
27. Sahali D, Pawlak A, Valanciute A, Grimbert P, Lang P, Remy P, et al. A novel approach to investigation of the pathogenesis of active minimal-change nephrotic syndrome using subtracted cDNA library screening. *J Am Soc Nephrol.* (2002) 13:1238–47.
28. Mundel P, Heid HW, Mundel TM, Kruger M, Reiser J, Kriz W. Synaptopodin: an actin-associated protein in telencephalic dendrites and renal podocytes. *J Cell Biol.* (1997) 139:193–204. doi: 10.1083/jcb.139.1.193
29. Record M, Subra C, Silvente-Poirot S, Poirot M. Exosomes as intercellular signalosomes and pharmacological effectors. *Biochem Pharmacol.* (2011) 81:1171–82. doi: 10.1016/j.bcp.2011.02.011
30. Ghossoub R, Lembo F, Rubio A, Gaillard CB, Bouchet J, Vitale N, et al. Syntenin-ALIX exosome biogenesis and budding into multivesicular bodies are controlled by ARF6 and PLD2. *Nat Commun.* (2014) 5:3477. doi: 10.1038/ncomms4477

31. Benigni A, Gagliardini E, Remuzzi G. Abatacept in B7-1-positive proteinuric kidney disease. *N Engl J Med.* (2014) 370:1261–3. doi: 10.1056/NEJMc1400502
32. Delville M, Baye E, Durrbach A, Audard V, Kofman T, Braun L, et al. B7-1 Blockade Does Not Improve Post-Transplant Nephrotic Syndrome Caused by Recurrent FSGS. *J Am Soc Nephrol.* (2016) 27:2520–7. doi: 10.1681/ASN.2015091002
33. Ziegler-Heitbrock HW, Definition of human blood monocytes. *J Leukocyte Biol.* (2000) 67:603–6. doi: 10.1002/jlb.67.5.603
34. Wolf AA, Yanez A, Barman PK, Goodridge HS. The ontogeny of monocyte subsets. *Front Immunol.* (2019) 10:1642. doi: 10.3389/fimmu.2019.01642
35. Le Berre L, Herve C, Buzelin F, Usal C, Soulillou JP, Dantal J. Renal macrophage activation and Th2 polarization precedes the development of nephrotic syndrome in Buffalo/Mna rats. *Kidney Int.* (2005) 68:2079–90. doi: 10.1111/j.1523-1755.2005.00664.x
36. J.G. van den Berg, Weening JJ. Role of the immune system in the pathogenesis of idiopathic nephrotic syndrome. *Clin Sci.* (2004) 107:125–36. doi: 10.1042/CS20040095
37. Qu Y, Tang Y, Cao D, Wu F, Liu J, Lu G, et al. Genetic polymorphisms in alveolar macrophage response-related genes, and risk of silicosis and pulmonary tuberculosis in Chinese iron miners. *Int J Hyg Environ Health.* (2007) 210:679–89. doi: 10.1016/j.ijheh.2006.11.010
38. Baietti MF, Zhang Z, Mortier E, Melchior A, Degeest G, Geeraerts A, et al. Syndecan-syntenin-ALIX regulates the biogenesis of exosomes. *Nat Cell Biol.* (2012) 14:677–85. doi: 10.1038/ncb2502
39. Bernfield M, Gotte M, Park PW, Reizes O, Fitzgerald ML, Lincecum J, et al. Functions of cell surface heparan sulfate proteoglycans. *Ann Rev Biochem.* (1999) 68:729–77. doi: 10.1146/annurev.biochem.68.1.729

Conflict of Interest: The authors declare that the research was conducted in the absence of any commercial or financial relationships that could be construed as a potential conflict of interest.

frontiers in Immunology

ORIGINAL RESEARCH
published: 19 May 2020
doi: 10.3389/fimmu.2020.00800

Fli1 Downregulation in Scleroderma Myeloid Cells Has Profibrotic and Proinflammatory Effects

Andreea M. Bujor[1], Fatima El Adili[1,2], Arshi Parvez[1], Grace Marden[1] and Maria Trojanowska[1]*

[1] Division of Rheumatology, Department of Medicine, Arthritis and Autoimmune Diseases Research Center, Boston University School of Medicine, Boston, MA, United States, [2] Division of Rheumatology, Department of Medicine, Whitaker Cardiovascular Institute, Boston University School of Medicine, Boston, MA, United States

Scleroderma (SSc) is an autoimmune connective tissue disease characterized by immune dysregulation, vasculopathy, and fibrosis. We have previously demonstrated that low Fli1 expression in SSc fibroblasts and endothelial cells plays an important role in SSc pathogenesis. Cells of myeloid and lymphoid origin also express Fli1 and are dysregulated in patients with SSc, playing key roles in disease pathogenesis. However, the role for immune Fli1 in SSc is not yet clear. Our aim was to elucidate whether Fli1 contributes to the immune dysregulation seen in SSc. Comparison of the expression of Fli1 in monocytes, B- and T-cell fractions of PBMCs isolated from SSc patients and healthy controls (HC), showed an increase in Fli1 levels in monocytes. We used siRNA transfected human myeloid cells and mouse peritoneal macrophages obtained from *Fli1*$^{flox/flox}$*LysMCre*$^{+/+}$ mice, and found that markers of alternative macrophage activation were increased with Fli1 deletion. Coculture of Fli1-deficient myeloid cells and primary human or mouse fibroblasts resulted in a potent induction of collagen type I, independent of TGFβ upregulation. We next analyzed global gene expression profile in response to Fli1 downregulation, to gain further insight into the molecular mechanisms of this process and to identify differentially expressed genes in myeloid cells. Of relevance to SSc, the top most upregulated pathways were hallmark IFN-γ and IFN-α response. Additionally, several genes previously linked to SSc pathogenesis and fibrosis in general were also induced, including CCL2, CCL7, MMP12, and CXCL10. ANKRD1, a profibrotic transcription co-regulator was the top upregulated gene in our array. Our results show that Fli1-deficient myeloid cells share key features with cells from SSc patients, with higher expression of profibrotic markers and activation of interferon responsive genes, thus suggesting that dysregulation of Fli1 in myeloid cells may contribute to SSc pathogenesis.

Keywords: scleroderma, Fli1, monocytes, macrophages, fibroblasts, fibrosis

OPEN ACCESS

Edited by:
Anna-Maria Hoffmann-Vold, Oslo University Hospital, Norway

Reviewed by:
Andras Perl, Upstate Medical University, United States
Sun Jung Kim, Northwell Health, United States

****Correspondence:***
Andreea M. Bujor
andreea@bu.edu

Specialty section:
This article was submitted to Autoimmune and Autoinflammatory Disorders, a section of the journal Frontiers in Immunology

Received: *31 January 2020*
Accepted: *07 April 2020*
Published: *19 May 2020*

Citation:
Bujor AM, El Adili F, Parvez A, Marden G and Trojanowska M (2020) Fli1 Downregulation in Scleroderma Myeloid Cells Has Profibrotic and Proinflammatory Effects. Front. Immunol. 11:800. doi: 10.3389/fimmu.2020.00800

INTRODUCTION

Scleroderma (SSc) is an autoimmune connective tissue disease characterized by immune dysregulation, vasculopathy, and fibrosis. There is no cure for SSc and therapies are at best modestly effective. Immune cell dysregulation occurs early in the course of the disease and it involves both the innate and adaptive systems (1, 2). Despite significant advances in the field, the exact mechanism by which immune dysregulation contributes to vasculopathy and fibrosis is currently unclear.

Depending on the environment, macrophages (Mø) can acquire distinct functional phenotypes: classical, proinflammatory Mø (C-Mø), and alternative, pro-fibrotic Mø (A-Mø), which are just extremes on a continuum of activation states (3). In response to Th_1 cytokines, including IL-1 and IFNγ, Mø secrete proinflammatory cytokines IL-12, IL-23, IL-1, and TNFα. In contrast, Th_2 type cytokine (IL-4/13) stimulation leads to differentiation into the profibrotic Mø phenotype, with expression of the CD163 and CD204 markers and secretion of the IL-10, TGFβ, and CCL18, followed by tissue fibrosis (4). Flow cytometry analysis of SSc-PBMCs (peripheral blood mononuclear cells) revealed a higher proportion of monocytes (Mo), which showed expression of CD163 and CD204, while these markers were not present in PBMCs from healthy controls (HC) (5). CD163+/CD204 + cells were also identified in SSc skin biopsies, not only in the perivascular regions, but also between thickened collagen bundles (5). When SSc Mo from ILD patients were stimulated *in vitro* with LPS (lipopolysaccharide), which normally induces differentiation into C-Mø, there was increased expression of CD163 compared to control Mo (6). A comprehensive meta-analysis of transcriptomic data sets from skin biopsies of three large independent SSc patient populations identified a conserved set of genes across the SSc patients, with one subset containing genes characteristic of alternative Mø activation (7).

Monocytes derived from SSc patients may contribute to fibrogenesis via secretion of profibrotic factors, elevated in the skin and serum of SSc patients, is expressed by fibroblasts in SSc and plays an active role early in the disease pathogenesis by recruiting Mo and fibrocytes into tissues. Blockade of CCL2 prevented fibrosis in several animal models of SSc, including sclerodermatous graft-versus-host disease and bleomycin induced skin fibrosis (8, 9). Monocytes also secrete CCL2, which in turn may act as a profibrotic stimulus on fibroblasts, leading to secretion of TGFβ and extracellular matrix production (10). TGFβ further enhances CCL2 production, leading to a complex cascade of feedback regulation. CCL7/MCP-3 (monocyte chemoattractant protein-3), a chemotactic protein closely related to CCL2, is overexpressed by mononuclear cells and fibroblasts in SSc. Apart from promoting the recruitment of immune cells, CCL7 also has direct profibrotic effects on fibroblasts, and its expression is stimulated by TGFβ (11). Another characteristic of SSc Mo is enhanced migration. SSc-interstitial lung disease Mo express higher levels of CCR2 (receptor for CCL2) and lower levels of caveolin-1, both proven to increase the Mo migratory capacity (12, 13). Up-regulation of CCL2 and CCR2 was also reported on macrophages in the skin of early diffuse SSc (14). While all these studies strongly support a role for the mononuclear phagocytic system in SSc, their pathogenetic mechanism is far from clear.

Fli1, a member of the Ets family of transcription factors, is expressed in endothelial cells, fibroblasts and immune cells. Fli1 knockout mice die during embryogenesis due to a defect in vessel maturation (15). Abnormal expression of Fli1 is seen in autoimmune diseases, including systemic lupus erythematosus and SSc, where it plays important roles in pathogenesis (16, 17). Fli1 plays a key role in repressing collagen genes in healthy tissues and its deficiency likely contributes to the upregulated matrix production in SSc (18). Recent studies also suggest that Fli1 is critical for vessel maturation and stabilization. Mice with a conditional knockout of Fli1 in endothelial cells displayed abnormal skin vasculature, with greatly compromised vessel integrity and markedly increased vessel permeability, similar to SSc vasculopathy (19). Fli1 plays an important role in regulating mononuclear phagocyte cell development. Monocytes, Mø and dendritic cells populations were increased in the $Fli1^{\Delta CTA/\Delta CTA}$ mice (lacking the C-terminal regulatory domain) compared with wild-type littermates, via de-repression of the Flt3L promoter (20). Additionally, Fli1 deficiency induced CXCL13 expression in murine peritoneal macrophages (21). Given the important role that it plays in SSc pathogenesis, our aim was to elucidate whether Fli1 contributes to the immune dysregulation seen in this disease.

MATERIALS AND METHODS

Cell Isolation and Culture

Informed consent was obtained from all subjects, and the study was conducted in compliance with Institutional Review Board guidelines. PBMCs from SSc and HC were isolated by Ficoll Paque gradient centrifugation. CD14+ monocytes were isolated via positive selection from fresh PBMCs using EasyStep human monocyte isolation kit (Stem Cell Technologies, Cambridge, MA catalog # 18058) according to manufacturer's instructions. B cells were then isolated from remaining PBMCs using EasySep Human CD19 positive selection kit II (Stem Cell Technologies, Cambridge, MA catalog # 17754), and T cells through negative selection (CD14-/CD19- cells). Human dermal fibroblasts were isolated from the forearm of HC and cultured as previously described (22). Cells in passages 2–5 were used for experiments. For experiments using mouse cells, dermal fibroblasts were isolated from the back of the mice after shaving and overnight collagenase digestion. Mature quiescent resident mouse peritoneal macrophages were isolated according to a previously published protocol (23). For coculture experiements, THP1 cells, or mouse peritoneal macrophages were either directly seeded on top of fibroblasts or inside cell inserts with 0.4 μm membrane pore size (Corning, NY, product number 353493).

Generation of Myeloid-Cell Specific Fli1-Knockout Mice

All experimental procedures were approved by the Boston University Animal Care and Use Committee and conducted in accordance with the guidelines of the National Institutes of Health. The floxed Fli1 mice was generated using a Fli1 targeting vector purchased from the KOMP repository (UCDavis, Sacramento,CA, Clone name: HTGR06010_A_1_C02, **Figure 1**). 129 agouti embryonic stem cell lines harboring an insertion with

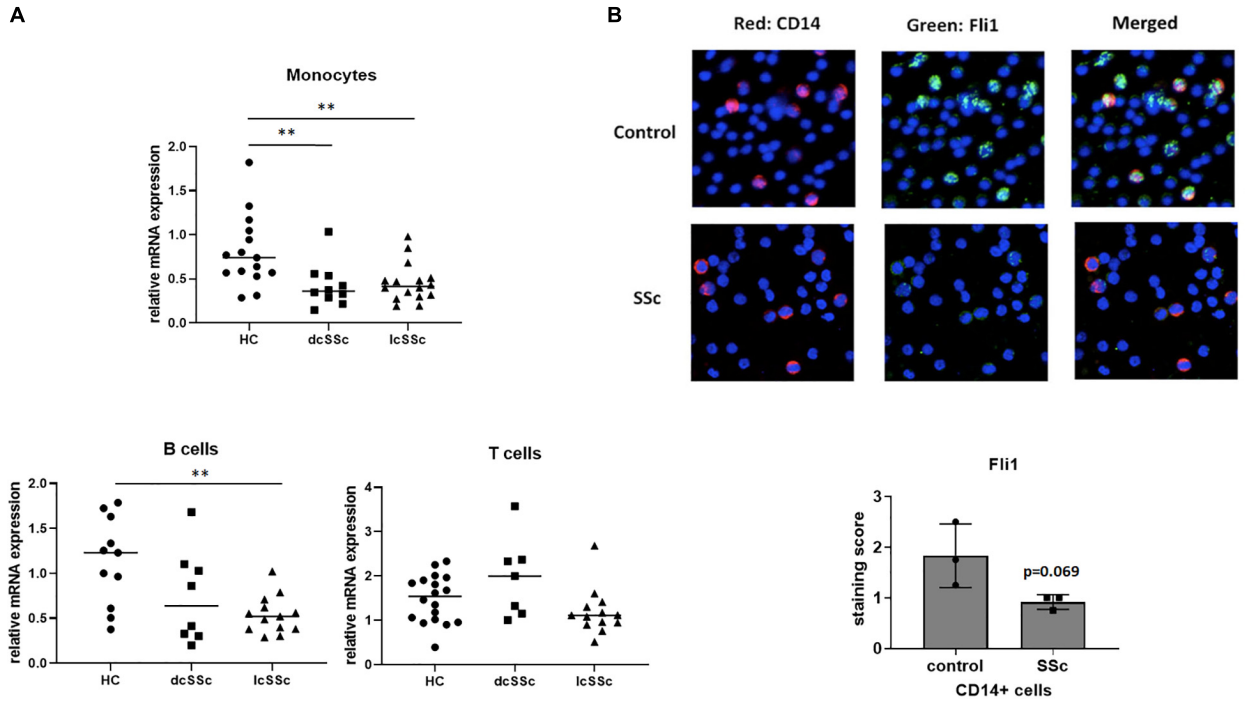

FIGURE 1 | Monocytes isolated from SSc patients have low levels of Fli1. **(A)** Monocytes, T and B lymphocytes were isolated from healthy controls (HC) and SSc patients (diffuse-dcSSc or limited-lcSSc) and mRNA levels of Fli1 were analyzed using quantitative RT-PCR. One way ANOVA (GraphPad Prims 7) was used to compare SSc to control. **(B)** Isolated peripheral blood mononuclear cells (PBMCs) from SSc and healthy controls (HC) were stained with CD14 for monocytes (red) and Fli1 (green) antibodies, and DAPI was used to counterstain the nuclei. Representative images and quantification are shown ($n = 3$ each). $^{**}p < 0.01$.

the KOMP vector were generated at the Transgenic Mouse Core at Harvard Medical School (Boston, MA, United States) and used for blastocyst injection to generate chimeric mice, which were then selected for germline transmission. Heterozygous mice with the targeted gene mutation were then crossed with transgenic C57BL/6J mice expressing *FLP1* recombinase (FlpE) in all tissues, under the human β-actin promoter (transgenic B6.Cg-Tg (ACT*FlpE*)9205Dym/J, available from The Jackson Laboratory, United States, Stock number 005703). The resultant Fli1$^{flox/flox}$ mice were further crossed to C57BL/6 mice for 10 generations.

For the generation of Fli1 conditional knockout mice, mice expressing the Cre recombinase under the control of the myeloid-specific Lyz2 promoter were purchased from the Jackson Laboratory (B6.129P2-*Lyz2*$^{TM1(cre)Ifo}$/J, Bar Harbor, ME, United States) and crossed with Fli1$^{flox/flox}$ mice.

Six to eight-week-old homozygous mice were used for all experiments. The genotyping primers suggested by Jackson Laboratory were used for the Cre mice and for the Fli1$^{flox/flox}$ mice the following primers were used: gactcaaaccagggaaagttgc (3′ loxP site, forward), ttgggaaggtggaatctagcag (3′ loxP site, reverse), acctttgctccacacatctga (5′ loxP site, forward), accttggttacaggactgagtg (5′ loxP, reverse).

Isolation of Peritoneal Macrophages From Mice

Mice were euthanized following an IACUC approved animal protocol, then 5 cc germ-free PBS was flushed into the peritoneal cavity and the peritoneal lavage fluid was collected. Cells were centrifuged (350 *g* for 5 min at 4°), and plated in RPMI media for 2 h, then unattached cells were washed twice with sterile PBS. Attached macrophages were then harvested using trypsin.

Immunofluorescence

Cells were washed twice with 1 × PBS and fixed in acetone:methanol 1:1 for 15 min at room temperature, followed by three washes in PBS. Cells were permeabilized with 0.25% Triton X-100 for 15 min followed by three washes in PBS and 1 h blocking in 3% bovine serum albumin (BSA) in PBS at room temperature. Cells were incubated with anti- Fli1 (mouse anti-human, BD Bioscience #554266), CD14 (rabbit monoclonal, Abcam, Cambridge, MA, United States) and Collagen type I (Southern Biotech, #1310-01), and CD163 (mouse antihuman #MCA1853, BioRad, hercules, CA, United States) primary antibodies (1:100 in 1% BSA in PBS) at 4°C overnight followed by three washes in PBS. The bound antibody was detected using anti-rabbit (Alexa Fluor 594, Invitrogen) and anti-mouse (Alexa Fluor 488, Invitrogen) secondary antibodies (1:500 each) for 1 h. Coverslips were washed three times in PBS in the dark and then mounted on glass slides using Vectashield mounting medium with DAPI (Vector Laboratories Inc, Burlingame, CA, United States). Slides were blinded, and ten random fields were examined using an Olympus microscope attached to a digital camera. Semi-quantitative evaluation of staining results for Fli1 expression in CD14 positive cells from SSc patients and controls

PBMCs was independently assessed in a blind manner by two experienced investigators. Staining was scored using 7 scores: 0, 0.5, 1, 1.5, 2, 2.5, and 3, according to the intensity, with results expressed as the mean ± standard deviation.

Inhibition of Protein Expression by Small Interfering RNA (siRNA)

For the inhibition of Fli1 expression using siRNA, THP1 cells or dermal fibroblasts were grown to 80% confluence and transiently transfected with 50 nm Fli1 siRNA (Dharmacon, Fli1 ON-TARGETplus SMARTpool – a mixture of 4 siRNAs provided as a single reagent for enhanced potency and specificity), or the corresponding concentration of scrambled non-silencing siRNA (Scr, Dharmacon, On-TARGETplus Non-targeting Control Pool) for 48 h. Cells were then serum starved overnight and treated as indicated.

Quantitative RT-PCR

Total RNA was extracted using TRI Reagent and 1 μg was converted to cDNA as previously described (22). Quantitative real time RT–PCR was performed using SYBR Green mixture (Applied Biosystems, Carlsbad, CA, United States) on a StepOnePlus Real-Time PCR system using 1 μl of cDNA in triplicate with beta actin as internal control. The sequences of the primers used are provided in **Supplementary Table S1**.

Global Gene Expression Profile

THP1 cells were grown in RPMI media and Fli1 expression was inhibited using siRNA as described above. Cells were then converted to M_0 macrophages 24 h later using 10 ng/ml PMA (Phorbol 12-myristate 13-acetate) for 4 h, then media changed and cells treated with 100 ng/ml M-CSF (macrophage colony stimulating factor) for 48 h. Cells were lysed using TRIzol and RNA was then extracted using Zymo Research kit and integrity analyzed using Agilent Bioanalyzer. Purity of the RNA samples was confirmed using a NanoDrop spectrophotometer.100 ng of high quality RNA (RIN > 9.0) with Biotin labeling was performed using the WT Plus reagent kit (Affymetrix, Santa Clara, CA, United States) according to the manufacturer's protocol. The labeled, fragmented DNA was hybridized to the Affymetrix Human Gene 2.0 ST Array for 18 h in a GeneChip Hybridization oven 640 at 45°C with rotation (60 rpm). The hybridized samples were washed and stained using an Affymetrix fluidics station 450. Raw Affymetrix CEL files were normalized to produce Entrez Gene-identifier-specific expression values using the implementation of the Robust Multiarray Average (RMA) in the affy Bioconductor package (version 1.36.1), using R version 2.15.1 and the Brainarray hugene20sthsentrezgcdf R package (version 23.0.0). Raw and processed microarray data have been deposited in the Gene Expression Omnibus (GEO), Series GSE144625.

Statistical Analysis

One-way analysis of variance (ANOVA) followed by Tukey's multiple comparisons test was used for comparisons of differences between three or more groups. Unpaired *t*-test was used when only two groups were compared. All statistical analyses were performed using *GraphPad Prism 8* software (La Jolla, CA, United States). A p value of <0.05 was considered significant.

RESULTS

Monocytes Isolated From Scleroderma Patients Have Low Levels of Fli1

To investigate whether Fli1 contributes to immune abnormalities in SSc, we first evaluated the expression levels of Fli1 in T cell, B cells and monocytes isolated from SSc patients and healthy controls (HC). The mRNA levels of Fli1 were decreased in monocytes isolated from both limited and diffuse SSc patients, compared to HC (**Figure 1A**). The levels of Fli1 were not significantly different in T or B cells, except for B cells from limited SSc patients, which had lower Fli1 compared to controls. The protein levels of Fli1 were then investigated in patient's monocytes by immunofluorescence staining using CD14 and Fli1 specific antibodies and PBMCs, confirming the downregulation in SSc patients (**Figure 1B**).

Conditioned Media From Fli1 Deficient Mø Has Profibrotic Effects on Fibroblasts

Scleroderma monocytes can contribute to fibrosis and fibroblast activation via several mechanisms, including enhanced differentiation into alternatively activated macrophages and secretion of profibrotic molecules. We next treated human dermal fibroblasts with conditioned media from Fli1 depleted THP1 cells to assess whether low levels of Fli1 contributes to their ability to enhance fibrosis. As seen in **Figure 2A**, conditioned media from Mø with low Fli1 induced periostin and type I collagen gene expression in human dermal fibroblasts, supporting a profibrotic role for Fli1 deletion in Mø. Interestingly, CCL2 was upregulated in fibroblasts treated with Fli1 siRNA, suggesting that Fli1-deficient fibroblasts could recruit monocytes in early disease stages (**Figure 2B**). In turn, a soluble factor secreted by Fli1-deficient Mø may induce expression of profibrotic genes in fibroblasts, thus potentially contributing to SSc fibrosis.

Expression of the Alternative Macrophage Activation Markers Is High in Fli1 Deficient Cells

To assess whether low Fli1 seen in SSc monocytes skews them toward differentiation into A-Mø, we next used Fli1-depleted THP1 cells, and treated them with 10 ng/ml phorbol-12-myristate-13-acetate (PMA) for 4 h to induce transdifferentiation into Mø (24). Downregulation of Fli1 in these cells resulted in an induction of the mRNA levels of CD163, MRC1, both linked to A-Mø (**Figure 3A**).

While wildly used for the study of the myeloid cell functions *in vitro*, THP1 cells are secondary, immortalized

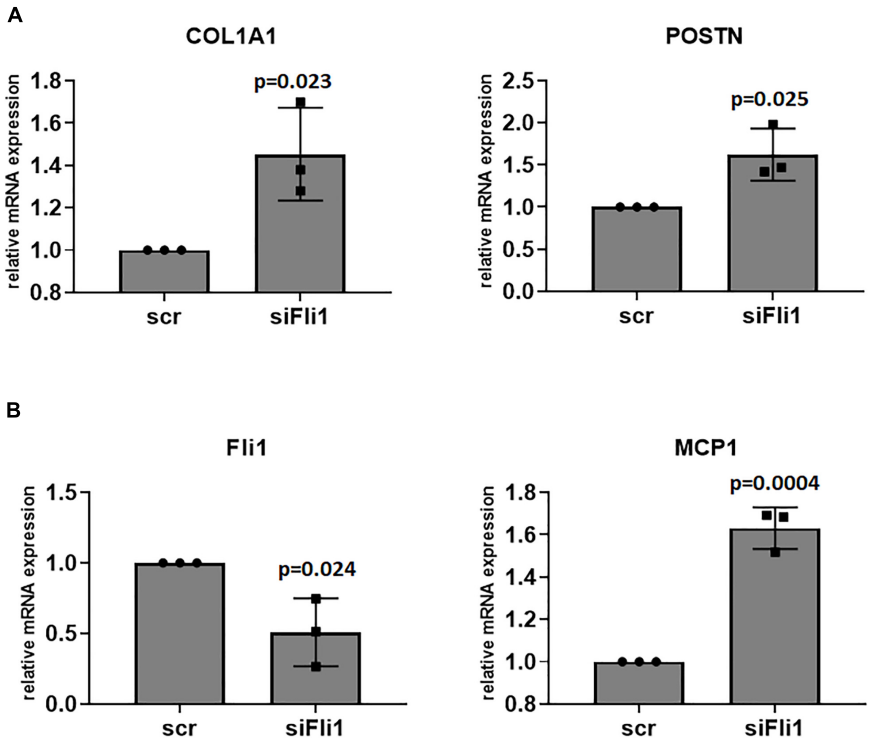

FIGURE 2 | (A) Conditioned media from Fli1 deficient Mø has profibrotic effects on fibroblasts. Confluent, serum starved human dermal fibroblast were treated with conditioned media from scr and siFli1 treated THP1 cells, and after 6 h cell pellets were collected and mRNA levels of Collagen (COL1A1) and POSTN (periostin) were analyzed via RT-PCR. **(B)** Downregulation of Fli1 in fibroblasts induces CCL2/MCP1 mRNA levels. Confluent, serum starved human dermal fibroblast were treated with scr and siFli1 for 48 h then cell pellets were collected and mRNA levels of CCL2 were analyzed via RT-PCR. Mean ± SD.

cells, phenotypically, and functionally different from primary Mo. To validate these findings, we asked whether deletion of Fli1 in primary mouse Mø would skew them toward an alternative activation phenotype and influence development of fibrosis.

Targeted Ablation of the Fli1 Gene in Mouse Myeloid Cells

Fli1 knockout mice die during embryogenesis due to a defect in vessel maturation (15), precluding assessment of the function of Fli1 in myeloid cells in these mice. To examine the function of Fli1 in mouse myeloid cells, we generated mice with *Fli1* gene selectively ablated in cells of myeloid origin. $Fli1^{flox/flox}$ mice were generated as described in section "Materials and Methods," and crossed with LysMCre transgenic mice that express the Cre-recombinase under the transcriptional control of the myeloid-specific Lyz2 promoter. Cre-mediated recombination in the resultant $Fli1^{flox/flox}LysMCre^{+/+}$ mice results in excision of exon 3 from the Fli1 gene (**Figure 3B**). To confirm that excision of the exon 3 of Fli1 results in a corresponding loss of Fli1 protein, we performed western blot analysis on protein extracts from peritoneal Mø harvested from the $Fli1^{flox/flox}LysMCre^{+/+}$. **Figure 3B** (right, bottom) shows that Fli1 was significantly downregulated in the transgenic mice compared to wild types.

Next, we compared the expression of A-Mø markers in peritoneal Mø isolated from wild type and $Fli1^{flox/flox}LysMCre^{+/+}$mice. Similar to results in THP1 cells, the mRNA levels of CD163 and the mouse specific A-Mø marker FIZZ1 were significantly induced in mice with conditional Fli1 deletion (**Figure 3C**).

Collectively, these results suggest that decreased expression of Fli1 in SSc monocytes may directly contribute to fibrogenesis via imparting cells a selective bias toward alternative macrophage activation and secretion of soluble profibrotic mediators.

Depletion of Fli1 in Myeloid Cells Does Not Induce TGFβ Gene Expression

TGFβ is a central mediator of fibrosis and a key molecule involved in SSc pathogenesis (25, 26). Secretion of TGFβ by myeloid cells has been implicated in the induction of fibrogenesis (27). As an initial step to test whether these molecules mediate the profibrotic phenotype induced by Fli1 downregulation in myeloid cells, we measured the mRNA levels after siRNA mediated depletion of Fli1 in THP1 cells and in peritoneal $Fli1^{flox/flox}LysMCre^{+/+}$ macrophages compared to wild type mice. No significant changes in the levels of TGFβ were found (**Figure 4A**). TGFβ patway activation can be a result of either increased TGFβ protein levels, enhanced

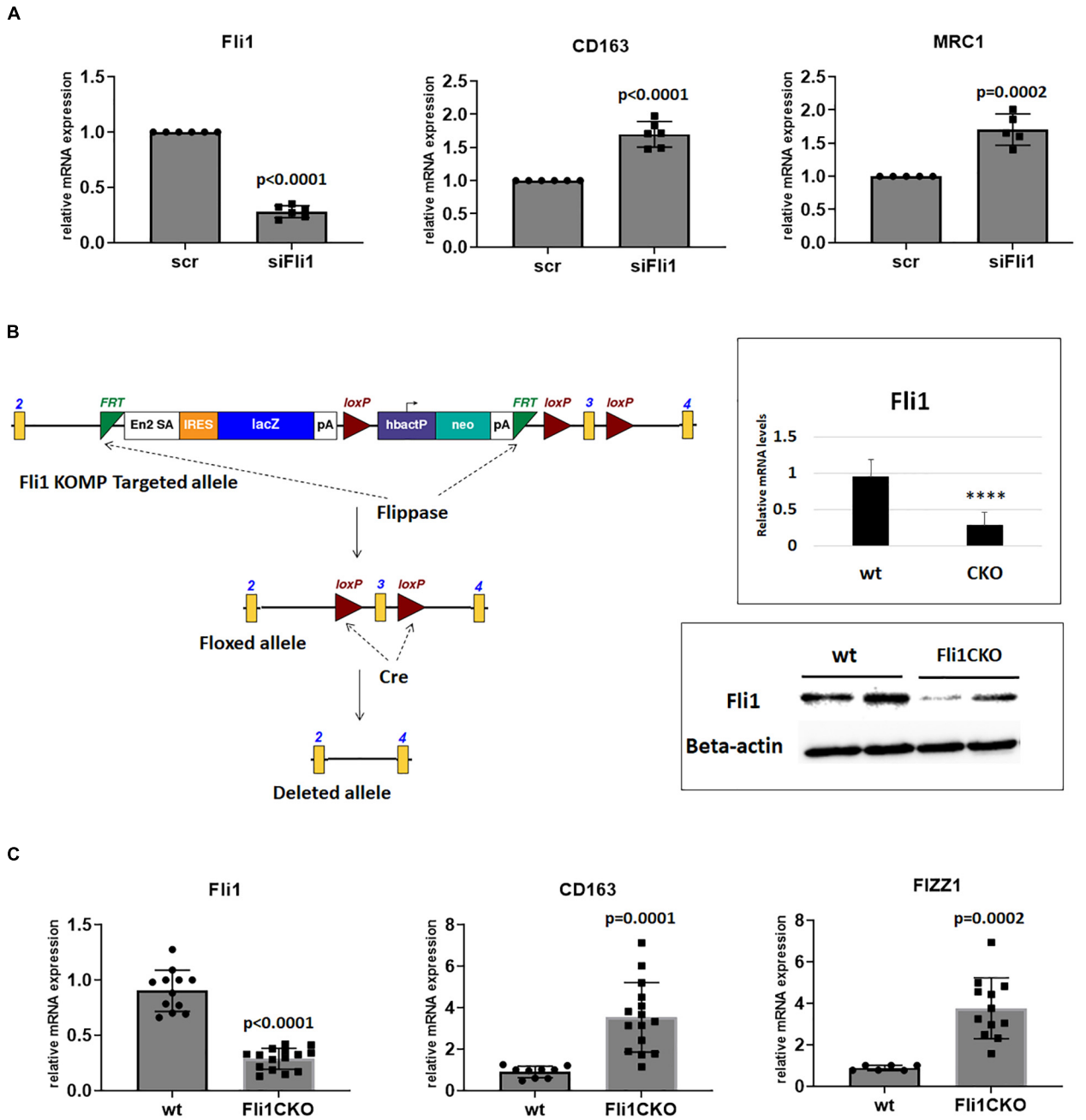

FIGURE 3 | Expression of the A-Mø markers is high in Fli1 deficient cells. **(A)** Human THP1 cells were treated with Fli1 and scr siRNA and then 24 h later with 10 ng PMA for 4 h, then mRNA extracted after total 48 h, and relative mRNA levels of CD163 and MRC1 were quantified by RT-PCR (n = 4). Mean ± SD. **(B)** Generation of myeloid specific Fli1 knockout mice (*Fli1*$^{flox/flox}$*LysMCre*$^{+/+}$, Fli1 CKO). Schematic outline of the Fli1 KOMP targeting construct and Fli1 floxed allele. Neo: neomycin resistance gene. Flippase: FLP recombinase to remove the Neo cassette. The structures of the mutant allele after *in vivo* Cre-mediated recombination in myeloid cells lacks exon 3. Upper right panel shows relative mRNA levels of Fli1 in peritoneal macrophages isolated from wt and Fli1CKO mice, and bottom right panel shows protein levels of Fli1 in wt and Fli1CKO. Two mice were pooled for protein levels in each group. Beta actin was used as control for loading. **(C)** Peritoneal macrophages were collected from wt and Fli1 CKO mice and mRNA extracted and RT-PCR used to quantify levels of CD163, and FIZZ1. Individual mice used for each sample. ****$p < 0.0001$.

activation of latent TGFβ, or enhanced receptor expression. To further explore a potential contribution of the TGFβ pathway in this process, we next assessed phosphorylation levels of its main downstream target, Smad2. There was no induction in P-Smad2 in fibroblasts cocultured with Fli1-depleted THP1 cells (**Figure 4B**). Collectively, these results suggest that a TGFβ-independent mechanism may be responsible for the fibrogenic effects of low Fli1 in myeloid cells.

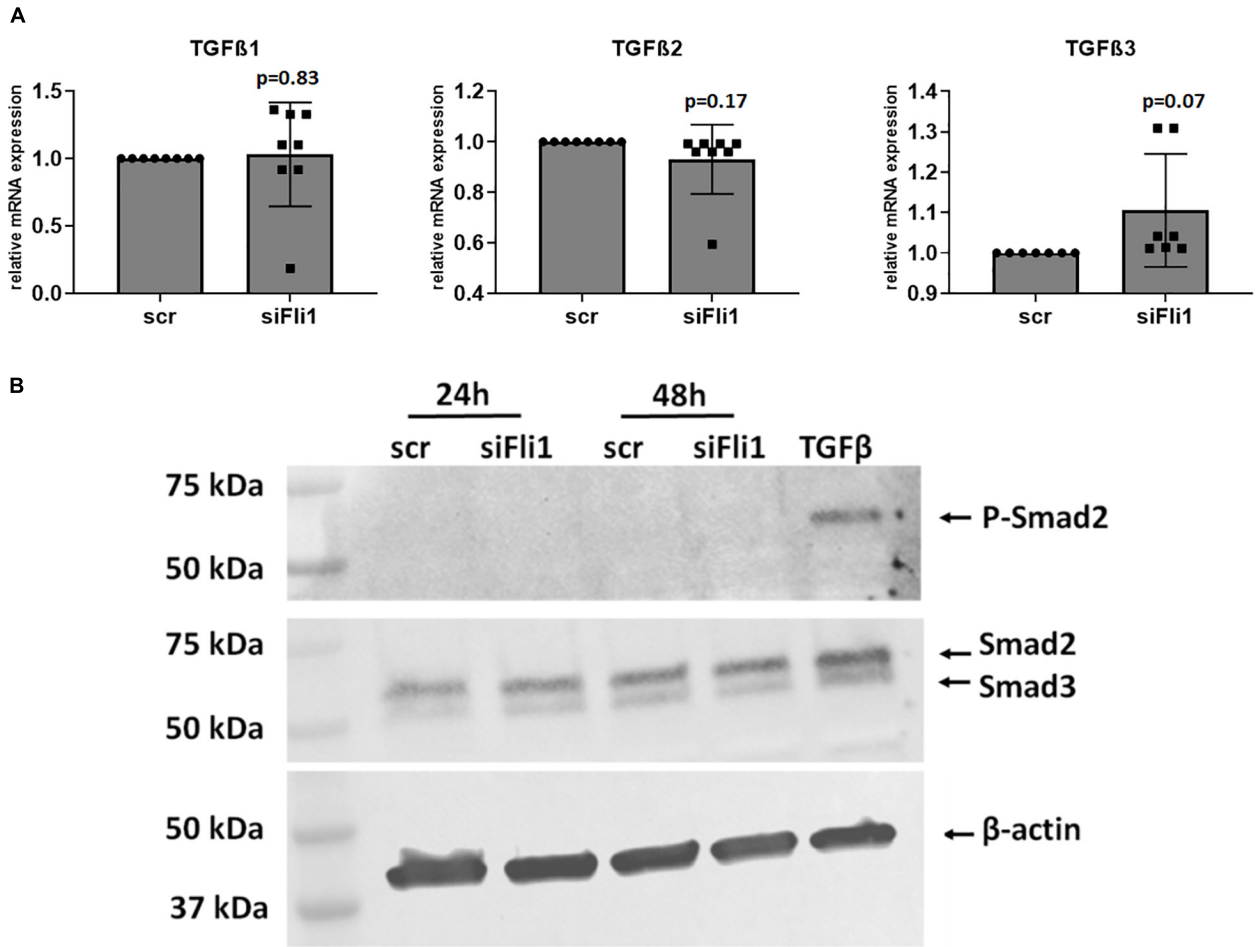

FIGURE 4 | Fli1 downregulation in myeloid cells does not induce TGFβ pathway. **(A)** THP1 cells were transfected as described with scr and Fli1 siRNA and levels of TGFβ isoforms 1, 2, and 3 were measured at the mRNA levels 48 h later using RT-PCR. $n > 3$ each, not statistically significant. **(B)** THP1 monocytes were transfected with siRNA and 48 h later they were plated directly over confluent, serum starved human dermal fibroblasts. After 24 and 48 h, cells were washed and cell layers collected and protein extracted. Levels of P-Smad2 (Ser465/467) and total Smad2/3 were assessed by Western Blot, with TGFβ as positive control.

Coculture of Myeloid Cells and Fibroblasts Enhances the Profibrotic Effects Seen With Low Fli1

Isolated cell cultures do not reflect the complexity of cell-cell interaction *in vivo*, and direct contact of myeloid cells and fibroblasts may be required to fully achieve the profibrotic phenotype. To better assess paracrine and juxtacrine effects of myeloid-fibroblast cell-cell signaling, we used an experimental model of both non-contacting and direct contact co-culturing. To study the paracrine effects of myeloid-fibroblast co-cultures, we used transwell inserts that provided physical separation of the two cell types while allowing free cytokine transport between them. When cells were co-cultured in direct, physical contact with each other, there was a potent induction of collagen (**Figure 5A**, right panel). Similar, but less pronounced upregulation of collagen was seen when the two cells types were not in direct contact with each other (**Figure 5A**, left panel). In a separate experiment, we assessed the expression of CD163 on THP1 cells with low Fli1 in coculture with fibroblasts, and confirmed at the protein levels by immunofluorescent staining that this marker of alternative macrophage activation is induced under these experimental conditions as well (**Figure 5B**). Altogether, these results indicate that direct cell-cell contact between activated macrophages and fibroblasts may be required for the full fibrogenic effect of Fli1 depletion in myeloid cells.

Global Gene Expression Profile in Fli1-siRNA Treated THP1 Cells Reveals Upregulation of Pro-Inflammatory and Migration-Related Genes

Identification of molecular pathways and genes that are significantly associated with Fli1 downregulation might help unravel the mechanisms of myeloid-induced fibrosis. We next downregulated Fli1 expression via siRNA in PMA-treated THP1 monocytes (24), then performed microarray analysis using the Affimetrix GeneChip human 2.0 ST gene array. The expression

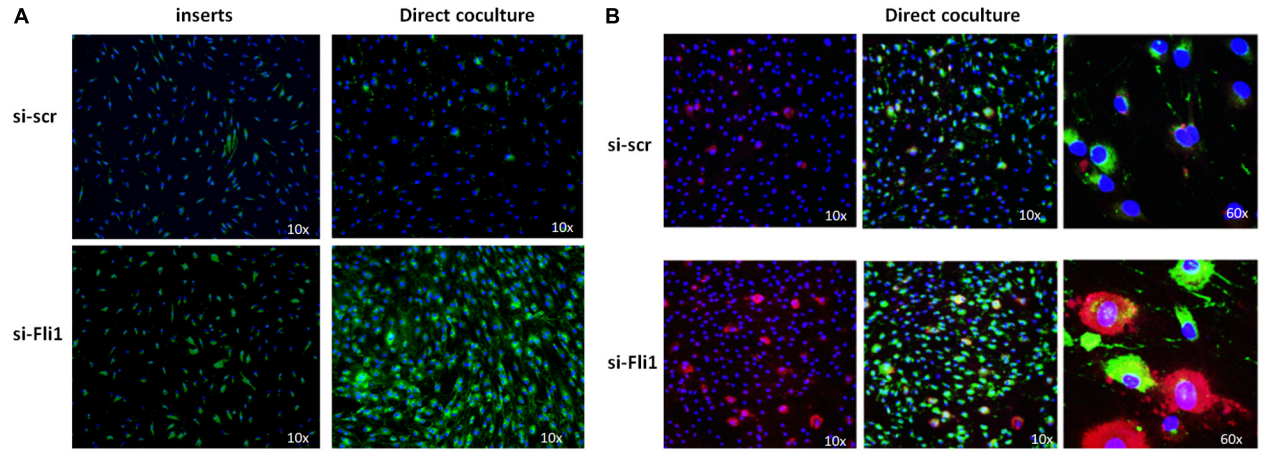

FIGURE 5 | (A) Effects on collagen deposition in indirect (inserts) and direct coculture of human dermal fibroblasts and siRNA-treated THP1 cells. THP1 monocytes were transfected with siRNA and 48 h later they were plated either inside inserts or directly over confluent, serum starved fibroblasts. Cells were washed and immunofluorescent staining using specific anti-Collagen type I antibodies was done on day 5. DAPI was used to counterstain the nuclei. Representative images sown, $n = 3$ each. **(B)** Chamber slides were used for direct coculture experiments as described above and cells were stained with CD163 for A-Mø (red) and Collagen type I (green) antibodies, and DAPI was used to counterstain the nuclei. Representative images are shown ($n = 3$ each).

of Fli1 was reduced approximately 3.7-fold in the samples treated with siFli1 compared to the scrambled controls. A total of 778 genes were identified as significantly differentially expressed in cells with low Fli1 ($p < 0.005$). The top twenty most up and down-regulated genes ($p > 0.001$) are shown in **Figure 6A**. Gene ontology analysis revealed multiple biological functions that were significantly enriched with siRNA treatment. Notably, several pathways related to activation of inflammatory programs (hallmark IFN-γ & IFN-α response, and hallmark TNFα signaling via NFKB), as well as pathways related to immune cell migration, were among the top upregulated biological pathways (**Figure 6B**). Amongst the alternative activation markers only CD163 was significantly upregulated in the microarray analysis (1.5 fold, $p = 0.00073$). Detailed heatmaps of the leading edge genes of all gene sets with FDR $q < 0.25$ are available in **Supplementary Data Sheet S1**.

Validation of the Differentially Expressed Genes by Real-Time PCR

In order to assess the validity of the microarray results, we used QRT-PCR to compare the expression of top genes of interest that had significant expression changes in the microarray analyses. The following genes were selected: ANKRD1, CCL2, CCL7, CCL8, CXCL10, HMOX1, and MMP12. Results are presented in **Figure 7A**. The top differentially expressed gene in the microarray was ANKRD1, which was induced by 11-fold in cells with low Fli1. This upregulation was confirmed by quantitative RT-PCR analysis, and analysis of CT values revealed that ANKRD1 is expressed at very low levels in primary Mo, and not expressed in quiescent human dermal fibroblasts (data not shown). Next, we used peritoneal macrophages from $Fli1^{flox/flox}LysMCre^{+/+}$ mice and validated our microarray results for the genes presented in **Figure 7B**. Of note, several interferon response genes, including CCL7, CCL2, and CXCL10 were upregulated in these mice, similar to published results in SSc patients. Our microarray data identified multiple Fli1 targets in myeloid cells that had differential expression compared to controls and that are relevant to SSc, thus potentially mediating the altered phenotype of myeloid cells with low Fli1 expression seen in our study.

DISCUSSION

We show here that monocytes from patients with systemic sclerosis have decreased levels of the transcription factor Fli1, and provide new evidence for an antifibrotic role for Fli1 in these cells. SiRNA mediated downregulation of Fli1 in human myeloid cells, and via Cre mediated targeted disruption in mouse myeloid cells resulted in key changes in their phenotype, with acquisition of alternative, profibrotic features and activation of key interferon regulated genes, similar to what has been described in SSc patients. This suggested that decreased levels of Fli1 in Mo/Mø in SSc patients may contribute to fibrosis via alternative Mø activation and secretion of pro-fibrotic and pro-inflammatory cytokines, with paracrine activation of fibroblasts.

The mononuclear phagocytic system in SSc is central to fibrogenesis, and may contribute to fibrosis via enhanced Mo migration into injured tissues, differentiation of Mo into fibrocytes or A-Mø, and secretion of various pro-fibrotic mediators (28).

It is challenging to elucidate the diverse role of myeloid cells in driving fibrosis, due to their vast plasticity and functional diversity, all depending on a multitude of variables, including tissue environment, injury specific co-signals, and particular disease etiology. Alterations in Mø polarization may contribute to SSc pathogenesis, with a higher proportion of CD163 and CD204 positive Mo reported in SSc blood and skin biopsies (5, 7, 29). However, the mechanism that drives this phenotypic change is

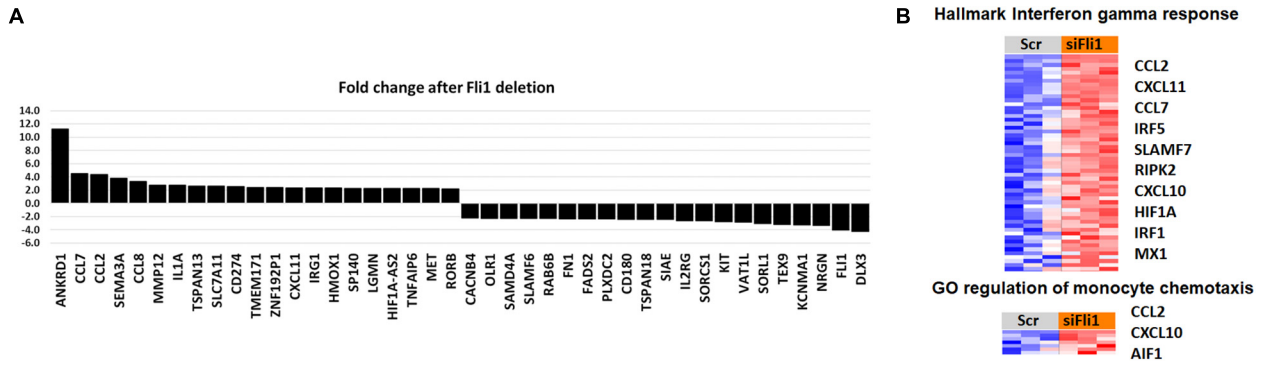

FIGURE 6 | Global gene expression profile in Fli1-siRNA treated myeloid cells. **(A)** The top twenty most up and down-regulated genes after Fli1 deletion in myeloid cells ($p > 0.001$). **(B)** Heatmap of gene-expression of IFN-γ and monocyte migration pathways. Blue indicates repressed mRNA levels and red elevated levels.

still elusive. We found low levels of Fli1 in SSc monocytes and increased expression of A-Mø markers in cells with low Fli1, both in human and mice. Our observations thus identify Fli1 as one of the factors that possibly orchestrates the changes described in SSc myeloid cells.

While helpful to appreciate the heterogeneity and functions of Mø, characterizing them as classical vs. alternatively activated based on the initial stimulus or a mere handful of markers is not ideal and does not reflect the complex *in vivo* microenvironment. There are likely differences in Mø phenotype that span beyond this classification. While this study shows that the expression of alternative activation markers is elevated in cells with low Fli1, the observation that cells have a profibrotic phenotype is of particular relevance, as it implies that decreased Fli1 in myeloid cells has distinctive consequences on cell function.

Myeloid cells derived from SSc patients may contribute to fibrosis via secretion of profibrotic factors, including TGFβ (25). Although we found that conditioned media from Mo with low Fli1 induced fibrosis via direct stimulation of fibroblasts, we failed to find an increase in mRNA levels of TGFβ in Fli1-depleted myeloid cells, and there was no activation of the TGFβ/Smad2 pathway, suggesting that other factors might mediate their profibrotic effects on fibroblasts. Based on the microarray analysis, we identified further potential candidates. To that extent, CCL2 and CCL7 were among the top upregulated genes after Fli1 downregulation in Mø in our study. Earlier reports showed that both these chemokines are increased in SSc serum and can enhance collagen synthesis, but a direct role for CCL2 on fibroblasts is controversial (9–11). Using quantitative RT-PCR analysis, we were unable to find expression of the CCL2 receptor CCR2 in human dermal fibroblasts (data not shown), suggesting that secretion of CCL2 by myeloid cells with low Fli1 does not directly contribute to collagen upregulation. This is in agreement with previously published studies that found no expression of CCL2 receptors and no direct effect of CCL2 stimulation or CCL2 blocking on collagen production by fibroblasts (30, 31). However, indirect fibrogenic effects of CCL2 may still contribute to SSc tissue fibrosis, and there is abundant published evidence to support this notion (32). Fibroblasts serve as a source of cytokines and chemokines that influence the microenvironment, and earlier studies have shown that coculture of myeloid cells and fibroblasts enhances fibrosis (33). SSc fibroblasts are known to secrete CCL2, which attracts monocytes to the site of injury. In our study deletion of Fli1 in both myeloid cells and fibroblasts enhanced CCL2 mRNA levels, thus potentially creating an unbalanced cytokine response that could lead to tissue damage and fibrosis. While the profibrotic phenotype of myeloid cells in SSc may be due to a combination of factors, our finding suggest that the increased CCL2 and CCL7 levels in SSc patients (31, 34–36) may be in part due to Fli1 downregulation in Mo and could contribute to fibrosis.

Of relevance to SSc, CXCL10 and CXCL11 are IFN-γ inducible chemokines that are upregulated in SSc (37, 38) and that showed a twofold induction in response to Fli1 deletion in our study. Interestingly, it was previously found that CXCL10 is expressed early in the disease and associated with a worse outcome, including more severe pulmonary fibrosis (39). Whether overexpression of or CXCL11 contributes to fibrosis remains to be determined.

MMP12 is a matrix metalloproteinase produced at high levels by IL-4- and IL-13- alternative-activated macrophages, and has been implicated in development of fibrosis. MMP-12 deficiency reduced myocardial fibrosis following myocardial infarction and angiotensin II infusion, liver, and lung fibrosis after Schistosoma mansoni infection and lung fibrosis after bleomycin infusion in mice. Proposed mechanisms are via suppression of specific ECM-degrading MMPs and decreased matrix degradation, induction of alternative-macrophage infiltration and PDGF production, and activation of TGF-β signaling pathway (40–43). Importantly, MMP-12 was increased in the serum, alveolar macrophages and dermal inflammatory infiltrates in SSc patients, and its expression correlated with the severity of skin and lung fibrosis (44). MMP12 was induced in response to Fli1 downregulation in myeloid cells, suggesting that MMP12 may contribute to the profibrotic effects we observed in our system. However, MMP12 expression was not enhanced in mice with deletion of Fli1, suggesting there are differences the response to Fli1 downregulation between mice and human cells.

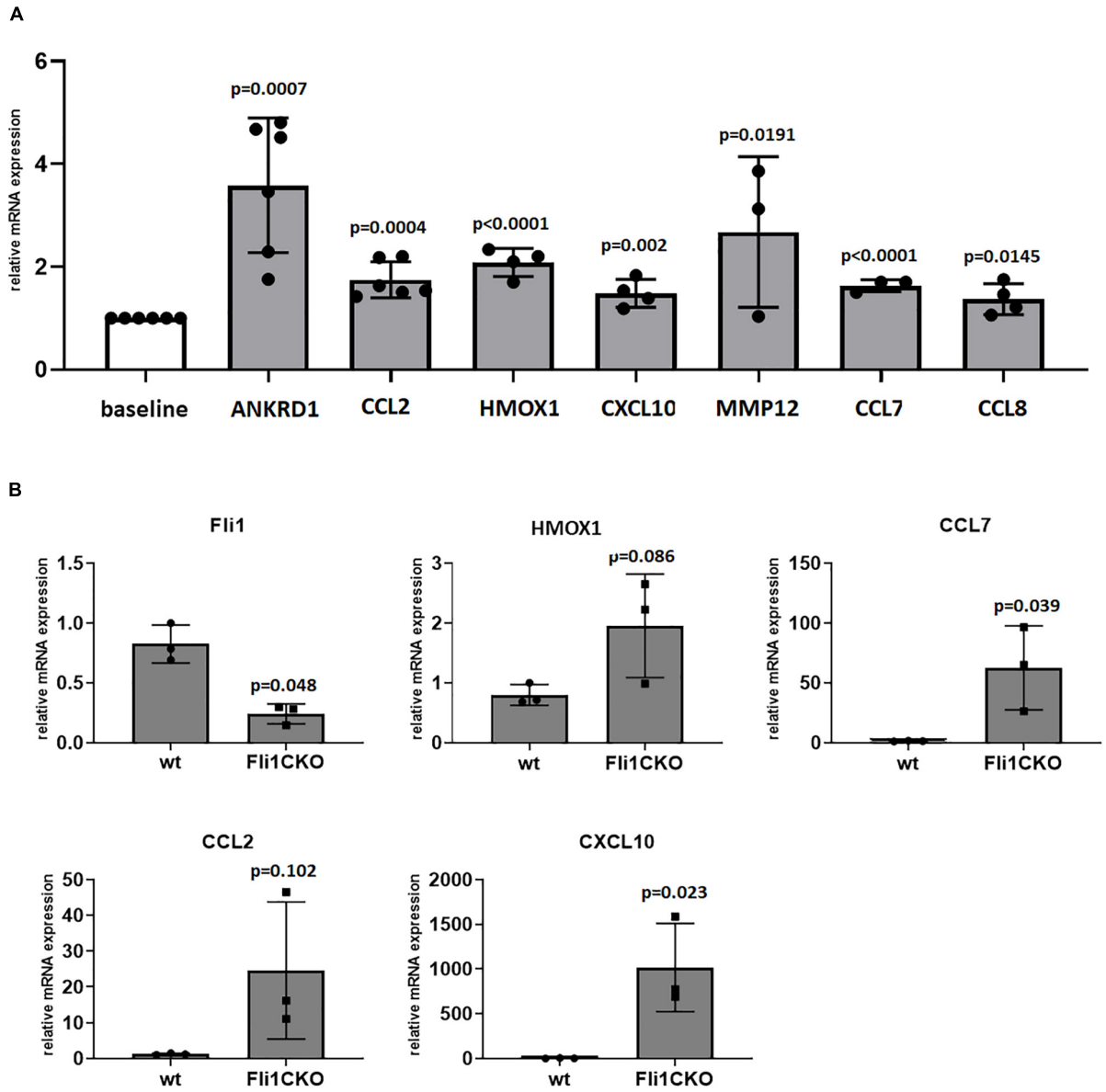

FIGURE 7 | Validation of differentially expressed genes via quatitative RT-PCR. Results in THP1 cells treated with siRNA in **(A)** or peritoneal macrophages isolated from Fli1CKO mice and wt mice in **(B)**. mRNA levels of selected genes of interest were analyzed by RT-PCR in ≥3 separate experiments and the results are presented as bar graphs with controls arbitrarily set at 1. scr, scrambled.

We also found elevated expression of HMOX1, a stress-inducible protein upregulated by various oxidative and inflammatory signals, with immunomodulatory and anti-inflammatory properties. It has been reported that HMOX-1 induction drives the phenotypic shift to M2 macrophages, however, a previous study found that HMOX-1 was expressed at lower levels in SSc compared to controls.

Interestingly, the top, most highly expressed gene in our microarray was ANKRD1 (ankryn repeat domain 1), a transcription co-regulator expressed predominantly in cardiac muscle, with roles in heart and skin fibrosis (45, 46). Very little is known about the role of ANKRD1 in immune cells. We found that ANKRD1 is expressed in cells with low Fli1, but is found at very low levels or not expressed in primary monocytes. This is consistent with previous studies showing that ANKRD1 was sharply and dramatically induced in immune cells during wound healing, but mostly absent in intact skin (47). Interestingly, the profibrotic molecule TGFβ was also shown to induce ANKRD1 expression in vascular smooth muscle cells (48). Given the importance of ANKRD1 in regulating fibrosis and cardiac hypertrophy, further studies are required to assess if its induction in response to low Fli1 in Mo/Mø contributes to their fibrogenic effects.

A number of studies looking at transcriptional profiling of peripheral blood cells from SSc patients revealed significantly increased expression of both type I and type II IFN-inducible genes (49, 50). High levels of both IFN-regulated genes and alternative Mo/Mø activation markers were shown in SSc PBMCs and fibrotic lung tissue (51, 52). It has been suggested that IFN-γ may play a role in the early stages of SSc, in which inflammation and vasculopathy are predominant features (53, 54). Our microarray data shows that downregulation of Fli1 in myeloid cells resulted in induction of numerous interferon-regulated genes, with both type I and type II interferon responses being recorded. Significantly, mice with targeted deletion of Fli1 in myeloid cells showed similar response in the interferon related genes CCL2, CCL7, and CXCL10, confirming microarray data.

Beyond regulating the expression of alternative activation markers and other profibrotic genes, we recorded Fli1 regulation of migration-associated genes, which may control the migratory properties of monocytes *in vivo*, allowing infiltration of tissues and thus potentially contributing to the inflammatory infiltrates seen in the lesional skin in SSc and to exaggerated tissue fibrosis.

Our study has several limitations. Firstly, THP1 cells were used for the experiments involving the effects of Fli1 downregulation in human myeloid cells. While widely used in published studies, these are immortalized cells and may not accurately reflect what occurs in primary cell lines. Nevertheless, we were able to reproduce our results in macrophages from mice with conditional deletion of Fli1, suggesting that findings in human cells could be accurate. Moving forward, it will be of interest to characterize the *in vivo* consequences in loss of Fli1 in myeloid cells, however, this was beyond the scope of this paper. Secondly, while we provide solid evidence that the loss of Fli1 in myeloid cells is profibrotic, we failed to unravel the exact mechanism that leads to this outcome. Our results however, suggest that a number of genes could contribute to this effect, including CCL2, CCL7, MMP12, CXCL10, and ANKRD1.

In summary, myeloid cells with low Fli1 reproduce key features with myeloid cells from SSc patients, with higher expression of profibrotic markers and activation of interferon responsive genes, thus suggesting that Fli1-deficient Mø may contribute to SSc fibrosis. Further work will be required to establish the exact mechanistic details of these findings, but microarray analyses suggests that a combination of factors could be responsible for the modulation of the observed profibrotic effects of myeloid cells with low Fli1 on fibroblasts.

DATA AVAILABILITY STATEMENT

The datasets generated for this study can be found in the NCBI Gene Expression Omnibus (GEO: Series GSE144625) database.

ETHICS STATEMENT

The studies involving human participants were reviewed and approved by the Boston University, IRB. The patients/participants provided their written informed consent to participate in this study. The animal study was reviewed and approved by Boston University Institutional Animal Care & Use (IACUC).

AUTHOR CONTRIBUTIONS

AB contributed to the study design, data curation, statistical analysis and interpretation of the data, and drafted and revised the manuscript. FE performed the staining, coculture, Q-PCR experiments, and participated in the analysis interpretation and revised the manuscript. AP performed Q-PCR experiments in THP1 cells and revised the manuscript. GM participated breeding and genotyping of the mice, and Q-PCR analyses, and in the analysis interpretation, and critically revised the manuscript. MT contributed to the study conceptions and design and revised the manuscript. All authors read and approved the final manuscript.

FUNDING

This study was supported from internal funding (AB) and generation of Fli1 floxed mice was supported from NIH NIAMS R01 AR42334 (MT).

ACKNOWLEDGMENTS

We would like to thank the BU Microarray and Sequencing Resource Data Core for their excellent service provided in the global gene expression analysis described in this manuscript.

SUPPLEMENTARY MATERIAL

The Supplementary Material for this article can be found online at: https://www.frontiersin.org/articles/10.3389/fimmu.2020.00800/full#supplementary-material

REFERENCES

1. Laurent P, Sisirak V, Lazaro E, Richez C, Duffau P, Blanco P, et al. Innate immunity in systemic sclerosis fibrosis: recent advances. *Front Immunol*. (2018) 9:1702. doi: 10.3389/fimmu.2018.01702
2. Chizzolini C, Brembilla NC, Montanari E, Truchetet ME. Fibrosis and immune dysregulation in systemic sclerosis. *Autoimmun Rev*. (2011) 10:276–81. doi: 10.1016/j.autrev.2010.09.016
3. Martinez FO, Gordon S. The M1 and M2 paradigm of macrophage activation: time for reassessment. *F1000Prime Rep*. (2014) 6:13. doi: 10.12703/P6-13
4. Shapouri-Moghaddam A, Mohammadian S, Vazini H, Taghadosi M, Esmaeili SA, Mardani F, et al. Macrophage plasticity, polarization, and function in health and disease. *J Cell Physiol*. (2018) 233:6425–40. doi: 10.1002/jcp.26429
5. Higashi-Kuwata N, Jinnin M, Makino T, Fukushima S, Inoue Y, Muchemwa FC, et al. Characterization of monocyte/macrophage subsets in the skin and

peripheral blood derived from patients with systemic sclerosis. *Arthritis Res Ther*. (2010) 12:R128. doi: 10.1186/ar3066
6. Mathai SK, Gulati M, Peng X, Russell TR, Shaw AC, Rubinowitz AN, et al. Circulating monocytes from systemic sclerosis patients with interstitial lung disease show an enhanced profibrotic phenotype. *Lab Invest*. (2010) 90:812–23. doi: 10.1038/labinvest.2010.73
7. Mahoney JM, Taroni J, Martyanov V, Wood TA, Greene CS, Pioli PA, et al. Systems level analysis of systemic sclerosis shows a network of immune and profibrotic pathways connected with genetic polymorphisms. *PLoS Comput Biol*. (2015) 11:e1004005. doi: 10.1371/journal.pcbi.1004005
8. Greenblatt MB, Sargent JL, Farina G, Tsang K, Lafyatis R, Glimcher LH, et al. Interspecies comparison of human and murine scleroderma reveals IL-13 and CCL2 as disease subset-specific targets. *Am J Pathol*. (2012) 180:1080–94. doi: 10.1016/j.ajpath.2011.11.024
9. Kimura M, Kawahito Y, Hamaguchi M, Nakamura T, Okamoto M, Matsumoto Y, et al. SKL-2841, a dual antagonist of MCP-1 and MIP-1 beta, prevents bleomycin-induced skin sclerosis in mice. *Biomed Pharmacother*. (2007) 61:222–8. doi: 10.1016/j.biopha.2006.10.002
10. Chujo S, Shirasaki F, Kondo-Miyazaki M, Ikawa Y, Takehara K. Role of connective tissue growth factor and its interaction with basic fibroblast growth factor and macrophage chemoattractant protein-1 in skin fibrosis. *J Cell Physiol*. (2009) 220:189–95. doi: 10.1002/jcp.21750
11. Ong VH, Evans LA, Shiwen X, Fisher IB, Rajkumar V, Abraham DJ, et al. Monocyte chemoattractant protein 3 as a mediator of fibrosis: overexpression in systemic sclerosis and the type 1 tight-skin mouse. *Arthritis Rheum*. (2003) 48:1979–91. doi: 10.1002/art.11164
12. Lee R, Reese C, Perry B, Heywood J, Bonner M, Zemskova M, et al. Enhanced chemokine-receptor expression, function, and signaling in healthy African American and scleroderma-patient monocytes are regulated by caveolin-1. *Fibrogenesis Tissue Repair*. (2015) 8:11. doi: 10.1186/s13069-015-0028-7
13. Tourkina E, Bonner M, Oates J, Hofbauer A, Richard M, Znoyko S, et al. Altered monocyte and fibrocyte phenotype and function in scleroderma interstitial lung disease: reversal by caveolin-1 scaffolding domain peptide. *Fibrogenesis Tissue Repair*. (2011) 4:15. doi: 10.1186/1755-1536-4-15
14. Carulli MT, Ong VH, Ponticos M, Shiwen X, Abraham DJ, Black CM, et al. Chemokine receptor CCR2 expression by systemic sclerosis fibroblasts: evidence for autocrine regulation of myofibroblast differentiation. *Arthritis Rheum*. (2005) 52:3772–82. doi: 10.1002/art.21396
15. Spyropoulos DD, Pharr PN, Lavenburg KR, Jackers P, Papas TS, Ogawa M, et al. Hemorrhage, impaired hematopoiesis, and lethality in mouse embryos carrying a targeted disruption of the Fli1 transcription factor. *Mol Cell Biol*. (2000) 20:5643–52. doi: 10.1128/mcb.20.15.5643-5652.2000
16. Georgiou P, Maroulakou I, Green J, Dantis P, Romanospica V, Kottaridis S, et al. Expression of ets family of genes in systemic lupus erythematosus and Sjogren's syndrome. *Int J Oncol*. (1996) 9:9–18.
17. Kubo M, Czuwara-Ladykowska J, Moussa O, Markiewicz M, Smith E, Silver RM, et al. Persistent down-regulation of Fli1, a suppressor of collagen transcription, in fibrotic scleroderma skin. *Am J Pathol*. (2003) 163:571–81. doi: 10.1016/S0002-9440(10)63685-1
18. Asano Y, Bujor AM, Trojanowska M. The impact of Fli1 deficiency on the pathogenesis of systemic sclerosis. *J Dermatol Sci*. (2010) 59:153–62. doi: 10.1016/j.jdermsci.2010.06.008
19. Asano Y, Stawski L, Hant F, Highland K, Silver R, Szalai G, et al. Endothelial Fli1 deficiency impairs vascular homeostasis: a role in scleroderma vasculopathy. *Am J Pathol*. (2010) 176:1983–98. doi: 10.2353/ajpath.2010.090593
20. Suzuki E, Williams S, Sato S, Gilkeson G, Watson DK, Zhang XK. The transcription factor Fli-1 regulates monocyte, macrophage and dendritic cell development in mice. *Immunology*. (2013) 139:318–27. doi: 10.1111/imm.12070
21. Taniguchi T, Miyagawa T, Toyama S, Yamashita T, Nakamura K, Saigusa R, et al. CXCL13 produced by macrophages due to Fli1 deficiency may contribute to the development of tissue fibrosis, vasculopathy and immune activation in systemic sclerosis. *Exp Dermatol*. (2018) 27:1030–7. doi: 10.1111/exd.13724
22. Bujor AM, Pannu J, Bu S, Smith EA, Muise-Helmericks RC, Trojanowska M. Akt blockade downregulates collagen and upregulates MMP1 in human dermal fibroblasts. *J Invest Dermatol*. (2008) 128:1906–14. doi: 10.1038/jid.2008.39
23. Zhang X, Goncalves R, Mosser DM. The isolation and characterization of murine macrophages. *Curr Protoc Immunol*. (2008):
24. Tsuchiya S, Kobayashi Y, Goto Y, Okumura H, Nakae S, Konno T, et al. Induction of maturation in cultured human monocytic leukemia cells by a phorbol diester. *Cancer Res*. (1982) 42:1530–6.
25. Hasegawa M, Sato S, Takehara K. Augmented production of transforming growth factor-beta by cultured peripheral blood mononuclear cells from patients with systemic sclerosis. *Arch Dermatol Res*. (2004) 296:89–93. doi: 10.1007/s00403-004-0472-5
26. Gay S, Jones RE Jr., Huang GQ, Gay RE. Immunohistologic demonstration of platelet-derived growth factor (PDGF) and sis-oncogene expression in scleroderma. *J Invest Dermatol*. (1989) 92:301–3. doi: 10.1111/1523-1747.ep12276895
27. Wynn TA, Barron L. Macrophages: master regulators of inflammation and fibrosis. *Semin Liver Dis*. (2010) 30:245–57. doi: 10.1055/s-0030-1255354
28. Kania G, Rudnik M, Distler O. Involvement of the myeloid cell compartment in fibrogenesis and systemic sclerosis. *Nat Rev Rheumatol*. (2019) 15:288–302. doi: 10.1038/s41584-019-0212-z
29. Naik PK, Bozyk PD, Bentley JK, Popova AP, Birch CM, Wilke CA, et al. Periostin promotes fibrosis and predicts progression in patients with idiopathic pulmonary fibrosis. *Am J Physiol Lung Cell Mol Physiol*. (2012) 303:L1046–56. doi: 10.1152/ajplung.00139.2012
30. Distler JH, Jungel A, Caretto D, Schulze-Horsel U, Kowal-Bielecka O, Gay RE, et al. Monocyte chemoattractant protein 1 released from glycosaminoglycans mediates its profibrotic effects in systemic sclerosis via the release of interleukin-4 from T cells. *Arthritis Rheum*. (2006) 54:214–25. doi: 10.1002/art.21497
31. Distler O, Pap T, Kowal-Bielecka O, Meyringer R, Guiducci S, Landthaler M, et al. Overexpression of monocyte chemoattractant protein 1 in systemic sclerosis: role of platelet-derived growth factor and effects on monocyte chemotaxis and collagen synthesis. *Arthritis Rheum*. (2001) 44:2665–78. doi: 10.1002/1529-0131(200111)44:11<2665::aid-art446>3.0.co;2-s
32. Distler JHW, Akhmetshina A, Schett G, Distler O. Monocyte chemoattractant proteins in the pathogenesis of systemic sclerosis. *Rheumatology*. (2009) 48:98–103. doi: 10.1093/rheumatology/ken401
33. Lodyga M, Cambridge E, Karvonen HM, Pakshir P, Wu B, Boo S, et al. Cadherin-11-mediated adhesion of macrophages to myofibroblasts establishes a profibrotic niche of active TGF-beta. *Sci Signal*. (2019) 12:eaao3469. doi: 10.1126/scisignal.aao3469
34. Yamamoto T, Eckes B, Hartmann K, Krieg T. Expression of monocyte chemoattractant protein-1 in the lesional skin of systemic sclerosis. *J Dermatol Sci*. (2001) 26:133–9. doi: 10.1016/s0923-1811(00)00169-9
35. Hasegawa M, Sato S, Takehara K. Augmented production of chemokines (monocyte chemotactic protein-1 (MCP-1), macrophage inflammatory protein-1alpha (MIP-1alpha) and MIP-1beta) in patients with systemic sclerosis: MCP-1 and MIP-1alpha may be involved in the development of pulmonary fibrosis. *Clin Exp Immunol*. (1999) 117:159–65. doi: 10.1046/j.1365-2249.1999.00929.x
36. Galindo M, Santiago B, Rivero M, Rullas J, Alcami J, Pablos JL. Chemokine expression by systemic sclerosis fibroblasts: abnormal regulation of monocyte chemoattractant protein 1 expression. *Arthritis Rheum*. (2001) 44:1382–6. doi: 10.1002/1529-0131(200106)44:6<1382::AID-ART231>3.0.CO;2-T
37. Crescioli C, Corinaldesi C, Riccieri V, Raparelli V, Vasile M, Del Galdo F, et al. Association of circulating CXCL10 and CXCL11 with systemic sclerosis. *Ann Rheum Dis*. (2018) 77:1845–6. doi: 10.1136/annrheumdis-2018-213257
38. Tiev KP, Chatenoud L, Kettaneh A, Toledano C, Bach JF, Cabane J. [Increase of CXCL10 serum level in systemic sclerosis interstitial pneumonia]. *Rev Med Interne*. (2009) 30:942–6. doi: 10.1016/j.revmed.2009.05.001
39. Antonelli A, Ferri C, Fallahi P, Ferrari SM, Giuggioli D, Colaci M, et al. CXCL10 (alpha) and CCL2 (beta) chemokines in systemic sclerosis–a longitudinal study. *Rheumatology*. (2008) 47:45–9. doi: 10.1093/rheumatology/kem313
40. Stawski L, Haines P, Fine A, Rudnicka L, Trojanowska M. MMP-12 deficiency attenuates angiotensin II-induced vascular injury, M2 macrophage accumulation, and skin and heart fibrosis. *PLoS One*. (2014) 9:e109763. doi: 10.1371/journal.pone.0109763

41. Kubota A, Suto A, Suzuki K, Kobayashi Y, Nakajima H. Matrix metalloproteinase-12 produced by Ly6C (low) macrophages prolongs the survival after myocardial infarction by preventing neutrophil influx. *J Mol Cell Cardiol*. (2019) 131:41–52. doi: 10.1016/j.yjmcc.2019.04.007
42. Madala SK, Pesce JT, Ramalingam TR, Wilson MS, Minnicozzi S, Cheever AW, et al. Matrix metalloproteinase 12-deficiency augments extracellular matrix degrading metalloproteinases and attenuates IL-13-dependent fibrosis. *J Immunol*. (2010) 184:3955–63. doi: 10.4049/jimmunol.0903008
43. Manoury B, Nenan S, Guenon I, Boichot E, Planquois JM, Bertrand CP, et al. Macrophage metalloelastase (MMP-12) deficiency does not alter bleomycin-induced pulmonary fibrosis in mice. *J Inflamm*. (2006) 3:2. doi: 10.1186/1476-9255-3-2
44. Manetti M, Guiducci S, Romano E, Bellando-Randone S, Conforti ML, Ibba-Manneschi L, et al. Increased serum levels and tissue expression of matrix metalloproteinase-12 in patients with systemic sclerosis: correlation with severity of skin and pulmonary fibrosis and vascular damage. *Ann Rheum Dis*. (2012) 71:1064–72. doi: 10.1136/annrheumdis-2011-200837
45. Ling SSM, Chen YT, Wang J, Richards AM, Liew OW. Ankyrin repeat domain 1 protein: a functionally pleiotropic protein with cardiac biomarker potential. *Int J Mol Sci*. (2017) 18:1362. doi: 10.3390/ijms18071362
46. Samaras SE, Almodovar-Garcia K, Wu N, Yu F, Davidson JM. Global deletion of Ankrd1 results in a wound-healing phenotype associated with dermal fibroblast dysfunction. *Am J Pathol*. (2015) 185:96–109. doi: 10.1016/j.ajpath.2014.09.018
47. Shi Y, Reitmaier B, Regenbogen J, Slowey RM, Opalenik SR, Wolf E, et al. CARP, a cardiac ankyrin repeat protein, is up-regulated during wound healing and induces angiogenesis in experimental granulation tissue. *Am J Pathol*. (2005) 166:303–12. doi: 10.1016/S0002-9440(10)62254-7
48. Kanai H, Tanaka T, Aihara Y, Takeda S, Kawabata M, Miyazono K, et al. Transforming growth factor-beta/Smads signaling induces transcription of the cell type-restricted ankyrin repeat protein CARP gene through CAGA motif in vascular smooth muscle cells. *Circ Res*. (2001) 88:30–6. doi: 10.1161/01.res.88.1.30
49. Tan FK, Zhou X, Mayes MD, Gourh P, Guo X, Marcum C, et al. Signatures of differentially regulated interferon gene expression and vasculotrophism in the peripheral blood cells of systemic sclerosis patients. *Rheumatology*. (2006) 45:694–702. doi: 10.1093/rheumatology/kei244
50. Assassi S, Mayes MD, Arnett FC, Gourh P, Agarwal SK, McNearney TA, et al. Systemic sclerosis and lupus: points in an interferon-mediated continuum. *Arthritis Rheum*. (2010) 62:589–98. doi: 10.1002/art.27224
51. Christmann RB, Hayes E, Pendergrass S, Padilla C, Farina G, Affandi AJ, et al. Interferon and alternative activation of monocyte/macrophages in systemic sclerosis-associated pulmonary arterial hypertension. *Arthritis Rheum*. (2011) 63:1718–28. doi: 10.1002/art.30318
52. Christmann RB, Sampaio-Barros P, Stifano G, Borges CL, de Carvalho CR, Kairalla R, et al. Association of Interferon- and transforming growth factor beta-regulated genes and macrophage activation with systemic sclerosis-related progressive lung fibrosis. *Arthritis Rheumatol*. (2014) 66:714–25. doi: 10.1002/art.38288
53. Capaldo CT, Nusrat A. Cytokine regulation of tight junctions. *Biochim Biophys Acta*. (2009) 1788:864–71. doi: 10.1016/j.bbamem.2008.08.027
54. Chrobak I, Lenna S, Stawski L, Trojanowska M. Interferon-gamma promotes vascular remodeling in human microvascular endothelial cells by upregulating endothelin (ET)-1 and transforming growth factor (TGF) beta2. *J Cell Physiol*. (2013) 228:1774–83. doi: 10.1002/jcp.24337

Conflict of Interest: The authors declare that the research was conducted in the absence of any commercial or financial relationships that could be construed as a potential conflict of interest.

frontiers in Immunology

REVIEW
published: 19 June 2020
doi: 10.3389/fimmu.2020.01249

The Role of Endogenous Eicosapentaenoic Acid and Docosahexaenoic Acid-Derived Resolvins in Systemic Sclerosis

Aslıhan Avanoğlu Güler[1,2], Francesca Wanda Rossi[3], Silvia Bellando-Randone[1], Nella Prevete[3], Abdurrahman Tufan[2], Mirko Manetti[1], Amato de Paulis[3] and Marco Matucci-Cerinic[1]*

[1] Department of Experimental and Clinical Medicine, University of Florence and Department of Geriatric Medicine, Division of Rheumatology AOUC, Florence, Italy, [2] Department of Internal Medicine, Division of Rheumatology, Gazi University Faculty of Medicine, Ankara, Turkey, [3] Department of Internal Medicine, Clinical Immunology and Rheumatology, University of Naples Federico II, Naples, Italy

OPEN ACCESS

Edited by:
Dimitrios Petrou Bogdanos, University of Thessaly, Greece

Reviewed by:
Dimitrios Daoussis, University of Patras Medical School, Greece
Sun Jung Kim, Northwell Health, United States

***Correspondence:**
Silvia Bellando-Randone
s.bellandorandone@gmail.com

Specialty section:
This article was submitted to Autoimmune and Autoinflammatory Disorders, a section of the journal Frontiers in Immunology

Received: *12 February 2020*
Accepted: *18 May 2020*
Published: *19 June 2020*

Citation:
Avanoğlu Güler A, Rossi FW, Bellando-Randone S, Prevete N, Tufan A, Manetti M, de Paulis A and Matucci-Cerinic M (2020) The Role of Endogenous Eicosapentaenoic Acid and Docosahexaenoic Acid-Derived Resolvins in Systemic Sclerosis. Front. Immunol. 11:1249. doi: 10.3389/fimmu.2020.01249

Resolvins, the member of specialized pro-resolving mediators, are produced from omega-3 polyunsaturated fatty acids as a response to an acute inflammatory process in that termination and resolution of inflammation. In the acute inflammation, these lipid mediators limit polymorphonuclear cells infiltration, proinflammatory cytokine production; promote efferocytosis, and regulate several cell types being important roles in innate and adaptive immunity. Any dysregulation or defect of the resolution phase result in prolonged, persistent inflammation and eventually fibrosis. Resolvins are implicated in the development of various chronic autoimmune diseases. Systemic sclerosis (SSc) is a very complicated, chronic autoimmune disorder proceeding with vasculopathy, inflammation, and fibrosis. Dysregulation of innate and adaptive immunity is another important contributing factor in the pathogenesis of SSc. In this review, we will focus on the different roles of this new family of lipid mediators, characterized by the ability to prevent the spread of inflammation and its chronicity in various ways and how they can control the development of fibrotic diseases like SSc.

Keywords: resolvins, resolution of inflammation, systemic sclerosis, innate immunity, adaptive immunity, fibrosis

Systemic sclerosis (SSc) is a complex immune-mediated connective tissue disorder characterized by microvascular damage, inflammatory cell infiltration, and excessive deposition of extracellular matrix proteins (ECMs) in the skin and various internal organs (1–3). Over the course of the disease, these pathologic alterations cause severe organ dysfunctions such as pulmonary fibrosis, pulmonary arterial hypertension, cardiac arrhythmias and heart failure, which are the major causes of mortality in SSc (4). Identification of the immune, vasculopathic, and fibrotic mechanisms involved in the pathogenesis of SSc is critical for the understanding of disease progression and developing new disease-modifying therapies (5). Despite the fact that innate and adaptive immunity components, including T cells, B cells, macrophages, dendritic cells (DCs), and multiple cytokines (e.g., interleukin (IL)-4, IL-6, transforming growth factor (TGF)-β) play roles in both the onset and the progression of SSc, the exact etiopathogenesis of the disease still remains elusive (1, 2).

It is well-known that acute inflammatory responses, triggered by a variety of noxious stimuli, including endogenous and exogenous signals, are protective, self-limited reactions that are essential for restoring homeostasis in the affected tissues. However, this benign process may not subside, leading to chronic systemic inflammatory disorders (6, 7). In fact, in a few autoimmune and chronic inflammatory diseases, including SSc, perturbation is observed in inflammation resolution (8). Until recently, termination of acute inflammation was considered as a passive process. However, the latest investigations have demonstrated that the resolution of inflammation is an active process controlled by the local release of various mediators called specialized pro-resolving mediators (SPMs). The biosynthesis of SPMs is induced by pro-inflammatory stimuli as a compensatory mechanism to downregulate the inflammatory response (7). In general, SPMs bind to G protein-coupled receptors (GPRs) to exert anti-inflammatory and pro-resolving biological actions; inhibition of polymorphonuclear leukocyte (PMNs) infiltration and pro-inflammatory cytokine/mediator secretion; promote bacterial removal; and evoke the efferocytosis of apoptotic PMNs through macrophages (9, 10). Thus, far, more than 20 different SPMs have been explored using lipid mediator metabolon lipidomics and proteomics, and these SPMs have been subdivided into four main classes based on distinct biosynthetic pathways and target receptors: lipoxins, resolvins (Rvs), protectins, and maresins (11, 12). The discovery of Rvs attracted significant interest because these lipid mediators play prominent roles in different pathological conditions by sustaining homeostasis owing to their anti-inflammatory properties (13). It is widely accepted that Rvs play significant roles in several chronic inflammatory diseases, such as rheumatoid arthritis, Sjogren's syndrome, and inflammatory bowel disease (14–17). Although many experimental studies have been conducted to define the preventive role of Rvs in pulmonary fibrosis and ischemia-reperfusion injury in animal models, their contribution to the pathogenesis of SSc is yet to be clarified (18, 19). In this review, we will focus on this new family of lipid mediators that can control the propagation and prolongation of inflammation, as well as their possible roles in the pathogenesis of fibrotic diseases such as SSc.

BIOSYNTHESIS OF RESOLVINS AND THEIR RECEPTORS

For the first time, Rvs were identified in inflammatory exudates triggered by tumor necrosis alpha (TNF-α) in mice exposed to omega (Ω)-3 polyunsaturated fatty acids (PUFAs) and aspirin. Usually, different immune cells, such as macrophages and PMNs generate Rvs from Ω-3 PUFAs, namely docosahexaenoic acid (DHA) and eicosapentaenoic acid (EPA), originating from the dietary sources and cell membranes through phospholipase enzyme pathways (20). Two classes of Rvs have been identified: D-series resolvins (RvD1-6) derived from DHA through lipoxygenase (LO)-initiated pathways during the inflammation-resolution phase and the E-series family of Rvs (RvE1-4) produced from EPA via 5-LO and cytochrome P450 (12, 21–23). It has been shown that Rvs signal through specific GPRs (23–26).

RvD1 exerts anti-inflammatory and inflammation-resolution effects via A lipoxin and formyl peptide receptor 2 (ALX/FPR2), as well as via GPR32 (24, 25). RvD2 interacts with GPR18 expressed on PMNs, monocytes, and macrophages (26). In addition to RvD1, RvD3, and RvD5 activate GPR32 and enhance the phagocytosis and inhibition of neutrophil transmigration (27, 28). Furthermore, RvEs exert their function through GPCRs. Chemerin receptor 23 (ChemR23), which is selectively expressed on antigen-presenting cells (APCs), is a binding site for RvE1 (29). Additionally, RvE1 also interacts with leukotriene B_4 receptor 1 (BLT1), as a partial agonist, which mediates the potent inflammatory effects of leukotriene B4 (LTB_4) (30).

ROLE OF RESOLVINS IN THE INNATE IMMUNITY

In SSc, endothelial cell activation is one of the earliest events, along with immune cell activation and inflammation (31). Unresolved or prolonged inflammation and immune cell activation could result in chronic inflammation and, subsequently, in fibrosis (7). The inflammatory process is characterized by the production of various mediators (e.g., cytokines, chemokines, vasoactive amines, and eicosanoids) by the innate immune cells, including PMNs, macrophages, dendritic cells, lymphocytes, endothelial cells, and fibroblasts, in the damaged tissue. This occurs concomitantly with the upregulation of cell-adhesion molecules on leukocytes and endothelial cells, and continue with the infiltration of neutrophils, monocytes, and phagocytes. It is now recognized that Rvs, which are produced by immune cells such as macrophages and PMNs, are pivotal in the resolution of acute inflammatory reactions. They significantly limit acute inflammation response and promote tissue repair (32) (**Figure 1**). Each type of Rvs is considered to have a unique role in the resolution phase of inflammation (**Table 1**). Therefore, the role of Rvs and their possible failure to resolve local inflammatory responses should be investigated in the pathogenesis of SSc.

Effect of Resolvin E-series on Inflammation

RvE1 inhibits human neutrophil transendothelial migration and infiltration *in vivo* (20). RvE1 is characterized by the modulation of leukocytes adhesion molecules through the enhancement of L-selectin shedding, which inhibits the aggregation of leukocytes and reduces CD18 (LFA-1) expression, which is required for neutrophils adhesion and transmigration (30, 33). Animal studies have elucidated that RvE1 enhances efferocytosis through macrophages and reduces pro-inflammatory cytokines, including IL-1β, IL-6, and TNF-α, in zymosan-induced peritonitis (40, 41). Similarly, the result of a mice animal model study indicated that the exogenous RvE1 induces the phagocytosis of neutrophil apoptosis via macrophages in pulmonary inflammation (45). Similar to RvE1, RvE2 actively participates in the resolution of inflammation by blocking neutrophil infiltration through chemotaxis modulation, reinforcement of phagocytosis, and

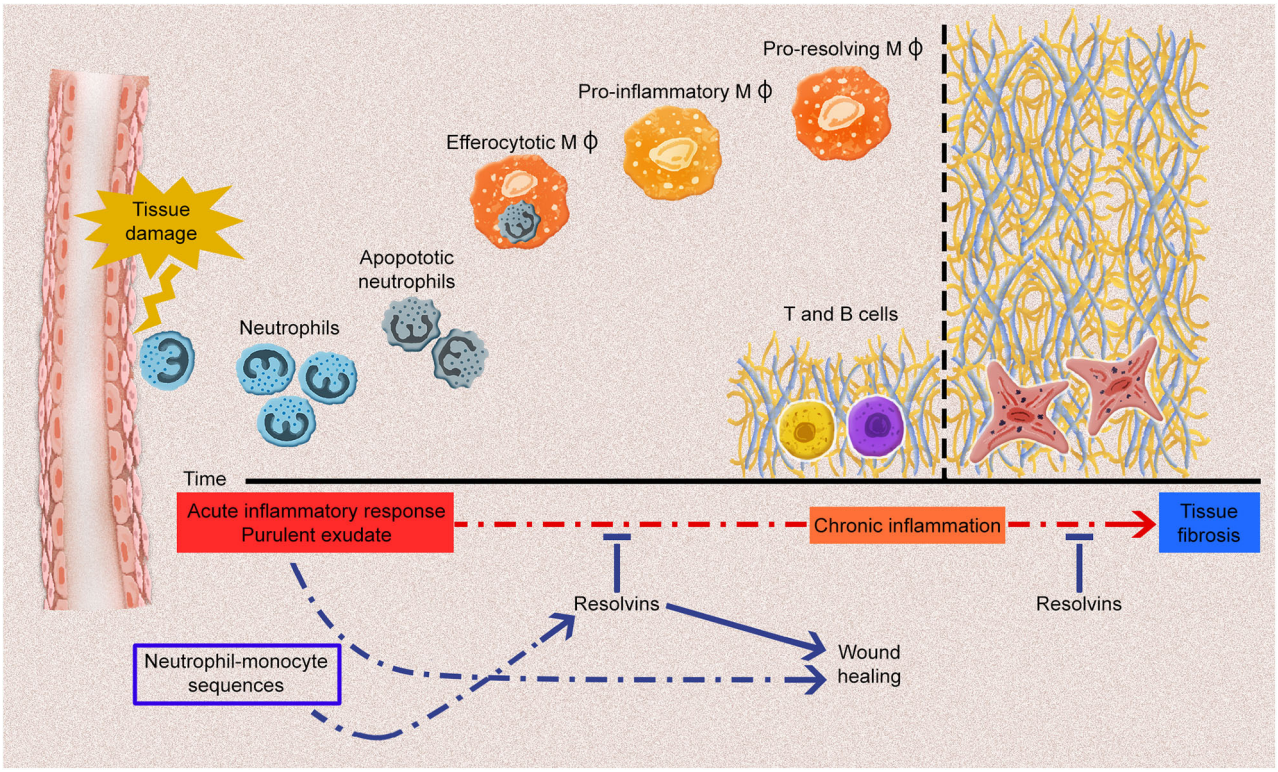

FIGURE 1 | The acute inflammatory response and potential fates for the acute inflammatory process. Tissue damage induced by endogenous or exogenous stimuli leads to the generation of acute inflammatory responses, including various types of proinflammatory cell infiltrations and the production of plenty of proinflammatory mediators. Polymorphonuclear leukocytes infiltration especially neutrophils induce the influx of monocyte-derived macrophages to remove apoptotic cells and debris. Throughout the resolution phase of inflammation, resolvins (Rvs) promote the efferocytosis of macrophages and differentiation of proinflammatory macrophages (MΦ) into anti-inflammatory macrophages. At the post-resolution phase of inflammation, adaptive immunity response (B and T cells) establishes which contributes the wound healing. Any dysregulation of these processes may lead to chronic inflammation and fibrosis. Rvs limit the acute inflammatory process, thus, they prevent the development of chronic inflammation and fibrosis.

macrophages-dependent production of IL-10 (34). Eosinophils mainly release RvE3, which limits the infiltration of PMNs in zymosan triggered peritonitis (55). In an allergic lung inflammation model, RvE3 significantly reduced the number of inflammatory cells and the secretion of pro-inflammatory cytokines in bronchoalveolar lavage (35). Recently, it has been demonstrated that the production of new RvE4 is accelerated by hypoxia, which induces the efferocytosis of neutrophils and erythrocytes through macrophages and inhibits the infiltration of neutrophil in hemorrhagic exudates *in vivo* (23).

Effect of Resolvin D-series on Inflammation

RvD1 modulates the regulatory action of PMNs by inhibiting rolling and adhesion to endothelium via GPR32, in addition to limiting the infiltration of leukocytes and neutrophils via FPR2/ALX and the production of pro-inflammatory mediators in zymosan-induced peritonitis (36). Through this binding with FPR2/ALX, RvD1 inhibits lipopolysaccharide (LPS)-induced acute lung inflammation. This is realized because of reduced neutrophil infiltration due to the suppression of macrophage inflammatory protein (MIP)2-α (CXCL2) expression on alveolar macrophages (56). Similarly, RvD2 plays an effective role in the resolution phase of inflammation by reducing neutrophil recruitment, increasing mononuclear and macrophage phagocytosis by binding with GPR18, and suppressing the pro-inflammatory mediators (26). Additionally, RvD2 suppresses pro-inflammatory mediators by decreasing the plasma levels of IL-1β, IL-6, IL-17, IL-23, and TNF-α, as well as the levels of prostaglandin (PG)E2 and LTB_4 in peritoneal exudates, as demonstrated using an animal sepsis model Interestingly, RvD2 decreases the plasma levels of the potent anti-inflammatory cytokine IL-10, which is of interest because of its detrimental impact on survival in sepsis (42). By contrast, RvD2 increases the level of IL-10 mRNA in the porphyromonas gingivalis-induced periodontitis (43). RvD3, which appears later than RvD1 and RvD2 in the resolution phase of inflammation, has potent local and systemic anti-inflammatory activities, such as decreasing the recruitment of PMNs and reducing the levels of IL-6 and LTB_4 and matrix-degrading enzymes (MMP-2 and MMP-9). This enhances the level of IL-10 and stimulates macrophage efferocytosis (28, 37). Moreover, RvD4 decreases PMNs infiltration and promotes macrophage efferocytosis in zymosan-induced peritonitis and

TABLE 1 | Resolvins and their functions on immune cells.

Immune cells	Resolvin D-series					Resolvin E-series				
	RvD1	**RvD2**	**RvD3**	**RvD4**	**RvD5**	**RvE1**	**RvE2**	**RvE3**	**RvE4**	**References**
PMNs migration infiltration	↓	↓	↓	↓	↓	↓	↓	↓	↓	(23, 26, 28, 30, 33–39)
Mediators	↑IL-10 ↓LTB_4	↓IL-1β ↓IL-6 ↓IL-17 ↓IL-23 ↓TNFα ↓LTB_4 ↓↑IL10	↓IL-6 ↓LTB_4 ↑IL-10			↓IL-1β ↓IL-6 ↓TNFα	↑IL-10	↓IL-4 ↓IL-5 ↓IL-13 ↓IL-23		(24, 26, 28, 34, 35, 37, 40–44)
Mφ efferocytosis	↑	↑	↑	↑	↑	↑	↑		↑	(23, 28, 34, 37, 38, 41, 45)
Mφ polarization	↑M2	↑M2								(46–49)
DCs						↓Migration ↓IL-12 ↓IL-23	↓IL-23	↓IL-23		(29, 35)
T cells	↓$CD4^+$T ↓Th1 ↓Th17 ↓IFN-ɤ ↓IL-17 ↓$CD8^+$T ↑Treg	↓$CD4^+$T ↓Th1 ↓Th17 ↓IFN-ɤ ↓IL-17 ↓$CD8^+$T ↑Treg				↓$CD4^+$T ↓ IL-4 ↓IFN-ɤ ↓$CD8^+$T				(44, 50, 51)
B cells	↑IgM ↑IgG ↓IgE									(52–54)

DCs, dendritic cells; IL, interleukin; Ig, immunoglobulin; IFN-ɤ, interferon-gamma; LTB_4, leukotriene B_4; Mφ, macrophages; PMNs, polymorphonuclear leukocytes; RvD, resolvin D; RvE, resolvin E; Th, T helper; TNF-α tumor necrosis factor alpha; Treg, T regulatory cell.

Staphylococcus aureus-triggered skin infection, in addition to inducing the phagocytosis of dermal fibroblasts (38). Several studies have elucidated the dysregulation of neutrophils in SSc and the relationship between neutrophil infiltration in lung tissue and lung fibrosis or disease severity (57–61). Considering all of these results, it seems that blocking of neutrophil migration and infiltration from most of Rvs might be beneficial for SSc or dysregulation of these mediators might contribute to the pathogenesis of SSc. As mentioned above, most of Rvs stimulate macrophage efferocytosis, which has been found to be dysfunctional in autoimmune diseases (systemic lupus erythematosus, Sjogren's syndrome, and SSc) (62–64).

Polarization of Macrophages

From the onset of inflammation to its resolution, macrophages, as a part of innate immunity, play a significant role in inflammatory responses because they have possessed a diversity of phenotypes and polarization abilities. Based on responses to various signals from the environment, macrophages convert into classically activated M1 or alternatively activated M2 phenotypes that are mainly stimulated by interferon (IFN)-ɤ/LPS and IL-4/IL-13, respectively (65, 66). M1 macrophages contribute to the initiation and progression of inflammation by secreting pro-inflammatory mediators (IL-12, IL-1β, IL-6, and TNF-α). M2 macrophages, by contrast, are implicated in the tissue repair, wound healing, and resolution phase of the inflammation through the production of cytokines (IL-4, IL-10, IL-13) and growth factors (TGF-β, vascular endothelial growth factor (VEGF), and endothelial growth factor (EGF) (67). Alternatively activated M2 macrophages may have four subtypes: M2a stimulated by IL-4 or IL-13, M2b stimulated by immune complex and LPS, M2c stimulated by IL-10 and TGF-β1, and M2d stimulated by IL-6 and adenosine (68). Activated macrophages may change their polarization in accordance with new environmental stimuli (69). In autoimmune diseases, an M1/M2 imbalance has been detected. In SSc, M2 macrophages produce profibrotic cytokines that promote ECM synthesis (31). The M2 polarization observed in SSc seems to be induced by increased IL-6 and IL-4 levels (2). Although previous results are mainly consistent with M2 activation, recent evidence has suggested that macrophages express mixed surface markers of the M1 and M2 phenotypes in SSc (70–72).

During the resolution phase of inflammation, M1 macrophages change into the M2 phenotype owing to the action of specific mediators, especially SPMs. It has been shown that RvD1 significantly reduces the expression of M1 phenotype markers (TNF-α, IL-6, monocyte chemoattractant protein (MCP)-1 expression) and increases the expression of M2 markers in peritoneal macrophages obtained from obese mice (46). In the mouse carotid ligation model, systemic RvD2 markedly enhanced the proportion of M2 macrophages among

the monocytes/macrophages present in the injured arterial wall (47). Recently, an assessment of inflammation in an abdominal aortic aneurysm model animal study demonstrated that RvD2 improved M2 polarization and ameliorated pro-inflammatory markers (IL-1β, IL-6, MCP-1, and MIP-1α) (73). Moreover, RvD1 reinforced the activation of M2 macrophages in acute smoke-induced lung inflammation (48). The animal study has indicated that long-term treatment with aspirin-triggered (AT) RvD1 does not influence macrophage polarization in long-term smoke-induced lung inflammation. Additionally, tissue fibrosis is not observed with long-term AT-RvD1 treatment (49). These effects could suggest that the effects of RvD1 on macrophage polarization may be associated with the type of inflammation (acute or chronic) or the duration of Rvs exposure. At the moment, we don't have enough data to disclosure if M2 differentiation may be a negative event in the pathogenic cascade of SSc linked to the activity of Rvs. Therefore, it is still very difficult to regard M2 differentiation as in those by Rvs as beneficial or pathogenic.

Dendritic Cells

Dendritic cells (DCs) are an important component of innate immunity. They recognize and present damage-associated molecular patterns and pathogens, as well as induce the adaptive immune response. Usually, DCs are composed of two main cell types: conventional (cDC) and plasmacytoid (pDC), which, especially, secretes interferon-alpha (IFN-α). Recent studies have revealed that pDCs infiltrate the skin and the lungs of SSc patients, and contribute to fibrosis and that the number of pDCs in the lungs of SSc patients correlates with the severity of the lung disease (74, 75). ChemR23, a receptor of RvEs, is highly expressed in pDCs, and it mediates the migration of pDCs to inflammatory sites (76, 77). In an animal study, ChemR23 deficiency in knockout mice reduced the migration of pDCs to atherosclerotic lesions (78). Only RvE1 restrained the migration of DCs and inhibited their production of IL-12 via ChemR23 (29, 79). The serum level of IL-12 is increased in patients with SSc (79). Although the role of cDCs in SSc is not as known as pDCs, the increase in the production of proinflammatory cytokines from cDCs is demonstrated in SSc (80).

ROLE OF RESOLVINS IN ADAPTIVE IMMUNITY

T Cells

Several reports have suggested that T cells, particularly $CD4^+$ T helper 2 (Th2), play a significant role in both the inflammatory and fibrotic processes of SSc (81). Activated $CD4^+$ Th2 cells produce the predominantly potent profibrotic cytokines IL-4 and IL-13, which induce fibroblast proliferation, their differentiation into myofibroblasts, and polarization of M2 macrophages. All of these features are implicated in the pathogenesis of SSc (2, 82, 83). Furthermore, IL-13 producing $CD8^+$ T cells have been detected in the skin in the early phases of SSc (84). Studies have highlighted the importance of Rvs in T cell regulation. Exogenous RvD1 diminishes the infiltration of $CD4^+$ and $CD8^+$ T lymphocytes in endotoxin-induced uveitis (50). Similarly, in an animal study, it was found that exogenous RvE1 suppressed the infiltration of $CD4^+$ and $CD8^+$ T cells in atopic dermatitis in a dose-dependent manner. In addition, RvE1 treatment reduced the IL-4 and IFN-ɤ production of activated $CD4^+$ T cells (51). Abnormal Th17 cell responses are encountered in many chronic inflammatory and autoimmune diseases (85). Th17 and IL-17 may play an important role in SSc due to proinflammatory and profibrotic effects. Some evidence has demonstrated that the level of Th17 and IL-17 increased in SSc (86–88). However, the results of several studies have not found an increase in the level of IL-17 in SSc. Therefore, the role of Th17 and IL-17 have not completely understood in the pathogenesis of SSc yet (89–91). RvD1 and RvD2 abate the inflammatory responses of activated $CD8^+$ T, Th1, and Th17 cells by decreasing the production of TNF-α, IFN-ɤ, IL-2, and IL-17. RvD1 and RvD2 inhibit the differentiation of naïve $CD4^+$ T cells into Th1 and Th17 cells while they improve the differentiation of $CD4^+$ T cells into regulatory T (Treg) cells. However, they do not exert any effect on the apoptosis of both $CD8^+$ and $CD4^+$ cells (44). In contrast to RvD1-2, RvE1 amplifies the T cell apoptotic activity of DCs through indolamine 2,3 dioxygenase induction (92). Although the effect of RvE1 on Th17 is undefined, RvE1 diminishes the production of IL-23 and IL-6, which are crucial for the survival of Th17 cell, in allergic lung inflammation (93). Recently, it has been demonstrated that RvE1, RvE2, and RvE3 decrease the production of IL-23 from bone marrow DCs *in vitro*. In particular, the treatment of house dust-mite-sensitized mice with RvE3 promoted the reduction of inflammatory cells, including eosinophils, and decreased IL-23 and IL-17 levels in lavage fluid, thus supporting the role of RvE3 in the resolution of allergic airway inflammation (35). These effects of Rvs on T cell regulation might create a protective mechanism against the dysregulation of T cells in SSc.

B Cells

In recent studies on SSc, the role of the B cells in the generation of fibrosis has been highlighted, especially in the lungs and the gastrointestinal tract (94, 95). In fact, an increase in the naive B cell count and a decrease in memory and regulatory B cell counts has been found in SSc. These impairments of B cell homeostasis result in the decline in the production of potent anti-inflammatory and anti-fibrotic cytokines (i.e., IL-10) and the enhancement of production of proinflammatory cytokines (i.e., IL-6) (96). However, information on the effects of Rvs on B cells is scarce. In the mouse spleen, 17-hydroxydosahexaenoic acid (17-HDHA) (a biomarker of Rvs), RvD1, and RvE1, but not RvD2 and RvD5, have been detected (52, 53). In activated B cells, RvD1 elevates antibody production, notably immunoglobulin (Ig)M, while 17-HDHA increases both IgM and IgG in proportion to the increasing differentiation of B cells into the antibody-secreting B cell phenotype (52). Interestingly, it has been found that RvD1 and 17-HDHA suppress the differentiation of naïve B cells into IgE-secreting cells, which induce a specific block of the epsilon germline transcription (54).

EFFECT OF RESOLVINS ON ISCHEMIA-REPERFUSION-INDUCED INFLAMMATION

Raynaud's phenomenon (RP) is frequently encountered in SSc, and it influences the acral blood flow (97). In primary RP, impaired arterial inflow induced by sympathetic vasoconstriction causes mild reversible microvascular sufferance. In SSc, the impairment of arteriolar inflow is not compensated for by endothelial-dependent vasodilation. In fact, the disease affects the endothelial cells that are injured or dysfunctional (98, 99). Therefore, prolonged vasoconstriction leads to a loss of endothelial junctions, enhanced inflammatory immune cell migration and infiltration, and microvessel permeability (100). Moreover, repeated and sustained vasoconstriction attacks result in ischemia-reperfusion (IR) injury, which promotes the production of various proinflammatory mediators and reactive oxygen species, activation and migration of PMNs, and interaction with endothelial cells. This causes further microvascular damage (101, 102).

In this context, based on the data available about Rvs role in IR-induced injury models, they can be considered operative in a condition such as RP in SSc as well. In the IR-induced model, the levels of endogenous DHA and all types

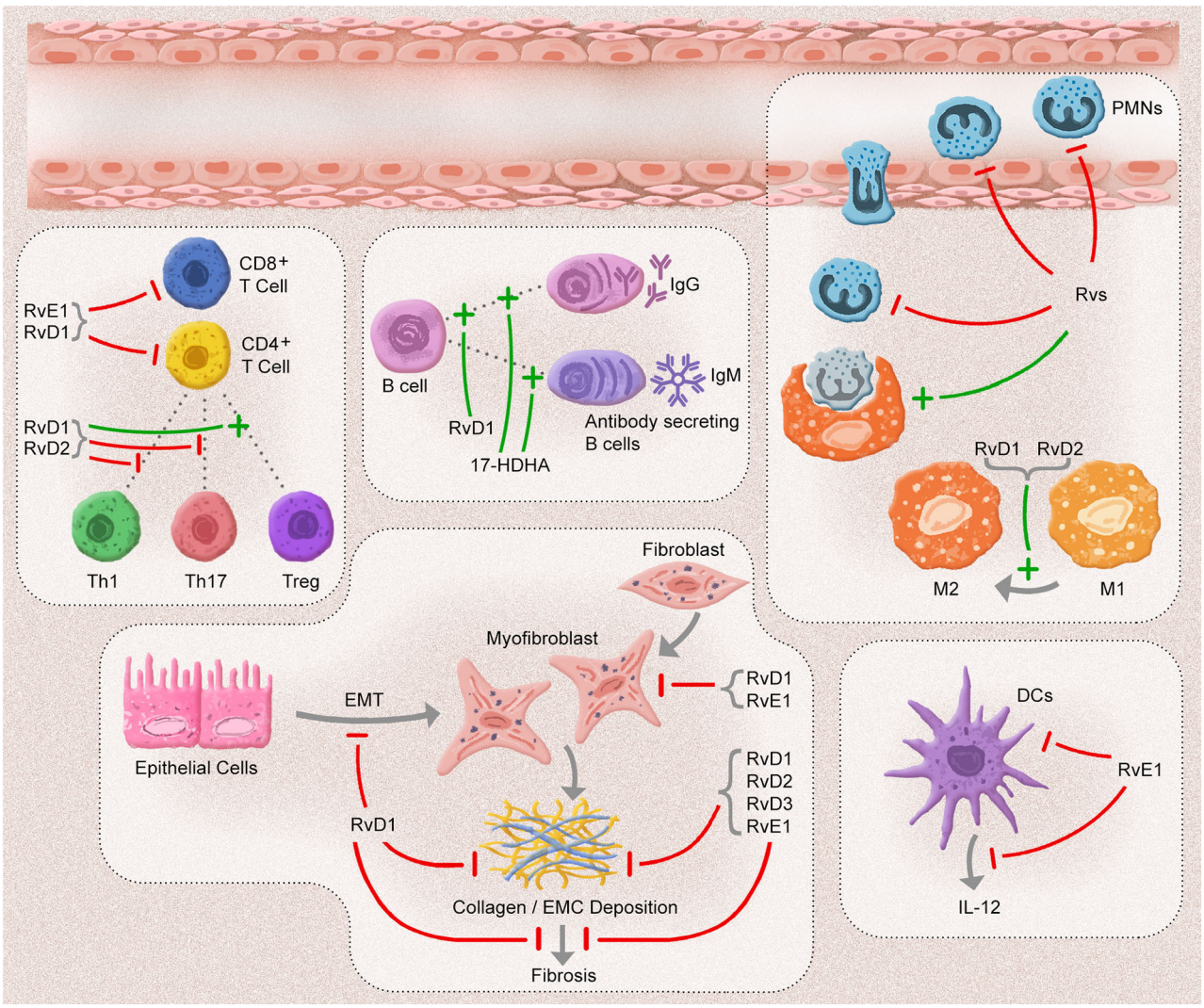

FIGURE 2 | The anti-inflammatory, pro-resolution, and anti-fibrotic effects of Resolvins. In an acute inflammatory response, resolvins (Rvs) inhibit the adhesion, migration, and infiltration of polymorphonuclear leukocytes (PMNs) and enhance the efferocytosis capacity of macrophages. D-series Rvs (RvD1 and RvD2) induce the polarization of macrophages toward to phenotype M2. One of the E-series Rvs, RvE1 blocks the migration and production of interleukin (IL)-12 in dendritic cells (DCs) and the infiltration of $CD8^+$ and $CD4^+$ cells. RvD1 and RvD2 suppress the inflammatory responses of $CD8^+$ T, T helper (Th)1, and Th17 cells, in addition to limiting the differentiation of $CD4^+$ T cells into T helper (Th)1 and Th17 cells and promoting the conversion of T regulatory (Treg) cells. 17-hydroxydosahexaenoic acid (17-HDHA) and RvD1 enhance the antibody secretion of B cells. After an inflammatory response, most of Rvs block the development of fibrosis by decreasing collagen deposition and myofibroblast infiltration, as well as by inhibiting epithelial-mesenchymal cell transition (EMT).

of RvDs, apart from RvD1 and RvD3, are known to increase in the plasma, while only DHA, RvD1, and RvD3 are detected in the affected kidney tissue. Exogenous Rvs (composed of RvD1-3) limit the infiltration of PMNs, and the deposition of interstitial collagen. RvD1 has a protective capacity for the kidney when administered after the development of IR (39). It has been shown that RvD1 treatment protects the lung tissue from IR-induced inflammation, thus limiting the homing of inflammatory cells, production of proinflammatory mediators, and apoptosis (19). IR injury elicits mitochondrial dysfunction and augments excessive ROS production (103). RvD1 limits IR-triggered liver damage by reducing mitochondrial oxidative stress and regulating mitochondrial homeostasis (104). Furthermore, RvD2 diminishes the infiltration of PMNs through GPR18 in IR-induced lung injury (26).

ROLE OF RESOLVINS IN FIBROSIS

Fibrosis is the main eventual hallmark of SSc. Vasculopathy; immune dysregulation, including innate and adaptive immunity; and several cytokines contribute to the process leading to fibrosis. However, the exact mechanisms of fibrosis in SSc still remain undefined.

Rvs are mainly known for their anti-inflammatory and pro-resolutive effects. They prevent fibrosis by limiting inflammation, supporting efferocytosis, and suppressing proinflammatory and profibrotic cytokines. Furthermore, Rvs have direct anti-fibrotic effects: RvE1 prevents hepatic fibrosis induced by Schistosoma japonicum infection by decreasing the levels of fibrotic markers such as laminin, hyaluronic acid, procollagen type III, and type IV collagen (105). In the animal model study, the anti-fibrotic effects of RvE1 were evaluated by inducing unilateral ureteric obstruction. The interstitial fibrosis obtained using this model was driven not by an inflammatory process but by an irreversible surgical insult, and it was characterized by collagen deposition and the proliferation of α-smooth muscle actin $(SMA)^+$ myofibroblasts. RvE1 treatment dramatically attenuated the accumulation of α-SMA^+ myofibroblasts, deposition of type IV collagen, and production of platelet-derived growth factor (PDGF)-BB, which is a potent inducer of fibroblast proliferation through activation of the AKT and ERK pathways. Moreover, RvD1 markedly reduced myofibroblast accumulation, and mRNA levels of type I and III collagens in an injured kidney (106). In bleomycin-induced lung tissue, treatment with 17(R)-RvD1, an epimer of RvD1, diminished the mRNA-expression of IL-1β, TGF-β1, and connective tissue growth factor, in addition to sharply reducing the numbers of macrophages and neutrophils in the bronchoalveolar fluid. The anti-fibrotic capacity of 17(R)-RvD1 has been confirmed based on reductions in hydroxyproline content (marker of collagen deposition), type I collagen mRNA expression, and score of the fibrotic changes (via Ashcroft scale) in the lung tissue. Moreover, 17(R)-RvD1 treatment has anti-inflammatory and anti-fibrotic effects even when it is administered in the established fibrotic stage in lung tissue (18). Besides, RvD1 alleviates collagen deposition in heart tissue after a myocardial infarction (107).

Epithelial-mesenchymal transition (EMT) is thought to be a crucial mechanism in the development of fibrosis, particular in the lungs and kidneys (97, 98). In general, EMT is closely related to embryonic development, tissue repair, wound healing, and cell migration. During tissue repair or wound healing, epithelial cells lose their phenotype and gain mesenchymal phenotypes to produce fibroblasts and myofibroblasts (108). EMT may be a part of the cellular origins of fibrosis in SSc (109). The potent pro-resolving activity of RvD1 has been further investigated in a model of acute respiratory distress syndrome (ARDS) in which it was demonstrated that RvD1 can prevent EMT of lung epithelial cells with reversal of the TGF-β-smad2/3 signaling pathway and lung fibrosis via the FPR2/ALX receptor (110). Endothelial-to-mesenchymal (EndoMT) transition is also thought to play an important role in both SSc-related fibrosis and vasculopathy (101, 102). Of note, RvD1 has also been reported to significantly inhibit TGF-β1-induced EndoMT through increasing the expression of Smad7 (39).

CONCLUSION

The resolution of inflammation is vital for ensuring tissue homeostasis. Any defects in the resolution phase could lead to a prolonged inflammatory response, including increasing PMNs, exaggerated proinflammatory mediator production, increase in the number of apoptotic cells, and inappropriate activation of adaptive immune cells. This unresolved inflammation results in fibrosis of the affected tissue. After the identification of SPMs, many investigators have focused on the effects of SPM on the resolution of inflammation. Rvs are efficacious anti-inflammatory and pro-resolving mediators that play various roles in innate immunity cells. A myriad of studies has confirmed that they influence adaptive immune cells (**Figure 2**). This exciting anti-fibrotic effect has been supported by the direct effect of these mediators on the regulation of fibrotic cells and cytokines.

The pathogenesis of SSc is associated with vasculopathy, immune dysregulation, and fibrosis (1). It is well-known that progressive chronic inflammation is a part of the disease, while the connection between the resolution of inflammation and SSc still remains unclear. From this viewpoint, any dysfunction of the well-defined anti-fibrotic, anti-inflammatory, and pro-resolving abilities of Rvs may contribute to the progression of SSc. In the future, an accurate understanding of Rvs in SSc may foster the development of novel treatment strategies (4, 111).

AUTHOR CONTRIBUTIONS

AA: substantial contributions to the conception of the work, acquisition, and interpretation of data, drafting the article, revising the manuscript critically, providing approval for publication of the content. FR: acquisition of data, drafting the article, revising the manuscript critically, providing approval for publication of the content. SB-R and NP: revising the manuscript critically, providing approval for publication of the content. AT: drafting the article, revising the manuscript critically, providing approval for publication

of the content. MM: drafting the article, revising the manuscript critically, providing approval for publication of the content. AP: substantial contributions to the conception of the work, revising the manuscript critically, providing approval for publication of the content. MM-C: substantial contributions to the conception of the work, revising the manuscript critically, providing approval for publication of the content.

REFERENCES

1. Varga J, Trojanowska M, Kuwana M. Pathogenesis of systemic sclerosis: recent insights of molecular and cellular mechanisms and therapeutic opportunities. *J Scleroderma Relat Disord*. (2017) 2:137–52. doi: 10.5301/jsrd.5000249
2. Brown M, O'Reilly S. The immunopathogenesis of fibrosis in systemic sclerosis. *Clin Exp Immunol*. (2019) 195:310–21. doi: 10.1111/cei.13238
3. Hamaguchi Y, Takehara K. Anti-nuclear autoantibodies in systemic sclerosis: news and perspectives. *J Scleroderma Relat Disord*. (2018) 3:201–13. doi: 10.1177/2397198318783930
4. Tyndall AJ, Bannert B, Vonk M, Airo P, Cozzi F, Carreira PE, et al. Causes and risk factors for death in systemic sclerosis: a study from the EULAR scleroderma trials and research (EUSTAR) database. *Ann Rheum Dis*. (2010) 69:1809–15. doi: 10.1136/ard.2009.114264
5. Volkmann ER, Varga J. Emerging targets of disease-modifying therapy for systemic sclerosis. *Nat Rev Rheumatol*. (2019) 15:208–24. doi: 10.1038/s41584-019-0184-z
6. Medzhitov R. Origin and physiological roles of inflammation. *Nature*. (2008) 454:428–35. doi: 10.1038/nature07201
7. Ariel A, Timor O. Hanging in the balance: endogenous anti-inflammatory mechanisms in tissue repair and fibrosis. *J Pathol*. (2013) 229:250–63. doi: 10.1002/path.4108
8. Abdolmaleki F, Kovanen PT, Mardani R, Gheibi-Hayat SM, Bo S, Sahebkar A. Resolvins: emerging players in autoimmune and inflammatory diseases. *Clin Rev Allergy Immunol*. (2019) 58:82–91. doi: 10.1007/s12016-019-08754-9
9. Serhan CN. A search for endogenous mechanisms of anti-inflammation uncovers novel chemical mediators: missing links to resolution. *Histochem Cell Biol*. (2004) 122:305–21. doi: 10.1007/s00418-004-0695-8
10. Serhan CN, Chiang N, Van Dyke TE. Resolving inflammation: dual anti-inflammatory and pro-resolution lipid mediators. *Nat Rev Immunol*. (2008) 8:349–61. doi: 10.1038/nri2294
11. Bannenberg GL, Chiang N, Ariel A, Arita M, Tjonahen E, Gotlinger KH, et al. Molecular circuits of resolution: formation and actions of resolvins and protectins. *J Immunol*. (2005) 174:4345–55. doi: 10.4049/jimmunol.174.7.4345
12. Serhan CN. Pro-resolving lipid mediators are leads for resolution physiology. *Nature*. (2014) 510:92–101. doi: 10.1038/nature13479
13. Fetterman JW Jr, Zdanowicz MM. Therapeutic potential of n-3 polyunsaturated fatty acids in disease. *Am J Health Syst Pharm*. (2009) 66:1169–79. doi: 10.2146/ajhp080411
14. Arnardottir HH, Dalli J, Norling LV, Colas RA, Perretti M, Serhan CN. Resolvin D3 is dysregulated in arthritis and reduces arthritic inflammation. *J Immunol*. (2016) 197:2362–8. doi: 10.4049/jimmunol.1502268
15. Dean S, Wang CS, Nam K, Maruyama CL, Trump BG, Baker OJ. Aspirin triggered resolvin D1 reduces inflammation and restores saliva secretion in a sjogren's syndrome mouse model. *Rheumatology (Oxford)*. (2019) 58:1285–92. doi: 10.1093/rheumatology/kez072
16. Schwanke RC, Marcon R, Bento AF, Calixto JB. EPA- and DHA-derived resolvins' actions in inflammatory bowel disease. *Eur J Pharmacol*. (2016) 785:156–64. doi: 10.1016/j.ejphar.2015.08.050
17. Serhan CN, Levy BD. Resolvins in inflammation: emergence of the pro-resolving superfamily of mediators. *J Clin Invest*. (2018) 128:2657–69. doi: 10.1172/JCI97943
18. Yatomi M, Hisada T, Ishizuka T, Koga Y, Ono A, Kamide Y, et al. 17(R)-resolvin D1 ameliorates bleomycin-induced pulmonary fibrosis in mice. *Physiol Rep*. (2015) 3:e12628. doi: 10.14814/phy2.12628
19. Xia J, Xue JY, Du J, Wu GW, Hu XT, Zhao QF. [Role and related mechanism of resolvin D1 in lung ischemia reperfusion injury in rats]. *Zhonghua yi xue za zhi*. (2019) 99:1111–5. doi: 10.3760/cma.j.issn.0376-2491.2019.14.015
20. Serhan CN, Clish CB, Brannon J, Colgan SP, Chiang N, Gronert K. Novel functional sets of lipid-derived mediators with antiinflammatory actions generated from omega-3 fatty acids via cyclooxygenase 2-nonsteroidal antiinflammatory drugs and transcellular processing. *J Exp Med*. (2000) 192:1197–204. doi: 10.1084/jem.192.8.1197
21. Serhan CN, Hong S, Gronert K, Colgan SP, Devchand PR, Mirick G, et al. Resolvins: a family of bioactive products of omega-3 fatty acid transformation circuits initiated by aspirin treatment that counter proinflammation signals. *J Exp Med*. (2002) 196:1025–37. doi: 10.1084/jem.20020760
22. Norris PC, Libreros S, Chiang N, Serhan CN. A cluster of immunoresolvents links coagulation to innate host defense in human blood. *Sci Signal*. (2017) 10:eaan1471. doi: 10.1126/scisignal.aan1471
23. Norris PC, Libreros S, Serhan CN. Resolution metabolomes activated by hypoxic environment. *Sci Adv*. (2019) 5:eaax4895. doi: 10.1126/sciadv.aax4895
24. Krishnamoorthy S, Recchiuti A, Chiang N, Fredman G, Serhan CN. Resolvin D1 receptor stereoselectivity and regulation of inflammation and proresolving microRNAs. *Am J Pathol*. (2012) 180:2018–27. doi: 10.1016/j.ajpath.2012.01.028
25. Prevete N, Liotti F, Amoresano A, Pucci P, de Paulis A, Melillo RM. New perspectives in cancer: modulation of lipid metabolism and inflammation resolution. *Pharmacol Res*. (2018) 128:80–7. doi: 10.1016/j.phrs.2017.09.024
26. Chiang N, Dalli J, Colas RA, Serhan CN. Identification of resolvin D2 receptor mediating resolution of infections and organ protection. *J Exp Med*. (2015) 212:1203–17. doi: 10.1084/jem.20150225
27. Chiang N, Fredman G, Backhed F, Oh SF, Vickery T, Schmidt BA, et al. Infection regulates pro-resolving mediators that lower antibiotic requirements. *Nature*. (2012) 484:524–8. doi: 10.1038/nature11042
28. Dalli J, Winkler JW, Colas RA, Arnardottir H, Cheng CY, Chiang N, et al. Resolvin D3 and aspirin-triggered resolvin D3 are potent immunoresolvents. *Chem Biol*. (2013) 20:188–201. doi: 10.1016/j.chembiol.2012.11.010
29. Arita M, Bianchini F, Aliberti J, Sher A, Chiang N, Hong S, et al. Stereochemical assignment, antiinflammatory properties, and receptor for the omega-3 lipid mediator resolvin E1. *J Exp Med*. (2005) 201:713–22. doi: 10.1084/jem.20042031
30. Arita M, Ohira T, Sun YP, Elangovan S, Chiang N, Serhan CN. Resolvin E1 selectively interacts with leukotriene B4 receptor BLT1 and ChemR23 to regulate inflammation. *J Immunol*. (2007) 178:3912–7. doi: 10.4049/jimmunol.178.6.3912
31. Dowson C, Simpson N, Duffy L, O'Reilly S. Innate immunity in systemic sclerosis. *Curr Rheumatol Rep*. (2017) 19:2. doi: 10.1007/s11926-017-0630-3
32. Fullerton JN, Gilroy DW. Resolution of inflammation: a new therapeutic frontier. *Nat Rev Drug Discov*. (2016) 15:551–67. doi: 10.1038/nrd.2016.39
33. Dona M, Fredman G, Schwab JM, Chiang N, Arita M, Goodarzi A, et al. Resolvin E1, an EPA-derived mediator in whole blood, selectively counterregulates leukocytes and platelets. *Blood*. (2008) 112:848–55. doi: 10.1182/blood-2007-11-122598
34. Oh SF, Dona M, Fredman G, Krishnamoorthy S, Irimia D, Serhan CN. Resolvin E2 formation and impact in inflammation resolution. *J Immunol*. (2012) 188:4527–34. doi: 10.4049/jimmunol.1103652
35. Sato M, Aoki-Saito H, Fukuda H, Ikeda H, Koga Y, Yatomi M, et al. Resolvin E3 attenuates allergic airway inflammation via the interleukin-23-interleukin-17A pathway. *FASEB J*. (2019) 33:12750–9. doi: 10.1096/fj.201900283R
36. Norling LV, Dalli J, Flower RJ, Serhan CN, Perretti M. Resolvin D1 limits polymorphonuclear leukocyte recruitment to inflammatory loci: receptor-dependent actions. *Arterioscler Thromb Vasc Biol*. (2012) 32:1970–8. doi: 10.1161/ATVBAHA.112.249508
37. Norris PC, Arnardottir H, Sanger JM, Fichtner D, Keyes GS, Serhan CN. Resolvin D3 multi-level proresolving actions are host protective during infection. *Prostag Leukot Essent Fatty Acids*. (2018) 138:81–9. doi: 10.1016/j.plefa.2016.01.001

38. Winkler JW, Orr SK, Dalli J, Cheng CY, Sanger JM, Chiang N, et al. Resolvin D4 stereoassignment and its novel actions in host protection and bacterial clearance. *Sci Rep*. (2016) 6:18972. doi: 10.1038/srep18972
39. Duffield JS, Hong S, Vaidya VS, Lu Y, Fredman G, Serhan CN, et al. Resolvin D series and protectin D1 mitigate acute kidney injury. *J Immunol*. (2006) 177:5902–11. doi: 10.4049/jimmunol.177.9.5902
40. Schwab JM, Chiang N, Arita M, Serhan CN. Resolvin E1 and protectin D1 activate inflammation-resolution programmes. *Nature*. (2007) 447:869–74. doi: 10.1038/nature05877
41. Oh SF, Pillai PS, Recchiuti A, Yang R, Serhan CN. Pro-resolving actions and stereoselective biosynthesis of 18S E-series resolvins in human leukocytes and murine inflammation. *J Clin Invest*. (2011) 121:569–81. doi: 10.1172/JCI42545
42. Spite M, Norling LV, Summers L, Yang R, Cooper D, Petasis NA, et al. Resolvin D2 is a potent regulator of leukocytes and controls microbial sepsis. *Nature*. (2009) 461:1287–91. doi: 10.1038/nature08541
43. Mizraji G, Heyman O, Van Dyke TE, Wilensky A. Resolvin D2 restrains Th1 immunity and prevents alveolar bone loss in murine periodontitis. *Front Immunol*. (2018) 9:785. doi: 10.3389/fimmu.2018.00785
44. Chiurchiu V, Leuti A, Dalli J, Jacobsson A, Battistini L, Maccarrone M, et al. Proresolving lipid mediators resolvin D1, resolvin D2, and maresin 1 are critical in modulating T cell responses. *Sci Transl Med*. (2016) 8:353ra111. doi: 10.1126/scitranslmed.aaf7483
45. El Kebir D, Gjorstrup P, Filep JG. Resolvin E1 promotes phagocytosis-induced neutrophil apoptosis and accelerates resolution of pulmonary inflammation. *Proc Natl Acad Sci U S A*. (2012) 109:14983–8. doi: 10.1073/pnas.1206641109
46. Titos E, Rius B, Gonzalez-Periz A, Lopez-Vicario C, Moran-Salvador E, Martinez-Clemente M, et al. Resolvin D1 and its precursor docosahexaenoic acid promote resolution of adipose tissue inflammation by eliciting macrophage polarization toward an M2-like phenotype. *J Immunol*. (2011) 187:5408–18. doi: 10.4049/jimmunol.1100225
47. Akagi D, Chen M, Toy R, Chatterjee A, Conte MS. Systemic delivery of proresolving lipid mediators resolvin D2 and maresin 1 attenuates intimal hyperplasia in mice. *FASEB J*. (2015) 29:2504–13. doi: 10.1096/fj.14-265363
48. Hsiao HM, Sapinoro RE, Thatcher TH, Croasdell A, Levy EP, Fulton RA, et al. A novel anti-inflammatory and pro-resolving role for resolvin D1 in acute cigarette smoke-induced lung inflammation. *PLoS ONE*. (2013) 8:e58258. doi: 10.1371/journal.pone.0058258
49. Hsiao HM, Thatcher TH, Colas RA, Serhan CN, Phipps RP, Sime PJ. Resolvin D1 reduces emphysema and chronic inflammation. *Am J Pathol*. (2015) 185:3189–201. doi: 10.1016/j.ajpath.2015.08.008
50. Settimio R, Clara DF, Franca F, Francesca S, Michele D. Resolvin D1 reduces the immunoinflammatory response of the rat eye following uveitis. *Mediat Inflamm*. (2012) 2012:318621. doi: 10.1155/2012/318621
51. Kim TH, Kim GD, Jin YH, Park YS, Park CS. Omega-3 fatty acid-derived mediator, Resolvin E1, ameliorates 2,4-dinitrofluorobenzene-induced atopic dermatitis in NC/Nga mice. *Int Immunopharmacol*. (2012) 14:384–91. doi: 10.1016/j.intimp.2012.08.005
52. Ramon S, Gao F, Serhan CN, Phipps RP. Specialized proresolving mediators enhance human B cell differentiation to antibody-secreting cells. *J Immunol*. (2012) 189:1036–42. doi: 10.4049/jimmunol.1103483
53. Hong S, Porter TF, Lu Y, Oh SF, Pillai PS, Serhan CN. Resolvin E1 metabolome in local inactivation during inflammation-resolution. *J Immunol*. (2008) 180:3512–9. doi: 10.4049/jimmunol.180.5.3512
54. Kim N, Ramon S, Thatcher TH, Woeller CF, Sime PJ, Phipps RP. Specialized proresolving mediators (SPMs) inhibit human B-cell IgE production. *Eur J Immunol*. (2016) 46:81–91. doi: 10.1002/eji.201545673
55. Isobe Y, Arita M, Matsueda S, Iwamoto R, Fujihara T, Nakanishi H, et al. Identification and structure determination of novel anti-inflammatory mediator resolvin E3, 17,18-dihydroxyeicosapentaenoic acid. *J Biol Chem*. (2012) 287:10525–34. doi: 10.1074/jbc.M112.340612
56. Zhang HW, Wang Q, Mei HX, Zheng SX, Ali AM, Wu QX, et al. RvD1 ameliorates LPS-induced acute lung injury via the suppression of neutrophil infiltration by reducing CXCL2 expression and release from resident alveolar macrophages. *Int Immunopharmacol*. (2019) 76:105877. doi: 10.1016/j.intimp.2019.105877
57. Maugeri N, Capobianco A, Rovere-Querini P, Ramirez GA, Tombetti E, Valle PD, et al. Platelet microparticles sustain autophagy-associated activation of neutrophils in systemic sclerosis. *Sci Transl Med*. (2018) 10:eaao3089. doi: 10.1126/scitranslmed.aao3089
58. Barnes TC, Anderson ME, Edwards SW, Moots RJ. Neutrophil-derived reactive oxygen species in SSc. *Rheumatology (Oxford, England)*. (2012) 51:1166–9. doi: 10.1093/rheumatology/ker520
59. Kowal-Bielecka O, Kowal K, Highland KB, Silver RM. Bronchoalveolar lavage fluid in scleroderma interstitial lung disease: technical aspects and clinical correlations: review of the literature. *Semin Arthritis Rheum*. (2010) 40:73–88. doi: 10.1016/j.semarthrit.2008.10.009
60. Cakmak G, Selcuk Can T, Gundogdu S, Akman C, Ikitimur H, Musellim B, et al. Relationship between abnormalities on high-resolution computerized tomography, pulmonary function, and bronchoalveolar lavage in progressive systemic sclerosis. *Sarcoidosis Vasc Diffuse Lung Dis*. (2016) 33:349–54.
61. Antoniou KM, Wells AU. Scleroderma lung disease: evolving understanding in light of newer studies. *Curr Opin Rheumatol*. (2008) 20:686–91. doi: 10.1097/BOR.0b013e3283126985
62. Janko C, Schorn C, Grossmayer GE, Frey B, Herrmann M, Gaipl US, et al. Inflammatory clearance of apoptotic remnants in systemic lupus erythematosus (SLE). *Autoimmun Rev*. (2008) 8:9–12. doi: 10.1016/j.autrev.2008.07.015
63. Manoussakis MN, Fragoulis GE, Vakrakou AG, Moutsopoulos HM. Impaired clearance of early apoptotic cells mediated by inhibitory IgG antibodies in patients with primary sjogren's syndrome. *PLoS ONE*. (2014) 9:e112100. doi: 10.1371/journal.pone.0112100
64. Ballerie A, Lescoat A, Augagneur Y, Lelong M, Morzadec C, Cazalets C, et al. Efferocytosis capacities of blood monocyte-derived macrophages in systemic sclerosis. *Immunol Cell Biol*. (2019) 97:340–7. doi: 10.1111/imcb.12217
65. Sica A, Bronte V. Altered macrophage differentiation and immune dysfunction in tumor development. *J Clin Invest*. (2007) 117:1155–66. doi: 10.1172/JCI31422
66. Mantovani A, Sozzani S, Locati M, Allavena P, Sica A. Macrophage polarization: tumor-associated macrophages as a paradigm for polarized M2 mononuclear phagocytes. *Trends Immunol*. (2002) 23:549–55. doi: 10.1016/S1471-4906(02)02302-5
67. Lech M, Anders HJ. Macrophages and fibrosis: how resident and infiltrating mononuclear phagocytes orchestrate all phases of tissue injury and repair. *Biochim Biophys Acta*. (2013) 1832:989–97. doi: 10.1016/j.bbadis.2012.12.001
68. Funes SC, Rios M, Escobar-Vera J, Kalergis AM. Implications of macrophage polarization in autoimmunity. *Immunology*. (2018) 154:186–95. doi: 10.1111/imm.12910
69. Stout RD, Jiang C, Matta B, Tietzel I, Watkins SK, Suttles J. Macrophages sequentially change their functional phenotype in response to changes in microenvironmental influences. *J Immunol*. (2005) 175:342–9. doi: 10.4049/jimmunol.175.1.342
70. Higashi-Kuwata N, Jinnin M, Makino T, Fukushima S, Inoue Y, Muchemwa FC, et al. Characterization of monocyte/macrophage subsets in the skin and peripheral blood derived from patients with systemic sclerosis. *Arthritis Res Ther*. (2010) 12:R128. doi: 10.1186/ar3066
71. Trombetta AC, Soldano S, Contini P, Tomatis V, Ruaro B, Paolino S, et al. A circulating cell population showing both M1 and M2 monocyte/macrophage surface markers characterizes systemic sclerosis patients with lung involvement. *Respir Res*. (2018) 19:186. doi: 10.1186/s12931-018-0891-z
72. Soldano S, Trombetta AC, Contini P, Tomatis V, Ruaro B, Brizzolara R, et al. Increase in circulating cells coexpressing M1 and M2 macrophage surface markers in patients with systemic sclerosis. *Ann Rheum Dis*. (2018) 77:1842–5. doi: 10.1136/annrheumdis-2018-213648
73. Pope NH, Salmon M, Davis JP, Chatterjee A, Su G, Conte MS, et al. D-series resolvins inhibit murine abdominal aortic aneurysm formation and increase M2 macrophage polarization. *FASEB J*. (2016) 30:4192–201. doi: 10.1096/fj.201600144RR
74. Ah Kioon MD, Tripodo C, Fernandez D, Kirou KA, Spiera RF, Crow MK, et al. Plasmacytoid dendritic cells promote systemic sclerosis with a key role for TLR8. *Sci Transl Med*. (2018) 10:eaam8458. 10:eaam8458. doi: 10.1126/scitranslmed.aam8458
75. Kafaja S, Valera I, Divekar AA, Saggar R, Abtin F, Furst DE, et al. pDCs in lung and skin fibrosis in a bleomycin-induced model and patients with systemic sclerosis. *JCI Insight*. (2018) 3:e98380. doi: 10.1172/jci.insight.98380
76. Zabel BA, Silverio AM, Butcher EC. Chemokine-like receptor 1 expression and chemerin-directed chemotaxis distinguish plasmacytoid from

myeloid dendritic cells in human blood. *J Immunol*. (2005) 174:244–51. doi: 10.4049/jimmunol.174.1.244
77. Vermi W, Riboldi E, Wittamer V, Gentili F, Luini W, Marrelli S, et al. Role of chemr23 in directing the migration of myeloid and plasmacytoid dendritic cells to lymphoid organs and inflamed skin. *J Exp Med*. (2005) 201:509–15. doi: 10.1084/jem.20041310
78. van der Vorst EPC, Mandl M, Muller M, Neideck C, Jansen Y, Hristov M, et al. Hematopoietic chemr23 (chemerin receptor 23) fuels atherosclerosis by sustaining an M1 macrophage-phenotype and guidance of plasmacytoid dendritic cells to murine lesions-brief report. *Arterioscler Thromb Vasc Biol*. (2019) 39:685–93. doi: 10.1161/ATVBAHA.119.312386
79. Sato S, Hanakawa H, Hasegawa M, Nagaoka T, Hamaguchi Y, Nishijima C, et al. Levels of interleukin 12, a cytokine of type 1 helper T cells, are elevated in sera from patients with systemic sclerosis. *J Rheumatol*. (2000) 27:2838–42.
80. Carvalheiro T, Zimmermann M, Radstake T, Marut W. Novel insights into dendritic cells in the pathogenesis of systemic sclerosis. *Clin Exp Immunol*. (2020). doi: 10.1111/cei.13417. [Epub ahead of print].
81. Gasparini G, Cozzani E, Parodi A. Interleukin-4 and interleukin-13 as possible therapeutic targets in systemic sclerosis. *Cytokine*. (2020) 125:154799. doi: 10.1016/j.cyto.2019.154799
82. Salmon-Ehr V, Serpier H, Nawrocki B, Gillery P, Clavel C, Kalis B, et al. Expression of interleukin-4 in scleroderma skin specimens and scleroderma fibroblast cultures. Potential role in fibrosis. *Arch Dermatol*. (1996) 132:802–6. doi: 10.1001/archderm.132.7.802
83. Huang XL, Wang YJ, Yan JW, Wan YN, Chen B, Li BZ, et al. Role of anti-inflammatory cytokines IL-4 and IL-13 in systemic sclerosis. *Inflamm Res*. (2015) 64:151–9. doi: 10.1007/s00011-015-0806-0
84. Fuschiotti P, Larregina AT, Ho J, Feghali-Bostwick C, Medsger TA Jr. Interleukin-13-producing CD8+ T cells mediate dermal fibrosis in patients with systemic sclerosis. *Arthritis Rheum*. (2013) 65:236–46. doi: 10.1002/art.37706
85. Korn T, Bettelli E, Oukka M, Kuchroo VK. IL-17 and Th17 cells. *Annu Rev Immunol*. (2009) 27:485–517. 27:485–517. doi: 10.1146/annurev.immunol.021908.132710
86. Kurasawa K, Hirose K, Sano H, Endo H, Shinkai H, Nawata Y, et al. Increased interleukin-17 production in patients with systemic sclerosis. *Arthritis Rheum*. (2000) 43:2455–63. 43:2455–63. doi: 10.1002/1529-0131(200011)43:11<2455::AID-ANR12>3.0.CO;2-K
87. Rolla G, Fusaro E, Nicola S, Bucca C, Peroni C, Parisi S, et al. Th-17 cytokines and interstitial lung involvement in systemic sclerosis. *J Breath Res*. (2016) 10:046013. 10:046013. doi: 10.1088/1752-7155/10/4/046013
88. Yang X, Yang J, Xing X, Wan L, Li M. Increased frequency of Th17 cells in systemic sclerosis is related to disease activity and collagen overproduction. *Arthritis Res Ther*. (2014) 16:R4. doi: 10.1186/ar4430
89. Chizzolini C, Dufour AM, Brembilla NC. Is there a role for IL-17 in the pathogenesis of systemic sclerosis? *Immunol Lett*. (2018) 195:61–7. doi: 10.1016/j.imlet.2017.09.007
90. Gourh P, Arnett FC, Assassi S, Tan FK, Huang M, Diekman L, et al. Plasma cytokine profiles in systemic sclerosis: associations with autoantibody subsets and clinical manifestations. *Arthritis Res Ther*. (2009) 11:R147. doi: 10.1186/ar2821
91. Olewicz-Gawlik A, Danczak-Pazdrowska A, Kuznar-Kaminska B, Gornowicz-Porowska J, Katulska K, Trzybulska D, et al. Interleukin-17 and interleukin-23: importance in the pathogenesis of lung impairment in patients with systemic sclerosis. *Int J Rheum Dis*. (2014) 17:664–70. doi: 10.1111/1756-185X.12290
92. Vassiliou EK, Kesler OM, Tadros JH, Ganea D. Bone marrow-derived dendritic cells generated in the presence of resolvin E1 induce apoptosis of activated CD4+ T cells. *J Immunol*. (2008) 181:4534–44. doi: 10.4049/jimmunol.181.7.4534
93. Haworth O, Cernadas M, Yang R, Serhan CN, Levy BD. Resolvin E1 regulates interleukin 23, interferon-γ and lipoxin A4 to promote the resolution of allergic airway inflammation. *Nat Immunol*. (2008) 9:873–9. doi: 10.1038/ni.1627
94. Manetti M, Neumann E, Muller A, Schmeiser T, Saar P, Milia AF, et al. Endothelial/lymphocyte activation leads to prominent CD4+ T cell infiltration in the gastric mucosa of patients with systemic sclerosis. *Arthritis Rheum*. (2008) 58:2866–73. doi: 10.1002/art.23806
95. Lafyatis R, O'Hara C, Feghali-Bostwick CA, Matteson E. B cell infiltration in systemic sclerosis-associated interstitial lung disease. *Arthritis Rheum*. (2007) 56:3167–8. doi: 10.1002/art.22847
96. Sanges S, Guerrier T, Launay D, Lefevre G, Labalette M, Forestier A, et al. Role of B cells in the pathogenesis of systemic sclerosis. *Rev Med Interne*. (2017) 38:113–24. doi: 10.1016/j.revmed.2016.02.016
97. Wigley FM, Flavahan NA. Raynaud's phenomenon. *N Engl J Med*. (2016) 375:556–65. doi: 10.1056/NEJMra1507638
98. Cutolo M, Smith V, Furst DE, Khanna D, Herrick AL. Points to consider-Raynaud's phenomenon in systemic sclerosis. *Rheumatology (Oxford)*. (2017) 56(suppl. 5):v45–v8. doi: 10.1093/rheumatology/kex199
99. Cutolo M, Soldano S, Smith V. Pathophysiology of systemic sclerosis: current understanding and new insights. *Expert Rev Clin Immunol*. (2019) 15:753–64. doi: 10.1080/1744666X.2019.1614915
100. Bruni C, Frech T, Manetti M, Rossi FW, Furst DE, De Paulis A, et al. Vascular leaking, a pivotal and early pathogenetic event in systemic sclerosis: should the door be closed? *Front Immunol*. (2018) 9:2045. doi: 10.3389/fimmu.2018.02045
101. Flavahan NA. A vascular mechanistic approach to understanding raynaud phenomenon. *Nat Rev Rheumatol*. (2015) 11:146–58. doi: 10.1038/nrrheum.2014.195
102. Collard CD, Gelman S. Pathophysiology, clinical manifestations, and prevention of ischemia-reperfusion injury. *Anesthesiology*. (2001) 94:1133–8. doi: 10.1097/00000542-200106000-00030
103. Wu MY, Yiang GT, Liao WT, Tsai AP, Cheng YL, Cheng PW, et al. Current mechanistic concepts in ischemia and reperfusion injury. *Cell Physiol Biochem*. (2018) 46:1650–67. doi: 10.1159/000489241
104. Kang JW, Choi HS, Lee SM. Resolvin D1 attenuates liver ischaemia/reperfusion injury through modulating thioredoxin 2-mediated mitochondrial quality control. *Br J Pharmacol*. (2018) 175:2441–53. doi: 10.1111/bph.14212
105. Qiu W, Guo K, Yi L, Gong Y, Huang L, Zhong W. Resolvin E1 reduces hepatic fibrosis in mice with schistosoma japonicum infection. *Exp Ther Med*. (2014) 7:1481–5. doi: 10.3892/etm.2014.1641
106. Qu X, Zhang X, Yao J, Song J, Nikolic-Paterson DJ, Li J. Resolvins E1 and D1 inhibit interstitial fibrosis in the obstructed kidney via inhibition of local fibroblast proliferation. *J Pathol*. (2012) 228:506–19. doi: 10.1002/path.4050
107. Kain V, Ingle KA, Colas RA, Dalli J, Prabhu SD, Serhan CN, et al. Resolvin D1 activates the inflammation resolving response at splenic and ventricular site following myocardial infarction leading to improved ventricular function. *J Mol Cell Cardiol*. (2015) 84:24–35. doi: 10.1016/j.yjmcc.2015.04.003
108. Rout-Pitt N, Farrow N, Parsons D, Donnelley M. Epithelial mesenchymal transition (EMT): a universal process in lung diseases with implications for cystic fibrosis pathophysiology. *Respir Res*. (2018) 19:136. doi: 10.1186/s12931-018-0834-8
109. Postlethwaite AE, Shigemitsu H, Kanangat S. Cellular origins of fibroblasts: possible implications for organ fibrosis in systemic sclerosis. *Curr Opin Rheumatol*. (2004) 16:733–8. doi: 10.1097/01.bor.0000139310.77347.9c
110. Yang Y, Hu L, Xia H, Chen L, Cui S, Wang Y, et al. Resolvin D1 attenuates mechanical stretch-induced pulmonary fibrosis via epithelial-mesenchymal transition. *Am J Physiol Lung Cell Mol Physiol*. (2019) 316:L1013–l24. doi: 10.1152/ajplung.00415.2018
111. Khanna D, Distler JH, Sandner P, Distler O. Emerging strategies for treatment of systemic sclerosis. *J Scleroderma Relat Disord*. (2016) 1:186–93. doi: 10.5301/jsrd.5000207

Conflict of Interest: The authors declare that the research was conducted in the absence of any commercial or financial relationships that could be construed as a potential conflict of interest.

frontiers in Immunology

MINI REVIEW
published: 14 August 2020
doi: 10.3389/fimmu.2020.01394

Fibrotic Scar in Neurodegenerative Diseases

Nadia D'Ambrosi and Savina Apolloni**

Department of Biology, Tor Vergata University, Rome, Italy

The process of uncontrolled internal scarring, called fibrosis, is now emerging as a pathological feature shared by both peripheral and central nervous system diseases. In the CNS, damaged neurons are not replaced by tissue regeneration, and scar-forming cells such as endothelial cells, inflammatory immune cells, stromal fibroblasts, and astrocytes can persist chronically in brain and spinal cord lesions. Although this process was extensively described in acute CNS damages, novel evidence indicates the involvement of a fibrotic reaction in chronic CNS injuries as those occurring during neurodegenerative diseases, where inflammation and fibrosis fuel degeneration. In this mini review, we discuss recent advances around the role of fibrotic scar formation and function in different neurodegenerative conditions, particularly focusing on the rising role of scarring in the pathogenesis of amyotrophic lateral sclerosis, multiple sclerosis, and Alzheimer's disease and highlighting the therapeutic relevance of targeting fibrotic scarring to slow and reverse neurodegeneration.

Keywords: Alzheimer's disease, amyotrophic lateral sclerosis, astrocytes, fibroblasts, microglia, multiple sclerosis

OPEN ACCESS

Edited by:
Anna-Maria Hoffmann-Vold,
Oslo University Hospital, Norway

Reviewed by:
Carlo Chizzolini,
Université de Genève, Switzerland
Zoltan Jakus,
Semmelweis University, Hungary

****Correspondence:***
Nadia D'Ambrosi
nadia.dambrosi@uniroma2.it
Savina Apolloni
savina.apolloni@uniroma2.it

Specialty section:
This article was submitted to Autoimmune and Autoinflammatory Disorders, a section of the journal Frontiers in Immunology

Received: *31 March 2020*
Accepted: *01 June 2020*
Published: *14 August 2020*

Citation:
D'Ambrosi N and Apolloni S (2020) Fibrotic Scar in Neurodegenerative Diseases. Front. Immunol. 11:1394. doi: 10.3389/fimmu.2020.01394

INTRODUCTION

Fibrosis identifies a condition marked by an increase of interstitial fibrous tissue in the parenchyma, induced by an uncontrolled inflammatory reaction derived by a wound healing response to tissue injury. While wound healing represents a necessary action to contain and repair damage, the cellular and molecular events characterizing the fibrotic response can evolve in time and can lead to the distortion of tissue architecture, followed by a loss of organ function with pathophysiological consequences that may even be severe (1, 2). The wound healing response, resulting from neurodegeneration, recruits local and infiltrating immune cells, as well as extracellular matrix (ECM)-producing stromal fibroblasts and astrocytes. Typically, damaged neurons are not replaced by tissue regeneration, and scar-forming cells can persist chronically in brain and spinal cord lesions. Fibrotic scarring, also called mesenchymal scarring, represents the central core of the CNS acute lesions and it mainly consists of endothelial cells and inflammatory immune cells, including monocyte-derived macrophages, stromal fibroblasts, and ECM deposits. The fibrotic core is closely bordered by the so-called glial scar, mainly consisting of astrocytes. CNS responses to acute lesions can be divided into partially overlapping but functionally distinct temporal phases: cell death and inflammation, cell proliferation and tissue replacement, ECM degradation, an tissue remodeling. Chronic injuries of the CNS, occurring in most neurodegenerative diseases, do not display and overt fibrotic condition. Major differences with acute injuries concern the lower intensity of the initial damage which accumulates only gradually, and, as it becomes more severe gives rise to small individual lesions displaying reactive gliosis, multicellular responses and ECM deposits, similarly to acute damages, albeit in a smaller scale, in a wider time-range and in an interspersed manner (3, 4). Pieces of evidence indeed indicate the involvement of a fibrotic reaction in chronic diseases,

such as activation of cells of mesenchymal origin, astrocytes, and a redefinition of the ECM. Specifically, myofibroblasts (mainly deriving from endothelial vasculature, meninges, pericytes or infiltrated stromal cells), astrocytes and macrophages contribute to the disproportionate deposition of connective tissue matrix proteins, consisting predominantly of fibronectin, collagen and laminin, as well as glycosaminoglycans (GAGs) (5, 6) that delay tissue repair by stimulating further scarring and fibrosis through communication with inflammatory cells (7, 8). ECM components form dense lattice-like structures surrounding neurons, termed perineuronal nets (PNNs), that in the long-term hamper neural plasticity and axon regeneration and growth (9).

Rising evidence supports a double, and apparently contrasting, role of the CNS scar, in both promoting tissue protection as well as in inhibiting repair. Indeed, scar-forming astrocytes have been extensively studied and regarded as one of the main sources of the axon growth inhibitory mechanism (10) by acting as a physical barrier that delays rather than supporting axon regeneration. At the injury margins, reactive astrocytes reorganize their structure, becoming hypertrophic, with elongated overlapping processes, and display a strong upregulation of intermediate filament proteins such as glial fibrillary acidic protein (GFAP), vimentin and nestin (1). In addition, in the site of CNS damage, reactive macrophages and microglia play crucial roles in driving secondary injury through a vicious neuroinflammatory cycle. Indeed, ECM molecules released by reactive cells activate receptors on macrophages and microglia to induce a pro-inflammatory phenotype that leads to further astrocytic reactivity and matrix molecules deposition. It is reported that in neurodegenerative diseases including amyotrophic lateral sclerosis (ALS), multiple sclerosis (MS), and Alzheimer's disease (AD), activated microglia, secreting pro-inflammatory cytokines, induce the so called "A1" reactive astrocytes. These astrocytes fail to support the survival and differentiation of neuronal cells, and start to drive neuron and oligodendrocyte death (11). Conversely, it has also been reported that astrocytic scar formation may not only have a detrimental role, but it also helps CNS axonal regeneration by forming permissive bridges *in vivo*, known as glial bridges, along which injured CNS axons can regrow and cross the scar when stimulated with appropriate growth factors and by transcriptional activation of neuronal-intrinsic growth pathways (12). For instance, reactive astrocytes appearing after a stroke acquire a repairing phenotype, characterized by the upregulation of neurotrophic factors expression and by the translocation of mitochondrial particles to damaged neurons (13).

Microglia and macrophages promote tissue remodeling and repair by clearance of cellular and myelin debris, degradation of scar tissue and production of neurotrophic factors (14). Depending on the time/phase of the disease, and type of injury (acute vs. chronic) these cells can be involved in a composite response. They participate in secondary tissue damage with consequent glial scar formation, and at the same time they assume an anti-inflammatory phenotype with increased phagocytic activity, producing growth factors and anti-inflammatory cytokines and stimulating tissue repair and regeneration (15). Therefore, a categorization of glial functions is an oversimplification, since their responses (16), characterized simultaneously by both detrimental and protective features, are closely linked and mutually dependent.

Besides astrocytes and microglia, reactive NG2-glia are reported to contribute to the formation of the scar, migrating toward the site of injury and increasing the proliferation and the expression of ECM molecules, as proteoglycans. Moreover, oligodendrocytes precursor cells change their gene expression following CNS damage, starting to express cytokines, and perpetuating the immune response. On the other hand, oligodendrocyte progenitor cells participate in the resolution of the scar, limiting the extent of neurotoxic inflammatory lesion core cells (17).

Recent evidence has shown that, following CNS injury, pericytes, perivascular cells located on microvessels, partake in the fibrotic scar formation by proliferating and differentiating into scar-forming myofibroblasts (18–20).

This mini review aims at summarizing and discussing the current evidence regarding the role of fibrotic scar in the context of neurodegenerative diseases.

FIBRO-GLIAL SCAR IN ALS

Amyotrophic lateral sclerosis (ALS) is characterized by motor neuron degeneration in the motor cortex, brainstem, and anterior horns of the spinal cord. Motor neuron loss is a complex phenomenon, where different cell types actively contribute to the pathological mechanism, establishing a non-cell autonomous disease, implying a comprehensive analysis to understand how changes in the function of individual cell types can affect the behavior of other cells. In the CNS, motor neuron loss is indeed accompanied by glial cells activation, oligodendrocyte pathology and toxicity, blood-brain and -spinal barrier permeabilization, and peripheral immune cells infiltration (21). Astrocytosis has a particular impact on the disease, since it is characterized by a massive response of hypertrophic protoplasmic astrocytes surrounding degenerating motor neurons, and intense fibrotic astrocyte reactivity in the white matter (22). This process involves numerous molecular changes toward a reactive phenotype, such as production and secretion of pro-inflammatory cytokines, chemokines, and growth factors, in particular, IL-6, CXCL1, 10, 12, tumor necrosis factor-α, transforming growth factor β (TGFβ), nerve growth factor, interferon γ, prostaglandin D2 (23), as well as ECM components (24, 25). During ALS, such activation could have the protective purpose to circumvent the degeneration spreading and to restrict inflammation by contrasting the infiltration of active immune cells into the injured tissue, preventing further tissue damage. However, the presence of glial scarring, excessive microgliosis and accumulation of

Abbreviations: AD, Alzheimer's disease; ALS, amyotrophic lateral sclerosis; CSPGs, chondroitin sulfate proteoglycans; EAE, experimental autoimmune encephalomyelitis; ECM, extracellular matrix; GFAP, glial fibrillary acidic protein; hFUS, human FUS; HS, heparan sulfate; HSPGs, heparan sulfate proteoglycans; MS, multiple sclerosis; PNN, perineuronal net; PDGFR, platelet-derived growth factor receptor β; α-SMA, α-smooth muscle actin; TGFβ, transforming growth factor (TGF)β.

ECM into a disorganized PNN structure around motor neurons, actually form a non-permissive environment that is hostile to neuron survival and regeneration, thus resulting in a harmful reaction (26). Therefore, the fibro-gliotic response could have a dual role, where the contribution of the two processes is continuously remodeled over time, eventually shifting the subtle equilibrium between two possible opposite outcomes toward a detrimental one.

It has been demonstrated that in tissues derived from ALS patients and from the SOD1-G93A mouse model, increased levels of TGFβ correlate with disease progression. Persistent elevated amounts of TGFβ are supposed to be responsible for a decrease in neurogenesis, pro-inflammatory reactions, and fibrosis. This latter might promote the progression of ALS indirectly by replacing areas of motor neuron loss with excessive scar tissue. In this respect, mainly astrocytes and microglia produce and release TGFβ that may act on myofibroblasts precursors to induce a profibrotic phenotype (27, 28). Indeed, the motor cortex of ALS patients displays significantly increased levels of fibronectin and collagen IV, indicating fibrotic activity (27). Moreover, the ECM characterizing spinal cord in ALS H46R rats is also increased in chondroitin sulfate proteoglycans (CSPGs), which are supposed to behave as hindering matrices toward any cell-restorative therapy with both cell transplantation and endogenous neural progenitor activation (26). The analysis performed with confocal Raman spectra of spinal cord tissues from SOD1-G93A mice shows that the signature of the gray matter, both in early symptomatic and presymptomatic mice, is markedly different from the one obtained from healthy mice. In addition to axon demyelination and loss of lipid structural order, these spectra differences account for proliferation and aggregation of branched CSPGs that, moreover, appear to be early events in the progression of the disease (29). Furthermore, CSPGs receptors are increased in reactive astrocytes from diseased rats, and this may contribute to further inhibition of neuronal regeneration, through a signaling mechanism induced by CSPGs (25). Accumulation of ECM is moreover testified by the downregulation of the ADAMTS-4 proteoglycanase activity, particularly at the end stage of the disease in SOD1-G93A mice lumbar spinal cord. However, differently from spinal cord injury, the decrease of the metalloproteinase could be a protective tissue response to maintain a robust ECM envelope, with the aim to render neurons less vulnerable to degeneration (30), although it cannot be excluded that, the downregulation of ADAMTS-4 and the consequent thickening of the PNN could be a neuron regeneration-opposing process. With a supposed protective extent, semaphorin Sema3A, an extracellular matrix molecule mainly expressed by meningeal fibroblasts and involved in the inhibition of axonal degeneration, decreases progressively in SOD1-G93A mice spinal cord, highlighting the remodeling of the ECM as an attempt to rescue the inhibition of axonal regeneration and growth cone collapse (31). Elevated levels of connective tissue growth factor (CTGF) a protein involved in different processes, among which adhesion, migration, and synthesis of ECM components is increased in the spinal cord of ALS patients (32). Although it can be speculated that this protein may exert non-fibrotic roles in the CNS, i.e., interfering with oligodendrocyte maturation and proper axon myelination, it cannot be excluded that it could be involved in ECM remodeling function in the CNS of ALS patients.

Although the remodeling of the ECM in ALS is attributed mainly to astrocytes (33, 34), other cell types can contribute to this phenomenon. Mesenchymal cells of meningeal and perivascular origin could have a major role in creating a fibrotic environment in the CNS. In this regard, S100A4, a member of the S100 Ca^{2+}-binding protein family, is strongly upregulated in ALS models, starting from presymptomatic stages (35, 36) and its overexpression, mainly ascribable to spinal astrocytes and microglia (35), occurs likewise in other cell types. S100A4 is well-known to exhibit a pivotal role in promoting changes in cellular phenotype, as it is highly expressed in cells that are undergoing a mesenchymal transition or are converting into a more reactive state (37). Moreover, S100A4 favors ECM deposition in tissues, contributing to the scar formation (38). Therefore, the increase in S100A4 during ALS could be related to inflammation, fibrosis and tissue remodeling in disease progression. Furthermore, vimentin, a type III intermediate filament protein, shared by reactive astrocytes and mesenchymal cells, increases its expression in SOD1-G93A mice (39, 40), as well as in the spinal cord of symptomatic ALS transgenic mice overexpressing wild-type human FUS (hFUS) (**Figure 1A**). Together with S100A4, vimentin and fibronectin, α-smooth muscle actin (α-SMA) is commonly used to identify activated mesenchymal cells surrounding CNS blood vessels which are a major source of injury-induced myofibroblasts after damage (41, 42). In the spinal cord of ALS models, α-SMA increases in thickened blood vessels of SOD1-G93A mice (43) and in vessels in close proximity to astrocytes in the formation of the neurovascular unit of hFUS mice (**Figure 1B**). This evidence suggests that in ALS CNS there is an increase of mesenchymal cells, such as myofibroblasts derived from perivascular and endothelial cells, which could contribute to a pro-fibrotic environment. Indeed, elevated levels of various inflammatory cytokines in ALS patients could induce a pro-inflammatory endothelial cell response promoting the synthesis of monocyte-attracting chemokines and vascular cell-adhesion molecules, leading to parenchymal invasion of inflammatory and immune cells (44). Furthermore, the loss of pericytes in the blood-brain and blood-spinal cord barrier, a well-established pathogenic mechanism in ALS, correlated with the worsening of the disease, leads to accumulation of blood cells and proteins (such as immunoglobulin G, fibrin and thrombin) in the CNS (45). In a similar way to what occurs in AD (18), we can speculate that pericytes can actively contribute to the fibrotic scar by transforming into myofibroblasts.

FIBRO-GLIAL SCAR IN MS

Multiple sclerosis (MS) is a neuroinflammatory CNS disease where white matter axonal demyelination, accompanied by the disruption of the blood-brain barrier and consequent infiltration of monocyte-derived macrophages and lymphocytes, causes multiple white matter scars in the brain and spinal cord (46).

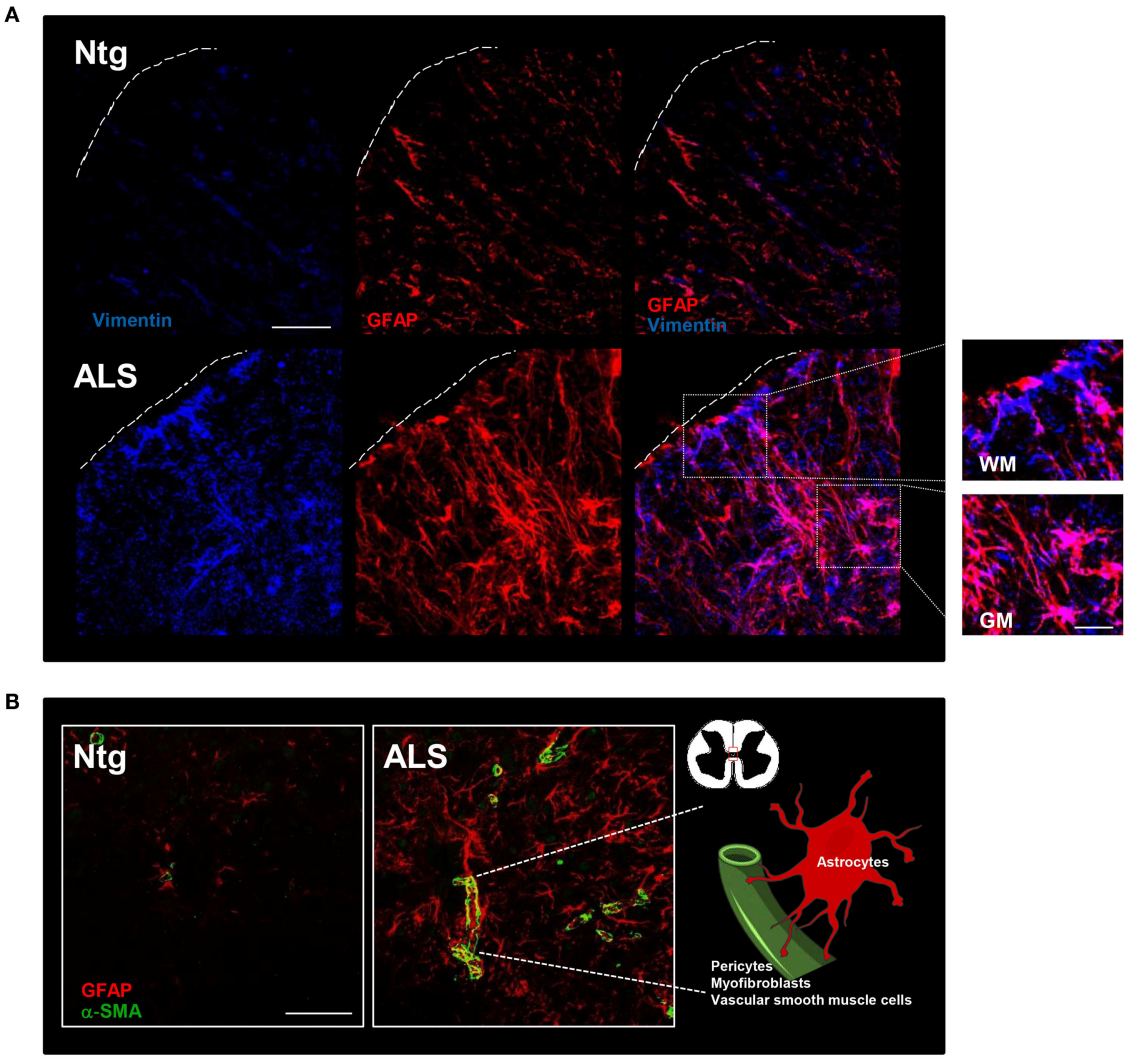

FIGURE 1 | Fibrotic and glial scar in ALS mice. **(A)** Representative confocal images of lumbar spinal cord sections from non-transgenic (Ntg) and hFUS (ALS) mice at end stage of the disease. ALS section displays abundant vimentin-immunoreactive cells (blue) and glial fibrillary acidic protein (GFAP)-immunoreactive astroglial cells organized in a scar-like fashion (red). Scale bar = 20 μm. A higher magnification of the area marked by the white square is shown on the right and displays cells stained by both vimentin and GFAP in the gray matter (GM) and vimentin-positive cells closely associated to GFAP-positive astrocytes in the white matter (WM) Scale bar = 100 μm. **(B)** Representative confocal images of lumbar spinal cord sections from non-transgenic (Ntg) and hFUS (ALS) mice at end stage of the disease. ALS section displays an increase in α-smooth muscle actin (α-SMA)-immunoreactive cells (green) closely surrounded by GFAP-positive cells (red). Scale bar = 100 μm.

A large amount of literature describes in both MS patients and experimental autoimmune encephalomyelitis (EAE) animal models, the formation of a fibrotic scar near the well-known glial scar. Particularly, in the active MS brain lesions and in EAE mouse spinal cord, besides the neuroinflammatory component, a widespread deposition of ECM, pro-fibrotic factors, collagens and fibronectin aggregates has been observed, all concurring to impair the remyelination process (8, 47). Moreover, biglycan and decorin are up-regulated in the demyelinated regions closely associated with immune cells infiltrates in the parenchyma (48). In addition, recent papers have shown the presence of brain mesenchymal perivascular aggregates of platelet-derived growth factor receptor (PDGFR)β-positive cells in MS patients and in the EAE model, where they contribute to fibrotic scar tissue generation, active inflammation and demyelination (49). In brain demyelinated plaques of MS patients and in leucocyte-containing perivascular cuff, an important portal where immune cells infiltrate into the CNS parenchyma, CSPGs are up-regulated. In this context they increase the activation and transmigratory capacity of macrophages and impair remyelination by interfering with the migration of pro-regenerative neural and oligodendrocyte precursor cells into lesions (50, 51).

The emerging novel function of microvascular endothelial cells in boosting secondary injury by promoting inflammation, microvessel dilation, and fibrotic scar formation is recently

described by Zhou and co-authors in the EAE model. They show that endothelial cells exert critical functions beyond myelin clearance in promoting the progression of demyelination disorders, by regulating macrophage infiltration, pathologic angiogenesis and fibrosis. Particularly, they demonstrate that the engulfment of myelin debris induces a mesenchymal transition, transforming endothelial cells into a source of fibrotic molecules as collagen and fibronectin (52). Therefore, both inflammation and ECM deposition contribute to impair the regenerative ability of oligodendrocyte progenitor cells to replace mature oligodendrocytes, thus prolonging the demyelination of lesions. Recently, Yan and colleagues, by using Col1α1GFP transgenic mice to visualize scar-forming cells in the lesioned tissue, showed that perivascular fibroblasts are activated in the EAE model at the onset of the disease and infiltrate the parenchyma next to the areas of demyelination and the ECM deposition. Moreover, they showed that both fibroblast conditioned medium and fibroblast ECM hinder the differentiation of oligodendrocyte progenitor cells into mature oligodendrocytes (53).

FIBRO-GLIAL SCAR IN AD

Alzheimer's disease (AD) is a neurodegenerative disorder characterized by the formation of "plaques" constituted by an excess of fibrous tissue in the brain. Brain tissue from AD patients indeed shows extensive deposition of extracellular β-amyloid aggregates accumulating into toxic fibrils, along with several other extracellular molecules, including GAGs and proteoglycans, with a prevalence of heparan sulfate proteoglycans (HSPGs) (54). HSPGs exert a critical role in amyloid precursor protein cleavage and the resulting β-amyloid fibrillization (55, 56). Remarkably, the study of Garcia et al. (57) reports that the expression of heparanase, an endoglucuronidase that specifically degrades heparan sulfate (HS) side chains, is upregulated in the brain of AD patients both within intracellular deposits of degenerating neurons and in extracellular plaques. Yet, in the brains of mice overexpressing heparanase, the recruitment and activation of inflammatory cells are significantly attenuated as well as immune cell-mediated clearance of β-amyloid deposits, proving that intact HS chains are required to mediate neuroinflammatory responses and highlighting a possible beneficial role of HS in the disease (58, 59). These apparently contradictory results are nevertheless in line with the dual role of the fibrotic process particularly linked to the inflammatory responses activated during the progression of neurodegenerative pathologies. The importance of interfering with HSPGs is supported by novel studies showing that this mechanism could represent a possible therapeutic approach in the control of fibrotic and glial scarring in AD pathology. Consistently, an antibody targeting extracellular tau is able to potently inhibit its neuronal internalization by masking epitopes that are important for the interaction with neuron surface HSPGs, constituting therefore a potential strategy in hampering AD (60). Moreover, HSPGs-mediated tau internalization is inhibited by the sulfated glycosaminoglycan heparin that, however, is characterized by a low brain penetration and strong anticoagulant properties (61). Stopschinski et al. (62) recently developed a synthetic heparinoid devoid of anticoagulant activity able to inhibit tau binding to GAGs and consequently its cellular uptake.

An increasing attention is now given to the role of pericyte cells as an attractive target involved in the pathogenesis, progression and potential treatment of AD (18). In AD patients, pericyte density is associated with blood-brain barrier breakdown, reported to be strongly responsible for the cognitive deficits characterizing the disease and identified as an early biomarker. Moreover, pericytes and vascular smooth muscle cells constitute the major cellular phenotypes expressing PDGFRβ, the levels of which in the cerebrospinal fluid positively correlate with clinical dementia rating in AD patients (63).

CONCLUSIONS

A fibrotic environment within the CNS can be a consequence of infections, parasite infestations, and neuronal injury. While acute brain and spinal cord traumas generate a well-defined fibrotic scar, where ECM, myofibroblasts, and astrocytes are clearly organized into a discernible structure, in neurodegenerative diseases the formation of a fibrotic environment in neuronal tissue is less obvious. However, a number of evidence indicates that in chronic situations of neuron loss, as those occurring in neurodegenerative conditions, there is a progressive replacement

TABLE 1 | Synoptic view of main features of acute and chronic CNS fibro-glial scar.

CNS disease	Responder cells	Mediators	ECM component
Acute damage	Astrocytes, microglia, leukocytes, meningeal cells, fibroblasts, pericytes	Thrombin, MMP-9, ATP, PDGFRβ, TGFβ	Fibronectin, laminin, collagen, CSPGs, tenascin, HSPGs
ALS	Astrocytes, microglia, leukocytes, oligodendrocytes, meningeal cells, fibroblasts, pericytes	IL-6, CXCL1, CXCL10, CXCL12, TNFα, TGFβ, NGF, INFγ, PGD2, ADAMTS-4, CTGF, S100A4, MMP-9	Fibronectin, collagen IV, CSPGs, Sema3A, fibrin, vimentin, thrombin
MS	Astrocytes, microglia, leukocytes, endothelial cells, meningeal cells, fibroblasts, pericytes, oligodendrocytes	PDGFRβ, TGFβ, myelin	Collagen, fibronectin, biglycan, decorin, CSPGs
AD	Astrocytes, microglia, leukocytes, smooth muscle cells, fibroblasts, pericytes	PDGFRβ, TGFβ	GAGs, HSPGs

The table summarizes the main cellular components, mediators and ECM molecules involved in ALS, MS, and AD as well as in acute CNS damage. For a more extensive review of the many specific molecules that regulate or influence CNS cellular responses to acute conditions see (3, 4). CTGF, connective tissue growth factor; INFγ, interferon γ; MMP-9, matrix metalloprotease-9; NGF, nerve growth factor; PGD2, prostaglandin D2; TNFα, tumor necrosis factor α.

of damaged tissue with ECM components, mainly produced by activated fibroblasts and astrocytes and this leads to a secondary response involving microglia and peripheral immune cells. Nevertheless, the outcome of acute injury and the progression of chronic disease such as ALS, MS, and AD share most responder cells and many of the principal mediators and extracellular components, some of which have been described in this review and summarized in **Table 1**.

Although the purpose of fibrotic material deposition is to limit damage spreading, the prolonged, and massive response that often characterizes this process eventually impedes tissue regeneration and axons preservation. Thus, while wound healing is an advisable event in neurodegenerative conditions, it would be therapeutically helpful to try to modify and resolve scarring toward a beneficial pro-axon regeneration feature, by manipulating for instance myofibroblasts, originating from perivascular or meningeal tissues or from pericytes, and glial cells, with the overall aim to improve the outcome of diseases (2). Since neurodegenerative diseases are mediated by multifactorial pathways and are characterized by multicellular responses, it is now clear that their successful treatment should necessarily be multi-targeted. Toward this end, strategies aimed at removing excessive fibrotic matrix and slowing-down the relentless deposition of ECM by reactive glia and fibroblasts, could be promising because they could limit the chronic inflammation that is associated to fibrosis.

By targeting the molecular mechanisms which are involved in the process of fibrotic scar formation as inflammatory responses, autophagy, debris uptake, and mesenchymal reactivity, it could be possible to reverse the effects of CNS associated fibrosis. In this regard, future directions could be represented by anti-fibrotic agents acting as novel potential therapeutic targets for the treatment of MS, re-establishing an environment where the remyelination is not hindered by the formation of a fibrotic scar, followed by the appearance of neuroinflammatory lesions. In ALS and AD, where both inflammation and fibrosis strongly contribute to the pathogenesis of the diseases, switching cells such as astrocytes and myofibroblasts from a matrix-depositing state that supports fibrosis to a matrix-degrading state that promotes resolution or reversal of fibrosis may contribute to ameliorate pathological conditions.

AUTHOR CONTRIBUTIONS

All authors listed have made a substantial, direct and intellectual contribution to the work, and approved it for publication.

FUNDING

Research in NDA lab was supported by the Italian Research Foundation for Amyotrophic Lateral Sclerosis-AriSLA (Project SPLICEALS).

ACKNOWLEDGMENTS

We are grateful to Dr. Mauro Cozzolino for helping with confocal microscope images.

REFERENCES

1. Bradbury EJ, Burnside ER. Moving beyond the glial scar for spinal cord repair. *Nat Commun*. (2019) 10:3879. doi: 10.1038/s41467-019-11707-7
2. Jun JI, Lau LF. Resolution of organ fibrosis. *J Clin Invest*. (2018) 128:97–107. doi: 10.1172/JCI93563
3. Burda JE, Sofroniew MV. Reactive gliosis and the multicellular response to CNS damage and disease. *Neuron*. (2014) 81:229–48. doi: 10.1016/j.neuron.2013.12.034
4. Kawano H, Kimura-Kuroda J, Komuta Y, Yoshioka N, Li HP, Kawamura K, et al. Role of the lesion scar in the response to damage and repair of the central nervous system. *Cell Tissue Res*. (2012) 349:169–80. doi: 10.1007/s00441-012-1336-5
5. Hamill KJ, Kligys K, Hopkinson SB, Jones JC. Laminin deposition in the extracellular matrix: a complex picture emerges. *J Cell Sci*. (2009) 122:4409–17. doi: 10.1242/jcs.041095
6. Fernandez-Klett F, Priller J. The fibrotic scar in neurological disorders. *Brain Pathol*. (2014) 24:404–13. doi: 10.1111/bpa.12162
7. O'Shea TM, Burda JE, Sofroniew MV. Cell biology of spinal cord injury and repair. *J Clin Invest*. (2017) 127:3259–70. doi: 10.1172/JCI90608
8. Dias DO, Goritz C. Fibrotic scarring following lesions to the central nervous system. *Matrix Biol*. (2018) 69:561–70. doi: 10.1016/j.matbio.2018.02.009
9. Soleman S, Filippov MA, Dityatev A, Fawcett JW. Targeting the neural extracellular matrix in neurological disorders. *Neuroscience*. (2013) 253:194–213. doi: 10.1016/j.neuroscience.2013.08.050
10. Yiu G, He Z. Glial inhibition of CNS axon regeneration. *Nat Rev Neurosci*. (2006) 7:617–27. doi: 10.1038/nrn1956
11. Liddelow SA, Guttenplan KA, Clarke LE, Bennett FC, Bohlen CJ, Schirmer L, et al. Neurotoxic reactive astrocytes are induced by activated microglia. *Nature*. (2017) 541:481–7. doi: 10.1038/nature21029
12. Anderson MA, Burda JE, Ren Y, Ao Y, O'Shea TM, Kawaguchi R, et al. Astrocyte scar formation aids central nervous system axon regeneration. *Nature*. (2016) 532:195–200. doi: 10.1038/nature17623
13. Hayakawa K, Esposito E, Wang X, Terasaki Y, Liu Y, Xing C, et al. Transfer of mitochondria from astrocytes to neurons after stroke. *Nature*. (2016) 535:551–5. doi: 10.1038/nature18928
14. Milich LM, Ryan CB, Lee JK. The origin, fate, and contribution of macrophages to spinal cord injury pathology. *Acta Neuropathol*. (2019) 137:785–97. doi: 10.1007/s00401-019-01992-3
15. Adams KL, Gallo V. The diversity and disparity of the glial scar. *Nat Neurosci*. (2018) 21:9–15. doi: 10.1038/s41593-017-0033-9
16. Ransohoff RM. A polarizing question: do M1 and M2 microglia exist? *Nat Neurosci*. (2016) 19:987–91. doi: 10.1038/nn.4338
17. Duncan GJ, Manesh SB, Hilton BJ, Assinck P, Plemel JR, Tetzlaff W. The fate and function of oligodendrocyte progenitor cells after traumatic spinal cord injury. *Glia*. (2020) 68:227–45. doi: 10.1002/glia.23706
18. Laredo F, Plebanski J, Tedeschi A. Pericytes: problems and promises for CNS repair. *Front Cell Neurosci*. (2019) 13:546. doi: 10.3389/fncel.2019.00546
19. Goritz C, Dias DO, Tomilin N, Barbacid M, Shupliakov O, Frisen J. A pericyte origin of spinal cord scar tissue. *Science*. (2011) 333:238–42. doi: 10.1126/science.1203165
20. Harrell CR, Simovic Markovic B, Fellabaum C, Arsenijevic A, Djonov V, Volarevic V. Molecular mechanisms underlying therapeutic potential of pericytes. *J Biomed Sci*. (2018) 25:21. doi: 10.1186/s12929-018-0423-7
21. Greenhalgh AD, David S, Bennett FC. Immune cell regulation of glia during CNS injury and disease. *Nat Rev Neurosci*. (2020) 21:139–52. doi: 10.1038/s41583-020-0263-9
22. D'Ambrosi N, Cozzolino M, Carri MT. Neuroinflammation in amyotrophic lateral sclerosis: role of redox (dys)regulation. *Antioxid Redox Signal*. (2018) 29:15–36. doi: 10.1089/ars.2017.7271

23. Yamanaka K, Komine O. The multi-dimensional roles of astrocytes in ALS. *Neurosci Res*. (2018) 126:31–8. doi: 10.1016/j.neures.2017.09.011
24. Mizuno H, Warita H, Aoki M, Itoyama Y. Accumulation of chondroitin sulfate proteoglycans in the microenvironment of spinal motor neurons in amyotrophic lateral sclerosis transgenic rats. *J Neurosci Res*. (2008) 86:2512–23. doi: 10.1002/jnr.21702
25. Shijo T, Warita H, Suzuki N, Kitajima Y, Ikeda K, Akiyama T, et al. Aberrant astrocytic expression of chondroitin sulfate proteoglycan receptors in a rat model of amyotrophic lateral sclerosis. *J Neurosci Res*. (2018) 96:222–33. doi: 10.1002/jnr.24127
26. Forostyak S, Homola A, Turnovcova K, Svitil P, Jendelova P, Sykova E. Intrathecal delivery of mesenchymal stromal cells protects the structure of altered perineuronal nets in SOD1 rats and amends the course of ALS. *Stem Cells*. (2014) 32:3163–72. doi: 10.1002/stem.1812
27. Peters S, Zitzelsperger E, Kuespert S, Iberl S, Heydn R, Johannesen S, et al. The TGF-β system as a potential pathogenic player in disease modulation of amyotrophic lateral sclerosis. *Front Neurol*. (2017) 8:669. doi: 10.3389/fneur.2017.00669
28. Endo F, Komine O, Fujimori-Tonou N, Katsuno M, Jin S, Watanabe S, et al. Astrocyte-derived TGF- β1 accelerates disease progression in ALS mice by interfering with the neuroprotective functions of microglia and T cells. *Cell Rep*. (2015) 11:592–604. doi: 10.1016/j.celrep.2015.03.053
29. Picardi G, Spalloni A, Generosi A, Paci B, Mercuri NB, Luce M, et al. Tissue degeneration in ALS affected spinal cord evaluated by Raman spectroscopy. *Sci Rep*. (2018) 8:13110. doi: 10.1038/s41598-018-31469-4
30. Lemarchant S, Pomeshchik Y, Kidin I, Karkkainen V, Valonen P, Lehtonen S, et al. ADAMTS-4 promotes neurodegeneration in a mouse model of amyotrophic lateral sclerosis. *Mol Neurodegener*. (2016) 11:10. doi: 10.1186/s13024-016-0078-3
31. Miyazaki K, Nagai M, Morimoto N, Kurata T, Takehisa Y, Ikeda Y, et al. Spinal anterior horn has the capacity to self-regenerate in amyotrophic lateral sclerosis model mice. *J Neurosci Res*. (2009) 87:3639–48. doi: 10.1002/jnr.22156
32. Gonzalez D, Brandan E. CTGF/CCN2 from skeletal muscle to nervous system: impact on neurodegenerative diseases. *Mol Neurobiol*. (2019) 56:5911–6. doi: 10.1007/s12035-019-1490-9
33. Wiese S, Karus M, Faissner A. Astrocytes as a source for extracellular matrix molecules and cytokines. *Front Pharmacol*. (2012) 3:120. doi: 10.3389/fphar.2012.00120
34. Jayakumar AR, Apeksha A, Norenberg MD. Role of matricellular proteins in disorders of the central nervous system. *Neurochem Res*. (2017) 42:858–75. doi: 10.1007/s11064-016-2088-5
35. Serrano A, Apolloni S, Rossi S, Lattante S, Sabatelli M, Peric M, et al. The S100A4 transcriptional inhibitor niclosamide reduces pro-inflammatory and migratory phenotypes of microglia: implications for amyotrophic lateral sclerosis. *Cells*. (2019) 8:1261. doi: 10.3390/cells8101261
36. Sun S, Sun Y, Ling SC, Ferraiuolo L, McAlonis-Downes M, Zou Y, et al. Translational profiling identifies a cascade of damage initiated in motor neurons and spreading to glia in mutant SOD1-mediated ALS. *Proc Natl Acad Sci USA*. (2015) 112:E6993–7002. doi: 10.1073/pnas.1520639112
37. Schneider M, Hansen JL, Sheikh SP. S100A4: a common mediator of epithelial-mesenchymal transition, fibrosis and regeneration in diseases? *J Mol Med (Berl)*. (2008) 86:507–22. doi: 10.1007/s00109-007-0301-3
38. Fei F, Qu J, Li C, Wang X, Li Y, Zhang S. Role of metastasis-induced protein S100A4 in human non-tumor pathophysiologies. *Cell Biosci*. (2017) 7:64. doi: 10.1186/s13578-017-0191-1
39. Tang C, Zhu L, Zhou Q, Li M, Zhu Y, Xu Z, et al. Altered features of vimentin-containing cells in cerebrum of Tg(SOD1*G93A)1gur mice: a preliminary study on cerebrum endogenous neural precursor cells in amyotrophic lateral sclerosis. *Int J Biol Sci*. (2019) 15:2830–43. doi: 10.7150/ijbs.33461
40. Zhou Y, Lu Y, Fang X, Zhang J, Li J, Li S, et al. An astrocyte regenerative response from vimentin-containing cells in the spinal cord of amyotrophic lateral sclerosis's disease-like transgenic (G93A SOD1) mice. *Neurodegener Dis*. (2015) 15:1–12. doi: 10.1159/000369466
41. Di Carlo SE, Peduto L. The perivascular origin of pathological fibroblasts. *J Clin Invest*. (2018) 128:54–63. doi: 10.1172/JCI93558
42. Piera-Velazquez S, Jimenez SA. Endothelial to mesenchymal transition: role in physiology and in the pathogenesis of human diseases. *Physiol Rev*. (2019) 99:1281–324. doi: 10.1152/physrev.00021.2018
43. Crivello M, O'Riordan SL, Woods I, Cannon S, Halang L, Coughlan KS, et al. Pleiotropic activity of systemically delivered angiogenin in the SOD1(G93A) mouse model. *Neuropharmacology*. (2018) 133:503–11. doi: 10.1016/j.neuropharm.2018.02.022
44. Garbuzova-Davis S, Ehrhart J, Sanberg PR, Borlongan CV. Potential role of humoral IL-6 cytokine in mediating pro-inflammatory endothelial cell response in amyotrophic lateral sclerosis. *Int J Mol Sci*. (2018) 19:423. doi: 10.3390/ijms19020423
45. Winkler EA, Sengillo JD, Sullivan JS, Henkel JS, Appel SH, Zlokovic BV. Blood-spinal cord barrier breakdown and pericyte reductions in amyotrophic lateral sclerosis. *Acta Neuropathol*. (2013) 125:111–20. doi: 10.1007/s00401-012-1039-8
46. van Horssen J, Dijkstra CD, de Vries HE. The extracellular matrix in multiple sclerosis pathology. *J Neurochem*. (2007) 103:1293–301. doi: 10.1111/j.1471-4159.2007.04897.x
47. Stoffels JM, de Jonge JC, Stancic M, Nomden A, van Strien ME, Ma D, et al. Fibronectin aggregation in multiple sclerosis lesions impairs remyelination. *Brain*. (2013) 136:116–31. doi: 10.1093/brain/aws313
48. Mohan H, Krumbholz M, Sharma R, Eisele S, Junker A, Sixt M, et al. Extracellular matrix in multiple sclerosis lesions: fibrillar collagens, biglycan and decorin are upregulated and associated with infiltrating immune cells. *Brain Pathol*. (2010) 20:966–75. doi: 10.1111/j.1750-3639.2010.00399.x
49. Iacobaeus E, Sugars RV, Tornqvist Andren A, Alm JJ, Qian H, Frantzen J, et al. Dynamic changes in brain mesenchymal perivascular cells associate with multiple sclerosis disease duration, active inflammation, and demyelination. *Stem Cells Transl Med*. (2017) 6:1840–51. doi: 10.1002/sctm.17-0028
50. Stephenson EL, Mishra MK, Moussienko D, Laflamme N, Rivest S, Ling CC, et al. Chondroitin sulfate proteoglycans as novel drivers of leucocyte infiltration in multiple sclerosis. *Brain*. (2018) 141:1094–110. doi: 10.1093/brain/awy033
51. Lau LW, Keough MB, Haylock-Jacobs S, Cua R, Doring A, Sloka S, et al. Chondroitin sulfate proteoglycans in demyelinated lesions impair remyelination. *Ann Neurol*. (2012) 72:419–32. doi: 10.1002/ana.23599
52. Zhou T, Zheng Y, Sun L, Badea SR, Jin Y, Liu Y, et al. Microvascular endothelial cells engulf myelin debris and promote macrophage recruitment and fibrosis after neural injury. *Nat Neurosci*. (2019) 22:421–35. doi: 10.1038/s41593-018-0324-9
53. Yahn SL, Li J, Goo I, Gao H, Brambilla R, Lee JK. Fibrotic scar after experimental autoimmune encephalomyelitis inhibits oligodendrocyte differentiation. *Neurobiol Dis*. (2020) 134:104674. doi: 10.1016/j.nbd.2019.104674
54. Zhang GL, Zhang X, Wang XM, Li JP. Towards understanding the roles of heparan sulfate proteoglycans in Alzheimer's disease. *Biomed Res Int*. (2014) 2014:516028. doi: 10.1155/2014/516028
55. Alavi Naini SM, Soussi-Yanicostas N. Heparan sulfate as a therapeutic target in tauopathies: insights from zebrafish. *Front Cell Dev Biol*. (2018) 6:163. doi: 10.3389/fcell.2018.00163
56. Heindryckx F, Li JP. Role of proteoglycans in neuro-inflammation and central nervous system fibrosis. *Matrix Biol*. (2018) 69:589–601. doi: 10.1016/j.matbio.2018.01.015
57. Garcia B, Martin C, Garcia-Suarez O, Muniz-Alonso B, Ordiales H, Fernandez-Menendez S, et al. Upregulated expression of heparanase and heparanase 2 in the brains of alzheimer's disease. *J Alzheimers Dis*. (2017) 58:185–92. doi: 10.3233/JAD-161298
58. Zhang X, Wang B, O'Callaghan P, Hjertstrom E, Jia J, Gong F, et al. Heparanase overexpression impairs inflammatory response and macrophage-mediated clearance of amyloid-β in murine brain. *Acta Neuropathol*. (2012) 124:465–78. doi: 10.1007/s00401-012-0997-1
59. Farrugia BL, Lord MS, Melrose J, Whitelock JM. The role of heparan sulfate in inflammation, and the development of biomimetics as anti-inflammatory strategies. *J Histochem Cytochem*. (2018) 66:321–36. doi: 10.1369/0022155417740881
60. Weisova P, Cehlar O, Skrabana R, Zilkova M, Filipcik P, Kovacech B, et al. Therapeutic antibody targeting microtubule-binding domain prevents neuronal internalization of extracellular tau via masking

neuron surface proteoglycans. *Acta Neuropathol Commun*. (2019) 7:129. doi: 10.1186/s40478-019-0770-y

61. Timmer NM, van Dijk L, van der Zee CE, Kiliaan A, de Waal RM, Verbeek MM. Enoxaparin treatment administered at both early and late stages of amyloid β deposition improves cognition of APPswe/PS1dE9 mice with differential effects on brain Aβ levels. *Neurobiol Dis*. (2010) 40:340–7. doi: 10.1016/j.nbd.2010.06.008
62. Stopschinski BE, Thomas TL, Nadji S, Darvish E, Fan L, Holmes BB, et al. A synthetic heparinoid blocks Tau aggregate cell uptake and amplification. *J Biol Chem*. (2020) 295:2974–83. doi: 10.1074/jbc.RA119.010353
63. Nation DA, Sweeney MD, Montagne A, Sagare AP, D'Orazio LM, Pachicano M, et al. Blood-brain barrier breakdown is an early biomarker of human cognitive dysfunction. *Nat Med*. (2019) 25:270–6. doi: 10.1038/s41591-018-0297-y

Conflict of Interest: The authors declare that the research was conducted in the absence of any commercial or financial relationships that could be construed as a potential conflict of interest.

frontiers in Immunology

MINI REVIEW
published: 04 September 2020
doi: 10.3389/fimmu.2020.01990

Interstitial Lung Disease in Patients With Systemic Sclerosis: Toward Personalized-Medicine-Based Prediction and Drug Screening Models of Systemic Sclerosis-Related Interstitial Lung Disease (SSc-ILD)

Padmini Khedoe†, Emiel Marges†, Pieter Hiemstra, Maarten Ninaber and Miranda Geelhoed*

Department of Pulmonology, Leiden University Medical Center (LUMC), Leiden, Netherlands

OPEN ACCESS

Edited by:
Oliver Distler,
University of Zurich, Switzerland

Reviewed by:
Elizabeth Volkmann,
University of California, Los Angeles, United States
David Launay,
Université de Lille, France

***Correspondence:**
Padmini Khedoe
p.p.s.j.khedoe@lumc.nl

† These authors have contributed equally to this work

Specialty section:
This article was submitted to Autoimmune and Autoinflammatory Disorders, a section of the journal Frontiers in Immunology

Received: *13 March 2020*
Accepted: *23 July 2020*
Published: *04 September 2020*

Citation:
Khedoe P, Marges E, Hiemstra P, Ninaber M and Geelhoed M (2020) Interstitial Lung Disease in Patients With Systemic Sclerosis: Toward Personalized-Medicine-Based Prediction and Drug Screening Models of Systemic Sclerosis-Related Interstitial Lung Disease (SSc-ILD). Front. Immunol. 11:1990. doi: 10.3389/fimmu.2020.01990

Systemic sclerosis (SSc) is an autoimmune connective tissue disease, characterized by immune dysregulation and progressive fibrosis. Interstitial lung disease (ILD) is the most common cause of death among SSc patients and there are currently very limited approved disease-modifying treatment options for systemic sclerosis-related interstitial lung disease (SSc-ILD). The mechanisms underlying pulmonary fibrosis in SSc-ILD are not completely unraveled, and knowledge on fibrotic processes has been acquired mostly from studies in idiopathic pulmonary fibrosis (IPF). The incomplete knowledge of SSc-ILD pathogenesis partly explains the limited options for disease-modifying therapy for SSc-ILD. Fibrosis in IPF appears to be related to aberrant repair following injury, but whether this also holds for SSc-ILD is less evident. Furthermore, immune dysregulation appears to contribute to pro-fibrotic responses in SSc-ILD, perhaps more than in IPF. In addition, SSc-ILD patient heterogeneity complicates the understanding of the underlying mechanisms of disease development, and more importantly, limits correct clinical diagnosis and treatment effectivity. Therefore, there is an unmet need for patient-relevant (*in vitro*) models to examine patient-specific disease pathogenesis, predict disease progression, screen appropriate treatment regimens and identify new targets for treatment. Technological advances in *in vitro* patient-relevant disease modeling, including (human induced pluripotent stem cell (hiPSC)-derived) lung epithelial cells, organoids and organ-on-chip technology offer a platform that has the potential to contribute to unravel the underlying mechanisms of SSc-ILD development. Combining these models with state-of-the-art analysis platforms, including (single cell) RNA sequencing and (imaging) mass cytometry, may help to delineate pathogenic mechanisms and define new treatment targets of SSc-ILD.

Keywords: systemic sclerosis, interstitial lung disease, idiopathic pulmonary fibrosis, pathogenesis, organoids, human disease models

INTRODUCTION

Systemic sclerosis (SSc) is a devastating disease of unknown etiology, characterized by systemic, immunological, vascular, and fibrotic abnormalities, with a heterogeneous clinical course. Fibrosis, the hallmark of the disease, can affect skin and internal organs, including the lung (1). SSc-related interstitial lung disease (SSc-ILD) is one of the most severe complications and is the main cause of SSc-related deaths (2, 3). Treatment options are limited, although the FDA has recently approved nintedanib for progressive SSc-ILD. The limitation in options for disease-modifying treatments may partly be explained by the incomplete knowledge of the mechanisms underlying lung fibrosis development in SSc-ILD and the heterogeneous course of disease. Furthermore, the optimal type and timing of treatment of SSc-ILD is unknown and it is becoming increasingly clear that the treatment of SSc-ILD patients requires a personalized approach. An unknown subgroup of patients with SSc may benefit from antifibrotic drugs such as nintedanib and related compounds, in addition to their immunosuppressive therapy. Therefore, there is an unmet need for novel biomarkers to predict disease progression and response to treatment (4). As a result, the prognosis for SSc-ILD patients remains extremely poor, and there is an urgent need for better disease-relevant models to identify new treatment targets and for (personalized) drug screening.

Although various experimental animal models of human ILD are currently available, they do not fully represent human disease development, and fibrosis is often reversible (5). Furthermore, whereas pathogenic mechanisms can be studied to some extent using inflammatory cells derived from peripheral blood and bronchoalveolar lavage (BAL) from SSc-ILD patients, insight into the interaction between key players in the pathogenesis of fibrosis is often lacking. Currently, there are only a few available preclinical human *in vitro* models which recapitulate features of fibrosis, including the complex interplay between (myo)fibroblasts, epithelial cells, inflammatory cells and endothelial cells, and these are reviewed elsewhere (5). The extent to which these models recapitulate fibrosis development in SSc-ILD is unclear.

Here, we discuss how recent advances in human preclinical models may help to unravel pathogenic mechanisms and new treatment targets of SSc-ILD by shortly reviewing the cellular processes that lead to fibrosis in IPF and SSc-ILD (**Figure 1**).

COMMON FIBROTIC PATHWAYS

SSc-ILD can be regarded as an impaired or otherwise aberrant repair response in the alveolar areas. Proposed mechanisms of fibrosis development and progression include profibrotic responses following lung alveolar epithelial cell (AEC) damage, aberrant alveolar repair (6, 7) and accelerated lung epithelial aging (8). Impaired regenerative capacity of lung progenitor cells, mainly the type 2 alveolar cells (AEC2), are suggested to be key players in the aberrant repair response. In concert with activated endothelial cells (EC) and recruited inflammatory cells, AEC2 orchestrate a profibrotic niche leading to fibroblast activation, myofibroblast formation and excessive extracellular matrix (ECM) deposition. Increased numbers of (myo)fibroblasts and their activation is mainly driven by transforming growth factor-β (TGF-β), whereas in alveolar epithelial type 1 and 2 cells (AEC1/2) and EC, excessive TGF-β may result in epithelial-to-mesenchymal transition (EMT) and endothelial-to-mesenchymal transition (endoMT) (9–12). TGF-β, produced by various cells types, is the central regulator of fibrotic processes and its levels are increased in both IPF and SSc-ILD lungs (13, 14). TGF-β enhances expression of profibrotic and pro-inflammatory cytokines and growth factors, such as tumor necrosis factor-α (TNF-α), platelet derived growth factor (PDGF), Interleukin-1β (IL-1β), and IL-13 (15). Target genes of TGF-β include e.g., α-smooth muscle actin (α-SMA) and connective tissue growth factor (CTGF), which are increased in fibrosis (12). Plasma CTGF levels were reported to be elevated in IPF patients (16) and, together with Vascular Endothelial Growth Factor (VEGF) and TGF-β, act as central mediators in fibrosis (14, 17–19). Altogether, the profibrotic niche leads to aberrant alveolar repair responses, fibroblast foci and excessive extracellular matrix (ECM) production, causing extensive pulmonary remodeling resulting in impairment of lung function.

Since one of the key players in this aberrant repair response is the AEC2, lung organoid assays provide a tool to study the regenerative ability of these lung progenitor cells. Organoids are three-dimensional (3D) self-organizing structures of multiple cell types grown in 3-D matrices, as opposed to a 2D cell culture on culture plates. The 3D matrix contains a mixture of ECM proteins and various growth factors, necessary for expansion, proliferation and differentiation of lung epithelial (progenitor) cells (20). Lung organoids can be cultured for prolonged periods of time, currently up to 2 years, without changes in their karyotype, whilst preserving original (patient) characteristics. An important feature of organoids is that progenitor cells are retained in culture, and have the capacity to proliferate and differentiate into various specialized cell types (21). Furthermore, when generating lung epithelial organoids, the differentiation into bronchial, alveolar or mixed cell types can be achieved by selection of cells, manipulating the cultures with cocktails of cytokines and growth factors, stimulating or inhibiting signaling pathways, and/or by including mesenchymal cells that provide supporting signals for differentiation. Organoid differentiation and behavior may alter in response to a variety of injuries including exposure to SSc-ILD-related cytokines, infectious agents, tobacco smoke, high levels of oxygen and bleomycin (22, 23). This way, lung organoid models are well suited to study early phases of the fibrotic process. TGF-β treatment of airway organoids, for example, resulted in enhanced αSMA expression, and upregulated pro-fibrotic genes including CTGF and fibronectin (24, 25). Importantly, the complexity of the cross-talk between epithelial cells, fibroblasts and inflammatory cells that occur in ILD, can be mimicked in organoid models containing epithelial cells and surrounding cells, including fibroblasts and endothelial cells. This is also illustrated by a study showing that pretreatment of MRC-5 fibroblasts with TGF-β decreases their ability to support mouse epithelial organoid formation (26). Finally, recent advances

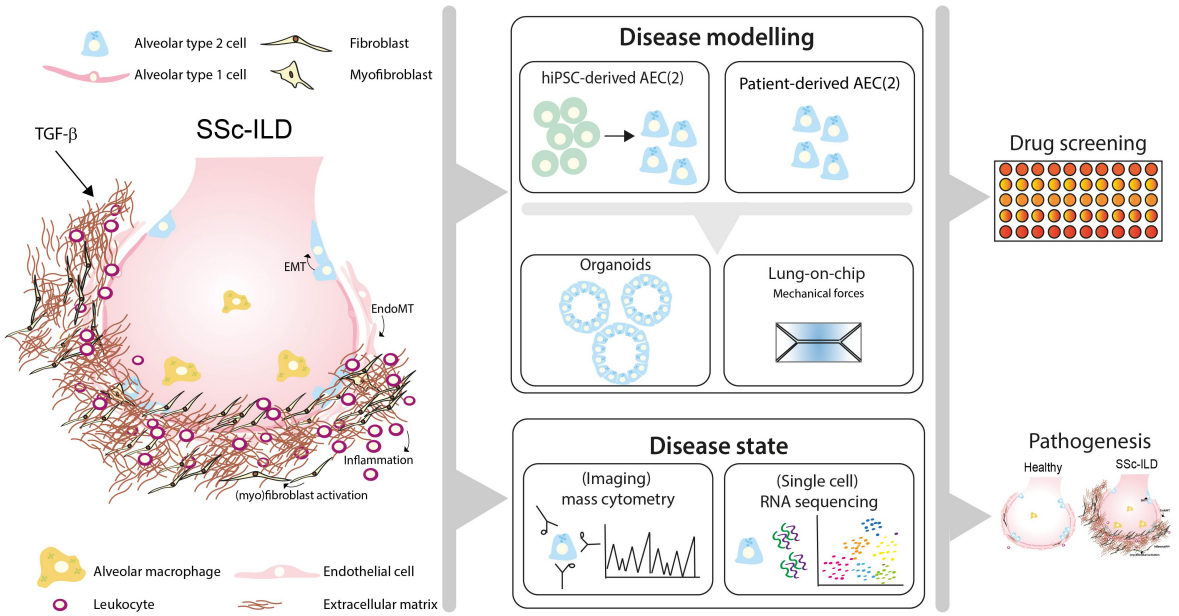

FIGURE 1 | Toward personalized-medicine-based prediction, target identification and drug screening models of SSc-ILD. In SSc-ILD, the interactions and cross-talk between various cell types, including in type 2 alveolar cells (AEC2), AEC1, endothelial cells, fibroblasts and immune cells is disturbed. This may be partly explained by excessive TGF-β signaling activation, leading to AEC1/2 and endothelial cell (EC) transition into a mesenchymal phenotype, (myo)fibroblast activation and proliferation and excessive interstitial extracellular matrix (ECM) deposition. Recruited leukocytes further contribute to the profibrotic environment, leading to lung tissue remodeling and fibrosis. Patient-derived pulmonary cells, either isolated from lung tissue or derived from human induced pluripotent stem cells (hiPSC), can be used to study patient-specific responses *in vitro* using organoid SSc-ILD disease models. Lung-chip models may add another layer of complexity containing physiological ques, including breathing motions, air-blood flow and stretch, which are often lacking in current available *in vitro* lung models. Disease-specific features can be measured using cutting-edge techniques such as single-cell-RNA-sequencing and (imaging) mass cytometry. Integrating information derived from SSc-ILD disease models using cells derived from SSc-ILD patients and triggers implicated in disease pathogenesis may lead to novel mechanistic insight and offer a platform for identification of pathogenic processes and drug screening for SSc-ILD.

allowing incorporation of inflammatory cells in lung organoid cultures may contribute to patient-relevant SSc-ILD models.

INFLAMMATION AND IMMUNITY

Fibrosis in SSc-ILD may result from an interplay between autoimmunity, inflammation, alveolar epithelial- and vascular injury (27), which may result in alveolitis. The alveolar and microvascular injurious events drive activation and proliferation of lung-resident immune cells and recruitment of inflammatory cells, including monocytes, neutrophils, mast cells and NK cells (28, 29). Interestingly, monocytes derived from SSc-ILD patients, which were increased in both the circulation and in lungs, exhibit pro-fibrotic properties *in vitro* upon pro-inflammatory stimulation (30). In addition, fibrotic mediators in SSc-ILD, including fibronectin-EDA and tenascin-C, may trigger activation of Toll Like Receptor 4 (TLR4) (31, 32) and cause uncontrolled ECM deposition in SSc (33), which subsequently potentiates TGF-β signaling, thereby enhancing fibrotic responses (15, 34).

Circulating and pulmonary (auto-reactive) B lymphocytes are important features in SSc-ILD (28, 35, 36) and produce pro-fibrotic mediators including TGF-β and Th2 cytokines (28). Furthermore, auto-antibodies, which are a characteristic feature of SSc, are produced by these autoreactive B cells and may cause local pulmonary damage and are associated with distinct clinical phenotypes of SSc (37). Development of ILD in SSc patients is strongly correlated with the presence of auto-antibodies against topoisomerase I, U11/12, Th/To,PL-7, U1-RNP, whereas anti-RNA polymerase III antibodies are associated with reduced risk of ILD in SSc (38). Also, anti-C1q antibodies were shown in a subgroup of SSc-ILD patients, and were found to be the most important predicting factor for pulmonary fibrosis development in SSc (39). Collectively, especially in SSc-ILD patients these autoreactive B cells may contribute to a profibrotic environment.

In IPF, the contribution of inflammation to IPF pathogenesis is less clear. Whereas the proportion of T- and B- cells was similar in IPF lungs compared to healthy lungs, both $CD71^{-}$ alveolar- and *SPP1*/osteopontin^{+} interstitial macrophages were found to be associated with disease severity (40, 41), suggesting that lung-resident macrophages contribute to fibrosis in IPF. In addition, circulating monocytes in patients with IPF appear to be programmed to express fibroblast-stimulating properties prior to entering the lung (42). The contribution of macrophage subtypes in fibrosis development is controversial. Whereas pro-inflammatory M1 macrophages may contribute to dysregulated repair (e.g., in acute exacerbations of IPF) (43, 44), anti-inflammatory M2 macrophages may promote fibroproliferation and progressive fibrosis (42, 44). Furthermore, dysregulated

apoptotic cell clearance and imbalanced ECM production and degradation by macrophages may contribute to fibrosis (45, 46).

In addition to enhanced levels of pro-fibrotic mediators, levels of pro-inflammatory cytokines and chemokines (including IL-8, IL-1α, IL-10, macrophage inflammatory protein-1α and MCP-1) and neutrophil-derived alpha-defensins (human neutrophil peptides (HNP), are increased in BALF from SSc-ILD patients (29, 47). In addition, also circulating levels of pro- and anti-inflammatory mediators, including IL-6, IL-10, MCP-1, IL-1RA and TNFα, were found to be increased. Some of these mediators correlate significantly with disease-relevant parameters (47, 48), and especially serum IL-6 is increased in both SSc-ILD and IPF, and may serve as a predictor of fibrosis progression (49). Recent studies intriguingly suggested both in IPF and SSc-ILD patients, an inverse correlation between lung function and myeloid-derived suppressor cell (MDSC) levels, highlighting their potential contribution to lung fibrosis (50). Thus, targeting the MDSC activity may be a novel approach to disease modification, and combined organoid models of epithelial and inflammatory cells may be useful tools to study this. This is illustrated by a study showing that lung organoids, comprised of epithelial and mesenchymal cells, respond to TLR- stimulation by releasing pro−inflammatory cytokines. Addition of primary human monocytes to these stimulated organoids, resulted in their migration toward the organoids and altered their phenotype to an "intermediate−like" phenotype, expressing increased levels of CD14, CD16 and HLA-DR compared to monocytes cultured alone (51).

Collectively these studies show that there are differences in the proposed role of inflammatory and immune cells in the pathogenesis of SSc-ILD and IPF. More complex organoid models, as outlined above, may help to further dissect the specific role of these cells, and the contribution of profibrotic and pro-inflammatory triggers in SSC-ILD. Indeed, whereas incorporation of patient-derived inflammatory and immune cells in organoids is logistically challenging, this may potentially provide preclinical personalized prediction models of disease development, and models for drug screening. In the tumor field, co-culture models of immune cells and tumor cells are used to assess effectivity of immunotherapy (52). Cattaneo et al. showed for example that effector function of autologous tumor-specific T cells could be assessed using peripheral blood-derived T cells and tumor organoids at a personalized level (53). Furthermore, efforts have been made to establish immune-engineered organoid models to study B-cell responses and antibody production (54, 55). Application of such combined organoid models to study (patient-specific) epithelial-inflammatory cell interactions in SSc-ILD, may provide an important step forward in our understanding of this devastating disease.

GENETICS

Accelerated lung aging and senescence of AEC and fibroblasts appear central phenotypes that promote lung fibrosis (8). Polymorphisms in genes involved in the maintenance of telomere length (mutations in TERT, TERC, PARN and RTEL1) are associated with an increased risk of IPF (56). Shortened telomeres, oxidative injury, endoplasmic reticulum (ER) stress, and mitochondrial dysfunction lead to decreased AEC proliferation and secretion of profibrotic mediators (8). In addition, genetic variants in the genes encoding e.g., surfactant protein C (SFPTC) (57, 58) and in the promotor region of mucin 5B (MUC5B), increase the risk of IPF development (59–61), while MUC5B has shown not to contribute to SSc-ILD (62). Whereas genetic susceptibility may be an important driver in IPF, for SSc, this is less clear. Several genetic factors may predispose to development of SSc, of which genetic variants in immune-related genes, including HLA and interferon-related genes, have been found (37). Genetic associations that predispose for development of SSc-ILD specifically, have been found in interferon regulatory factor 5 (IRF5), signal transducer and activator of transcription 4 (STAT4), DNAX accessory molecule 1 (CD226) and interleukin-1 receptor-associated kinase-1 (IRAK1) (63). Genetic variants in monocyte chemoattractant protein (MCP-1) and CTLA-4 were also associated with SSc-ILD (64). Especially, polymorphisms in CTLA-4, which acts as a checkpoint inhibitor, may be of relevance in SSc-ILD patients at risk for developing lung cancer.

Even though adult human cells can be isolated from lungs to study lung epithelial (progenitor) function, (altered) repair and regeneration, in SSc-ILD these are often derived from end-stage disease patients undergoing lung transplantation. To overcome this issue, human induced pluripotent stem cells (hiPSC)-derived lung epithelial cells may provide a personalized platform for assessing disease risk and potential treatment for SSc-ILD. One of the advantages of hiPSC-derived AEC2 is that they can be derived from individual patients from relatively easily accessible sources (urine, blood), enabling a personalized disease and medicine approach. Importantly, hiPSC-AEC2 can be genetically engineered by introducing or correcting mutations using CRISPR-based technology, which may be relevant to study genetic factors contributing to fibrosis in IPF and SSc-ILD (65). These hiPSC-derived AEC2 can be applied in lung organoids which can model pathogenetic processes occurring in ILD (66). Similar to hiPSC, lung organoids can also be derived from embryonic stem cells (ESC). A recent study used this approach with embryonic stem cells in which mutations were introduced in genes associated with Hermansky-Pudlak syndrome, that strongly predisposes to lung fibrosis, and thus demonstrated an essential role for IL-11 in the fibrotic process (67). Whereas generation of hiPSC- or ESC-derived AEC2 can be performed successfully, derivation of long-term primary AEC2 cultures from human lung tissue still is challenging. Recently, Shiraisi et al. successfully cultured AEC2 from human lungs using organoid expansion, which they were able to passage (68). More importantly, they transduced a pulmonary fibrosis-associated mutant SpC ($SFPTC^{\Delta\ exon4}$) protein into AEC2, resulting in the development of similar AEC2 features also observed in IPF patients (68). Combinations of hiPSC-derived AEC2 and lung organoid models may therefore offer a personalized platform to study the contribution of genetic predisposition and environmental cues to fibrosis development in SSc.

BIOMARKERS AND TREATMENT

Markers of alveolar epithelial injury, including Krebs von den Lungen-6 (KL-6) and surfactant protein-D (SP-D) (27), are increased in serum and may serve as biomarkers in identifying and monitoring SSc-ILD (69, 70). Importantly, exhaled nitric oxide (Fe_{NO}) has been proposed as a marker of (alveolar) inflammation in SSc-ILD. Fe_{NO} levels were shown to be increased in SSc compared to IPF patients, although it did not discriminate between SSc-patients with or without ILD (71, 72). In addition to the diagnostic potency of the circulating biomarkers and Fe_{NO}, microvascular abnormalities are detectable before clinical presentation of fibrosis (28, 73), and may serve as a prognostic marker to monitor disease progression in subgroups of SSc-ILD patients. Furthermore, levels of smooth muscle cells and myofibroblasts are increased in SSc-ILD lung tissue compared to healthy controls, and may also contribute to fibrosis. Finally, pro-fibrotic mediators, including TGF-β, PDGF, CTGF and thrombin, are increased in bronchoalveolar lavage fluid (BALF) or cells derived from BALF (29) and may contribute to altered cellular composition and phenotype in SSc-ILD. Several other potential serum biomarkers are under current investigation, among which serum chemokine [C-C motif] ligand 2 and 18 (74, 75), matrix metalloproteinase-7 and 12 (76, 77) and chemokine [C-X-C motif] ligand 4 (78, 79). Because a complete overview of current serum biomarkers is beyond the scope of this review, we refer the interested reader to a recently published comprehensive review summarizing the clinically used biomarkers, biomarkers under investigation and their link to mechanistic pathways (80). Interestingly, lung organoid models may contribute to identification of novel biomarkers, as was shown by the identification of the essential profibrotic role of IL-11, upon introduction of genes associated with Hermansky-Pudlak syndrome (67).

In addition to providing mechanistic insight into SSc-ILD pathogenesis, and biomarker identification, preclinical lung organoid models may also be applied to identify new treatment targets and for (personalized) drug screening platforms. So far, treatment of SSc-.ILD is targeted at alveolitis and includes non-selective immunomodulatory drugs like cyclophosphamide, azathioprine and mycophenolate (81, 82), all of which target (T- and/or) B lymphocyte proliferation or trigger cell death (83), as B-lymphocytes have a pivotal role in the pro-inflammatory and profibrotic pathway in SSc-ILD. Standard therapy combined with rituximab, also targeting CD20 on B cells, was shown to be beneficial, with a lower decline of FVC (84), whereas moderate effects were seen on FVC levels and HRCT fibrosis scores (35). The observation that anti-inflammatory and immune suppressive treatment with e.g., prednisone and azathioprine (85), or administration of interferon gamma (86), are clinically not effective, suggests that (late/end-stage) IPF does not result from a primary immunopathogenic process. Recently approved antifibrotic drugs that target selected profibrotic mediators has improved the treatment of IPF (87). The most widely studied drugs in this category are pirfenidone and nintedanib, which were shown to be safe and effective in IPF treatment. Pirfenidone acts through anti-inflammatory and antifibrotic effects, including down-regulation of TGF-β and TNF-α (88), whereas. Nintedanib is a tyrosine kinase inhibitor that inhibits activation of e.g., VEGF, fibroblast growth factor (FGF), and PDGF pathways (89). As nintedanib was recently approved for IPF treatment (90), its effectivity was also examined in SSc-ILD patients (91). Nintedanib demonstrated a clear effect on the annual rate of decline in FVC in SSc-ILD patients (91, 92), suggesting that targeting common pro-fibrotic pathways of lung fibrosis may be of therapeutic relevance (28, 93). Therapeutic targets (under investigation) for IPF may be therefore also be considered for treatment of SSc-ILD.

Regarding treatments under evaluation for IPF, a potential therapeutic target is autotaxin, an enzyme responsible for lysophosphatidic acid (LPA) production (94), both of which are increased in IPF, suggesting that the autotaxin-LPA pathway has a pathogenic role in this disorder (95, 96). Results from a phase-2 trial with GLPG1690, targeting autotaxin, were encouraging, especially regarding decline in FVC (97). Clinical assessment of GLPG1690 as treatment for IPF patients is currently ongoing in a phase-3 trial. A phase 2 trial of pamrevlumab, targeting CTGF (16, 17), also showed a decreased rate in decline of forced vital capacity (FVC) as compared with placebo (98). However, the results of this phase-2 trial must be treated with caution, pending an adequately powered phase 3 study. Furthermore, pentraxin-2, which inhibits differentiation of monocytes toward profibrotic fibrocytes and inhibits TGF-β production (41, 44, 99), may be targeted to stabilize or restore lung function. Results from a phase-2 trial with pentraxin-2 showed a slower decline of FVC compared to placebo (99).

Other treatments that have been evaluated in SSc-ILD include abatacept, tocilizumab, and autologous stem-cell transplantation, and are reviewed elsewhere (6, 7, 84, 91). In daily practice, however, there is no consensus about the right timing of initiating anti-inflammatory and/or antifibrotic treatment and exact patient selection. Furthermore, up to date there are no accepted prognostic models available to identify SSc patients at high risk for the development of lung fibrosis (100). Lung organoid models may therefore be applied to identify new treatment targets and for (personalized) drug screening platforms. Importantly, these models may be used to examine the effect of combined therapies targeting pro-fibrotic and pro-inflammatory pathways simultaneously. Patient-derived lung cancer organoids, for example, were able to predict patient-specific drug responses and drug resistance (101). Such patient-specific models in the future may be used to test drug combinations, drug toxicity and identification of novel drug targets. Furthermore, new pre-clinical models may aid in discriminating SSc patients at high risk for development of ILD.

FUTURE DIRECTIONS

Current concepts state that impaired or otherwise dysregulated repair of lung epithelial injury is an important driver of (progression of) fibrosis in SSc-ILD, but this is likely not unique to SSc-ILD. Delineating the triggers and/or the dysregulation

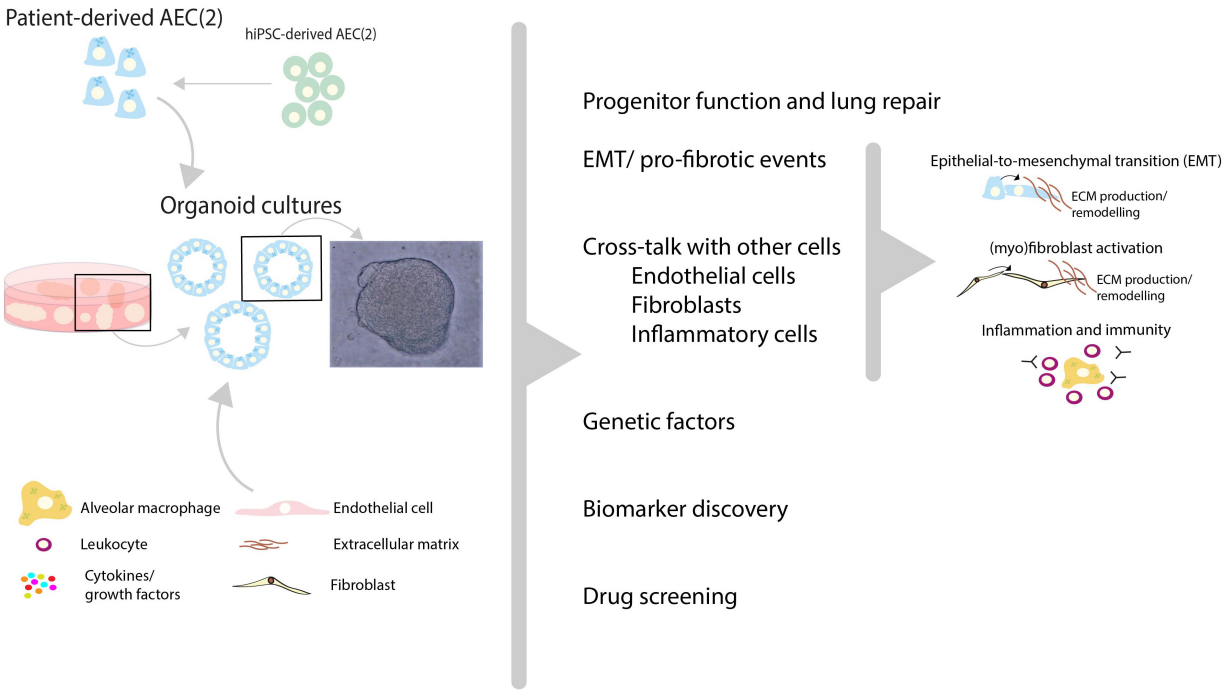

FIGURE 2 | Recent advances in human lung organoid models may help to unravel pathogenic mechanisms and new treatment targets of SSc-ILD. Patient-derived pulmonary cells, either isolated from lung tissue or derived from human induced pluripotent stem cells (hiPSC), can be expanded *in vitro* using 3D organoid culture models. In these models, a variety of (disease-)relevant characteristics including progenitor cell function, profibrotic features, interactions with other cells (endothelial cells, fibroblasts etc.) and inflammatory cell recruitment can be studied. In addition, in such models the contribution of genetic factors to SSc-ILD can be studied using either patient-derived cells with specific genetic features, or by genetic editing of primary AEC (2) or hiPSC-derived AEC. These 3D lung organoid cultures can be applied to study various aspects of SSc-ILD pathogenic mechanisms and may therefore provide patient-relevant models which may contribute to biomarker and target discovery and aid in personalized drug screening for SSc-ILD.

of repair may reveal features that distinguish SSc-ILD from other ILD. Furthermore, exhaustion and dysfunction of progenitor cells may contribute to the failure in resolving damage. Pharmacological activation of lung progenitor cells may thus be a promising approach for treatment of especially early stage SSc-ILD.

To address these questions, a human lung model that recapitulates essential features of SSc-ILD is required to help understanding mechanisms underlying SSc-ILD and develop new treatments. Availability of such a model, that is also suitable for e.g., screening small-molecule libraries, would be a major step forward. In addition, such a model may provide novel tools for personalized medicine to identify those that may benefit from an anti-inflammatory or an antifibrotic treatment or combined treatment strategies. The need for this is further illustrated by the recent introduction of the antifibrotic drug nintenadib in the treatment of SSc-ILD patients, based on clinical trials showing clear efficacy with a similar slowdown in the rate of lung function decline as found in IPF patients treated with antifibrotic agents (91). SSc-ILD patients with progressive fibrosis may therefore be selected for treatment with these drugs.

The concept of using organoid cultures for selecting individual patients for the optimal treatment is illustrated by the recent publication by Berkers and co-workers (102), in which rectal organoids grown from stem cells provide a tool for personalized medicine in patients suffering from cystic fibrosis. Organoids in this study showed a high correlation between *in vitro* and *in vivo* effects of drugs and demonstrated good to excellent predictive value for preclinical identification of response to treatment. Studies such as those by Strikoudis et al., showed that organoids can also be used to study fibrotic lung disease, indicating that organoid technology may help to understand underlying mechanisms of SSc-ILD (**Figure 2**) (67).

Important features of fibrotic lung diseases include matrix abnormalities, leading to increased tissue stiffness and consequent altered mechanical forces to which pulmonary cells are exposed, resulting in e.g., increased TGF-β signaling and fibroblast activation (46, 103). These alterations can be mimicked with state-of-the art organs-on-chips (including lung-chips) platforms, which provide us with unprecedented combinations of important features in the lung, including matrix stiffness, mechanical force (breathing pattern), air exposure and co-culture with various relevant cell types (5, 104). Combining organoid and organ-on-chip technology may lead to better patient-relevant culture models, which can be used for drug screening purposes and research into the pathogenesis.

In addition to these advances in *in vitro* modeling, there are also important developments in analysis of cells in lung tissue that can also be applied in the analysis of the above-mentioned cellular models. Patient-derived cells can for instance be analyzed using

single-cell-based RNA sequencing, which has already resulted in the identification of previously undescribed cell populations in SSc-ILD (105). Furthermore, patient-derived cells can now be analyzed at the protein level using (imaging) mass cytometry, enabling multidimensional unbiased analysis of more than 40 markers simultaneously (106) and an unprecedented potential for discovery of molecular culprits of disease. Mass cytometry analyses already revealed distinct immune cell signatures in patients with SSc (107).

In conclusion, the mechanisms underlying pulmonary fibrosis in SSc-ILD are not completely unraveled, and knowledge on fibrotic processes have been acquired mostly from studies in idiopathic pulmonary fibrosis (IPF). Recent advances in human preclinical models and biomedical technology may be used to unravel pathogenic mechanisms and new treatment targets of SSc-ILD (summarized in **Figure 1**). Developments in *in vitro* modeling using patient-derived organoid-based culture models and lung-chip platforms, as well as single cell analysis using e.g., single-cell RNA sequencing and (imaging) mass cytometry will be important to further broaden our insight in SSc-ILD pathogenesis and develop better and personalized treatments.

AUTHOR CONTRIBUTIONS

PK and EM drafted the manuscript. PK prepared the figures. PK, EM, PH, MN, and MG edited and revised the manuscript, and approved the final version of the manuscript. All authors contributed to the article and approved the submitted version.

FUNDING

Research conducted by PK is supported by a grant from TAS-ZonMW (40414009816007).

REFERENCES

1. Varga J. Systemic sclerosis: an update. *Bull NYU Hosp Jt Dis.* (2008) 66:198–202.
2. Steen VD, Medsger TA. Changes in causes of death in systemic sclerosis, 1972-2002. *Ann Rheum Dis.* (2007) 66:940–4. doi: 10.1136/ard.2006.066068
3. Tyndall AJ, Bannert B, Vonk M, Airo P, Cozzi F, Carreira PE, et al. Causes and risk factors for death in systemic sclerosis: a study from the EULAR Scleroderma Trials and Research (EUSTAR) database. *Ann Rheum Dis.* (2010) 69:1809–15.
4. Kowal-Bielecka O, Fransen J, Avouac J, Becker M, Kulak A, Allanore Y, et al. Update of EULAR recommendations for the treatment of systemic sclerosis. *Ann Rheum Dis.* (2017) 76:1327–39.
5. Sundarakrishnan A, Chen Y, Black LD, Aldridge BB, Kaplan DL. Engineered cell and tissue models of pulmonary fibrosis. *Adv Drug Deliv Rev.* (2018) 129:78–94. doi: 10.1016/j.addr.2017.12.013
6. Richeldi L, Collard HR, Jones MG. Idiopathic pulmonary fibrosis. *Lancet.* (2017) 389:1941–52. doi: 10.1016/S0140-6736(17)30866-8
7. Lederer DJ, Martinez FJ. Idiopathic pulmonary fibrosis. *N Engl J Med.* (2018) 378:1811–23. doi: 10.1056/NEJMra1705751
8. Selman M, Pardo A. Revealing the pathogenic and aging-related mechanisms of the enigmatic idiopathic pulmonary fibrosis. an integral model. *Am J Respir Crit Care Med.* (2014) 189:1161–72. doi: 10.1164/rccm.201312-2221PP
9. Winters NI, Burman A, Kropski JA, Blackwell TS. Epithelial injury and dysfunction in the pathogenesis of idiopathic pulmonaryfibrosis. *Am J Med Sci.* (2019) 357:374–8. doi: 10.1016/j.amjms.2019.01.010
10. Salton F, Volpe MC, Confalonieri M. Epithelial(-)mesenchymal transition in the pathogenesis of idiopathic pulmonary fibrosis. *Medicina (Kaunas).* (2019) 55:83. doi: 10.3390/medicina55040083
11. Hill C, Jones MG, Davies DE, Wang Y. Epithelial-mesenchymal transition contributes to pulmonary fibrosis via aberrant epithelial/fibroblastic cross-talk. *J Lung Health Dis.* (2019) 3:31–5. doi: 10.29245/2689-999X/2019/2.1149
12. Saito A, Horie M, Nagase T. TGF-beta signaling in lung health and disease. *Int J Mol Sci.* (2018) 19:2460. doi: 10.3390/ijms19082460
13. Dantas AT, Goncalves SM, de Almeida AR, Goncalves RS, Sampaio MC, Vilar KM, et al. Reassessing the role of the active TGF-beta1 as a biomarker in systemic sclerosis: association of serum levels with clinical manifestations. *Dis Markers.* (2016) 2016:6064830. doi: 10.1155/2016/6064830
14. Fernandez IE, Eickelberg O. The impact of TGF-beta on lung fibrosis: from targeting to biomarkers. *Proc Am Thorac Soc.* (2012) 9:111–6. doi: 10.1513/pats.201203-023AW
15. Zhao X, Kwan JYY, Yip K, Liu PP, Liu FF. Targeting metabolic dysregulation for fibrosis therapy. *Nat Rev Drug Discov.* (2020) 19:57–75. doi: 10.1038/s41573-019-0040-5
16. Kono M, Nakamura Y, Suda T, Kato M, Kaida Y, Hashimoto D, et al. Plasma CCN2 (connective tissue growth factor; CTGF) is a potential biomarker in idiopathic pulmonary fibrosis (IPF). *Clinica Chimica Acta.* (2011) 412:2211–5. doi: 10.1016/j.cca.2011.08.008
17. Lipson KE, Wong C, Teng Y, Spong S. CTGF is a central mediator of tissue remodeling and fibrosis and its inhibition can reverse the process of fibrosis. *Fibrogenesis Tissue Repair.* (2012) 5(Suppl. 1):S24. doi: 10.1186/1755-1536-5-S1-S24
18. Barratt SL, Blythe T, Jarrett C, Ourradi K, Shelley-Fraser G, Day MJ, et al. Differential expression of VEGF-Axxx isoforms is critical for development of pulmonary fibrosis. *Am J Respir Crit Care Med.* (2017) 196:479–93. doi: 10.1164/rccm.201603-0568OC
19. Barratt SL, Flower VA, Pauling JD, Millar AB. VEGF (vascular endothelial growth factor) and fibrotic lung disease. *Int J Mol Sci.* (2018) 19:1269. doi: 10.3390/ijms19051269
20. Gkatzis K, Taghizadeh S, Huh D, Stainier DYR, Bellusci S. Use of three-dimensional organoids and lung-on-a-chip methods to study lung development, regeneration and disease. *Eur Respir J.* (2018) 52:1800876. doi: 10.1183/13993003.00876-2018
21. Van Der Vaart J, Clevers H. Airway organoids as models of human disease. *J Intern Med.* (2020).
22. Hogan BL, Barkauskas CE, Chapman HA, Epstein JA, Jain R, Hsia CC, et al. Repair and regeneration of the respiratory system: complexity, plasticity, and mechanisms of lung stem cell function. *Cell Stem Cell.* (2014) 15:123–38. doi: 10.1016/j.stem.2014.07.012
23. Paolicelli G, Luca A, Jose SS, Antonini M, Teloni I, Fric J, et al. Using lung organoids to investigate epithelial barrier complexity and IL-17 signaling during respiratory infection. *Front Immunol.* (2019) 10:323. doi: 10.3389/fimmu.2019.00323
24. Tan Q, Choi KM, Sicard D, Tschumperlin DJ. Human airway organoid engineering as a step toward lung regeneration and disease modeling. *Biomaterials.* (2017) 113:118–32. doi: 10.1016/j.biomaterials.2016.10.046
25. Tan Q, Ma XY, Liu W, Meridew JA, Jones DL, Haak AJ, et al. Nascent lung organoids reveal epithelium- and bone morphogenetic protein-mediated suppression of fibroblast activation. *Am J Respir Cell Mol Biol.* (2019) 61:607–19. doi: 10.1165/rcmb.2018-0390OC
26. Ng-Blichfeldt JP, de Jong T, Kortekaas RK, Wu X, Lindner M, Guryev V, et al. TGF-beta activation impairs fibroblast ability to support adult lung epithelial progenitor cell organoid formation. *Am J Physiol Lung Cell Mol Physiol.* (2019) 317:L14–28. doi: 10.1152/ajplung.00400.2018

27. Akter T, Silver RM, Bogatkevich GS. Recent advances in understanding the pathogenesis of scleroderma-interstitial lung disease. *Curr Rheumatol Rep.* (2014) 16:411. doi: 10.1007/s11926-014-0411-1
28. Bagnato G, Harari S. Cellular interactions in the pathogenesis of interstitial lung diseases. *Eur Respir Rev.* (2015) 24:102–14. doi: 10.1183/09059180.00003214
29. Kowal-Bielecka O, Kowal K, Highland KB, Silver RM. Bronchoalveolar lavage fluid in scleroderma interstitial lung disease: technical aspects and clinical correlations: review of the literature. *Semin Arthritis Rheum.* (2010) 40:73–88. doi: 10.1016/j.semarthrit.2008.10.009
30. Tourkina E, Bonner M, Oates J, Hofbauer A, Richard M, Znoyko S, et al. Altered monocyte and fibrocyte phenotype and function in scleroderma interstitial lung disease: reversal by caveolin-1 scaffolding domain peptide. *Fibrogenesis Tissue Repair.* (2011) 4:15. doi: 10.1186/1755-1536-4-15
31. Bhattacharyya S, Wang W, Morales-Nebreda L, Feng G, Wu M, Zhou X, et al. Tenascin-C drives persistence of organ fibrosis. *Nat Commun.* (2016) 7:11703. doi: 10.1038/ncomms11703
32. Kelsh R, You R, Horzempa C, Zheng M, McKeown-Longo PJ. Regulation of the innate immune response by fibronectin: synergism between the III-1 and EDA domains. *PLoS One.* (2014) 9:e102974. doi: 10.1371/journal.pone.0102974
33. Bhattacharyya S, Varga J. Endogenous ligands of TLR4 promote unresolving tissue fibrosis: Implications for systemic sclerosis and its targeted therapy. *Immunol Lett.* (2018) 195:9–17. doi: 10.1016/j.imlet.2017.09.011
34. Kang H. Role of MicroRNAs in TGF-beta signaling pathway-mediated pulmonary fibrosis. *Int J Mol Sci.* (2017) 18:2527. doi: 10.3390/ijms18122527
35. Jordan S, Distler JH, Maurer B, Huscher D, van Laar JM, Allanore Y, et al. Effects and safety of rituximab in systemic sclerosis: an analysis from the European Scleroderma Trial and Research (EUSTAR) group. *Ann Rheum Dis.* (2015) 74:1188–94. doi: 10.1136/annrheumdis-2013-204522
36. Lafyatis R, O'Hara C, Feghali-Bostwick CA, Matteson EB. cell infiltration in systemic sclerosis-associated interstitial lung disease. *Arthritis Rheum.* (2007) 56:3167–8. doi: 10.1002/art.22847
37. Pattanaik D, Brown M, Postlethwaite BC, Postlethwaite AE. Pathogenesis of systemic sclerosis. *Front Immunol.* (2015) 6:272. doi: 10.3389/fimmu.2015.00272
38. Wells AU, Denton CP. Interstitial lung disease in connective tissue disease–mechanisms and management. *Nat Rev Rheumatol.* (2014) 10:728–39. doi: 10.1038/nrrheum.2014.149
39. Liaskos C, Rentouli S, Simopoulou T, Gkoutzourelas A, Norman GL, Brotis A, et al. Anti-C1q autoantibodies are frequently detected in patients with systemic sclerosis associated with pulmonary fibrosis. *Br J Dermatol.* (2019) 181:138–46. doi: 10.1111/bjd.17886
40. Allden SJ, Ogger PP, Ghai P, McErlean P, Hewitt R, Toshner R, et al. The transferrin receptor CD71 delineates functionally distinct airway macrophage subsets during idiopathic pulmonary fibrosis. *Am J Respir Crit Care Med.* (2019) 200:209–19. doi: 10.1164/rccm.201809-1775OC
41. Morse C, Tabib T, Sembrat J, Buschur KL, Bittar HT, Valenzi E, et al. Proliferating SPP1/MERTK-expressing macrophages in idiopathic pulmonary fibrosis. *Eur Respir J.* (2019) 54:1802441. doi: 10.1183/13993003.02441-2018
42. Zhou Y, Peng H, Sun H, Peng X, Tang C, Gan Y, et al. Chitinase 3-like 1 suppresses injury and promotes fibroproliferative responses in Mammalian lung fibrosis. *Sci Transl Med.* (2014) 6:240ra76. doi: 10.1126/scitranslmed.3007096
43. Pechkovsky DV, Prasse A, Kollert F, Engel KM, Dentler J, Luttmann W, et al. Alternatively activated alveolar macrophages in pulmonary fibrosis-mediator production and intracellular signal transduction. *Clin Immunol.* (2010) 137:89–101. doi: 10.1016/j.clim.2010.06.017
44. Reyfman PA, Walter JM, Joshi N, Anekalla KR, McQuattie-Pimentel AC, Chiu S, et al. Single-cell transcriptomic analysis of human lung provides insights into the pathobiology of pulmonary fibrosis. *Am J Respir Crit Care Med.* (2019) 199:1517–36.
45. Kolb M, Gauldie J, Bellaye PS. Editorial: extracellular matrix: the common thread of disease progression in fibrosis? *Arthritis Rheumatol.* (2016) 68:1053–6. doi: 10.1002/art.39569
46. Upagupta C, Shimbori C, Alsilmi R, Kolb M. Matrix abnormalities in pulmonary fibrosis. *Eur Respir Rev.* (2018) 27:180033. doi: 10.1183/16000617.0033-2018
47. Sakamoto N, Kakugawa T, Hara A, Nakashima S, Yura H, Harada T, et al. Association of elevated alpha-defensin levels with interstitial pneumonia in patients with systemic sclerosis. *Respir Res.* (2015) 16:148. doi: 10.1186/s12931-015-0308-1
48. Mathai SK, Gulati M, Peng X, Russell TR, Shaw AC, Rubinowitz AN, et al. Circulating monocytes from systemic sclerosis patients with interstitial lung disease show an enhanced profibrotic phenotype. *Lab Invest.* (2010) 90:812–23. doi: 10.1038/labinvest.2010.73
49. De Lauretis A, Sestini P, Pantelidis P, Hoyles R, Hansell DM, Goh NS, et al. Serum interleukin 6 is predictive of early functional decline and mortality in interstitial lung disease associated with systemic sclerosis. *J Rheumatol.* (2013) 40:435–46. doi: 10.3899/jrheum.120725
50. Fernandez IE, Greiffo FR, Frankenberger M, Bandres J, Heinzelmann K, Neurohr C, et al. Peripheral blood myeloid-derived suppressor cells reflect disease status in idiopathic pulmonary fibrosis. *Eur Respir J.* (2016) 48:1171–83. doi: 10.1183/13993003.01826-2015
51. Jose SS, De Zuani M, Tidu F, Hortova Kohoutkova M, Pazzagli L, Forte G, et al. Comparison of two human organoid models of lung and intestinal inflammation reveals Toll-like receptor signalling activation and monocyte recruitment. *Clin Transl Immunol.* (2020) 9:e1131. doi: 10.1002/cti2.1131
52. Tuveson D, Clevers H. Cancer modeling meets human organoid technology. *Science.* (2019) 364:952–5. doi: 10.1126/science.aaw6985
53. Cattaneo CM, Dijkstra KK, Fanchi LF, Kelderman S, Kaing S, van Rooij N, et al. Tumor organoid-T-cell coculture systems. *Nat Protoc.* (2020) 15:15–39. doi: 10.1038/s41596-019-0232-9
54. Purwada A, Jaiswal MK, Ahn H, Nojima T, Kitamura D, Gaharwar AK, et al. Ex vivo engineered immune organoids for controlled germinal center reactions. *Biomaterials.* (2015) 63:24–34. doi: 10.1016/j.biomaterials.2015.06.002
55. Purwada A, Singh A. Immuno-engineered organoids for regulating the kinetics of B-cell development and antibody production. *Nat Protoc.* (2017) 12:168–82. doi: 10.1038/nprot.2016.157
56. Armanios MY, Chen JJ, Cogan JD, Alder JK, Ingersoll RG, Markin C, et al. Telomerase mutations in families with idiopathic pulmonary fibrosis. *N Engl J Med.* (2007) 356:1317–26. doi: 10.1056/NEJMoa066157
57. Burman A, Tanjore H, Blackwell TS. Endoplasmic reticulum stress in pulmonary fibrosis. *Matrix Biol.* (2018) 68-69:355–65. doi: 10.1016/j.matbio.2018.03.015
58. Dickens JA, Malzer E, Chambers JE, Marciniak SJ. Pulmonary endoplasmic reticulum stress-scars, smoke, and suffocation. *FEBS J.* (2019) 286:322–41. doi: 10.1111/febs.14381
59. Seibold MA, Wise AL, Speer MC, Steele MP, Brown KK, Loyd JE, et al. A common MUC5B promoter polymorphism and pulmonary fibrosis. *N Engl J Med.* (2011) 364:1503–12.
60. Roy MG, Livraghi-Butrico A, Fletcher AA, McElwee MM, Evans SE, Boerner RM, et al. Muc5b is required for airway defence. *Nature.* (2014) 505:412–6. doi: 10.1038/nature12807
61. Heukels P, Moor CC, von der Thusen JH, Wijsenbeek MS, Kool M. Inflammation and immunity in IPF pathogenesis and treatment. *Respir Med.* (2019) 147:79–91. doi: 10.1016/j.rmed.2018.12.015
62. Peljto AL, Steele MP, Fingerlin TE, Hinchcliff ME, Murphy E, Podlusky S, et al. The pulmonary fibrosis-associated MUC5B promoter polymorphism does not influence the development of interstitial pneumonia in systemic sclerosis. *Chest.* (2012) 142:1584–8. doi: 10.1378/chest.12-0110
63. Stock CJW, De Lauretis A, Visca D, Daccord C, Kokosi M, Kouranos V, et al. Defining genetic risk factors for scleroderma-associated interstitial lung disease : IRF5 and STAT4 gene variants are associated with scleroderma while STAT4 is protective against scleroderma-associated interstitial lung disease. *Clin Rheumatol.* (2020) 39:1173–9. doi: 10.1007/s10067-019-04922-6
64. Song GG, Lee YH. The CTLA-4 and MCP-1 polymorphisms and susceptibility to systemic sclerosis: a meta-analysis. *Immunol Invest.* (2013) 42:481–92. doi: 10.3109/08820139.2013.789910
65. Jacob A, Morley M, Hawkins F, McCauley KB, Jean JC, Heins H, et al. Differentiation of human pluripotent stem cells into functional lung alveolar

epithelial cells. *Cell Stem Cell.* (2017) 21:472–88.e10. doi: 10.1016/j.stem.2017.08.014
66. McCauley KB, Hawkins F, Serra M, Thomas DC, Jacob A, Kotton DN. Efficient derivation of functional human airway epithelium from pluripotent stem cells via temporal regulation of wnt signaling. *Cell Stem Cell.* (2017) 20:844–57.e6. doi: 10.1016/j.stem.2017.03.001
67. Strikoudis A, Cieslak A, Loffredo L, Chen YW, Patel N, Saqi A, et al. Modeling of fibrotic lung disease using 3D organoids derived from human pluripotent stem cells. *Cell Rep.* (2019) 27:3709–23.e5. doi: 10.1016/j.celrep.2019.05.077
68. Shiraishi K, Nakajima T, Shichino S, Deshimaru S, Matsushima K, Ueha S. In vitro expansion of endogenous human alveolar epithelial type II cells in fibroblast-free spheroid culture. *Biochem Biophys Res Commun.* (2019) 515:579–85. doi: 10.1016/j.bbrc.2019.05.187
69. Yanaba K, Hasegawa M, Takehara K, Sato S. Comparative study of serum surfactant protein-D and KL-6 concentrations in patients with systemic sclerosis as markers for monitoring the activity of pulmonary fibrosis. *J Rheumatol.* (2004) 31:1112–20.
70. Bonella F, Volpe A, Caramaschi P, Nava C, Ferrari P, Schenk K, et al. Surfactant protein D and KL-6 serum levels in systemic sclerosis: correlation with lung and systemic involvement. *Sarcoidosis Vasc Diffuse Lung Dis.* (2011) 28:27–33.
71. Girgis RE, Gugnani MK, Abrams J, Mayes MD. Partitioning of alveolar and conducting airway nitric oxide in scleroderma lung disease. *Am J Respir Crit Care Med.* (2002) 165:1587–91. doi: 10.1164/rccm.2104003
72. Paredi P, Kharitonov SA, Loukides S, Pantelidis P, du Bois RM, Barnes PJ. Exhaled nitric oxide is increased in active fibrosing alveolitis. *Chest.* (1999) 115:1352–6. doi: 10.1378/chest.115.5.1352
73. Trojanowska M. Cellular and molecular aspects of vascular dysfunction in systemic sclerosis. *Nat Rev Rheumatol.* (2010) 6:453–60. doi: 10.1038/nrrheum.2010.102
74. Elhai M, Hoffmann-Vold AM, Avouac J, Pezet S, Cauvet A, Leblond A, et al. Performance of candidate serum biomarkers for systemic sclerosis-associated interstitial lung disease. *Arthritis Rheumatol.* (2019) 71:972–82. doi: 10.1002/art.40815
75. Wu M, Baron M, Pedroza C, Salazar GA, Ying J, Charles J, et al. CCL2 in the circulation predicts long-term progression of interstitial lung disease in patients with early systemic sclerosis: data from two independent cohorts. *Arthritis Rheumatol.* (2017) 69:1871–8. doi: 10.1002/art.40171
76. Kennedy B, Branagan P, Moloney F, Haroon M, O'Connell OJ, O'Connor TM, et al. Biomarkers to identify ILD and predict lung function decline in scleroderma lung disease or idiopathic pulmonary fibrosis. *Sarcoidosis Vasc Diffuse Lung Dis.* (2015) 32:228–36.
77. Manetti M, Guiducci S, Romano E, Bellando-Randone S, Conforti ML, Ibba-Manneschi L, et al. Increased serum levels and tissue expression of matrix metalloproteinase-12 in patients with systemic sclerosis: correlation with severity of skin and pulmonary fibrosis and vascular damage. *Ann Rheum Dis.* (2012) 71:1064–72. doi: 10.1136/annrheumdis-2011-200837
78. Kafaja S, Clements PJ, Wilhalme H, Tseng CH, Furst DE, Kim GH, et al. Reliability and minimal clinically important differences of forced vital capacity: Results from the Scleroderma Lung Studies (SLS-I and SLS-II). *Am J Respir Crit Care Med.* (2018) 197:644–52.
79. van Bon L, Affandi AJ, Broen J, Christmann RB, Marijnissen RJ, Stawski L, et al. Proteome-wide analysis and CXCL4 as a biomarker in systemic sclerosis. *N Engl J Med.* (2014) 370:433–43. doi: 10.1056/NEJMc1402401
80. Khanna D, Tashkin DP, Denton CP, Renzoni EA, Desai SR, Varga J. Etiology, risk factors, and biomarkers in systemic sclerosis with interstitial lung disease. *Am J Respir Crit Care Med.* (2020) 201:650–60. doi: 10.1164/rccm.201903-0563CI
81. Tashkin DP, Roth MD, Clements PJ, Furst DE, Khanna D, Kleerup EC, et al. Mycophenolate mofetil versus oral cyclophosphamide in scleroderma-related interstitial lung disease (SLS II): a randomised controlled, double-blind, parallel group trial. *Lancet Respir Med.* (2016) 4:708–19.
82. Khanna D, Tashkin DP, Denton CP, Lubell MW, Vazquez-Mateo C, Wax S. Ongoing clinical trials and treatment options for patients with systemic sclerosis-associated interstitial lung disease. *Rheumatology (Oxford).* (2019) 58:567–79. doi: 10.1093/rheumatology/key151
83. Hall AG, Tilby MJ. Mechanisms of action of, and modes of resistance to, alkylating agents used in the treatment of haematological malignancies. *Blood Rev.* (1992) 6:163–73. doi: 10.1016/0268-960X(92)90028-O
84. Misra DP, Ahmed S, Agarwal V. Is biological therapy in systemic sclerosis the answer? *Rheumatol Int.* (2020) 40:679–94. doi: 10.1007/s00296-020-04515-6
85. Idiopathic Pulmonary Fibrosis Clinical Research Network, Raghu G, Anstrom KJ, King TE Jr., Lasky JA, Martinez FJ. Prednisone, azathioprine, and N-acetylcysteine for pulmonary fibrosis. *N Engl J Med.* (2012) 366:1968–77. doi: 10.1056/NEJMoa1113354
86. King TE Jr., Albera C, Bradford WZ, Costabel U, Hormel P, Lancaster L, et al. Effect of interferon gamma-1b on survival in patients with idiopathic pulmonary fibrosis (INSPIRE): a multicentre, randomised, placebo-controlled trial. *Lancet.* (2009) 374:222–8. doi: 10.1016/S0140-6736(09)60551-1
87. Wuyts WA, Antoniou KM, Borensztajn K, Costabel U, Cottin V, Crestani B, et al. Combination therapy: the future of management for idiopathic pulmonary fibrosis? *Lancet Respir Med.* (2014) 2:933–42. doi: 10.1016/S2213-2600(14)70232-2
88. Kolb M, Bonella F, Wollin L. Therapeutic targets in idiopathic pulmonary fibrosis. *Respir Med.* (2017) 131:49–57. doi: 10.1016/j.rmed.2017.07.062
89. Richeldi L, du Bois RM, Raghu G, Azuma A, Brown KK, Costabel U, et al. Efficacy and safety of nintedanib in idiopathic pulmonary fibrosis. *N Engl J Med.* (2014) 370:2071–82. doi: 10.1056/NEJMoa1402584
90. Wollin L, Wex E, Pautsch A, Schnapp G, Hostettler KE, Stowasser S, et al. Mode of action of nintedanib in the treatment of idiopathic pulmonary fibrosis. *Eur Respir J.* (2015) 45:1434–45. doi: 10.1183/09031936.00174914
91. Distler O, Highland KB, Gahlemann M, Azuma A, Fischer A, Mayes MD, et al. Nintedanib for systemic sclerosis-associated interstitial lung disease. *N Engl J Med.* (2019) 380:2518–28. doi: 10.1056/NEJMoa1903076
92. Distler O, Brown KK, Distler JHW, Assassi S, Maher TM, Cottin V, et al. Design of a randomised, placebo-controlled clinical trial of nintedanib in patients with systemic sclerosis-associated interstitial lung disease (SENSCIS). *Clin Exp Rheumatol.* (2017) 35(Suppl. 106):75–81.
93. Renaud L, da Silveira WA, Takamura N, Hardiman G, Feghali-Bostwick C. Prominence of IL6, IGF, TLR, and bioenergetics pathway perturbation in lung tissues of scleroderma patients with pulmonary fibrosis. *Front Immunol.* (2020) 11:383. doi: 10.3389/fimmu.2020.00383
94. Nakanaga K, Hama K, Aoki J. Autotaxin–an LPA producing enzyme with diverse functions. *J Biochem.* (2010) 148:13–24. doi: 10.1093/jb/mvq052
95. Montesi SB, Mathai SK, Brenner LN, Gorshkova IA, Berdyshev EV, Tager AM, et al. Docosatetraenoyl LPA is elevated in exhaled breath condensate in idiopathic pulmonary fibrosis. *BMC Pulm Med.* (2014) 14:5. doi: 10.1186/1471-2466-14-5
96. Oikonomou N, Mouratis MA, Tzouvelekis A, Kaffe E, Valavanis C, Vilaras G, et al. Pulmonary autotaxin expression contributes to the pathogenesis of pulmonary fibrosis. *Am J Respir Cell Mol Biol.* (2012) 47:566–74. doi: 10.1165/rcmb.2012-0004OC
97. Maher TM, van der Aar EM, Van de Steen O, Allamassey L, Desrivot J, Dupont S, et al. Safety, tolerability, pharmacokinetics, and pharmacodynamics of GLPG1690, a novel autotaxin inhibitor, to treat idiopathic pulmonary fibrosis (FLORA): a phase 2a randomised placebo-controlled trial. *Lancet Respir Med.* (2018) 6:627–35. doi: 10.1016/S2213-2600(18)30181-4
98. Richeldi L, Fernandez Perez ER, Costabel U, Albera C, Lederer DJ, Flaherty KR, et al. Pamrevlumab, an anti-connective tissue growth factor therapy, for idiopathic pulmonary fibrosis (PRAISE): a phase 2, randomised, double-blind, placebo-controlled trial. *Lancet Respir Med.* (2020) 8:25–33. doi: 10.1016/S2213-2600(19)30262-0
99. Raghu G, van den Blink B, Hamblin MJ, Brown AW, Golden JA, Ho LA, et al. Effect of recombinant human pentraxin 2 vs placebo on change in forced vital capacity in patients with idiopathic pulmonary fibrosis: a randomized clinical trial. *JAMA.* (2018) 319:2299–307. doi: 10.1001/jama.2018.6129
100. Cottin V, Brown KK. Interstitial lung disease associated with systemic sclerosis (SSc-ILD). *Respir Res.* (2019) 20:13. doi: 10.1186/s12931-019-0980-7

101. Kim M, Mun H, Sung CO, Cho EJ, Jeon HJ, Chun SM, et al. Patient-derived lung cancer organoids as in vitro cancer models for therapeutic screening. *Nat Commun.* (2019) 10:3991. doi: 10.1038/s41467-019-11867-6
102. Berkers G, Van Mourik P, Vonk AM, Kruisselbrink E, Dekkers JF, De Winter-de Groot KM, et al. Rectal organoids enable personalized treatment of cystic fibrosis. *Cell Rep* (2019) 26:1701–8.e3. doi: 10.1016/j.celrep.2019.01.068
103. Froese AR, Shimbori C, Bellaye PS, Inman M, Obex S, Fatima S, et al. Stretch-induced activation of transforming growth factor-beta1 in pulmonary fibrosis. *Am J Respir Crit Care Med.* (2016) 194:84–96. doi: 10.1164/rccm.201508-1638OC
104. Nawroth JC, Barrile R, Conegliano D, van Riet S, Hiemstra PS, Villenave R. Stem cell-based lung-on-chips: the best of both worlds? *Adv Drug Deliv Rev.* (2019) 140:12–32. doi: 10.1016/j.addr.2018.07.005
105. Valenzi E, Bulik M, Tabib T, Morse C, Sembrat J, Trejo Bittar H, et al. Single-cell analysis reveals fibroblast heterogeneity and myofibroblasts in systemic sclerosis-associated interstitial lung disease. *Ann Rheum Dis.* (2019) 78:1379–87. doi: 10.1136/annrheumdis-2018-214865
106. Ijsselsteijn ME, van der Breggen R, Farina Sarasqueta A, Koning F, De Miranda NA. 40-marker panel for high dimensional characterization of cancer immune microenvironments by imaging mass cytometry. *Front Immunol.* (2019) 10:2534. doi: 10.3389/fimmu.2019.02534
107. Van Der Kroef M, Van Den Hoogen LL, Mertens JS, Blokland SLM, Haskett S, Devaprasad A, et al. Cytometry by time of flight identifies distinct signatures in patients with systemic sclerosis, systemic lupus erythematosus and Sjogrens syndrome. *Eur J Immunol.* (2020) 50:119–29.

Conflict of Interest: The authors declare that the research was conducted in the absence of any commercial or financial relationships that could be construed as a potential conflict of interest.

frontiers in Immunology

METHODS
published: 07 October 2020
doi: 10.3389/fimmu.2020.566607

A Method for Isolating and Culturing Skin Cells: Application to Endothelial Cells, Fibroblasts, Keratinocytes, and Melanocytes From Punch Biopsies in Systemic Sclerosis Skin

Pauline Henrot[1,2]*, *Paôline Laurent*[3], *Emeline Levionnois*[3], *Damien Leleu*[3], *Catherine Pain*[1], *Marie-Elise Truchetet*[2,3] *and Muriel Cario*[1,4,5]

[1] Univ. Bordeaux, Inserm, BMGIC, UMR1035, Bordeaux, France, [2] Department of Rheumatology, National Reference Center for Systemic Autoimmune Rare Diseases, Hopital Pellegrin, Bordeaux, France, [3] Univ. Bordeaux, CNRS, Immunoconcept, UMR 5164, Bordeaux, France, [4] Department of Dermatology and Pediatric Dermatology, National Center for Rare Skin Disorders, Hôpital Saint André, Bordeaux, France, [5] AquiDerm, Univ. Bordeaux, Bordeaux, France

OPEN ACCESS

Edited by:
Anna-Maria Hoffmann-Vold, Oslo University Hospital, Norway

Reviewed by:
Jillian M. Richmond, University of Massachusetts Medical School, United States
Umesh S. Deshmukh, Oklahoma Medical Research Foundation, United States

***Correspondence:**
Pauline Henrot
pauline.henrot@u-bordeaux.fr

Specialty section:
This article was submitted to Autoimmune and Autoinflammatory Disorders, a section of the journal Frontiers in Immunology

Received: *28 May 2020*
Accepted: *31 August 2020*
Published: *07 October 2020*

Citation:
Henrot P, Laurent P, Levionnois E, Leleu D, Pain C, Truchetet M-E and Cario M (2020) A Method for Isolating and Culturing Skin Cells: Application to Endothelial Cells, Fibroblasts, Keratinocytes, and Melanocytes From Punch Biopsies in Systemic Sclerosis Skin. Front. Immunol. 11:566607. doi: 10.3389/fimmu.2020.566607

Systemic Sclerosis (SSc) is a complex auto-immune connective tissue disease combining inflammatory, vasculopathic and fibrotic manifestations. Skin effectively recapitulates the main pathogenic processes and therefore is a good organ to decipher the disease pathophysiology, which remains unclear. However, culturing primary skin cells is SSc can be a major issue due to small sample size combined to skin fibrosis. Here, we present a protocol allowing to isolate and culture the four main types of skin cells: dermal cells (microvascular dermal endothelial cells—HDMECs—and fibroblasts) and epidermal cells (keratinocytes and melanocytes), from a single 4 mm-punch biopsy, at a low cost. The present protocol has been optimized to fit SSc skin cells particularities. Such technique allows to culture primary cells, crucial to study the disease pathophysiology, as well as to isolate cells in order to perform immediate molecular biology experiments such as single-cell transcriptomic. Cells grown from biopsies are also suitable for various types of experiments such as immunocytochemistry, Western blot, RT-qPCR or functional *in vitro* assays (angiogenesis, migration, etc.). Ultimately, they can be used for experimental 3D cell culture models such as reconstructed skin.

Keywords: scleroderma, cell culture, human microvascular dermal endothelial cells, dermis, epidermis

INTRODUCTION

Systemic Sclerosis (SSc) is a rare auto-immune connective tissue disease combining autoimmune features, widespread vasculopathy, and systemic fibrosis (1). Despite recent therapeutic advances, the morbidity and mortality remain high, with a standardized mortality ratio up to 7.2-fold according to studies (2). Skin manifestations, which give the original name to the disease (scleroderma), are considered as diagnostic, subclassification, severity, and prognostic markers (3). SSc skin effectively recapitulates the main pathogenic processes of the disease, while being the most accessible organ to biopsy. Therefore, SSc skin cells are extremely helpful to decipher the disease pathophysiology, which remains unclear. However,

due to ethical issues, only small biopsies can be performed in patients, contrary to healthy skin, which can usually be obtained in larger samples; moreover, SSc skin features (notably fibrosis and vasculopathy) further add to the difficulty of isolating and culturing cells.

Here, we propose a technique allowing the isolation and primary cell culture of the four main types of skin cells: epidermal cells (keratinocytes and melanocytes) and dermal cells (fibroblasts and human dermal microvascular endothelial cells or HDMECs). This protocol, which is applicable to every skin disease, has been applied to fit the particularities of SSc skin cells. Briefly, the protocol consists in splitting the epidermis from the dermis after an incubation with dispase, and separately seeding epidermal cells (keratinocytes and melanocytes) and dermal cells (HDMECs and fibroblasts). Endothelial cells are obtained by a mechanical extraction combined with immuno-magnetic cell sorting, thus avoiding contamination by fibroblasts, which is a major issue. Fibroblasts are further obtained by digesting the dermis in collagenase. Keratinocytes and melanocytes are purifiedafter a few days of primary culture by means of a "differential trypsinization" technique. All cells can be passaged rapidly after the initial seeding and used for cell culture experiment as well as molecular and biochemical analysis (immunocytochemistry, Western blotting, qPCR). Such technique also allows performing immediate molecular biology experiments such as single-cell transcriptomic. Finally, cultured cells can be implemented into skin equivalents models, such as reconstructed skin, in order to reproduce the complex cellular interactions within the skin microenvironment.

MATERIALS AND EQUIPMENT

Material for Tissue Digestion and Primary Cells Seeding

Day 0 (D0): sample arrival, tissue digestion

Equipment: Ethanol 70°, simple clamp

Reagents:

- Hank's Balanced Salt Solution (HBSS) with calcium and magnesium (optional: with phenol red): e.g., Gibco
- Dispase II solution: 25 UI/mL in HBSS, e.g., 4942078001, Roche

Day 1 (D1): primary cells seeding

Equipment:

- Ethanol 70°
- curved clamp
- gripped clamp
- sterile surgical scalpel blade (we recommend size 24, which makes cutting easier) and blade holder
- Falcon 70 μm cell strainer: e.g., 352350, Corning

Reagents:

- HBSS
- Fetal Calf Serum (FCS): sterile and heat inactivated at 56° during 30 min, e.g., CVFSVF00-01, Eurobio
- Trypsin-EDTA (TE): Trypsin 0.25%, e.g., T9201, Sigma—Ethylenediaminetetraacetic acid (EDTA) 0.1%, e.g., E4884, Sigma in HBSS

Q-medium:

Reagents:

- Iscove's Modified Dulbecco's Media (IMDM), optional: with phenol red, e.g., Gibco
- Fetal Calf Serum (FCS), sterile and heat inactivated at 56° during 30 min, e.g., CVFSVF00-01, Eurobio
- Penicilline-Streptomycine (PS), e.g., CABPES01-0U, Eurobio

Q-medium composition: IMDM + 10% FCS + 1% PS

- Collagenase solution: 40 UI/mL in HBSS, e.g., C-9891, Sigma
- Cell culture media: (add 1% PS for each)
  - Melanocytes: Melanocyte Growth Medium (MGM), C-24010, Promocell
  - Endothelial cells: Endothelial Cell Growth Medium (MV2), C-22022, Promocell
  - Fibroblasts: Dulbecco's Modified Eagle's medium, e.g., Gibco + 10% FCS

All reagents prepared from powders must be sterile filtered through a 0.22 μm-filter.

Further cell culture and amplification:

- Keratinocyte Growth Medium 2 (KGM2), Promocell
- For cell passaging:

TE 10%: 0.025% Trypsin-0.01 % EDTA diluted $1/10^e$ in HBSS

FCS 10%: FCS diluted $1/10^e$ in HBSS

Nota bene: for cell culture flasks, better use vented caps.

All human material was obtained thanks to the biomedical research cohort VISS (Vasculopathy and Inflammation in Systemic Sclerosis) approved by the institutional ethical committee (CPP, 2012 A00081-42, Aquitaine). All patients provided written and informed consent before the biopsy.

Material for Immunomagnetic HDMECs Sorting

For $CD31^+$ cells sorting:

- Manual separator, e.g., QuadroMACS™ Separator (MACS)
- Immunomagnetic sorting anti-CD31 microbeads: e.g., 130-091-935, Miltenyi.
- LS columns (Miltenyi)
- TE 10%
- FCS 10%
- HBSS
- Sorting buffer (optional): Phosphate-Buffered Saline (PBS) + 2 mM EDTA + 0.5% Bovine Serum Albumin (BSA)

(NB: for a low number of cells, MS columns are usually recommended. However, we found that LS columns were more efficient for HDMECs sorting, possibly due to a quicker flow of cell suspension through the column, exposing cells to a shorter duration of stressful conditions).

Additional material for $CD45^-$ cells sorting:

- LD columns (Miltenyi).
- anti-CD45 microbeads (e.g., 130-045-801, Miltenyi).

Material for HDMECs Phenotyping (by Fluorescence-Activated Cell Sorting)

- anti-CD31 fluorochrome-conjugated antibody: e.g., APC-conjugated anti-CD31 antibody, clone AC128, Miltenyi
- anti-CD45 fluorochrome-conjugated antibody: e.g., FITC-conjugated anti-CD45 antibody, clone 5B1, Miltenyi
- FACS buffer: e.g., PBS + 2 mM EDTA + 0.5% BSA
- Flow cytometer: e.g., Canto I, BD.

METHODS

Figure 1 outlines skin cells *in situ* and protocol principle. Steps of the whole protocol are presented **Figure 2** (for whole protocol outlining) and **Figure 3** (for day 1: cell seeding).

Day 0: Sample Arrival, Tissue Digestion

The sample (ideally a 4-mm biopsy punch minimum, but smaller punch such as 3-mm should do as well) should have been conserved in a sterile pad soaked with saline solution (alternatively, submerged in sterile saline solution).

Dip the sample rapidly in ethanol (to avoid future contamination), then rinse thoroughly in HBSS. Incubate the whole sample in dispase solution (25 UI/mL), overnight à 4°C (the sample can be put in a 1.5 mL tube containing 1 mL dispase) (maximal incubation time: 15 h).

Alternatively, if necessary: incubate the sample in dispase for 90 min at 37°C.

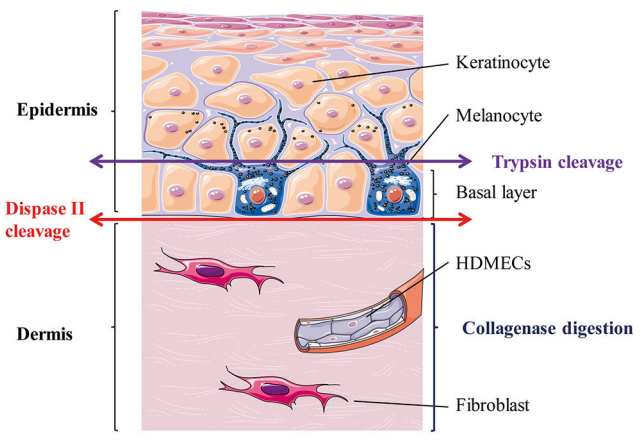

FIGURE 1 | Skin layers and general principle of the enzymatic dissociation used in the protocol. HDMECs, human dermal microvascular endothelial cells. The epithelial layer is the epidermis and is composed mostly of keratinocytes (90%) and melanocytes (5%). Melanocytes sit at the epidermal basal layer, which also contains keratinocytes stem cells, which differentiate as they reach upper layers. The connective tissue layer is the dermis and is composed mostly of extra-cellular matrix secreted by fibroblasts and is perfused with blood vessels, whose internal layer is composed of dermal microvascular endothelial cells (HDMECs).

Day 1: Primary Cells Seeding

Prepare sterile material and reagents according to the procedure described in section Material for Tissue Digestion and Primary Cells Seeding. For clamps: dip in ethanol before and after each use to ensure sterility, then dip in sterile HBSS before using again.

Cell seeding: (protocol illustration: **Figures 2**,**3**):

1. Transfer the tube content into a Petri dish. Inactivate the enzymatic digestion (dispase) by adding the same volume of FCS 10% in HBSS.
2. Mechanically separate the epidermis from the dermis. The epidermis should be a very thin sheet, easily peeled off the dermal part.

   Tip: for an easy separation, hold the dermal part with the gripper clamp whilst grasping and peeling the epidermis off (in one piece) with the curved clamp (**Supplementary Video 1**).
3. (Epidermal layer) Transfer the epidermal sheet into a 1.5 mL tube containing 1 mL Trypsin-EDTA and incubate at 37°C for 10 min (incubator or water bath).
4. (Dermal layer) Meanwhile: in a Petri dish filled with Q-medium, dip the dermal part and mechanically extract HDMECs.

   To this end, apply gently but firmly the curved clamp on the dermal surface (cf **Supplementary Video 2**). Best results are obtained if you look for and press against microvessels on the deep dermal part, and rinse the dermal surface with Q-medium afterwards.

   This step is highly critical, as too much pressure will result in fibroblasts contamination, while too few pressure will not extract enough HDMECs. Several tests with healthy skin are advised in order for experimentators to fine-tune their gesture before starting with patient's samples.

   Collect the Q-medium in a 50 mL tube and set aside the dermal piece in a Petri dish filled with HBSS.
5. (Epidermal layer) Shake vigorously the tube containing the epidermal sheet after the 10 min incubation of step 3 and transfer the tube content in a Petri dish filled with HBSS. Inactivate the enzymatic digestion of the epidermis by adding the same volume of FCS. Then, dissociate the epidermal cells by trimming the epidermis in a Petri dish filled with HBSS.

   Tip: for an easy cutting, hold the epidermal sheet with the curved clamp while trimming with the scalpel blade until maximum shredding. This step is easier in the lid of the Petri dish, as the edges are lower.

   Collect the epidermal pieces as well as the supernatant in a 50 mL tube.

   If necessary, adjust the volume of the two tubes with HBSS before centrifugation.
6. Centrifugate epidermal and endothelial cells at the appropriate speed for cells [e.g., 5 min, 1,200 rotations per minute (rpm)].
7. (Dermal layer) Meanwhile, cut the remaining dermal part into 1 mm^3 pieces using the scalpel blade. Transfer the pieces in a 50 mL tube containing 5 mL of collagenase solution. Incubate for 90 min at 37°C under mechanical shaking.

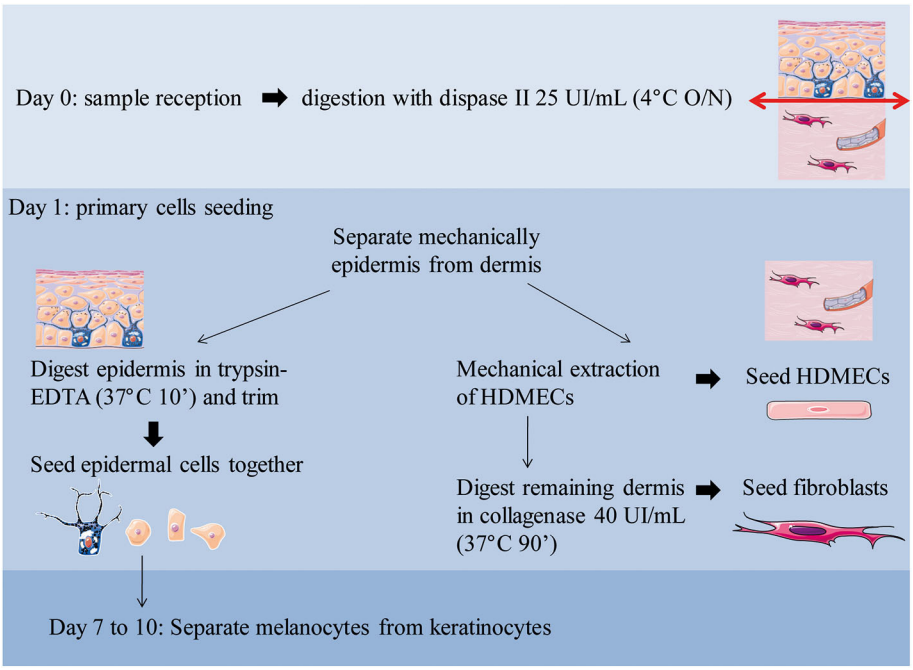

FIGURE 2 | Overview of the workflow with daily steps. O/N, overnight.

Alternatively, if no mechanical shaker is available, incubate the tube at 37°C and manually shake it every 10–15 min.

8. After the centrifugation of step 6, do not discard the supernatant!

   For HDMECs: Collect the supernatant and seed into a 6-wells plate: two wells filled with 1 mL of endothelial cells culture medium. Resuspend the cell pellet with 2 mL of culture medium and seed in a third well (named "pellet"). Seeding three separate wells maximizes the chances to obtain a pure HDMECs culture afterwards.

   For epidermal cells: Collect the supernatant and seed into 2–4 wells (depending on the initial volume) filled with 1 mL of melanocytes culture medium. Resuspend the cell pellet with 4 mL of culture medium and seed in two to four separate wells.
9. After the 90 min incubation of remaining dermal cells (fibroblasts) described in step 7, inactive the enzymatic digestion by adding the same amount of FCS 10% directly into the tube. Then, filter the cell suspension through a 70 µm-cell strainer. To this end, gently press the skin pieces above the filter using the plunger from a 10 mL-syringe. Rinse two to three times with HBSS.
10. Centrifugate the filtered suspension 5 min at 1,200 rpm. Resuspend the cell pellet with 3 mL of fibroblasts culture medium and seed into a 12.5 cm^2-flask.

Day 2 (to 4 if Necessary): First Cell Medium Renewal

- For the epidermal cells (keratinocytes/melanocytes) plate: collect the supernatant of all wells and rinse with HBSS; centrifugate the collected supernatant and resuspend the pellet with fresh medium before distributing it equally inside all wells (new wells in case of many adhered cells). This step is to ensure optimal adhesion of initially seeded cells.
- For the endothelial cells plate: add 1 mL of fresh medium to the well named "pellet." Collect the supernatant of the two other wells, centrifuge and resuspend the pellet with fresh medium before distributing it equally between all others wells.
- For the fibroblast flask (optional): if a lot of floating debris are present, collect the supernatant, rinse the flask with HBSS; centrifuge the collected medium, discard the supernatant of the centrifuged tube and resuspend the pellet with fresh medium before adding it again into the flask.

Fibroblasts Amplification

When fibroblasts reach 70–80% confluence, detach cells using the following procedure:

- Aspirate and discard the supernatant, rinse the flask with HBSS, add 0.5 mL of TE 10%
- Incubate at 37°C during 3–5 min, regularly check under the microscope if cells are detached; gently tap the flask if necessary
- When cells are detached, block TE action with FCS 10%. Collect the cell suspension, centrifuge 5 min at 1,500 rpm. Discard the supernatant, resuspend the cell pellet into 8 mL of fibroblasts culture medium and seed into 2 T25 cm^2 flasks (or 6-wells plates depending on further experiments).

Alternatively, freeze the cells if necessary. A minimum of 100 000–200 000 cells per vial is necessary to ensure that cells will grow back after thawing (concentration minimum: 1 million cells/mL of freezing medium). An example of freezing

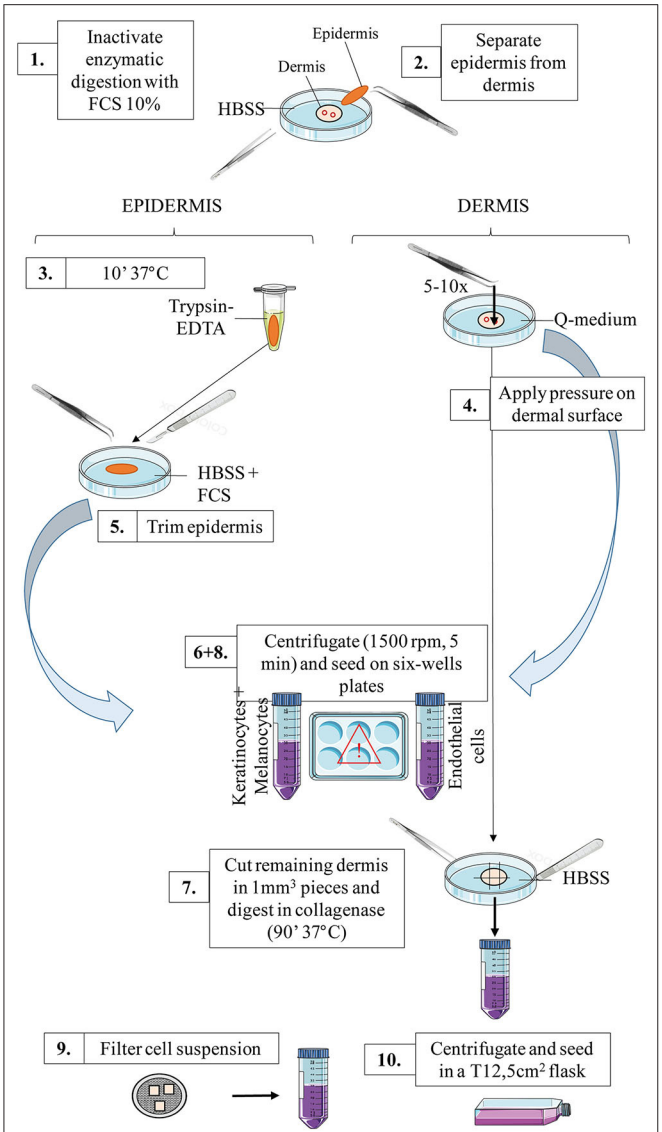

FIGURE 3 | Schematic representation of the workflow for day 1: primary cells seeding. For a detailed explanation of each step, cf section Day 1: Primary Cells Seeding.

medium is culture medium supplemented with FCS + 10% dimethylsulfoxyde (DMSO).

HDMECs Amplification ± Purification

HDMECs primoculture gives rise to several HDMECs islets which will grow independently in a concentric manner. When the islets have sufficiently grown, even if the well is not confluent (**Supplementary Figure 1**), each well can be passaged into a 25 cm^2-flask according to the procedure described in section Fibroblasts Amplification.

Important point: always check the phenotype of HDMECs culture by labeling cells with an anti-CD31 fluorochrome-conjugated antibody and performing fluorescence-activated cell sorting. A minimum of 10 000 labeled cells is needed for this experiment (see protocol in **Supplementary Material**). A purity of >90% $CD31^+$-cells is acceptable. As immune cells can also express CD31 (4), it is best to perform a simultaneous labeling with an anti-CD45 fluorochrome-conjugated antibody to rule out the presence of double-positive cells (which would be immune cells).

This mechanical extraction of HDMECs is very efficient and fibroblasts contamination is rare (**Figure 4**). However, if fibroblasts contamination occurs, which is easy to spot by observing cell culture, as HDMECs islets and fibroblasts differ in shape, two additional methods are possible:

- "differential trypsinization" technique:

This technique is usually efficient within 5–7 days of primary cell culture, before fibroblasts grow too much and HDMECs adhesion is too strong. When several islets of HDMECs appear, try to detach selectively HDMECs by applying TE 10% and checking under the microscope that fibroblasts remain attached. Collect the cell suspension and seed with a 1:2 split ratio.

- immunomagnetic cell sorting:

This technique can be used in case of failure of differential trypsinization or in later stages of cell culture. If the culture is still not pure afterwards, perform one immunomagnetic cell sorting with anti-CD31 microbeads (see protocol in **Supplementary Material**). The CD31 negative cells are fibroblasts and can be cultured in the appropriate medium after cell sorting.

Another possible contamination would be the presence of immune cells, such as lymphocytes or dendritic cells. To avoid this, another immunomagnetic cell sorting can also be performed at that stage in order to deplete CD45-positive cells (immune cells) (see protocol in **Supplementary Material**).

If necessary, HDMECs can be freezed until further use. A minimum of 100 000–200 000 cells per vial is necessary to ensure that cells will grow back after thawing (concentration minimum: 1 million cells/mL of freezing medium). An example of freezing medium is culture medium + 10% FCS + 10% DMSO.

Keratinocytes and Melanocytes Separation

When epidermal cells reach 60–70% confluence (this should be about 7–10 days from the initial seeding), separate melanocytes from keratinocytes (**Figure 5**). This is facilitated by the weaker adhesion system of melanocytes compared to keratinocytes; therefore, melanocytes detach before keratinocytes when challenged with trypsin.

To this end, apply TE 10% (e.g., 500 µL per well) in the wells and check under the microscope for dendrites retraction (the melanocytes will become round). After 1 or 2 min, collect the detached cells (which are the melanocytes)—do not wait too much, as you will get keratinocytes coming along—and block TE 10% with FCS 10% poured directly into the collection tube. Centrifugate this collection tube (5 min, 1,200 rpm).

Meanwhile, if necessary, apply again TE 10% on the initial well to ensure getting rid of every melanocyte (check under the microscope). Then, rinse the well (which contains only keratinocytes) with 10% FCS. Rinse again with HBSS, as

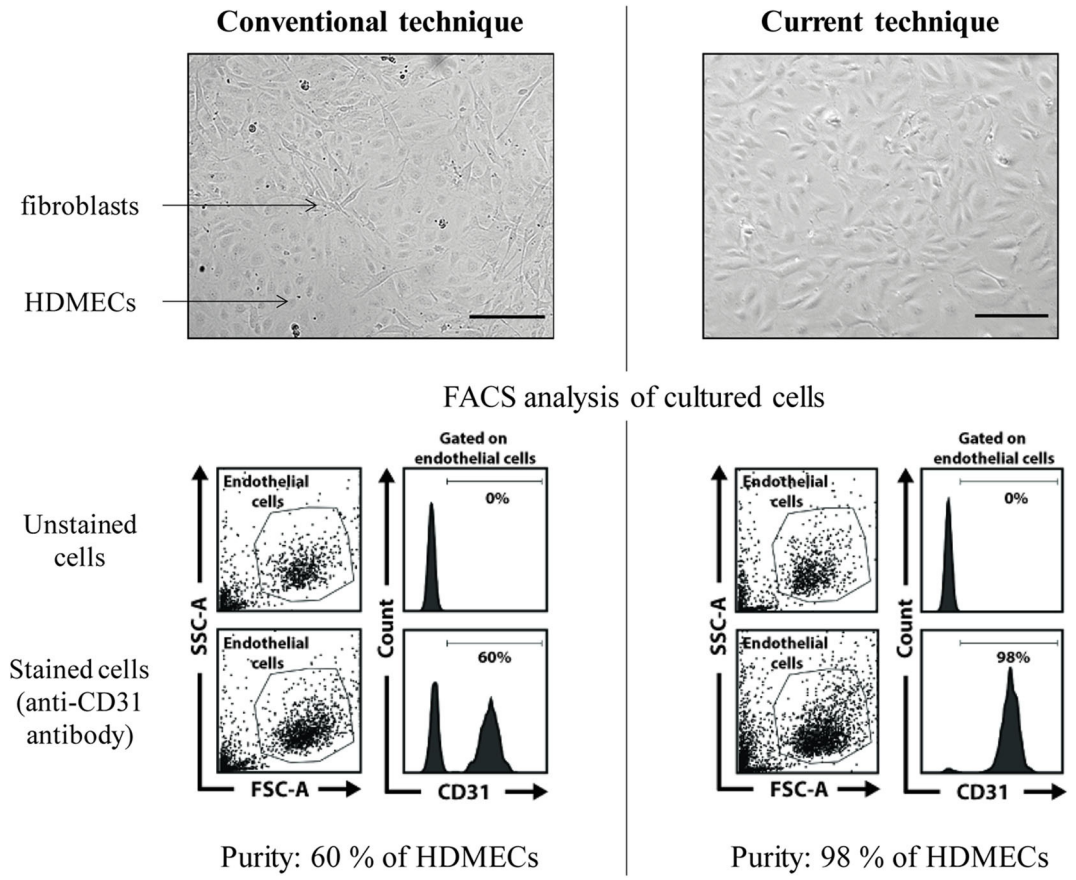

FIGURE 4 | HDMECs culture: efficacy of the proposed protocol (mechanical extraction) vs. conventional technique (dermal digestion with collagenase). FACS, fluorescence-activated cell sorting. Scale bar, 100 μm. In the conventional technique example picture, HDMECs islets (plain arrow) are surrounded by fibroblasts (dotted arrow). FACS analysis of cultured cells shows a proportion of 60% of HDMECs, identified thanks to CD31 surface marker expression. In the proposed technique, pure HDMECs culture can be seen, as confirmed by FACS analysis showing 98% of CD31+ cells in the culture plate.

prolonged FCS exposure leads to keratinocytes differentiation. Carefully pour fresh keratinocytes culture medium on the well and put the plate back into the incubator.

After centrifugation of the melanocytes tube, resuspend the cell pellet with Melanocyte Growth Medium, count the cells and seed into a 12-wells plate at the concentration of minimum 50 000 cells per well. Alternatively, seed them in order to perform immunocytochemistry experiment, for example in lab-tek^{TM} chamber slides.

Tip: melanocytes do not grow very well in very large culture flasks; best results are obtained when they are cultured in small spaces such as 12 or 24-wells plates.

From our personal experience, melanocytes do not grow back well after freezing.

Keratinocytes Culture and Amplification

After a few days, the keratinocytes will be ready to be expanded into a bigger flask (usually one T25 cm^2-flask starting from the whole 6-wells-plate), according to the procedure described in section Fibroblasts Amplification. For further experiments, use keratinocytes of passage 2 or fewer. Further passages might compromise the results as it favors cell differentiation.

If necessary, keratinocytes can be freezed until further use, although it should be avoided if possible, or done at the earliest passage. A minimum of 100 000–200 000 cells per vial is necessary to ensure that cells will grow back after thawing (concentration minimum: 1 million cells/mL of freezing medium). An example of freezing medium is culture medium + 10% FCS + 10% DMSO.

RESULTS

Cell Purification and Culture

The present protocol allows isolation and culture of HDMECs, fibroblasts, keratinocytes, and melanocytes (illustration of cultured cells: **Figure 6**). Pitfalls, when they exist, are outlined directly in the protocol described above. The major advantage is to obtain patients' cells which can be either grown, either analyzed with single-cell transcriptomics. However, the latter is not possible on freshly isolated cells for epidermal cells, as the present technique implies that they are separated later on.

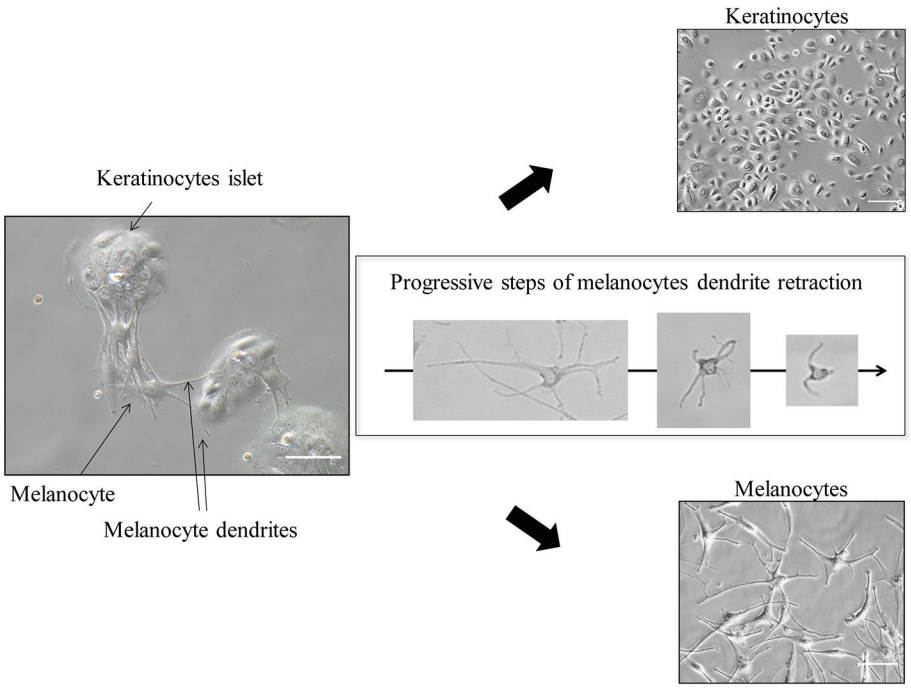

FIGURE 5 | Keratinocytes and Melanocytes separation (≪ differential trypsinization ≫). Scale bar for co-culture and for keratinocytes alone (upper right), 100 μm; for melanocytes alone (lower right), 50 μm. After trypsin application, melanocytes dendrites progressively retract within a few minutes, allowing easy detachment and leaving pure keratinocytes culture in the initial dish.

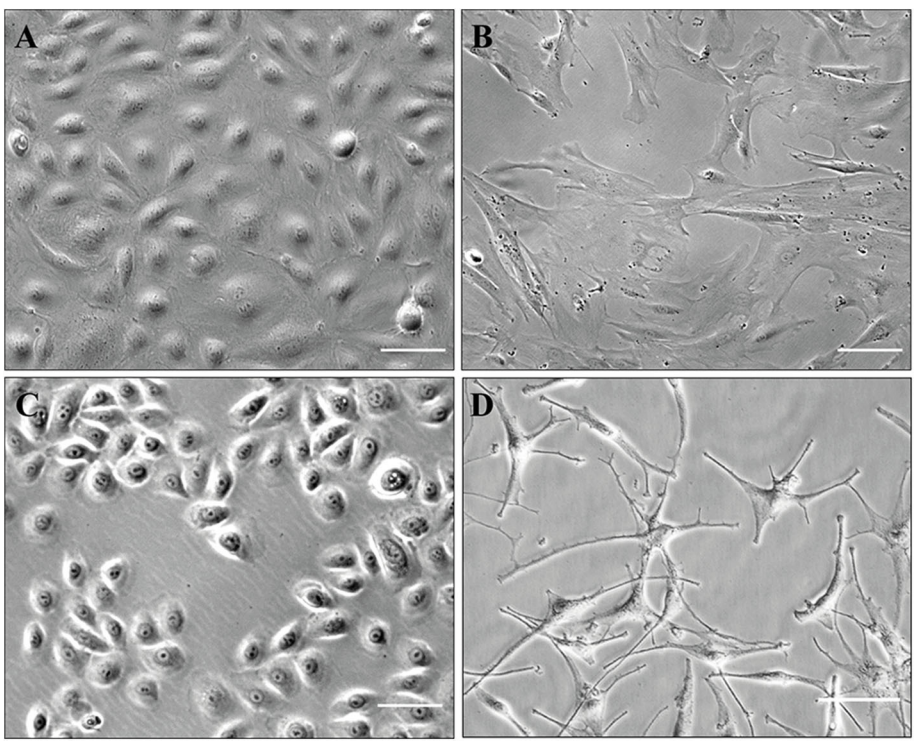

FIGURE 6 | Illustration of cultured cells (brightfield phase-contrast images). Scale, 100 μm **(A–C)** or 50 μm **(D)**. **(A)** HDMECs (initial seeding); **(B)** fibroblasts (passage number 5); **(C)** keratinocytes (passage number 1); **(D)** melanocytes (passage number 1).

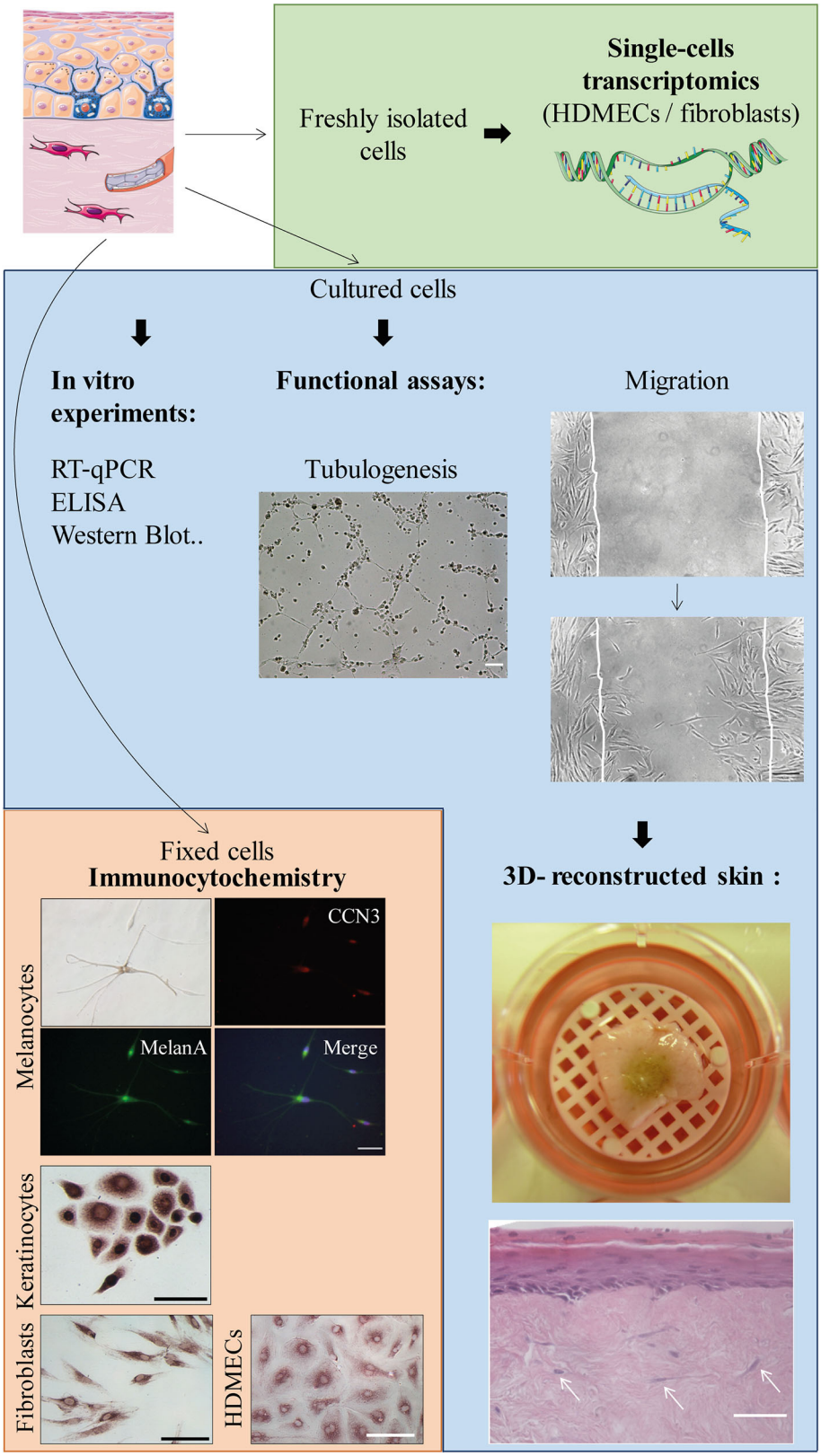

FIGURE 7 | Possible applications of the protocol (non-exhaustive list). Scale bars, 100 μm unless notified otherwise. From upper to lower panels: Tubulogenesis assay on Matrigel™ (or *in vitro* angiogenesis assay): picture taken 6 h after the beginning of the experiment with SSc HDMECs. Migration (or scratch assay) with

(Continued)

FIGURE 7 | fibroblasts: second picture taken 22 h after the beginning of the experiment. Skin equivalent (reconstructed epidermis): picture shows the macroscopical aspect of a pigmented reconstructed epidermis on a matrix of dead de-epithelialized dermis (DDD) implemented with fibroblasts. Histological image shows Hematoxylin-Eosin staining of the reconstructed skin with a multilayered differentiated epidermis and dermal fibroblasts within the DDD matrix (white arrows). Scale bar, 20 μm. Immunocytochemistry: experiments were performed to evidence CCN3, an ubiquitous multimodular protein implicated in melanocyte adhesion to the basal epidermal layer as well as angiogenesis [Ricard et al. *Experimental Dermatology* 2012 (6)—Henrot et al. *Journal of Investigative Dermatology* 2020 (7)]. Melanocytes (upper panel): double immunocytochemistry staining using antibodies against CCN3 and MelanA, which is a specific cytoplasmic marker. Nuclei are stained in blue with DAPI. Keratinocytes, fibroblasts, and HDMECs: immunostaining with anti-CCN3 antibody and revelation with horseradish-peroxydase and ImmPACT VIP™ as a substrate.

Concerning HDMECs, the proposed technique (mechanical extraction) allows efficient purity of HMECs culture, with an overall success rate of around 80 % (from our personal experience) as opposed to the conventional technique (dermal digestion with collagenase) (5), which gives pure and sustained HDMECs culture in about 30 % of the cases (also personal experience) (**Figure 4**). Cells obtained with our technique are in sufficient number for Western Blot or RT-qPCR experiments, as well as functional assays such as migration or *in vitro* angiogenesis assays (**Figure 7**). Also from personal experience, mechanical extraction of HDMECs directly gives a pure HDMECs culture in around 80% of the cases—for the 20% remaining cases, additional purification methods such as differential trypsinization and/or immunomagnetic cell sorting have to be used in order to obtain a pure culture. Directly obtaining a pure HDMECs culture is of major interest in order to use cells at early passages for subsequent experiments. From our personal experience, HDMECs should not be used beyond the 6th passage.

Fibroblast culture is relatively easy and the present protocol allows the isolation and culture of SSc fibroblasts with a success rate close to 100% from our personal experience. Cells are also in sufficient number for Western Blot, RT-qPCR, or functional assays. From our personal experience, fibroblasts should not be used beyond the 6th or 7th passage.

Both HDMECs and fibroblasts can be kept frozen and grow back correctly once thawed.

Keratinocytes can be obtained from most samples, with a success rate of about 90% from our personal experience. However, cells should be used immediately as they do not grow well after freezing. Best results are also obtained if cells are used within the second passage, in order to avoid keratinocytes differentiation. Keratinocytes differentiation is easy to spot as cells become visibly bigger and stop growing (**Supplementary Figure 1**).

Melanocytes can also be grown from most samples, with a success rate of around 60% (personal experience). Of note, difficulties to obtain SSc melanocytes are also applicable to healthy skin, particularly from small skin samples as melanocytes represent around 5% of epidermal cells. Cells grow in sufficient number for immunocytochemistry or ELISA experiments. However, given the small sample size, it is quite difficult to obtain enough cells to perform Western Blot or RT-qPCR experiments. SSc melanocytes also do not grow back very well after freezing (which is also true for melanocytes grown from healthy skin). For detailed explanations concerning melanocytes culture in general, see (8).

Of note, as showed in **Figure 1**, trypsin usually allows separating the epidermis in two parts: the basal layer, constituted by melanocytes and keratinocytes stem cells. When only epidermal cells are required, conventional protocols use skin digestion with trypsin in order to seed only the cells from the basal layer. However, in the current protocol, a digestion with dispase is needed in order to separate the epidermal sheet from the dermis. Therefore, trypsin is used here in order to help digesting inter-cellular adhesions between epidermal cells. Some of the cells that are seeded afterwards may not be stem cells as they originate from upper layers of the epidermis, but this should not be a limitation as they will quickly be overgrown by keratinocytes stem cells.

Applications

All cells grown from the biopsy are suitable for immunocytochemistry, whether fluorescent or using enzyme-labeled detection system. Cultured cells can also be used for functional assays such as migration (scratch assays) or *in vitro* angiogenesis assays. Finally, cultured cells can be implemented in 3D-skin models (or skin equivalents) (**Figure 7**). For example, our lab has a long-lasting experience of reconstructed epidermis on a matrix of dead de-epithelialized dermis. Such model allows the formation of a multi-layered epidermis containing both keratinocytes and melanocytes (seeded at a respective proportion of 95/5%). The underlying matrix can also be implemented with dermal cells (fibroblasts and HDMECs) in order to expose the epidermis to secretions from dermal cells (**Figure 7** and **Supplementary Figure 2**). Such model would highly benefit from SSc cells, in order to reproduce the complex interactions between dermal and epidermal cells.

DISCUSSION

Isolating primary skin cells in SSc can be a struggle due to small sample size as well as skin condition. Here, we present a protocol allowing the isolation of the four main types of skin cells: HDMECs, fibroblasts, keratinocytes, and melanocytes, from a single 4 mm-punch biopsy. Dermal cells (fibroblasts and HDMECs) can be immediately used after skin dissociation, notably for molecular biology experiments such as single-cell transcriptomics; they can also be used for functional assays or 3D-skin models after a few passages. Epidermal cells (keratinocytes and melanocytes) are initially cultured together and can be separated at the first passage in order to be used for functional assays.

Fibroblasts are relatively easy to culture and many protocols describe their isolation (9). However, culturing HDMECs is a more delicate issue. Most published protocols use foreskin tissue, which gives highly proliferative HDMECs culture but poorly reflects adult skin characteristics (10). Yet, HDMECs are cells of major importance concerning SSc pathophysiology: it is currently discussed whether they are key cells initiating fibrotic events, as vascular manifestations such as Raynaud's phenomenon often precede the development of the disease (11). Therefore, having access to patients' cells is a crucial challenge. A well-known problem for HDMECs culture is contamination by surrounding fibroblasts, an issue further enhanced in SSc skin where activated fibroblasts bear extensive proliferative capacity over HDMECs (12). A mechanical extraction of HDMECs possibly combined to immunomagnetic cell sorting, as proposed in the current technique, ultimately allows better specificity of HDMECs culture. If the experimentator is properly trained for mechanical extraction, the immunomagnetic cell sorting can be dispensable; the extracted HDMECs population can be immediately used with a high purity ratio if single-cell experiments are planned. Avoiding immunomagnetic cell sorting could also be useful due to the potential influence of anti-CD31 antibodies coupled to microbeads on HDMECs function (13). Other protocols also describe isolation of HDMECs, such as a protocol using enzymatic digestion and the perfusion technique, specifically designed for SSc skin (14); however, this protocol does not allow culture of epidermal cells. More recently, another protocol has been published allowing culturing of HDMECs and also using mechanical extraction (15); however, this protocol was not specifically optimized for SSc cells, did not allow epidermal cell culture, and requires bigger pieces of skin than a punch biopsy.

Several protocols also well describe epidermal cells culture, such as the paper from Tsuji and Karasek back in 1983, describing melanocytes isolation from newborn skin (16), or the more recent protocol from Wang et al. (17). However in the latter, minimal required biopsy size was 6 × 3-mm punch biopsies (e.g., 42 mm2), which is bigger than the current proposed biopsy size. Morevoer, to our knowledge, no report specifically concerns SSc keratinocytes and melanocytes.

Finally, to our knowledge, only one report describes a protocol aiming to culture keratinocytes, fibroblasts and HDMECs from a single punch biopsy (18). This method already included the mechanical extraction of HDMECs. However, the protocol was not optimized for SSc cells (in particular, HDMECs culture was not detailed) and the possibility to culture melanocytes was not addressed. Altogether, we believe that the current protocol is the only one allowing isolating the four main types of skin cells from a small biopsy in SSc patients.

Epidermal cells, namely keratinocytes and melanocytes, are initially cultured together. Indeed, this step is essential to favor melanocytes growth, which is almost impossible without keratinocytes. However, they are easily separated after a few days, also allowing single-cell experiments, even if such experiments would not be performed directly on freshly isolated cells. After this first passage, keratinocytes and melanocytes are cultivated separately. As melanocytes do not proliferate highly on their own, a pure melanocytes culture could be mostly used to perform immunocytochemistry experiments. However, they can also be used in co-culture experiments (for example with keratinocytes), using a controlled combination of healthy and SSc cells.

Of course, skin cells are prone to lose their original phenotype during successive passages. This is particularly true for keratinocytes, which differentiate rapidly in culture. For these reasons, experimentators are advised to use cells within a few passages, and to favor experiments performed immediately after cell extraction whenever possible. We also recommend to check the morphology of cultured cells and to monitor their growth rate in order to ensure the viability of the culture.

Skin 3D models, or skin equivalents, are a powerful tool in translational research, allowing to test the effects of drugs or to modelize the cellular cross-talk in complex diseases such as SSc (19). This kind of model can highly benefit from primary cells incorporation, thus better reflecting cellular interactions, and even more if primary cells come from patients. Our team has a long-lasting experience in 3D skin models such as reconstructed multi-layered epidermis on a matrix of dead de-epithelialized dermis (DDD) (20). This kind of model, initially aimed at studying epidermal homeostasis, has then been implemented with dermal cells such as fibroblasts and HDMECs (**Figure 7** and **Supplementary Figure 2**). Other 3D models could benefit from patient's cells. Recently, an elegant paper reported a skin equivalent using primary HDMECs forming a functionally vascular network, fibroblasts, and keratinocytes (21). In this model, fibrosis was induced with TGF-β exposure. Thus, such model could highly benefit from the implementation of patients' cells, as well as the addition of melanocytes. Another very interesting report showed the generation of a skin organoid using SSc patients induced pluripotent stem cells (iPSCs), which had been differentiated into fibroblasts and keratinocytes (22). However, iPSCs culture is very delicate and costly, and do not allow the complete control of the differentiation state. Altogether, our protocol provides a quick and efficient way to obtain a primary culture of the four main types of skin cells, allowing their use in skin equivalents.

Our protocol has been adapted to fit the particularities of SSc cells, but works quite efficiently with healthy skin, from our personal experience. Moreover, although we have not tried it directly, it could also be used with any other skin disease. Indeed, many skin diseases rely on abnormalities of several skin cells, such as vitiligo where both epidermal and dermal cells are affected (23). Moreover, dermal digestion with collagenase also allows isolating other cells than HDMECs and fibroblasts. Theoretically, immune cells such dendritic cells or cutaneous T lymphocytes could further be extracted from the dermis in order to be used for characterization or functional experiments, for example by combining our method to other published protocols (24, 25). Such additional methods should not alter the performance of our protocol concerning HDMECs culture (as it represents the first step of dermal digestion) nor fibroblasts

culture (as this part is relatively easy). However, the yield of immune cells extraction is probably more hazardous and will possibly require additional digestion enzymes. Ultimately, the current protocol could be adapted to other tissues, by dissociating and cultivating separately epithelial and connective tissue cells.

To conclude, performing experiments on primary cells is essential in the field of translational research, especially for diseases whom pathophysiology is complex and where different cell types may be simultaneously affected. Cells isolated from patients' samples can be further used in 3D skin models, in order to better reproduce the disease complex pathophysiology.

DATA AVAILABILITY STATEMENT

The original contributions presented in the study are included in the article/**Supplementary Material**, further inquiries can be directed to the corresponding author/s.

ETHICS STATEMENT

The studies involving human participants were reviewed and approved by the appropriate institutional ethical committee (CPP, 2012 A00081-42, Aquitaine). The patients/participants provided their written informed consent to participate in this study.

AUTHOR CONTRIBUTIONS

PH, MC, CP, PL, M-ET, and EL contributed to the conception of the protocol. PH, PL, MC, DL, and EL contributed to data acquisition. PH wrote the first draft of the manuscript. All authors contributed to manuscript revision, read, and approved the submitted version.

FUNDING

This research was funded by Association des Sclérodermiques de France (Convention 18-7-16) and Société Française de Dermatologie et de Vénérologie (Convention n°3 -AO septembre 2018).

ACKNOWLEDGMENTS

The authors wish to thank every clinician and patient who contributed to the local SSc cohort (SSc-VISS) coordinated by Dr. Marie-Elise Truchetet, as well as the Plastic Surgery Department of Bordeaux Universitary Hospital (head: Dr. Vincent Casoli) who provided healthy skin, which was necessary to develop the protocol. The authors also wish to thank Mrs. Vanessa Bergeron for technical assistance in skin reconstruction with HDMECs. **Figures 1–3**, **7** were created using images from Servier Medical Art Commons Attribution 3.0 Unported License. (http://smart.servier.com). Servier Medical Art by Servier is licensed under a Creative Commons Attribution 3.0 Unported License.

SUPPLEMENTARY MATERIAL

The Supplementary Material for this article can be found online at: https://www.frontiersin.org/articles/10.3389/fimmu.2020.566607/full#supplementary-material

Supplementary Figure 1 | HDMECs passaging.

Supplementary Figure 2 | differentiated keratinocytes.

Supplementary Figure 3 | skin equivalent with HDMECs.

Supplementary Video 1 | epidermal sheet separation.

Supplementary Video 2 | endothelial cells mechanical extraction. Text: protocol for CD31 and CD45 labeling before FACS analysis and immunomagnetic cell sorting.

REFERENCES

1. Gabrielli A, Avvedimento EV, Krieg T. Scleroderma. *N Engl J Med.* (2009) 360:1989–2003. doi: 10.1056/NEJMra0806188
2. Poudel DR, Derk CT. Mortality and survival in systemic sclerosis: a review of recent literature. *Curr Opin Rheumatol.* (2018) 30:588–93. doi: 10.1097/BOR.0000000000000551
3. Krieg T, Takehara K. Skin disease: a cardinal feature of systemic sclerosis. *Rheumatology.* (2009) 48(Suppl. 3):iii14–8. doi: 10.1093/rheumatology/kep108
4. Marelli-Berg FM, Clement M, Mauro C, Caligiuri G. An immunologist's guide to CD31 function in T-cells. *J Cell Sci.* (2013) 126:2343–52. doi: 10.1242/jcs.124099
5. Monsuur HN, Weijers EM, Niessen FB, Gefen A, Koolwijk P, Gibbs S, et al. Extensive characterization and comparison of endothelial cells derived from dermis and adipose tissue: potential use in tissue engineering. *PLoS ONE.* (2016) 11:e167056. doi: 10.1371/journal.pone.0167056
6. Ricard AS, Pain C, Daubos A, Ezzedine K, Lamrissi-Garcia I, Bibeyran A, et al. Study of CCN3 (NOV) and DDR1 in normal melanocytes and vitiligo skin. *Exp Dermatol.* (2012) 21:411–6.
7. Henrot P, Moisan F, Laurent P, Manicki P, Kaulanjan-Checkmodine P, Jolivel V, et al. Decreased CCN3 in Systemic Sclerosis Endothelial Cells Contributes to Impaired Angiogenesis. *J Invest Dermatol.* (2020) 140:1427–1434.e5.
8. Cario M, Taieb A. Isolation and culture of epidermal melanocytes. *Methods Mol Biol.* (2019) 1993:33–46. doi: 10.1007/978-1-4939-9473-1_3
9. *Isolation and Culture of Skin Fibroblasts | Springer Nature Experiments*. Available online at: https://experiments.springernature.com/articles/10.1385/1-59259-940-0:083 (accessed May 15, 2020).
10. Richard L, Velasco P, Detmar M. Isolation and culture of microvascular endothelial cells. *Methods Mol Med.* (1999) 18:261–9. doi: 10.1385/0-89603-516-6:261
11. Mostmans Y, Cutolo M, Giddelo C, Decuman S, Melsens K, Declercq H, et al. The role of endothelial cells in the vasculopathy of systemic sclerosis: A systematic review. *Autoimmun Rev.* (2017) 16:774–86. doi: 10.1016/j.autrev.2017.05.024
12. Gilbane AJ, Denton CP, Holmes AM. Scleroderma pathogenesis: a pivotal role for fibroblasts as effector cells. *Arthritis Res Ther.* (2013) 15:215. doi: 10.1186/ar4230
13. Plouffe BD, Murthy SK, Lewis LH. Fundamentals and application of magnetic particles in cell isolation and enrichment. *Rep Prog Phys.* (2015) 78:016601. doi: 10.1088/0034-4885/78/1/016601
14. Kräling BM, Jimenez SA, Sorger T, Maul GG. Isolation and characterization of microvascular endothelial cells from the adult human dermis and from skin biopsies of patients with systemic sclerosis. *Lab Invest.* (1994) 71:745–54.
15. *Isolation and Culture of Human Dermal Microvascular Endothelial Cells | Springer Nature Experiments*. Available online at: https://experiments.

springernature.com/articles/10.1007/978-1-4939-9473-1_7 (accessed May 15, 2020).
16. Tsuji T, Karasek M. A procedure for the isolation of primary cultures of melanocytes from newborn and adult human skin. *J Invest Dermatol.* (1983) 81:179–80. doi: 10.1111/1523-1747.ep12543633
17. Wang Y, Tissot M, Rolin G, Muret P, Robin S, Berthon JY, et al. Development and validation of a simple method for the extraction of human skin melanocytes. *Cytotechnology.* (2018) 70:1167–76. doi: 10.1007/s10616-018-0207-7
18. Normand J, Karasek MA. A method for the isolation and serial propagation of keratinocytes, endothelial cells, and fibroblasts from a single punch biopsy of human skin. *In Vitro Cell Dev Biol Anim.* (1995) 31:447–55. doi: 10.1007/BF02634257
19. Ali N, Hosseini M, Vainio S, Taïeb A, Cario-André M, Rezvani HR. Skin equivalents: skin from reconstructions as models to study skin development and diseases. *Br J Dermatol.* (2015) 173:391–403. doi: 10.1111/bjd.13886
20. Cario-André M, Briganti S, Picardo M, Nikaido O, Gall Y, Ginestar J, et al. Epidermal reconstructs: a new tool to study topical and systemic photoprotective molecules. *J Photochem Photobiol B Biol.* (2002) 68:79–87. doi: 10.1016/S1011-1344(02)00328-7
21. Matei AE, Chen CW, Kiesewetter L, Györfi AH, Li YN, Trinh-Minh T, et al. Vascularised human skin equivalents as a novel *in vitro* model of skin fibrosis and platform for testing of antifibrotic drugs. *Ann Rheum Dis.* (2019) 78:1686–92. doi: 10.1136/annrheumdis-2019-216108
22. Kim JW, Kim Y, Kim J, Park MJ, Kwon E, Lee J, et al. AB0189 3d skin organoid mimicking systemic sclerosis generated by patient-derived induced pluripotent stem cells: 'disease in a dish' and development of animal model. *Ann Rheum Dis.* (2018) 77(Suppl. 2):1281. doi: 10.1136/annrheumdis-2018-eular.4502
23. Ezzedine K, Eleftheriadou V, Whitton M, van Geel N. Vitiligo. *Lancet.* (2015) 386:74–84. doi: 10.1016/S0140-6736(14)60763-7
24. Lorenz B, von Stebut E. Isolation of T cells from the skin. *Methods Mol Biol.* (2014) 1193:3–13. doi: 10.1007/978-1-4939-1212-4_1
25. Kashem SW, Kaplan DH. Isolation of murine skin resident and migratory dendritic cells via enzymatic digestion. *Curr Protoc Immunol.* (2018) 121:e45. doi: 10.1002/cpim.45

Conflict of Interest: The authors declare that the research was conducted in the absence of any commercial or financial relationships that could be construed as a potential conflict of interest.

frontiers in Immunology

ORIGINAL RESEARCH
published: 23 October 2020
doi: 10.3389/fimmu.2020.532177

Elevated Circulatory Levels of Microparticles Are Associated to Lung Fibrosis and Vasculopathy During Systemic Sclerosis

*Damien Leleu[1,2], Emeline Levionnois[1], Paoline Laurent[1], Estibaliz Lazaro[1,3,4], Christophe Richez[1,4,5], Pierre Duffau[1,3], Patrick Blanco[1,2], Vanja Sisirak[1], Cecile Contin-Bordes[1,2] and Marie-Elise Truchetet[1,4,5]*on behalf of the Fédération Hospitalo Universitaire ACRONIM Aquitaine's Care and Research Organization for Inflammatory and Immune-Mediated Diseases*

[1] University of Bordeaux, CNRS, ImmunoConcEpT, UMR 5164, Bordeaux, France, [2] Immunology and Immunogenetic Department, Bordeaux University Hospital, Bordeaux, France, [3] Internal Medicine Department, Bordeaux University Hospital, Bordeaux, France, [4] Centre national de reference des maladies auto-immunes systémiques rares de l'Est et du Sud-Ouest (RESO), Bordeaux, France, [5] Rheumatology Department, Bordeaux University Hospital, Bordeaux, France

OPEN ACCESS

Edited by:
Anna-Maria Hoffmann-Vold, Oslo University Hospital, Norway

Reviewed by:
Serena Vettori, University of Campania Luigi Vanvitelli, Italy
Francesco Del Galdo, University of Leeds, United Kingdom

***Correspondence:**
Marie-Elise Truchetet
marie-elise.truchetet@chu-bordeaux.fr

Specialty section:
This article was submitted to Autoimmune and Autoinflammatory Disorders, a section of the journal Frontiers in Immunology

Received: *05 March 2020*
Accepted: *01 October 2020*
Published: *23 October 2020*

Citation:
Leleu D, Levionnois E, Laurent P, Lazaro E, Richez C, Duffau P, Blanco P, Sisirak V, Contin-Bordes C and Truchetet M-E (2020) Elevated Circulatory Levels of Microparticles Are Associated to Lung Fibrosis and Vasculopathy During Systemic Sclerosis. Front. Immunol. 11:532177. doi: 10.3389/fimmu.2020.532177

Background: Microparticles (MPs) are vesicular structures that derive from multiple cellular sources. MPs play important roles in intercellular communication, regulation of cell signaling or initiation of enzymatic processes. While MPs were characterized in Systemic Sclerosis (SSc) patients, their contribution to SSc pathogenesis remains unknown. Our aim was to investigate the potential role of MPs in SSc pathophysiology and their impact on tissue fibrosis.

Methods: Ninety-six SSc patients and 37 sex-matched healthy donors (HD) were enrolled in this study in order to quantify and phenotype their plasmatic MPs by flow cytometry. The ability of MPs purified from SSc patients and HD controls to modulate fibroblast's extra-cellular matrix genes expression was evaluated *in vitro* by reverse transcriptase quantitative polymerase chain reaction.

Results: SSc patients exhibited a higher concentration of circulatory MPs compared to HD. This difference was exacerbated when we only considered patients that were not treated with methotrexate or targeted disease-modifying antirheumatic drugs. Total circulatory MPs were associated to interstitial lung disease, lung fibrosis and diminished lung functional capacity, but also to vascular involvement such as active digital ulcers. Finally, contrary to HD MPs, MPs from SSc patients stimulated the production of extracellular matrix by fibroblast, demonstrating their profibrotic potential.

Conclusions: In this study, we provide evidence for a direct profibrotic role of MPs from SSc patients, underpinned by strong clinical associations in a large cohort of patients.

Keywords: microparticles (MPs), systemic sclerosis (scleroderma), fibrosis, platelets, endothelial cells (ECs), immunosuppressive agent

BACKGROUND

Systemic Sclerosis (SSc) is a rare and complex autoimmune disease that involves immune activation, microvascular dysfunction and perivascular fibrosis affecting both the skin and internal organs. SSc is associated with serious complications that severely impact patients' quality of life and vital prognosis. Among them are vasculopathies (Raynaud's phenomenon, digital ulcers), gastrointestinal complications, cardiovascular damage (pulmonary arterial hypertension, cardiac fibrosis) and interstitial lung disease (ILD) that can lead to pulmonary fibrosis. The pathophysiology of SSc remains poorly understood, however the systemic nature of the disease may be due, in part, to aberrant immune stimulation, as well as to platelets and endothelial cells hyperactivation (1, 2). Microparticles (MPs) generated from these activated immune cells, platelets and endothelial cell, were shown in inflammatory and autoimmune diseases to display pathogenic properties across multiple tissues, and may as well contribute to SSc pathogenesis (3).

Virtually all eukaryotic cells shed submicron vesicles constitutively, upon activation or during apoptosis. It is only recently that their potential roles in physiology and pathophysiology have been appreciated, including their involvement in blood coagulation, inflammation, and intercellular signaling (3). MPs are vesicular structures that derive from multiple cellular sources and in the circulation, they notably originate from platelets (4, 5) and endothelial cell (6). There are two principal types of MPs identified according to their size and content. Large MPs (0.1 to 1 μm) that arise from outward budding of the plasma membrane, and small MPs also called exosomes (50 to 150 nm) which are manufactured within multivesicular bodies of the endocytic tract (7). MPs can play many roles in intercellular communication, regulation of cell signaling or initiation of enzymatic processes (3). Interestingly, large extracellular MPs were shown as a major carrier of self-DNA and thus may represent an important self-antigen involved in the loss of tolerance mechanisms, and the development of autoimmune diseases, when improperly cleared (8). Therefore, MPs represent functional units with a disseminated storage pool of bioactive effectors that are starting to be recognized as important players in different autoimmune diseases including Systemic Lupus Erythematosus (SLE) and SSc (9–11). MPs can originate from every type of cells, particularly under stress conditions. Endothelial cell (EC) damage is one major hallmark of SSc and lead to the shedding of endothelial MPs [EMPs; (12, 13)]. *Batteux* et al. showed in a murine model of SSc, that inhibiting MPs shedding either chemically or genetically diminishes the hallmarks of oxidative and endothelial stress but also skin and lung fibrosis (14). However, the underlying mechanisms of MPs impact on SSc pathogenesis in these animal models were not characterized. Nomura et al. measured circulatory MPs originating from platelets (PMPs) and monocytes, on a small cohort of SSc patients with pulmonary disease, and showed that they were both increased compared to healthy donors [HD; (15)]. Furthermore, Maugeri et al. have recently shown that PMPs that accumulate in SSc patients promote neutrophil autophagy and the formation of neutrophil extracellular traps (NETs) upon stimulation by PMPs-associated HMGB1 [High-Mobility Group Box 1; (16)]. However, associations between PMPs, their content in HMGB1, circulatory NETs byproducts and specific SSc clinical features were not described. It is only recently that pulmonary arterial hypertension (PAH) in a very small cohort of SSc patients was associated with elevated levels of circulatory EMPs. Such contribution of EMP to PAH was proposed to rely on SSc patients MPs ability to stimulate EC capacity to produce inflammatory cytokines (17). Furthermore, MPs containing mitochondrial DNA were recently suggested to contribute to ILD in SSc patients through their ability to activate inflammatory immune responses (18). Although these studies support the importance of MPs in SSc pathophysiology, human data on MPs in SSc and their involvement in fibrotic process is remain scarce.

Taking into account the previously described involvement of platelets and endothelial cell in the SSc physiopathology (1, 2) and the previous observation of the total MPs, EMPs and PMPs elevations during SSc (10, 16, 17), we decided to analyze all circulatory MPs and those derived from platelet and endothelial cells, in our patient cohort. Our objective was to investigate total numbers of these MPs in SSc patients compared to HD, and to study whether MPs counts were associated to specific clinical features. We also investigated the impact of purified total MPs from SSc patients and HD on fibroblasts production of extracellular matrix components. We report evidence for a direct profibrotic role specifically of SSc patients' MPs *in vitro* underpinned by clear clinical associations between SSc patients' MPs numbers with lung involvement in a large cohort.

METHODS

Study Population

Patients with SSc have been included in the biomedical research project "MICROLUPS" (Microparticles in lupus and SSc), approved by the institutional ethics committee (CPP, SUD-EST IV, 18/024) at the university hospital of Bordeaux. All patients satisfied the American College of Rheumatology/European League Against Rheumatism 2013 classification criteria for SSc (19) and provided written informed consent before inclusion. Clinical (age, sex, disease duration, skin disease, articular disease, heart disease, lung disease, kidney disease, and gastrointestinal disease) and biologic (anti-nuclear serology, creatinine clearance) features of each patient were recorded, as well as their respiratory function tests and treatments. Values of the modified Rodnan skin score (MRSS) and right ventricular systolic pressure (RVSP), that were recorded were the one that were the closest to the collection time of the sample. ILD was diagnosed if respiratory function tests showed a restrictive effect with a decrease in carbon monoxide diffusion capacity (DLCO < 80% and/or FVC < 70%) associated with damages (such as ground-glass opacities, honeycombing or reticular infiltrations) on high-resolution computed tomography (HRCT) and stratified

into limited and extensive ILD, according to Goh et al. and Roofeh D. et al. (20, 21). Diagnosis of PAH was based on the assessment of mean pulmonary arterial pressure (PAPm > 25mmHg) by right heart catheterization (22). Severe SSc phenotypes were defined as SSc with ILD, PAH, cardiac disease, renal crisis, and active digital ulcers. The control group consisted of sex-matched healthy donors (mean age = 45 years; 72,72% of women) obtained from the local Blood Transfusion Center (Etablissement Français du Sang, University Hospital of Bordeaux).

Pre-Analytical Sample Processing

SSc Patients and HD's blood were collected in 7 ml EDTA tubes, without applying the tourniquet and with a needle of at least 21 gauges. Samples were kept upright and rapidly conveyed to the laboratory without being shaken and then processed within 2 h of collection. Blood was gently transferred into a 15 ml tube and spun at 3500g for 15 minutes (without brakes). Platelet-poor plasma (PPP) was gently collected leaving a minimum of 1 ml of plasma above the pellet. The PPP was then spun again at 3500g for 15 minutes (without brakes). Platelet-free plasma (PFP) was collected leaving a minimum of 500 µl above the platelet pellet. PFP was then aliquoted in 1 ml aliquots and stored at −80°C.

Microparticles Phenotyping

Patient and control samples of PFP were thawed at room temperature and spun at 21,000 g for 1 h at 4°C. The pellet containing MPs was resuspended in 1 ml of 0.1µm filtered Phosphate Salt Buffer (PBS) and 100 µl of this suspension was labeled with 5 ng/µl of anti-CD235a Pacific Blue (Mouse IgG1, κ, Biolegend), anti-CD41 APC (Mouse IgG1, κ, Biolegend), anti-CD31 PE-Cy7 antibodies (Mouse IgG1, κ, Biolegend), and lactadherin (Hematologic Technologies, diluted at 1/50) or with 5 ng/µl anti-CD45 FITC (Mouse IgG1, Beckman Coulter), anti-CD66b PerCP (Mouse IgG1, κ, Biolegend), anti-CD3 BV510 (Mouse IgG1, κ BD biosciences) or with anti-CD19 PE (Mouse IgG1, Beckman Coulter) for 30 minutes, in the dark at room temperature. MPs count-beads® (Biocytex, diluted at 1/10), for MPs counting, and 100 µl of filtered PBS were added after the labeling. Samples were then analyzed by flow cytometry on a FACS canto II (Becton Dickinson). Megamix-Plus SSC® (Biocytex) was used to set up the threshold in side scatter (SSC) and place the MPs gate in accordance with the manufacturer's protocol. A second threshold was set on forward scatter (FSC) using a tube containing only 0.1µm filtered PBS together with the antibody mix, according to the protocol from Burbano et al. (23). All the background noise generated by the buffer was thus eliminated. These settings allowed us to define the total MPs among which two sub-populations were characterized: the EMPs ($CD235a^-CD41^-CD31^+$) and the PMPs ($CD235a^-CD41^+$).

Fibroblast Culture With Microparticles

Fibroblasts extracted from mammoplasty were cultured in 24-well plates with 50,000 cells per well. Fibroblasts were allowed to adhere for 24 h in Dulbecco's Modified Eagle Medium (DMEM, Gibco), containing 10% fetal bovine serum (FBS, GE Healthcare Bio-Sciences), 1% penicillin/streptomycin (Gibco) and 1% Pyruvate (complete DMEM medium). Then, the medium was replaced by the same medium without FBS overnight to starve the cells, in order to promote their stimulation.

Patient and control samples were thawed at room temperature and centrifuged at 21,000g for 1 h at 4°C to pellet the MPs. The supernatant was removed to leave only 50 µl above the MPs pellet. The MPs were then resuspended in 950 µl of filtered PBS and centrifuged again at 21,000g for 1 h at 4°C. The MPs concentration was adjusted after quantification by flow cytometry on the FACS Canto II (Becton Dickinson) with complete DMEM medium to obtain a concentration of 1,000 MPs/µl (corresponding to 10 times the cell concentration). MPs were then cultured with the fibroblasts at 10 MPs/µl, 100 MPs/µl, and 1,000 MPs/µl. As a positive control, fibroblasts were treated with 10 ng/ml of TGF-β (Miltenyi Biotec), which is known to induce collagen expression (**Figure S3**). Fibroblasts and MPs were co-cultured for 24 h before RNA extraction.

Reverse Transcription Quantitative PCR (RT qPCR)

mRNA was purified from fibroblasts using an RNeasy Plus Micro Kit (Qiagen), and mRNA concentration and purity were quantified with a Spectrophotometer DS11 (Denovix). RNA integrity number (RIN) was assessed using an Agilent 2200 TapeStation (Agilent Technologies). All procedures were performed according to the manufacturer's instructions. Total mRNA was converted to cDNA using GoScript Reverse Transcription (Promega TM). qPCR was performed using GoTaq Master Mix (Promega TM). The following targets were analyzed: 18s, RPLP0, Col1A1, Col1A2, MMP1and CCL2. The 18s-specific primers used were 5'-TGCCATCACTGCCATTAAG-3' (forward) and 5'-TGCTTTCCTCAACACCACATG-3' (reverse), the RPLP0-specific primers used were 5'-GCAGCATCTACAACCCTGAAG-3' (forward) and 5'-CACTGGCAACATTGCGGAC-3' (reverse), the Col1A1-specific primers used were 5'-CCCTCCTGACGCACGG-3' (forward) and 5'-GTGATTGGTGGGATGTCTTCGT-3' (reverse), the Col1A2-specific primers used were 5'-CTGTAAGAAAGGGCCCAGCC-3' (forward) and 5'-GACCCCTTTCTCCACGTGG-3' (reverse), the MMP1-specific primers used were 5'-GGAGGAAAAGCAGCTCAAGAAC-3' (forward) and 5'-TCCAGGGTGACACCAGTGACT-3' (reverse) and the CCL2-specific primers used were 5'-AACCACAGTTCTACCCCTGGG-3' (forward) and 5'-TAATGATTCTTGCAAAGACCCTCAA-3' (reverse). Samples were distributed in duplicate in a 384-well plate using an Epmotion 5073 automated pipetting system (Eppendorf). Real-time quantitative PCR was performed using a CFX384 thermocycler (Bio-Rad TM), the data were analyzed using Bio-Rad TM CFX Manager software (Bio-Rad TM). mRNA differential expression was evaluated according to the normalization of the mean housekeeping genes expression (18s and RPLP0) and the DMEM 10% FBS condition (ΔΔCt method: $2^{-\Delta\Delta Ct}$, $\Delta\Delta Ct = Ct_{target} - Ct_{mean\ 18s\ \&\ RPLP0} - Ct_{target\ DMEM\ 10\%\ FBS\ condition}$).

Statistical Analysis

Statistical analyses were performed using GraphPad Prism (La Jolla, CA). For populations who satisfied the Kolmogorov–Smirnov normality test, a two-tailed Student's t-test for unpaired or paired samples and one-way repeated-measures ANOVA test followed by the Bonferroni correction were used to compare the different populations according to the experimental design. When the normality test was not satisfied, the Mann-Whitney, Wilcoxon and Kruskal Wallis tests were used. Correlations were analyzed using the Spearman test. A p-value <0.05 was considered statistically significant.

RESULTS

Cohort Description

From December 2018 to December 2019, 96 SSc patients were included in this study. Approximately 2/3 of the cohort presented a limited form of the disease (n=57, 59%) while the rest of the patients had a diffuse form of the disease (n=39, 41%). The demographic characteristics and main clinical or biological features of the entire cohort are presented in **Table 1**. Thirty-two patients were treated with methotrexate, 22 patients received steroids, 13 patients received a targeted disease-modifying antirheumatic drugs (tDMARDs; eight Tocilizumab, three Rituximab, and two Baricitinib), 5 received mycophenolate mofetil (MMF), and 8 received Hydroxychloroquine (HCQ) at the time of collection. Thirty-seven sex-matched healthy donors (HDs) served as controls. Overall, healthy donors were on average younger than SSc patients (mean HD = 45 years *vs* mean SSc = 61 years). Nevertheless, MPs levels were previously reported as unaffected by age (24, 25) and when we analyzed total MPs, EMPs and PMPs in our cohorts of SSc patients and HD controls we haven't observed any correlation between MPs counts and age (**Figure S1**). Therefore, we have a large cohort of SSc patients with multiples phenotypes and treatments that can be extensively analyzed and compared to HD controls.

Circulatory MPs Are Increased in SSc Patients, Especially Those of Originating From Platelets

Plasma levels of MPs were assessed by flow cytometry. Anti-CD45, CD3, CD19, and CD66b antibodies labeled only a very minor MP fraction and were thus not retained in subsequent experiments (data not shown). Representative gating strategy of blood MPs was shown in **Figure 1A**. Even though mean levels of total MPs were not significantly different between SSc patients and HDs (mean ± SEM of 16859 ± 2528 MPs/µl *vs.* 10408 ± 1827 MPs/µl, respectively, data not shown), a higher proportion of SSc patients exhibited increased levels of MPs compared to HD (median of 8444 *vs.* 5331, **Figure 1B**, p=0.04). More than half of the patients presented over than 8,000 MPs/µl vs. one third of HDs. This increase was independent of the mechanism leading to their generation, since both MPs originating from dying (phosphatidylserine $(PS)^+$) (26) and living (PS^-) cells were significantly increased in SSc patients compared to HD (median of 429.0 MPs/µl *vs.* 208.5 MPs/µl, and of 5042 MPs/µl *vs.* 2217 MPs/µl, respectively, p<0.05, data not shown). Among total MPs, we particularly analyzed those originating from platelets (PMPs) and endothelial cells (EMPs). These two populations were defined by the absence of red blood cell marker (CD235) expression. PMPs were further characterized by the

TABLE 1 | Main characteristics of SSc patients included in the study.

	lcSSc (n=57)	dcSSc (n=39)	All SSc patients (n=96)	P
Age at onset, median ± SD years	61 (13.68)	62 (10.88)	59 (12.87)	ns
Gender (Female) (%)	51 (80.95)	16 (41.03)	67 (73.63)	0.02
Disease duration, mean ± SD years	7.89 ± 7.34	7.5 ± 5.55	7.77 ± 6.53	ns
MRSS, mean ± SD	4 ± 5.11	16.93 ± 10.03	8.4 ± 8.01	<0.0001
Active smokers (%)	17 (26.98)	8 (20.51)	25 (27.47)	ns
Active disease (%)	8 (12.7)	8 (20.51)	16 (17.58)	0.0795
Digestive disease (%)	28 (44.44)	17 (43.59)	45 (49.45)	ns
Cardiac involvement (%)	4 (6.35)	2 (5.13)	6 (6.59)	ns
Raynaud phenomenon (%)	55 (93.65)	25 (64.10)	84 (92.31)	ns
Digital ulcers (%)	6 (9.52)	8 (20.51)	14 (15.38)	0.0286
Synovitis/tenosynovitis (%)	15 (23.81)	4 (41.02)	19 (20.88)	ns
Interstitial lung disease (%)	17 (26.98)	16 (41.02)	33 (36.26)	0.009
TLC, mean ± SD	1.01 ± 0.15	0.95 ± 0.18	0.98 ± 0.18	ns
DLCO/VA, mean ± SD	0.67 ± 0.16	0.61 ± 0.19	0.65 ± 0.18	ns
FVC, mean ± SD	1.13 ± 0.21	0.88 ± 0.24	1.05 ± 0.25	<0.0001
PAPS, mean ± SD	32.8 ± 9.05	33 ± 10.4	32.87 ± 10.92	ns
ANA (%)	57 (100%)	39 (100%)	96 (100%)	ns
Anti-scl70 Ab (%)	5 (7.94)	19 (48.71)	20 (21.98)	<0.0001
Anti-centromeres Ab (%)	39 (61.9)	2 (5.13)	41 (45.05)	<0.0001
Anti-ARNpolIII Ab (%)	1 (1.59)	3 (7.69)	4 (4.4)	0.0849
Methotrexate (%)	19 (33.33)	13 (33.33)	32 (33.33)	ns
tDMARDs (%)	6 (10.53)	7 (17.95)	13 (13.54)	ns

SSc, Systemic Sclerosis; lcSSc, limited cutaneous systemic sclerosis; dcSSc, diffuse cutaneous systemic sclerosis; SD, standard deviation; mRSS, modified Rodnan skin score; TLC, total lung capacity; DLCO, volume-corrected carbon monoxide diffusing capacity; FVC, forced vital capacity; PAPs, systolic pulmonary arterial pressure; ANA, Anti-Nuclear antibody; Ab, antibody; tDMARDs, targeted disease-modifying antirheumatic drugs; ns, not significant.

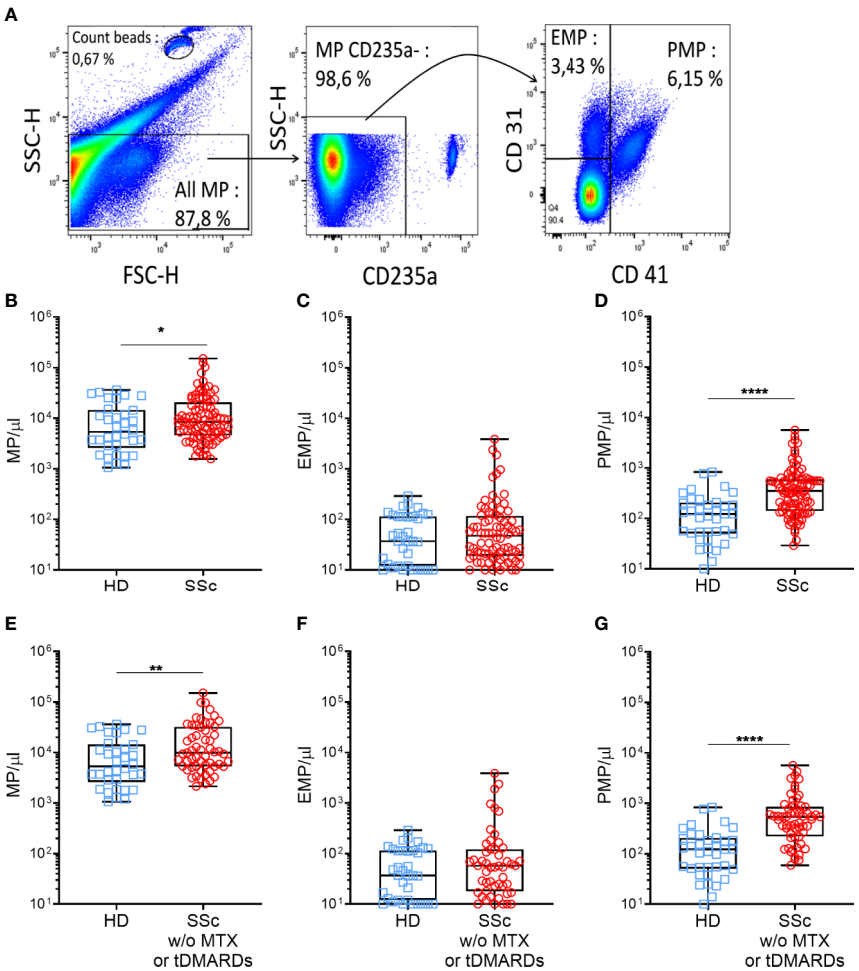

FIGURE 1 | Circulating MPs are increased in SSc patients compared to HD. MPs were gated on their scatter property, then among the CD235a-, the PMPs (CD41+) and the EMPs (CD41-CD31+) were defined **(A)**. Plasma MPs **(B)**, EMPs **(C)**, PMPs **(D)**, levels were compared between HDs and SSc patients (HDs = 37, SSc = 96). Same comparison of MPs **(E)**, EMPs **(F)** and PMPs **(G)** levels between HDs and SSc was made, taking into account only those patients not treated with methotrexate or tDMARDs (HDs = 37, SSc = 60); Box-plots represent the extreme values, the first and third quartiles and the medians. *p < 0.05 **(B)**, **p < 0.01 **(E)**, ****p < 0.0001 **(D, G)** by Mann-Whitney. MPs, microparticles; EMPs, endothelial cells derived microparticles; PMPs, platelets derived microparticles; HD, healthy donors; SSc, systemic sclerosis; MTX, methotrexate; tDMARDS, targeted disease-modifying antirheumatic drugs.

expression of CD41, with or without CD31, and EMPs by the expression of CD31 without CD41 (**Figure 1A**). Although no overall difference in EMPs concentration between HD and SSc was observed (**Figure 1C**), PMPs concentration was significantly higher in SSc patients compared to HD (median of 352.0 *vs* 122.0 PMPs/µl, respectively, **Figure 1D**, $p<0.0001$). The numbers of these PMP were elevated in SSc patients regardless of their PS expression (median of 108 PMPs PS^-/µl *vs*. 50 PMPs PS^-/µl, and of 192 PMPs PS^+/µl *vs*. 88 PMPs PS^+/µl, respectively, p<0.001, data not shown).

We next investigated whether specific therapeutic regimens administered to SSc patients could impact MPs circulatory levels. As shown in **Figure S2A**, total MPs concentration did not differ between patients without immunosuppressive (IS) therapy (10512 MPs/µl), with corticosteroids (9379 MPs/µl), with non-specific immunosuppressive drugs including MMF (7188 MPs/µl), HCQ (9385 MPs/µl) or methotrexate (7693 MPs/µl) and those with tDMARDs (8878 MPs/µl). While total MPs (**Figure S2A**) and EMPs concentration (data not shown) were similar in treated and untreated patients, PMPs concentration was significantly decreased in patients treated with methotrexate and tDMARDs, compared to untreated patients (median of 230 PMPs/µl, 187 PMPs/µl, and 544 PMPs/µl, respectively, p<0.01, **Figure S2B**). Based on these observations and to avoid any confounding effect of the patient's treatment regimens, we excluded from our initial comparison patients treated by methotrexate or tDMARDs (n=36). As shown in **Figures 1E, G**, we observed a greater increase in total MPs (mean ± SEM of 21567 ± 3686 MPs/µl *vs*. 10408 ± 1827 MPs/µl, respectively, p<0.01, **Figure 1E**) and PMPs (mean ± SEM of 828.6 ± 141.4 *vs* 167.0 ± 30.76 PMPs/µl, respectively, $p<0.0001$, **Figure 1G**) concentrations in SSc patients compared to HD controls.

However, irrelevant of the treatment, EMPs concentration between SSc patients and HD controls remained comparable (**Figure 1F**). Altogether, these results indicate an increase of circulatory MPs in SSc patients, in particular of those with a platelet origin, questioning their association to specific clinical features of SSc patients and their functional role in SSc pathogenesis.

High MPs Concentrations Are Associated With Severe SSc Phenotypes

To evaluate the impact of MPs on SSc pathogenesis, we evaluated if there were any associations and/or correlations between circulating MPs numbers and patients' clinical parameters, particularly among patient not treated with methotrexate or tDMARDs. No correlation was observed between total circulatory MPs levels and mRSS, or the limited or diffuse form of the disease (median of 9815 MPs/µl *vs.* 9947 MPs/µl, respectively, data not shown), or even with the SSc serology (data not show). There were also no association between circulatory MPs levels and disease duration, presence of active smoking, heart disease, gastrointestinal involvement, synovitis or tenosynovitis (data not shown). We observed a weak but significant inverse correlation between Raynaud's phenomenon duration and EMPs concentration ($r=-0.369$, $p=0.01$, data not shown) while no association were observed between SSc patients' clinical parameters tested and PMPs levels (data not shown). Moreover, we observed a significant association between total MPs concentration and the pulmonary disease. Indeed, a higher concentration of MPs was observed for patients with ILD on HRCT, compared with other SSc patients and HD (median of 10880 MPs/µl vs 6700 MPs/µl vs 5331 MPs/µl, respectively, **Figure 2A**, $p<0.05$). Looking at patients without PAH, those with ILD present a higher EMPs concentration than the other SSc patients and HD (median of 69 EMP/µl vs 18 EMP/µl vs 37 EMP/µl, $p<0.01$ and $p<0.05$, respectively, Data not shown). Furthermore, SSc patients with lung fibrosis showed as well elevated MPs concentration compared to patients without lung fibrosis (median of 17,177 vs 8,052, respectively, **Figure 2B**, $p<0.05$). Accordingly, total MPs concentration was inversely correlated to SSc patients' respiratory function tests (RFT). Particularly, total MPs levels were moderately but significantly inversely correlated with Total Lung Capacity (TLC; $r=-0.3934$, $p<0,005$, **Figure 2C**) and forced vital capacity ($r=-0.4376$, $p<0,005$, **Figure 2D**). Although weak, we also observed a significant inverse correlation of the total MPs concentration to the volume-corrected carbon monoxide diffusing capacity (DLCO/VA; $r=-0.3274$, **Figure 2E**, $p<0.05$). EMPs level was also weakly but significantly inversely correlated with FVC ($r=-0.3312$, $p<0,05$, data not shown). No other correlations between MPs, EMPs or PMPs with clinical features were observed. Vascular damage was also associated to total MPs levels, as they were significantly higher in SSc patients with active digital ulcers (DU), at the time of sampling, than in the rest of the patients (median of 27275 MPs/µl *vs.* 7504 MPs/µl, **Figure 2F**, $p<0.01$). Among patients without ILD, patients with high PAH were more likely to present high levels of MPs (median of 22237 MPs/µl *vs.* 6666 MPs/µl, $p<0.05$, respectively, **Figure 2G**) and high levels of EMPs (median of 152 EMPs/µl *vs.* 21 MPs/µl, $p<0.01$, respectively, Data not shown). Taken together, these results suggest that total circulating MPs and EMPs are associated with ILD and vascular damage.

MPs From SSc Patients Induce a Profibrotic Profile in Human Dermal Fibroblasts

MPs were differently represented in HD and SSc patients and the accumulation of MPs in SSc patients correlates with certain clinical features associated with tissue fibrosis. Therefore, we assessed whether MPs may directly contribute to tissue fibrosis through the production of extra cellular matrix (ECM) by dermal fibroblasts. We thus examined the expression of the genes involved in collagen synthesis (Collagen Type I Alpha 1, Col1a1, and Collagen Type I Alpha 2, Col1a2) or its degradation (Matrix Metallopeptidase 1, MMP1) and in recruitment of immune cells (C-C Motif Chemokine Ligand 2, CCL2) in HD dermal fibroblasts upon stimulation with HD or SSc patients-derived MPs.

Dermal HD fibroblasts were first stimulated with the transforming growth factor (TGF)-β as a positive control. As expected, TGFβ induced Col1a1 (mean ± SEM of fold change: 2.33 ± 0.39-fold increase *vs.* the medium condition, **Figure S3A**) and Col1a2 (2.03 ± 0.34-fold increase *vs.* the medium condition, **Figure S3A**) mRNA expression in HD dermal fibroblasts while MMP1 and CCL2 were only slightly affected. To further address the reproducibility of the fibroblast co-culture with MPs, we repeated the co-culture three times, using fibroblasts from three healthy donors and different concentration of purified total MPs from a single healthy donor. We did not observe any significant variation in the expression of mRNAs coding for Col1a1, Col1a2 and CCL2 (**Figures S3B, C, E**). Concerning the expression of MMP1, we observed an increase of mRNA expression although not significant (mean ± sem of fold change for 10 MPs/µl: 1.62 ± 0.25; for 100 MPs/µl: 2.12 ± 0.34; for 1,000 MPs/µl: 1.50 ± 0.09, **Figure S2D**). These optimization steps, showed that fibroblasts responded as expected to TGFβ stimulation and that the impact of HD MPs on fibrotic properties was stable in our experimental settings, allowing us to further evaluate the fibrotic potential of SSc patients-derived MPs.

Therefore, we stimulated HD dermal fibroblasts with increasing numbers of MPs from healthy donors and SSc patients (**Figure 3**). We tested MPs from three HD and three SSc patients at the three concentrations that were previously used during the optimization step. As expected, we did not observed any effect of MPs from HD on Col1a1 (mean ± sem of fold change for 10 MPs/µl: 1.18 ± 0.14; for 100 MPs/µl: 1.21 ± 0.19; for 1,000 MPs/µl: 1.19 ± 0.08, **Figure 3A**) and Col1a2 (mean ± sem of fold change for 10 MPs/µl: 1.46 ± 0.43; for 100 MPs/µl: 1.16 ± 0.16; for 1,000 MPs/µl: 1.81 ± 1.37, **Figure 3B**), at the tested concentrations. This was also true for MMP1 (mean ± sem of fold change for 10 MPs/µl: 1.02 ± 0.22; for 100 MPs/µl: 1.19 ± 0.36; for 1,000 MPs/µl: 0.97 ± 0.26, **Figure 3C**) and CCL2 expression (mean ± sem of fold change for 10 MPs/µl: 0.69 ±

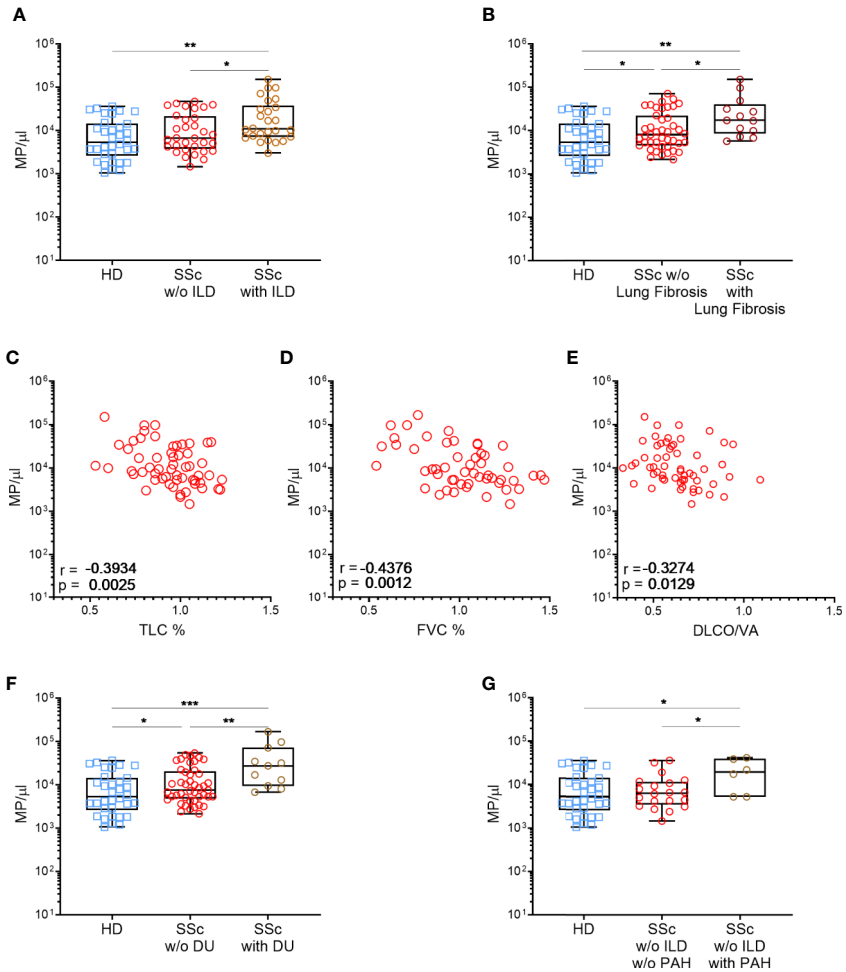

FIGURE 2 | High MPs concentrations are associated with severe SSc phenotypes. Circulating MPs were compared between HD, patients with and without diffuse interstitial lung disease [Normal = 32, interstitial lung disease = 26; **(A)**], and lung fibrosis [HD = 37, SSc =43, SSc with lung fibrosis=13; **(B)**]. The concentration of circulating MPs is compared to the lung function test of SSc patients (SSc=59): TLC **(C)**, FVC **(D)** and DLCO/VA **(E)**. Circulating MPs were compared between HD, patients with or without vascular injury like digital ulcers [HD = 37, SSc =47, SSc with digital ulcers = 11; **(F)**] or pulmonary arterial hypertension without interstitial lung disease [HD = 37, SSc = 20, SSc with PAH = 6; **(H)**]. In **(A**, **B**, **F**, **G)** symbols represent individual subjects; Box-plots represent the extreme values, the first and third quartiles and the medians. In **(C–E)**, Correlations were determined using Spearman's test. *p<0.05 by Mann-Whitney **(A–C, F–H)**, **p<0.01 by Mann-Whitney **(A–E, G)**, ***p<0,001 **(G)**. MPs, microparticles; HD, healthy donors; SSc, systemic sclerosis; ILD, interstitial lung disease; TLC, total lung capacity; FVC, forced vital capacity; DLCO/VA, diffusing capacity of the lung for carbon monoxide; DU, active digital ulcers; PAH, pulmonary arterial hypertension.

0.35; for 100 MPs/µl: 1.01 ± 0.10; for 1,000 MPs/µl: 0.93 ± 0.06, **Figure 3D**).

Conversely, MPs from SSc patients upregulated Col1a1 (mean ± sem of fold change for 10 MPs/µl: 1.41 ± 0.37; for 100 MPs/µl: 2.03 ± 0.35; for 1,000 MPs/µl: 2.47 ± 0.7, **Figure 3A**) and Col1a2 expression (mean ± sem of fold change for 10 MPs/µl: 3.74 ± 1.00; for 100 MPs/µl: 6.56 ± 1.95; for 1,000 MPs/µl: 8.32 ± 3.32, **Figure 3B**) in a dose dependent manner. MMP1 (mean ± sem of fold change for 10 MPs/µl: 1.25 ± 0.05; for 100 MPs/µl: 1.41 ± 0.05; for 1,000 MPs/µl: 0.92 ± 0.19, **Figure 3C**) and CCL2 expression (mean ± sem of fold change for 10 MPs/µl: 0.80 ± 0.01; for 100 MPs/µl: 0.78 ± 0.08; for 1,000 MPs/µl: 1.23 ± 0.08, **Figure 3D**), as with HD MPs, were not affected by SSc MPs.

Given the dose dependent impact of SSc MPs on the fibrotic potential of fibroblasts, we decided to extend our analysis using the highest concentration of MPs (1,000/µl) to 12 HD and 12 SSc patients. We observed a significant increase of Col1a1 and CCL2 expression induced by MPs from SSc patients compared to HD (median of 1.55 *vs.* 1.06 for Col1a1, respectively, p<0.05, **Figure 3E**, and median of 1.21 *vs.* 0.98, for CCL2, respectively, p<0.05, **Figure 3H**), and a trend toward for the increased of Col1a2 expression induced by MPs from SSc patients compared to HD (median of 2.05 *vs.* 0.935, respectively, p=0.1, **Figure 3F**). We haven't observed any difference between MPs from SSc patients and HD on MMP1 expression (median of 1.23 *vs.* 1.54, respectively, **Figure 3G**). Our findings thus suggest that MPs

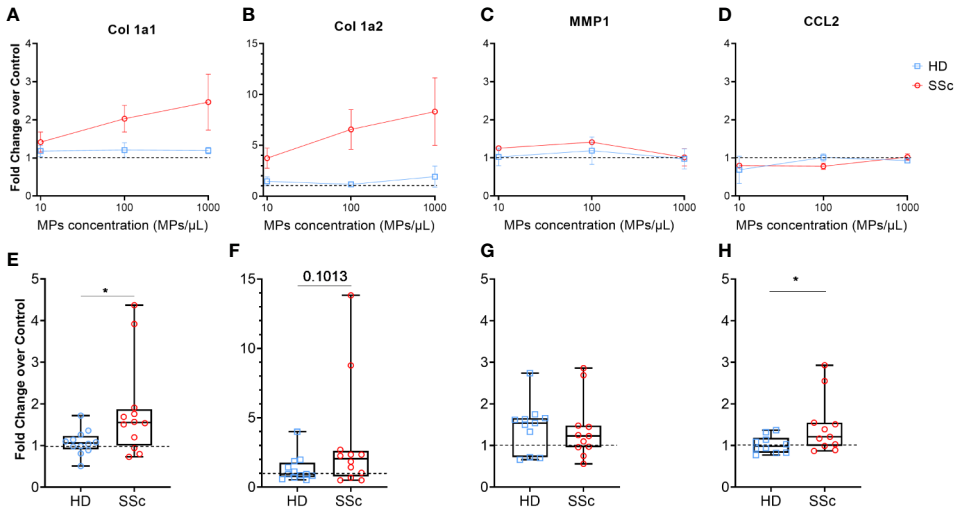

FIGURE 3 | MPs activated human dermal fibroblasts to produce extracellular matrix. Levels of Col1A1 mRNA **(A, E)**, Col1A2 **(B, F)**, MMP1 **(C, G)** and CCL2 **(D, H)** expression were assessed in fibroblasts stimulated with an increasing concentration of MPs from HD (n = 3) and from SSc patients (n= 3) **(A–D)**, or with 1,000 MPs/µl of HD (n=12) or SSc (n=12) **(E–H)** by reverse transcriptase quantitative polymerase chain reaction (RT qPCR) and expressed in ΔΔCt toward housekeeping gene and DMEM 10% FBS. The dashed line represents the fibroblast condition treated only with DMEM 10% FBS; In **(A–D)**, Dot and error bars show the meanSEM. In **(E–H)**, Box-plots represent the extreme values, the first and third quartiles and the medians. *p < 0.05 **(A, D, E, H)** by Mann-Whitney test. MPs, microparticles; HD, healthy donors; SSc, systemic sclerosis; Col1a1, Type 1 Collagen a1; Col1a2, Type 1 Collagen a2; MMP1, Matrix Metallopeptidase 1; CCL2, C-C Motif Chemokine Ligand 2; FBS, fetal bovine serum.

from SSc patients promote a pro-fibrotic response in human dermal fibroblasts.

Differential Profibrotic Effects of MPs According to SSc Patients Disease Duration, Presence of Pulmonary Fibrosis, and Treatment With Methotrexate

We next investigated whether the profibrotic effect of MPs that we observed was associated to any clinical parameters in the 12 SSc patients tested. For this purpose, the profibrotic potential of MPs from HD and SSc patients was expressed as the ratios between Col1a1/MMP1 or Col1a2/MMP1 expression.

First, we compared the MPs profibrotic effect based on whether they were coming from patients that have been diagnosed with another symptoms than Raynaud phenomenon for less than 3 years (early disease) or for more than 3 years (late disease). We observed that Col1a1/MMP1 and Col1a2/MMP1 ratios were increased when HD fibroblast were stimulated with MPs from SSc patients with a longer disease duration compared to those with a shorter disease duration (median of 1.60 *vs.* 0.60, respectively, p<0.05, **Figure 4A** and 4.80 *vs.* 0.82, p<0.01, respectively, **Figure 4B**). Conversely, we observed a statistically higher expression of CCL2 for patients with a shorter disease duration compared to patients with a longer disease duration, which showed a similar profile than healthy donors (median of 1.53 *vs.* 1.03 *vs.* 0.96, respectively, p<0.05 & p<0.005, **Figure 4C**).

Next, we distinguished between patients with and without pulmonary fibrosis. Similarly, MPs isolated from SSc patients with lung fibrosis showed a greater profibrotic profile, with an upward trend for Col1a1/MMP1 (median of 1.59 *vs.* 0.65, p=0.1, **Figure 4D**) and Col1a2/MMP1 ratio (median of 2.42 *vs.* 0.91, p=0.07, **Figure 4E**), but reduced ability to induce CCL2 (median of 0.89 *vs.* 1.51, p<0.05, **Figure 4F**).

Among the tested patients, none were treated by tDMARDs, but 6 was treated with methotrexate. Interestingly, when we compared MPs from patients treated or not with methotrexate, we observe the opposite results to our previous observations. Indeed, MPs from SSc patients treated with methotrexate showed a reduced profibrotic potential, with Col1a1/MMP1 and Col1a2/MMP1 ratios close to those of HD (median of 0.49 *vs.* 0.68, respectively, **Figure 4G** and median of 0.72 *vs.* 0.98, respectively, **Figure 4H**), while they upregulated CCL2 expression, compared to the untreated patients and HD (median of 2.05 vs. 1.10 vs. 0.96, respectively, p<0.05 and p<0.005, **Figure 4I**).

Thus, patients with a longer disease duration and with a lung fibrosis have MPs that display an elevated profibrotic potential, and treatment with methotrexate seems to limit MPs profibrotic potential.

DISCUSSION

In our study, we have shown that there is an increase in circulatory MPs in SSc patients especially those shedding from platelets, but not from EC, compared to HD. This increase is especially observed in patients without methotrexate or

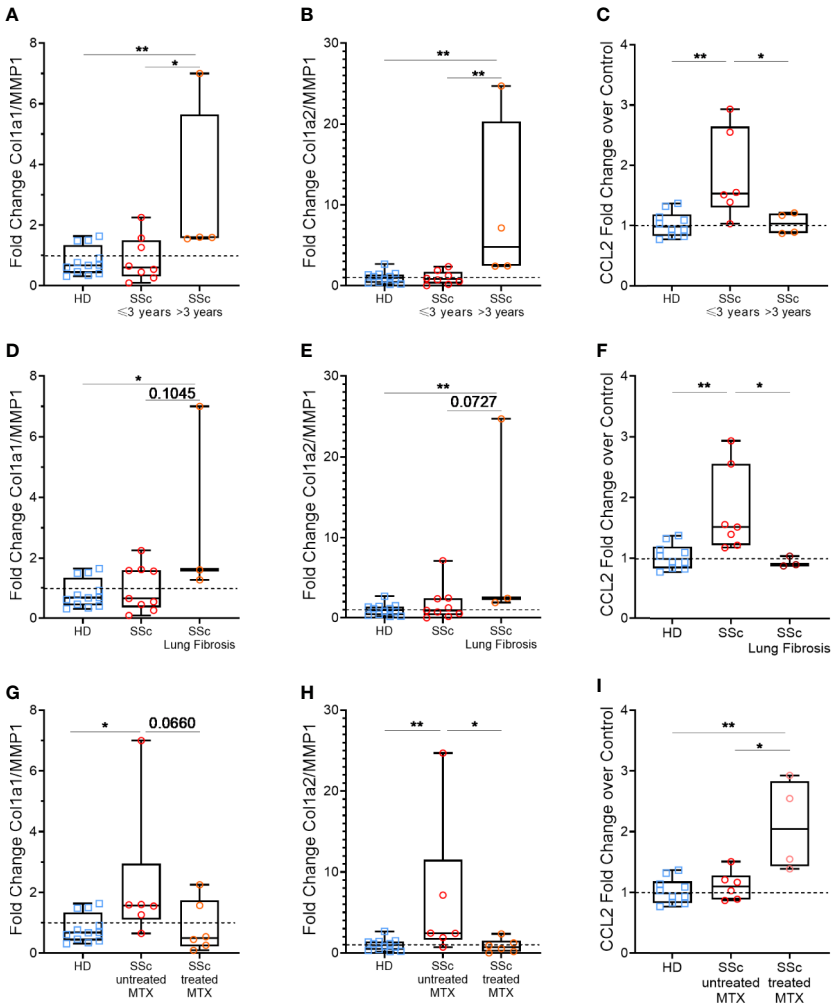

FIGURE 4 | Effects of patients' according to clinical features: disease duration, pulmonary fibrosis and methotrexate intake. Levels of Col1A1 mRNA, Col1A2, MMP1, and CCL2 were assessed in fibroblasts stimulated with 1,000 MPs/µl of HD (n=12) or SSc (n=12) by reverse transcriptase quantitative polymerase chain reaction (RT qPCR) and expressed as a Col1a1/MMP1 **(A, D, G)** or Col1a2/MMP1 ratio **(B, E, H)**, or in relation to ΔΔCt for housekeeping gene and for DMEM 10% FBS as the baseline condition for CCL2 **(C, F, I)**. Then, for each analysis, we compared the effect of MPs from HD or SSc patient according to different clinical parameters: duration between the onset of the first symptoms other than Raynaud's phenomenon less than (n=8) or greater than (n=4) 3 years **(A–C)**, presence (n=3) or absence (n=9) of lung fibrosis **(D–F)** and patients treated (n=6) or not treated (n=6) with methotrexate **(G–I)**. The dashed line represents the fibroblast condition treated only with DMEM 10% FBS; Box-plots represent the extreme values, the first and third quartiles and the medians. **p < 0,01 **(A–C, E, F, H, I)**, *p < 0.05 **(A, C, D, F–I)** by Mann-Whitney test. MPs, microparticles; HD, healthy donors; SSc, systemic sclerosis; Col1a1, Type 1 Collagen a1; Col1a2, Type 1 Collagen a2; MMP1, Matrix Metallopeptidase 1; CCL2, C-C Motif Chemokine Ligand 2; MTX, methotrexate; FBS, fetal bovine serum.

tDMARDs. We also demonstrated a profibrotic effect of MPs on dermal fibroblasts specifically of those from SSc patients.

Our results on PMPs were comparable to the study of Nomura et al. that showed increased levels of PMPs in 42 SSc patients compared to 30 HD (15). They also showed an increase in monocytes-derived MPs, however due to the detection of low number of MPs derived from immune cells, we were unable to quantify monocytes-derive MPs in our cohort.

Interestingly, we found in patients treated with immunosuppressive agents such as methotrexate or tDMARDs, that there was a decrease in circulatory PMP concentration. Two tDMARDs used in SSc patients, tocilizumab or baricitinib, target respectively IL6 receptor and the Jak1-2 Stat3 signaling pathway that indirectly affects IL6 and type I interferon signaling. Furthermore, methotrexate was also previously reported to reduce the IL6 expression in rheumatoid arthritis patients (27–29). It was previously reported that IL6 circulatory levels, in patients with coronary heart disease, are correlated to PMP and EMP levels (30). Therefore, blocking this IL6 pathway either directly or indirectly may affect MPs shedding.

Altogether, observations in human studies on MPs are heterogenous due to low number of patients, specific disease

subtypes and technical procedures, but our results provide robust data on a large number of patients that reinforce and clarify existing data (31). Elevated levels of total MPs and EMPs were associated with an interstitial lung disease phenotype and were inversely correlated with respiratory function test, suggesting their involvement in the pathophysiology of the disease. Additionally, we confirmed that total MPs and EMPs counts were associated to PAH as already described on a very small cohort of SSC patients (17). Total MP were also associated to digital ulcers, reinforcing their potential role in the vasculopathy. Prospective studies are ongoing to identify whether more than being a witness, MPs levels could help to predict the onset of severe complications of SSc notably vascular such as PAH or digital ulcers. In the majority of our analyses, it is the total MPs level that is significantly associated with SSc patients' clinical parameters studied, and to lesser extent EMPs. We did not find any association between circulatory PMP levels and the vascular or fibrotic features of SSc patients. Among the $CD235a^-$ MPs, EMP and PMP proportion represent less 10-20% of total MPs, which means that the cellular origin of almost 80-90% MPs has unfortunately not been identified. Identifying the remaining fraction of MP would be of great interest to further identify the source of circulatory MPs that are pathogenic in SSc patients. Another hypothesis would be that, rather than the number of individual MPs, their content would be of major importance. Accordingly PMPs associated HMGB1was recently shown to contribute to vasculopathy during SSc by Maugeri et al. (16). PMPs from SSc patients induced neutrophil activation and the extrusion of NETS in a HMGB1-dependent manner which consequently induced endothelial cell damage and subsequent fibrosis in mice. However, the *in vivo* experiments were conducted using injection of human MPs in a mouse strain lacking adaptive immunity that limits the full elucidation of the role of MPs during the course of SSc either on vascular damage and fibrosis and no specific association between HMGB1 content on PMPs with SSc patients clinical outcomes were established. Therefore our results suggest a more direct role of MPs in SSc pathophysiology, however it will be of great importance to analyze MPs content in our patients and seek any association with clinical parameters in order to shed light on mechanisms of MPs profibrotic properties.

A previous study has described that EMPs from idiopathic pulmonary fibrosis patients stimulated the migration of normal human lung fibroblast (32) and other reports suggest direct implication of MP in fibrosis genesis, through their content or their surface markers [DAMPs, metabolite implied in the ROS production or nuclear factor B pathway, plasmin expression etc.; (33)]. Another recent observation, provided by Wermuth et al., show the profibrotic effect of exosomes from SSc patients (34). Interestingly, the authors showed that SSc exosome had a profibrotic effect in a dose response dependent, especially on Col1a1 expression. Here, we provide new evidence that purified MPs from SSc patient exert a pro-fibrotic impact on human primary fibroblasts compared to MPs from HD, notably in the induction of type 1 collagen expression, but also in the recruitment of the immune system by increasing CCL2 expression. Our results, in addition to exosome's profibrotic effect already published, reinforce the role of extracellular vesicles, like exosomes or MPs, on fibrosis induction during SSc. Our *in-vitro* data are in accordance with our observations that increased circulatory MPs numbers in SSc patients are associated to lung fibrosis, such as fibrotic lung disease in HRCT, DLCO/VA and dyspnea. So far MPs role in SSc lung fibrosis was described to be indirect, through neutrophils activation (16) and endothelial cells damage being followed by pulmonary fibrosis (17). In accordance with our results, it was recently been demonstrated that plasma MPs containing mitochondrial DNA were increase in SSc patient with ILD, and stimulated inflammatory responses that may contribute to lung fibrosis (18). Our data shed new light on the potential direct contribution of MPs to lung fibrosis by modulating fibroblast activation.

Finally, we have observed differential pro-fibrotic effects of MPs according to clinical manifestations of SSc patients. Among them, MPs from patients with a longer disease duration or pulmonary fibrosis presented a higher profibrotic profile and a lesser capacity to express CCL2, implied in the recruitment of immune cells. Interestingly the response induced by MPs from patients treated with methotrexate on HD fibroblast did not impact CM production by fibroblasts as MPs purified from HD. Patients treated with methotrexate show less MPs or PMPs and those MPs are also less pro-fibrotic. Direct action of methotrexate on fibroblast-like synovial cells has already been described in rheumatoid arthritis (35), showing the importance of its action on the extracellular matrix, and this drug is given as a first-line treatment for early cutaneous sclerosis (36). We observed that methotrexate treatment increases the potential of SSc patients MPs to induce CCL2 a chemokine involved in the recruitment of immune cells, which may seem contradictory in light of what has already been described (37). One interesting avenue to study would be the impact of methotrexate on the MPs content, particularly their load of DNA. Methotrexate is a dihydrofolate reductase inhibitor, enzyme involved in the reduction of folic acid to tetrahydro-folic acid and then to folinic acid, and inhibits amido-phosphoryl transferase which converts phosphoribosyl-pyrophosphate to phosphoribosylamine, implied in the formation of inosine monophosphate (IMP). These two mechanisms of action leading to a decrease in the formation of purine base and thymidine, inhibit the formation of DNA and RNA. Given That, methotrexate may impact the overall DNA and RNA content of MPs. This observation is in line with the work of Ryu et al. on the link between MPs containing mitochondrial DNA from SSc patients and ILD (18). Wermuth et al. showed that exosomes purified from SSc patients have altered profile of microRNA (miRNA) derived from several anti and pro-fibrotic genes (34). They observed an increase of six profibrotic miRNA and a decrease of ten antifibrotic miRNA in SSc exosomes compared to HD. It is tempting to speculate that methotrexate might modify RNA or miRNA content in SSc derived exosomes. Whether MPs have similar miRNA alterations and whether

methotrexate could impact is still to be explored. Although these results are in line with our observation indicating that MPs levels are associated with lung fibrosis, it appears that given the small number of patients tested (n=12), possible bias may exist. The representativity of patients in the study is not ideal, we need to increase the patients' number, notably to ascertain the impact of methotrexate on MPs fibrotic potential. In addition, pro-fibrotic effect of the MPs that we showed was obtained using skin fibroblasts. However, our results show mostly an association with lung disease. Thus it would be relevant to address the impact of MPs also on lung fibroblasts. Apart from this direct role, it is worthwhile to pursue the study of the indirect and complementary role of MPs. Polymorphisms in the gene encoding the secreting desoxyribonuclease DNASE1L3 have been observed in both SSc and SLE diseases, suggesting a new potential common pathway important for the loss of tolerance (38, 39). DNASE1L3 is specifically secreted by macrophages and dendritic cells, and with DNase1, is responsible for the entirety of DNase activity in the serum (40). Sisirak et al. recently showed that the loss of DNASE1L3 in mice causes a rapid antibody response to double stranded DNA and chromatin (41). Mechanistically, DNASE1L3 was shown to digest chromatin in apoptotic cell-derived MPs, and its absence and/or downregulation caused the accumulation of DNA within MPs that ultimately lead to the break of tolerance to self-DNA. Reduction of DNASE1L3 activity in SSc could be responsible for the accumulation of immunogenic MPs that may represent the initial process governing the occurrence of inflammatory process in human, and eventually play a role as pro-fibrotic factors.

In conclusion, we show that circulatory MPs were increased in SSc patients, especially those with ILD, lung fibrosis and vasculopathy. Moreover, it seems that immunosuppressive treatments present an impact on their concentration. In contrast to HD MPs, MPs from SSc patients induced the extracellular matrix production and the CCL2 gene expression. To establish the potential of MPs as a biomarker in vascular or fibrotic phenotype in SSc, analysis of longitudinal cohorts should be performed to uncover potential correlations with disease severity or prognosis. Moreover, in-depth subtyping of the pro-fibrotic MPs and unraveling mechanisms involved in their production could pave the road to new therapeutic avenues.

DATA AVAILABILITY STATEMENT

All datasets generated for this study are included in the article/ **Supplementary Material**.

ETHICS STATEMENT

The studies involving human participants were reviewed and approved by CPP, SUD-EST IV, 18/024. The patients/ participants provided their written informed consent to participate in this study.

AUTHOR CONTRIBUTIONS

DL, VS, CC-B, and M-ET designed the experiments. DL, ELe, and PL performed the experiments. VS, CR, ELa, PD, PB, CC-B, and M-ET wrote the paper. All authors contributed to the article and approved the submitted version.

FUNDING

This work was supported by the Fondation pour la recherche Médicale (FRM) and the Association des Sclérodermiques de France (ASF).

ACKNOWLEDGMENTS

We thank the TBMCore cytometry and qPCR platforms of the University of Bordeaux for their help in the realization of this work, Thomas Barnetche and Gael Galli for their help and advice.

SUPPLEMENTARY MATERIAL

The Supplementary Material for this article can be found online at: https://www.frontiersin.org/articles/10.3389/fimmu.2020.532177/full#supplementary-material

SUPPLEMENTARY FIGURE 1 | Correlation between age and MPs levels. Levels of total MPs **(A, D)**, EMPs **(B, E)** and PMPs **(C, F)** from HD **(A–C)** and SSc patients **(D–F)** were put in relation to the age of the subject at the time of sampling. Correlation was determined using Spearman's test. MPs, microparticles; EMPs,: endothelial cells derived microparticles; PMPs, platelets derived microparticles; HD, healthy donors; SSc, systemic sclerosis.

SUPPLEMENTARY FIGURE 2 | Effects of immunosuppressant agents on level of circulatory MPs. Circulatory MPs and PMPs levels were compared between HD, SSc patients without immunosuppressive therapy, with steroids, hydroxychloroquine, mycophenolate mofetil, methotrexate and tDMARDs. Box-plot represents the extreme values, the first and third quartile and the median. ***p<0,0005 **(D)**, **p<0,001 **(C)** by Mann-Whitney. MPs, microparticles; PMPs, platelets derived microparticles; HD, healthy donors; SSc, systemic sclerosis; w/o IS, without immunosuppressor; HCQ, hydroxychloroquine; MMF, mycophenolate mofetil; MTX, methotrexate; tDMARD,: targeted disease-modifying antirheumatic drugs.

SUPPLEMENTARY FIGURE 3 | Positive and reproducibility controls of fibroblasts and MPs co-culture. Levels of Col1A1 mRNA, Col1A2, MMP1 & CCL2 were assessed in fibroblasts stimulated with TGF as a positive control (10 ng/ml, n=4; **A**). The same levels of Col1A1 mRNA **(B)**, Col1A2 **(C)**, MMP1**(D)** & CCL2 **(E)** were assessed in fibroblasts stimulated with an increasing concentration of MPs of the same HD three times to test the reproducibility of the experience. The analysis was carried out by reverse transcriptase quantitative polymerase chain reaction (RT qPCR) and expressed in relation to ΔΔCt for DMEM as the baseline condition. The dashed line represents the fibroblast condition treated only with DMEM 10% FBS. Dot and error bars show the meanSEM. MPs, microparticles; Col1a1, Type 1 Collagen a1; Col1a2, Type 1 Collagen a2; TGFβ, Tumor Growth Factor ; MMP1, Matrix Metallopeptidase 1; CCL2, C-C Motif Chemokine Ligand 2; HD, healthy donors.

REFERENCES

1. Truchetet M-E, Demoures B, Eduardo Guimaraes J, Bertrand A, Laurent P, Jolivel V, et al. Platelets Induce Thymic Stromal Lymphopoietin Production by Endothelial Cells: Contribution to Fibrosis in Human Systemic Sclerosis. *Arthritis Rheumatol (Hoboken NJ)* (2016) 68(11):2784–94. doi: 10.1002/art.39817
2. Mostmans Y, Cutolo M, Giddelo C, Decuman S, Melsens K, Declercq H, et al. The role of endothelial cells in the vasculopathy of systemic sclerosis: A systematic review. *Autoimmun Rev* (2017) 16(8):774–86. doi: 10.1016/j.autrev.2017.05.024
3. Turpin D, Truchetet M-E, Faustin B, Augusto J-F, Contin-Bordes C, Brisson A, et al. Role of extracellular vesicles in autoimmune diseases. *Autoimmun Rev* (2016) 15(2):174–83. doi: 10.1016/j.autrev.2015.11.004
4. Scherlinger M, Guillotin V, Truchetet M-E, Contin-Bordes C, Sisirak V, Duffau P, et al. Systemic lupus erythematosus and systemic sclerosis: All roads lead to platelets. *Autoimmun Rev* (2018) 17(6):625–35. doi: 10.1016/j.autrev.2018.01.012
5. Arraud N, Linares R, Tan S, Gounou C, Pasquet J-M, Mornet S, et al. Extracellular vesicles from blood plasma: determination of their morphology, size, phenotype and concentration. *J Thromb Haemostasis* (2014) 12(5):614–27. doi: 10.1111/jth.12554
6. Michalska-Jakubus M, Kowal-Bielecka O, Smith V, Cutolo M, Krasowska D. Plasma endothelial microparticles reflect the extent of capillaroscopic alterations and correlate with the severity of skin involvement in systemic sclerosis. *Microvascular Res* (2017) 110:24–31. doi: 10.1016/j.mvr.2016.11.006
7. Colombo M, Raposo G, Théry C. Biogenesis, secretion, and intercellular interactions of exosomes and other extracellular vesicles. *Annu Rev Cell Dev Biol* (2014) 30:255–89. doi: 10.1146/annurev-cellbio-101512-122326
8. Pisetsky DS, Gauley J, Ullal AJ. Microparticles as a source of extracellular DNA. *Immunol Res* (2011) 49(0):227–34. doi: 10.1007/s12026-010-8184-8
9. Mobarrez F, Vikerfors A, Gustafsson JT, Gunnarsson I, Zickert A, Larsson A, et al. Microparticles in the blood of patients with systemic lupus erythematosus (SLE): phenotypic characterization and clinical associations. *Sci Rep* (2016) 6:36025. doi: 10.1038/srep36025
10. Guiducci S, Distler JHW, Jüngel A, Huscher D, Huber LC, Michel BA, et al. The relationship between plasma microparticles and disease manifestations in patients with systemic sclerosis. *Arthritis Rheumatol* (2008) 58(9):2845–53. doi: 10.1002/art.23735
11. McCarthy EM, Moreno-Martinez D, Wilkinson FL, McHugh NJ, Bruce IN, Pauling JD, et al. Microparticle subpopulations are potential markers of disease progression and vascular dysfunction across a spectrum of connective tissue disease. *BBA Clin* (2017) 7:16–22. doi: 10.1016/j.bbacli.2016.11.003
12. Jung C, Drummer K, Oelzner P, Figulla HR, Boettcher J, Franz M, et al. The association between endothelial microparticles and inflammation in patients with systemic sclerosis and Raynaud's phenomenon as detected by functional imaging. *Clin Hemorheol Microcirc* (2015) 61(3):549–57. doi: 10.3233/CH-151956
13. Benyamine A, Magalon J, Sabatier F, Lyonnet L, Robert S, Dumoulin C, et al. Natural Killer Cells Exhibit a Peculiar Phenotypic Profile in Systemic Sclerosis and Are Potent Inducers of Endothelial Microparticles Release. *Front Immunol* (2018) 9:1665. doi: 10.3389/fimmu.2018.01665
14. Kavian N, Marut W, Servettaz A, Nicco C, Chéreau C, Lemaréchal H, et al. Pantethine Prevents Murine Systemic Sclerosis Through the Inhibition of Microparticle Shedding. *Arthritis Rheumatol (Hoboken NJ)* (2015) 67(7):1881–90. doi: 10.1002/art.39121
15. Nomura S, Inami N, Ozaki Y, Kagawa H, Fukuhara S. Significance of microparticles in progressive systemic sclerosis with interstitial pneumonia. *Platelets* (2008) 19(3):192–8. doi: 10.1080/09537100701882038
16. Maugeri N, Capobianco A, Rovere-Querini P, Ramirez GA, Tombetti E, Valle PD, et al. Platelet microparticles sustain autophagy-associated activation of neutrophils in systemic sclerosis. *Sci Transl Med* (2018) 25:10(451). doi: 10.1126/scitranslmed.aao3089
17. Lammi MR, Saketkoo LA, Okpechi SC, Ghonim MA, Wyczechowska D, Bauer N, et al. Microparticles in systemic sclerosis: Potential pro-inflammatory mediators and pulmonary hypertension biomarkers. *Respirology* (2019) 24(7):675–83. doi: 10.1111/resp.13500
18. Ryu C, Walia A, Ortiz V, Perry C, Woo S, Reeves BC, et al. Bioactive Plasma Mitochondrial DNA is Associated with Disease Progression in Scleroderma Associated Interstitial Lung Disease. *Arthritis Rheumatol* (2020). doi: 10.1002/art.41418
19. van den Hoogen F, Khanna D, Fransen J, Johnson SR, Baron M, Tyndall A, et al. 2013 classification criteria for systemic sclerosis: an American college of rheumatology/European league against rheumatism collaborative initiative. *Ann Rheum Dis* (2013) 72(11):1747–55. doi: 10.1136/annrheumdis-2013-204424
20. Goh NSL, Desai SR, Veeraraghavan S, Hansell DM, Copley SJ, Maher TM, et al. Interstitial Lung Disease in Systemic Sclerosis. *Am J Respir Crit Care Med* (2008) 177(11):1248–54. doi: 10.1164/rccm.200706-877OC
21. Roofeh D, Jaafar S, Vummidi D, Khanna D. Management of systemic sclerosis-associated interstitial lung disease. *Curr Opin Rheumatol* (2019) 31(3):241–9. doi: 10.1097/BOR.0000000000000592
22. Galiè N, Humbert M, Vachiery J-L, Gibbs S, Lang I, Torbicki A, et al. 2015 ESC/ERS Guidelines for the diagnosis and treatment of pulmonary hypertension. *Eur Heart J* (2016) 37(1):67–119. doi: 10.1093/eurheartj/ehv317
23. Burbano C, Villar-Vesga J, Orejuela J, Muñoz C, Vanegas A, Vásquez G, et al. Potential Involvement of Platelet-Derived Microparticles and Microparticles Forming Immune Complexes during Monocyte Activation in Patients with Systemic Lupus Erythematosus. *Front Immunol* (2018) 9. doi: 10.3389/fimmu.2018.00322
24. Amabile N, Cheng S, Renard JM, Larson MG, Ghorbani A, McCabe E, et al. Association of circulating endothelial microparticles with cardiometabolic risk factors in the Framingham Heart Study. *Eur Heart J* (2014) 35(42):2972–9. doi: 10.1093/eurheartj/ehu153
25. Owen BAL, Xue A, Heit JA, Owen WG. Procoagulant activity, but not number, of microparticles increases with age and in individuals after a single venous thromboembolism. *Thromb Res* (2011) 127(1):39–46. doi: 10.1016/j.thromres.2010.10.018
26. Denecker G, Vercammen D, Steemans M, Berghe TV, Brouckaert G, Loo GV, et al. Death receptor-induced apoptotic and necrotic cell death: differential role of caspases and mitochondria. *Cell Death Differ* (2001) 8(8):829–40. doi: 10.1038/sj.cdd.4400883
27. Sung JY, Hong JH, Kang HS, Choi I, Lim SD, Lee JK, et al. Methotrexate suppresses the interleukin-6 induced generation of reactive oxygen species in the synoviocytes of rheumatoid arthritis. *Immunopharmacology* (2000) 47(1):35–44. doi: 10.1016/S0162-3109(99)00185-X
28. Lacki JK, Klama K, Mackiewicz SH, Mackiewicz U, Müller W. Circulating interleukin 10 and interleukin-6 serum levels in rheumatoid arthritis patients treated with methotrexate or gold salts: Preliminary report. *Inflammation Res* (1995) 44(1):24–6. doi: 10.1007/BF01630483
29. Aggarwal A, Misra R. Methotrexate inhibits interleukin-6 production in patients with juvenile rheumatoid arthritis. *Rheumatol Int* (2003) 23(3):134–7. doi: 10.1007/s00296-002-0267-y
30. Cui Y, Zheng L, Jiang M, Jia R, Zhang X, Quan Q, et al. Circulating microparticles in patients with coronary heart disease and its correlation with interleukin-6 and C-reactive protein. *Mol Biol Rep* (2013) 40(11):6437–42. doi: 10.1007/s11033-013-2758-1
31. Iversen LV, Ullman S, Østergaard O, Nielsen CT, Halberg P, Karlsmark T, et al. Cross-sectional study of soluble selectins, fractions of circulating microparticles and their relationship to lung and skin involvement in systemic sclerosis. *BMC Musculoskelet Disord* (2015) 16:191. doi: 10.1186/s12891-015-0653-8
32. Bacha NC, Blandinieres A, Rossi E, Gendron N, Nevo N, Lecourt S, et al. Endothelial Microparticles are Associated to Pathogenesis of Idiopathic Pulmonary Fibrosis. *Stem Cell Rev Rep* (2018) 14(2):223–35. doi: 10.1007/s12015-017-9778-5
33. Čolić J, Cerinic MM, Guiducci S, Damjanov N. Microparticles in systemic sclerosis, targets or tools to control fibrosis: This is the question! *J Scleroderma Related Disord* (2019) 5(1):6–20. doi: 10.1177/2397198319857356
34. Wermuth PJ, Piera-Velazquez S, Jimenez SA. Exosomes isolated from serum of systemic sclerosis patients display alterations in their content of profibrotic and antifibrotic microRNA and induce a profibrotic phenotype in cultured normal dermal fibroblasts. *Clin Exp Rheumatol* (2017) 35(Suppl 106):21–30.
35. Lories R, Derese I, De Bari C, Luyten F. In vitro growth rate of fibroblast-like synovial cells is reduced by methotrexate treatment. *Ann Rheum Dis* (2003) 62(6):568–71. doi: 10.1136/ard.62.6.568

36. Kowal-Bielecka O, Fransen J, Avouac J, Becker M, Kulak A, Allanore Y, et al. Update of EULAR recommendations for the treatment of systemic sclerosis. *Ann Rheumatic Dis* (2017) 76(8):1327–39. doi: 10.1136/annrheumdis-2016-209909
37. Lu Z-Y, Jensen LE, Huang Y, Kealey C, Blair IA, Whitehead AS. The up-regulation of monocyte chemoattractant protein-1 (MCP-1) in Ea.hy 926 endothelial cells under long-term low folate stress is mediated by the p38 MAPK pathway. *Atherosclerosis* (2009) 205(1):48–54. doi: 10.1016/j.atherosclerosis.2008.12.008
38. Ueki M, Takeshita H, Fujihara J, Iida R, Yuasa I, Kato H, et al. Caucasian-specific allele in non-synonymous single nucleotide polymorphisms of the gene encoding deoxyribonuclease I-like 3, potentially relevant to autoimmunity, produces an inactive enzyme. *Clin Chim Acta* (2009) 407(1–2):20–4. doi: 10.1016/j.cca.2009.06.022
39. Zochling J, Newell F, Charlesworth JC, Leo P, Stankovich J, Cortes A, et al. An Immunochip-based interrogation of scleroderma susceptibility variants identifies a novel association at DNASE1L3. *Arthritis Res Ther* (2014) 16 (5):438. doi: 10.1186/s13075-014-0438-8
40. Napirei M, Ludwig S, Mezrhab J, Klöckl T, Mannherz HG. Murine serum nucleases–contrasting effects of plasmin and heparin on the activities of DNase1 and DNase1-like 3 (DNase1l3). *FEBS J* (2009) 276(4):1059–73. doi: 10.1111/j.1742-4658.2008.06849.x
41. Sisirak V, Sally B, D'Agati V, Martinez-Ortiz W, Özçakar ZB, David J, et al. Digestion of Chromatin in Apoptotic Cell Microparticles Prevents Autoimmunity. *Cell* (2016) 166(1):88–101. doi: 10.1016/j.cell.2016.05.034

Conflict of Interest: The authors declare that the research was conducted in the absence of any commercial or financial relationships that could be construed as a potential conflict of interest.

frontiers in Immunology

ORIGINAL RESEARCH
published: 30 March 2021
doi: 10.3389/fimmu.2021.595811

Disparate Interferon Signaling and Shared Aberrant Basaloid Cells in Single-Cell Profiling of Idiopathic Pulmonary Fibrosis and Systemic Sclerosis-Associated Interstitial Lung Disease

Eleanor Valenzi[1]*, *Tracy Tabib*[2], *Anna Papazoglou*[2], *John Sembrat*[1], *Humberto E. Trejo Bittar*[3], *Mauricio Rojas*[1] and *Robert Lafyatis*[2]

[1] Division of Pulmonary, Allergy and Critical Care Medicine, University of Pittsburgh, Pittsburgh, PA, United States, [2] Division of Rheumatology and Clinical Immunology, University of Pittsburgh, Pittsburgh, PA, United States, [3] Department of Pathology, University of Pittsburgh, Pittsburgh, PA, United States

OPEN ACCESS

Edited by:
Oliver Distler,
University of Zurich, Switzerland

Reviewed by:
Mojca Frank-Bertoncelj,
University Hospital Zurich and University of Zurich, Switzerland
Victor J. Thannickal,
University of Alabama at Birmingham, United States

***Correspondence:**
Eleanor Valenzi
valenzie@upmc.edu

Specialty section:
This article was submitted to Autoimmune and Autoinflammatory Disorders, a section of the journal Frontiers in Immunology

Received: 17 August 2020
Accepted: 11 March 2021
Published: 30 March 2021

Citation:
Valenzi E, Tabib T, Papazoglou A, Sembrat J, Trejo Bittar HE, Rojas M and Lafyatis R (2021) Disparate Interferon Signaling and Shared Aberrant Basaloid Cells in Single-Cell Profiling of Idiopathic Pulmonary Fibrosis and Systemic Sclerosis-Associated Interstitial Lung Disease. Front. Immunol. 12:595811. doi: 10.3389/fimmu.2021.595811

Idiopathic pulmonary fibrosis (IPF) and systemic sclerosis-associated interstitial lung disease (SSc-ILD) differ in the predominant demographics and identified genetic risk alleles of effected patients, however both diseases frequently progress to respiratory failure and death. Contrasting advanced SSc-ILD to IPF provides insight to the role dysregulated immunity may play in pulmonary fibrosis. To analyze cell-type specific transcriptome commonalities and differences between IPF and SSc-ILD, we compared single-cell RNA-sequencing (scRNA-seq) of 21 explanted lung tissue specimens from patients with advanced IPF, SSc-ILD, and organ donor controls. Comparison of IPF and SSc-ILD tissue identified divergent patterns of interferon signaling, with interferon-gamma signaling upregulated in the *SPP1*^{hi} and *FABP4*^{hi} macrophages, cytotoxic T cells, and natural kill cells of IPF, while type I interferon signaling and production was upregulated in the corresponding SSc-ILD populations. Plasmacytoid dendritic cells were found in diseased lungs only, and exhibited upregulated cellular stress pathways in SSc-ILD compared to IPF. Alveolar type I cells were dramatically decreased in both IPF and SSc-ILD, with a distinct transcriptome signature separating these cells by disease. *KRT5*$^{-}$/*KRT17*$^{+}$ aberrant basaloid cells exhibiting markers of cellular senescence and epithelial-mesenchymal transition were identified in SSc-ILD for the first time. In summary, our study utilizes the enriched capabilities of scRNA-seq to identify key divergent cell types and pathways between IPF and SSc-ILD, providing new insights into the shared and distinct mechanisms between idiopathic and autoimmune interstitial lung diseases.

Keywords: systemic sclerosis, systemic sclerosis (scleroderma), idiopathic pulmonary fibrosis, interstitial lung disease (ILD), single-cell RNA-sequencing (scRNA-seq)

INTRODUCTION

Pulmonary fibrosis can occur as a consequence of autoimmunity, environmental exposures, or genetic mutations, as well as idiopathic disease. Idiopathic pulmonary fibrosis (IPF) is a progressive interstitial lung disease (ILD) of unknown etiology primarily occurring in the elderly, invariably progressing to respiratory failure, resulting in lung transplant or death. While some overlap exists between the clinical features, pathogenesis, and more recently the approved anti-fibrotic therapies for IPF and the connective tissue disease-associated ILDs, significant heterogeneity exists amongst the incidence and morbidity and mortality of the various autoimmune ILDs (1–3). In systemic sclerosis (SSc), an autoimmune disorder involving fibrosis and vasculopathy of the skin, lungs, and other organs, interstitial lung disease (ILD) occurs in up to 80% of patients, with 25-30% developing progressive disease resulting in respiratory failure (4). SSc predominantly occurs in women, although men with the disease have an increased risk for developing ILD, with an age of presentation between 30-55 years, while IPF predominantly occurs in men, with age of presentation between 60-75 years (5, 6). As it carries the highest rates of disease-associated mortality, primarily driven by pulmonary complications, examining advanced SSc-ILD in comparison to IPF presents a unique window into the role dysregulated immunity may play in pulmonary fibrosis (7, 8).

While the specific pathogenesis of both diseases remains unknown, current paradigms suggest that in IPF, repetitive epithelial cell microinjuries induce dysregulated restoration of the alveolar epithelium, activating a fibrotic response *via* the expansion of aberrant myofibroblasts, overproducing extracellular matrix (9). In SSc-ILD, activation of the innate and adaptive immune systems is hypothesized to result in endothelial and epithelial cell injury resulting in vasculopathy, aberrant transforming growth factor-beta (TGF-β) signaling, and the transformation to and expansion of myofibroblasts (10–12). In both diseases, resulting structural changes to the fibrotic lung parenchyma, including increasing tissue stiffness and hypoxia, generate a feed forward loop further promoting fibroblast activation and cellular injury (13–15). The significant role of inflammation is more established in the pathogenesis of SSc-ILD, with randomized clinical trials demonstrating modest therapeutic efficacy of the immunosuppressive agents cyclophosphamide and mycophenolate (16, 17). More recently, randomized trials in both Europe and the United States identified a mortality benefit for autologous stem cell transplantation in SSc, expanding therapeutic options for those with severe, progressive disease (18–20). Conversely, neither cyclophosphamide nor mycophenolate showed benefit in IPF clinical trials, and a trial of combined prednisone and azathioprine demonstrated increased mortality in those receiving immunosuppressive therapy (21–23).

The occurrence of pulmonary fibrosis within several rare genetic disorders, as well as the presence of familial pulmonary fibrosis have contributed to the increasing recognition that host genetic background influences the development and course of IPF and SSc-ILD for many patients (24). Rare variants in telomere-related (*TERT,TERC,PARN,RTEL1,DKC1,TINF2*) and surfactant-encoding genes (*SFTPC,SFTPA1,SFTPA2*), along with single nucleotide polymorphisms (SNPs) identified by genome-wide association studies (GWAS) in 20 independent loci currently account for 25-30% of the sporadic IPF disease risk (25, 26). The genes associated with these loci implicate a key role for telomere integrity, cell adhesion, and fibrogenic and host defense pathways in the pathogenesis of IPF. In SSc, a 2019 GWAS of 10,000 European patients identified 23 independent loci associated with SSc, increasing the total known SSc risk loci to 28 (27). The majority of gene products associated with these SSc risk loci are related to inflammation and autoimmunity, underscoring the immune etiology of SSc (28). Surprisingly, despite the similarities between the two diseases, there is no current overlap between the genetic variants or the identified HLA alleles associated with IPF and SSc-ILD. This is in contrast to ILD associated with rheumatoid arthritis (RA-ILD). The common *rs35705950* polymorphism in the promoter of MUC5B is associated with an increased risk of developing IPF as well as RA-ILD with a usual interstitial pneumonia (UIP) pattern, but not SSc-ILD (29, 30).

While the current paradigm for pathogenesis and genetic contribution to IPF and SSc-ILD differ, both diseases lead to a final common pathway of respiratory failure resulting in lung transplant or death. Investigating the shared and disparate mechanisms between SSc-ILD and IPF may yield important new insights influencing therapeutic development for both diseases. Previous microarray and bulk RNA-sequencing technologies are limited by their inherent averaging of gene expression across multiple disparate cell types. To examine transcriptomic commonalities and differences between advanced IPF and SSc-ILD, we compared single-cell RNA-sequencing (scRNA-seq) of peripheral parenchymal lung tissue obtained at the time of lung transplant from patients with IPF and SSc-ILD, and control lung tissue from organ donors without pre-existing lung disease. Comparison of IPF and SSc-ILD tissue identified divergent patterns of interferon signaling in IPF and SSc-ILD, increased cellular stress pathways in the plasmacytoid dendritic cells of SSc-ILD, a profound loss of alveolar type 1 (AT1) cells in both IPF and SSc-ILD with a distinct transcriptome signature defining each AT1 subset by disease, as well as identified aberrant basaloid cells in SSc-ILD for the first time.

MATERIALS AND METHODS

The University of Pittsburgh Institutional Review Board approved procedures involving human samples. Explanted subpleural peripheral lung tissue was digested and scRNA-sequencing performed as previously described (**Supplementary File 1**) (31, 32). All samples were processed in the same manner using 10X Genomics 3' v2 chemistry reagents. Raw data was demultiplexed using Cell Ranger 3.0.2 mkfastq function and aligned to the human reference genome GRCh38. Data analysis was performed with the R package Seurat V3.1.1 and R V3.6.0

(33, 34). Cells were filtered for greater than 200 genes, less than 50,000 unique molecular identifiers (UMI), and less than 15 percent mitochondrial genes. To reduce batch effects in analyzing multiple samples, all control, IPF, and SSc-ILD samples were combined into 3 objects by disease status using Seurat's IntegrateData function, followed by integration of these 3 objects (35). Following clustering and visualization with uniform manifold approximation and projection (UMAP) (36), cell populations were classified using multiple gene markers in the transcriptome. Doublet cells were manually identified as expressing markers of multiple cell types with elevated UMI counts and subsequently removed. Cell cycle phase was predicted using Seurat's CellCycleScoring function. To better define individual cell types, the myeloid, lymphoid, epithelial, and stromal populations were then separately reclustered. Differential gene expression analysis for IPF versus SSc-ILD cells for each cluster was performed using the Wilcoxon rank-sum statistical test. Differences in mean proportions of cells comprising each cell type were compared with the non-parametric Kruskal-Wallis test with Dunn's multiple comparison test. P-values less than 0.05 were considered to be statistically significant. Differentially expressed genes with a p-value less than 0.05 and absolute value natural log fold change greater than 0.5 were used as input for pathway enrichment analyses. Enriched gene ontology biological processes with a false discovery rate less than 5 percent were identified using the Gene Ontology Resource (37, 38). Hierarchical tree clustering of the epithelial cells was performed on gene average expression levels by Euclidean distance using Cluster 3.0, filtering out genes expressed at an average expression level less than 0.2 in fewer than 3 clusters (39).

TABLE 1 | Characteristics of Patient Samples Demographics, the number of cells analyzed after filtering in the scRNA-seq analysis, pathological review of adjacent tissue, and clinical characteristics of the patient samples included.

Variable	IPF	SSc-ILD	Control
N	8	8	5
Cells post-filtering, mean (SD)	3995.88 [1031]	4039.63 [609.48]	4521.4 [959.79]
Age (years), mean (SD)	68.75 [1.09]	56.75 [9.5]	35.2 [17.09]
Male, n (%)	4 (50%)	6 (75%)	2 (40%)
FEV1 (L), mean (SD)	1.29 [0.66]	2.03 [0.51]	
FEV1 predicted %, mean (SD)	50.25 [19.21]	60.75 [11.32]	
FVC (L), mean (SD)	1.46 [0.81]	2.70 [0.88]	
FVC predicted %, mean (SD)	39.25 [14.45]	58.25 [11.54]	
DLCO (ml), mean (SD)	7.34 [3.34]	6.15 [3.33]	
DLCO predicted %, mean (SD)	33.75[13.74]	20.25 [9.23]	
Mean PAP (mmHg), mean (SD)	20.25 [6.91]	39.75 [12.58]	
Specific therapies:			
Mycophenolate, n (%)		4 (50%)	
Rituximab, n (%)		2 (25%)	
Cyclophosphamide, n (%)		2 (25%)	
Prednisone, n (%)		2 (25%)	
Pirfenidone, n(%)	4 (50%)		
Usual interstitial pneumonia on explant pathology, n (%)	8 (100%)	7 (87.5%)	

FEV1: forced expiratory volume in 1 second; FVC: forced vital capacity; DLCO: diffusion capacity of the lungs for carbon monoxide; PAP: pulmonary artery pressure.
Mean pulmonary artery pressure (mPAP) measurement is from the last right heart catheterization preceding lung transplantation. Immunosuppression listed includes the medications received in the 90 days preceding lung transplantation. Data presented as means (standard deviation [SD]) or N (%).

RESULTS

Study Population

In order to determine commonalities and differences between IPF and SSc-ILD, we performed single-cell RNA-sequencing (scRNA-seq) on 21 peripheral lung tissue specimens obtained at the time of lung transplant from patients with IPF (n=8 samples) and SSc-ILD (n=8) and control lung tissue from organ donors without pre-existing lung disease whose lungs were declined for transplant (n=5). Separate upper and lower lobe samples were included for each IPF and SSc-ILD patient and from one control patient, with only lower lobe samples available from the other 3 controls. For these analyses we added 2 not previously analyzed IPF samples with previously described samples (31, 32). The histopathology of adjacent lung tissue and clinical information for all samples was reviewed (**Table 1**, **Supplemental Figure 1**). All of the IPF and 7 of the SSc-ILD samples showed usual interstitial pneumonia (UIP) on histology, with varied amounts of diffuse alveolar damage, lymphoid aggregates, and myointimal thickening of the pulmonary arteries. The remaining SSc-ILD sample exhibited nonspecific interstitial pneumonia (NSIP) with acute lung injury. Although NSIP is traditionally regarded as the most common histopathology pattern in SSc-ILD (40), the high prevalence of UIP within our samples is consistent with the histopathology of most patients at the time of end-stage SSc-ILD resulting in respiratory failure (41).

In total, we analyzed 85,756 cells, with individual cell types identified by multiple distinct markers (**Figure 1A**, **Supplemental Figure 2A** and **3**) and samples well-integrated by disease status and sample (**Figure 1B**, **Supplemental Figure 2B**). Myeloid, lymphoid, epithelial, and stromal populations were separately reclustered to identify more distinct cell phenotypes and allow for differential gene expression comparisons between IPF and SSc-ILD for all cell types. Evaluating the proportion of total cells present in each population by sample and disease status revealed many similar trends in the shifts of cell populations between control and fibrotic lungs (**Figure 1C**). Ciliated, club, goblet, basal, and the intermediate secretory cells all trended towards increased frequency in the fibrotic lower lobes, compared to the fibrotic upper lobes and control samples, reflecting the basal and mixed bronchial epithelial populations lining honeycomb cysts (42). Basal cells in SSc-ILD lower lobes were significantly increased in comparison to control lungs (p=0.0266). Alveolar type 1 and alveolar type 2 cells both trended towards a graded decrease, with the most dramatic loss of alveolar type 1 cells (p=0.0230) and alveolar type 2 cells (p=0.0365) occurring in the IPF lower lobes in comparison to controls. Amongst the lymphoid populations, natural killer cells were decreased in IPF and SSc-ILD compared to controls, with a significant change between controls and SSc-ILD lower lobes (p=0.0379). T regulatory, plasma, and

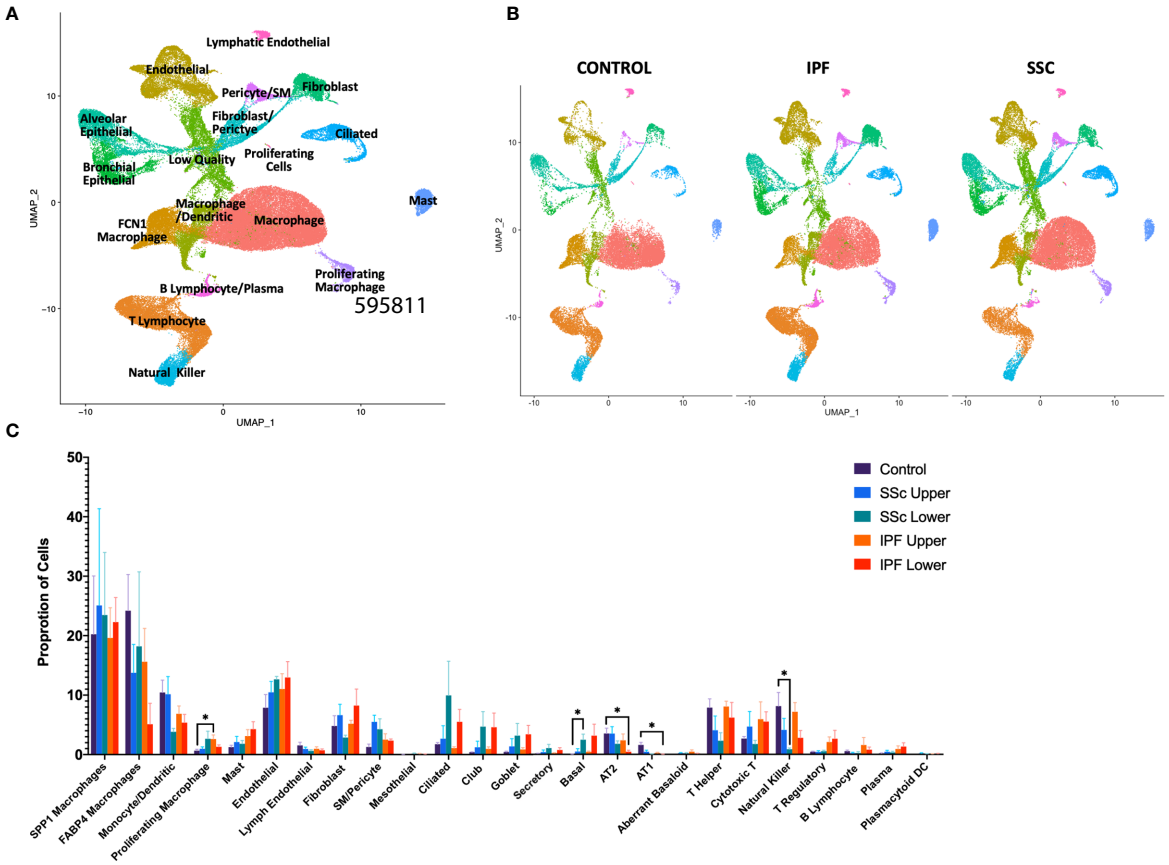

FIGURE 1 | ScRNA-seq analysis of 8 IPF, 8 SSc-ILD, and 5 organ donor control lung samples. **(A)** UMAP plot of all 21 integrated samples, identified by cell type. **(B)** UMAP plots of all samples, divided by disease status. **(C)** Mean percentage of total cells comprised of each cell type, comparing, control, upper lobe IPF, lower lobe IPF, upper lobe SSc-ILD, and lower lobe SSc-ILD. Bars represent the mean percentage of total cells, with error bars representing the standard error of the mean. *=p-value<0.05. scRNA-seq, single-cell RNA-sequencing; IPF, idiopathic pulmonary fibrosis; SSc-ILD, systemic sclerosis-associated interstitial lung disease; UMAP, uniform manifold approximation and projection.

plasmacytoid dendritic cells trended towards increase in IPF and SSc-ILD compared to controls. The smooth muscle and pericyte population was increased amongst the SSc-ILD samples, possibly related to the elevated pulmonary pressures of these patients (mean pulmonary artery pressure 39.75 mmHg vs 20.25 mmHg in IPF).

Myeloid Cells

Consistent with our previous scRNA-seq analyses, macrophages appeared in three primary phenotypes: *SPP1*^{hi} macrophages, *FABP4*^{hi} macrophages, and a population of monocyte-derived macrophages (*FCN1*^{hi}) (**Figure 2A**, **Supplemental Figure 4**) (31, 32). A small population of dendritic cells clustered within the *FCN1*^{hi} macrophages. While all three subpopulations of macrophages have been identified in the bronchoalveolar lavage (BAL) fluid of the healthy human lung, *FABP4*^{hi} macrophages comprised the majority of BAL macrophages, and likely most closely approximate the traditionally designated alveolar macrophages (31). Proliferating macrophages were expanded in IPF and SSc-ILD, compared to controls, with *FABP4*^{hi} the predominant proliferating phenotype in SSc-ILD and controls, and a similar proportion of proliferating *SPP1*^{hi} and *FABP4*^{hi} phenotype cells in IPF. (**Supplemental Figure 5A, B**). Differentially expressed genes and their enhanced gene ontology biological processes were examined between IPF and SSc-ILD lungs for each myeloid population, with the most distinct differences noted amongst the *SPP1*^{hi} and *FABP4*^{hi} macrophages (**Figures 2C–H**, **Supplemental Figure 6A, B**). Complete differential expression and gene ontology results for all compared cell populations are included in **Supplemental Files 2** and **3**.

Interferon-gamma (IFN-γ) mediated signaling was distinctly upregulated amongst *SPP1*^{hi} and *FABP4*^{hi} macrophages in IPF, compared to SSc-ILD (**Figures 2C, F**). This upregulation included expression of multiple IFN-γ primary response genes such as *IRF1, MT2A, GBP2* and numerous HLA class II antigens within the *SPP1*^{hi} macrophages and *IRF9, IRF1, CCL3, CCL4*, and *CCL23* within the *FABP4*^{hi} macrophages (**Figures 2E, H**). Interferon-gamma (*IFNG*) was primarily expressed by natural killer cells and to a lesser extent by T lymphocytes, with

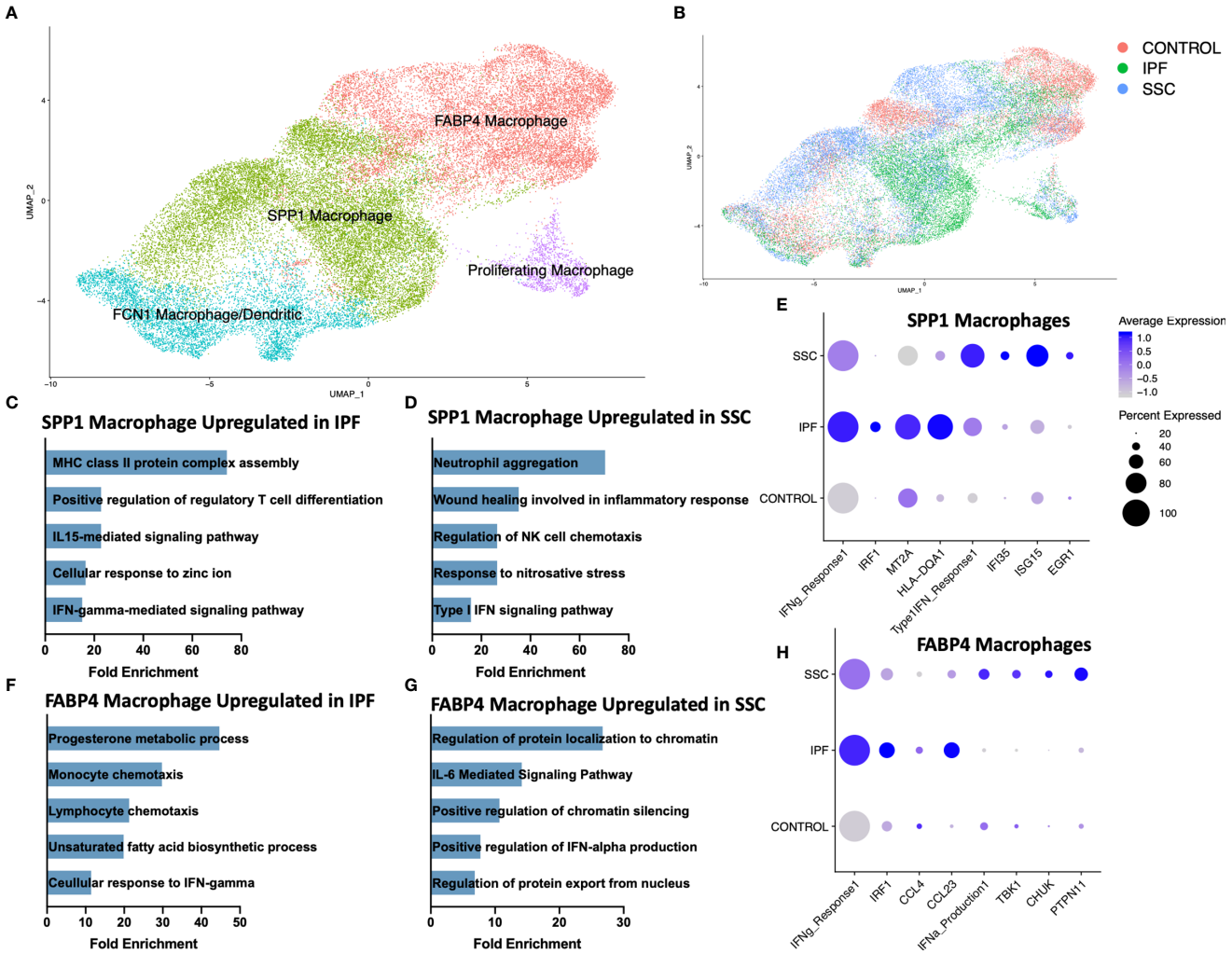

FIGURE 2 | ScRNA-seq analysis of IPF, SSc-ILD, and control myeloid populations. **(A)** UMAP plot of macrophage and dendritic cell populations, identified by cell type. **(B)** UMAP plot of macrophage and dendritic cell populations, identified by disease status. **(C)** Pathways upregulated in IPF *SPP1*^{hi} macrophages compared to SSc-ILD *SPP1*^{hi} macrophages **(D)** Pathways upregulated in SSc-ILD *SPP1*^{hi} macrophages compared to IPF *SPP1*^{hi} macrophages **(E)** Expression of selected genes and pathways in *SPP1*^{hi} macrophages, separated by disease state. Pathway expression depicted as a module score of all genes in the specific GO biological process. **(F)** Pathways upregulated in IPF *FABP4*^{hi} macrophages compared to SSc-ILD *FABP4*^{hi} macrophages. **(G)** Pathways upregulated in SSc-ILD *FABP4*^{hi} macrophages compared to IPF *FABP4*^{hi} macrophages. **(H)** Expression of selected genes and pathways in *FABP4*^{hi} macrophages, separated by disease state. scRNA-seq, single-cell RNA-sequencing; IPF, idiopathic pulmonary fibrosis; SSc-ILD, systemic sclerosis-associated interstitial lung disease; UMAP, uniform manifold approximation and projection; GO, gene ontology.

macrophages its primary target *via* their expression of the heterodimeric receptor comprised of IFNGR1 and IFNGR2 (**Supplemental Figure 7A, B**). Regulation of T cell differentiation, including that of regulatory T cells, IL-15 mediated signaling, and cellular response to zinc and cadmium ion pathways were also upregulated in IPF macrophages compared to SSc-ILD. Cadmium exposure has recently been implicated as potential exogenous risk factor for pulmonary fibrosis *via* its activation of SMAD2/3/4-dependent signaling in the murine lung (43).

Conversely, type I interferon signaling and production was significantly upregulated amongst *SPP1*^{hi} and *FABP4*^{hi} macrophages in SSc-ILD (**Figures 2E, H**), compared to IPF, including expression of multiple interferon-induced transmembrane proteins, *IFI35, ISG15*, and *EGR1* within the *SPP1*^{hi} macrophages and *TBK1, CHUK*, and *PTPN11*, amongst others, within the *FABP4*^{hi} macrophages. IL-6 mediated signaling, chromatin silencing, and p53 signal transduction were also upregulated in SSc-ILD *FABP4*^{hi} macrophages compared to IPF.

Lymphoid Cells

Reclustering the lymphoid populations, allowed for identification of the three primary T cell populations, as well as improved separation of the natural killer cells, plasma cells, and B lymphocytes (**Figure 3A**, **Supplemental Figure 8**). Natural killer

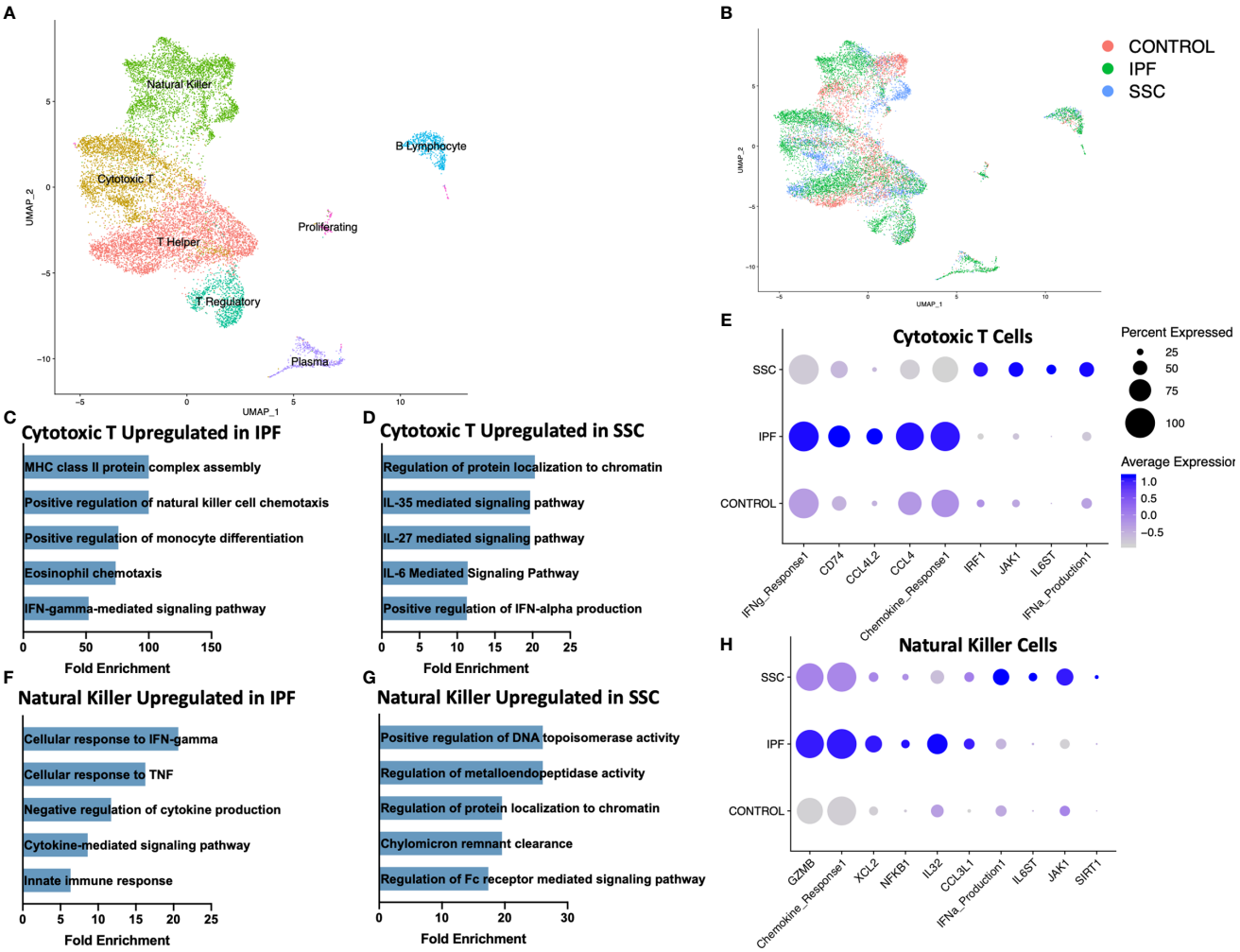

FIGURE 3 | ScRNA-seq analysis of IPF, SSc-ILD, and control lymphoid populations. **(A)** UMAP plot of lymphoid subpopulations, identified by cell type. **(B)** UMAP plot of lymphoid subpopulations, identified by disease status. **(C)** Pathways upregulated in IPF cytotoxic T cells compared to SSc-ILD cytotoxic T cells. If fold enrichment was calculated as >100 it is depicted as 100 for visualization. **(D)** Pathways upregulated in SSc-ILD cytotoxic T cells compared to IPF cytotoxic T cells **(E)** Expression of selected genes and pathways in cytotoxic T cells, separated by disease state. Pathway expression depicted as a module score of all genes in the specific GO biological process. **(F)** Pathways upregulated in IPF NK cells compared to SSc-ILD NK cells **(G)** Pathways upregulated in SSc-ILD NK cells compared to IPF NK cells **(H)** Expression of selected genes and pathways in NK cells, separated by disease state. scRNA-seq, single-cell RNA-sequencing; IPF, idiopathic pulmonary fibrosis; SSc-ILD, systemic sclerosis-associated interstitial lung disease; UMAP, uniform manifold approximation and projection; NK, natural killer.

cells and cytotoxic T cells demonstrated the greatest geographic separation in UMAP clustering between IPF and SSc-ILD. We examined differentially expressed genes and their enhanced pathways for each lymphoid population (**Supplemental File 2, 3**, **Supplemental Figure 9**). Amongst the cytotoxic T cells, IFN-γ mediated signaling, regulation of natural killer cell and eosinophil chemotaxis, the ERK1/ERK2 cascade, and responses to IL-1 and tumor necrosis factor (TNF) were distinctly upregulated in IPF compared to SSc-ILD (**Figures 3C, E**, **Supplemental File 3**); identification of these pathways was largely driven by increased expression of numerous major histocompatibility complex (MHC) class II cell surface receptors and several chemokines in IPF cytotoxic T cells. Conversely, IL-6 family mediated signaling pathways (including IL-27 and the related IL-35), as well as positive regulation of type I interferon production were upregulated in SSc-ILD cytotoxic T cells compared to IPF (**Figure 3D**). The proportion of natural killer cells trended toward a graded decline in fibrotic lower lobes compared to fibrotic upper lobes and controls, with a significant decline between controls and SSc-ILD lower lobes (p=0.0379). Cellular response pathways to IFN-γ and TNF, and chemokine response were upregulated in IPF compared to SSc-ILD natural killer cells (**Figures 3F, H**); whereas regulation of metalloendopeptidase activity, and positive regulation of type I interferon production were upregulated in SSc-ILD compared to IPF natural killer cells (**Figures 3G, H**, **Supplemental File 3**).

On separately reclustering the original B Lymphocyte/ plasma cell cluster only, we identified a small population of

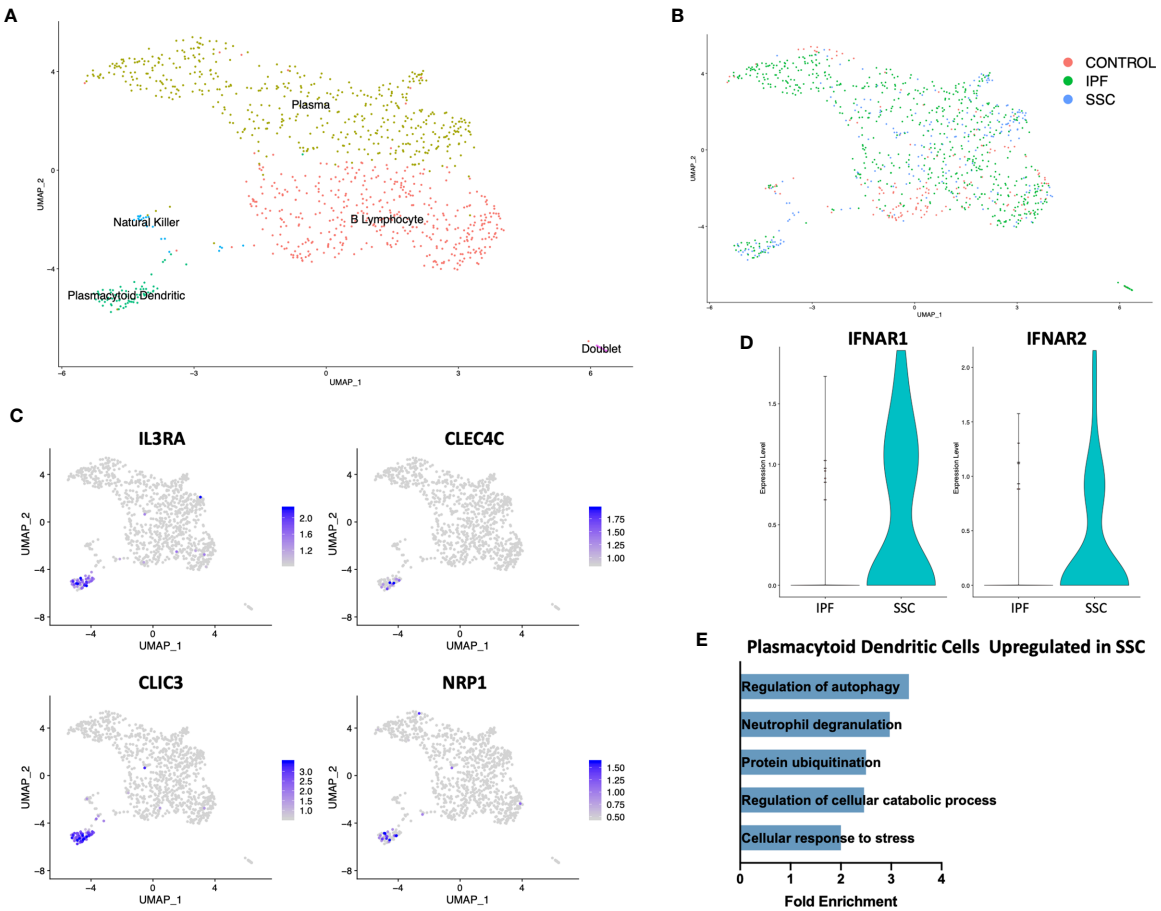

FIGURE 4 | ScRNA-seq analysis of IPF, SSc-ILD, and control plasmacytoid dendritic cell populations. **(A)** UMAP plot of the reclustered original B lymphocyte and plasma cell cluster, identified by cell type. **(B)** UMAP plot of the reclustered original B lymphocyte and plasma cell cluster, identified by disease status. **(C)** Expression of *IL3RA, CLEC4C, CLIC3*, and *NRP1*, identifying pDCs. **(D)** Expression of *IFNAR1*and *IFNAR2* in IPF versus SSc-ILD pDCs. **(E)** Pathways upregulated in SSc-ILD pDCs compared to IPF pDCs. scRNA-seq, single-cell RNA-sequencing; IPF, idiopathic pulmonary fibrosis; SSc-ILD, systemic sclerosis-associated interstitial lung disease; UMAP, uniform manifold approximation and projection; pDCs, plasmacytoid dendritic cells.

plasmacytoid dendritic cells (pDC) expressing *IL3RA* (CD123), *CLEC4C, CLIC3*, and *NRP1* (**Figures 4A, C**). This population originated only from IPF and SSc-ILD lungs, with no pDCs identified from control lungs (**Figure 4B**). Multiple cellular stress related pathways including the regulation of autophagy, protein ubiquitination, and response to cellular stress were up-regulated in SSc-ILD pDCs compared to IPF (**Figure 4E**, **Supplemental Figure 10A**), possibly indicating an activated aberrant phenotype amongst the SSc-ILD pDCs. Type 1 interferon receptor expression (*IFNAR1, IFNAR2*) was also increased in SSc-ILD pDCs compared to IPF (**Figure 4D**). We were unable to detect expression of type I IFNs by these cells.

Epithelial Cells

Although genetic evidence has implicated a more central role for epithelial cells in IPF than SSc-ILD, the dramatic loss of alveolar type 1 (AT1) cells and increase in cells originating from the bronchial epithelium was consistent in both diseases (**Figure 1C**, **5B**). Sample digestion and processing may differentially impact the survival of particular cell populations, however the robust presence of AT1 cells within the control samples suggests there is a true loss within the diseased lungs. A population of secretory cells present in disease and controls expressed transcripts associated with both goblet and ciliated cells, including airway mucin *MUC5B*, goblet cell marker *SCGB1A1* and ciliated markers *FOXJ1* and *RSPH1* (**Figure 5A**, **Supplemental Figure 11**).

Upon hierarchical clustering of the epithelial cells by the average expression of genes within control, IPF, and SSc-ILD samples for each cell type, AT1 cells exhibited the most distinct expression patterns between IPF and SSc-ILD (**Figures 6A, B**). Analyzing the gene signature best distinguishing IPF from SSc-ILD AT1 cells, pathways involved in stress DNA damage response were upregulated in IPF compared to SSc-ILD (**Figures 5D, E**, **Supplemental File 3**), supporting the response to AT1 cellular injury. Multiple E3 ubiquitin-protein ligase genes, including *RNF168, TRIM37, RNF40*, and *HUWE1*, as

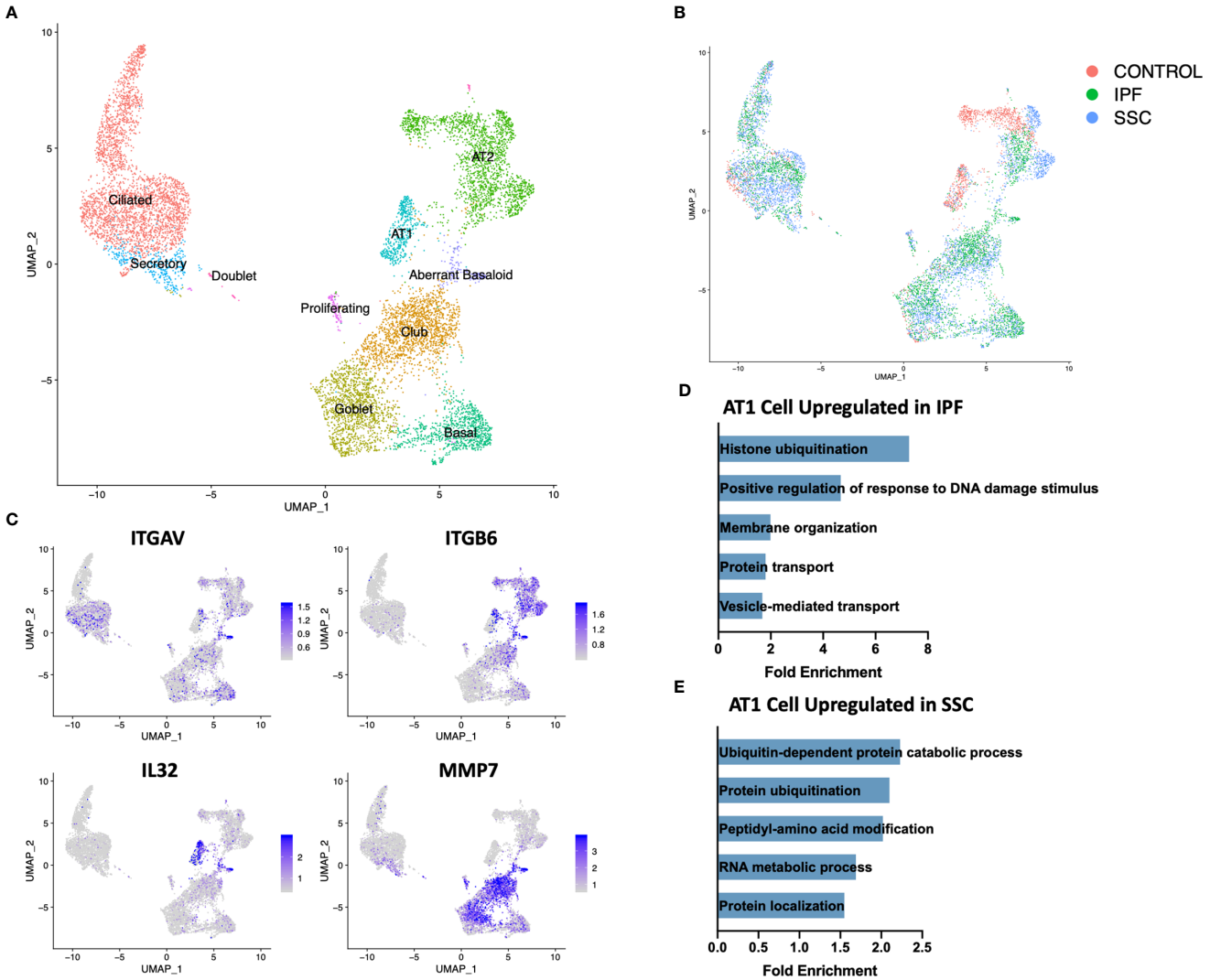

FIGURE 5 | ScRNA-seq analysis of IPF, SSc-ILD, and control epithelial cell populations. **(A)** UMAP plot of epithelial cell populations, identified by cell type **(B)** UMAP plot of epithelial cell populations, identified by disease status. **(C)** Expression of *ITGAV, ITGB6, IL32*, and *MMP7*, highlighting the aberrant basaloid population. **(D)** Pathways upregulated in IPF AT1 cell gene signature compared to SSc-ILD AT1 cell gene signature. **(E)** Pathways upregulated in SSc-ILD AT1 cell gene signature compared to IPF AT1 cell gene signature. scRNA-seq, single-cell RNA-sequencing; IPF, idiopathic pulmonary fibrosis; SSc-ILD, systemic sclerosis-associated interstitial lung disease; UMAP, uniform manifold approximation and projection; AT1, alveolar type 1.

well as the deubiquitinase *BAP1* were upregulated in IPF AT1 cells, implicating the histone ubiquitination pathway which has been linked to double-stranded DNA break repair as well as transcription repression and activation (44). Other proteins involved in ubiquitination and deubiquitination have been linked to pulmonary fibrosis by both TGF-β dependent and independent mechanisms (45), and further investigation of these AT1 associated ubiquitin proteins may be of particular interest as druggable targets by small molecule inhibitors (46). On the other hand, pathway analysis of SSc AT1 cells indicated altered protein ubiquitination and catabolism, as well as cellular response to oxygen levels, suggesting that cell stress, possibly oxidative stress, leads to death of AT1 cells in SSc-ILD. The distinct transcriptional signatures of AT1 cells between diseases suggests the loss of these cells may results from distinct mechanisms in IPF and SSc-ILD.

AT2 cells, depleted more dramatically in IPF than SSc-ILD, were more transcriptionally similar between IPF and SSc-ILD samples, with few significant pathways identified by genes differentially expressed between IPF and SSc-ILD. The inositol-requiring enzyme 1 (IRE-1) mediated unfolded protein response was upregulated in IPF. IRE1 is an endoplasmic reticulum (ER) stress sensor previously identified to signal through the transcription factor XBP1, as well as the JNK and NF-κB pathways (47). Murine studies suggest a causative role for ER stress in AT2 cell dysfunction, and ER stress is a proposed

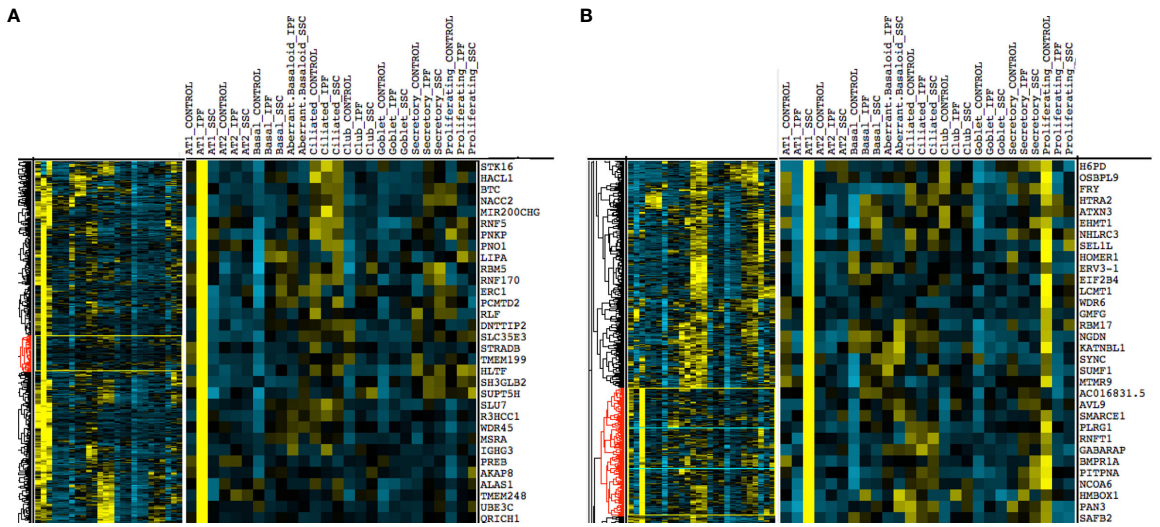

FIGURE 6 | Hierarchical clustering on gene average expression levels of epithelial cell subtypes divided by disease status, demonstrating distinct gene signatures of IPF and SSc-ILD AT1 cells. Yellow indicates positive and blue indicates negative scaled expression. **(A)** Partial gene signature of IPF AT1 cells **(B)** Partial gene signature of SSc-ILD AT1 cells. IPF, idiopathic pulmonary fibrosis; SSc-ILD, systemic sclerosis-associated interstitial lung disease; AT1, alveolar type 1; AT2, alveolar type 2.

connection between IPF and multiple fibrosis risk factors including aging, the *MUC5B* risk allele, hypoxia, and infection (47, 48).

Within both the IPF and SSc-ILD samples we identified a small population of the recently described aberrant basaloid cells (or *KRT5*$^{-}$/*KRT17*$^{+}$ cells), with no cells sharing this distinct transcriptome amongst the control samples (**Figures 5A, B**) (49, 50). Consistent with recent descriptions in IPF, these cells express traditional basal genes including *KRT17* and *TP63*, but do not express *KRT5, KRT15*, or *SOX2* (**Figure 5C**). In both IPF and SSc-ILD they express elevated *MMP7*, a peripheral blood IPF biomarker, elevated integrin αVβ6, a potent activator of latent TGF-β also implicated in matrix metalloproteinase expression (51), markers of epithelial-mesenchymal transition (such as *COL1A1, CDH2*, and *FN1*), and markers of cellular senescence (including *CDKN2A*(p16), *CDKN1A*(p21), and *GDF15*) (**Supplemental Figure 12**). *IL32* was the top differentially expressed gene amongst the aberrant basaloid cells, compared to the other epithelial cell populations. The presence of aberrant basaloid cells in both IPF and SSc-ILD as well as the severe loss of alveolar type 1 cells, despite purported different drivers, may indicate that both are features of an unsuccessful repair process in advanced lung disease.

Stromal Populations

On reclustering the stromal populations, three major subpopulations of fibroblasts, pericytes, smooth muscle cells, four major subpopulations of vascular endothelial cells, lymphatic endothelial cells, and mesothelial cells were identified (**Figure 7A**, **Supplemental Figure 13**). A separate cluster of proliferating cells contained myofibroblasts and mixed endothelial cells nearly exclusively originating from IPF and SSc-ILD samples (**Figure 7B**). The major fibroblast subpopulations (myofibroblast, *MFAP5*^{hi}, and *SPINT2*^{hi}) as well as the presence of a small control only *WIF1*^{hi} population clustering within the myofibroblasts, mirrored those defined in our previous analysis of fibroblasts in SSc-ILD and control lungs (32), even with the addition of cells from the eight IPF samples. The control cells falling within the myofibroblast cluster overall do not express the myofibroblast transcriptome of increased *COL1A1, COL1A2, CTHRC1*, and *POSTN* and instead are more transcriptionally similar to the *SPINT2*^{hi} fibroblasts.

In comparing all IPF endothelial cells to all SSc-ILD endothelial cells, multiple pathways for cellular responses to metallic ions were distinctly upregulated in IPF (**Figure 7C**, **Supplemental Figure 10B**), driven by the increased expression of multiple metallothionine genes including *MT1A, MT1X, MT1E*, and *MT1M* in IPF endothelial cells, although all were expressed at even higher levels in control cells (**Figure 7E**). Vasculogenesis, prostaglandin biosynthesis, and platelet derived growth factor receptor-signaling were all increased in SSc-ILD compared to IPF (**Figure 7D**, **Supplemental File 3**), reflecting a more active expansion of the endothelium in SSc-ILD. Vasculopathy is understood to play a more central role in the pathogenesis of SSc (12). Thus, these changes may represent important drivers of SSc-PAH associated with SSc-ILD, but also indicate an altered endothelial cell transcriptome that may also play a central role in SSc-ILD pathogenesis. However, since the samples are not matched for physiologic parameters, the observed changes, as well as those of each endothelial subpopulation, (**Supplemental Figures 14**, **15**) cannot be definitively attributed to disease-specific differences.

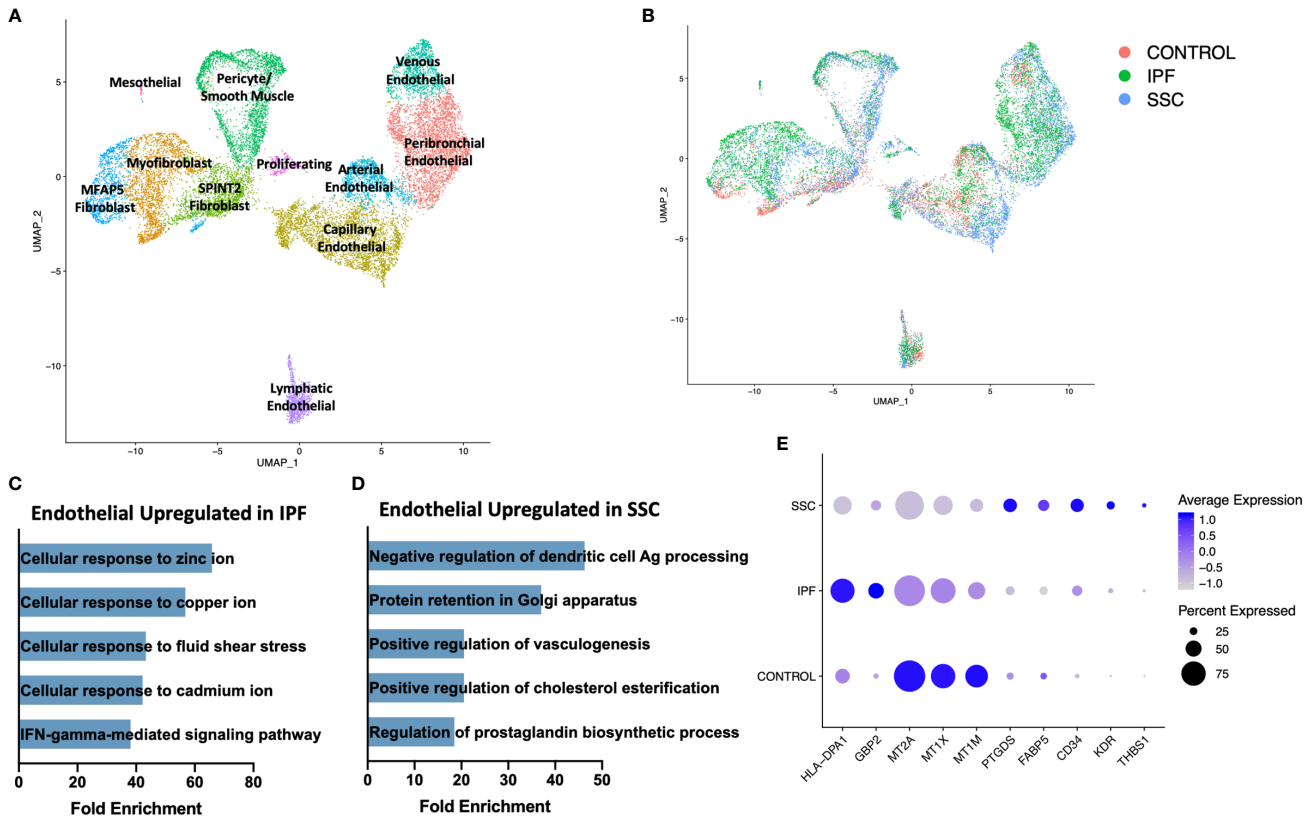

FIGURE 7 | ScRNA-seq analysis of IPF, SSc-ILD, and control stromal cell populations. **(A)** UMAP plot of stromal cell populations, identified by cell type. **(B)** UMAP plot of stromal cell populations, identified by disease status. **(C)** Pathways upregulated in IPF endothelial cells compared to SSc-ILD endothelial cells **(D)** Pathways upregulated in SSc-ILD endothelial cells compared to IPF endothelial cells **(E)** Expression of selected genes in all non-lymphatic endothelial cells, separated by disease state. scRNA-seq, single-cell RNA-sequencing; IPF, idiopathic pulmonary fibrosis; SSc-ILD, systemic sclerosis-associated interstitial lung disease; UMAP, uniform manifold approximation and projection.

DISCUSSION

As the progression of disease can be variable in both IPF and SSc-ILD, our analysis focuses on patients with severe disease resulting in respiratory failure by utilizing only explanted tissues from the time of lung transplant. Although the majority (7 of 8) of our SSc-ILD samples showed UIP on histopathology, we identified significant systematic differences compared to IPF, supporting the notion that many distinct disease mechanisms remain despite the shared histopathologic pattern. Thus, all UIP is not the same at the molecular level, and there is potential loss of scientific knowledge and treatment opportunities in the inclination to think of it as such. The similarities and differences identified between diseases could lead to additional hypotheses regarding treatments that will have a benefit in both diseases versus only IPF or SSc-ILD. We believe that even greater differences could be present in a comparison of early stage disease tissue, however due to the associated risks, patients with SSc-ILD rarely undergo surgical lung biopsy, resulting in no early disease tissue available for research studies.

IPF and SSc-ILD myeloid and lymphoid cells exhibited disparate patterns of interferon signaling, with IFN-γ signaling amplified in IPF *SPP1*^{hi} and *FABP4*^{hi} macrophages and cytotoxic T and natural killer cells, while Type 1 IFN signaling was amplified in the analogous SSc-ILD populations. In up to 50% of patients with SSc, even early in disease, a type I IFN signature is identifiable in the peripheral blood and correlates with other mediators of fibrosis and inflammation (52, 53). Polymorphisms in several interferon regulatory factors (IRFs) including *IRF4*, *IRF5*, *IRF7*, and *IRF8* have been associated with the development of SSc (24, 54). Type I IFNs in SSc have multiple supported effects including the activation of monocytes, the differentiation and activation of T lymphocytes, B lymphocytes, and dendritic cells, stimulation of the expression of Toll-like receptors by dendritic cells, and increasing the expression of fibrotic effectors such as *CTGF* and *ACTA* in endothelial cells and fibroblasts, amongst others (53). Though the UIP histopathology identified in most of our SSc-ILD samples is often thought of as correlating with less "active inflammation", and thus being less likely to respond to immunomodulatory therapies, our finding of upregulation of type I IFN in SSc-ILD myeloid and lymphoid populations suggests that type I IFN signaling and inflammation remain an active mechanism in advanced SSc-ILD.

The realm of interferon has previously been considered for therapeutics in IPF, however with a focus on delivering IFN-γ. The 2009 INSPIRE trial evaluated the use of subcutaneous IFN-γ1b in IPF, but was terminated early due to a lack of benefit at interim analysis (55). Inhalational delivery of IFN-γ in IPF has been assessed for safety, and is now being evaluated for a larger trial, with the goal of stimulating macrophages and inhibiting fibrosis *via* this cytokine (56, 57). Albiet aerosolized delivery will likely avoid many of the systemic side effects of parenteral IFN-γ, our findings of upregulation of IFN-γ signaling in the macrophages and selected lymphoid populations of advanced IPF warrant caution in further augmenting this pathway. Although the timing of upregulation of type I and II IFNs during ILD, as well as their role(s) as primary versus secondary drivers of disease is not precisely known, and may vary between IPF and SSc-ILD, ultimately the upregulation of both IFN-γ and Type I IFN signaling may be detrimental in human lung fibrosis.

Plasmacytoid dendritic cells provide a connection between innate and adaptive immunity, and have been identified as producing type 1 interferons during viral infection, and fostering autoimmunity, as well as tolerogenic responses (58). Compared to healthy controls, pDCs are depleted in the blood of patients with SSc, likely secondary to their accumulation within target organs. The frequency of pDCs in BAL fluid correlates with severity of fibrosis on chest CT in SSc-ILD patients (59), while in SSc skin lesions, pDCs accumulate in perivascular regions and produce increased IFN-α and chemokine ligand 4 (CXCL4) *via* TLR8 and phosphoinositide 3-kinase-δ signaling (60, 61). In the murine bleomycin skin and lung fibrosis models, reduction of pDCs results in decreased inflammation and fibrosis, indicating their potential as a therapeutic target in fibrosis (59). Murine studies and the accumulation of conventional dendritic cells (cDCs) in the BAL fluid of patients with IPF have implicated cDC dysfunction in the pathogenesis of IPF, however the role of pDCs in IPF is much less defined (62, 63). In our analysis, although pDCs were recovered from the lung at similar frequencies for both IPF and SSc-ILD, the SSc-ILD pDCs were more transcriptionally active, expressed greater type 1 interferon receptor, and upregulation of multiple cellular stress response pathways. Whether these differences reflect an activated aberrant phenotype of the SSc-ILD pDCs or a failure to act (i.e. senescent-like phenotype) by the IPF pDCs is unclear. Further studies to define the precise function of pDCs and their crosstalk with other cell types within the human fibrotic lung are necessary to discern if these cells are a potential therapeutic target in disease.

Our analysis is the first description of aberrant basaloid cells within the SSc-ILD lung. Although our study includes samples previously analyzed in prior publications by our group, these unique cells were not apparent at that time due to their low cell numbers in analyses with fewer samples. These transcriptionally discrete cells were recently first identified by Adams et al. in a large scRNA-seq analysis of IPF and chronic obstructive pulmonary disease (COPD) lungs (50), as well as by Habermann et al. in a separate large scRNA-seq analysis of pulmonary fibrosis lungs (referred to as *KRT5*$^{-}$*/KRT17*$^{+}$ cells by the latter group) (49). The aberrant basaloid cells express some typical basal cell markers including *TP63* and *KRT17*, but lack others such as *KRT5* and *KRT15*, and also express multiple markers of cellular senescence and epithelial-mesenchymal transition, the highest expression of the IPF biomarker *MMP7*, and elevated expression of the TGF-β activator integrin αVβ6. The lack of aberrant basaloid cells from all control samples and their presence within all IPF and SSc-ILD samples suggests these are a consistent feature of advanced fibrotic disease. Histopathologic examination has suggested these cells localize to the areas of fibroblastic foci in IPF and may activate TGF-β locally *via* their integrin expression (49, 50), now a possible feature in SSc-ILD as well. These cells may exhibit a unique link in the epithelial-mesenchymal transition during which evolving cells lose epithelial characteristics and develop mesenchymal polarity as part of a transition from inflammation to fibrosis (64). The relative proportion of these cells in early versus late disease of both IPF and SSc-ILD is currently unknown, but could help clarify if these cells support ongoing damage and thus are a potential target for therapeutics in both diseases.

Akin to what other scRNA-seq analyses have observed in IPF (50, 65), our analysis identified a dramatic loss of alveolar type I cells in both IPF and SSc-ILD lungs, most significantly in the lower lobes. Despite a similar shift in population prevalence, amongst the epithelial populations the AT1 cells exhibited the most distinct transcriptional signatures between diseases, with upregulation of multiple cellular stress and DNA damage response pathways in IPF compared to SSc-ILD. Current models of IPF pathogenesis suggest repetitive epithelial cell microinjuries induce a dysregulated repair response, prompting a pathological fibrotic response, with the (potentially) intermediary roles for myeloid and lymphoid cells less clear (9). Preclinical models support that epithelial cell injury from environmental exposures may trigger fibrosis, with genetic predisposition and aging creating a more susceptible host to such dysregulated repair (66). Aspiration related to gastroesophageal reflux and esophageal dysmotility is one potential shared injurious mechanism to AT1 cells in IPF and SSc-ILD, although not present in all patients with either disease. While multiple sources of environmental injuries to AT1 cells may exist in SSc-ILD, the downregulation of damage response pathways relative to IPF suggests that their loss may be a secondary effect, rather than an initiating mechanism in SSc-ILD, or occurring due to a very different mechanism, such as injury from immune and/or secondary to endothelial cell dysfunction.

Our study was limited by its small sample size and exclusive use of advanced disease tissue. As patients with IPF and SSc-ILD now rarely undergo surgical lung biopsy, there was no early-stage disease tissue available for analysis. Pulmonary fibrosis, in particular IPF, often develops along an apicobasal gradient, thus we instead included samples from both the upper and lower lobes to capture a greater spectrum of disease. The graded shifts in cell populations most pronounced in the lower lobes, such as the loss of alveolar type 1 and natural killer cells, suggest

that this method may enable the identification of progressive changes in the disease course for at least some samples. All IPF and SSc-ILD samples are from patients with end-stage disease receiving care at a tertiary medical center and may not reflect the comprehensive IPF and SSc-ILD population. Due to the limited number of samples, we were unable to perform matching for age, sex, or the degree of pulmonary hypertension. Specifically, the sizeable difference in mean pulmonary artery pressure between the IPF and SSc-ILD patients (20.25 vs 39.75 mmHg) precluded us from determining if differences identified in the endothelial cells, smooth muscle cells, and pericytes are truly disease-specific versus secondary effects of increased pulmonary vascular pressures. To limit confounding from differences in experimental technique, we have chosen to limit our analysis to samples processes with the same digestion protocol and reagent chemistry. Due to the limited number of alveolar type 1 and plasmacytoid dendritic cells recovered from IPF and SSc-ILD samples, analysis of differentially expressed genes may have a higher false positive rate in these populations.

In summary, our analysis utilizes the enhanced capabilities of scRNA-seq to discriminate disease-specific alterations in explanted SSc-ILD and IPF lungs. Macrophages exhibit distinct interferon signatures in IPF versus SSc-ILD, with cytotoxic T cell and natural killer cells expressing similar patterns. The striking loss of alveolar type 1 cells in both diseases likely results from distinct mechanisms, with the presence of aberrant basaloid cells transcriptionally similar to those in IPF now confirmed in SSc-ILD as well. Focusing on shared and unique mechanisms of pathology in IPF and SSc-ILD provides improved insight to identifying treatments that may benefit both diseases. Improved phenotyping of patients with IPF and SSc-ILD to indicate those at highest risk for progressive disease, as well as those with a predominance of specific pathologic mechanisms (such as myofibroblast proliferation or Type 1 IFN signaling) is needed to better guide treatment choices throughout the disease course. Expanding existing lung scRNA-seq datasets and linking these to peripheral blood biomarkers may be a unique opportunity to link pathologic alterations in the tissue to clinically accessible biomarkers, allowing such improved phenotyping.

DATA AVAILABILITY STATEMENT

The datasets presented in this study can be found in online repositories. The names of the repository/repositories and accession number(s) can be found below: https://www.ncbi.nlm.nih.gov/geo, GSE 128169, GSE 128033, and GSE 156310.

AUTHOR CONTRIBUTIONS

EV: design of study, data generation, data analysis, writing of manuscript. TT, AP, JS, HB, MR: data generation and analysis. RL: design of study, interpretation of data and editing manuscript. All authors contributed to the article and approved the submitted version.

FUNDING

Research reported in this publication was supported by the National Institutes of Health NIAMS 2P50AR060780 (RL) and NHLBI 2T32HL007563-31 (EV). The content is solely the responsibility of the authors and does not necessarily represent the official views of the National Institutes of Health.

ACKNOWLEDGMENTS

The authors would like to acknowledge the University of Pittsburgh Medical Center lung transplantation team for procurement of lung tissue, the Center for Organ Recovery and Education, and the organ donors and their families for the generous donation of tissues utilized in this study.

SUPPLEMENTARY MATERIAL

The Supplementary Material for this article can be found online at: https://www.frontiersin.org/articles/10.3389/fimmu.2021.595811/full#supplementary-material

REFERENCES

1. Distler O, Highland KB, Gahlemann M, Azuma A, Fischer A, Mayes MD, et al. Nintedanib for Systemic Sclerosis-Associated Interstitial Lung Disease. *N Engl J Med* (2019) 380(26):2518–28. doi: 10.1056/NEJMoa1903076
2. Richeldi L, du Bois RM, Raghu G, Azuma A, Brown KK, Costabel U, et al. Efficacy and safety of nintedanib in idiopathic pulmonary fibrosis. *N Engl J Med* (2014) 370(22):2071–82. doi: 10.1056/NEJMoa1402584
3. Mathai SC, Danoff SK. Management of interstitial lung disease associated with connective tissue disease. *BMJ* (2016) 352:h6819. doi: 10.1136/bmj.h6819
4. Denton CP, Khanna D. Systemic sclerosis. *Lancet* (2017) 390(10103):1685–99. doi: 10.1016/S0140-6736(17)30933-9
5. Herzog EL, Mathur A, Tager AM, Feghali-Bostwick C, Schneider F, Varga J. Review: interstitial lung disease associated with systemic sclerosis and idiopathic pulmonary fibrosis: how similar and distinct? *Arthritis Rheumatol* (2014) 66(8):1967–78. doi: 10.1002/art.38702
6. Winstone TA, Assayag D, Wilcox PG, Dunne JV, Hague CJ, Leipsic J, et al. Predictors of mortality and progression in scleroderma-associated interstitial lung disease: a systematic review. *Chest* (2014) 146(2):422–36. doi: 10.1378/chest.13-2626
7. Wu W, Jordan S, Becker MO, Dobrota R, Maurer B, Fretheim H, et al. Prediction of progression of interstitial lung disease in patients with systemic sclerosis: the SPAR model. *Ann Rheum Dis* (2018) 77(9):1326–32. doi: 10.1136/annrheumdis-2018-213201
8. Steen VD, Medsger TA. Changes in causes of death in systemic sclerosis, 1972-2002. *Ann Rheum Dis* (2007) 66(7):940–4. doi: 10.1136/ard.2006.066068
9. Bagnato G, Harari S. Cellular interactions in the pathogenesis of interstitial lung diseases. *Eur Respir Rev* (2015) 24(135):102–14. doi: 10.1183/09059180.00003214
10. Dowson C, Simpson N, Duffy L, O'Reilly S. Innate Immunity in Systemic Sclerosis. *Curr Rheumatol Rep* (2017) 19(1):2. doi: 10.1007/s11926-017-0630-3

11. Lafyatis R. Transforming growth factor beta–at the centre of systemic sclerosis. *Nat Rev Rheumatol* (2014) 10(12):706–19. doi: 10.1038/nrrheum.2014.137
12. Korman B. Evolving insights into the cellular and molecular pathogenesis of fibrosis in systemic sclerosis. *Transl Res* (2019) 209:77–89. doi: 10.1016/j.trsl.2019.02.010
13. Liu F, Mih JD, Shea BS, Kho AT, Sharif AS, Tager AM, et al. Feedback amplification of fibrosis through matrix stiffening and COX-2 suppression. *J Cell Biol* (2010) 190(4):693–706. doi: 10.1083/jcb.201004082
14. Santos A, Lagares D. Matrix Stiffness: the Conductor of Organ Fibrosis. *Curr Rheumatol Rep* (2018) 20(1):2. doi: 10.1007/s11926-018-0710-z
15. Lokmic Z, Musyoka J, Hewitson TD, Darby IA. Hypoxia and hypoxia signaling in tissue repair and fibrosis. *Int Rev Cell Mol Biol* (2012) 296:139–85. doi: 10.1016/B978-0-12-394307-1.00003-5
16. Goldin J, Elashoff R, Kim HJ, Yan X, Lynch D, Strollo D, et al. Treatment of scleroderma-interstitial lung disease with cyclophosphamide is associated with less progressive fibrosis on serial thoracic high-resolution CT scan than placebo: findings from the scleroderma lung study. *Chest* (2009) 136(5):1333–40. doi: 10.1378/chest.09-0108
17. Volkmann ER, Tashkin DP, Li N, Roth MD, Khanna D, Hoffmann-Vold AM, et al. Mycophenolate Mofetil Versus Placebo for Systemic Sclerosis-Related Interstitial Lung Disease: An Analysis of Scleroderma Lung Studies I and II. *Arthritis Rheumatol* (2017) 69(7):1451–60. doi: 10.1002/art.40114
18. Sullivan KM, Goldmuntz EA, Keyes-Elstein L, McSweeney PA, Pinckney A, Welch B, et al. Myeloablative Autologous Stem-Cell Transplantation for Severe Scleroderma. *N Engl J Med* (2018) 378(1):35–47. doi: 10.1056/nejmoa1703327
19. Burt RK, Shah SJ, Dill K, Grant T, Gheorghiade M, Schroeder J, et al. Autologous non-myeloablative haemopoietic stem-cell transplantation compared with pulse cyclophosphamide once per month for systemic sclerosis (ASSIST): an open-label, randomised phase 2 trial. *Lancet* (2011) 378(9790):498–506. doi: 10.1016/S0140-6736(11)60982-3
20. van Laar JM, Farge D, Sont JK, Naraghi K, Marjanovic Z, Larghero J, et al. Autologous hematopoietic stem cell transplantation vs intravenous pulse cyclophosphamide in diffuse cutaneous systemic sclerosis: a randomized clinical trial. *JAMA* (2014) 311(24):2490–8. doi: 10.1001/jama.2014.6368
21. Kondoh Y, Taniguchi H, Yokoi T, Nishiyama O, Ohishi T, Kato T, et al. Cyclophosphamide and low-dose prednisolone in idiopathic pulmonary fibrosis and fibrosing nonspecific interstitial pneumonia. *Eur Respir J* (2005) 25(3):528–33. doi: 10.1183/09031936.05.00071004
22. Tzouvelekis A, Bouros E, Oikonomou A, Ntolios P, Zacharis G, Kolios G, et al. Effect and safety of mycophenolate mofetil in idiopathic pulmonary fibrosis. *Pulm Med* (2011) 2011:849035. doi: 10.1155/2011/849035
23. Idiopathic Pulmonary Fibrosis Clinical Research N, Raghu G, Anstrom KJ, King TEJr, Lasky JA, Martinez FJ. Prednisone, azathioprine, and N-acetylcysteine for pulmonary fibrosis. *N Engl J Med* (2012) 366(21):1968–77. doi: 10.1056/NEJMoa1113354
24. Distler JHW, Gyorfi AH, Ramanujam M, Whitfield ML, Konigshoff M, Lafyatis R. Shared and distinct mechanisms of fibrosis. *Nat Rev Rheumatol* (2019) 15(12):705–30. doi: 10.1038/s41584-019-0322-7
25. Allen RJ, Guillen-Guio B, Oldham JM, Ma SF, Dressen A, Paynton ML, et al. Genome-Wide Association Study of Susceptibility to Idiopathic Pulmonary Fibrosis. *Am J Respir Crit Care Med* (2020) 201(5):564–74. doi: 10.1164/rccm.201905-1017OC
26. Lorenzo-Salazar JM, Ma SF, Jou J, Hou PC, Guillen-Guio B, Allen RJ, et al. Novel idiopathic pulmonary fibrosis susceptibility variants revealed by deep sequencing. *ERJ Open Res* (2019) 5(2):00071-2019. doi: 10.1183/23120541.00071-2019
27. Lopez-Isac E, Acosta-Herrera M, Kerick M, Assassi S, Satpathy AT, Granja J, et al. GWAS for systemic sclerosis identifies multiple risk loci and highlights fibrotic and vasculopathy pathways. *Nat Commun* (2019) 10(1):4955. doi: 10.1038/s41467-019-12760-y
28. Angiolilli C, Marut W, van der Kroef M, Chouri E, Reedquist KA, Radstake T. New insights into the genetics and epigenetics of systemic sclerosis. *Nat Rev Rheumatol* (2018) 14(11):657–73. doi: 10.1038/s41584-018-0099-0
29. Borie R, Crestani B, Dieude P, Nunes H, Allanore Y, Kannengiesser C, et al. The MUC5B variant is associated with idiopathic pulmonary fibrosis but not with systemic sclerosis interstitial lung disease in the European Caucasian population. *PLoS One* (2013) 8(8):e70621. doi: 10.1371/journal.pone.0070621
30. Juge PA, Lee JS, Ebstein E, Furukawa H, Dobrinskikh E, Gazal S, et al. MUC5B Promoter Variant and Rheumatoid Arthritis with Interstitial Lung Disease. *N Engl J Med* (2018) 379(23):2209–19. doi: 10.1056/NEJMoa1801562
31. Morse C, Tabib T, Sembrat J, Buschur KL, Bittar HT, Valenzi E, et al. Proliferating SPP1/MERTK-expressing macrophages in idiopathic pulmonary fibrosis. *Eur Respir J* (2019) 54(2):1802441. doi: 10.1183/13993003.02441-2018
32. Valenzi E, Bulik M, Tabib T, Morse C, Sembrat J, Trejo Bittar H, et al. Single-cell analysis reveals fibroblast heterogeneity and myofibroblasts in systemic sclerosis-associated interstitial lung disease. *Ann Rheum Dis* (2019) 78(10):1379–87. doi: 10.1136/annrheumdis-2018-214865
33. Macosko EZ, Basu A, Satija R, Nemesh J, Shekhar K, Goldman M, et al. Highly Parallel Genome-wide Expression Profiling of Individual Cells Using Nanoliter Droplets. *Cell* (2015) 161(5):1202–14. doi: 10.1016/j.cell.2015.05.002
34. Satija R, Farrell JA, Gennert D, Schier AF, Regev A. Spatial reconstruction of single-cell gene expression data. *Nat Biotechnol* (2015) 33(5):495–502. doi: 10.1038/nbt.3192
35. Stuart T, Butler A, Hoffman P, Hafemeister C, Papalexi E, Mauck WM,3, et al. Comprehensive Integration of Single-Cell Data. *Cell* (2019) 177(7):1888–902.e21. doi: 10.1016/j.cell.2019.05.031
36. Becht E, McInnes L, Healy J, Dutertre CA, Kwok IWH, Ng LG, et al. Dimensionality reduction for visualizing single-cell data using UMAP. *Nat Biotechnol* (2019) 37:38–44. doi: 10.1038/nbt.4314
37. Ashburner M, Ball CA, Blake JA, Botstein D, Butler H, Cherry JM, et al. Gene ontology: tool for the unification of biology. The Gene Ontology Consortium. *Nat Genet* (2000) 25(1):25–9. doi: 10.1038/75556
38. The Gene Ontology C. The Gene Ontology Resource: 20 years and still GOing strong. *Nucleic Acids Res* (2019) 47(D1):D330–D8. doi: 10.1093/nar/gky1055
39. de Hoon MJ, Imoto S, Nolan J, Miyano S. Open source clustering software. *Bioinformatics* (2004) 20(9):1453–4. doi: 10.1093/bioinformatics/bth078
40. Bouros D, Wells AU, Nicholson AG, Colby TV, Polychronopoulos V, Pantelidis P, et al. Histopathologic subsets of fibrosing alveolitis in patients with systemic sclerosis and their relationship to outcome. *Am J Respir Crit Care Med* (2002) 165(12):1581–6. doi: 10.1164/rccm.2106012
41. Hsu E, Shi H, Jordan RM, Lyons-Weiler J, Pilewski JM, Feghali-Bostwick CA. Lung tissues in patients with systemic sclerosis have gene expression patterns unique to pulmonary fibrosis and pulmonary hypertension. *Arthritis Rheumatol* (2011) 63(3):783–94. doi: 10.1002/art.30159
42. Seibold MA, Smith RW, Urbanek C, Groshong SD, Cosgrove GP, Brown KK, et al. The idiopathic pulmonary fibrosis honeycomb cyst contains a mucocilary pseudostratified epithelium. *PLoS One* (2013) 8(3):e58658. doi: 10.1371/journal.pone.0058658
43. Hu X, Fernandes J, Jones DP, Go YM. Cadmium stimulates myofibroblast differentiation and mouse lung fibrosis. *Toxicology* (2017) 383:50–6. doi: 10.1016/j.tox.2017.03.018
44. So CC, Ramachandran S, Martin A. E3 Ubiquitin Ligases RNF20 and RNF40 Are Required for Double-Stranded Break (DSB) Repair: Evidence for Monoubiquitination of Histone H2B Lysine 120 as a Novel Axis of DSB Signaling and Repair. *Mol Cell Biol* (2019) 39(8):e00488-18. doi: 10.1128/MCB.00488-18
45. Li S, Zhao J, Shang D, Kass DJ, Zhao Y. Ubiquitination and deubiquitination emerge as players in idiopathic pulmonary fibrosis pathogenesis and treatment. *JCI Insight* (2018) 3(10):e120362. doi: 10.1172/jci.insight.120362
46. Lear T, McKelvey AC, Rajbhandari S, Dunn SR, Coon TA, Connelly W, et al. Ubiquitin E3 ligase FIEL1 regulates fibrotic lung injury through SUMO-E3 ligase PIAS4. *J Exp Med* (2016) 213(6):1029–46. doi: 10.1084/jem.20151229
47. Hetz C, Martinon F, Rodriguez D, Glimcher LH. The unfolded protein response: integrating stress signals through the stress sensor IRE1alpha. *Physiol Rev* (2011) 91(4):1219–43. doi: 10.1152/physrev.00001.2011
48. Winters NI, Burman A, Kropski JA, Blackwell TS. Epithelial Injury and Dysfunction in the Pathogenesis of Idiopathic PulmonaryFibrosis. *Am J Med Sci* (2019) 357(5):374–8. doi: 10.1016/j.amjms.2019.01.010
49. Habermann AC, Gutierrez AG, Bui LT, Yahn SL, Winters NI, Calvi CL, et al. Single-cell RNA sequencing reveals profibrotic roles of distinct epithelial and

mensenchymal lineages in pulmonary fibrosis. *Sci Adv* (2020) 6(28):eaba1972. doi: 10.1126/sciadv.aba1972
50. Adams TS, Schupp JC, Poli S, Ayaub EA, Neumark N, Ahangari F, et al. Single-cell RNA-seq reveals ectopic and aberrant lung-resident cell populations in idiopathic pulmonary fibrosis. *Sci Adv* (2020) 6(28): eaba1983. doi: 10.1126/sciadv.aba1983
51. Dutta A, Li J, Fedele C, Sayeed A, Singh A, Violette SM, et al. alphavbeta6 integrin is required for TGFbeta1-mediated matrix metalloproteinase2 expression. *Biochem J* (2015) 466(3):525–36. doi: 10.1042/BJ20140698
52. Brkic Z, van Bon L, Cossu M, van Helden-Meeuwsen CG, Vonk MC, Knaapen H, et al. The interferon type I signature is present in systemic sclerosis before overt fibrosis and might contribute to its pathogenesis through high BAFF gene expression and high collagen synthesis. *Ann Rheum Dis* (2016) 75 (8):1567–73. doi: 10.1136/annrheumdis-2015-207392
53. Sierra-Sepulveda A, Esquinca-Gonzalez A, Benavides-Suarez SA, Sordo-Lima DE, Caballero-Islas AE, Cabral-Castaneda AR, et al. Systemic Sclerosis Pathogenesis and Emerging Therapies, beyond the Fibroblast. *BioMed Res Int* (2019) 2019:4569826. doi: 10.1155/2019/4569826
54. Wu M, Assassi S. The role of type 1 interferon in systemic sclerosis. *Front Immunol* (2013) 4:266. doi: 10.3389/fimmu.2013.00266
55. King TEJr, Albera C, Bradford WZ, Costabel U, Hormel P, Lancaster L, et al. Effect of interferon gamma-1b on survival in patients with idiopathic pulmonary fibrosis (INSPIRE): a multicentre, randomised, placebo-controlled trial. *Lancet* (2009) 374(9685):222–8. doi: 10.1016/S0140-6736 (09)60551-1
56. Diaz KT, Skaria S, Harris K, Solomita M, Lau S, Bauer K, et al. Delivery and safety of inhaled interferon-gamma in idiopathic pulmonary fibrosis. *J Aerosol Med Pulm Drug Deliv* (2012) 25(2):79–87. doi: 10.1089/jamp.2011.0919
57. Smaldone GC. Repurposing of gamma interferon *via* inhalation delivery. *Adv Drug Deliv Rev* (2018) 133:87–92. doi: 10.1016/j.addr.2018.06.004
58. Swiecki M, Colonna M. The multifaceted biology of plasmacytoid dendritic cells. *Nat Rev Immunol* (2015) 15(8):471–85. doi: 10.1038/nri3865
59. Kafaja S, Valera I, Divekar AA, Saggar R, Abtin F, Furst DE, et al. pDCs in lung and skin fibrosis in a bleomycin-induced model and patients with systemic sclerosis. . *JCI Insight* (2018) 3(9):e98380. doi: 10.1172/jci.insight.98380
60. Rossato M, Affandi AJ, Thordardottir S, Wichers CGK, Cossu M, Broen JCA, et al. Association of MicroRNA-618 Expression With Altered Frequency and Activation of Plasmacytoid Dendritic Cells in Patients With Systemic Sclerosis. *Arthritis Rheumatol* (2017) 69(9):1891–902. doi: 10.1002/art.40163
61. Takahashi T, Asano Y, Nakamura K, Yamashita T, Saigusa R, Ichimura Y, et al. A potential contribution of antimicrobial peptide LL-37 to tissue fibrosis and vasculopathy in systemic sclerosis. *Br J Dermatol* (2016) 175(6):1195–203. doi: 10.1111/bjd.14699
62. Tort Tarres M, Aschenbrenner F, Maus R, Stolper J, Schuette L, Knudsen L, et al. The FMS-like tyrosine kinase-3 ligand/lung dendritic cell axis contributes to regulation of pulmonary fibrosis. *Thorax* (2019) 74(10):947–57. doi: 10.1136/thoraxjnl-2018-212603
63. Tsoumakidou M, Karagiannis KP, Bouloukaki I, Zakynthinos S, Tzanakis N, Siafakas NM. Increased bronchoalveolar lavage fluid CD1c expressing dendritic cells in idiopathic pulmonary fibrosis. *Respiration* (2009) 78 (4):446–52. doi: 10.1159/000226244
64. Hewlett JC, Kropski JA, Blackwell TS. Idiopathic pulmonary fibrosis: Epithelial-mesenchymal interactions and emerging therapeutic targets. *Matrix Biol* (2018) 71-72:112–27. doi: 10.1016/j.matbio.2018.03.021
65. Reyfman PA, Walter JM, Joshi N, Anekalla KR, McQuattie-Pimentel AC, Chiu S, et al. Single-Cell Transcriptomic Analysis of Human Lung Provides Insights into the Pathobiology of Pulmonary Fibrosis. *Am J Respir Crit Care Med* (2019) 199(12):1517–36. doi: 10.1164/rccm.201712-2410OC
66. Chambers RC, Mercer PF. Mechanisms of alveolar epithelial injury, repair, and fibrosis. *Ann Am Thorac Soc* (2015) 12(Suppl 1):S16–20. doi: 10.1513/AnnalsATS.201410-448MG

Conflict of Interest: RL reports grants from Bristol Myers Squibb, Corbus, Formation, Elpidera, Regeneron, Pfizer, and Kiniksa outside the submitted work; personal fees from Bristol Myers Squibb, Formation, Sanofi, Biocon, Boehringer Mannheim, Merck, and Genentech/Roche outside the submitted work.

The remaining authors declare that the research was conducted in the absence of any commercial or financial relationships that could be construed as a potential conflict of interest.

frontiers in Immunology

ORIGINAL RESEARCH
published: 21 July 2021
doi: 10.3389/fimmu.2021.665100

Dual Effect of Bleomycin on Histopathological Features of Lungs and Mediastinal Fat-Associated Lymphoid Clusters in an Autoimmune Disease Mouse Model

Yaser Hosny Ali Elewa[1,2*], *Osamu Ichii*[2,3], *Teppei Nakamura*[2,4] *and Yasuhiro Kon*[2]

[1] *Department of Histology and Cytology, Faculty of Veterinary Medicine, Zagazig University, Zagazig, Egypt,* [2] *Laboratory of Anatomy, Department of Basic Veterinary Sciences, Faculty of Veterinary Medicine, Hokkaido University, Sapporo, Japan,* [3] *Laboratory of Agrobiomedical Science, Faculty of Agriculture, Hokkaido University, Sapporo, Japan,* [4] *Section of Biological Safety Research, Chitose Laboratory, Japan Food Research Laboratories, Hokkaido, Japan*

Mediastinal fat-associated lymphoid clusters (MFALCs) are novel immune clusters that function in the pathogenesis of bleomycin (BLM)-induced pneumonitis in a C57BL/6 mouse model. However, we lack literature on the effects of BLM in an autoimmune disease mouse model (AIDM). In the present study, BLM sulfate (BLM group) or phosphate-buffered saline (PBS group) were intranasally administered in BXSB/MpJ-Yaa (Yaa) AIDM and its wild-type strains (BXSB/MpJ "BXSB") and the histopathology of MFALCs and lungs were examined on days 7 and 21 days. Immunohistochemical analysis was performed to detect lymphatic vessels (LVs), high endothelial venules (HEVs), proliferating, and immune cells. Furthermore, the mRNA expression of Yaa locus genes (*TLR7*, *TLR8*, *Arhgap6*, *Msl3*, and *Tceanc*) was detected in the lung tissues. Here, we show a dual effect of BLM on intra-thoracic immune hemostasis among Yaa AIDM and its corresponding wild-type strain (BXSB mice). The BLM group of BXSB mice displayed significantly higher values of lung injury scores (LIS) and size of MFALCs as compared with the corresponding PBS group. However, an opposite effect was detected in Yaa mice. Furthermore, Yaa mice displayed decreased serum autoantibody titers and downregulated expression of *TLR7*, *TLR8*, *Msl3*, and *Tceanc* in the lungs following BLM administration, especially on day 21. Interestingly, significant positive correlations were detected in both strains between the LIS and the size of MFALCs, LVs, HEVs, and proliferating cells. Conclusively, our findings revealed a crucial function of HEVs on the extent of lung injury and the development of MFALCs in BLM-administered Yaa AIDM and control BXSB mice with dual effects. Moreover, our data suggest that down regulation of Yaa locus genes could contribute as an important attributing factor leading to decrease in the degree of autoimmunity and lung injury in AIDM. Therefore, we suggest that genetic background contributes to BLM diversity among AIDM and the wild-type strain. Targeting some genes or venules could provide novel therapeutic approaches for some autoimmune-associated respiratory diseases *via* controlling the MFALCs development.

Keywords: bleomycin, immune cell infiltration, lung injury score, mediastinal adipose tissue, high endothelial venules

OPEN ACCESS

Edited by:
Anna-Maria Hoffmann-Vold, Oslo University Hospital, Norway

Reviewed by:
Christoph Hudemann, Philipps-University Marburg, Germany
Hongbing Guan, Guangzhou Medical University, China

***Correspondence:**
Yaser Hosny Ali Elewa
yaserelewa@yahoo.com

Specialty section:
This article was submitted to Autoimmune and Autoinflammatory Disorders, a section of the journal Frontiers in Immunology

Received: *07 February 2021*
Accepted: *23 June 2021*
Published: *21 July 2021*

Citation:
Elewa YHA, Ichii O, Nakamura T and Kon Y (2021) Dual Effect of Bleomycin on Histopathological Features of Lungs and Mediastinal Fat-Associated Lymphoid Clusters in an Autoimmune Disease Mouse Model. Front. Immunol. 12:665100. doi: 10.3389/fimmu.2021.665100

INTRODUCTION

Fat-associated lymphoid clusters (FALCs) are atypical lymphoid clusters (LCs) associated with adipose tissues on various mucosal surfaces, including the mediastinum, pericardium, mesenteries, omentum, and gonadal fat in humans and mice (1–4). FALCs were first identified in healthy mouse and human mediastinal and mesenteric adipose tissues and consist of numerous macrophages, T and B lymphocytes, as well as a small number of granulocytes. Moreover, these are enriched with blood vessels, lymphatic vessels (LVs), and high endothelial venules (HEVs) (1, 2, 5). FALCs have been recently implicated in the progression of several diseases in both mice and humans and in protecting against helminth infections (1). In addition, mesenteric FALCs markedly increase in number and size on day 3 following zymosan-induced peritoneal inflammation (3). Furthermore, our previous studies have suggested a possible function of mediastinal FALCs (MFALCs) in the pathogenesis of lung injuries in both autoimmune mouse model (MRL/MpJ-*lpr* mice "Lpr" and BXSB/MpJ-*Yaa* "Yaa" mice) (6) and bleomycin (BLM)-induced pneumonitis C57BL/6 (B6) mice model (7).

BLM is an antitumor drug that has been used successfully to treat a variety of malignancies, including Hodgkin's lymphoma that usually affects young individuals and germ cell testicular tumors. However, its therapeutic use in humans is associated with the development of pulmonary toxicity and fibrosis in up to 10% of patients receiving it (8). Similarly, differences in the susceptibility to fibrosis of mouse strains following administration of a single dose of BLM have been reported in which C57BL/6 (B6) mice were susceptible to BLM-induced lung injury and developed pneumonitis and lung fibrosis (7, 9). In contrast, other strains, such as DBA/2 (DBA), BALB/c, and C3H/HeJ mice, are resistant to BLM-induced lung injury and fibrosis (10, 11). Interestingly, our previous study revealed a difference in the size of MFALCs between different strains in which the DBA mice showed less developed MFALCs than B6 mice (2). Furthermore, we have recently reported a dramatic increase in the size of MFALCs following administration of a single dose of BLM in B6 mice at both 7 and 21 days. In addition, we have reported a significant positive correlation between the size of MFALCs and lung injury following BLM administration, suggesting the involvement of MFALCs in the pathogenesis of BLM-induced fibrosis (7). Although genetic susceptibility is an important risk factor for several diseases as well as susceptibility to BLM-induced fibrotic lung injury (10), the effect of BLM on both lung injury and size of MFALCs in both the autoimmune disease mouse model (that showed severe lung injury and well-developed MFALCs) and its control strains (that showed normal lung architecture and less developed MFALCs) (6) has not yet been established.

Numerous autoimmune murine models are currently being used to understand the cellular and genetic aspects of the progression of autoimmune disease in humans, such as Lpr and Yaa, along with a comparison with their healthy control mice MRL/MpJ "MpJ" and BXSB/MpJ "BXSB,", respectively (12). Such autoimmune mouse models develop lupus-like diseases with symptoms similar to those of human systemic lupus erythematosus (SLE) (13). The autoimmune lesions in the Lpr mouse developed in both sexes and resulted from a mutation in a single gene (Fas receptor gene) (14), and defects in this gene resulted in marked lymphadenopathy and splenomegaly (15). In contrast, the autoimmune disease occurred only in male Yaa mice due to the translocation of an X chromosomal region onto the Y chromosome (16), resulting in 15 duplicated genes on the Y chromosome (17).

Interestingly, we have recently reported high expression of certain genes on Yaa locus, such as Toll-like receptor 7 (*Tlr7*) and *Tlr8*, in Yaa mice than in BXSB mice at both young (three months) and old (six months) ages. Moreover, the expression of other Yaa locus genes, such as male-specific lethal-subunit 3 (*Msl3*), Rho GTPase activating protein 6 (*Arhgap6*), and transcription elongation factor A (SII) N-terminal (*Tceanc)* was significantly increased with the progression of autoimmune disease (18).

The genetic basis of susceptibility to BLM-induced pulmonary fibrosis in several healthy strains has been established (10). Our previous report in genetically mutated autoimmune mouse models (Lpr and Yaa) indicated more developed MFALCs and severe lung injury in comparison with the control strains (MpJ and BXSB) (6). However, it is still unknown whether such genetic mutations in autoimmune mouse models could affect their response to BLM. Therefore, in the present study, we used the autoimmune disease model strain (Yaa) and their control strain (BXSB) to study the genetic variations regulating the response of BLM-induced pulmonary fibrosis.

MATERIALS AND METHODS

Ethics Statement

The animal experiments were performed under a protocol approved by the Institutional Animal Care and Use Committee of the Graduate School of Veterinary Medicine, Hokkaido University (approval no. 15–0079).

Experimental Animals and Design

We used the autoimmune mouse model established in adult Yaa male mice of 12 weeks of age and its control strain (BXSB mice). Mice were purchased from Japan SLC, Inc. (Shizuoka, Japan) and housed in a specific pathogen-free facility with free access to water and chow. Sixteen mice belonging to each strain were used and divided into two groups, including BLM and phosphate-buffered saline (PBS). In the BLM group, 50 μL of BLM sulfate (LKT Laboratories, Inc., catalog number: B4518, lot number: 2599253) was diluted in sterile PBS at a concentration of 5 mg/kg, was administered as a single intranasal dose. The control group received 50 μL of sterile PBS intranasally. on days 7 and 21, four mice from each group were subjected to deep anesthesia using a mixture of medetomidine (0.3 mg/kg), butorphanol (5.0 mg/kg), and midazolam (4.0 mg/kg). At the same time, the blood was collected by cutting of femoral artery, and transcardial perfusion with PBS was performed. Then the spleens were harvested from mice and weighted in all groups, and both mediastinal fat tissues (MFTs) and right lung lobes were immediately collected and fixed in 4% paraformaldehyde

overnight at 4°C. The left lung lobe from different groups was immediately inserted into liquid nitrogen and stored at −80°C until further analysis.

Tissue Preparation for Histopathological Analysis

The specimens were washed following overnight fixation, dehydrated in ascending grades (70, 80, 90, 95%, absolute I, II, and III) of alcohol, cleared in xylene, and subsequently embedded in paraffin. Paraffin sections (3 μm) of MFTs were prepared for histopathological analysis. Sections were stained with H&E and Masson's trichrome (MT). Furthermore, immunohistochemistry was performed using 3 μm thick sections to detect different vessels ($PNAd^+$ HEVs and $LYVE\text{-}1^+$ LVs), immune cells ($B220^+$ B cells, $CD3^+$ T cells, $Iba1^+$ macrophages, and $Gr1^+$ granulocytes), and $BrdU^+$ proliferating cells. BrdU-incorporating cells were detected as described in our previous study (2). Immunohistochemical staining was performed following the method described in our previous study (19). The details of antigen retrieval and optimal primary antibody dilutions are summarized in **Table 1**. Additionally, the lung sections of different studied groups were stained with rabbit polyclonal anti-collagen I antibody, and anti-COL3A1 to detect degree of collagen depositions for different collagen types according to our recent report (20). Furthermore, double immunofluorescence staining was performed to reveal the occurrence of $B220^+$ B cells and $CD3^+$ T cells in both MFALCs and the lungs of different groups in both studied strains. The immunofluorescent images were captured by a fluorescence microscope (BZX-710; Keyence; Osaka, Japan).

Quantitative Polymerase Chain Reaction Analysis

Total RNA was purified from the frozen lung samples of each group using TRIzol reagent (Thermo Fisher Scientific; Waltham, MA, USA) according to the manufacturer's instructions. The purified total RNA of each sample was used as a template to synthesize cDNA using ReverTra Ace qPCR RT Master Mix (Toyobo Co., Osaka, Japan). Thereafter, the cDNA (20 ng/μL) from each sample was used for qPCR analysis using either TaqMan PCR method (for analysis of fibrosis genes: actin, alpha 2, smooth muscle, aorta [*Acta2*]; collagen, type I, alpha 1 [*Col1a1*]; and collagen, type III, alpha 1 [*Col3a1*]) as we previously described (7) or THUNDERBIRD® SYBR® qPCR Mix (Toyobo Co., Ltd.) for the analysis of Yaa locus genes (*TLR7*, *TLR8*, *Arhgap6*, *Msl3*, and *Tceanc*) as we recently reported (18). The gene expression data were normalized using the housekeeping β-actin (*ACTB*) gene.

Enzyme-Linked Immunosorbent Assay for Serum Autoantibody Measurement

To evaluate the extent of systemic autoimmune conditions, the titers of anti-dsDNA autoantibodies in the sera of mice were measured by enzyme-linked immunosorbent assay (ELISA) using the Alpha Diagnostic International Inc. mouse anti-dsDNA ELISA Kit (M-5110; San Antonio, TX, USA) according to the manufacturer's instructions.

Histomorphometric Measurements

For histoplanimetry, four mice were analyzed per group on day 7 (early time points) and day 21 (late time points). Using the BZ-X710 microscope (Keyence; Osaka, Japan), digital images from H&E, MT, and immune-stained tissue sections were captured for further analysis. The ratio of lymphoid clusters (LCs) area/total MFTs area was calculated from the H&E-stained digital images using the ImageJ software (ver. 1.32j, http://rsb.info.nih.gov/ij), as described in our previous reports (7, 20). Furthermore, the extent of lung injury was measured using images of MT-stained lung sections from grade 0 to 8 according to the scoring criteria reported by Ashcroft et al. (21), and the average of such scores per mouse was recorded. Briefly, different digital images from microscopic fields of all lung tissues for each mouse belonging to different groups were captured. Thereafter, we graded the field with normal lung structure as grade 0 and scored the field with lung lesions as grades 1 to 8. In grade 1, the lesions corresponded to a slight thickening of the alveolar wall with a few cellular infiltrations. In grade 3, the lesions were characterized by a slight thickening of the alveolar wall with moderate cellular infiltrations. In grade 5, numerous cellular infiltrations with mild fibrosis and damage to the lung architecture were observed. In grade 7, severe damage of lung tissue with clear fibrous masses was observed. Grade 8 showed total replacement of lung tissues with fibrous tissue. We used the odd number grade for scaling of the extent of lung injury; however, in case of difficulty in distinguishing between the two odd number grades, we used the intervening even-numbered grades. Subsequently, the scores of different microscopic fields/mice were recorded, and the average score of all grades was quantified. Furthermore, the lung injury scores of different groups from both studied strains (Yaa, and BXSB mice) were compared to that of photographs captured from MT-stained lung sections from the wild-type strain (B6 mice) treated with either BLM or PBS in our previous study at the indicated time points (**Supplementary Figure 1**).

For immune-stained MFTs and lung tissue sections, digital images were captured at ×200 power field using the BZ-X710

TABLE 1 | List of antibodies, working dilutions, and methods for antigen retrieval.

Antibody	Source	Dilution	Antigen retrieval	Heating condition
Rat anti-BrdU	Abcam (Tokyo, Japan)	1:200	10 mM citrate buffer (pH 6.0)	105°C, 20 min
Rabbit anti-CD3	Nichirei (Tokyo, Japan)	1:200	10 mM Tris-HCl buffer (pH 7.4)	105°C, 20 min
Rat anti-B220	Cedarlane (Ontario, Canada)	1:1600	10 mM citrate buffer (pH 6.0)	105°C, 20 min
Rabbit anti-Iba1	Wako (Osaka, Japan)	1:1200	10 mM citrate buffer (pH 6.0)	105°C, 20 min
Rat anti-Gr1	R and D system (Minneapolis, USA)	1:800	0.1% pepsin/0.2 N HCl	37°C, 5 min
Rabbit anti-LYVE-1	Adipogen (San Diego, CA, USA)	1:500	10 mM citrate buffer (pH 6.0)	105°C, 20 min
Rat anti-PNAd	BioLegend (San Diego, CA, USA)	1:500	10 mM Tris-HCl buffer (pH 7.4)	105°C, 20 min

(Keyence, Osaka, Japan), and the following measurements were performed using the BZ-X analyzer (Keyence): percentage of positive area ratio of collagen I, and COL3A1 immuno-stained lung sections, relative area ratio of LYVE-1$^+$ LVs in the lungs and MFALCs and PNAd$^+$ HEVs in MFALCs (as previously described (7), PNAd$^+$ HEVs number/mice in the lung field, and the positive area ratio of different immune cells (B and T lymphocytes, macrophages, and granulocytes) in both MFALCs and lung fields in different groups. To analyze the extent of proliferation within both MFALCs and lung lobes, the number of BrdU$^+$ proliferative cells was counted and represented as the percentage of either cell density ratio in MFALCs (number of positive cells divided by the total number of cells within the clusters) or as a positive index ratio in lung (number of positive cells divided by the field area of different lung fields). Such percentages were compared between the two groups. Furthermore, we examined the spleen/body weight (B.W.) ratios.

Statistical Analysis

Differences between the groups were compared using the Kruskal–Wallis test, followed by Scheffé's method for multiple comparisons when significant differences were observed. Numerical data are presented as mean± standard error. *P*-values < 0.05 were considered statistically significant. To analyze the correlation between two variables, Spearman's correlation test was used (*significant value, $P < 0.05$, **highly significant value, $P < 0.01$).

RESULTS

Morphological Features of MFALCs in BLM Mouse Model Versus the Phosphate-Buffered Saline Control Group

Examination of hematoxylin and eosin (H&E)-stained sections of MFTs in BXSB mice revealed more developed MFALCs in the BLM groups than in the PBS groups at both time points (days 7 and 21) (**Figure 1A**). However, a remarkable decrease in such clusters was observed in Yaa mice following BLM administration when compared with the PBS groups on days 7 and 21 (**Figure 1B**). To assess the histological index of development of MFALCs, we measured the area ratio of LCs/MFTs in H&E-stained sections. As shown in **Figure 1C**, the sizes of MFALCs were significantly larger in the BLM group of BXSB mice at both time points in comparison with those in the PBS-treated control group. In contrast, a significant decrease in the LCs/MFTs area ratios in the BLM group of Yaa mice was observed on both 7 and 21 days than in the PBS group. Furthermore, such ratios were significantly lower in the BLM group on day 21 than that on day 7 (**Figure 1D**).

Histopathological Analysis of the Degree of Lung Injury in BLM and PBS-Treated Groups

H&E-stained lung tissue sections in PBS groups of BXSB mice (days 7 and 21) showed the normal histological structure of the lung tissues, including thin-walled alveoli with scarce mononuclear cellular infiltration. However, disruption of the normal lung architecture was observed in the BLM group. Examination of the lung sections of the BLM group on day 7 revealed high cellular infiltration in the interstitial tissue, thickening of the inter-alveolar space, and a few collapsed alveoli. On day 21, the BLM group showed severely distorted parenchyma with an increased disposition of connective tissue (CT), replacing the normal alveoli and numerous collapsed alveoli (**Figure 2A**).

As shown in **Figure 2B**, the lung tissues of the PBS group in Yaa mice showed numerous mononuclear cellular infiltrations into the lung parenchyma and several collapsed alveoli with thickening of the interalveolar septa on day 7. On day 21, the lung tissues in the PBS group showed severe lung lesions represented by high cellular infiltration that replaced most of the lung parenchyma with a few collapsed alveoli. Interestingly, moderate cellular infiltration with a slight thickening of the alveolar wall and interalveolar septum were observed following BLM administration in the lung tissues of Yaa mice on day 7. On day 21, the lung tissues in the BLM group of Yaa mice showed restoration of the normal lung architecture with little cellular infiltration and thin alveolar wall, suggesting the recovery of lung inflammation after BLM exposure.

To detect the extent of lung injury, we graded several MT-stained lung microscopic fields from PBS and BLM groups in both BXSB and Yaa mice on days 7 and 21 into scores according to the criteria described by Ashcroft et al. (22). The average of scores was compared between the groups in both the strains. Interestingly, the average lung injury score in BXSB mice increased significantly in the BLM group on days 7 and 21 than those of the PBS group. Furthermore, the BLM group showed significantly higher lung injury scores on day 21 than on day 7 (**Figure 2C**). In contrast, a sharp significant decrease in the lung injury scores in the BLM group of Yaa mice on both days 7 and 21 was observed than those in the PBS group (**Figure 2D**). As shown in **Supplementary Figure 1**, the BLM group of wild-type strain (B6 mice) at 21d showed significant higher lung injury score than other studied groups. On the other hand, the BLM group of B6 mice at 7d revealed significant difference in such score when compared with that of BXSB (BLM, and PBS groups at both 7 and 21 d), B6 (PBS groups at both 7 and 21 d), and Yaa (BLM groups at both 7 and 21 d) mice, but not with the PBS groups (7 and 21d) of Yaa mice.

Extent of Lung Fibrosis in BLM and PBS-Treated Groups

To identify the effect of BLM on the progression of lung inflammation and fibrosis in both BXSB and Yaa mice, we compared the histopathology of MT-stained lung sections between the PBS and BLM groups at both early and late time points (days 7 and 21, respectively). The PBS groups in BXSB mice showed a normal lung architecture with a few aniline blue-positive collagen fibers around the bronchioles. The BLM group showed high cellular infiltration and few aniline blue-positive collagen fibers around the bronchioles on day 7 and more aniline blue-positive collagen fiber depositions around the large bronchioles and within the lung parenchyma on day 21

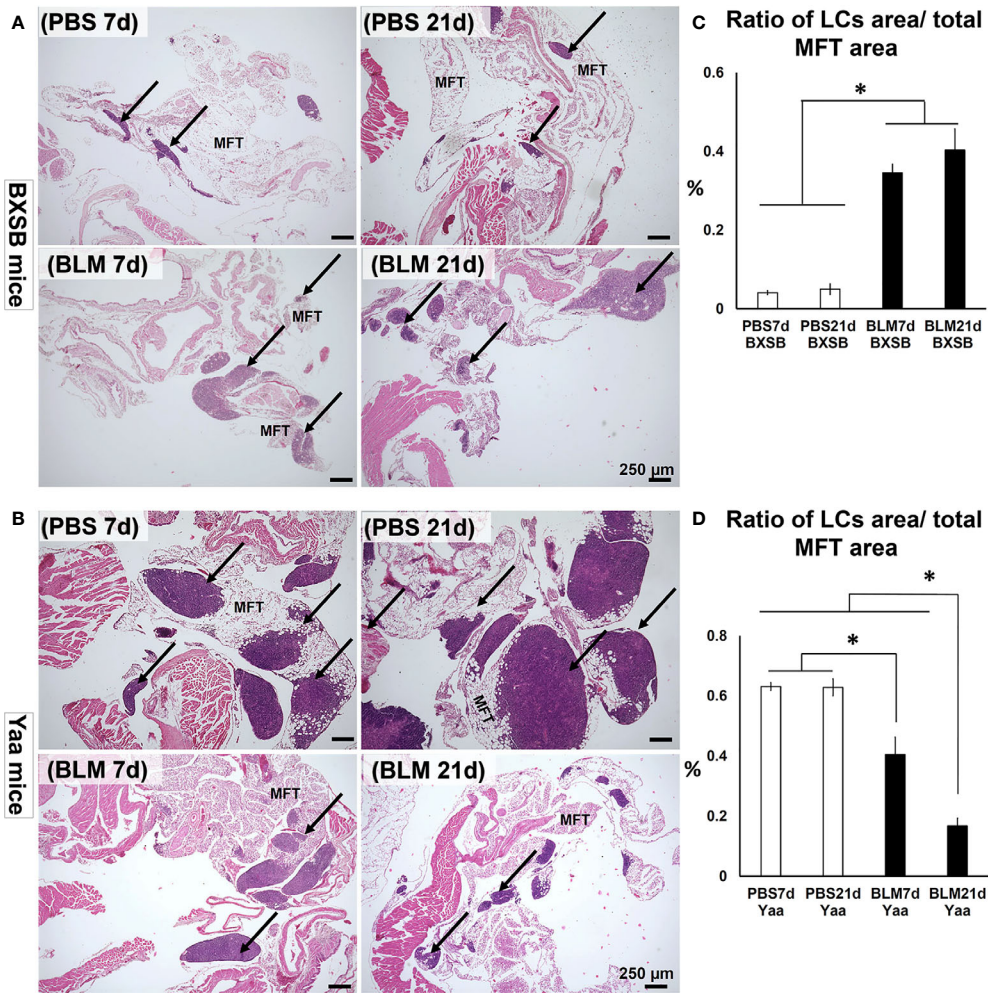

FIGURE 1 | Degree of mediastinal fat-associated lymphoid cluster (MFALC) development in BLM and PBS groups of both autoimmune disease mice model (Yaa) and their wild-type strain (BXSB) on days 7 and 21. **(A, B)** Representative histopathological images of H&E stained mediastinal fat tissue (MFT) sections in both BXSB **(A)** and Yaa **(B)**. Arrows indicate MFALCs. **(C, D)** Graphs showing the percentages of the ratio of lymphoid clusters (LCs) area/total mediastinal fat tissue (MFT) area in control strain "BXSB" **(C)** and its autoimmune disease mouse model "Yaa" **(D)**. Asterisk indicates significant differences between PBS and BLM groups, analyzed by the Kruskal–Wallis test, and followed by Scheffé's method. ($P < 0.05$); $n = 4$ in each experimental group. Values are expressed as mean ± standard error (SE).

(**Figure 3A**). The PBS groups in Yaa mice (on both days 7 and 21) showed high cellular infiltration and mild aniline blue-positive collagen fiber deposition around the bronchioles as well as within the parenchyma. However, the BLM groups at both time points showed a normal lung architecture with mild aniline blue-positive collagen fiber deposition around the large bronchioles (**Figure 3B**).

Interestingly, our previous studies have demonstrated significant upregulation of candidate fibrosis genes (*Acta2, Col1a1*, and *Col3a1*) in B6 mice at 21d following BLM administration (7). Therefore, to further explore the effects of BLM on the expression of such candidate fibrosis genes in autoimmune mouse model and their control strains, we compared the relative mRNA expression of these genes in the lung tissues of both BLM and PBS groups in Yaa and BXSB mice. The BLM group in BXSB mice showed significantly higher values for all studied fibrosis genes on day 21 than other BXSB and Yaa groups. Furthermore, the BLM administered-Yaa mice groups (on day 21) showed significantly reduced mRNA expression of *Col3a1* than the PBS-administered Yaa group on day 21 (**Figure 3C**). Similarly, immunohistochemical staining of lung sections with collagen I and COL3A1 antibodies among all studied groups revealed prominent collagen deposition in the lung sections of BLM group in BXSB mice at 21d than other studied groups (**Supplementary Figures 2A, B, D, E**). Morphometric measurement of the percentages of collagen I and COL3A1 positive area ratios revealed significant higher values than that of other groups in BXSB (**Supplementary Figure 2C**) and Yaa (**Supplementary Figure 2F**) mice. However, among the Yaa groups, no significant difference was observed among the PBS and BLM groups for collagen I positive area ratios at different time points (**Supplementary Figure 2C**). But for COL3A1 positive area ratios

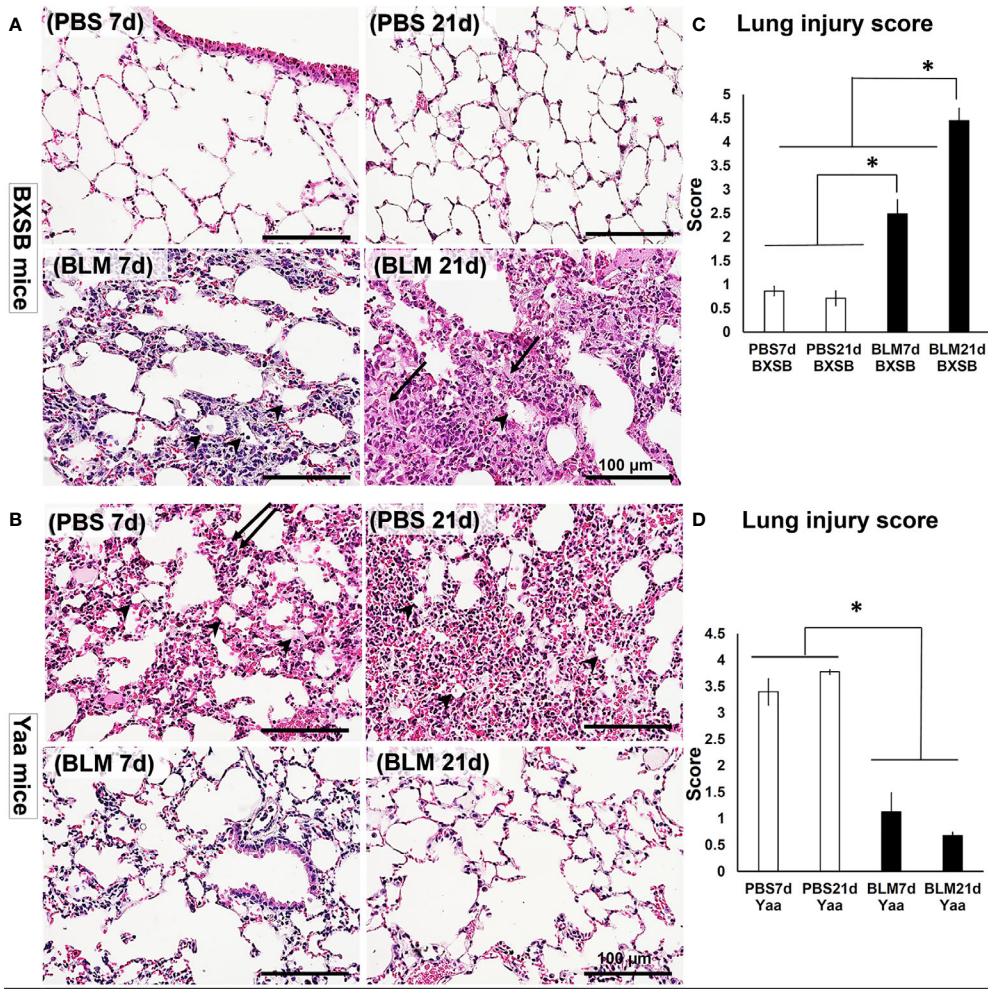

FIGURE 2 | Degree of lung injury in BLM and PBS groups of both autoimmune disease mice model (Yaa) and their wild-type strain (BXSB) on days 7 and 21. **(A, B)** Representative histopathological images of H&E-stained lung tissue sections in both BXSB **(A)** and Yaa **(B)**. More connective tissue deposition in the parenchyma of BLM group in BXSB mice on day 21 (arrows), collapsed alveoli (arrow heads), and thickening of the inter-alveolar space (double arrows). **(C, D)** Graphs showing the average of lung injury score in control strain "BXSB" **(C)** and its autoimmune disease mouse model "Yaa" **(D)**. Asterisk indicates significant differences between PBS and BLM groups, analyzed by the Kruskal–Wallis test, and followed by Scheffé's method. ($P < 0.05$); $n = 4$ in each experimental group. Values are expressed as mean ± standard error (SE).

among Yaa studied groups, significant reduction was observed in the BLM group at both 7 and 21d than that of PBS at 21d (**Supplementary Figure 2F**).

Analysis of Immune Cells in MFALCs and Lung Infiltration Between BLM-and PBS-Treated Groups

To analyze the changes in immune cell populations in MFALCs and lung infiltrates following BLM administration, immunohistochemical analysis was performed that detected $B220^+$ B cells, $CD3^+$ T cells, $Iba1^+$ macrophages, and $Gr1^+$ granulocytes. We compared the percentages of positive area ratios (PARs) for several immune cell populations within the MFALCs (**Supplementary Figures 3A, B**, **4A, B**) and lungs (**Supplementary Figures 3C, D**, **4C, D**) among different groups. Concerning the PARs for $B220^+$ B cells and $CD3^+$ T cells within the MFALCs of BXSB mice, the BLM groups showed significantly higher percentages than PBS groups (**Figures 4A, B** and **Supplementary Figure 3A**). Furthermore, a significantly reduced percentage of PAR of $CD3^+$ T cells was observed in the BLM group on day 21 than on day 7 (**Figure 4B**). Also, the BLM group in Yaa mice showed a similar pattern of change for the percentage of PAR in both $B220^+$ B cells and $CD3^+$ T cells; however, there were no significant differences (**Figures 4A, B** and **Supplementary Figure 3A**). For the percentage of PAR of $Iba1^+$ macrophages within the MFALCs, the BLM group in the BXSB and Yaa mice showed a high percentage than the control group. Such increase was non-significant in BXSB mice. However, significant values were observed in Yaa mice between the BLM groups (on days 7 and 21) and the PBS group (on day 7) and

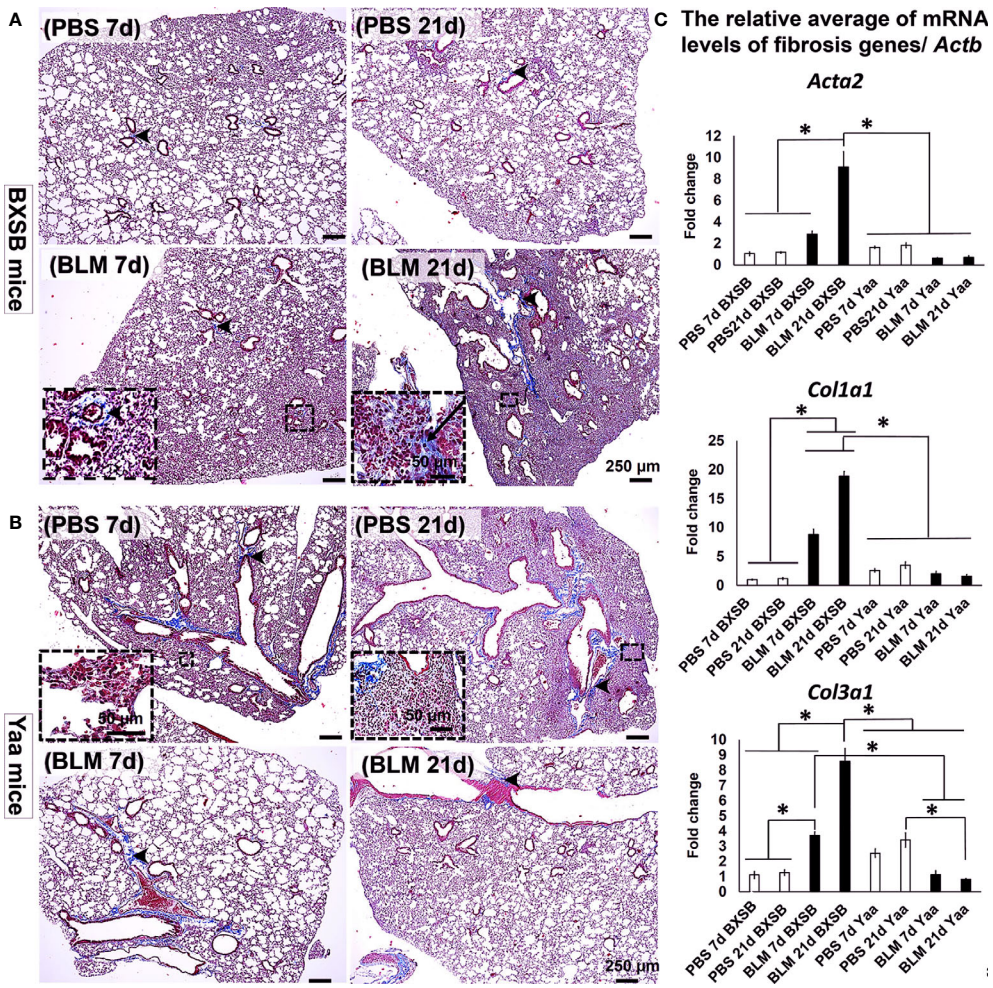

FIGURE 3 | Degree of lung fibrosis in BLM and PBS groups of both autoimmune disease mice model (Yaa) and their wild-type strain (BXSB) on days 7 and 21. **(A, B)** Representative histopathological images of Masson's trichrome (MT)-stained lung tissue sections in both BXSB **(A)** and Yaa **(B)**. C.T. Notice more aniline blue-positive deposition in the parenchyma of BLM group in BXSB mice on day 21 (arrows) and a few aniline blue-positive collagen fibers around the bronchioles (arrow heads). **(C)** Graphs showing the relative mRNA expression of candidate fibrosis genes (*Acta2, Col1a1*, and *Col3a1*) in the lung tissues of different groups in control strain "BXSB," and its autoimmune disease mouse model "Yaa." Asterisk indicates significant differences between the PBS and BLM groups, analyzed by the Kruskal–Wallis test, and followed by Scheffé's method. ($P < 0.05$); $n = 4$ in each experimental group. Values are expressed as mean ± standard error (SE).

between the BLM groups (day 7) and the PBS group (day 21) (**Figure 4C** and **Supplementary Figures 4A, B**). In contrast, no significant difference could be observed in the percentage of PAR of $Gr1^+$ granulocytes within the MFALCs among the groups in both the studied strains (**Figure 4D**).

With respect to infiltration of immune cells into the lungs (**Figures 4″A–″D**), the BLM group in BXSB mice showed a significant increase in the percentage of PAR of $B220^+$ B cells, $CD3^+$ T cells, and $Iba1^+$ macrophages on day 7 than PBS groups (days 7 and 21). Furthermore, the BLM group on day 21 showed a decrease in the percentage of PAR of such immune cells than that of the BLM group on day 7. Such a decrease was significant for the percentages of PAR of $B220^+$ B cells and $Iba1^+$ macrophages (**Figures 4″A–″C** and **Supplementary Figures 3C**, **4C**). For $Gr1^+$ granulocytes within the lungs, the BLM group showed a high percentage of PAR than the PBS groups. Such an increase was significant between the BLM group on day 21 and the PBS group on day 7 (**Figure 4″D**). On the contrary, a decrease in the percentages of PAR for the studied immune cell infiltration was observed in the BLM groups in the lungs of Yaa mice (on days 7 and 21) than in the PBS group on day 21. Such a decrease was significant for $B220^+$ B cells, $CD3^+$ T cells, and $Iba1^+$ macrophages but not for $Gr1^+$ granulocytes (**Figures 4″A–″D** and **Supplementary Figures 3D**, **4D**).

Role of Peripheral Node Addressin$^+$ HEVs in the Development of Lung Injury and MFALCs

Our previous studies have revealed a possible function of HEVs in the development of MFALCs and progression of pneumonitis

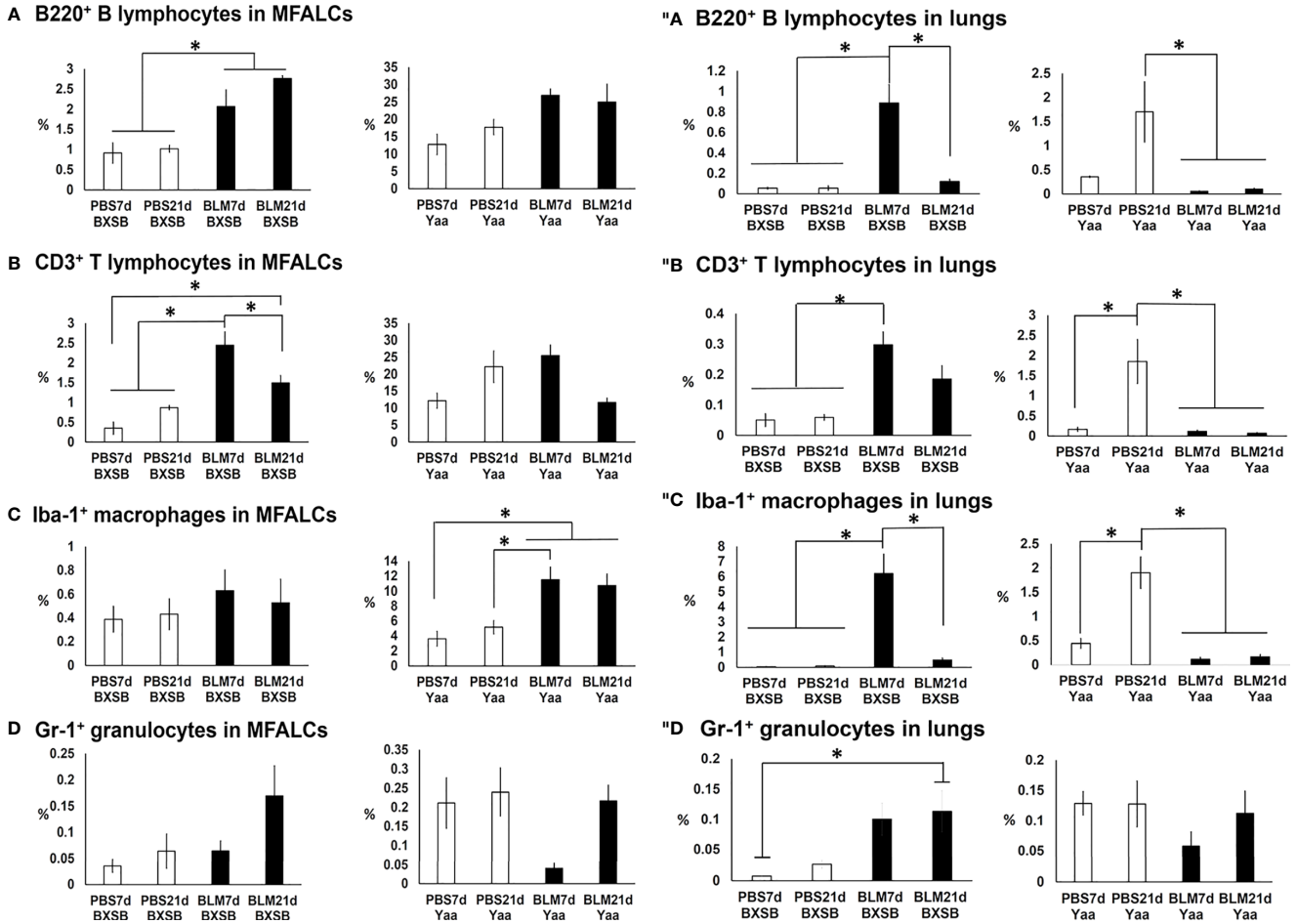

FIGURE 4 | Analysis of immune cells within the MFALCs **(A–D)** and lungs **(″A–″D)** in BLM and PBS groups of both autoimmune disease mice model (Yaa) and their wild-type strain (BXSB) on days 7 and 21. **(A–D)** Graphs showing the positive area ratio of B220$^+$ B cells **(A)**, CD3$^+$ T cells **(B)**, Iba1$^+$ macrophages **(C)**, and Gr1$^+$ granulocytes **(D)** within MFALCs among different groups in both BXSB and Yaa mice. **(″A–″D)** Graphs showing the positive area ratio of B220$^+$ B cells **(″A)**, CD3$^+$ T cells **(″B)**, Iba1$^+$ macrophages **(″C)**, and Gr1$^+$ granulocytes **(″D)** within the lung tissue sections among different groups in both BXSB and Yaa mice. Asterisk indicates significant differences between PBS and BLM groups, analyzed by the Kruskal–Wallis test, followed by Scheffé's method. ($P < 0.05$); $n = 4$ in each experimental group. Values are expressed as mean ± standard error (SE). Figures showing positive immune cells within MFALCs and lungs can be found in **Supplementay Figures 3**, **4**.

following BLM administration in B6 mice (7). In BXSB mice, highly developed PNAd$^+$ HEVs were observed in MFALCs following BLM administration (**Figure 5A**). Furthermore, well-developed HEVs were observed in the lungs of BLM groups (on days 7 and 21); however, they were not detected in the PBS groups (**Figure 5″A**). Similarly, the morphometric measurements of relative ratios of PNAd$^+$ HEVs in MFALCs and their numbers in the lungs revealed a significant increase following BLM administration. Furthermore, the BLM group on day 21 showed a significant increase in the relative ratios of PNAd$^+$ HEVs in MFALCs and a significant decrease in their numbers in the lungs of the BLM group on day 7 (**Figures 5C, ″C**). In contrast, less developed HEVs were observed in MFALCs and lung tissues of the BLM group than that of the PBS group in Yaa mice (**Figures 5B, ″B**). Interestingly, a significant decrease in the relative ratios of PNAd$^+$ HEVs in MFALCs and their numbers in the lungs was observed in the BLM group of Yaa mice on days 7 and 21 than in the PBS group. Furthermore, the PBS group showed a significant increase in the relative ratios of PNAd$^+$ HEVs in MFALCs and their numbers in the lungs on day 21 than the PBS group on day 7 (**Figures 5D, ″D**).

Analysis of LV Occurrence in Both MFALCs and Lungs

The occurrence of LVs was analyzed in MFALCs and lung tissues of both BLM and PBS groups in BXSB and Yaa mice. Furthermore, we measured the total areas of the lymphatic vessel endothelial hyaluronic acid receptor 1 (LYVE-1)$^+$ LVs and the total field

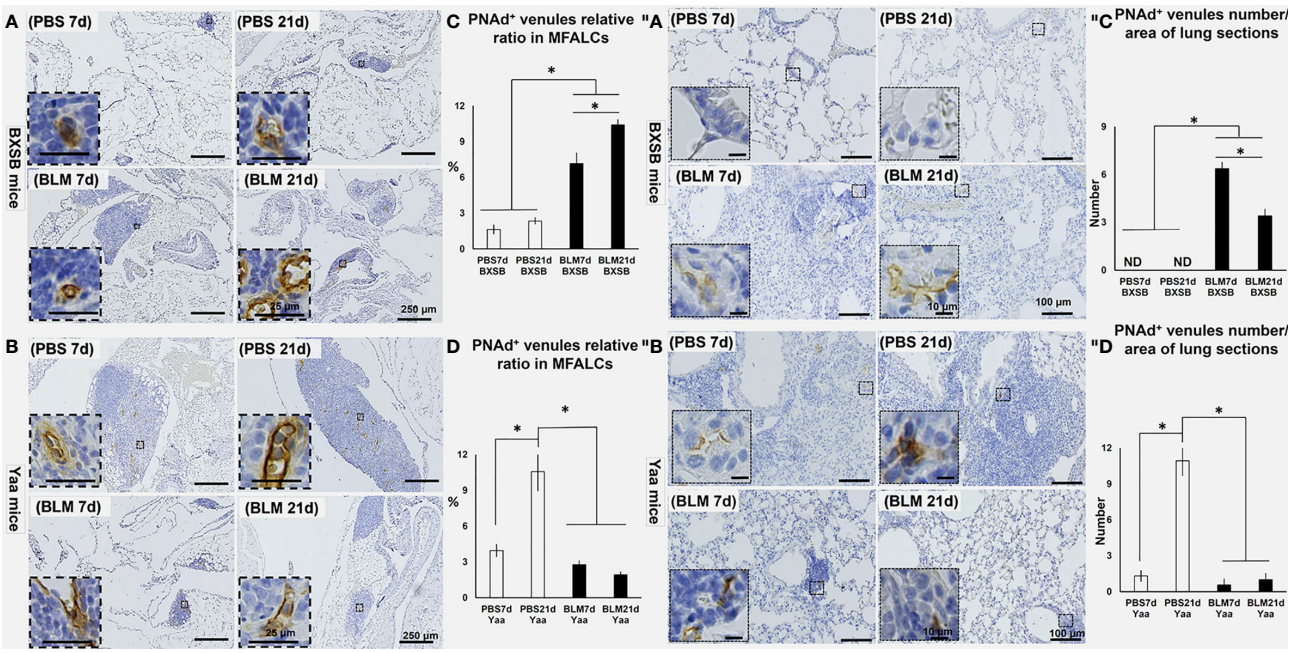

FIGURE 5 | Analysis of the degree of PNAd$^+$ HEVs development in MFALCs **(A–D)** and lungs **(″A–″D)** of BLM and PBS groups of both autoimmune disease mice model (Yaa) and their wild-type strain (BXSB) on days 7 and 21. **(A, B)** Representative histopathological images of immunohistochemically stained MFT sections with anti-PNAd antibody in both BXSB **(A)** and Yaa **(B)**. **(C, D)** Graphs showing the percentages of relative ratios of PNAd$^+$ HEVs in MFALCs of control strain "BXSB" **(C)** and its autoimmune disease mouse models "Yaa" **(D)**. **(″A, ″B)** Representative histopathological images of immunohistochemically stained lung tissue sections with anti-PNAd antibody in both BXSB **(″A)** and Yaa **(″B)**. **(″C, ″D)** Graphs showing the average of PNAd$^+$ HEVs number/lung field area of control strain "BXSB" **(″C)** and its autoimmune disease mouse models "Yaa" **(″D)**. Asterisk indicates significant differences between the PBS and BLM groups, analyzed by the Kruskal–Wallis test, followed by Scheffé's method. ($P < 0.05$); $n = 4$ in each experimental group. Values are expressed as mean ± standard error (SE).

areas of MFALCs and the lungs. To calculate the relative ratio of LYVE1$^+$ LVs areas, the total areas of LYVE-1$^+$ LVs were divided by the total field areas of MFALCs and the lungs, and the average relative ratios were measured among different groups and strains. As shown in **Figures 6A, ″A**, highly developed LYVE-1$^+$ LVs were observed in MFALCs (**Figure 6A**) and the lungs (**Figure 6″A**) of BXSB mice following BLM administration. The morphometrical analysis of the percentage of the relative ratio of the LYVE-1$^+$ LVs areas in MFALCs and the lungs revealed a significantly increased value in the BLM group (on days 7 and 21), compared with the PBS groups in both MFALCs and the lungs. Furthermore, a significantly higher percentage was observed in the BLM group on day 21 than on day 7 (**Figures 6C, ″C**). On the contrary, less developed LYVE-1$^+$ LVs were observed in the MFALCs (**Figure 6B**) and the lungs (**Figure 6″B**) of Yaa mice following BLM administration than the PBS groups, especially on day 21. Similarly, for the LVs in MFALCs and lungs, significant lower relative ratios of LYVE-1$^+$ LVs were observed in the BLM group of Yaa mice on both days 7 and 21 as compared to the PBS group on day 21. Furthermore, the PBS group showed significantly higher ratios of LYVE-1$^+$ LVs on day 21 than on day 7 (**Figures 6D, ″D**).

Analysis of the Degree of Proliferation in both MFALCs and Lungs

For detection of the degree of proliferation in either MFALCs or lungs, bromodeoxyuridine (BrdU)$^+$ cells were observed in both BXSB and Yaa mice. Moreover, the percentage of either cell density ratio or index ratio was compared between the BLM- and PBS-treated groups in MFALCs or lungs, respectively. In BXSB mice, numerous BrdU$^+$ proliferating cells were observed in MFALCs and the lungs of BLM as compared with the PBS group (**Figures 7A, ″A**). As shown in **Figures 7C, ″C**, the percentage of cell density ratio and index ratio within MFALCs and the lungs of the BLM group in BXSB mice on day 7 showed a higher percentage than those in the BLM group on day 21 and PBS group on days 7 and 21. On the contrary, the BLM groups in Yaa mice showed fewer BrdU$^+$ proliferating cells, especially on day 21 as compared with the PBS groups (**Figures 7B, ″B**). The MFALCs in the BLM group on day 21 showed a significantly reduced percentage of BrdU$^+$ proliferating cell density ratio than those in the PBS groups (days 7 and 21) (**Figure 7D**). Furthermore, the lungs in the PBS group on day 21 showed a significantly higher percentage of BrdU$^+$ proliferating cell density ratio than those in the BLM groups (days 7 and 21) and the PBS group on day 7 (**Figure 7″D**).

Autoimmune Indices (Spleen/BW Ratio And Serum Anti-Double Stranded DNA [anti-dsDNA] Autoantibodies)

To further examine the effects of BLM administration on the degree of autoimmunity, we compared the autoimmune indices among the BLM and PBS groups in both an autoimmune mouse

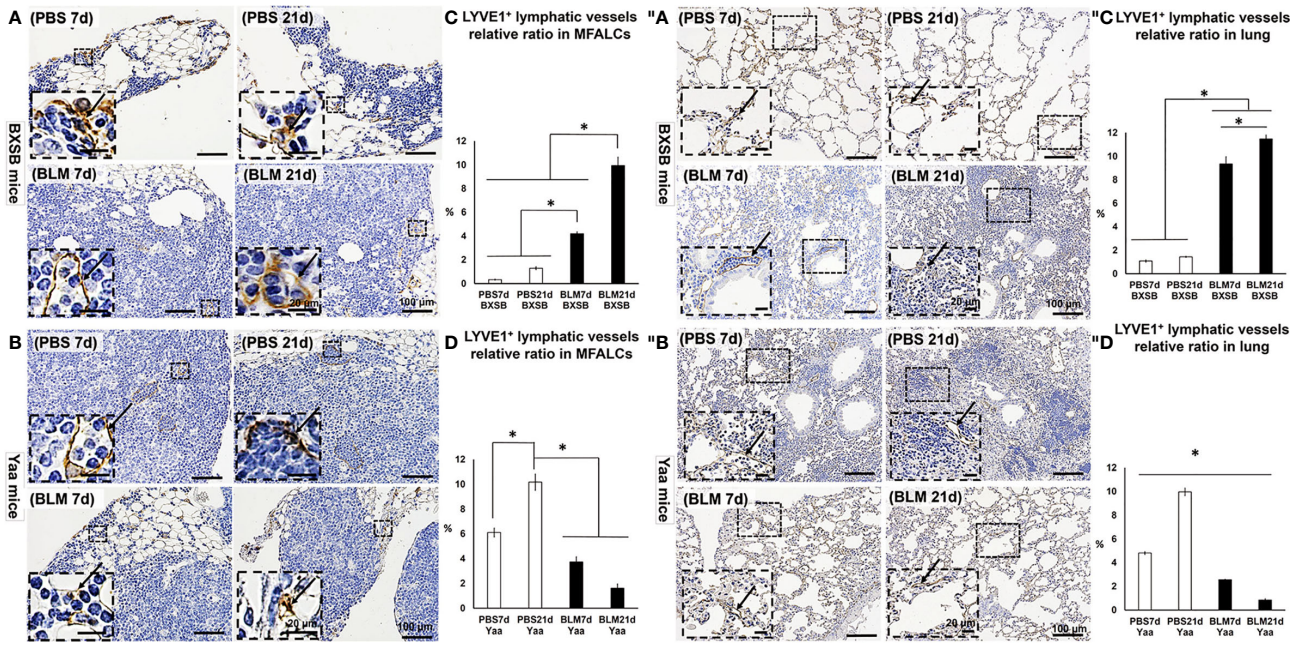

FIGURE 6 | Analysis of the degree of LYVE1$^+$ LV development in MFALCs **(A–D)** and lungs **(″A–″D)** of BLM and PBS groups of both autoimmune disease mice model (Yaa) and their wild-type strain (BXSB) on days 7 and 21. **(A, B)** Representative histopathological images of immunohistochemically stained MFT sections with anti-LYVE1 antibody in both BXSB **(A)** and Yaa **(B)**. **(C, D)** Graphs showing the percentages of average of relative ratios of LYVE1$^+$ LVs in MFALCs of control strain "BXSB" **(C)** and its autoimmune disease mouse model "Yaa" **(D)**. **(″A, ″B)** Representative histopathological images of immunohistochemically stained lung tissue sections with anti-LYVE1 antibody in both BXSB **(″A)** and Yaa **(″B)**. Arrows indicate positive LVs. **(″C, ″D)** Graphs showing the percentages of average of relative ratios of LYVE1$^+$ LVs in the control strain "BXSB" **(″C)** and its autoimmune disease mouse model "Yaa" **(″D)**. Asterisk indicates significant differences between PBS and BLM groups, analyzed by the Kruskal–Wallis test, followed by Scheffé's method. ($P < 0.05$); $n = 4$ in each experimental group. Values are expressed as mean ± standard error (SE).

model and their control strains. As shown in **Figure 8A**, the spleen/BW ratios of Yaa autoimmune mice were significantly higher in the PBS groups (on days 7 and 21) than in both the BLM and PBS groups (days 7 and 21) of its control (BXSB) mice strain. Furthermore, Yaa mice in the BLM group showed significantly reduced spleen/BW ratios on day 21 than the PBS group. Similarly, Yaa mice in the PBS groups (days 7 and 21) displayed significantly higher titers of serum anti-dsDNA autoantibodies than that in PBS and BLM groups in BXSB mice. Furthermore, a sharp and significant decrease in the titers of serum anti-double-stranded DNA (anti-dsDNA) autoantibodies was observed in the BLM group on day 21 than the PBS group on day 21 (**Figure 8B**).

Relative mRNA Expression of the Yaa Locus Genes in Lung Tissues

To further explore the effect of BLM on the expression of candidate Yaa locus genes (*TLR7, TLR8, Arhgap6, Msl3*, and *Tceanc)* associated with autoimmunity, quantitative real-time PCR (RT-qPCR) was performed to compare the mRNA expression of these genes in the lung tissues of both BLM and PBS groups in Yaa and BXSB mice. Except for *Msl3*, the PBS groups (days 7 and 21) in Yaa mice showed significantly higher expression of Yaa locus genes than the BXSB mice. The PBS groups (day 21) in Yaa mice showed significantly higher expression of Msl3 mRNA than in BXSB mice (on days 7 and 21) (**Figures 9A–C, E**). Moreover, the BLM group on day 21 in BXSB mice revealed a significant increase in the mRNA expression of *Msl3* than the other studied groups in both BXSB and Yaa mice (**Figure 9D**). As shown in **Figures 9A, B, D**, and 9E, the BLM groups (days 7 and 21) in Yaa mice revealed a significant decrease in the mRNA expression of *TLR7, TLR8, Msl3*, and *Tceanc* than the PBS groups, especially on day 21. However, elevated mRNA expression of *Arhgap6* was observed in the BLM group of Yaa mice as compared with the PBS groups although without any significant differences (**Figure 9C**).

Histopathological Correlations Between Autoimmune Parameters and Parameters for MFALCs and Lungs

As shown in **Tables 2A, B**, we examined the histopathological correlations between autoimmune parameters (SPW/BW, serum titer of anti-dsDNA antibodies) and parameters of MFALCs and the lungs (sizes of MFALCs, LIS, proliferating cells, and LVs and HEVs within MFALCs and the lungs) as well as between parameters of MFALCs and the lungs in both BLM and PBS groups on days 7 and 21 for autoimmune mouse model "Yaa" **Table 2A** and its control strain "BXSB" (**Table 2B**). To study correlations among different groups in Yaa mice (**Table 2A**), the SPW/BW autoimmune parameter was observed that showed a

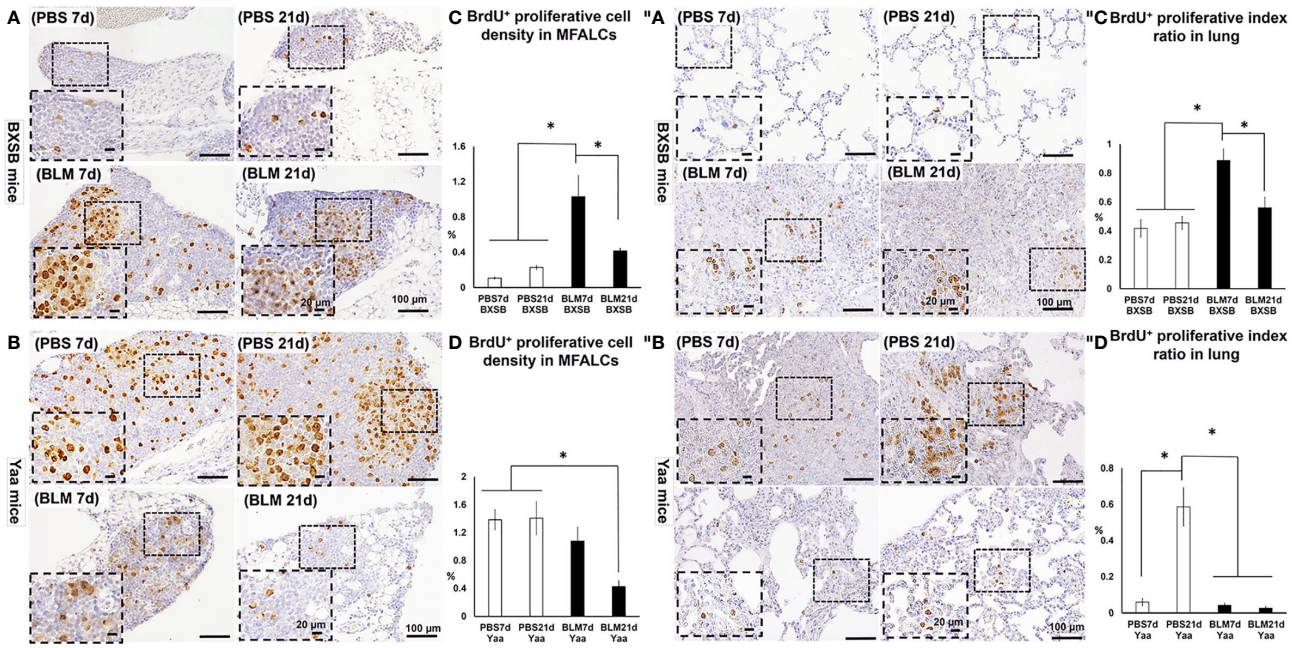

FIGURE 7 | Analysis of the degree of proliferation in MFALCs **(A–D)** and lungs **(″A–″D)** of BLM and PBS groups of both autoimmune disease mice model (Yaa) and their wild-type strain (BXSB) on days 7 and 21. **(A, B)** Representative histopathological images of immunohistochemically stained MFT sections with anti-bromodeoxyuridine "BrdU" antibody in both BXSB **(A)** and Yaa **(B)**. **(C, D)** Graphs showing the percentages of $BrdU^+$ proliferating cell density ratio in MFALCs of control strain "BXSB" **(C)** and its autoimmune disease mouse models "Yaa" **(D)**. **(″A, ″B)** Representative histopathological images of immunohistochemically stained lung tissue sections with anti-BrdU antibody in both BXSB **(″A)** and Yaa **(″B)**. **(″C, ″D)** Graphs showing the percentages of average of $BrdU^+$ proliferating cell index ratio in control strain "BXSB" **(″C)** and its autoimmune disease mouse model "Yaa" **(″D)**. Asterisk indicates significant differences between PBS and BLM groups, analyzed by the Kruskal–Wallis test, followed by Scheffé's method. ($P < 0.05$); $n = 4$ in each experimental group. Values are expressed as mean ± standard error (SE).

highly significant positive correlation with the size of MFALCs and $BrdU^+$ proliferative cell density in MFALCs. Furthermore, the serum titer of anti-dsDNA antibodies showed a significant positive correlation with the size of MFALCs and highly significant positive correlations with the relative ratios of $LYVE1^+$ LVs in MFALCs and the lungs, $BrdU^+$ proliferative cell density in MFALCs, and index ratio in the lungs, and $PNAd^+$ HEVs relative ratio in MFALCs. Interestingly, the size of MFALCs showed a significant positive correlation with lung $BrdU^+$ proliferative cells and highly significant positive correlations with LIS and lung LVs. Furthermore, our results indicated a significant positive correlation between the quantitative indices of LVs and HEVs in MFALCs with lung HEVs and highly significant positive correlations with LIS and lung LVs. Moreover, a significant positive correlation of proliferating cells of MFALCs was observed with those of the lungs, and a highly significant positive correlation was observed with LIS and lung LVs.

In addition, we examined the correlations between different parameters of MFALCs and the lungs in the control strain (BXSB). As shown in **Table 2B**, the LIS showed highly significant correlations with the size of MFALCs, and both the quantitative indices of LV and HEVs. In addition, the quantitative indices of LV and HEVs in the lungs revealed a highly significant positive correlation with those of the MFALCs as well as with the size of MFALCs.

DISCUSSION

Effect of BLM Administration on the Degree of Lung Injury and MFALC Development and Autoimmune Mice Model

Systemic autoimmune disorders constitute a group of immune-mediated inflammatory diseases affecting various organs, including the lungs, heart, kidneys, skin, brain, and hematopoietic system. They are characterized by the deposition of immune complexes or direct autoantibodies resulting in tissue inflammation and damage (22, 23). Several autoimmune diseases (AID) have been reported in humans, including SLE, systemic sclerosis, rheumatoid arthritis (RA), polymyositis/dermatomyositis, Wegener's granulomatosis, ankylosing spondylitis, and Sjögren syndrome (23). Recently, several autoimmune murine strains have been used as models to study the pathogenesis of AID development in humans, such as Lpr and male Yaa mice. These mice displayed lesions that closely mimicked human AID, especially in SLE and RA, including lymphadenopathy, splenomegaly, and hypergammaglobulinemia with anti-dsDNA antibodies (13, 24). Furthermore, pleuropulmonary involvement and the development of lung injury have been reported to occur in most AID in both humans and mouse models (6, 23, 25, 26).

Interestingly, we previously reported the presence of more prominent MFALCs in autoimmune disease mouse models (Lpr

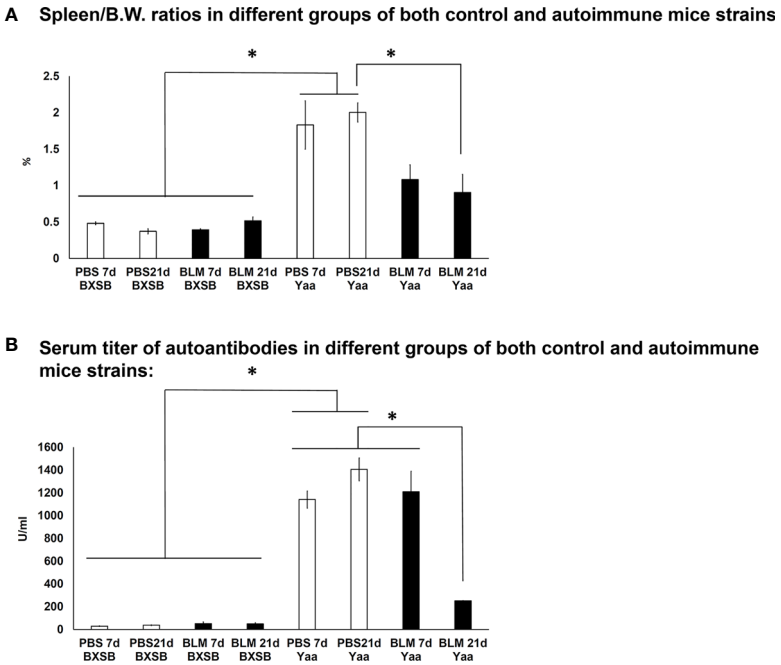

FIGURE 8 | Analysis of autoimmune indices (spleen/body weight ratios and serum titer of autoantibodies) among BLM and PBS groups of both autoimmune disease mice model (Yaa) and their wild-type strain (BXSB) on days 7 and 21. **(A)** Spleen/BW ratios among BLM and PBS groups in both autoimmune disease mouse model (Yaa) and their wild-type strain (BXSB) on days 7 and 21. **(B)** Serum titer of autoantibodies among BLM and PBS groups in both autoimmune disease mouse model (Yaa) and their wild-type strain (BXSB) on days 7 and 21. Asterisk indicates significant differences between PBS and BLM groups, analyzed by the Kruskal–Wallis test, followed by Scheffé's method. ($P < 0.05$); $n = 4$ in each experimental group. Values are expressed as mean ± standard error (SE).

and Yaa mice) as compared with control strains. The study showed a significant positive correlation between the size of MFALCs and cellular infiltration in the lungs of these models as well as with autoimmune disease indices, including the spleen/BW ratios and serum autoantibody levels, suggesting a possible function of MFALCs in the progression of lung lesions (6). Furthermore, previous studies have demonstrated that inflammation induced the development of FALCs in the mesentery and MFTs following peritoneal immunization with antigens and intranasal (i.n.) BLM administration, respectively (3, 5). In humans, BLM has been previously used as a successful therapeutic target for certain curable malignancies, such as germ cell tumors, and Hodgkin's and non-Hodgkin's lymphomas. However, its use is currently not recommended due to the development of pulmonary fibrosis in up to 10% of patients receiving the medication (9, 27). Altogether, differences in mouse strain have been reported to be susceptible to the development of pulmonary fibrosis following BLM administration. Specifically, A/J and Balb/c mice were found to be resistant to fibrosis, whereas both DBA and B6 mice were highly susceptible (11, 28). Furthermore, our recent study had demonstrated that BLM induced the development of pneumonitis in healthy B6 mice, concomitantly with an increased size of MFALCs when compared with the PBS-administered control group (7). However, the effect of BLM on the degree of lung injury and MFALCs remain largely unclear in Yaa autoimmune disease mouse models, characterized by lymphoproliferation and more developed MFALCs. Therefore, we examined the effect of BLM on the degree of lung injury in autoimmune disease mouse models (Yaa) and their corresponding control strain (BXSB) on days 7 and 21 following i.n. administration of either BLM sulfate (5 mg/kg) or vehicles (PBS group). The present study revealed a reduced degree of lung injury and size of MFALCs following BLM administration in Yaa mice as compared with the corresponding PBS group; however, contradictory results were observed in their wild-type control strain. These results suggest a dual effect of BLM on lung injury and intrathoracic immune hemostasis that could be attributed to strain differences in response to BLM administration.

Effect of BLM Administration on Immune Cells' Hemostasis in Both Lungs and MFALCs in the Autoimmune Mice Model

FALCs are immune cell aggregates that associate with mediastinal and mesenteric fat tissues. Both lineage-positive (B and T lymphocytes) and lineage-negative (macrophages and granulocyte) cells are enriched with FALCs (1, 2). The present investigation revealed a significant positive correlation between the size of MFALCs and the degree of lung injury in all analyzed groups, suggesting the possible function of MFALCs in immune cell recruitment into the lung tissues. Furthermore, we analyzed

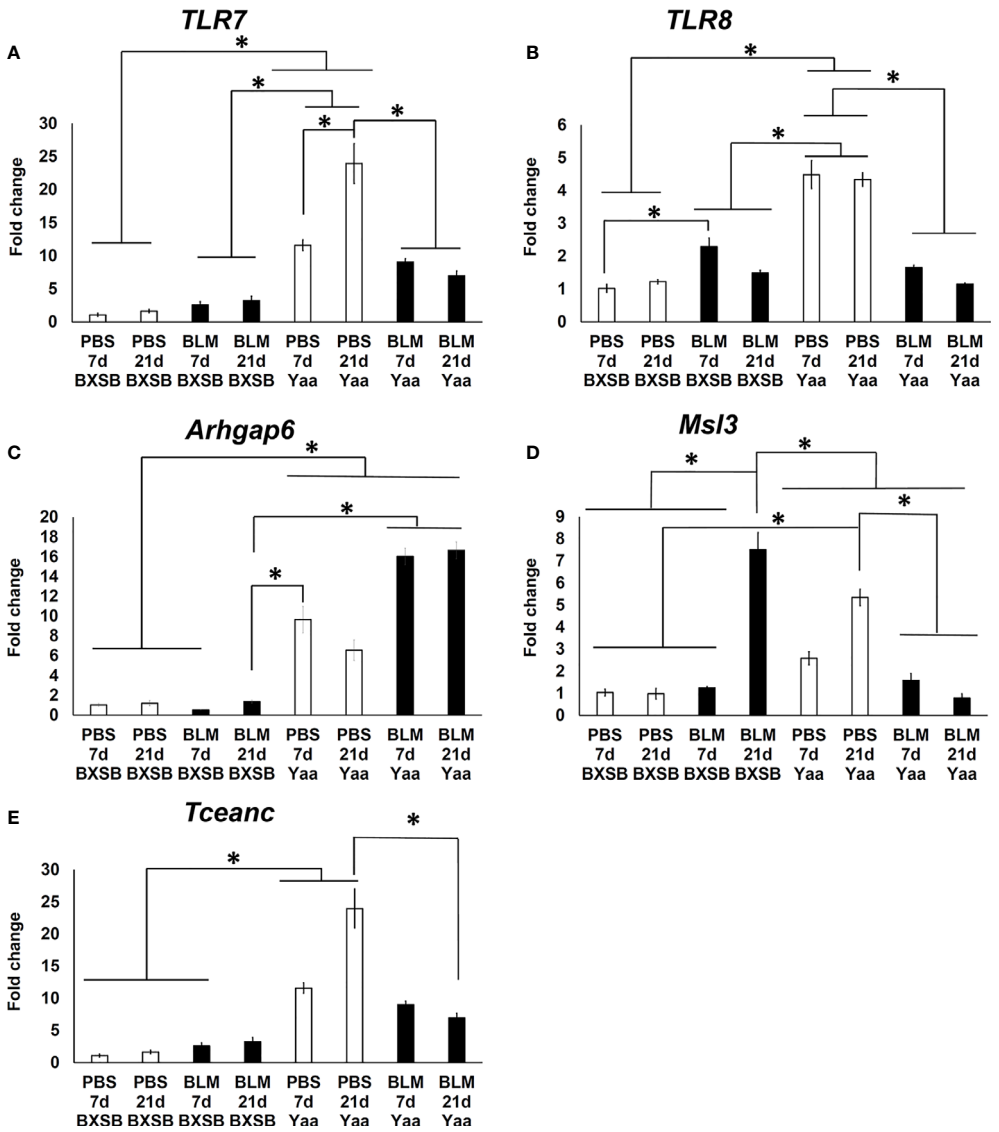

FIGURE 9 | Analysis of the relative mRNA expression of Yaa locus genes (*TLR7, TLR8, Arhgap6, Msl3*, and *Tceanc)* in the lung tissues among BLM and PBS groups of both autoimmune disease mice model (Yaa) and their wild-type strain (BXSB) on days 7 and 21. Graphs showing fold increase in the relative mRNA expression of *TLR7* **(A)**, *TLR8* **(B)**, *Arhgap6* **(C)**, *Msl3* **(D)**, and *Tceanc* **(E)** in the lung tissues of different groups in both control strain "BXSB" and its autoimmune disease mouse model "Yaa." Asterisk indicates significant differences between PBS and BLM groups, analyzed by the Kruskal–Wallis test, followed by Scheffé's method. ($P < 0.05$); $n = 4$ in each experimental group. Values are expressed as mean ± standard error (SE).

the positive area ratios for immune cells within both MFALCs and lung tissues among the BLM and PBS groups in all analyzed strains. Interestingly, the BLM group in BXSB mice showed significantly higher ratios for B and T lymphocytes, and macrophages and a higher tendency for granulocytes than the PBS group in both MFALCs and the lungs. However, a significantly lower positive area ratio for B and T lymphocytes and macrophages was observed in the lungs of Yaa mice in the BLM group as compared with the PBS control group. Furthermore, the ratios of B and T lymphocytes and macrophages within MFALCs were observed to be negatively and positively correlated with the degree of lung injury in Yaa and BXSB, respectively. Therefore, based on our findings, we suggest that BLM could exert different effects on the recruitment of immune cells into the lung tissues among various mouse strains, and thus a dual effect of BLM was observed on lung fibrosis. Consistent with our results showing a decrease in the quantitative indices of T and B lymphocytes, and macrophages in the lung tissues of Yaa mice following BLM administration, previous reports revealed the function of different immune cells in the progression of pulmonary fibrosis (29). Our results revealed a reduced ratio of T lymphocytes within MFALCs and the lungs of the BLM group on day 21 than on day 7 in both studied strains. Interestingly, a recent study demonstrated that

TABLE 2 | Spearman's correlations between autoimmune parameters (SPW/BW, serum titer of anti-dsDNA antibodies) and the parameters of MFALCs and lungs in Yaa (1A) and BXSB (1B) mice.

Table 2A			Parameters for autoimmune disease		Parameters for MFALCs							
			SPW/BW	Anti-dsDNA Abs	MFALC	LYVE-1	PNAd	Gr1	BrdU	CD3	B220	Iba1
Parameters for autoimmune disease in Yaa	**SPW/BW**	ρ	–	0.179	0.632**	0.412	0.235	-0.047	0.641**	-0.056	-0.541*	0.424
		P	–	0.506	0.009	0.113	0.113	0.863	0.007	0.837	0.030	0.102
	Anti-dsDNA	ρ	0.179	–	0.603*	0.765**	0.771**	-0.150	0.644**	0.344	-0.256	-0.344
	Abs	*P*	0.506	–	0.013	0.001	0.001	0.579	0.007	0.192	0.339	0.192
Parameters for lung in Yaa	**LIS**	ρ	0.494	0.390	0.868**	0.806**	0.711**	0.475	0.695**	-0.007	-0.604*	-0.669**
		P	0.052	0.136	0.001	0.001	0.002	0.063	0.003	0.978	0.013	0.005
	BrdU	ρ	0.188	0.641**	0.509*	0.762**	0.756**	0.050	0.544*	0.282	-0.332	-0.553*
		P	0.485	0.007	0.044	0.001	0.001	0.854	0.029	0.289	0.208	0.026
	Gr1	ρ	0.641**	0.009	0.350	0.162	0.074	0.053	0.365	-0.053	-0.476	-0.171
		P	0.007	0.974	0.184	0.549	0.787	0.846	0.165	0.846	0.062	0.528
	CD3	ρ	0.238	0.700**	0.697**	0.815**	0.811**	0.350	0.697**	0.279	-0.444	-0.465
		P	0.374	0.003	0.003	0.001	0.001	0.184	0.004	0.295	0.085	0.070
	B220	ρ	0.444	0.285	0.632**	0.724**	0.729**	0.509*	0.538*	-0.132	-0.694**	-0.803**
		P	0.085	0.284	0.009	0.002	0.003	0.044	0.031	0.625	0.003	0.001
	Iba1	ρ	0.365	0.474	0.691**	0.782**	0.768**	0.456	0.556*	0.006	-0.618*	-0.674**
		P	0.165	0.064	0.003	0.001	0.001	0.076	0.025	0.983	0.011	0.004
	LYVE-1	ρ	0.424	0.674**	0.874**	0.947**	0.911**	0.247	0.788**	0.159	-0.582*	-0.671**
		P	0.102	0.004	0.001	0.001	0.001	0.356	0.001	0.557	0.018	0.004
	PNAd	ρ	0.286	0.182	0.497	0.522*	0.544*	0.247	0.278	0.007	-0.478	-0.425
		P	0.284	0.500	0.050	0.038	0.029	0.356	0.297	0.978	0.061	0.101

*LIS, lung Injury Score. MFALC: % of LCs area/total MFTs area. P: Spearman's rank correlation coefficient. n= 4/group (PBS 7, 21 d and bleomycin7, 21 d. *: Significant, P <0.05. **: highly significant, P < 0.01.*

Table 2B			Parameters for autoimmune disease		Parameters for MFALCs							
			SPW/BW	Anti-dsDNA Abs	MFALC	LYVE-1	PNAd	Gr1	BrdU	CD3	B220	Iba1
Parameters for autoimmune disease in BXSB	**SPW/BW**	ρ	–	-0.132	0.085	0.150	0.053	0.253	0.459	-0.256	0.247	0.118
		P	–	0.625	0.753	0.579	0.846	0.345	0.074	0.339	0.356	0.664
	Anti-dsDNA	ρ	-0.132	–	0.388	0.391	0.409	0.444	0.459	0.329	0.262	-0.094
	Abs	*P*	0.625	–	0.137	0.213	0.116	0.085	0.074	0.213	0.327	0.729
Parameters for lung in BXSB	**LIS**	ρ	0.396	0.387	0.709**	0.876**	0.837**	0.711**	0.637**	0.620*	0.815**	0.165
		P	0.129	0.139	0.002	0.001	0.001	0.002	0.008	0.010	0.001	0.542
	BrdU	ρ	-0.135	0.179	0.529*	0.412	0.497	0.129	0.774**	0.747**	0.271	0.209
		P	0.617	0.506	0.035	0.113	0.050	0.633	0.001	0.001	0.311	0.438
	Gr1	ρ	0.106	0.450	0.768**	0.838**	0.712**	0.350	0.809**	0.729**	0.591*	0.341
		P	0.696	0.080	0.001	0.001	0.002	0.184	0.001	0.001	0.016	0.196
	CD3	ρ	-0.215	0.379	0.683**	0.706**	0.606*	0.315	0.853**	0.750**	0.538*	0.203
		P	0.425	0.147	0.008	0.002	0.013	0.235	0.001	0.001	0.031	0.451
	B220	ρ	-0.103	0.238	0.685**	0.556*	0.688**	0.421	0.818**	0.803**	0.406	0.182
		P	0.704	0.374	0.003	0.025	0.003	0.105	0.001	0.001	0.119	0.499
	Iba1	ρ	-0.218	0.432	0.624**	0.738**	0.676**	0.379	0.935**	0.856**	0.559*	0.200
		P	0.418	0.094	0.010	0.001	0.004	0.147	0.001	0.001	0.024	0.458
	LYVE-1	ρ	0.176	0.379	0.750**	0.953**	0.909**	0.644**	0.765**	0.741**	0.750**	0.362
		P	0.513	0.147	0.001	0.001	0.001	0.007	0.001	0.001	0.001	0.169
	PNAd	ρ	0.007	0.495	0.782**	0.478	0.475	0.301	0.760**	0.755**	0.441	0.115
		P	0.980	0.051	0.001	0.061	0.063	0.258	0.001	0.001	0.087	0.672

*LIS, lung Injury Score. MFALC: % of LCs area/total MFTs area. ρ: Spearman's rank order correlation coefficient. n= 4/group (PBS 7, 21 d &bleomycin7, 21 d. *: Significant, P < 0.05. **: highly significant, P < 0.01.*

infiltration of T lymphocytes in the lungs contributed to the progression of pulmonary fibrosis through a profibrotic function or recovery from fibrosis through an antifibrotic role (30). In addition, a dual effect of B lymphocytes on the progression of pulmonary fibrosis in a mouse model of BLM-induced fibrosis was reported where the progression of lung fibrosis was substantially exacerbated when B cell depletion occurred before inducing lung fibrosis lesions. However, this fibrosis was dramatically suppressed when B cell depletion occurred during the inflammatory phase (31).

Effect of BLM Administration on the Degree of Proliferation, Development of LVs, and HEVs in Both Lungs and MFALCs in the Autoimmune Mice Model and Its Control Wild Strain

Previous studies have implicated inflammation induced by chemicals or helminth or bacterial infections in the rapid formation and expansion of FALCs by triggering the proliferation of immune cells (1, 3, 5). Similarly, our recent study revealed a significant increase in the ratio of the proliferation of immune cells as well as the ratio of LV areas in both lungs and MFALCs following BLM administration, suggesting its function in the development of lung injury (7). Consistent with this speculation, we demonstrated a significant increase in the degree of proliferation ($BrdU^+$ proliferative cell density) and the relative ratio of $LYVE1^+$ LVs in both MFALCs and the lungs of the BLM group as compared with the PBS group in BXSB mice. However, an opposite trend was observed in the case of Yaa mice.

HEVs are specialized blood vessels that play a vital role in lymphocyte trafficking. HEVs were first reported in secondary lymphoid organs, such as lymph nodes (LN) and Peyer's patches of healthy individuals (32). A recent study reported that HEVs can develop during chronic inflammation associated with autoimmunity, allografts, and infection in non-lymphoid organs; thus, playing a significant function in the recruitment of lymphocytes at the inflamed sites (33). Furthermore, our recent study showed the development of HEVs and LVs in the lung tissues of B6 mice following BLM administration but not following PBS treatment, suggesting their function in the development of lung injury (7). Interestingly, the present study revealed higher quantitative values for HEVs within MFALCs of the BLM groups of the wild-type control BXSB mice and lower values in Yaa mice as compared with the PBS control groups. Furthermore, we demonstrated the presence of well-developed HEVs in the lungs of BLM groups in the control strain (BXSB mice); however, these were not detected in the PBS groups. Furthermore, less-developed HEVs were observed in the BLM group of Yaa mice in comparison with the corresponding PBS group. Therefore, our data suggest a possible function of HEVs in the development of lung injury. In addition, our study suggests that the dual effect of BLM on lung injury development could be related to their effect on HEV development. Therefore, HEVs may be considered as therapeutic targets for lung injuries associated with autoimmune diseases. However, further studies are required to explore other possible mechanisms and associated factors beyond the development of HEVs in the lungs following BLM administration, especially in the control strains.

Effect of BLM Administration on the Degree of Autoimmunity, Relative Expression of Both Candidate Fibrosis and Yaa Locus Genes in the Autoimmune Mice Model and Its Control Wild Strain

The present study revealed a dramatic decrease in the autoimmune indices (spleen/BW ratios and serum titers of anti-dsDNA autoantibodies) on day 21 following BLM administration in the Yaa autoimmune mouse model, suggesting reduced severity of autoimmunity-associated lesions. However, no significant change in such indices among BXSB groups was observed. Furthermore, we revealed a significant increase in candidate fibrosis genes (*Acta2, Col1a1*, and *Col3a1*) in the BLM groups of BXSB mice on day 21 than other groups in both BXSB and Yaa mice. However, reduced expression of such genes was observed following BLM administration in Yaa, as compared with the PBS groups. Consistent with our results, the role of different mouse strains in the susceptibility to BLM-induced pulmonary fibrosis have been reported (10, 11). Moreover, previous studies have reported that changes in the expression of certain genes in the lung tissues could enhance the progression of lung fibrosis (11, 28). Recently, it has been reported that the susceptibility of B6 mice to pulmonary fibrosis following BLM administration was linked to the major locus on chromosome 17, called BLM-induced pulmonary fibrosis 1 (*Blmpf1*) (11). For Yaa locus genes in the autoimmune mouse model (Yaa mice), the autoimmunity was observed only in the males due to translocation of a region of the X chromosome onto the Y chromosome, leading to the duplication of 16 genes on the Y chromosome (34, 35). Interestingly, in our recent study, we revealed *TLR7, TLR8, Arhgap6, Msl3*, and *Tceanc* as major candidate Yaa-associated locus genes associated with promoting severe autoimmune response with an increase in age (18). Furthermore, these genes play a vital role in the progression of various lung diseases, including chronic obstructive pulmonary diseases, idiopathic interstitial pneumonia, lung injury, and lung cancer (35–38). Nevertheless, the effect of BLM administration on the expression of Yaa locus genes has not been reported that could contribute to the diverse effects of BLM on the degree of lung injury among the autoimmune Yaa mouse model and its corresponding strain. Therefore, we compared the expression of these genes in the lung tissues of Yaa and BXSB mice in both BLM and PBS groups. Except for *Arhgap6*, our results revealed significant downregulation in the expression of other studied genes in the BLM group of Yaa mice as compared with the PBS groups, especially on day 21. In contrast, elevated relative expression of *Arhgap6* was observed in the BLM group of Yaa mice than in the PBS group. The upregulation of *Arhgap6* gene is critically important in preventing and treating lung cancer through the suppression of matrix metalloproteinase−9 (MMP9) and vascular endothelial growth factor (VEGF) (36). Interestingly, the inhibition of TLR-7 in experimental lupus attenuated glomerulonephritis and lung injury (39). Alveolar macrophages express higher levels of TLR1, TLR2, TLR4, TLR7, and TLR8 (40). The current study indicated a significant decrease in lung macrophages and in the relative expression of both TLR7 and TLR8 in Yaa mice following BLM administration when compared with PBS groups. In addition, the expression of *Msl3* gene was higher by 85.2 fold in patients with idiopathic interstitial pneumonia (IIP) when compared with the control (38). Similarly, the BLM group in BXSB mice on day 21 showed significant upregulation of the latter gene than other groups in

BXSB and Yaa mice. In contrast, the BLM groups (days 7 and 21) in Yaa mice showed significant downregulation of *Msl3* gene expression than the PBS group, as well as the BLM group (day 21) in BXSB mice. Thus, our results suggested that the upregulation of such genes contributed to a higher degree of lung fibrosis progression observed in BXSB on day 21 following BLM administration than other studied groups.

CONCLUSIONS

The present study sheds light on strain-related differences following BLM administration in an autoimmune mouse model (Yaa) and its control strain (BXSB). BLM dramatically increased and decreased lung injury in BXSB and Yaa mice, respectively. Our results described multifactorial roles of BLM, which could explain its ameliorative effect on the degree of lung injury in Yaa mice, including downregulation of certain Yaa locus genes as well as its suppressive effect on HEV development, proliferation activity of immune cells, and their recruitment activity into the lung tissue, especially for macrophages, and T and B lymphocytes. Therefore, the present study suggested that targeting these factors could be a novel strategy for therapeutic approaches for lung injury associated with autoimmune diseases.

DATA AVAILABILITY STATEMENT

The original contributions presented in the study are included in the article/**Supplementary Material**. Further inquiries can be directed to the corresponding author.

ETHICS STATEMENT

The animal study was reviewed and approved by Institutional Animal Care and Use Committee of the Graduate School of Veterinary Medicine, Hokkaido University (approval no. 15–0079).

AUTHOR CONTRIBUTIONS

YE designed the study and experiments, interpreted the data, conceived the article structure, and wrote the manuscript. OI designed the experiments and edited the manuscript. TN reviewed the manuscript. YK conceptualized the research, performed data interpretation, contributed to the discussion, and critically revised the manuscript draft. All authors contributed to the article and approved the submitted version.

FUNDING

This study was supported by the Hokkaido University Tenure Track Program (Research Support Program II for Young Researchers) and Grant-in-Aid for Scientific Research (KAKENHI "B" No. 19H03113 and KAKENHI "C" No. 20K07420).

SUPPLEMENTARY MATERIAL

The Supplementary Material for this article can be found online at: https://www.frontiersin.org/articles/10.3389/fimmu.2021.665100/full#supplementary-material

Supplementary Figure 1 | Comparison between the lung injury score of BLM and PBS groups in both autoimmune disease mice model (Yaa) and their wild-type strain (BXSB) and the wild-type strain (B6 mice) on days 7 and 21. Graphs showing the average of lung injury score among studied groups and the wild-type strain. Asterisk indicates significant difference, analyzed by the Kruskal–Wallis test, followed by Scheffé's method. ($P < 0.05$); $n = 4$ in each experimental group. Values are expressed as mean± standard error (SE).

Supplementary Figure 2 | Collagen fibers (collagen I, col3A1) deposition in the lung sections of BLM and PBS groups in both autoimmune disease mice model (Yaa) and their wild-type strain (BXSB) on days 7 and 21. **(A, B)** Representative lung sections immuno-stained with anti-collagen I in both BXSB **(A)** and Yaa **(B)**. **(D, E)** Representative lung sections immuno-stained with anti-col3A1 in both BXSB **(D)** and Yaa **(E)**. **(C, F)** Graphs showing the percentages of positive area ratios of collagen I **(C)**, and col3A1 **(F)** among studied groups. Asterisk indicates significant differences between PBS and BLM groups, analyzed by the Kruskal–Wallis test, followed by Scheffé's method. ($P < 0.05$); $n = 4$ in each experimental group. Values are expressed as mean± standard error (SE).

Supplementary Figure 3 | Double immunofluorescent staining of MFALCs and lung sections of BLM and PBS groups in both autoimmune disease mice model (Yaa) and their wild-type strain (BXSB) on days 7 and 21. **(A, B)** Representative immunofluorescent images of MFALCs stained with anti-B220 and anti-CD3 antibodies in both BXSB **(A)** and Yaa **(B)**. **(C, D)** Representative immunofluorescent images of lung sections stained with anti-B220 and anti-CD3 antibodies in both BXSB **(C)** and Yaa **(D)**. Notice $B220^+$ B cells (green) and $CD3^+$ T cells (red).

Supplementary Figure 4 | Immunohistochemical staining of macrophages in MFALCs and the lungs of BLM and PBS groups in both autoimmune disease mice model (Yaa) and their wild-type strain (BXSB) on days 7 and 21. **(A, B)** Representative histopathological images of immunohistochemically stained sections of MFALCs in both BXSB **(A)** and Yaa **(B)** and the lungs in both BXSB **(C)** and Yaa **(D)** with anti-Iba1 antibody.

REFERENCES

1. Moro K, Yamada T, Tanabe M, Takeuchi T, Ikawa T, Kawamoto H, et al. Innate Production of T(H)2 Cytokines by Adipose Tissue-Associated c-Kit(+)Sca-1(+) Lymphoid Cells. *Nature* (2010) 463(7280):540–4. doi: 10.1038/nature08636
2. Elewa YHA, Ichii O, Otsuka S, Hashimoto Y, Kon Y. Characterization of Mouse Mediastinal Fat-Associated Lymphoid Clusters. *Cell Tissue Res* (2014) 357(3):731–41. doi: 10.1007/s00441-014-1889-6
3. Benezech C, Luu NT, Walker JA, Kruglov AA, Loo Y, Nakamura K, et al. Inflammation-Induced Formation of Fat-Associated Lymphoid Clusters. *Nat Immunol* (2015) 16(8):819–28. doi: 10.1038/ni.3215
4. Horckmans M, Bianchini M, Santovito D, Megens RTA, Springael JY, Negri I, et al. Pericardial Adipose Tissue Regulates Granulopoiesis, Fibrosis, and Cardiac Function After Myocardial Infarction. *Circulation* (2018) 137 (9):948–60. doi: 10.1161/CIRCULATIONAHA.117.028833
5. Cruz-Migoni S, Caamano J. Fat-Associated Lymphoid Clusters in Inflammation and Immunity. *Front Immunol* (2016) 7:612. doi: 10.3389/fimmu.2016.00612
6. Elewa YH, Ichii O, Kon Y. Comparative Analysis of Mediastinal Fat-Associated Lymphoid Cluster Development and Lung Cellular Infiltration in Murine Autoimmune Disease Models and the Corresponding Normal Control Strains. *Immunology* (2016) 147(1):30–40. doi: 10.1111/imm.12539

7. Elewa YHA, Ichii O, Takada K, Nakamura T, Masum MA, Kon Y. Histopathological Correlations Between Mediastinal Fat-Associated Lymphoid Clusters and the Development of Lung Inflammation and Fibrosis Following Bleomycin Administration in Mice. *Front Immunol* (2018) 9:271. doi: 10.3389/fimmu.2018.00271
8. Meadors M, Floyd J, Perry MC. Pulmonary Toxicity of Chemotherapy. *Semin Oncol* (2006) 33(1):98–105. doi: 10.1053/j.seminoncol.2005.11.005
9. Izbicki G, Segel MJ, Christensen TG, Conner MW, Breuer R. Time Course of Bleomycin-Induced Lung Fibrosis. *Int J Exp Pathol* (2002) 83(3):111–9. doi: 10.1046/j.1365-2613.2002.00220.x
10. Schrier DJ, Kunkel RG, Phan SH. The Role of Strain Variation in Murine Bleomycin-Induced Pulmonary Fibrosis. *Am Rev Respir Dis* (1983) 127(1): 63–6. doi: 10.1164/arrd.1983.127.1.63
11. Bergeron ME, Stefanov A, Haston CK. Fine Mapping of the Major Bleomycin-Induced Pulmonary Fibrosis Susceptibility Locus in Mice. *Mamm Genome* (2018) 29(9-10):670–9. doi: 10.1007/s00335-018-9774-3
12. Theofilopoulos ANaK, D. H, Lahita RG. Murine Lupus Models:Gene-Specific and Genome-Wide Studies. In: . *Systemic Lupus Erythematosus*, *3rd edn*. San Diego, CA: Academic Press (1999). p. 145.
13. Kono DH, Theofilopoulos AN. Genetics of SLE in Mice. *Springer Semin Immunopathol* (2006) 28(2):83–96. doi: 10.1007/s00281-006-0030-7
14. Pisetsky DS, Caster SA, Roths JB, Murphy ED. Ipr Gene Control of the anti-DNA Antibody Response. *J Immunol* (1982) 128(5):2322–5.
15. Mountz JD, Zhou T, Bluethmann H, Wu J, Edwards CK. 3rd. Apoptosis Defects Analyzed in TcR Transgenic and Fas Transgenic Lpr Mice. *Int Rev Immunol* (1994) 11(4):321–42. doi: 10.3109/08830189409051178
16. Deane JA, Pisitkun P, Barrett RS, Feigenbaum L, Town T, Ward JM, et al. Control of Toll-Like Receptor 7 Expression Is Essential to Restrict Autoimmunity and Dendritic Cell Proliferation. *Immunity* (2007) 27 (5):801–10. doi: 10.1016/j.immuni.2007.09.009
17. Santiago-Raber ML, Kikuchi S, Borel P, Uematsu S, Akira S, Kotzin BL, et al. Evidence for Genes in Addition to Tlr7 in the Yaa Translocation Linked With Acceleration of Systemic Lupus Erythematosus. *J Immunol* (2008) 181 (2):1556–62. doi: 10.4049/jimmunol.181.2.1556
18. Namba T, Ichii O, Nakamura T, Masum MA, Otani Y, Otsuka-Kanazawa S, et al. Feature Article: Altered Morpho-Functional Features of Bones in Autoimmune Disease-Prone BXSB/MpJ- Yaa Mice. *Exp Biol Med (Maywood)* (2019) 244(5):333–43. doi: 10.1177/1535370219832810
19. Elewa YH, Bareedy MH, Abuel-Atta AA, Ichii O, Otsuka S, Kanazawa T, et al. Structural Characteristics of Goat (Capra Hircus) Parotid Salivary Glands. *Jpn J Vet Res* (2010) 58(2):121–35.
20. Elewa YHA, Ichii O, Nakamura T, Kon Y. Pathological Alternations of Mediastinal Fat-Associated Lymphoid Cluster and Lung in a Streptozotocin-Induced Diabetic Mouse Model. *Microscopy Microanalysis* (2021) 27(1):187–200. doi: 10.1017/S1431927620024824
21. Ashcroft T, Simpson JM, Timbrell V. Simple Method of Estimating Severity of Pulmonary Fibrosis on a Numerical Scale. *J Clin Pathol* (1988) 41(4):467–70. doi: 10.1136/jcp.41.4.467
22. El-Badri NS, Hakki A, Ferrari A, Shamekh R, Good RA. Autoimmune Disease: Is it a Disorder of the Microenvironment? *Immunologic Res* (2007) 41(1):79. doi: 10.1007/s12026-007-0053-8
23. Cojocaru M, Cojocaru IM, Silosi I, Vrabie CD. Pulmonary Manifestations of Systemic Autoimmune Diseases. *Maedica (Bucur)* (2011) 6(3):224–9.
24. Perry D, Sang A, Yin Y, Zheng YY, Morel L. Murine Models of Systemic Lupus Erythematosus. *J BioMed Biotechnol* (2011) 2011:271694. doi: 10.1155/2011/271694
25. Cheema GS, Quismorio FP Jr. Interstitial Lung Disease in Systemic Lupus Erythematosus. *Curr Opin Pulm Med* (2000) 6(5):424–9. doi: 10.1097/00063198-200009000-00007
26. Quadrelli SA, Alvarez C, Arce SC, Paz L, Sarano J, Sobrino EM, et al. Pulmonary Involvement of Systemic Lupus Erythematosus: Analysis of 90 Necropsies. *Lupus* (2009) 18(12):1053–60. doi: 10.1177/0961203309106601
27. O'Sullivan JM, Huddart RA, Norman AR, Nicholls J, Dearnaley DP, Horwich A. Predicting the Risk of Bleomycin Lung Toxicity in Patients With Germ-Cell Tumours. *Ann Oncol* (2003) 14(1):91–6. doi: 10.1093/annonc/mdg020
28. Haston CK, Tomko TG, Godin N, Kerckhoff L, Hallett MT. Murine Candidate Bleomycin Induced Pulmonary Fibrosis Susceptibility Genes Identified by Gene Expression and Sequence Analysis of Linkage Regions. *J Med Genet* (2005) 42(6):464–73. doi: 10.1136/jmg.2004.027938
29. Zhou Y, Peng H, Sun H, Peng X, Tang C, Gan Y, et al. Chitinase 3-Like 1 Suppresses Injury and Promotes Fibroproliferative Responses in Mammalian Lung Fibrosis. *Sci Transl Med* (2014) 6(240):240ra76. doi: 10.1126/scitranslmed.3007096
30. Luzina IG, Todd NW, Iacono AT, Atamas SP. Roles of T Lymphocytes in Pulmonary Fibrosis. *J Leukoc Biol* (2008) 83(2):237–44. doi: 10.1189/jlb.0707504
31. Hamaguchi Y, Tedder T, Fujimoto M. B Cells Have a Dual Effect on Pulmonary Fibrosis Induced by Bleomycin in a Mouse Model. *J Immunol* (2011) 186:1.
32. Girard JP, Moussion C, Forster R. Hevs, Lymphatics and Homeostatic Immune Cell Trafficking in Lymph Nodes. *Nat Rev Immunol* (2012) 12 (11):762–73. doi: 10.1038/nri3298
33. Ager A, May MJ. Understanding High Endothelial Venules: Lessons for Cancer Immunology. *Oncoimmunology* (2015) 4(6):e1008791. doi: 10.1080/2162402X.2015.1008791
34. Merino R, Fossati L, Izui S. The Lupus-Prone BXSB Strain: The Yaa Gene Model of Systemic Lupus Erythematosus. *Springer Semin Immunopathol* (1992) 14(2):141–57. doi: 10.1007/BF00195291
35. Fairhurst A-M, Hwang S-H, Wang A, Tian X-H, Boudreaux C, Zhou XJ, et al. Yaa Autoimmune Phenotypes Are Conferred by Overexpression of TLR7. *Eur J Immunol* (2008) 38(7):1971–8. doi: 10.1002/eji.200838138
36. Wu Y, Xu M, He R, Xu K, Ma Y. ARHGAP6 Regulates the Proliferation, Migration and Invasion of Lung Cancer Cells. *Oncol Rep* (2019) 41(4):2281–888. doi: 10.3892/or.2019.7031
37. Pomerenke A, Lea SR, Herrick S, Lindsay MA, Singh D. Characterization of TLR-induced Inflammatory Responses in COPD and Control Lung Tissue Explants. *Int J Chron Obstruct Pulmon Dis* (2016) 11:2409–17. doi: 10.2147/COPD.S105156
38. Horimasu Y, Ishikawa N, Taniwaki M, Yamaguchi K, Hamai K, Iwamoto H, et al. Gene Expression Profiling of Idiopathic Interstitial Pneumonias (Iips): Identification of Potential Diagnostic Markers and Therapeutic Targets. *BMC Med Genet* (2017) 18(1):88. doi: 10.1186/s12881-017-0449-9
39. Pawar R, Allam R, Kulkarni O, Lech M, Anders H-J. Inhibition of Toll-Like Receptor-7 (Tlr-7) or TLR-7 Plus TLR-9 Attenuates Glomerulonephritis and Lung Injury in Experimental Lupus. Journal of the American Society of Nephrology. *JASN* (2007) 18:1721–31. doi: 10.1681/ASN.2006101162
40. Lafferty EI, Qureshi ST, Schnare M. The Role of Toll-Like Receptors in Acute and Chronic Lung Inflammation. *J Inflammation* (2010) 7(1):57. doi: 10.1186/1476-9255-7-57

Conflict of Interest: The authors declare that the research was conducted in the absence of any commercial or financial relationships that could be construed as a potential conflict of interest.

frontiers in Immunology

ORIGINAL RESEARCH
published: 24 August 2021
doi: 10.3389/fimmu.2021.642891

Elevated Fibronectin Levels in Profibrotic CD14$^+$ Monocytes and CD14$^+$ Macrophages in Systemic Sclerosis

*Michał Rudnik[1], Amela Hukara[1], Ievgeniia Kocherova[1], Suzana Jordan[1], Janine Schniering[1], Vincent Milleret[2], Martin Ehrbar[2], Karin Klingel[3], Carol Feghali-Bostwick[4], Oliver Distler[1], Przemysław Błyszczuk[1,5] and Gabriela Kania[1]**

[1] Department of Rheumatology, Center of Experimental Rheumatology, University Hospital Zurich, University of Zurich, Zurich, Switzerland, [2] Department of Obstetrics, University Hospital Zurich, Zurich, Switzerland, [3] Department of Molecular Pathology, University Hospital Tuebingen, Tuebingen, Germany, [4] Division of Rheumatology, Medical University of South Carolina, Charleston, SC, United States, [5] Department of Clinical Immunology, Jagiellonian University Medical College, Krakow, Poland

OPEN ACCESS

Edited by:
Carmelo Carmona-Rivera, National Institute of Arthritis and Musculoskeletal and Skin Diseases (NIAMS), United States

Reviewed by:
José Jiram Torres-Ruiz, Instituto Nacional de Ciencias Médicas y Nutrición Salvador Zubirán (INCMNSZ), Mexico
Eduardo Patino Martinez, National Institutes of Health Clinical Center (NIH), United States
Yudong Liu, Peking University People's Hospital, China

***Correspondence:**
Gabriela Kania
gabriela.kania@uzh.ch

Specialty section:
This article was submitted to Autoimmune and Autoinflammatory Disorders, a section of the journal Frontiers in Immunology

Received: 17 December 2020
Accepted: 21 July 2021
Published: 24 August 2021

Citation:
Rudnik M, Hukara A, Kocherova I, Jordan S, Schniering J, Milleret V, Ehrbar M, Klingel K, Feghali-Bostwick C, Distler O, Błyszczuk P and Kania G (2021) Elevated Fibronectin Levels in Profibrotic CD14$^+$ Monocytes and CD14$^+$ Macrophages in Systemic Sclerosis. Front. Immunol. 12:642891. doi: 10.3389/fimmu.2021.642891

Background: Systemic sclerosis (SSc) is an autoimmune disease characterized by overproduction of extracellular matrix (ECM) and multiorgan fibrosis. Animal studies pointed to bone marrow-derived cells as a potential source of pathological ECM-producing cells in immunofibrotic disorders. So far, involvement of monocytes and macrophages in the fibrogenesis of SSc remains poorly understood.

Methods and Results: Immunohistochemistry analysis showed accumulation of CD14$^+$ monocytes in the collagen-rich areas, as well as increased amount of alpha smooth muscle actin (αSMA)-positive fibroblasts, CD68$^+$ and mannose-R$^+$ macrophages in the heart and lungs of SSc patients. The full genome transcriptomics analyses of CD14$^+$ blood monocytes revealed dysregulation in cytoskeleton rearrangement, ECM remodeling, including elevated *FN1* (gene encoding fibronectin) expression and TGF-β signalling pathway in SSc patients. In addition, single cell RNA sequencing analysis of tissue-resident CD14$^+$ pulmonary macrophages demonstrated activated profibrotic signature with the elevated *FN1* expression in SSc patients with interstitial lung disease. Peripheral blood CD14$^+$ monocytes obtained from either healthy subjects or SSc patients exposed to profibrotic treatment with profibrotic cytokines TGF-β, IL-4, IL-10, and IL-13 increased production of type I collagen, fibronectin, and αSMA. In addition, CD14$^+$ monocytes co-cultured with dermal fibroblasts obtained from SSc patients or healthy individuals acquired a spindle shape and further enhanced production of profibrotic markers. Pharmacological blockade of the TGF-β signalling pathway with SD208 (TGF-β receptor type I inhibitor), SIS3 (Smad3 inhibitor) or (5Z)-7-oxozeaenol (TGF-β-activated kinase 1 inhibitor) ameliorated fibronectin levels and type I collagen secretion.

Conclusions: Our findings identified activated profibrotic signature with elevated production of profibrotic fibronectin in CD14$^+$ monocytes and CD14$^+$ pulmonary macrophages in SSc and highlighted the capability of CD14$^+$ monocytes to acquire a

profibrotic phenotype. Taking together, tissue-infiltrating CD14$^+$ monocytes/macrophages can be considered as ECM producers in SSc pathogenesis.

Keywords: systemic sclerosis, CD14+ monocytes, CD14+ macrophages, fibrosis, fibronectin, TGF-β

INTRODUCTION

Systemic sclerosis (SSc) is an autoimmune disease, characterized by high morbidity and mortality and a significant reduction in quality of life. Microvascular damages, dysregulation of innate and adaptive immunity and multiorgan fibrosis are implicated in the pathophysiology of SSc (1). SSc is characterized by a patient-to-patient variability in clinical manifestations, autoantibody profiles, extent of disease, treatment response and reduced survival rate (2). Changes in internal organ architecture, leading to pulmonary and cardiac complications and dysfunction remains the major causes of deaths among SSc patients (3).

Fibrogenesis is a multistage process, considered as the result of impaired tissue repair responses, in which abnormal production of cytokines, growth factors and angiogenic factors turn tissue homeostasis towards the excessive accumulation of extracellular matrix (ECM) (4). Fibrosis is usually an outcome of prolonged and exaggerated activation of fibroblasts, which differentiate into myofibroblasts (5). In contrast to physiological wound healing, in which myofibroblast are present only transiently, in fibrosis myofibroblasts become a permanent cellular component of the tissue (6).

Myofibroblasts are characterized by expression of alpha smooth muscle actin (αSMA) forming stress fibers and exhibit an increased capacity to synthesize collagens, fibronectin, and other ECM components. Fibronectin is a high-molecular weight glycoprotein of the extracellular matrix, which binds to integrins and other extracellular matrix proteins such as collagen, fibrin, and heparan sulfate proteoglycans (7). Increased deposition of fibronectin, paralleled to accumulated collagen, has been reported in the SSc skin (8, 9).

The cellular source of myofibroblasts in wound healing and fibrotic lesions is still debatable. Although most evidence point to resident fibroblasts, other tissue-resident cell types or cells recruited from circulation have been shown to acquire a myofibroblast-like phenotype (10). In experimental models of lung and kidney fibrosis, bone marrow-derived fibrocytes have been shown to be recruited into injured or fibrotic tissues in response to chemokine signals, where they differentiate into fibroblasts or myofibroblasts (11). Lineage tracing experiments have provided convincing evidence that pericytes are an important source of myofibroblasts during renal fibrogenesis in animal models, and these cells might also be a source of myofibroblasts in SSc (12, 13). During fibrogenesis, epithelial cells have been hypothesized to undergo epithelial-to-mesenchymal transition and transdifferentiate into myofibroblasts in response to TGFβ and other profibrotic cytokines. Additionally, SSc tissues are chronically hypoxic, which can further promote the formation of myofibroblast-like cells (14). In addition to epithelial cells, endothelial cells have also been hypothesized to transdifferentiate into myofibroblasts through endothelial-mesenchymal transition (15).

The primary mechanism underlying excessive fibrosis in SSc remains unknown; however, TGFβ is one of the best-studied mediators regulating fibrotic processes, including fibroblast differentiation, ECM deposition and tissue contraction (16). Elevated levels of TGFβ-regulated genes (cartilage oligomeric matrix protein, thrombospondin-1) were reported in the skin lesions from SSc patients (17). TGFβ signalling regulates the expression of profibrotic genes mostly *via* the SMAD-dependent canonical pathway (18). However, the involvement of several non-canonical pathways in fibrotic processes was acknowledged. For example, activation of the ERK-MAPK signalling pathway leads to upregulation of type I collagen in SSc fibroblasts (19). Ultimately, inhibition of TGFβ signalling has been addressed as a potential treatment strategy; however, conflicting results were reported following TGFβ blockade (20).

Myeloid cells, including monocytes, have been shown to be essential regulators of fibrosis as producers of chemokines, inflammatory cytokines and growth factors (21, 22). Our group has previously reported that the microenvironment of inflamed lung induces myeloid progenitors to acquire a myofibroblast phenotype (23). Similarly, we showed that heart-infiltrating myeloid cells served as myofibroblast progenitors in the model of post-inflammatory cardiac fibrosis (24). In the present study, we evaluated the differentiation potential of circulating CD14$^+$ monocytes from healthy controls and SSc patients into a myofibroblast-like phenotype.

MATERIAL AND METHODS

SSc Patients and Healthy Controls

Human blood samples and skin biopsies collection were approved by the local ethics committee of the Canton Zurich (KEK-ZH 515, PB-2016-02014, KEK-Nr 2018-01873). All study subjects provided written informed consent. SSc patients and healthy controls were recruited at the Department of Rheumatology of University Hospital Zurich. All the patients fulfilled the ACR/EULAR 2013 classification criteria for SSc.

The patients diagnosed with SSc by experts with Raynaud syndrome and a least one other SSc characteristic such as: SSc specific antibodies, SSc characteristic capillaroscopy changes and/or puffy fingers. The patients not fulfilling the ACR/EULAR 2013 classification criteria for SSc were grouped as early-SSc. The patients fulfilling the criteria were further divided into lcSSc and dcSSc subgroups, according to Le Roy et al. (25). Detailed demographics and clinical characteristics of SSc patients are included in **Table 1**. Healthy control group was

TABLE 1 | Definitions of items and organ manifestation are according to EUSTAR.

Baseline demographic and clinical characteristics of the SSc patients	SSc pat (N = 37)
Demographics	
Age (mean ± SD)	54.0 ± 14.6
Female sex	32/37 (86.5%)
Disease duration (mean ± SD; years)	14.7 ± 12.5
ACR/EULAR criteria fulfilled	28/37 (75.7%)
Subtype	
Diffuse SSc	4/37 (10.8%)
Skin/Vascular	
Raynaud's Phenomenon	32/37 (86.5%)
Digital ulcers	12/37 (32.4%)
Active digital ulcers	3/35 (8.6%)
Pitting scars	11/35 (31.4%)
Scleredema	26/35 (74.2%)
Telangiectasia	20/37 (54.1)
mRSS (mean ± SD)	2.8 ± 4.1
Abnormal nailfoldcapillaroscopy	30/33 (90.6%)
Musculoskeletal	
Tendon friction rubs	1/35 (2.9%)
Joint synovitis	5/36 (13.9%)
Joint contractures	9/32 (42.0%)
Muscle weakness	0/31 (0)
Gastrointestinal	
Esophageal symptoms	20/37 (54.1%)
Stomach symptoms	8/33 (24.2%)
Intestinal symptoms	14/33 (42.4%)
Cardiopulmonary	
Dyspnea	
Stage 1	27/34 (79.4%)
Stage 2	5/34 (14.7%)
Stage 3/4	2/34 (5.9%)
Diastolic dysfunction	8/31 (25.8%9
Pericardial effusion	3/24 (12.5%)
Conduction blocks	2/35 (5.7%)
LVEF<45%	0/35 (0)
PAH by RHC	0/37 (0)
Lung fibrosis on HRCT	11/37 (29.7%)
FVC, % predicted (mean ± SD)	93.5 ± 15.4
FVC<70% predicted	1/37 (2.7%)
FEV, % predicted (mean ± SD)	93.2 ± 14.6
TLC, % predicted (mean ± SD)	103.5 ± 16.6
DLCO, % predicted (mean ± SD)	76.0 ± 18.8
DLCO<70% predicted	10/33 (30.3%)
Kidney	
Renal crisis	1/37 (2.7%)
Laboratory parameters	
ANA positive	37/37 (100%)
ACA	22/37 (59.5%)
Anti-Scl-70 positive	8/36 (22.2%)
Anti-U1RNP positive	0/37 (0)
Anti RNA-polymerase III positive	2/36 (5.5%)
Creatinine kinase elevation	2/27 (7.4%)
Proteinuria	2/35 (5.7%)
Hypocomplementaemia	2/36 (5.5%)
ESR>25 mm/h	9/31 (29.0%)
CRP elevation	5/26 (19.2%)
Active disease (VAI>3)	1/32 (3.1%)
Immunosuppressive therapy	5/37 (13.5%)

age- and gender matched (age mean=44.4 ± 10.8, female 17/20 (85%).

Data are presented as number (n)/total valid cases (N) (%). Disease duration was calculated as the difference between the date of the baseline visit and the date of the first non-Raynaud's symptom of the disease as reported by the patient. Pulmonary hypertension was judged on RHC. Active disease was defined as a score >3 by calculating European Scleroderma Study Group disease activity indices for systemic sclerosis proposed by Valentini. Immunosuppressive therapy was defined as treatment with corticosteroids (prednisone dose ≥10 mg/day or other dosage forms in equal dose) or any immunosuppressant.

ACA, anti-centromere antibody; ANA, antinuclear antibody; Anti-Scl-70, anti-topoisomerase antibody; CRP, C reactive protein; HRCT, computed tomography; DLCO, diffusing capacity for carbon monoxide; ESR, erythrocyte sedimentation rate; FEV1, forced expiratory volume in 1 sec; FVC, forced vital capacity; LVEF, left ventricular ejection fraction; mRSS, modified Rodnan skin score; NYHA, New York Heart Association; TLC, total lung capacity; VAI, Valentini activity index.

Human endomyocardial biopsies were provided by the University Hospital Tubingen, Germany. Samples were obtained from SSc patients with cardiac involvement (inflammatory dilated cardiomyopathy) and controls (patients with healed myocarditis). Lung biopsies were provided by the Division of Rheumatology, Medical University of South Carolina, Charleston, USA. The samples were obtained from SSc-related interstitial lung disease (SSc-ILD). Sample tissue from downsized lung transplants from healthy individuals served as controls. The experiments with re-use of human material were approved by Swissethics (KEK-Nr 2019-00058, KEK-Nr 2018-01873) and were performed in conformity with the principles outlined in the Declaration of Helsinki. Transcriptomic analysis of an already published dataset of human lung tissues has been included. For this, the University of Pittsburgh Institutional Review Board approved ethics of use the human lung samples as previously described (26).

CD14$^+$ Monocytes Isolation and Differentiation

Blood samples were collected in EDTA tubes (BD Vacutainer) and processed within 24h. Peripheral blood mononuclear cells (PBMCs) were isolated by gradient centrifugation on cell separation medium (Lympholyte, Cedarlane), followed by magnetic-activated cell sorting for CD14 using human microbeads and AutoMACS Pro device (Miltenyi Biotec). Cells were cultured in DMEM low glucose medium (Sigma) with the addition of 10% Foetal Bovine Serum (FBS) and 1% penicillin/streptomycin (both Gibco). To differentiate into myofibroblast-like cells, CD14$^+$ monocytes were stimulated with 10 ng/ml TGFβ (PeproTech), 10 ng/ml IL-4, 10 ng/ml IL-10 and 10 ng/ml IL-13 (Immunotools) for 7 days.

RNA Extraction

Total RNA was isolated using the Quick-RNA Microprep isolation kit (Zymo Research). Directly after monocyte treatment, cells were washed with PBS and lysed in RNA lysis buffer (Zymo Research). An equal volume of absolute ethanol (Millipore) was added and mixed. Lysates were further processed on the columns. Genomic DNA was removed by DNase I treatment. RNA was washed twice and eluted in 10-15 µl of nuclease-free water (Promega). RNA concentration and purity were assessed on NanoDrop 1000 (Thermo Fisher Scientific).

Bulk and Single Cell (sc) RNA Sequencing and Data Analysis

For RNA sequencing, RNA was isolated from SSc patients and healthy controls [as described previously in **Supplementary Table 1** in (27)] as described above, and RNA Integrity Number (RIN) was assessed by Tape Station (Agilent). Samples with RIN≥8 were further processed. RNA sequencing was performed by the Functional Genomics Centre Zurich. From 100 ng of total RNA, polyA libraries were prepared using the Illumina TruSeq RNA Stranded mRNA library Kit. Sequencing was performed on the Illumina HiSeq 4000 platform. Quality of the sequencing was controlled by FastQC package. Reads were aligned to the genome using the STAR algorithm. Gene expression profiles were next calculated by the FeatureCount algorithm. For differentially expressed genes, the DeSEQ2 algorithm was used with a threshold of minimum 10 reads for a transcript to be considered as present. Pathway enrichment analysis of differentially expressed genes ($p \leq 0.01$, $|\log_2 ratio| \geq 0.5$) was performed by the Metacore software, as described previously (27).

Human explanted lung tissues were digested and scRNA-sequencing was performed as previously described (26).

ScRNAseq Analysis of Each Sample

Raw count matrices produced from CellRanger were loaded from the dataset GSE128169. Empty droplets were distinguished from droplet-containing cells by using the emptyDrops function from the R package DropletUtils (28, 29). Only droplets that obtained an FDR <= 0.001 were called as cells. Doublets were also discarded from further analysis using the R package scDblFinder. Low quality cells were identified based on the number of reads, genes and mitochondrial content using the R package scuttle. We excluded cells that were outliers according to at least one of the following thresholds: number of reads < 3 MADs, number of gene < 3 MADs, mitochondrial content > 3 MADs. Additionally, we discarded genes with < 1 UMI count in < 0.01 of the remaining cells. We used the SCTransform (30) method from the R package Seurat (31) to normalize and scale the data.

Integration of Multiple Samples

Multiple samples were combined using the Seurat integration workflow (32). After integration we reduced the dimensionality of the data using Principal Component Analysis (PCA). The main 30 principal components were used to perfor unsupervised clustering with a resolution value of 0.8. After clustering and visualization with Uniform Manifold Approximation and Projection (UMAP), cell populations were identified through examination of gene markers in the associated transcriptome.

Cells that had > 0 counts for the CD14 gene were called as $CD14^+$ cells. All plots and downstream analysis were performed using Seurat.

RT-qPCR

For reverse transcription, 200-300ng of total RNA was used. The reaction was performed using MultiScribe reverse transcriptase (Thermo Fisher Scientific), random hexamers and RNAase inhibitor (both Roche). Subsequently, the qPCR reaction was performed using the SYBR green GoTaq qPCR master mix (Promega) on Agilent Stratagene Mx3005P qPCR instrument. Sequences of primers are listed in **Supplementary Table 1**. Relative gene expression was calculated using the $2^{-\Delta\Delta Ct}$ method. *GAPDH* was used as the reference gene.

Protein Extraction and Immunoblotting

After the stimulation with cytokines, cells were washed once with ice-cold PBS, collected, centrifuged and lysed for 30 minutes on ice in RIPA buffer (Sigma) supplemented with proteases and phosphatases inhibitors (Roche). An equal amount of the protein was loaded and separated by SDS-PAGE electrophoresis, followed by wet transfer on the nitrocellulose membrane (GE Healthcare). The membrane was further incubated for 1 hour in blocking buffer (5% BSA in TBS-T). Further, membranes were probed overnight with primary antibodies, listed in **Supplementary Table 2**, in blocking buffer at 4°C. Further, membranes were incubated for 1 hour at room temperature with secondary HRP-conjugated antibodies. Signal was developed with ECL substrate (SuperSignal West Pico PLUS, Thermo Scientific) and acquired on the Fusion fx (Vilber) device.

ELISA

For the detection of human pro-collagen 1α1 DuoSet ELISA (RnD Systems) was used according to the manufacturer's protocol. Briefly, 96-well plates were coated with capture antibodies overnight in room temperature and further blocked with 2% BSA in phosphate-buffered saline (PBS) supplemented with 0.05%Tween 20. Between each step, plates were washed three times with PBS. The protein standards and samples were applied and incubated for 2 hours. Next, plates were incubated with biotin-conjugated detection antibodies for 2 hours and streptavidin-HRP for 30 minutes in room temperature. Signal was developed with TMB substrate (Thermo Scientific), and 450 nm absorbance was measured on a BioTEK HT plate reader (Tecan). Concentrations were calculated according to the respective standard curves.

Treatment With Pharmacological Inhibitors and Cytotoxicity Assessment

SD208 [1 µM], SIS3 [2 µM], (5Z)-7-Oxozeaenol (OXO) [1 µM] pharmacological inhibitors used in the project were purchased

from Tocris Biosciences. To determine optimal non-toxic concentrations, we performed toxicity tests. $CD14^+$ monocytes were incubated with 2-fold dilutions of inhibitors starting from 5 or 10 μM. Cells were incubated for 24h, stained with propidium iodide (Biolegend), and cytotoxicity was evaluated by flow cytometry. The highest non-toxic concentration was used in further experiments.

2D and 3D Co-Culture With Dermal Fibroblasts

To distinguish cells in both systems, monocytes were stained with Cell Trace Violet (Thermo Scientific), and fibroblasts were stained with CFSE (Biolegend) according to the manufacturer's protocol. For 2D co-cultures, fibroblasts were plated 24h prior to the addition of monocytes. Cells were cultured for 7 days and sorted using FACSAria III cell sorter.

For the 3D co-culture model, 3DProSeed® hydrogel microtiter plate (Ectica Technologies) were used. Firstly, labelled fibroblasts were plated and allowed to penetrate hydrogels for 24h. Next, monocytes were added. Plates were incubated for 7 days, and anti-αSMA/phalloidin (both Sigma) staining was performed. Co-cultures were visualized using Leica SP8 confocal microscope.

Immunohistochemistry, Imaging and Quantification

Collected tissue samples were washed in PBS and fixed for 16 hours in 4% paraformaldehyde in PBS. Next, tissues were rinsed in distilled water and transferred to 50% ethanol. Biopsies were then dehydrated (three incubations in 80% ethanol for 1 hour, three incubations in 96% ethanol for 1 hour, two incubations in 100% ethanol for 1 hour). Tissues were cleared twice in xylene for 1 hour and subsequently incubated twice in a 56°C paraffin bath for 3 hours. After paraffin embedding, 4 μm thick sections were placed on Superfrost Plus slides (Thermo Scientific) and dried overnight. Lung sections were cut at a thickness of 4 μm and stained with hematoxylin and eosin (HE) for analysis of the lung architecture and the presence of cellular infiltrates, and with Picrosirius Red to detect collagen deposition using standard protocols (33).

For immunohistochemistry sections were deparaffinized in xylene for 10 minutes (3 times) and rehydrated by sequential incubations in ethanol solutions (100%, 100%, 96% and 80%) for 3 minutes each. Sections were eventually washed for 5 minutes in distilled water. Antigen retrieval was performed in citrate buffer (10 mM citrate, 0.05% Tween, pH=6), and incubated at 95°C for 15 minutes. Endogenous peroxidases were blocked by 3% H_2O_2 solution for 15 minutes. Unspecific antibody binding was blocked with 10% goat serum in Background Reducing Antibody Diluent (Dako). Endogenous biotin was blocked by Avidin-Biotin Block kit (Vector Laboratories). Sections were incubated with primary antibodies, listed in the **Supplementary Table 2**, in 4°C overnight. The appropriate biotinylated secondary antibodies (Vector Laboratories) were incubated for 30 minutes at room temperature, followed by 30 minutes incubation with VECTASTAIN Elite ABC kit (Vector Laboratories). Staining was developed using Vector DAB or Vector Red (Vector Laboratories) followed by a counterstaining of nuclei for 1 minute in Mayer's hematoxylin solution (J.T Baker). All sections were mounted using Pertex mounting medium (Dako). CD14-collagen-1 was performed by Sophistolab AG.

Full slide images were acquired using a Zeiss Axio Scan Z1 slide scanner. ImageJ software was used for relative quantification of the signal in the sections. For CD45, mannose-R, CD86, iNOS and arginase-1 staining analysis, the "HDAB" plug-in was applied, while for Picrosirius Red and α-SMA "Fast Red, Fast Blue" plug-in was used. Deconvoluted images were used to calculate the area of the nuclear staining and the area of the specific signal. The value for each section was calculated as the ratio of the specific signal to nuclei signal.

Statistical Analysis

Statistical analysis was performed using GraphPad Prism 8 software. Data distribution was calculated using the Shapiro-Wilk test. Normally distributed data were presented as mean ± standard deviation and analyzed by unpaired two-tailed parametric *t*-test. For non-normally distributed data, unpaired non-parametric Mann-Whitney *U* test was used, and medians were presented. For comparisons of more than two groups, two-way ANOVA test with multiple comparisons (normally distributed data) and Kruskal-Wallis test with multiple comparisons (non-normally distributed data) were used. Differences were considered statistically significant for $p<0.05$. n refers to the number of biological replicates.

Additional methods are described in the **Supplementary Material**.

RESULTS

Infiltration of $CD14^+$ Monocytes Into the Organs Co-Localizes With Fibrosis in SSc

In line with data published previously (34), we observed increased infiltration of $CD14^+$ cells into the heart and lungs of SSc patients compared to control tissues (**Figures 1A, B**). Moreover, CD14 signal co-localized with collagen-rich lesions in different SSc tissues (**Figure 1C**). This data suggests that monocytes may participate in fibrotic processes in many organs during pathological tissue remodeling in SSc. Furthermore, heart and lungs of SSc patients showed the increased levels of αSMA^+ (myo)fibroblasts, $CD68^+$ pro-inflammatory macrophages and mannose-R^+ (CD206) alternatively activated macrophages (**Figures 2A–C**) that reflects inflammatory and fibrotic microenvironment in different SSc tissues.

Activation of Profibrotic Pathways in $CD14^+$ Blood Monocytes in SSc

We compared the transcriptome profiles of the total pool of SSc $CD14^+$ monocytes in relation to $CD14^+$ monocytes obtained from healthy controls (HC). Pathway analysis revealed

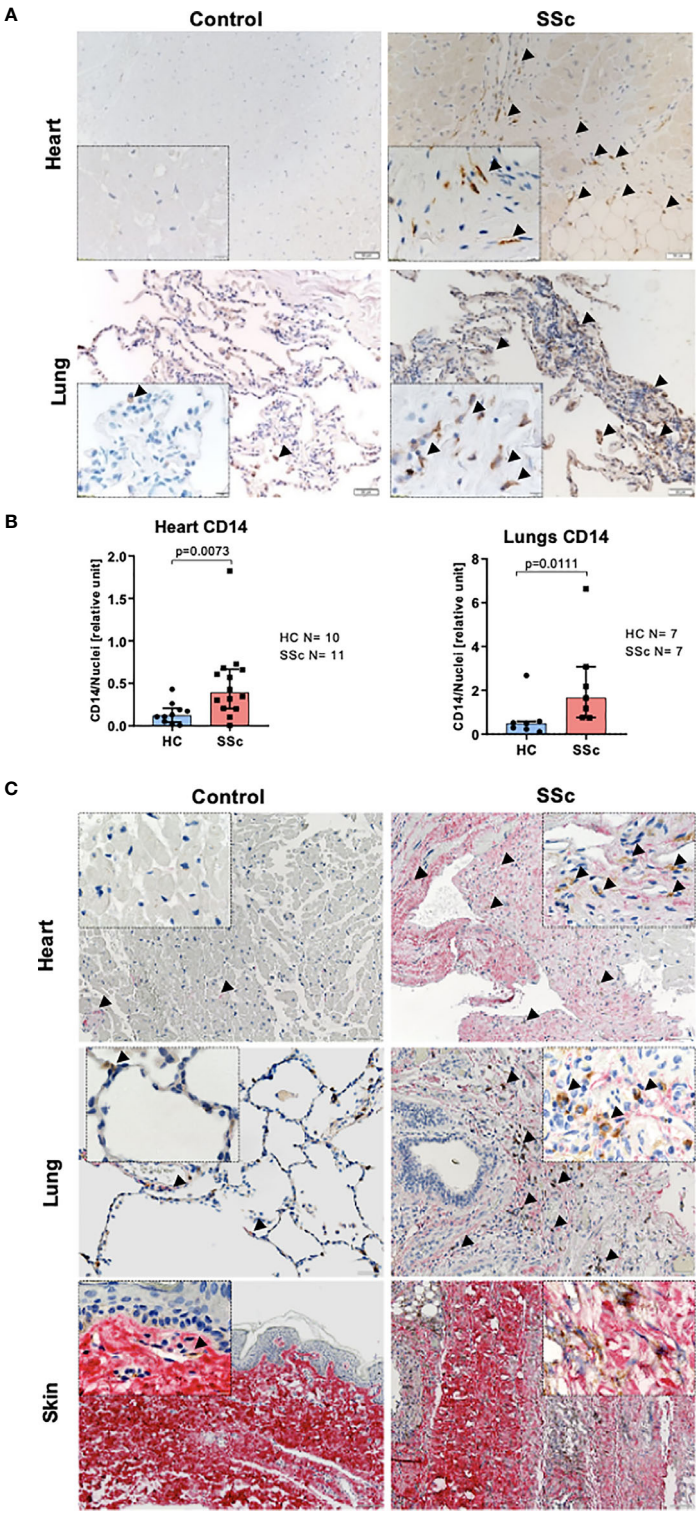

FIGURE 1 | Monocyte infiltration into the fibrotic lesion in SSc tissues. **(A)** Representative images of paraffin-embedded sections of the heart and lungs, and **(B)** corresponding quantification of IHC staining for CD14 (lungs HC N=7, SSc N=7, heart HC N=10, SSc N=11, *unpaired t-test).* **(C)** Representative images of paraffin-embedded sections of the heart, lungs and skin co-stained for pro-collagen I (red) and CD14 (brown). **(A, C)** Scale bar 100μm, scale bar in insert 20μm.

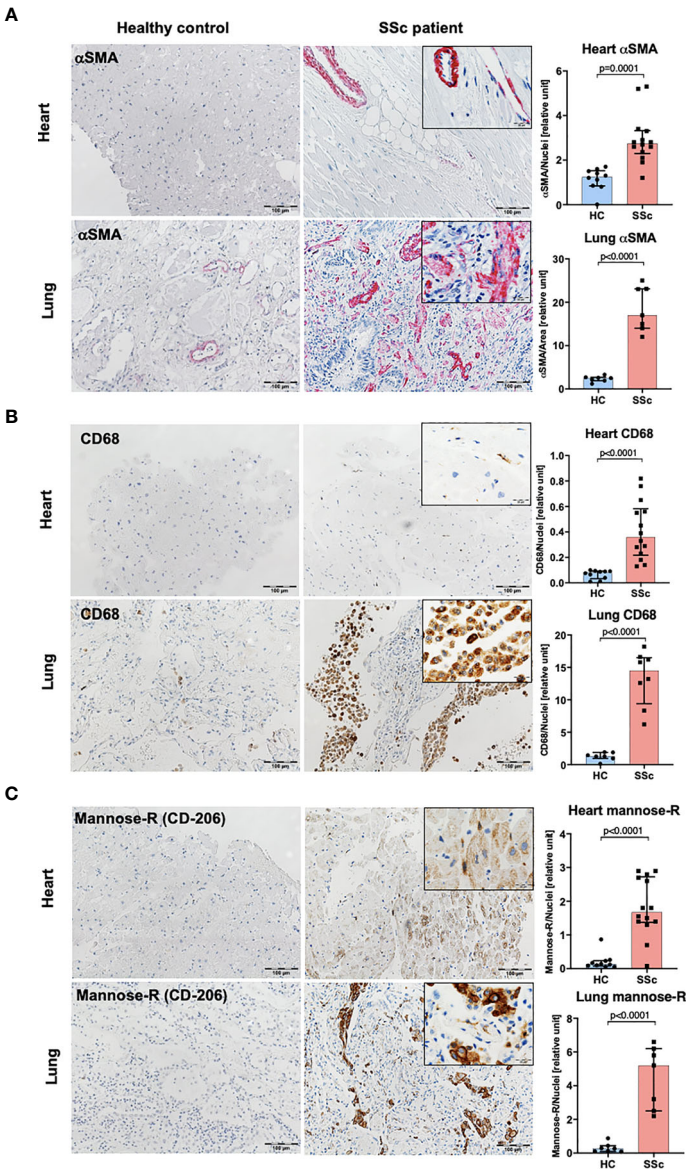

FIGURE 2 | Characteristic of human SSc lung and heart tissues. Representative images of paraffin-embedded sections of the heart and lungs and corresponding quantification of IHC staining for αSMA **(A)**, CD68 **(B)** and mannose-R (CD206) **(C)** (lung HC N=7, lung SSc N=7, heart HC N=10, heart SSc N=11, *unpaired t-test*; scale bar 100μm, scale bar in insert 20μm).

enrichment of SSc and fibrotic-associated processes, such as "TGF-beta signalling pathway", "Toll-like Receptor Signalling Pathway", "Angiogenesis" and "VEGF signalling pathway" in SSc $CD14^+$ monocytes (**Figure 3A**). At the transcription level, we observed dysregulated expression of essential profibrotic genes: *TGFBR2, MMP9, JUN, COL9A3, COL18A1, FN1* and *WNT5B* (**Figures 3B, C**). Further, we demonstrated that SSc $CD14^{++}CD16^-$ monocyte population showed significantly higher *FN1* expression than SSc $CD14^+CD16^+$ and $CD14l^{ow}CD16^+$ monocyte populations (**Figure 3D**). Of note, we did not notice any difference in *FN1* expression between these three monocyte populations in HC monocytes (**Figure 3D**). Importantly, SSc $CD14^{++}CD16^-$ and $CD14^+CD16^+$ monocyte populations revealed profibrotic features by expressing upregulated *FN1* levels compared to HC monocytes (**Figure 3D**).

This result indicated an activated, profibrotic phenotype of SSc $CD14^+$ monocytes in the circulation, which might predispose them to acquire pathogenic phenotype in the fibrotic tissue.

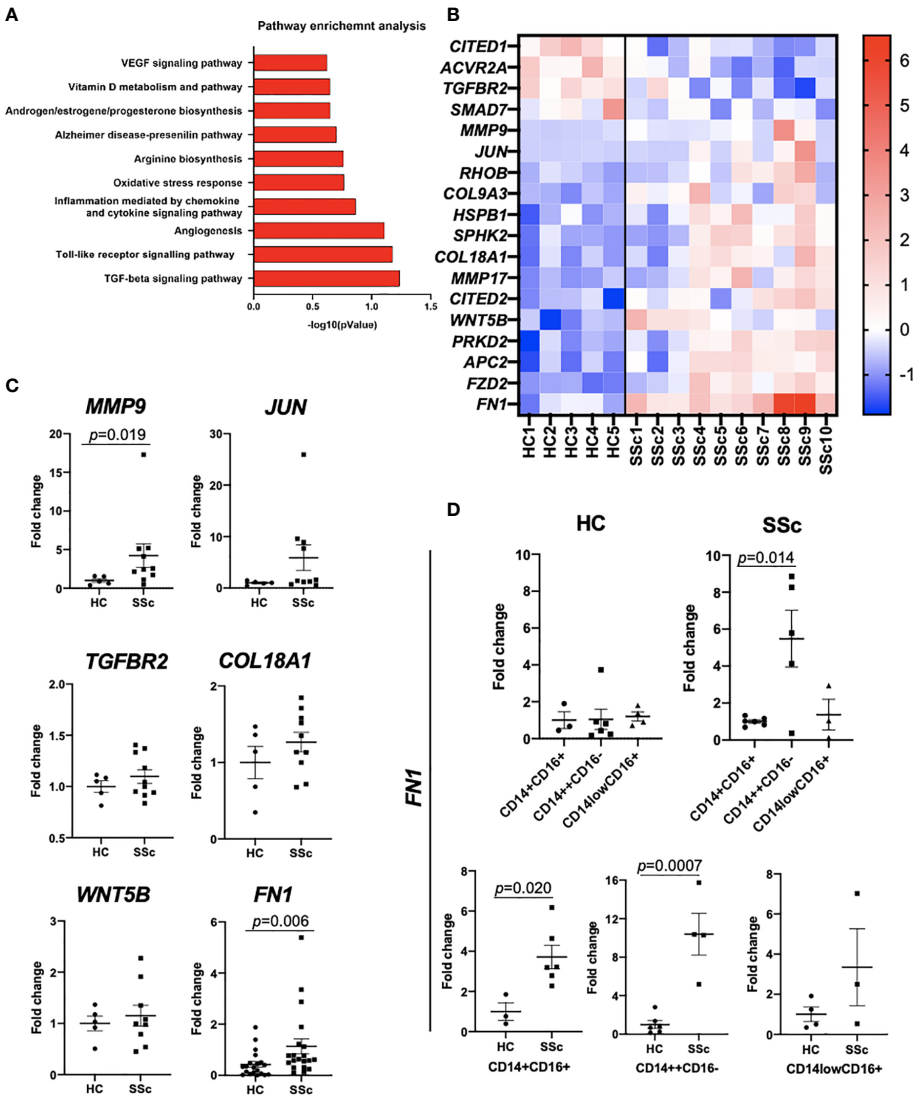

FIGURE 3 | Transcriptomic analysis of CD14$^+$ monocytes from SSc patients and HC. **(A)** Pathway enrichment analysis of SSc-related biological processes calculated based on differentially expressed gene sets (Metacore software). **(B)** Differentially expressed genes involved in fibrosis from RNAseq data. **(C)** qPCR confirmatory analyses of selected genes from RNAseq data (N=5-20, *Mann Whitney-U-test*). **(D)** qPCR analysis of *FN1* mRNA levels in sorted CD14^{++}CD16$^-$, CD14^{low}CD16$^+$ and CD14$^+$CD16$^+$ monocyte from SSc patients and HC (n=3-6, *Mann Whitney-U-test*).

Activation of Profibrotic Pathways in CD14$^+$ Pulmonary Macrophages in SSc

Transcriptomic analysis of an already published dataset of lung tissue from 4 HC and 4 SSc-ILD patients has been performed (26). CD14$^+$ cells were visualized in all macrophage clusters (FCN1hi, SPP1hi, FABP4hi and proliferating macrophages) (**Figure 4A**), determined as previously shown (26). Pathway analysis revealed enrichment of fibrosis-associated processes, such as "Extracellular matrix disassembly", "Extracellular matrix organization", "Cellular response to cytokine stimulus" and "Cytokine-mediated signalling pathway" in SSc CD14$^+$ cells (**Figure 4B**). At the transcription level, we noticed upregulation expression of several profibrotic genes, including *TGFβ1*, *TIPM1*, *TIPM2*, *FN1* and *ADAM10* (**Figure 4C**). Importantly, in all macrophage clusters in SSc lungs, we observed upregulated expression of *FN1* in CD14$^+$ cells (**Figures 4D, E**).

Profibrotic Cytokine Stimulation Induces Differentiation of Monocytes Into Myofibroblast-Like Cells

Bone marrow-derived cells have been proposed as one of the sources of myofibroblasts. Therefore, next, we evaluated the potential of CD14$^+$ monocytes to differentiate into myofibroblast-like cells in response to profibrotic stimulation with TGFβ, IL-4, IL-10 and IL-13 cytokines. We observed the induction of profibrotic gene expression including *ACTA2*, *COL1A1* and *FN1* (**Figure 5A**). Additionally, stimulated monocyte-derived cells secreted ECM components: type I collagen

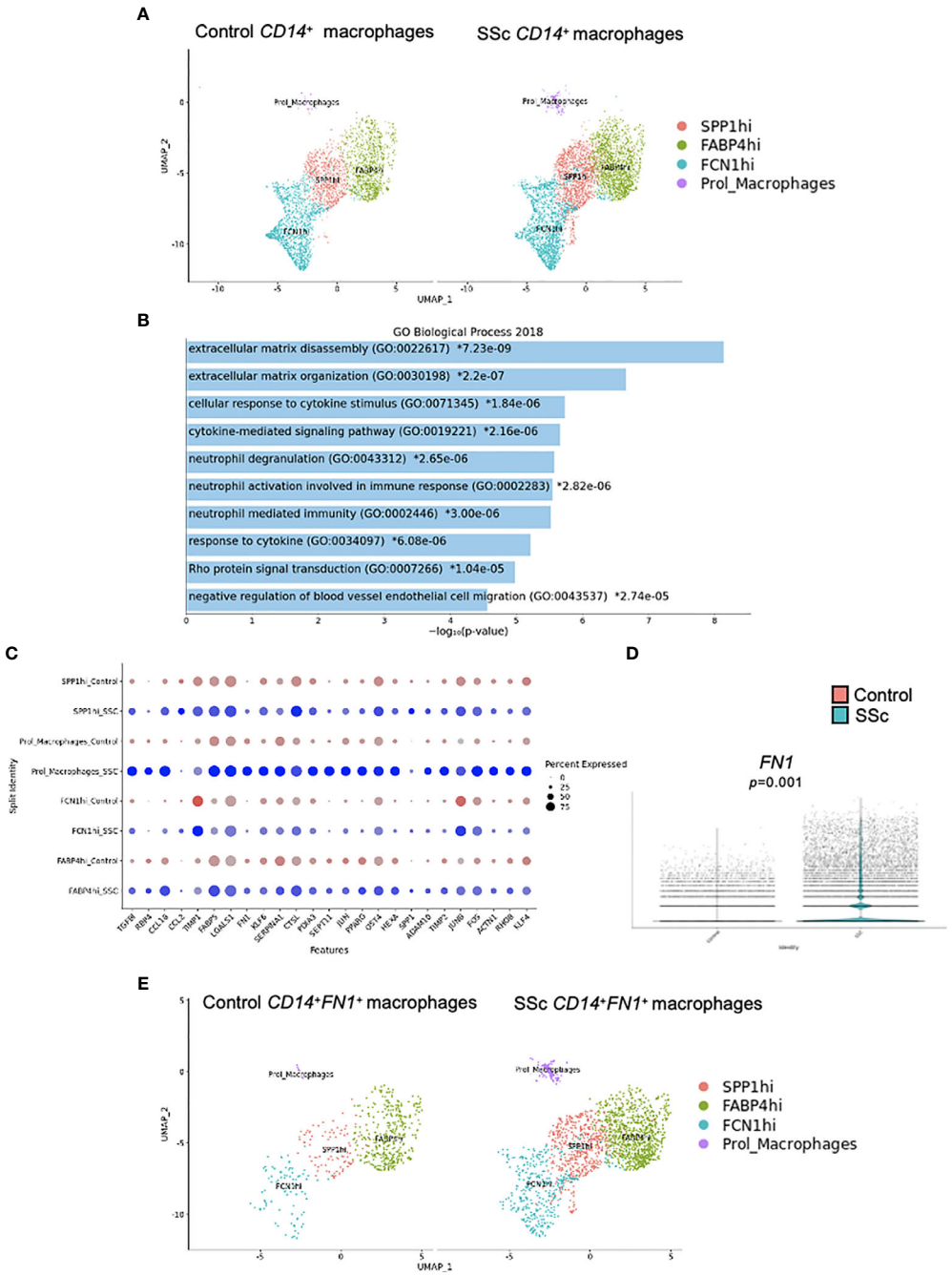

FIGURE 4 | Characteristic of CD14$^+$ macrophages in SSc-ILD lung tissues. Four human healthy control (HC) and 4 SSc-ILD lung tissue samples were used for a single-cell (sc) RNA-sequencing analysis according to Valenzi et al. (26). **(A)** UMAP plot visualization of CD14$^+$ cells in macrophage clusters in HC and SSc-ILD samples. **(B)** Pathway expression in the specific GO biological process (Enrichr 2018) and the expression of selected fibrotic-related genes **(C)** upregulated in SSc-ILD CD14$^+$fibronectin (FN1)$^+$ cells compared to HC CD14$^+$ cells in lungs. **(D)** *FN1* expression in SSc-ILD CD14$^+$ cells compared to HC CD14$^+$ cells in lungs (N=4, *Mann Whitney-U-test)*. **(E)** UMAP plot visualization of CD14$^+$ cells in macrophage clusters in HC and SSc-ILD samples. UMAP, uniform manifold approximation and projection; SSc-ILD, systemic sclerosis-associated interstitial lung disease.

and fibronectin (**Figures 5B, C**). Time-dependent profibrotic stimulation with TGFβ, IL-4, IL-10 and IL-13 cytokines revealed that CD14$^+$ monocytes upregulated profibrotic gene expression already after 24h and sustain these levels up to 7 days (**Figure 5D**). Of note, we did not observe any difference in the differentiation potential between CD14$^+$ monocytes obtained from SSc patients and healthy controls.

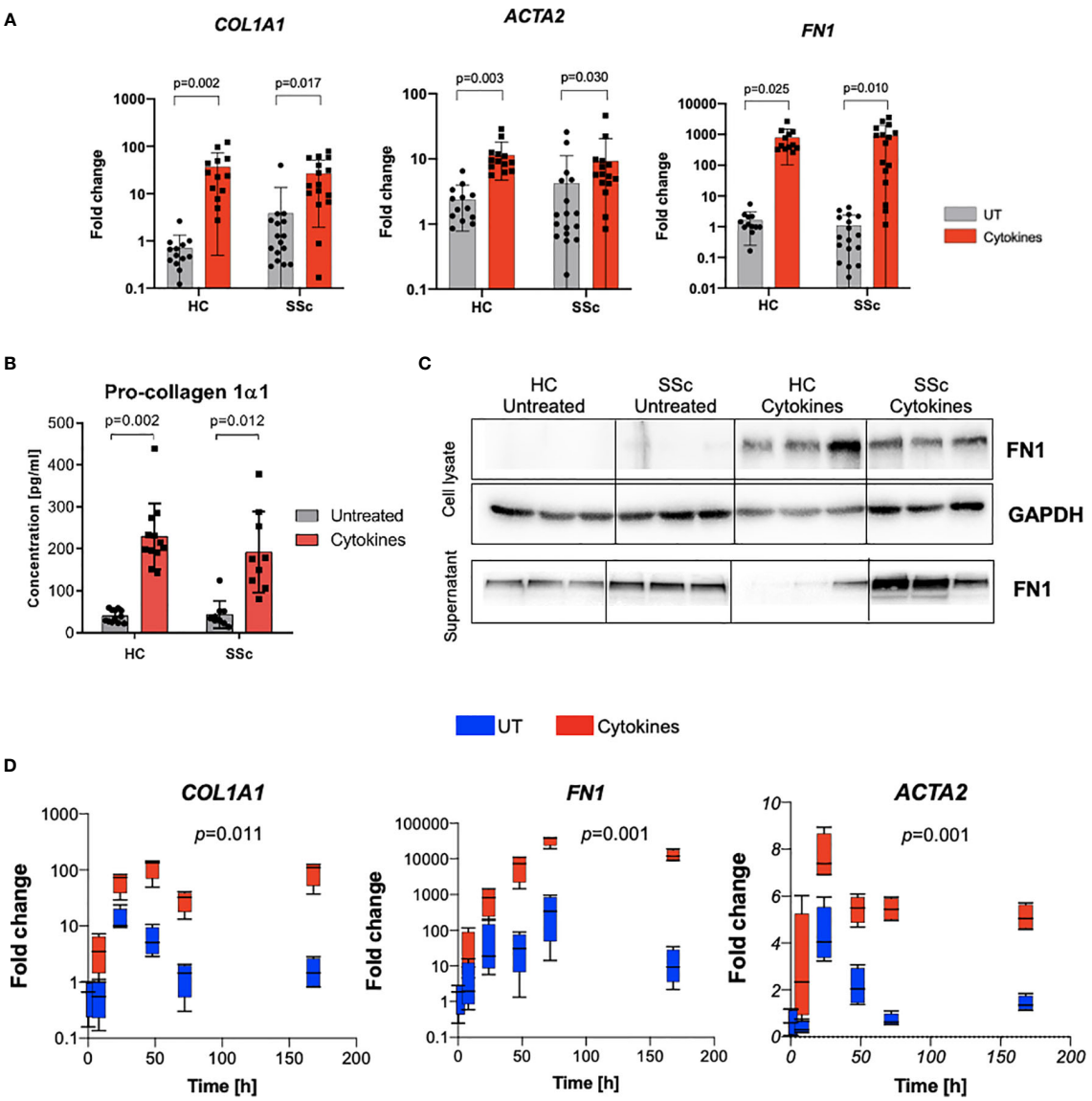

FIGURE 5 | Profibrotic stimulation induces differentiation of monocytes into fibroblast-like cells. **(A)** mRNA expression of *COL1A1, ACTA2 and FN1* after profibrotic cytokines stimulation (TGFβ, IL-4, IL-10, IL-13 [10 ng/ml each]) of HC and SSc monocytes (N=13, *two-way ANOVA with Benjamini, Krieger and Yekutieli post-hoc test*). **(B)** ELISA measurement of Pro-collagen 1α1 concentration in supernatants from CD14$^+$ monocytes after profibrotic cytokines stimulation (TGFβ, IL-4, IL-10, IL-13, [10 ng/ml each]) (N=13, *two-way ANOVA with Benjamini, Krieger and Yekutieli post-hoc test*). **(C)** Western blot assessment of fibronectin level in cell lysates and supernatants from CD14$^+$ monocytes stimulated with profibrotic cytokines (TGFβ, IL-4, IL-10, IL-13, [10 ng/ml each]) (N=3). **(D)** Time-dependent mRNA expression of *COL1A1, ACTA2 and FN1* after profibrotic cytokines stimulation (TGFβ, IL-4, IL-10, IL-13 [10 ng/ml each]) of HC monocytes at following time points: 0, 8, 24, 47, 72 and 168h (N=4, *two-way ANOVA with Tukey's multiple comparison test, p values for row factor*).

Co-Culture With Dermal Fibroblasts Enhances Profibrotic Phenotype of CD14$^+$ Monocytes

We hypothesized that the microenvironment might play a determinant role in the profibrotic response of CD14$^+$ monocytes. To test this hypothesis, we co-cultured CD14$^+$ monocytes with side-matched dermal fibroblast from SSc patients and HCs for 7 days. To analyze gene expression, cell types were separated using FACS sorting. We observed that co-culture with dermal fibroblasts induced expression of profibrotic genes *ACTA2*, *COL1A1* and *FN1* in both HC and SSc monocytes. Importantly, we noticed a significant induction of gene expression by SSc fibroblasts (**Figure 6A**).

Further, we aimed to observe phenotypic changes of CD14$^+$ monocytes after co-cultures in 2D and 3D models. Monocytes, which were sorted out after the 2D co-culture and re-plated in a chamber slide, were stained with phalloidin and anti-αSMA antibody. Compared to monocytes cultured alone, cells after

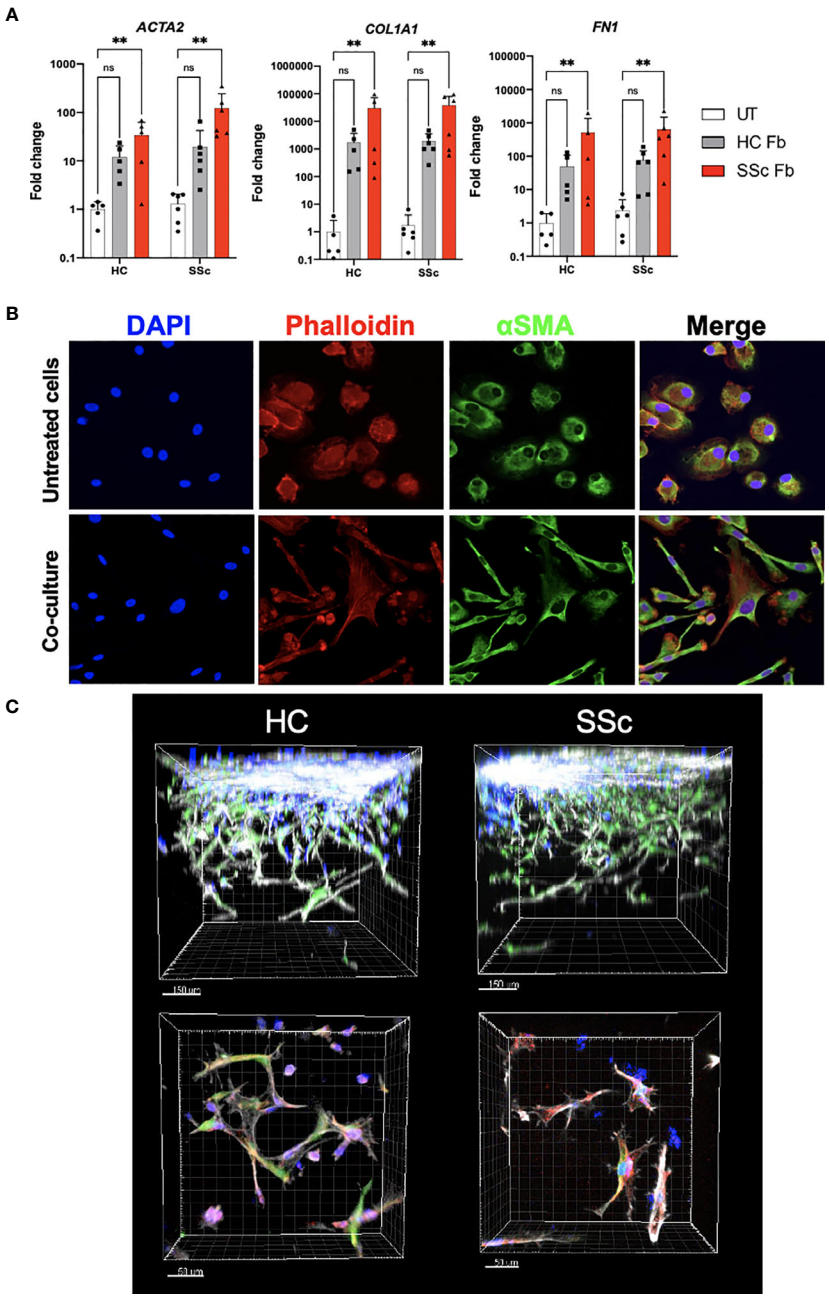

FIGURE 6 | Profibrotic microenvironment induces differentiation of monocytes into fibroblast-like cells. **(A)** mRNA expression of *ACTA2*, *COL1A1 and FN1* in $CD14^+$ monocytes from HC and SSc patients after co-culture with HC and SSc skin fibroblasts (HC N=5, SSc N=6, *two-way ANOVA with Uncorrected Fischer's LSD post-hoc test, **p < 0.005*). **(B)** Representative images of immunofluorescence staining of $CD14^+$ monocytes with and without co-culture with fibroblasts (blue– DAPI nuclear staining, red– Phalloidin staining, green- α-SMA staining). **(C)** Representative images of immunofluorescence staining of HC and SSc $CD14^+$ monocytes co-cultured with fibroblasts in 3D hydrogel model (blue– monocytes stained with Cell Trace Violet, green– fibroblasts stained with CFSE, red– α-SMA staining, grey- Phalloidin staining). ns, not significant.

the co-culture acquired spindle shape, however, they failed to form stress fibers (**Figure 6B**). Similar characteristics were observed for monocytes in 3D co-culture (**Figure 6C**). Taken together, the fibroblast microenvironment induced a change in monocyte gene expression and morphology towards myofibroblast-like cells.

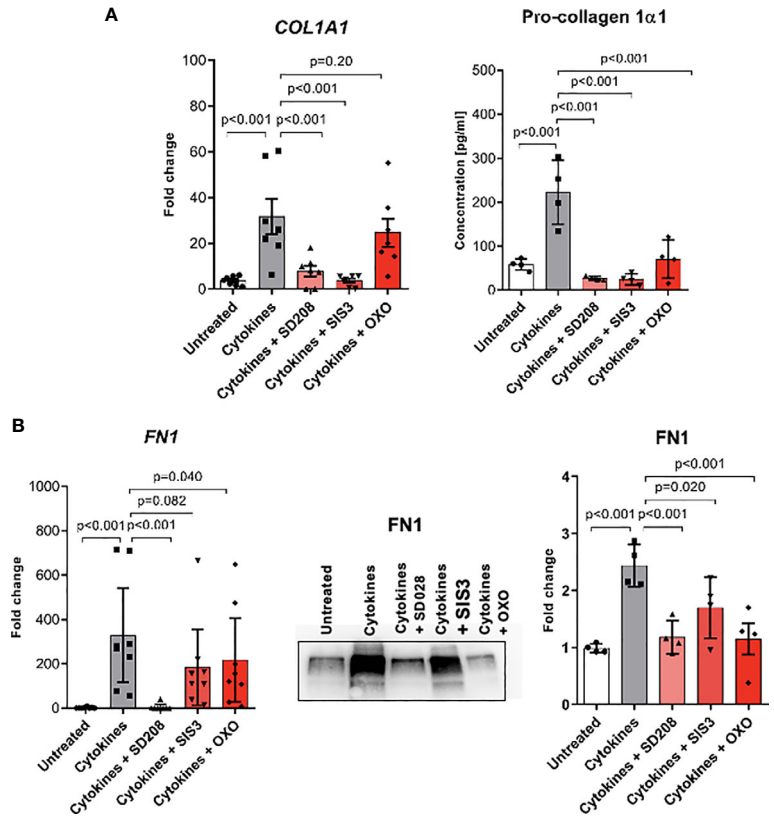

FIGURE 7 | Monocyte-to-fibroblast-like cells differentiation is dependent on TGFβ signalling pathways. **(A)** *COL1A1* mRNA expression level and ELISA measurements of Pro-collagen 1α1 protein level in supernatants after profibrotic cytokine stimulation (TGFβ, IL-4, IL-10, IL-13 [10 ng/ml each]) and treated with TGFβ signalling pathway inhibitors [SD208 and (5Z)-7-Oxozeaenol (OXO) 1 μM, SIS3 2 μM] (N=4-7, *one-way ANOVA with Benjamini, Krieger and Yekutieli post-hoc test*). **(B)** *FN1* mRNA expression level and Western Blot analysis, and corresponding densitometry of Fibronectin protein level in the supernatants after profibrotic cytokine stimulation (TGFβ, IL-4, IL-10, IL-13 [10 ng/ml each]) and treated with TGFβ signalling pathway inhibitors [SD208 and (5Z)-7-Oxozeaenol (OXO) 1 μM, SIS3 2 μM] (N=4-7, *one-way ANOVA with Benjamini, Krieger and Yekutieli post-hoc test*).

TGFβ Is a Key Regulator of Profibrotic Gene Expression in Monocyte-Derived Myofibroblast-Like Cells

Fibrotic processes might be driven by various stimuli; however, TGFβ is regarded as a pivotal mediator during SSc. To analyze the role of TGFβ signalling in monocyte-to-myofibroblast-like cell differentiation, we inhibited selected TGFβ downstream pathways in $CD14^+$ monocytes treated with the profibrotic cytokine cocktail (TGFβ, IL-4, IL-10 and IL-13). Treatment with the TGFBR1 kinase inhibitor SD-208 completely abolished expression of the ECM components collagen 1 and fibronectin on both mRNA and protein levels (**Figure 7**). Interestingly, TGFβ-induced expression of *COL1A1* was suppressed by the inhibitor of canonical SMAD-dependent pathway SIS3, but not by inhibition of TAK1-dependent non-canonical pathway with 5z-7-oxozeaenol (OXO). On the other hand, blocking of canonical and non-canonical TGFβ downstream pathways was sufficient to decrease expression and secretion of fibronectin (**Figure 7B**).

DISCUSSION

Our data demonstrated that human peripheral blood circulating $CD14^+$ monocytes exhibited profibrotic phenotype in SSc patients. Similarly, several reports indicated fibroblast-like/circulating Collagen I-producing $CD14^+$ monocytes or $CD14^-$ fibrocytes as profibrotic cell progeny in SSc (35). Likewise, the alternatively activated macrophages derived from circulating $CD14^+$ monocytes have also been considered as profibrotic cells in SSc (36). SSc patients have higher levels of circulating $CD34^+CD14^+$ cells, Collagen-I-producing $CD14^+$ monocytes and $CD163^+$ monocytes (36). Importantly, monocyte count could be incorporated into the clinical assessment of patients with fibro-proliferative disorders (37), including SSc patients with interstitial lung disease (ILD). Accordingly, the elevated numbers of Collagen-I-producing fibrocytes and profibrotic monocytes in SSc patients were associated with ILD progression and implicated in the pathogenesis of SSc-ILD (36). Circulating Collagen-I-producing fibrocytes have also been coupled with a growing repertoire of human diseases

including renal fibrosis (38), cirrhosis (39), nephrogenic systemic fibrosis (40), pulmonary fibrosis (41–43), and asthma (44).

It has been reported that the fibronectin splice variant-fibronectin extra domain A (FnEDA) is an endogenous TLR4 ligand. Importantly, elevated levels of FnEDA were demonstrated in the serum and skin lesions from SSc patients and in mouse model of cutaneous fibrosis (45). In chronic inflammatory diseases and during the healing phase of acute inflammatory reactions, the alternatively activated M(IL-4) macrophages showed significantly upregulated levels of fibronectin that suggest an active role of fibronectin$^+$ macrophages in the ECM deposition and tissue remodeling (46). Furthermore, the alveolar macrophages from lungs of SSc-ILD patients displayed elevated levels of fibronectin (47). These reports are in line with our results, which presented the elevated fibronectin levels in circulating CD14$^+$ monocytes and CD14$^+$ pulmonary macrophages in SSc patients and highlighted the capability of CD14$^+$ monocytes to acquire a profibrotic phenotype. Of note, monocyte-to-macrophage differentiation has been linked with the increase production of fibronectin (48). We, therefore, concluded that tissue-infiltrating CD14$^+$ monocytes/macrophages can be considered as ECM producers in the pathogenesis of fibrosis in SSc. All these data point to fibronectin as a potential target in therapeutic strategy in SSc.

Monocyte infiltration into the tissue affects the initiation of fibrotic processes in the skin and internal organs in SSc (49–51). Our data clearly presented infiltrating CD14$^+$ monocytes in the collagen-rich area in SSc-ILD lungs, myocardium of SSc patients with inflammatory dilated cardiomyopathy (iDCM) and in SSc skin (27). Increased numbers of spindle-shaped CD14$^+$CD34$^+$collagen-I$^+$ cells were found in the lungs of SSc-ILD patients (36). The bone marrow origin of fibroblasts or myofibroblasts in different tissues under homeostasis and disease condition has been debatable for many years now. *In vivo* data, with the use of cutaneous wound mouse model, confirmed that at least a part (15%-20%) of the spindle-shaped dermal fibroblasts were bone marrow origin (52). In contrast, another report suggested that bone marrow-derived progenitors contributed to the inflammatory cell pool infiltrating the wound area; however, they did not differentiate into dermal (myo) fibroblasts at the wound site (53, 54). In the bleomycin-induced skin fibrosis model, a significant number of CD45-positive collagen-producing cells of bone marrow origin contributed to collagen production during dermal fibrogenesis but not under homeostasis, indicating bone marrow originated cells as a cell source for (myo)fibroblasts under disease condition (55). Similarly, in bleomycin-induced lung fibrosis mouse model bone marrow-derived progenitors gave rise to collagen-producing cells but not to αSMA$^+$ myofiboblasts in the inflamed/fibrotic lungs (56, 57). Oppositely, in the renal fibrosis the inflammatory macrophages, characterized by alternatively activated macrophage markers, acquired fibroblast phenotype by collagen I and αSMA expression and actively contributed to the fibrogenesis (58).

Nevertheless, the transition of bone marrow-derived monocytes or macrophages (mainly alternatively activated macrophages) into functional myofibroblasts has been mediated by canonical SMAD2/3-dependent or non-canonical TAK-1-dependent TGFβ signal (24, 59–61). Accordingly, our results confirmed that both canonical and non-canonical TGFβ pathways were important to obtain the fibroblast-like phenotype of circulating CD14$^+$ monocytes, indicating the broad treatment options.

The pathophysiology of SSc is closely related to the activated TGFβ-dependent pathway. The levels of a latent, not-active form of TGFβ is similar in SSc and healthy serum samples. Active TGFβ serum levels were significantly higher in SSc, mainly in dcSSc, patients and correlated with clinical manifestations (digital ulcers, lung fibrosis, positive antitopoisomerase I and higher modified Rodnan score) (62). These results indicate TGFβ as a potential marker of fibrotic and vascular involvement in SSc on one side, and on the other side, it reflects an altered microenvironment, which may predispose circulating monocytes towards an activated and profibrotic phenotype. Accordingly, we used this cytokine, among others, to activate circulating monocytes towards a profibrotic phenotype. As expected, CD14$^+$ monocytes stimulated with TGFβ, IL-4, IL-10 and IL-13 or co-cultured in 2D and 3D model with human dermal fibroblasts were able to adopt a functional myofibroblast-like phenotype that may indicate these cells as one of the cellular sources of profibrotic cells upon their entrance into the tissues. The previous report indeed showed that GM-CSF, IL-4 and endothelin-1 alone or in combination induced myofibroblast-like differentiation of circulating SSc and healthy monocytes (63). Additionally, the profibrotic phenotype of circulating CD14$^+$ monocytes from SSc-ILD patients was confirmed by the expression of CD163 and boosted secretion of CCL18 and IL-10 in response to pro-inflammatory stimuli (36). However, as in our stimulation conditions, monocytes from SSc patients showed no differences in acquiring more pronounced profibrotic phenotype compared to monocytes from healthy donors. Therefore, we assume that under inflammatory conditions (i.e. in SSc) more circulating already activated monocytes are recruited to the injury site, where they play a profibrotic role, either by the transition into fibroblast-like cells or by the production of profibrotic stimuli. In line with this hypothesis, Bhandari et al. demonstrated that soluble factors in the local milieu are crucial for pro-fibrotic activation of SSc macrophages (measured as secretion of CCL2, IL-6, TGFβ), arisen from circulating monocytes either stimulated with SSc sera or conditioned media from indirect co-culture with dermal SSc fibroblasts (64). These results point to monocytes and monocyte-derived macrophages as probable key players in fibrogenesis in SSc, suggesting targeted cell therapeutic options as feasible and favorable in SSc.

Besides a known and active role of IL-6 and TGF-β signalling in the pathogenesis of SSc, there is increasing evidence that also Th-2 cytokines: IL-4 and IL-13, are involved in the pathology of

SSc (65, 66). Both cytokines relate to profibrotic responses, including connection with increased expression of novel myofibroblast marker: periostin, a matricellular protein important in fibrogenesis (67). Based on our data, the combination of TGFβ, IL-4, IL-10 and IL-13 was sufficient to obtain a fibroblast-like phenotype by circulating $CD14^+$ monocytes, indicating that IL-4/IL-13 targeted therapy might be an attractive option against fibrogenesis in SSc (68). Indeed, a randomized, double-blind, placebo-controlled, 24-week, phase II, proof-of-concept study (trial registration number: NCT02921971) with romilkimab (a bispecific immunoglobulin-G4 antibody that binds and neutralizes IL-4/IL-13; SAR156597) in early dcSSc patients revealed a beneficial effect of this treatment on skin disease changes, i.e. statistically significant decrease in mRSS from baseline to week 24 versus placebo (69).

Given the alerted activation status of circulating $CD14^+$ monocytes and their ability to accumulate in the affected organs in SSc, we believe that further research should focus on finding even more targeted therapies, which may invert the activation status of monocytes in the circulation.

DATA AVAILABILITY STATEMENT

The RNAseq datasets for this study can be found in the Gene Expression Omnibus under the accession numbers: GSE157840, GSE128169.

ETHICS STATEMENT

Human blood samples and skin biopsies collection were approved by the local ethics committee of the Canton Zurich (KEK-ZH 515, PB-2016-02014, KEK-Nr 2018-01873). All study subjects provided written informed consent. The experiments with re-use of human material were approved by Swissethics (KEK-Nr 2019-00058, KEK-Nr 2018-01873) and were performed in conformity with the principles outlined in the Declaration of Helsinki. The animal study was reviewed and approved by Commission on Animal Experimentation of the Canton Zurich.

AUTHOR CONTRIBUTIONS

GK directed the project and obtained funding. MR, AH, IK, SJ, and GK designed, analyzed, and interpreted experiments. MR, AH, IK, JS, and VM performed the experiments. CF-B and KK provided heart and lungs biopsies. MR, GK, and PB wrote the manuscript. OD, CF-B, ME contributed to final corrections of the drafted manuscript. All authors contributed to the article and approved the submitted version.

FUNDING

GK acknowledges support from the Swiss National Science Foundation (310030_152876/1; 310030_175663), Swiss Life Foundation and Swiss Heart Foundation.

ACKNOWLEDGMENTS

We thank Maria Comazzi-Fornallaz and Dr. Magdalena Diaz-Ovalle for performing immunohistochemistry, Functional Genomic Center University of Zurich for RNA sequencing and The Center for Microscopy and Image Analysis of University of Zurich for image scanning.

SUPPLEMENTARY MATERIAL

The Supplementary Material for this article can be found online at: https://www.frontiersin.org/articles/10.3389/fimmu.2021.642891/full#supplementary-material

REFERENCES

1. Allanore Y, Simms R, Distler O, Trojanowska M, Pope J, Denton CP, et al. Systemic Sclerosis. *Nat Rev Dis Primers* (2015) 1:15002. doi: 10.1038/nrdp.2015.2
2. Mayes MD, Lacey JV Jr, Beebe-Dimmer J, Gillespie BW, Cooper B, Laing TJ, et al. Prevalence, Incidence, Survival, and Disease Characteristics of Systemic Sclerosis in a Large US Population. *Arthritis Rheum* (2003) 48(8):2246–55. doi: 10.1002/art.11073
3. Elhai M, Meune C, Boubaya M, Avouac J, Hachulla E, Balbir-Gurman A, et al. Mapping and Predicting Mortality From Systemic Sclerosis. *Ann Rheum Dis* (2017) 76(11):1897–905. doi: 10.1136/annrheumdis-2017-211448
4. Bhattacharyya S, Wei J, Varga J. Understanding Fibrosis in Systemic Sclerosis: Shifting Paradigms, Emerging Opportunities. *Nat Rev Rheumatol* (2011) 8 (1):42–54. doi: 10.1038/nrrheum.2011.149
5. Garrett SM, Baker Frost D, Feghali-Bostwick C. The Mighty Fibroblast and Its Utility in Scleroderma Research. *J Scleroderma Relat Disord* (2017) 2(2):69–134. doi: 10.5301/jsrd.5000240
6. van Caam A, Vonk M, van den Hoogen F, van Lent P, van der Kraan P. Unraveling SSc Pathophysiology; The Myofibroblast. *Front Immunol* (2018) 9:2452. doi: 10.3389/fimmu.2018.02452
7. Pankov R, Yamada KM. Fibronectin at a Glance. *J Cell Sci* (2002) 115(Pt 20):3861–3. doi: 10.1242/jcs.00059
8. Xu WD, Leroy EC, Smith EA. Fibronectin Release by Systemic Sclerosis and Normal Dermal Fibroblasts in Response to TGF-Beta. *J Rheumatol* (1991) 18 (2):241–6.
9. Cooper SM, Keyser AJ, Beaulieu AD, Ruoslahti E, Nimni ME, Quismorio FP Jr. Increase in Fibronectin in the Deep Dermis of Involved Skin in Progressive Systemic Sclerosis. *Arthritis Rheum* (1979) 22(9):983–7. doi: 10.1002/art.1780220906
10. Falke LL, Gholizadeh S, Goldschmeding R, Kok RJ, Nguyen TQ. Diverse Origins of the Myofibroblast-Implications for Kidney Fibrosis. *Nat Rev Nephrol* (2015) 11(4):233–44. doi: 10.1038/nrneph.2014.246
11. Reilkoff RA, Bucala R, Herzog EL. Fibrocytes: Emerging Effector Cells in Chronic Inflammation. *Nat Rev Immunol* (2011) 11(6):427–35. doi: 10.1038/nri2990
12. Chang FC, Chou YH, Chen YT, Lin SL. Novel Insights Into Pericyte-Myofibroblast Transition and Therapeutic Targets in Renal Fibrosis. *J Formos Med Assoc* (2012) 111(11):589–98. doi: 10.1016/j.jfma.2012.09.008
13. Wilson CL, Stephenson SE, Higuero JP, Feghali-Bostwick C, Hung CF, Schnapp LM. Characterization of Human PDGFR-Beta-Positive Pericytes

From IPF and Non-IPF Lungs. *Am J Physiol Lung Cell Mol Physiol* (2018) 315 (6):L991–L1002. doi: 10.1152/ajplung.00289.2018
14. Hill C, Jones MG, Davies DE, Wang Y. Epithelial-Mesenchymal Transition Contributes to Pulmonary Fibrosis *via* Aberrant Epithelial/Fibroblastic Cross-Talk. *J Lung Health Dis* (2019) 3(2):31–5. doi: 10.29245/2689-999X/2019/2.1149
15. Jimenez SA, Piera-Velazquez S. Endothelial to Mesenchymal Transition (EndoMT) in the Pathogenesis of Systemic Sclerosis-Associated Pulmonary Fibrosis and Pulmonary Arterial Hypertension. Myth or Reality? *Matrix Biol* (2016) 51:26–36. doi: 10.1016/j.matbio.2016.01.012
16. Ayers NB, Sun CM, Chen SY. Transforming Growth Factor-Beta Signaling in Systemic Sclerosis. *J BioMed Res* (2018) 32(1):3–12. doi: 10.7555/JBR.31.20170034
17. Farina G, Lafyatis D, Lemaire R, Lafyatis R. A Four-Gene Biomarker Predicts Skin Disease in Patients With Diffuse Cutaneous Systemic Sclerosis. *Arthritis Rheum* (2010) 62(2):580–8. doi: 10.1002/art.27220
18. Walton KL, Johnson KE, Harrison CA. Targeting TGF-Beta Mediated SMAD Signaling for the Prevention of Fibrosis. *Front Pharmacol* (2017) 8:461. doi: 10.3389/fphar.2017.00461
19. Leask A. Scar Wars: Is TGFbeta the Phantom Menace in Scleroderma? *Arthritis Res Ther* (2006) 8(4):213. doi: 10.1186/ar1976
20. Varga J, Pasche B. Transforming Growth Factor Beta as a Therapeutic Target in Systemic Sclerosis. *Nat Rev Rheumatol* (2009) 5(4):200–6. doi: 10.1038/nrrheum.2009.26
21. Shi C, Pamer EG. Monocyte Recruitment During Infection and Inflammation. *Nat Rev Immunol* (2011) 11(11):762–74. doi: 10.1038/nri3070
22. Kania G, Rudnik M, Distler O. Involvement of the Myeloid Cell Compartment in Fibrogenesis and Systemic Sclerosis. *Nat Rev Rheumatol* (2019) 15(5):288–302. doi: 10.1038/s41584-019-0212-z
23. Blyszczuk P, Germano D, Stein S, Moch H, Matter CM, Beck-Schimmer B, et al. Profibrotic Potential of Prominin-1+ Epithelial Progenitor Cells in Pulmonary Fibrosis. *Respir Res* (2011) 12:126. doi: 10.1186/1465-9921-12-126
24. Kania G, Blyszczuk P, Stein S, Valaperti A, Germano D, Dirnhofer S, et al. Heart-Infiltrating Prominin-1+/CD133+ Progenitor Cells Represent the Cellular Source of Transforming Growth Factor Beta-Mediated Cardiac Fibrosis in Experimental Autoimmune Myocarditis. *Circ Res* (2009) 105 (5):462–70. doi: 10.1161/CIRCRESAHA.109.196287
25. LeRoy EC, Black C, Fleischmajer R, Jablonska S, Krieg T, Medsger TA Jr, et al. Scleroderma (Systemic Sclerosis): Classification, Subsets and Pathogenesis. *J Rheumatol* (1988) 15(2):202–5.
26. Valenzi E, Bulik M, Tabib T, Morse C, Sembrat J, Trejo Bittar H, et al. Single-Cell Analysis Reveals Fibroblast Heterogeneity and Myofibroblasts in Systemic Sclerosis-Associated Interstitial Lung Disease. *Ann Rheum Dis* (2019) 78(10):1379–87. doi: 10.1136/annrheumdis-2018-214865
27. Rudnik M, Rolski F, Jordan S, Mertelj T, Stellato M, Distler O, et al. CD52 Regulates Monocyte Adhesion and Interferon Type I Signalling in Systemic Sclerosis Patients. *Arthritis Rheumatol* (2021). doi: 10.1002/art.41737
28. Lun ATL, Riesenfeld S, Andrews T, Dao TP, Gomes Tparticipants in the 1st Human Cell Atlas J, et al. EmptyDrops: Distinguishing Cells From Empty Droplets in Droplet-Based Single-Cell RNA Sequencing Data. *Genome Biol* (2019) 20(1):63. doi: 10.1186/s13059-019-1662-y
29. Griffiths JA, Richard AC, Bach K, Lun ATL, Marioni JC. Detection and Removal of Barcode Swapping in Single-Cell RNA-Seq Data. *Nat Commun* (2018) 9(1):2667. doi: 10.1038/s41467-018-05083-x
30. Hafemeister C, Satija R. Normalization and Variance Stabilization of Single-Cell RNA-Seq Data Using Regularized Negative Binomial Regression. *Genome Biol* (2019) 20(1):296. doi: 10.1186/s13059-019-1874-1
31. Butler A, Hoffman P, Smibert P, Papalexi E, Satija R. Integrating Single-Cell Transcriptomic Data Across Different Conditions, Technologies, and Species. *Nat Biotechnol* (2018) 36(5):411–20. doi: 10.1038/nbt.4096
32. Stuart T, Butler A, Hoffman P, Hafemeister C, Papalexi E, Mauck WM3rd, et al. Comprehensive Integration of Single-Cell Data. *Cell* (2019) 177(7):1888–902 e21. doi: 10.1016/j.cell.2019.05.031
33. Schniering J, Benesova M, Brunner M, Haller S, Cohrs S, Frauenfelder T, et al. Visualisation of Interstitial Lung Disease by Molecular Imaging of Integrin Alphavbeta3 and Somatostatin Receptor 2. *Ann Rheum Dis* (2019) 78(2):218–27. doi: 10.1136/annrheumdis-2018-214322
34. Asano Y. The Pathogenesis of Systemic Sclerosis: An Understanding Based on a Common Pathologic Cascade Across Multiple Organs and Additional Organ-Specific Pathologies. *J Clin Med* (2020) 9(9):2687. doi: 10.3390/jcm9092687
35. Brunasso AM, Massone C. Update on the Pathogenesis of Scleroderma: Focus on Circulating Progenitor Cells. *F1000Res* (2016) 5:F1000 Faculty Rev-723. doi: 10.12688/f1000research.7986.1
36. Mathai SK, Gulati M, Peng X, Russell TR, Shaw AC, Rubinowitz AN, et al. Circulating Monocytes From Systemic Sclerosis Patients With Interstitial Lung Disease Show an Enhanced Profibrotic Phenotype. *Lab Invest* (2010) 90 (6):812–23. doi: 10.1038/labinvest.2010.73
37. Scott MKD, Quinn K, Li Q, Carroll R, Warsinske H, Vallania F, et al. Increased Monocyte Count as a Cellular Biomarker for Poor Outcomes in Fibrotic Diseases: A Retrospective, Multicentre Cohort Study. *Lancet Respir Med* (2019) 7(6):497–508. doi: 10.1016/S2213-2600(18)30508-3
38. Sakai N, Wada T, Yokoyama H, Lipp M, Ueha S, Matsushima K, et al. Secondary Lymphoid Tissue Chemokine (SLC/CCL21)/CCR7 Signaling Regulates Fibrocytes in Renal Fibrosis. *Proc Natl Acad Sci USA* (2006) 103 (38):14098–103. doi: 10.1073/pnas.0511200103
39. Kisseleva T, Uchinami H, Feirt N, Quintana-Bustamante O, Segovia JC, Schwabe RF, et al. Bone Marrow-Derived Fibrocytes Participate in Pathogenesis of Liver Fibrosis. *J Hepatol* (2006) 45(3):429–38. doi: 10.1016/j.jhep.2006.04.014
40. Bucala R. Circulating Fibrocytes: Cellular Basis for NSF. *J Am Coll Radiol* (2008) 5(1):36–9. doi: 10.1016/j.jacr.2007.08.016
41. Andersson-Sjoland A, de Alba CG, Nihlberg K, Becerril C, Ramirez R, Pardo A, et al. Fibrocytes Are a Potential Source of Lung Fibroblasts in Idiopathic Pulmonary Fibrosis. *Int J Biochem Cell Biol* (2008) 40(10):2129–40. doi: 10.1016/j.biocel.2008.02.012
42. Mehrad B, Burdick MD, Zisman DA, Keane MP, Belperio JA, Strieter RM. Circulating Peripheral Blood Fibrocytes in Human Fibrotic Interstitial Lung Disease. *Biochem Biophys Res Commun* (2007) 353(1):104–8. doi: 10.1016/j.bbrc.2006.11.149
43. Moeller A, Gilpin SE, Ask K, Cox G, Cook D, Gauldie J, et al. Circulating Fibrocytes Are an Indicator of Poor Prognosis in Idiopathic Pulmonary Fibrosis. *Am J Respir Crit Care Med* (2009) 179(7):588–94. doi: 10.1164/rccm.200810-1534OC
44. Wang CH, Huang CD, Lin HC, Lee KY, Lin SM, Liu CY, et al. Increased Circulating Fibrocytes in Asthma With Chronic Airflow Obstruction. *Am J Respir Crit Care Med* (2008) 178(6):583–91. doi: 10.1164/rccm.200710-1557OC
45. Bhattacharyya S, Tamaki Z, Wang W, Hinchcliff M, Hoover P, Getsios S, et al. FibronectinEDA Promotes Chronic Cutaneous Fibrosis Through Toll-Like Receptor Signaling. *Sci Transl Med* (2014) 6(232):232ra50. doi: 10.1126/scitranslmed.3008264
46. Gratchev A, Guillot P, Hakiy N, Politz O, Orfanos CE, Schledzewski K, et al. Alternatively Activated Macrophages Differentially Express Fibronectin and Its Splice Variants and the Extracellular Matrix Protein betaIG-H3. *Scand J Immunol* (2001) 53(4):386–92. doi: 10.1046/j.1365-3083.2001.00885.x
47. Kinsella MB, Smith EA, Miller KS, LeRoy EC, Silver RM. Spontaneous Production of Fibronectin by Alveolar Macrophages in Patients With Scleroderma. *Arthritis Rheum* (1989) 32(5):577–83. doi: 10.1002/anr.1780320511
48. Sudhakaran PR, Radhika A, Jacob SS. Monocyte Macrophage Differentiation *In Vitro*: Fibronectin-Dependent Upregulation of Certain Macrophage-Specific Activities. *Glycoconj J* (2007) 24(1):49–55. doi: 10.1007/s10719-006-9011-2
49. Gu YS, Kong J, Cheema GS, Keen CL, Wick G, Gershwin ME. The Immunobiology of Systemic Sclerosis. *Semin Arthritis Rheum* (2008) 38 (2):132–60. doi: 10.1016/j.semarthrit.2007.10.010
50. Bosello S, Angelucci C, Lama G, Alivernini S, Proietti G, Tolusso B, et al. Characterization of Inflammatory Cell Infiltrate of Scleroderma Skin: B Cells and Skin Score Progression. *Arthritis Res Ther* (2018) 20(1):75. doi: 10.1186/s13075-018-1569-0
51. Whitfield ML, Finlay DR, Murray JI, Troyanskaya OG, Chi JT, Pergamenschikov A, et al. Systemic and Cell Type-Specific Gene Expression Patterns in Scleroderma Skin. *Proc Natl Acad Sci USA* (2003) 100(21):12319–24. doi: 10.1073/pnas.1635114100

52. Fathke C, Wilson L, Hutter J, Kapoor V, Smith A, Hocking A, et al. Contribution of Bone Marrow-Derived Cells to Skin: Collagen Deposition and Wound Repair. *Stem Cells* (2004) 22(5):812–22. doi: 10.1634/stemcells.22-5-812
53. Barisic-Dujmovic T, Boban I, Clark SH. Fibroblasts/myofibroblasts That Participate in Cutaneous Wound Healing Are Not Derived From Circulating Progenitor Cells. *J Cell Physiol* (2010) 222(3):703–12. doi: 10.1002/jcp.21997
54. Ishii G, Sangai T, Sugiyama K, Ito T, Hasebe T, Endoh Y, et al. In Vivo Characterization of Bone Marrow-Derived Fibroblasts Recruited Into Fibrotic Lesions. *Stem Cells* (2005) 23(5):699–706. doi: 10.1634/stemcells.2004-0183
55. Higashiyama R, Nakao S, Shibusawa Y, Ishikawa O, Moro T, Mikami K, et al. Differential Contribution of Dermal Resident and Bone Marrow-Derived Cells to Collagen Production During Wound Healing and Fibrogenesis in Mice. *J Invest Dermatol* (2011) 131(2):529–36. doi: 10.1038/jid.2010.314
56. Hashimoto N, Jin H, Liu T, Chensue SW, Phan SH. Bone Marrow-Derived Progenitor Cells in Pulmonary Fibrosis. *J Clin Invest* (2004) 113(2):243–52. doi: 10.1172/JCI200418847
57. Habiel DM, Hogaboam CM. Heterogeneity of Fibroblasts and Myofibroblasts in Pulmonary Fibrosis. *Curr Pathobiol Rep* (2017) 5(2):101–10. doi: 10.1007/s40139-017-0134-x
58. Meng XM, Wang S, Huang XR, Yang C, Xiao J, Zhang Y, et al. Inflammatory Macrophages can Transdifferentiate Into Myofibroblasts During Renal Fibrosis. *Cell Death Dis* (2016) 7(12):e2495. doi: 10.1038/cddis.2016.402
59. Blyszczuk P, Muller-Edenborn B, Valenta T, Osto E, Stellato M, Behnke S, et al. Transforming Growth Factor-Beta-Dependent Wnt Secretion Controls Myofibroblast Formation and Myocardial Fibrosis Progression in Experimental Autoimmune Myocarditis. *Eur Heart J* (2017) 38(18):1413–25. doi: 10.1093/eurheartj/ehw116
60. Wang S, Meng XM, Ng YY, Ma FY, Zhou S, Zhang Y, et al. TGF-Beta/Smad3 Signalling Regulates the Transition of Bone Marrow-Derived Macrophages Into Myofibroblasts During Tissue Fibrosis. *Oncotarget* (2016) 7(8):8809–22. doi: 10.18632/oncotarget.6604
61. Lu J, Liu Q, Wang L, Tu W, Chu H, Ding W, et al. Increased Expression of Latent TGF-Beta-Binding Protein 4 Affects the Fibrotic Process in Scleroderma by TGF-Beta/SMAD Signaling. *Lab Invest* (2017) 97(9):1121. doi: 10.1038/labinvest.2017.43
62. Dziadzio M, Smith RE, Abraham DJ, Black CM, Denton CP. Circulating Levels of Active Transforming Growth Factor Beta1 Are Reduced in Diffuse Cutaneous Systemic Sclerosis and Correlate Inversely With the Modified Rodnan Skin Score. *Rheumatol (Oxford)* (2005) 44(12):1518–24. doi: 10.1093/rheumatology/kei088
63. Binai N, O'Reilly S, Griffiths B, van Laar JM, Hugle T. Differentiation Potential of CD14+ Monocytes Into Myofibroblasts in Patients With Systemic Sclerosis. *PloS One* (2012) 7(3):e33508. doi: 10.1371/journal.pone.0033508
64. Bhandari R, Ball MS, Martyanov V, Popovich D, Schaafsma E, Han S, et al. Profibrotic Activation of Human Macrophages in Systemic Sclerosis. *Arthritis Rheumatol* (2020) 72(7):1160–9. doi: 10.1002/art.41243
65. Jakubzick C, Choi ES, Joshi BH, Keane MP, Kunkel SL, Puri RK, et al. Therapeutic Attenuation of Pulmonary Fibrosis *via* Targeting of IL-4- and IL-13-Responsive Cells. *J Immunol* (2003) 171(5):2684–93. doi: 10.4049/jimmunol.171.5.2684
66. Hasegawa M, Fujimoto M, Kikuchi K, Takehara K. Elevated Serum Levels of Interleukin 4 (IL-4), IL-10, and IL-13 in Patients With Systemic Sclerosis. *J Rheumatol* (1997) 24(2):328–32. doi: 10.1016/0923-1811(96)89424-2
67. Okamoto M, Izuhara K, Ohta S, Ono J, Hoshino T. Ability of Periostin as a New Biomarker of Idiopathic Pulmonary Fibrosis. *Adv Exp Med Biol* (2019) 1132:79–87. doi: 10.1007/978-981-13-6657-4_9
68. Gasparini G, Cozzani E, Parodi A. Interleukin-4 and Interleukin-13 as Possible Therapeutic Targets in Systemic Sclerosis. *Cytokine* (2020) 125:154799. doi: 10.1016/j.cyto.2019.154799
69. Allanore Y, Wung P, Soubrane C, Esperet C, Marrache F, Bejuit R, et al. A Randomised, Double-Blind, Placebo-Controlled, 24-Week, Phase II, Proof-Of-Concept Study of Romilkimab (SAR156597) in Early Diffuse Cutaneous Systemic Sclerosis. *Ann Rheum Dis* (2020) 79(12):1600–7. doi: 10.1136/annrheumdis-2020-218447

Conflict of Interest: OD had consultancy relationship and/or has received research funding from Actelion, Acceleron Pharma, AnaMar, Bayer, Baecon Discovery, Blade Therapeutics, Boehringer, CSL Behring, ChemomAb, Curzion Pharmaceuticals, Ergonex, Galapagos NV, GSK, Glenmark Pharmaceuticals, Inventiva, Italfarmaco, iQvia, medac, Medscape, Mitsubishi Tanabe Pharma, MSD, Roche, Sanofi, UCBin the area of potential treatments of scleroderma and its complications. In addition, OD has a patent mir-29 for the treatment of systemic sclerosis issued (US8247389, EP2331143).

The remaining authors declare that the research was conducted in the absence of any commercial or financial relationships that could be construed as a potential conflict of interest.

Publisher's Note: All claims expressed in this article are solely those of the authors and do not necessarily represent those of their affiliated organizations, or those of the publisher, the editors and the reviewers. Any product that may be evaluated in this article, or claim that may be made by its manufacturer, is not guaranteed or endorsed by the publisher.

Advantages of publishing in Frontiers

OPEN ACCESS
Articles are free to read for greatest visibility and readership

FAST PUBLICATION
Around 90 days from submission to decision

HIGH QUALITY PEER-REVIEW
Rigorous, collaborative, and constructive peer-review

TRANSPARENT PEER-REVIEW
Editors and reviewers acknowledged by name on published articles

Frontiers
Avenue du Tribunal-Fédéral 34
1005 Lausanne | Switzerland

Visit us: www.frontiersin.org
Contact us: frontiersin.org/about/contact

REPRODUCIBILITY OF RESEARCH
Support open data and methods to enhance research reproducibility

DIGITAL PUBLISHING
Articles designed for optimal readership across devices

FOLLOW US
@frontiersin

IMPACT METRICS
Advanced article metrics track visibility across digital media

EXTENSIVE PROMOTION
Marketing and promotion of impactful research

LOOP RESEARCH NETWORK
Our network increases your article's readership